ANL/RAS 78-37

LIQUID-LIQUID CONTACT IN VAPOR EXPLOSION

by

Aryeh Segev

August 1978

Reactor Analysis and Safety Division
ARGONNE NATIONAL LABORATORY
9700 South Cass Avenue
Argonne, Illinois 60439

The facilities of Argonne National Laboratory are owned by the United States Government. Under the terms of a contract (W-31-109-Eng-38) between the U. S. Department of Energy, Argonne Universities Association and The University of Chicago, the University employs the staff and operates the Laboratory in accordance with policies and programs formulated, approved and reviewed by the Association.

MEMBERS OF ARGONNE UNIVERSITIES ASSOCIATION

The University of Arizona	Kansas State University	The Ohio State University
Carnegie-Mellon University	The University of Kansas	Ohio University
Case Western Reserve University	Loyola University	The Pennsylvania State University
The University of Chicago	Marquette University	Purdue University
University of Cincinnati	Michigan State University	Saint Louis University
Illinois Institute of Technology	The University of Michigan	Southern Illinois University
University of Illinois	University of Minnesota	The University of Texas at Austin
Indiana University	University of Missouri	Washington University
Iowa State University	Northwestern University	Wayne State University
The University of Iowa	University of Notre Dame	The University of Wisconsin

LIQUID-LIQUID CONTACT IN VAPOR EXPLOSION

A Thesis

Submitted to

The Graduate School

Northwestern University

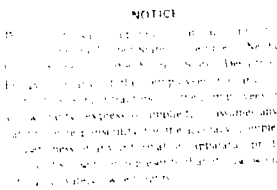

In Partial Fulfillment

of the Requirements for the Degree

Doctor of Philosophy

in the Field of Chemical Engineering

by

Aryeh Segev

August 1978

TABLE OF CONTENTS

LIST OF FIGURES

LIST OF TABLES

NOMENCLATURE

a	acceleration
A	atomic number
$A(T)$	constant
b	most dangerous wavelength growth rate parameter
C	specific heat
$C_\infty, C_i (i=0,3)$	constants
C_D	drag coefficient c
c	sound velocity
D	diameter
D_B	bubble diameter at point B
E_k	kinetic energy
E_m	mixing energy
F	force
g	gravity acceleration
h	film thickness
h_c	heat transfer coefficient
$\bar{h}_o$	dimensionless film thickness, defined in Eq. 3.42
I, I'	impulse per unit area
J	nucleation rate
Ja	Jacob number, defined in Eq. B.3
K	Boltzmann's constant
$K_i (i=1,4)$	constants
k	thermal conductivity
L	cold liquid column length
L'	distance

L_m	length of mixing zone
ℓ	length of liquid
m	mass
$\dot{m}_c$	condensation rate
$\dot{m}_\ell$	volumetric flow rate
N	sites density
N_h	number of intermixed particles
N_1, N_{We}	dimensionless numbers, defined in Eq. 3.42
P, P'	pressure
P^*	dimensionless pressure, defined in Eq. 6.26
P_1	pressure in interaction chamber
Q	heat flux
R	radius
R_t	transition radius
r	cylindrical coordinate
S	debris area
S_o	shock tube area
S_b	dimensionless number
T	temperature
T^*	temperature at point B
T_{eq}	equilibrium temperature
T_{hn}	homogeneous nucleation temperature
T_I	interface temperature
T_m	MFB temperature
$T_{m,i}$	isothermal MFB temperature
T_{sat}	saturation temperature
T_{sn}	spontaneous nucleation temperature

t	time
Δt	time between bounces
t^*	dimensionless time, defined in Eq. 6.27
t_a	acoustic relief time
t_g	inertially growth time
$t_n \equiv t_{sf} + t_a + t_w$	
t_p	pulse duration
t_{sf}	relief time of single-phase pressurization
t_w	growth time of single bubble
U	velocity
U^*	dimensionless velocity, defined in Eq. 6.29
u	velocity component
V	volume
v	velocity component
v	specific volume
v_e	evaporation velocity
$\bar{v}_o$	velocity
X_c	radius
x	distance
z	cylindrical coordinate

Greek Symbols

α	thermal diffusivity
α_p	thermal expansion coefficient
β	parameter $(=\rho Ck)^{-1}$
β_T	compressibility
γ	dimensionless parameter, defined in Eq. 6.2

δ	minimum film thickness
$\eta \equiv \frac{z}{L}$	dimensionless distance
ζ	dimensionless critical thickness defined in Eq. 3.40
θ	contact angle
λ	heat of evaporation
λ_{cr}	critical wave length
μ	viscosity
ν	kinematic viscosity
ρ	density
σ	surface tension
σ_{eq}	equivalent surface tension
τ	dimensionless time, defined in Eq. 6.24
$\psi \equiv \frac{P}{\rho}$	parameter

Subscripts

c	cold
cr	critical
d	drop
exp	experimental
h	hot
i	impact
l	liquid
m	mixing
max	maximum
s	initial
s	surface
th	theoretical

v	vapor
∞	ambient

Abbreviations

LMFBR	Liquid Metal Fast Breeder Reactor
LNG	Liquefied Natural Gas
LWR	Light Water Reactor
MFB	Minimum Film Boiling
PD	Percentage of Disintegration
PT	Pressure Transducer
PWR	Pressurized Water Reactor
TC	Thermocouple

LIQUID-LIQUID CONTACT IN VAPOR EXPLOSION

by

Aryeh Segev

ABSTRACT

The contact of two liquid materials, one of which is at a temperature substantially above the boiling point of the other, can lead to fast energy conversion and a subsequent shock wave. This well-known phenomenon is called a "vapor explosion." One method of producing intimate, liquid-liquid contact (which is known to be a necessary condition for vapor explosion) is a shock tube configuration. Such experiments in which water was impacted upon molten aluminum showed that very high pressures, even larger than the thermodynamic critical pressure, could occur. The mechanism by which such sharp pressure pulses are generated is not yet clear.

In this experiment cold liquids (Freon-11, Freon-22, water, or butanol) were impacted upon various hot materials (mineral oil, silicone oil, water, mercury, molten Wood's metal or molten salt mixture). Large pressures were obtained for systems of water-Wood's metal, butanol-Wood's metal and water-salt. With water-Wood's metal three separate regions were observed. When the hot liquid temperature was below 210°C (which can be identified as the spontaneous nucleation temperature T_{sn}) no thermal interaction occurred, and the cold liquid column only bounced if vapor was present initially (region A). When the hot liquid temperature was greater than the spontaneous nucleation temperature ($T_h > T_{sn}$) but the contact interface temperature was less than this value ($T_I < T_{sn}$), (region B) the low rate of vaporization results in bouncing of

the liquid column which in turn produced high pressures in the order of the theoretical "water hammer," (P_i), which are larger than the vapor pressure (P_v) corresponding to the bulk temperature. The third region observed when the hot liquid temperature was above the spontaneous nucleation temperature upon contact ($T_I > T_{sn}$) (region C) which resulted in fast production of vapor and impulses larger than the theoretical impulse for stopping the liquid column. The mechanism for producing the high pressures in region C is a combination of hydrodynamic impact and thermal interaction. Since pressures produced in region C are also in the order of impact pressures, the only indication for thermal interaction is a considerable increase in the resulted impulse of pressure pulses with short rise time (<1.0 msec).

When butanol was used as the cold liquid the same three regions were observed, and in addition, a fourth region (region D) was observed when the hot liquid temperature exceeded the critical temperature upon contact ($T_I > T_{cr}$). In this region the maximum pressures are lower and the growth and decay characteristics were much longer than in region C. Since the measured impulses in region C are of the same order as the possible hydrodynamic impulse it is highly suggestive that the pressures generated are a result of water hammer action.

Experiments with water and molten salt at 410°C and 600°C (eutectic mixture of LiCl-KCl) resulted in low yield thermal interactions.

When the initial pressure in the system was increased above 0.2 MPa (by means of a thicker diaphragm), the bouncing behavior exhibited by water and by butanol was suppressed. This was evident from the reduced number of bounces (if at all), the low relative pressures and impulses,

the temperature history, and the shape of pressure pulses. The experiments conducted with Freons and oils which did not result in any explosive type of interaction also fall in such a high pressure category and are in agreement with pouring experiments conducted by Henry and McUmber. By considering the theoretical transition radius between inertially and thermally dominated bubble growth as it relates to the "capture theory," good agreement was found between the experimental results and theoretical predictions.

The main conclusion from the experimental study is that hydrodynamic effects may be very significant in any shock tube analyses, especially when multiple interactions are observed.

A theoretical study was performed to check the possibility of vapor film squeezing (between a drop in film boiling and a surface) as a controlling mechanism for making liquid-liquid contact. Using experimental data, the film thickness was calculated and it was found to be too thick for any conceivable film rupture mechanism. It was suggested that the coalescence is a two-stage process, in which the controlling stage depends mainly on temperature and surface properties and can be described as the ability of cold liquid to spread on a hot surface.

I. INTRODUCTION

The contact of two liquid materials, one of which is at a temperature substantially above the boiling point of the other, can lead to vaporization on a time scale consistent with large shock wave formation. This well-known phenomenon, which is sometimes called a "vapor explosion," is characterized by sudden fragmentation of molten materials, fast energy conversion, and a subsequent shock wave. The occurrence of a vapor explosion was first reported in 1864 when an explosion occurred in the steel industry during the development of the Bessemer process.[1] In 1954, a titanium arc-melting furnace, which was water-cooled, exploded at a plant in Ohio. It was believed to result from water entering the melting crucible, and resulted in the death of four and $40,000 damage. Other explosions in the metal industry included the Reynolds Aluminum Incident in 1958 (46 injuries, including six fatalities, and approximately $1,000,000 in property damage), Quebec Foundry Incident[2] (one fatality and $150,000 damage) and several others. These accidents, including those in the paper industry (involving spillage of paper smelt on wet surfaces) have been documented by Epstein[3] and Witte et al.[4] Since the threat of an explosive incident exists in situations where hot molten materials are present, the subject is of concern in the safety analysis of nuclear reactors, such as the Liquid Metal Fast Breeder Reactors (LMFBR) and light water reactors, where molten core conditions are considered during the sequence of a hypothetical accident.

In 1961, SL-1, a small experimental boiling water nuclear reactor, was destroyed in an inadvertent transient, resulting in fuel-element failure and violent interaction between molten metal and water. The postaccident investigation[5] led to the conclusion that approximately 10-

15% of the potential thermal energy was released. This led to a series of tests on SPERT-1D, a light water test reactor with aluminum-clad fuel elements. In this series of tests, self-terminating power excursions were performed which resulted in a destructive transient. In one particular test the power excursion was self-terminating, but a sharp pressure pulse occurred about 1.5 msec after peak power, destroying the core. It was calculated that about one-third of the core was molten at the time that the destructive pressure pulse occurred, whereas only slight melting had occurred in previous transients. It is not clear whether there was chemical reaction between the molten aluminum and water, but fine dispersal and rapid heat transfer contributed to the destructive pulse.

In each of the incidents described above a hot molten material fell, dropped, or was injected into a mass of cooler liquid, resulting in a violent explosion. From the evidence which has been accumulated over the past 20 years, one can identify a class of violent nonchemical explosions caused by sudden generation of vapor. In these explosions a relatively large fraction of the total heat energy stored in the hot liquid may be converted into destructive mechanical energy. Sometimes, however, contacting of the two liquids merely leads to extensive fragmentation without a shock wave, or solidification into coarse masses with little fragmentation. A good deal of effort has therefore gone into elucidating the necessary and sufficient conditions for vapor explosions, as contrasted to merely violent boiling without harmful pressure shock waves. For a systematic tabulation of the large number of experiments conducted up to 1975, the attention of the reader is

directed to Ref. 6 and to a number of specialized reviews.[4,7,8]

II. VAPOR EXPLOSIONS - LITERATURE REVIEW

2.1 Experimental Studies

The experimental scale varies from laboratory experiments involving single drops of hot or cold liquid entering a pool of the second liquid, to large scale pouring experiments, in which thousands of kilograms of liquefied natural gas (LNG) have been poured onto water. Different modes of bringing the hot, nonvolatile liquid into contact with the cold vaporizable liquid were examined experimentally. The initial approach velocity of the two liquids may be large (as in shock tube experiments) or moderate (as in free-fall experiments).

2.1.1 Dropping and Injection Modes of Contact

The first large-scale pouring experiments were conducted by Long,[9] motivated by the occurrence of vapor explosions in the aluminum industry. The reference test, which always produced an explosion, involved the sudden discharge of 22.7 kg (50 lb) of commercially pure molten aluminum onto a clean steel container partially filled with water at temperatures between 12.8 and 25.6°C. Contrary to chemical explosions, no flash or fire could be detected during or after the explosions. The following parameters were changed: discharge rate and mass, height of dropping, water depth, and temperatures. Experiments were also conducted with different additives in the water and different solid surfaces. From those experiments Long concluded that in order to produce an aluminum/water explosion, three requirements must be met:

1. Molten metal in considerable quantities must penetrate to the bottom surface of the water container.
2. A triggering action must take place on this bottom surface when it is covered by the molten metal.

3. The water depth and temperature must lie within prescribed ranges.

A large number of experiments have been conducted by dropping small quantities of molten samples into water and other liquids ("dropping experiments"). Cho et al.[10,11] conducted some of the earliest experiments in dropping different molten materials (tin, bismuth, silver chloride, zinc, and lead) onto a pool of water. The water temperature varied and the total projected area of the resulting fragments was measured. It was found that fragmentation depends on the initial drop temperature as well as on the water subcooling, the extent of which decreases with water subcooling, and on the release height.

Small quantities (~4 ml) of liquid metals (tin, indium, aluminum, Wood's metal, lead, and two lead-tin alloys) were dropped into water and aqueous solutions by McCracken.[12] Some interesting results were obtained for fragmentation concerning surface and material property effects. The surface of the liquid metal was wiped clean immediately before each test, and if this was not done, inconsistent results were obtained. Those metals which have the highest rate of oxidation had also the lowest percentage of disintegration (PD). It was found that even small traces of oxide had an important effect. Observations with tap water (0-90°C) and tin at 600°C showed that at the higher water temperatures the tin fell to the bottom and solidified without an explosion, but as the water temperature decreased a high PD was observed. This gradual transition took place over the temperature range of 20-50°C. However, when oxide was removed before each test, the transition from a high to zero PD was very sharp, occurring over a temperature interval of 3-5°C.

Various solutions were examined in order to determine whether surface tension or viscosity of the cold liquid affects the interactions. For tin at 600°C neither the use of a 40% sugar solution nor a 10% glycerol solution affected the cutoff temperature of about 70°C, or the general shape of the curve of PD versus solution temperature. Adding detergent to the water had no effect on the metal/water interaction.

Tests with distilled water which had been degassed showed no appreciable difference from the results for untreated water. However, when carbon dioxide was dissolved in distilled water the critical temperature required for fragmentation was decreased by about 30°C and the threshold range was broadened.

It was thus concluded that the temperatures of the two liquids, the presence of oxide, the wetting properties, or dissolved gas in the water are important variables, while the viscosity and surface tension, together with the presence of dissolved solids in the water and metal melting temperature were relatively unimportant in determining the PD.

Another study of tin-water interactions in a dropping-mode of contact was carried out by Reynolds et al.[13] Degassed and distilled water was used in the pool, which was surrounded by a helium atmosphere in order to minimize oxide formation. About 12 g of tin were melted and poured into the water. An interaction was observed at a localized region on the drop after a penetration distance of a few centimeters. There was a growing oscillation, with tin being ejected from the bulk of the drop at each expansion, forming a cloud of small tin particles. Sometimes after a few oscillations, one or two other sites became active, but no correlation between the oscillations at neighboring sites

was observed. As in previous experiments, there is a definite range of tin temperatures for a particular water temperature over which rapid fragmentation occurred. For example, for water at 65°C there is a sharp cutoff at 727°C, below which the PD is nearly complete and above which self-triggered tin-water interactions never occur. A somewhat similar behavior was observed when the water temperature was varied at a constant tin temperature. These results are summarized in Fig. 2.1. Tin at 250°C (just above the melting temperature of 232°C), and water at 65°C resulted in no fragmentation. As the tin temperature increased the fraction of fine debris increased as the diagonal boundary is approached. At the boundary there was an abrupt cutoff, after which there was no fine debris. The delay time between the entrance into the water and the start of fragmentation was shown to depend on the initial tin and water temperatures. The sharp increase in dwell time as the diagonal of the tin-water interaction zone was approached corresponded to the zone where the most violent interactions occurred.

Mizuta[14] performed a series of 30 runs on the fragmentation of molten UO_2 dropped (as drops of about 2.6 mm) onto a liquid sodium bath at 200-300°C. Records were taken of the change in temperatures of the bath, together with photographs at 500-2000 frames/sec. The temperature of the droplet just before falling into the sodium was estimated to be 2840°C at the center and 2200-2500°C at the surface. Sometimes the UO_2 fragmented and sometimes it did not. In the cases where the UO_2 fragmented, the droplet first submerged completely in the sodium, the sodium bath temperature was raised quite abruptly and then cooled down slowly. A higher peak pressure was shown to be correlated with fine particle size.

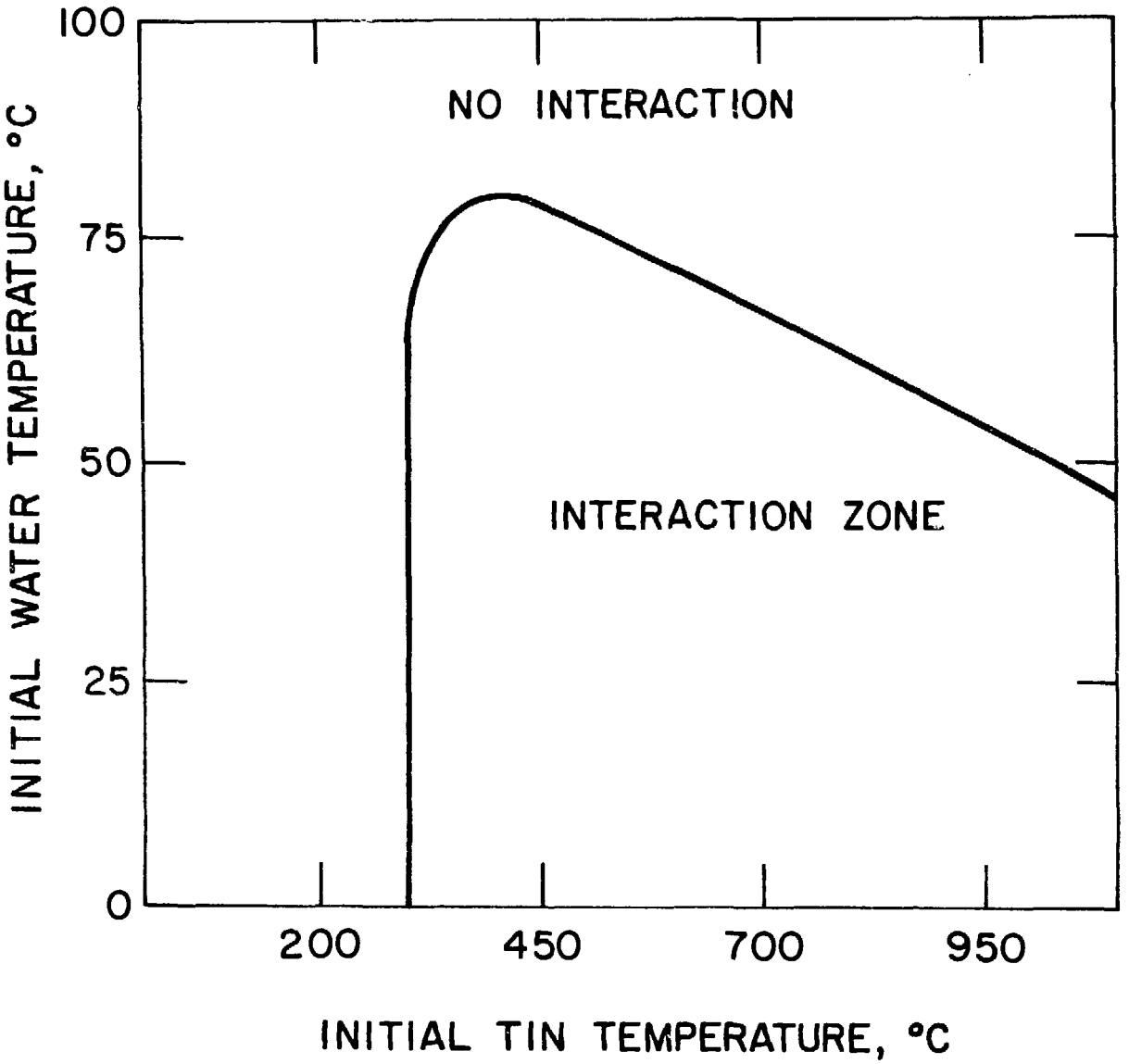

Fig. 2.1 Interaction Zone for Tin Dropped into Water (after Reynolds et al.[13])

From particle distribution measurements it was found that variation in the mean particle diameter between different runs are about an order of magnitude. It was observed that the larger particles (∿1 mm) were more or less spherical and smooth with internal cracks which were mainly transgranular, the fracture appearing to have taken place well below the brittle-to-ductile transition temperature (∿1600°C). The smaller particles (∿40 μ) were also smooth and spherical, and had appeared to freeze without further fragmentation. Only feeble pressure pulses were generated in the liquid bath, and it appeared that droplets whose surface had solidified during the free-fall could still be extensively fragmented.

Dropping experiments with UO_2 and stainless steel into sodium were conducted by Armstrong et al.[15] The melt was poured from a crucible over a period of 1/4 to 1 sec as streamlets and individual drops. It was estimated that the cooling rate of the UO_2 was about 100°C/sec. Several significant differences between UO_2 and stainless steel were noted. In the UO_2 experiments a relatively long delay occurred between the first contact of the hot drop and pressurization, while with stainless steel, pressurization occurred after a lesser delay and before complete submergence. As a result of the delay, the ejected UO_2 fragments were always surrounded by sodium vapor, while a little of the ejected stainless steel showed indications of having been in contact with sodium. The UO_2 runs showed much higher peak pressures, in accord with a higher melt temperature. The delay times for the UO_2 runs were in the neighborhood of 50-200 msec, while those with the stainless steel 3-20 msec.

For the UO_2 runs the residue found inside was angular and rough-surfaced while the particles collected outside the tank were rounded with smooth surfaces. With stainless steel, all particles were smooth and rounded. The implication is that fragmentation accompanying violent mixing occurred in the liquid state for stainless steel and also for the UO_2 particles, despite the fact that solidification proceeds as soon as contact is made with liquid sodium. The fragmentation of the UO_2 particles which remain in the vessel was attributed to thermal stresses.

Experiments showing an injection mode of contact have been conducted by Bradley and Witte.[16] Several metals and alloys were injected horizontally in a small diameter, 1.6 mm (1/16-in.) jet, into distilled water at 23.9°C. Three types of jet injection were identified, depending on the injection temperature. At low injection temperatures the jet material solidified into an irregular billet that was generally non-porous. At higher temperatures, the jet expanded into a 'popcorn' appearance and solidified in that configuration. At still higher temperatures for some metals the jet was actually fragmented; i.e., much of the molten metal was separated into discrete globules and flakes, and solidified into that configuration. In addition to the general behavior of the jet, the diameter to which the jet expanded as the interaction occurred was also dependent on injection temperature. The particles moved out into a well-defined radii band that could be obtained from an analysis of the high-speed films taken. For fragmented jets, the "effective" diameter included ∿95% of the metal particles.

It was shown that vapor production is not necessary for fragmentation, but the presence of vapor affects the jet-water interaction. In many cases, the jet was surrounded by a thick vapor 'shield' that was

conical in shape and behaved in a cyclic manner. As this shield was formed, the jet would pass stably through, with explosive action occurring just as the jet encountered the apex portion of the conical shield. Simultaneously, as the vapor collapsed on the jet, explosive action occurred and another cycle began. Experiments with tin at 600°C and different nozzle materials (copper and stainless steel) indicated that the explosive reaction for a jet is highly dependent on the instantaneous cooling rate of the jet, which depends on the jet surface temperature, i.e., with a copper nozzle (highly conductive) the tin solidified as a 'popcorn' strand but with stainless steel, extensive fragmentation was observed.

Injection experiments in which water was injected into molten NaCl were conducted by Anderson and Bova.[17] It was found that the H_2O/NaCl system is capable of producing thermal interactions with a time delay of 10-300 msec. The degree of the interaction violence can be related to the delay observed: longer delay times yielded more violent interactions. As is discussed later, those interactions are coherent and may be referred to as large scale explosions. The measured energy ranged up to 18% of the maximum theoretical energy that could be produced by the injected quantity of water. For the H_2O/NaCl system, subsurface movies showed (within the framing rate limitation) that:

a. The water mass was broken up into fine drops dispersed throughout the salt continuum prior to the explosions.

b. There was no evidence of a salt crust freezing around the water mass.

c. A gas and/or vapor layer formed between the two liquids during the injection process. This was obviously true during the

initial stage. The resolution of the pictures was not fine enough to distinguish very localized collapse of the gas layer and direct contact between the two interacting fluids.

d. The initiating interactions were always developed very rapidly (within 77 μsec).

Other injection experiments were conducted by Armstrong et al.[18] in which Na-UO_2 was studied. In each experiment, a small quantity of sodium was injected into a crucible filled with hot molten material. During some tests, the coolant quietly boiled away; in other tests, the coolant was relatively quiet for a delay period and then interacted. As is discussed later, those interactions are incoherent and may be referred to as small scale explosions.

Subsurface injection experiments were conducted by Asher et al.[19] and Abbey et al.[20] in which liquid sodium was injected beneath the surface of molten steel. Two experiments were performed. In the first one (Na-CS/1), 2 g of sodium at 380°C were injected into 54 g of steel at 1530°C. In the second experiment (Na-SS/1) ∿1.5 g of sodium at 400-450°C was injected into ∿80 g of stainless steel at 1750-1800°C. A sharp pressure pulse was observed less than 5 msec after the completion of the injection and 50-60 msec after the start of the injection (dwell time). It was assumed that an explosion had occurred. The magnitude of the pulses was less than that in Na-CS/1, even though the steel temperature was more than 200°C higher. It was noticed that in this experiment the sodium vaporized, when in Na-CS/1 much of it was recovered as droplets, and the steel was not so finely dispersed.

2.1.2 Experiments in Shock-tubes

In an attempt to understand the pressure generation by

the dispersal of molten fuel into coolant, experiments were performed by Wright et al.[21] using water impacting on molten aluminum. The aluminum was held in a 1-in. ID tapered crucible of molybdenum (TZM) and a thin stretched rubber served as a diaphragm. The volumes inside the crucible and on top of the water column were evacuated. The inside of the crucible was also connected to an evacuated water-filled flask at room temperature, so that the crucible volume contained about 1 cm Hg of water vapor which condensed on the advancing water column before impact. The presence of a noncondensible gas in the crucible was found to produce a soft bounce rather than a sharp impact.

The shape of a high pressure pulse resulting from the impact of water upon molten aluminum is shown by the graph of Fig. 2.2. This 20 MPa (2900 psia) pressure pulse, which resulted from water impact upon 950°C aluminum had an 80 μsec rise time and a time constant for pressure decay of about 3 msec. The notch after about 1 msec was the passage of the rarefaction wave from the top of the water column.

Some of the experiments gave extraneously low values of the peak pressure. In all these "anomalously low pressure" shots there was a "precursor" pressure before the impact. It may be that a slow diaphragm rupture occurred in those cases such that a sizable jet or stream of water sprayed the molten aluminum pool before impact and made sufficient steam to produce a soft impact, low dispersal, and low pressure.

The experimental data on peak pressure versus the molten metal (aluminum and silver) temperature are shown in Fig. 2.3.

Experiments have been carried out by Darby et al.[22] in a simple tube geometry using water and aluminum as the cold and hot liquids, respectively. The upper part consisted of a stainless steel tube, 91 cm

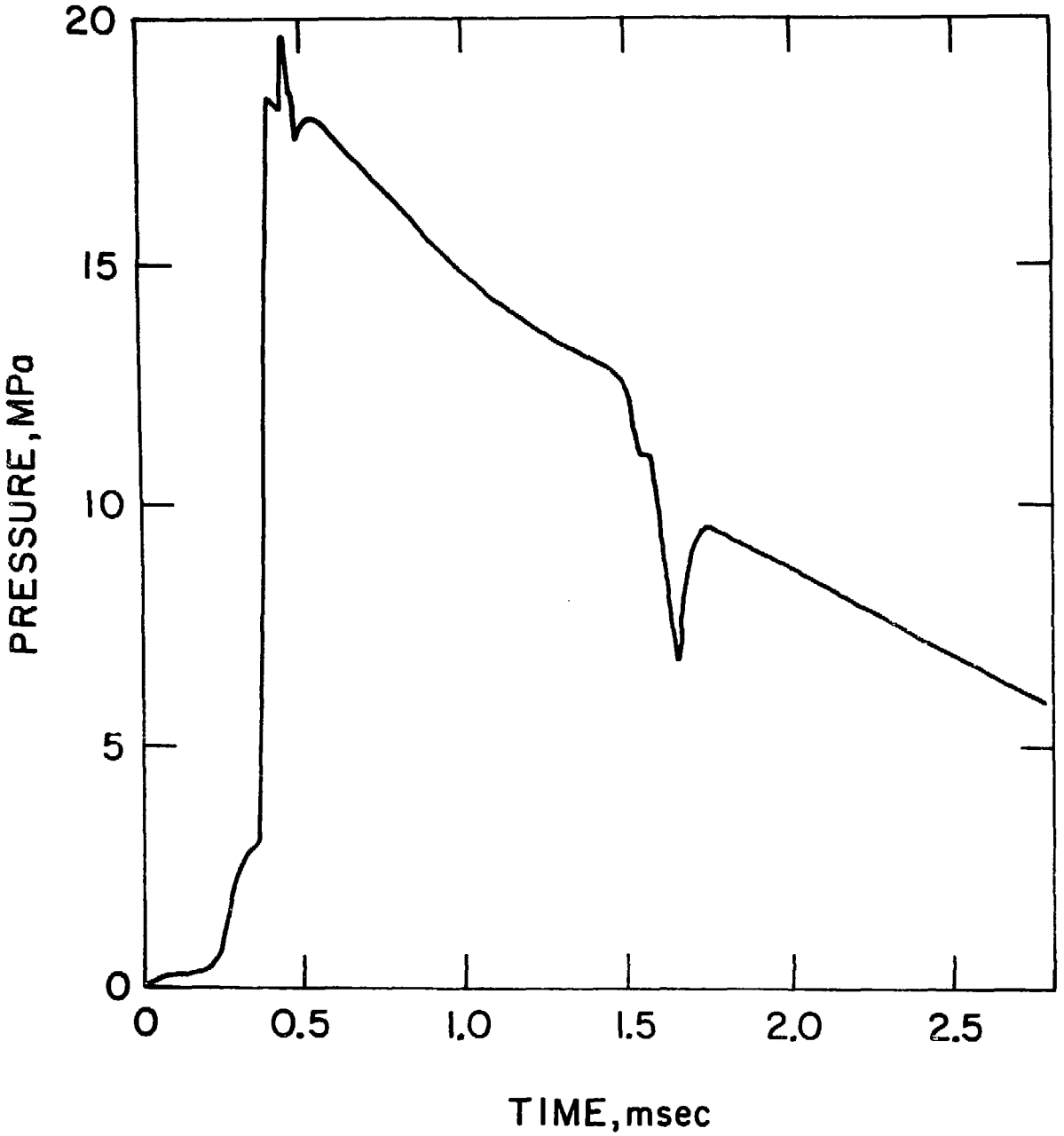

Fig. 2.2 Pressure Pulse from Water Impact on 950°C Aluminum (after Wright et al.[21])

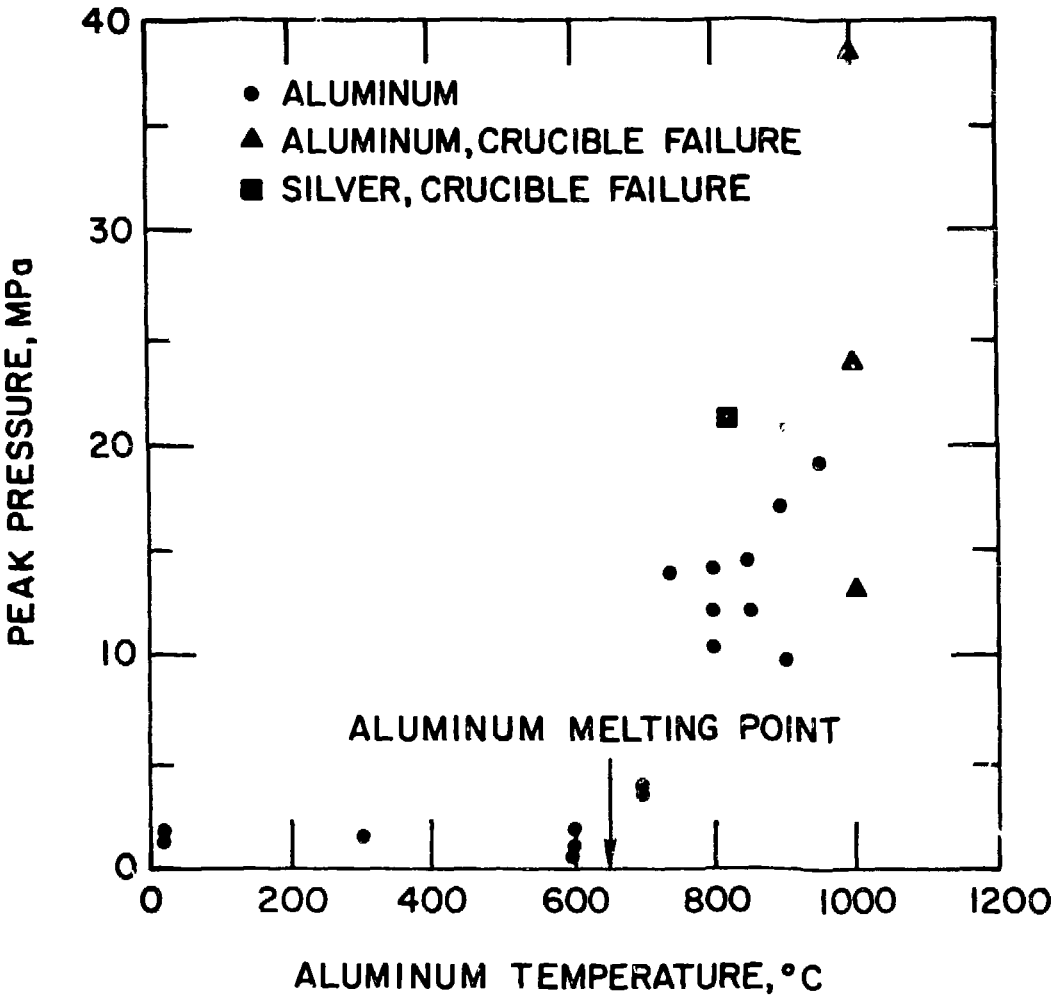

Fig. 2.3 Temperature Dependence of the Peak Pressure from Water Impact upon Aluminum or Silver (after Wright et al.[21])

(3 ft) long and of 2.54 cm (1-in.) bore, with up to eight pressure transducers mounted along the tube. The water was supported by a stretched rubber diaphragm clamped between two flanges and the molten aluminum was held in either a steel crucible or a section of transparent quartz.

Water vapor was introduced to the space between the diaphragm and aluminum just before firing, to prevent the water front from flashing off as it moves down. By opening a solenoid valve, pressure was applied on the water column, accelerating it downwards, rupturing the diaphragm and causing the water to impact on the molten aluminum.

The pressure pulses produced by a series of experiments at an aluminum temperature of 720°C and water at 20°C have usually produced maximum pressures on the impact of the second bounce of the series in each experiment, the highest pressure being in the range of 25.5-30.4 MPa (3700-4400 psi). A pressure pulse of run WHAM-9 is shown in Fig. 2.4. It has a small initial rise and plateau and then a rapid rise (200 μsec) to its maximum pressure, followed by a slow decay (∿2 msec) back to ambient pressure. Here also we notice the notch caused by the rarefaction wave travelling from the top of the water column. This shape is the most frequent type observed.

A few experiments have been performed using molten lead as the hot liquid. The same volume of molten material was used in both cases, and the temperatures for the lead shots were 473°C, 727°C, and 820°C. The results are substantially different from the aluminum-water interactions. The lead experiments produced far less fragmentation and the peak pressures measured were barely greater than the theoretical impact pressure.

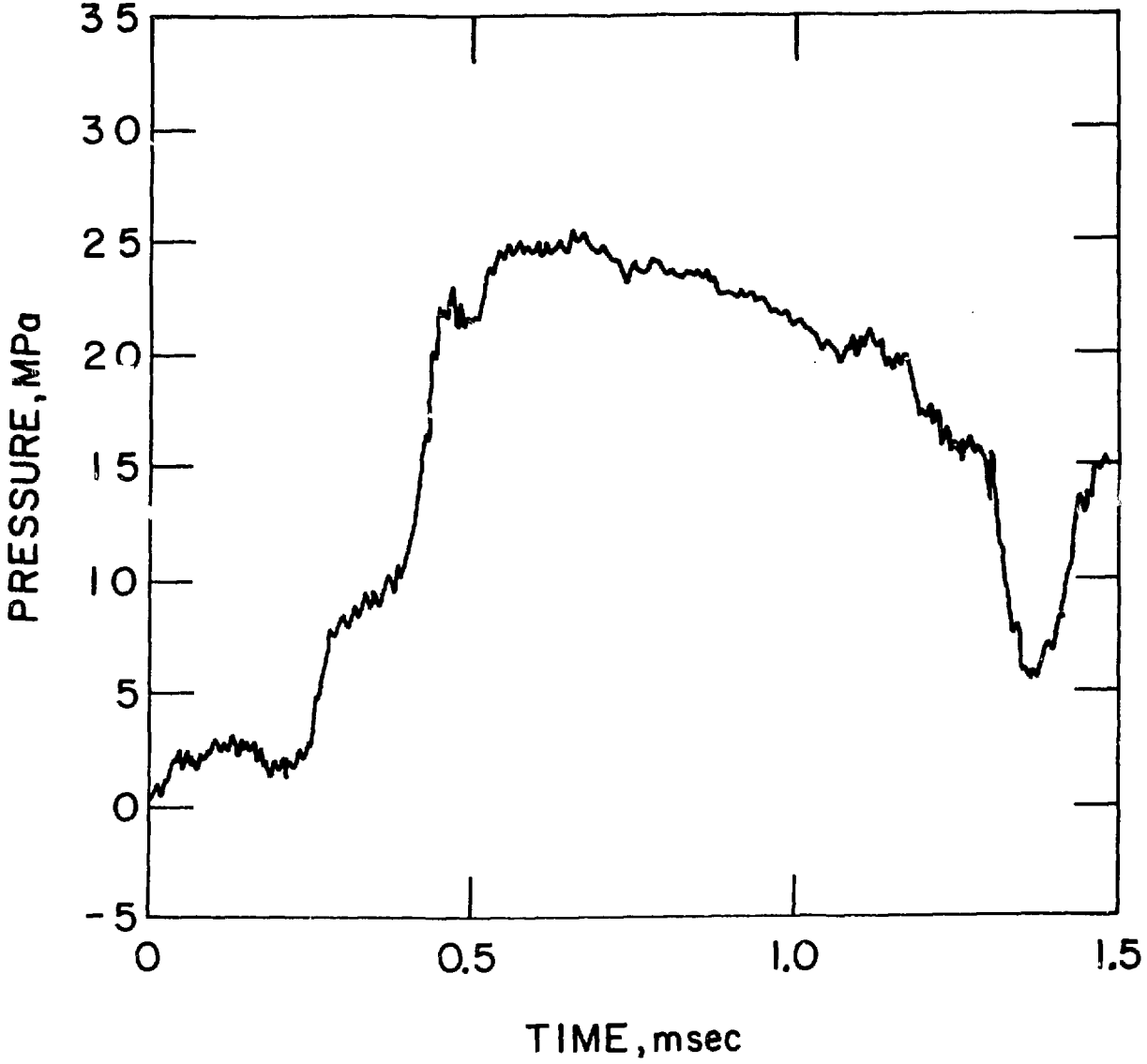

Fig. 2.4 Pressure History for the First Bounce in Round WHAM9 (after Darby et al.[22])

However, those experiments compare well with similar experiments done by Hilliary et al.[23] in which water was impacted on molten lead or a molten eutectic mixture of lithium and potassium chlorides. The experimental apparatus in the latter was essentially the same as the other shock tube systems discussed above. It is a 2.54 cm nominal bore stainless steel tube, 160 cm long, with a 2.0 cm diameter transparent silica mixing tube, 28 cm long. The cold fluid is contained in the upper tube and the hot fluid is normally 6 cm deep, in the lower tube.

Contact between the two liquids is achieved by the operation of a pneumatic piston which drives a steel cutter tube through a horizontal steel diaphragm, 0.13 mm thick. The diaphragm opens rapidly in about 1 msec, to lie as a flap against the wall. A reservoir of helium provides a driving pressure for accelerating the upper liquid. This accelerating force is applied simultaneously with diaphragm failure but takes ~175 msec to reach its maximum. The lower surface of the falling water column contacts the hot surface and the mixing process is recorded by a high-speed camera and pressure transducers. In experiments in which the water contacted molten material at a temperature which was well above the boiling point of water (in the absence of an inert noncondensible gas), the water was projected upwards after a brief mixing period. This 'bouncing' effect occurred at each successive contacting until the process reached equilibrium or was terminated by consumption of the molten material. A further important feature of this 'bouncing' phenomenon is that only a limited depth of the molten material was involved in each mixing stage. The mixing zone was approximately 15 mm deep. Its significance lies in the limited amount of thermal energy which may be available in a single contacting stage. On each subsequent contacting

in the same experiment, a further amount of molten lead was carried up the tube by the steam-driven water. In a test in which water contacted a molten salt mixture, almost identical behavior was observed, indicating a marginal effect of relative density on the depth of the mixing zone (density of molten lead at 470°C is about six times larger than LiCl/KCl density).

When a noncondensible gas (argon) was introduced between the two liquids at a pressure of 13.3 kPa no bouncing was observed and the appearance of the resolidified lead after the experiment was such that it was essentially in one piece with little deformation of the surface. This compares with the much more fragmented appearance when the noncondensible gas was absent and bouncing did occur. The elimination of bouncing and fragmentation by this means was also noted when argon at a pressure of 1.33 kPa was introduced below the diaphragm.

An attempt was made to examine the effect of deliberately varying the hot lead temperature through the critical temperature of water (374°C). No obvious effect on the pressure generated was noticed.

It was concluded from those experiments that, although in no case was the observed pressure greater than that expected from simple impact, the contacting of cold water with hot, molten lead or a salt mixture, resulted in some additional mechanical energy being transferred to the water column manifesting itself as a bouncing effect. This bouncing appeared to be eliminated if an inert noncondensible gas was present in the space separating the two liquids; deformation of the lead was also much reduced compared with the extensive fragmentation noted when bouncing occurred. An important feature of the contact appears to be the restricted mixing zone which limits the energy that can be transferred

to the water.

2.2 The Contact Stage

The main objective in studying the vapor explosion phenomenon is to develop a conservative model for predicting the pressure-time history resulting from a liquid-liquid interaction. For a conservative analysis it may be assumed that a given mass of molten liquid is suddenly released in small particles which coarsely intermixed in the cold liquid but separated by a gas and/or vapor film. In this initial configuration steady heat is transferred in a film boiling mode through the vapor film surrounding the particles.

The initial configuration, which exists before the explosion, must be stable for as long as it is necessary for the configuration to develop. This stable period is the dwell time, which is the observed delay before interaction occurs. In the case of large scale explosions in which the two materials are initially separate and are brought together by pouring, this may be a long time ($\sim$1 sec), though in other situations (e.g., in a shock tube geometry) the initial configuration may be achieved in only a few msec.

Consideration of the requirements for the initial configuration indicates that intermixing before the explosion such that the individual fuel and coolant regions are small compared with the size of the exploding region, and close enough together to give coupling for coherence, may be a necessary condition for high efficiency explosions. It seems likely that the initial mixing and break-up occur because of the initial kinetic energy of the pouring, and hydrodynamic breakup.[24],[25]

After the initial stage has been developed, intimate contact between the liquids is necessary. The contact stage allows a large

amount of energy to be rapidly transferred from the hot to the cold liquid. The necessity of intimate contact has been demonstrated in several experimental works. Fragmentation occurred readily and reproducibly when contact was initiated by rapid pressure increase. Board and Hall[26] conducted an experiment in which 50 g of molten tin at 800°C was placed in a shallow crucible located under water. Rupturing a diaphragm resulted in a sudden pressure increase and an explosion. A different way to initiate contact was demonstrated by the same authors.[26] Waves were transmitted into the cold liquid from a hammer blow on a rod or tapping on the tank resulting in an explosion. Zyszkowski[27] reported on a set of dropping experiments using several molten metals (silver, gold, copper, lead, tin, zinc, and stainless steel) and water. He claimed that vapor explosions occurred only when direct liquid-liquid contact was achieved and when the metal temperature exceeded a certain value. The Al/H_2O system is another example that liquid-liquid contact is necessary in order to produce explosion. Small scale dropping experiments of aluminum have not resulted in explosions or even fragmentation.[12] However, by impacting the cold liquid onto the hot metal as was done in the shock tube experiments[18],[19] or just by suddenly raising the pressure, as was done in the tin experiments, explosions and large pressures were produced.

Dropping experiments of tin (0.31 cm in radius) into water conducted by Bjornard et al.,[28] suggested that fragmentation is linked to the dynamics of the vapor film surrounding the drops. By measuring the pressures generated, it was found that a period of high frequency, low amplitude pressure oscillation followed by a lower frequency higher amplitude oscillation, accompanied the fragmentation event. The

duration, frequencies, and magnitudes of the two distinct portions of the waveforms were influenced by the initial tin and water temperatures. Thus, it was suggested that film boiling is possibly followed by film collapse and fragmentation.

Evidence of momentary contact between liquid drops and solids at temperatures well above the normal minimum film boiling temperature was reported by Bradfield.[29] The kind of contact (periodic or quasicontinuous) depends on surface roughness, subcooling and heating surface thermal conductivity. Explosive instabilities were observed under certain exceptional combinations of these parameters.

In general, when a body at sufficiently high temperature is suddenly immersed in a cool liquid, the body is at first surrounded by a shell of vapor, which acts as a thermal insulator. At a specific temperature, determined by the system characteristics, large-scale contact is made. Usually it is said that film boiling ceases and transition boiling begins. The temperature at which it occurs is called the "minimum heat flux point," "minimum film boiling (MFB)" point, or "Leidenfrost temperature" when small drops are concerned.

2.2.1 Minimum Film Boiling Point

Experiments to determine the parameters that govern drop collapse are usually one of two types. In the first, a drop is placed on a surface kept at constant temperature and the lifetime of the drop is measured. At a high plate temperature a vapor film is formed under the drop, the contact is random and evaporation is slow. At a particular plate temperature ("Leidenfrost temperature") the drop immediately makes contact, resulting in a short lifetime. In the second type of experiment a drop is established on a plate at high temperature, and the plate

temperature is then reduced gradually until collapse occurs. It was found that with this method drops may still exist with an intact vapor layer even when the plate is almost at the liquid saturation temperature.[30] While the "collapse temperature" in this type of experiments may span a wide range under apparently similar experimental conditions, it is very noticeable that the stability of the drop with respect to mechanical disturbances changes very markedly at about the same temperature as that which causes rapid evaporation in the first type of experiment.

Calculations of MFB point can be based on two models; hydrodynamic model[31] or thermodynamic model.[32]

Hydrodynamic Model

The minimum film boiling temperature can be derived from the expression given by Berenson[31] for pool boiling on a horizontal isothermal surface. The model assumes that: (1) vapor removal is governed by a Taylor instability. (2) The vapor flow is radial and laminar. (3) Vapor film thickness is constant. (4) Heat is transferred by conduction only across the film. (5) Vapor for a given bubble is generated in an area of $\lambda_{cr}^2/2$ where λ_{cr} is the critical wavelength (that with the fastest growth rate)

$$\lambda_{cr} = 2\pi \left[\frac{3\sigma}{g(\rho_\ell - \rho_v)}\right]^{1/2} \tag{2.1}$$

A prediction for the minimum temperature was given as

$$\Delta T_{m,i} = 0.127 \frac{\rho_v \lambda}{k_v} \left[\frac{g(\rho_\ell - \rho_v)}{\rho_\ell + \rho_v}\right]^{2/3} \left[\frac{\sigma}{g(\rho_\ell - \rho_v)}\right]^{1/2} \left[\frac{\mu_v}{g(\rho_\ell - \rho_v)}\right]^{1/3} \tag{2.2}$$

where $\Delta T_{m,i} = T_{m,i} - T_{sat}$ and $T_{m,i}$ is the minimum temperature to sustain film boiling with an isothermal surface.

Good results were obtained for n-pentane and carbon tetrachloride. However, it was found experimentally that this correlation is not accurate for liquid metals, water, Freons, and cryogenic fluids, since it is applicable only if the surface is isothermal, i.e., if thermal transients within the surface are negligible. In order to improve the correlation and include the transient effects, Henry[33] suggested that the occasional contact results from vapor bubble departure from the hot surface, caused by liquid rushing toward the surface which momentarily contacts portions of the solid surface. This short contact results in rapid evaporation which pushes the liquid off the surface, but a microlayer remains on the surface. If during contact the interface temperature is below $T_{m,i}$, transition will occur.

The transient wetting process is analyzed as a transient conduction process between two semi-infinite slabs (see Appendix A) and the microlayer evaporation is characterized by $\lambda/C_h\Delta T_{m,i}$. Using available solid-liquid data a correlation was found in the form;

$$\frac{T_m - T_{m,i}}{T_{m,i} - T_c} = 0.42 \left[\left(\frac{k_c \rho_c C_c}{k_h \rho_h C_h} \right)^{1/2} \frac{\lambda}{C_h \Delta T_{m,i}} \right]^{0.6}, \qquad (2.3)$$

where T_m = the real minimum temperature.

Equation 2.3 was found to correlate the solid-liquid data fairly well but since this model is based on wave behavior in pool boiling, it cannot be applied to single, small Leidenfrost drops. Calculated MFB points for some molten metals and water which are of interest in the present discussion are shown in Fig. 2.5.

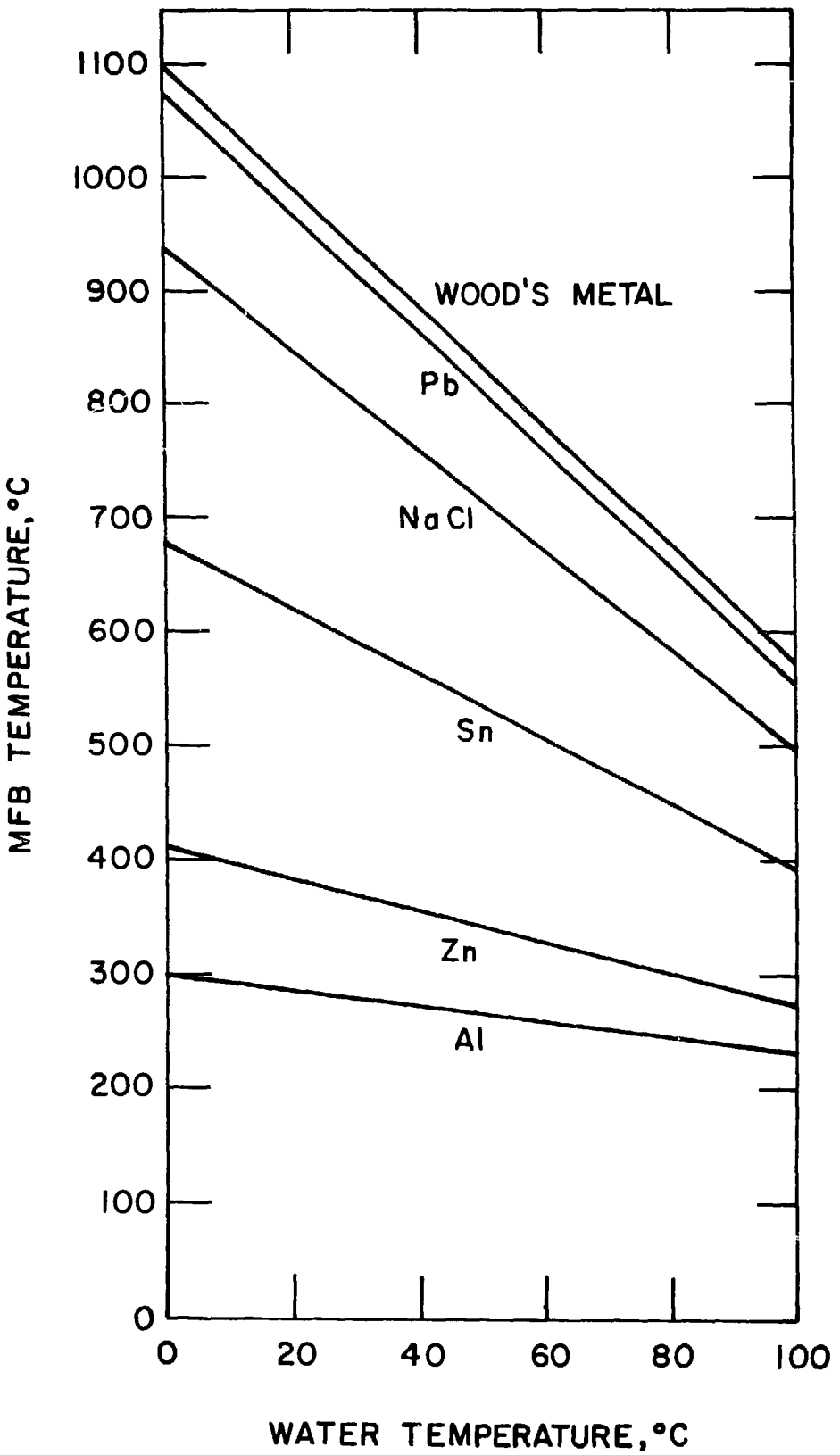

Fig. 2.5 Minimum Film Boiling Temperature for Various Hot Materials and Water

Thermodynamic model

Speigler et al.[32] suggested that the wall temperature at the minimum point corresponds to the maximum liquid superheat predicted by Van der Waal's equation of state. For pressures well below critical, maximum superheat is about $\frac{27}{32} T_{cr}$. It was shown that this prediction was in reasonable agreement with nitrogen, and hydrocarbon pool boiling data. However, a large discrepancy exists for liquid-metal data, carbon tetrachloride and water. The main drawback in this theory (as in Berenson's theory) is not taking into account the thermal properties of the solid, which experimentally have been proven to be important.

Baumeister and Simon[34] modified this model by assuming that local contact between liquid and solid will occur, lowering, consequently, the solid temperature sufficiently to permit spreading of the contact. The following correlation was developed for the minimum temperature:

$$T_m = \frac{\frac{27}{32} T_{cr} \left\{1 - \exp\left[-0.52\left(\frac{10^4 (\rho/A)^4/3}{\sigma}\right)^{1/3}\right]\right\} - T_c}{\exp(0.00175\beta)\operatorname{erfc}(0.042\sqrt{\beta})} + T_c \qquad (2.4)$$

where

A = atomic number

$\beta = (\rho Ck)^{-1}$ of solid in cgs units

In the case of liquid-liquid systems the question of predicting the MFB point seems more complicated. Boiling between two liquids is different in nature than between liquid and solid surfaces. The normal nucleate boiling regime is absent in a pure liquid-liquid system because of lack of preexisting nucleation sites resulting from surface cavities and gas bubbles. To achieve the ideal experimental conditions for

conducting minimum film boiling experiments purified surfaces such as oils or other pure liquids were used because of their excellent wetting properties. When using mercury as a surface even with great care, a clean liquid-liquid interface was never achieved.[35]

Film boiling experiments were conducted by Henry et al.[36] for liquid-liquid systems: drops of Freon-11, Freon-22, ethanol, and water on mercury. Minimum film boiling calculations based on the solid-liquid correlation predicted much greater temperatures than were measured experimentally. It was proposed that since the liquids do not wet mercury very well the microlayer evaporation does not apply thus, only the transient wetting was considered which results in:

$$\frac{T_m - T_{m,i}}{T_{m,i} - T_{sat}} = \sqrt{\frac{k_c \rho_c C_c}{k_h \rho_h C_h}} \qquad (2.5)$$

Minimum film boiling temperatures calculated from this equation and from the correlation given in Refs. 31 and 33 were compared to both visual assessments and evaluations via the experimentally minimum heat flux. The most significant point from the comparison is the large differences between the data and the correlation recommended by Henry which has demonstrated good agreement with the available liquid-solid film boiling results.

It is interesting to note that for water the visual mechanism of assessing the minimum temperature gave a lower value than the surface temperature at the minimum heat flux. At surface temperatures much less than the minimum heat flux point the liquid drop was clearly in film boiling, i.e., the edges demonstrated an unwetted curvature, the liquid

easily glided over the mercury surface and no nucleate boiling type sounds were observed. Contact measurements between the boiling liquids (water and ethanol) and mercury showed continuous intimate contact. Such contact was further evidenced by surface waves on the mercury which appeared to be generated following the bubble breakthrough in the boiling liquid.

Another experiment was conducted with a Freon-22/water system. Berenson's prediction for such a system is 20° and Eq. 2.5 yields a value of 33°C, but film boiling could not be sustained at water temperatures as high as 45°C, because of ice formation resulting in nucleate boiling. For water temperatures greater than 45°C small vapor explosions occurred.

The difference between the theoretical predictions and the experimental results was attributed to different buoyancy and wetting characteristics.

2.2.2. Mechanisms of Liquid-Liquid Contact

One of the problems in the formulation of vapor explosion is figuring out the conditions in which intimate contact is made between hot and cold liquids in connection with the triggering and propagation of the explosion. The problem is complicated and we suffer from a lack of knowledge about the exact mechanism which causes collapse, wetting, and nucleation characteristics in the different systems. One would expect to gain some knowledge and ideas about contact in relatively simple systems where no external velocities are present (Leidenfrost drop) but as we showed, even in those systems the problem is not yet resolved. However, it seems that hydrodynamic motion, instabilities, wetting characteristics, and thermal conditions are all involved in the

process.

One may assume that the governing process for making contact is the squeezing of the vapor film (see Chapter III). It may be due to random "tongues" of liquid or large liquid area pushed toward the surface by mechanical forces or disturbances (Taylor and Helmholtz instabilities). Another way for solving the problem is to assume that contact always exists and to study the thermal and hydrodynamic conditions for sustaining the contact.

In a study on vapor explosion mechanism Henry and Fauske[37] developed a model predicting the sizes of drops, as a function of surface temperature, which will result in liquid-liquid contact ("capture theory"). Based on experimental observations they assume that initial contact is always made and boiling is described by the spontaneous nucleation theory (see Appendix A). Upon this contact the interface temperature is established according to Eq. A.2 in Appendix A and the thermal boundary layer develops. The time for developing the boundary layer consists of: relief time necessitated by single-phase constant volume heating ($\sim 10^{-7}$ sec), the waiting time for the first nuclei ($=1/JV$), and the acoustic relief time required before that vapor bubble can grow ($t_a = 2\ell/c$). As illustrated in Fig. 2.6, this establishes not only the inception criterion for the vapor bubble but also the maximum diameter to which it can grow in a stable manner. Once this change in radius is evaluated, the time required for the growth can be evaluated from the inertial growth equation ($t_g = \frac{\Delta R}{\left(\frac{2\Delta P}{3\rho_\ell}\right)^{1/2}}$). On the other hand, if the boundary layer growth time is so short it cannot support a vapor bubble of the critical diameter, embryos will collapse before reaching

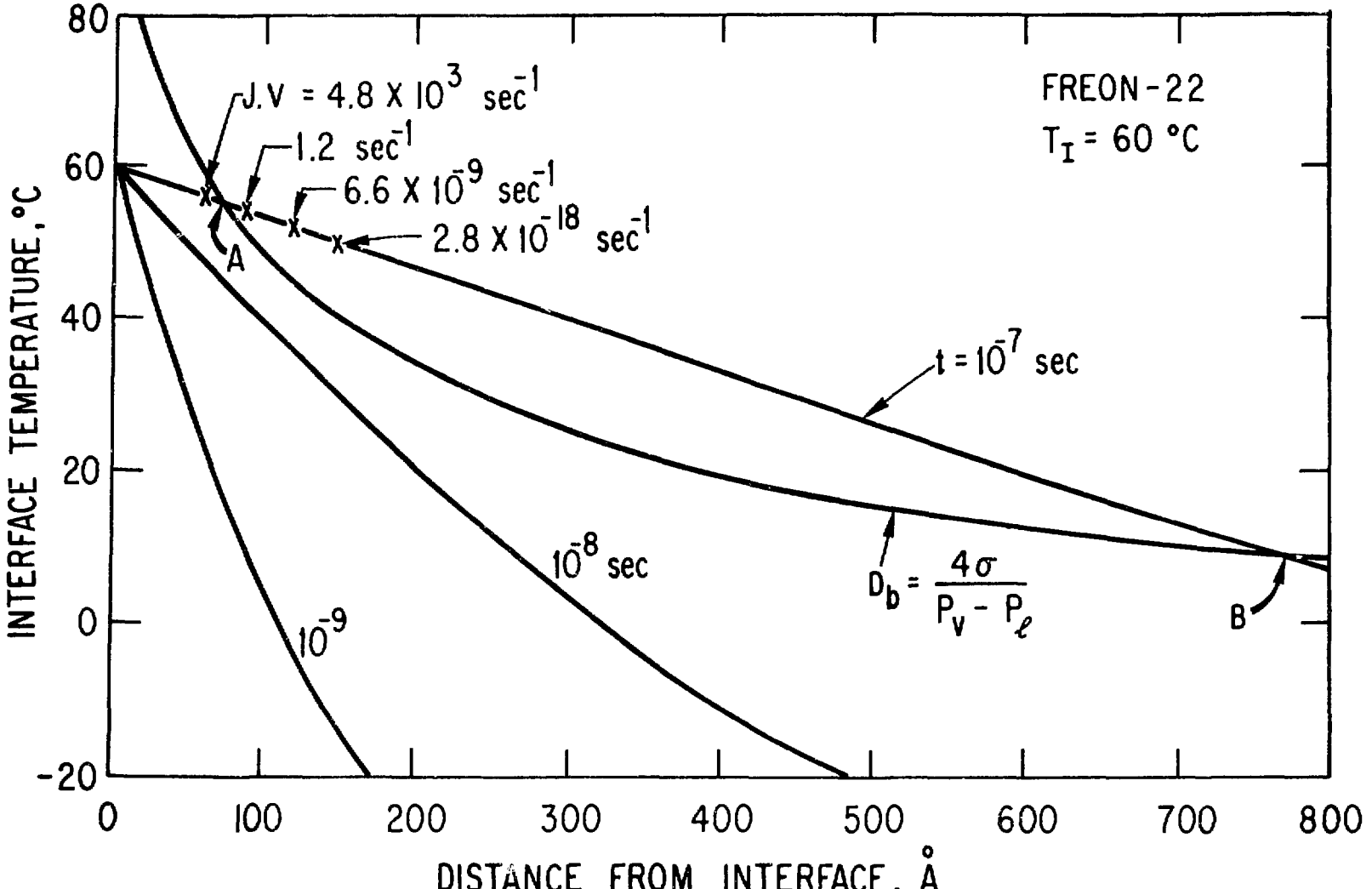

Fig. 2.6 Thermal Boundary Layer Development and Critical Cavity Size for Freon-22 (after Henry and Fauske[37])

the critical size (such conditions are shown in Fig. 2.6 for 10^{-9} and 10^{-8} sec.)

The number of bubbles that can exist simultaneously is obtained by the product of the nucleation frequency determined by the temperature at point A in Fig. 2.6, the volume per unit surface area between the interface and point A, and the growth time of a single bubble ($=JV\ t_g$). Because of mutual pressurization effects, the number of simultaneous nuclei is less than a predetermined number (in the case of Freon-22 it is 10^9 sites per sq cm of contact). If the number of nucleation sites that exist simultaneously result in interference at the maximum stable bubble diameter (point B in Fig. 2.6), the interface between the two liquids will be vapor blanketed and the energy transfer will be terminated for all practical purposes. This interference sites density (N) can be evaluated from the maximum stable diameter at point B (D_B) by

$$N = \frac{1}{D_B^2} \tag{2.6}$$

where

$$N \leq 10^9 \text{ sites/cm}^2$$

A schematic representation of the drop behavior for film boiling and capture is shown in Fig. 2.7.

Given the above information, the stability of a specified drop size, in terms of wetting and capture by the hot liquid or sustained film boiling, can be evaluated as a function of interface temperature. (On the stability line see Appendix B.)

An experiment was conducted to determine the viability of the above drop stability criteria. In this experiment, small drops of Freon-12

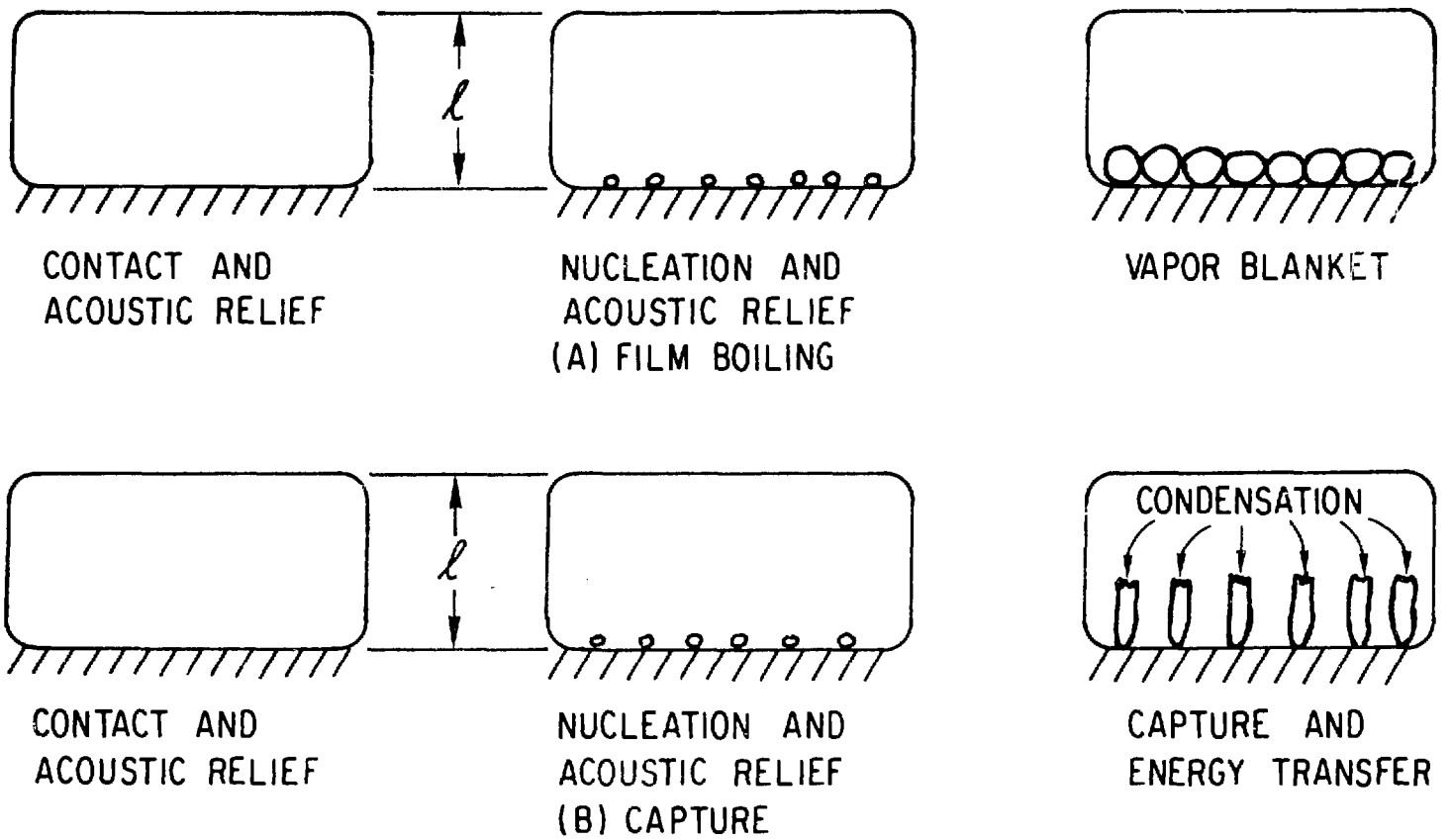

Fig. 2.7 Drop Behavior for (A) Film Boiling and (B) Capture (after Henry and Fauske[37])

were impinged upon a mineral oil surface and high speed movies (5,000 pps) were taken of the resulting interactions. For interface temperatures less than the homogeneous nucleation value, all sized drops wet the surface and proceeded to vaporize in thin film vaporization or by entrapment and incoherent nucleation (small scale explosive interactions). For interface temperatures greater than the homogeneous nucleation value large sized drops penetrated the surface and developed their own protective vapor film, which was clearly evident when the drops returned to the surface as drops floating in their own protective vapor pockets. When these large drops either fragmented or vaporized to a small enough size, they would become trapped on the surface and vaporize completely within 1 to 2 msec. This requires a heat flux which is approximately two orders of magnitude greater than the critical heat flux for the Freon. A summation of all these experimental results is shown in Fig. 2.8 along with the stability criteria for Freon-12 as a function of interface temperature. It is seen that the experimental results are in excellent agreement with the stability predictions arising from spontaneous nucleation and thermal boundary layer considerations.

Another theory suggested by Ochiai and Bankoff[38] is related to the last one. It assumes also that random contact is made by a tongue of cold liquid and the interface temperature is above the homogeneous nucleation temperature. In addition to thermal conditions, this model applies hydrodynamic consideration. After relieving the pressure, explosive growth and coalescence of the vapor bubbles results in a high pressure vapor layer at the liquid-liquid contact area. This amounts to an impact pressure applied to the free surface of the hot liquid, producing a "splash" with a resulting velocity distribution obtained from

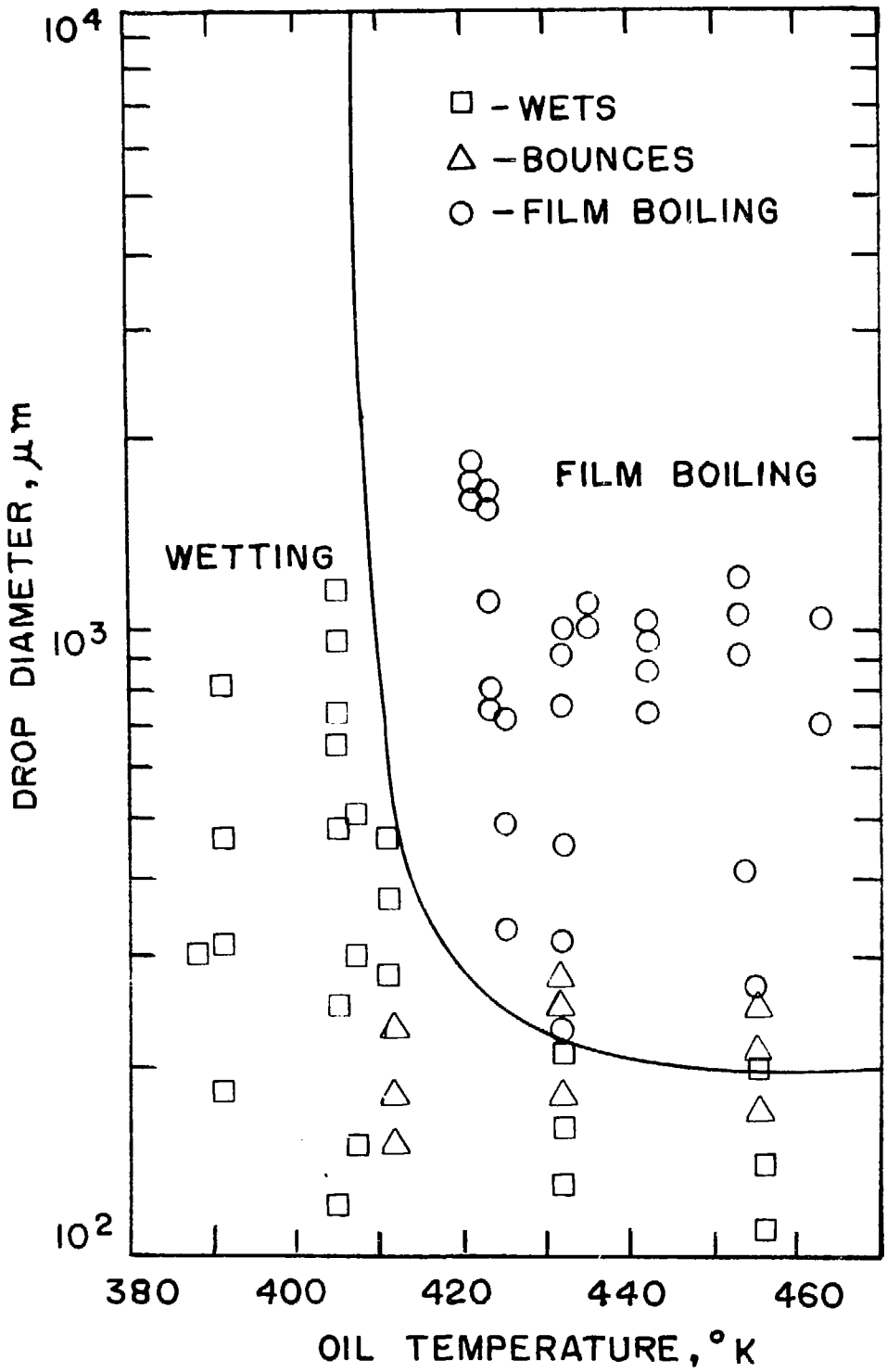

Fig. 2.8 Drop Stability Prediction and Experimental Data for Freon-12 (after Henry and Fauske[37])

potential flow theory. If the average Weber number in this "splash" is larger than some critical value (found from dropping experiments), contact will be sustained.

2.3 Mechanisms for Vapor Explosion

There have been many mechanisms proposed to describe the fragmentation process. Among them are

(1) Violent Boiling - Transition boiling between the two liquids may be violent enough to account for observed fragmentation.[39]

(2) The liquid entrapment model proposes that quenching liquid is drawn into the drop's interior or trapped between the drop and the container surface. The evaporation of that liquid is rapid, resulting in an explosion.[40]

(3) The solid shell model proposed that the drop solidifies on the surface upon contact. The solid shell thus formed shrinks, which consequently increases the pressure in the drop. This pressure increase causes an explosive rupture of the solidified shell.[41]

(4) Bubble Growth and Collapse - Microjets resulting from asymmetrical bubble growth and collapse at the liquid interface may produce a self-propagation formation of new interfacial area.[42]

(5) Violent Gas Release - Dissolved gases can precipitate out as the hot liquid cools and solidifies, resulting in rapid fragmentation.[43]

Among the models which have been proposed to describe the vapor explosion mechanisms, are the detonation model and spontaneous nucleation model.

Detonation model - The possibility of a steady-state Chapman-

Jouguet thermal detonation wave propagating through an initially coarse mixture of hot and cold liquids has been proposed by Board and Hall[44] as a mechanism for vapor explosion. The postulated mechanism is the breakup of single drops of hot liquid immersed in a vaporizable cold liquid (tin-water, or UO_2-sodium) due to passage of a shock wave. This fragmentation is accompanied by rapid mixing and heat transfer which sustains the shockwave. Very large peak pressures (~1500 MPa) were thus calculated for the initiation of such an event. For the LMFBR these pressures are in the neighborhood of the constant-volume temperature-equilibration pressure (Hicks and Menzies[45]), and hence, might conceivably be attained by a rapid local mixing with strong inertial and structural constraints. However, detailed calculations made by Bankoff et al.[46] show that an additional order-of-magnitude increase in peak pressures is required, making the possibility of such an event in a reactor accident even more remote.

Spontaneous Nucleation Model - From the LNG-water study done by Enger and Hartman[47] it was found that two physical phenomena are determining the conditions producing explosions: the boiling behavior in the interface region between the liquids and the maximum degree of superheating in the cold liquid (spontaneous nucleation). They suggested that explosions occur when the hot liquid temperature exceeds the cold liquid homogeneous nucleation temperature, i.e., $T_h \geq T_{hn}$. The results obtained by Enger and Hartman,[47] Nakanishi and Reid,[48] and Porteous and Reid[49] were shown to be in close proximity with that temperature threshold. Fauske[50] suggested that explosions occur if the interface temperature upon contact is equal to or above the spontaneous nucleation temperature of the cold liquid, i.e., $T_I \geq T_{sn}$. He also suggested that

three main stages exist in developing an explosion. In the first stage the two liquids coarsely intermix when the cold liquid is in film boiling. The second stage involves intimate contact between the liquids which results in vapor production in a short time scale and pressure, which should propagate (the third stage) through the system.

In the case of intermixing, when the hot liquid temperature is above the spontaneous nucleation temperature, but is not hot enough for resulting in an interface temperature above the spontaneous nucleation temperature, a possibility of entrapment and superheating of the cold liquid drops exists. In this case, the superheated drops explode like the classical physics experiments[51] but the result is an incoherent explosion, or a small scale event[52] in which the energy is transferred during a longer time than the explosion time scale. The difference between small scale and large scale explosions is described in Fig. 2.9. That explains some experimental observations, as the possibility of fragmentation occurrence which is not a consequence of an explosion and some of the observations which lead to the entrapment model.[40] Thus, when analyzing experimental results, one should be careful in deciding what scale of events has occurred. In some of the small-scale dropping experiments, this distinction may be somewhat difficult to observe experimentally because the small amount of thermal energy available, so that even if a large-scale event would be possible with large masses the observation is similar to the occurrence of a small-scale event.

As an example, large-scale explosive interactions, conducted by Henry et al.,[53] with saturated Freon-22 and saturated propane and mineral oil demonstrated excellent agreement with the model prediction of

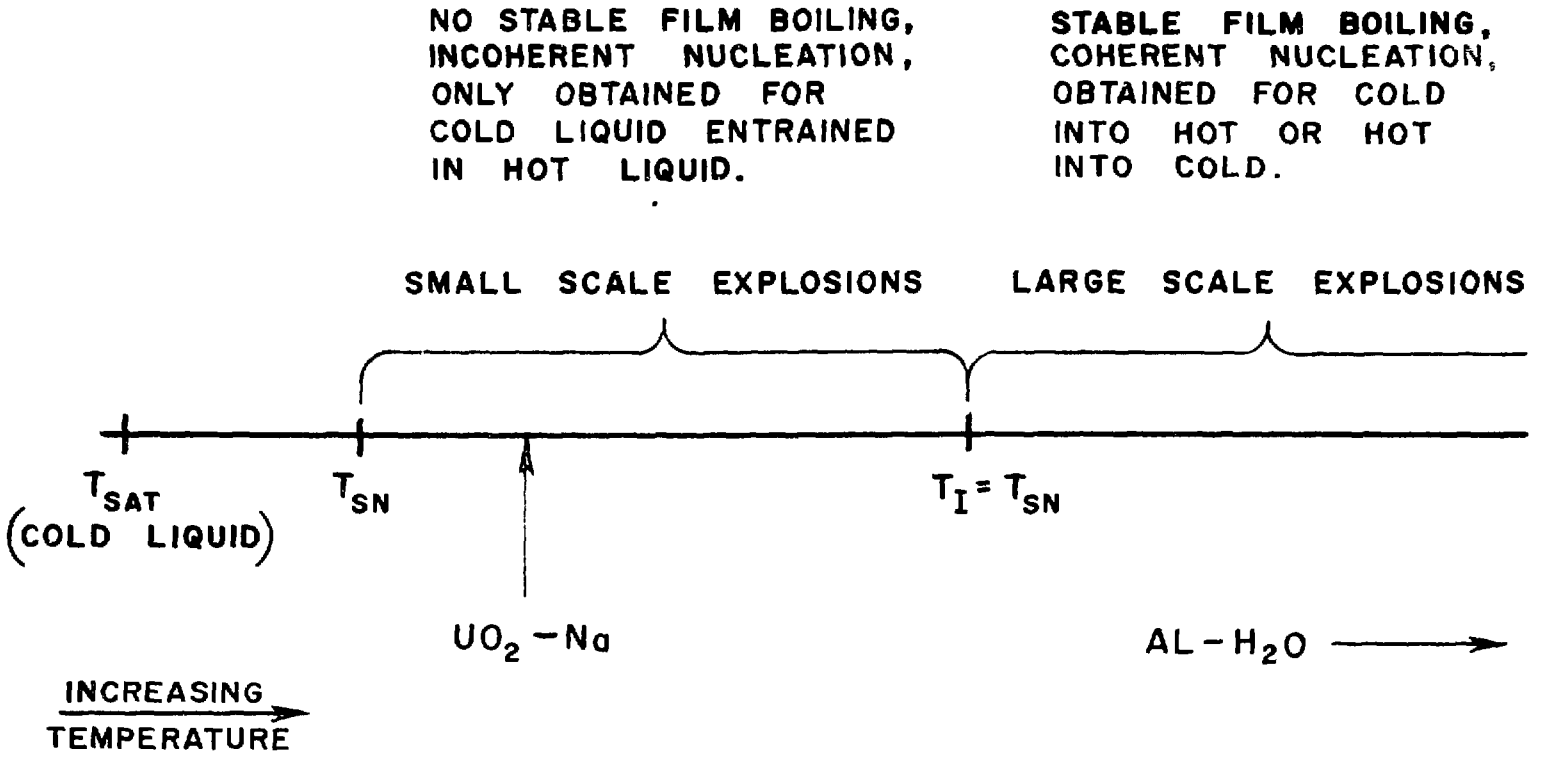

Fig. 2.9 Characterization of Temperature Requirements and Experimental Observations for Small and Large Scale Vapor Explosive Events (after Henry and Cho[52])

homogeneous nucleation temperature threshold as shown in Fig. 2.10 which is consistent with the fact that both systems are known to exhibit excellent wetting. On the other hand, for Freons using water as the host fluid, a definite threshold was found, and it corresponds to an interface temperature considerably lower than the homogeneous nucleation limit.[54],[55] This is again consistent with the wetting characteristics of these systems (Freons and water are poorly wetted systems) resulting in heterogeneous nucleation characteristics. In an effort to validate the interface criteria, Board et al.[54] conducted dropping experiments for Freon-22 into water. The Freon subcooling was varied and the conclusion was that the threshold temperature did not change with increasing Freon subcooling and hence with changing interface temperature. The disadvantage when dealing with poorly wetted system (as Freon-22-water) is that the wetting characteristics can be altered by changing the interface temperature which consequently changes the spontaneous nucleation temperature. Note that uncertainties in the initial Freon temperature are always inherent when dropping subcooled Freon, which is the method used by Board et al.[54] On the other hand, the resolution for the initial Freon temperature is much better when hot oil is dropped onto the subcooled Freon, a method used by Henry et al.[55] In a well-wetted system, which also has a greater sensitivity to Freon subcooling, Freon-22 and mineral oil did demonstrate a dependence on subcooling which is in good agreement with the interface temperature model (Fig. 2.11).

A recent paper by Corradini et al.[56] shows that the known experimental data for tin and water is consistent with the spontaneous nucleation theory.

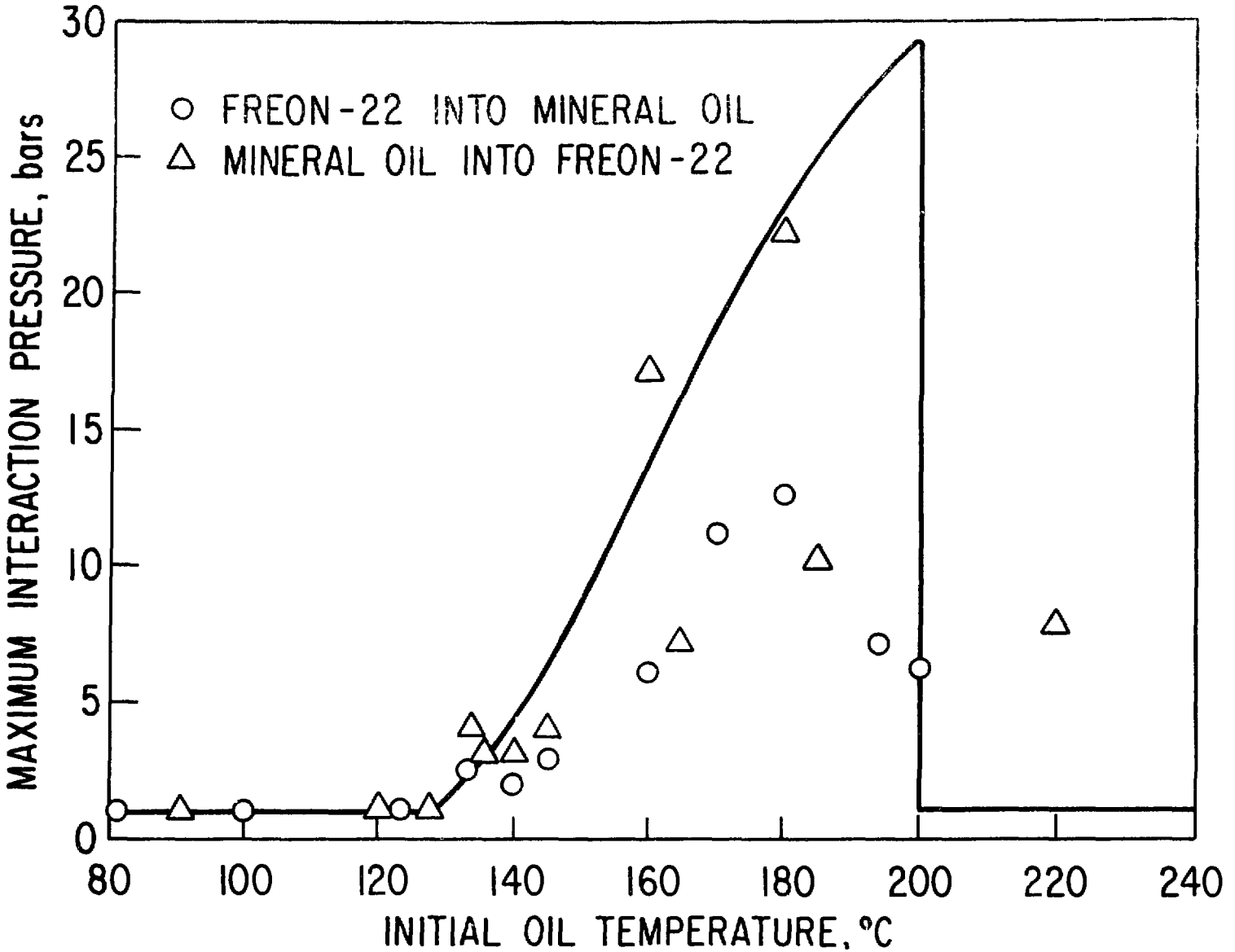

Fig. 2.10 Pressure Generation As a Function of Oil Temperature for the Freon-22-Mineral Oil System (after Henry et al.[53])

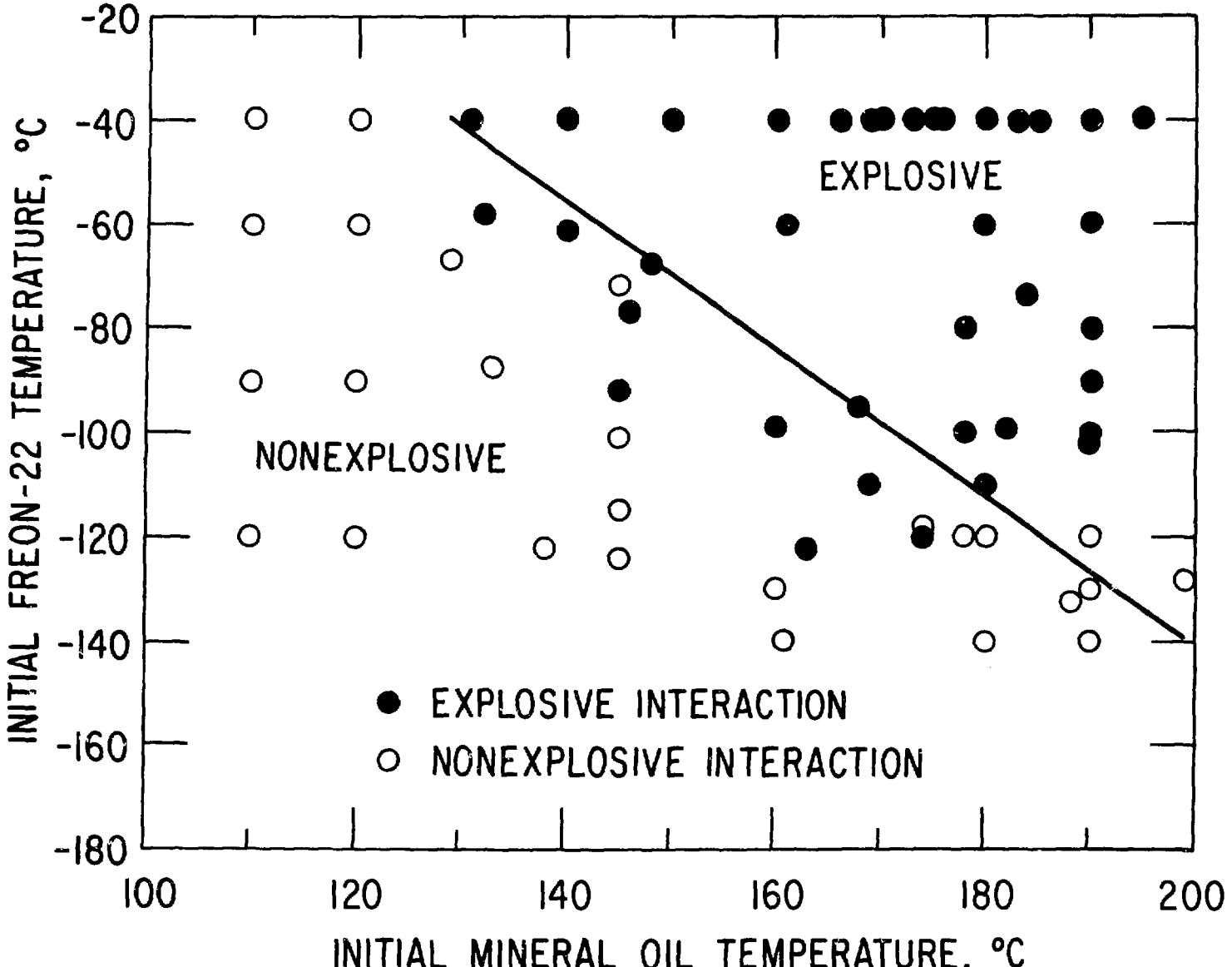

Fig. 2.11 Comparison Between the Interface Temperature Model and the Experimental Results (after Henry et al.[55])

Since a vapor explosion is a result of converting thermal energy to mechanical energy in a short time (less than the acoustic relief time characterizing the system), it is important to isolate the responsible mechanism for such transfer. According to Henry and McUmber[57] a high pressure source exists in the bubbles formed, particularly, in the inertially dominated period of the bubble growth. During that period the pressure in the bubble is the vapor pressure corresponding to the superheat. In the second growth period (the thermally dominated stage) the bubble pressure is essentially the same as the ambient pressure (see Appendix B). Thus, a possible way to sustain propagation in an explosive event is by internal fragmentation of liquid drops during the inertially dominated period. That leads us to the other related requirement which discusses the sizes of the cold liquid drops (the "capture theory") and the relative size of bubble formed in those drops, since pressure relief will not occur before the bubble becomes comparable to the drop in size.

In the intermixing stage a coarse mixing of cold and hot liquids is produced when the cold liquid is in film boiling. Since the minimum film boiling temperature for clean, nonsolidifying liquid-liquid systems (where no nucleation sites exist) is a contact temperature equal to the spontaneous nucleation temperature (at least for drop sizes usually formed by the dropping mode of contact), the hot liquid should be at a temperature such that the temperature upon contact is above the spontaneous nucleation temperature. During the intermixing stage, the drops evaporate and fragment slowly until contact occurs. If the temperature at the interface and the system pressure are such that bubbles are

capable of growing inertially up to the point they rupture the drop, the droplet is fragmented, and the high pressure is released[57] in the form of a small shock wave (Fig. 2.12). A possible propagation mechanism suggests that as a result of the drop rupture a fine spray of liquid is produced. Since the spray droplets size is much smaller than the parent droplet, they are capable of being "captured" and the bubbles will grow inertially even in a pressure field considerably higher than the initial pressure, which results in successive pressure release in a very short time scale. This process of nucleation, inertial growth and liquid fragmentation is terminated when the pressure in the system is such that the inertially dominated growth is essentially terminated at the bubble critical size.

In the dropping experiments of UO_2 and stainless steel into sodium conducted by Armstrong et al., and in the injection experiments of Na-UO_2 and Na-steel, the interface temperature is well below the homogeneous nucleation temperature of sodium. For homogeneous nucleation at the interface, the UO_2 and stainless steel temperature should be about 7000 and 3000°C, respectively, for sodium at ~400°C. In order to explain the interactions with sodium let us recall first that violent interaction has occurred only when the cold liquid (Na) was injected into the hot liquid (UO_2) and not when UO_2 or stainless steel were dropped into sodium. To explain the UO_2-Na experiments, Fauske[58] suggested an entrainment-wetting-superheat mechanism in which the liquid sodium globules can be entrained and wet the liquid UO_2 surface. The lack of nucleation sites in the liquid-liquid system results in an overheating of the liquid sodium until spontaneous nucleation occurs. The proposed mechanism is summarized in Fig. 2.13. Point I indicates

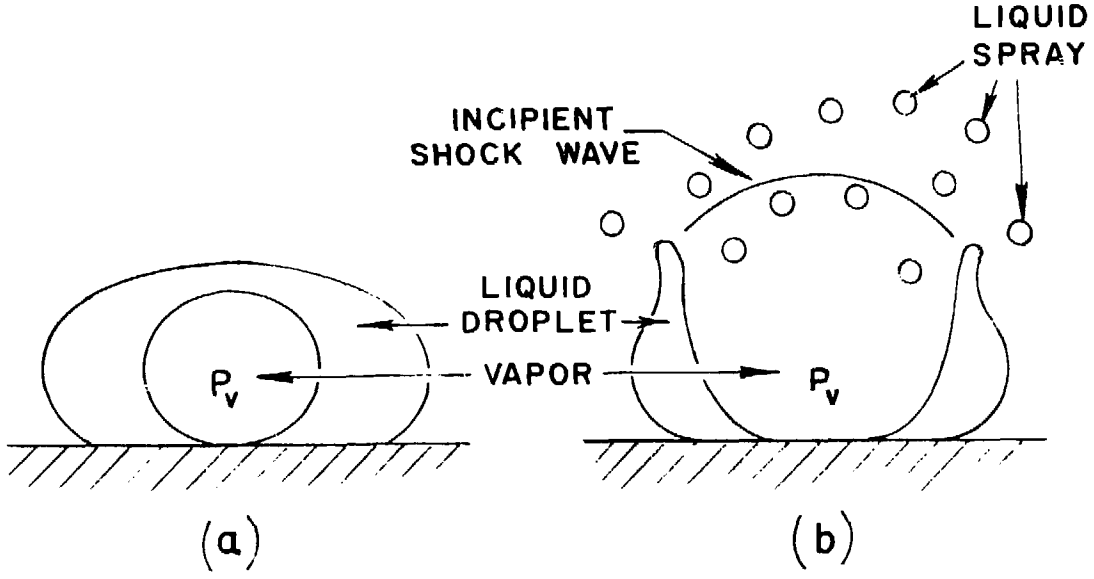

INERTIAL GROWTH

$P_v >> P_{ambient}$

$r_f > r_c$

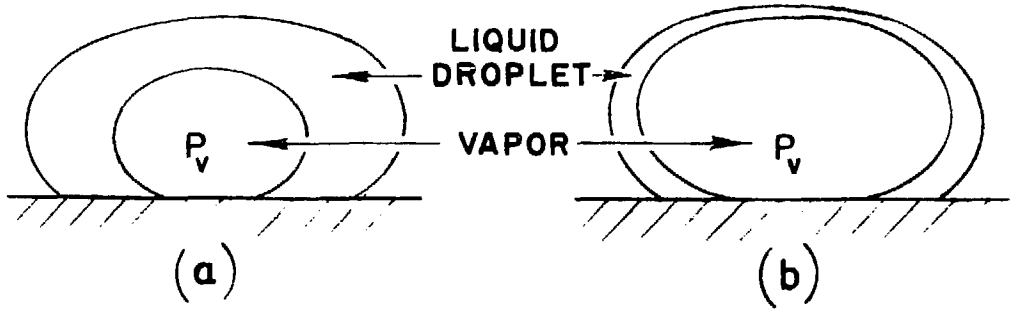

THERMAL GROWTH

$P_v = P_{ambient}$

$r_f < r_c$

Fig. 2.12 Liquid Drop Behavior for Inertial and Thermally Dominated Bubble Growth Behaviors (after Henry and McUmber[57])

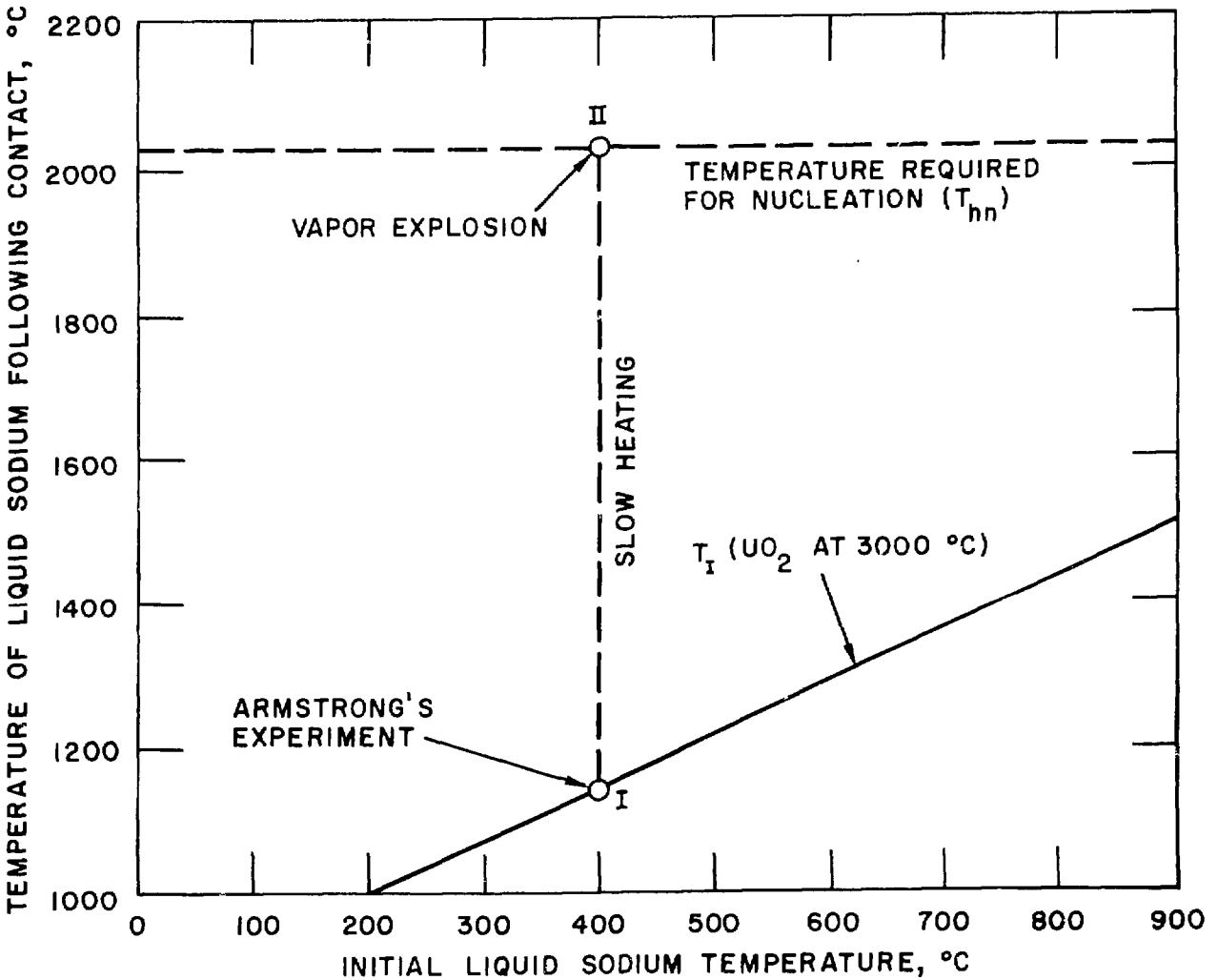

Fig. 2.13 Illustration of Proposed Mechanism for Armstrong's Observed Vapor Explosion (after Fauske[58])

roughly the initial temperature established upon contact. If the sodium is injected into the liquid UO_2, i.e., a limited amount of cold fluid is imbedded in the hot fluid, sodium can be heated to its superheat limit (Fig. 2.13, point II), which results in explosive vapor formation. The validity of the proposed mechanism has been demonstrated by above-surface injection of liquid Freon-11 (normal boiling point 23.8°C) into hot water (up to 90°C). This mechanism describes the "small-scale event" mode of interaction where incoherent interactions occur. Indeed, to date, no large-scale explosions have been reported when the predicted interface temperature was below the spontaneous nucleation temperature.

Considering the possibility that a small sodium drop becomes superheated up to its homogeneous nucleation temperature, the saturation pressure corresponding to this temperature is ∿11 MPa (see Table A.5) which is the maximum pressure in the bubble while it is inertially dominated. However, even a preferred site can result in nucleation and significant pressures in a highly superheated liquid even if the temperature of the hot material is below the spontaneous nucleation limit. The incoherent, small-scale event may also be an explanation for the Na-steel injection experimental observations discussed in Section 2.1.1.

The "capture theory" by Henry-Fauske also predicts that for non-chemically reacting systems in the free contacting mode the critical temperature at the interface, is an upper threshold for explosions. Excellent experimental agreement for the upper temperature threshold is shown to exist in Freon-oil and most of the LNG experiments. Liquid metals--water systems experience explosions well above an instantaneous

contact temperature equal to the thermodynamic critical temperature, e.g., Fe/H_2O, Al/H_2O, and Ag/H_2O in shock tubes and industrial explosions. Henry and Fauske pointed out that near the critical point strong variations in thermal conductivity, density, and specific heat must be accounted for. The thermal conductivity and specific heat can both increase by an order of magnitude resulting in an additional capability of the cold liquid to transfer and store energy. That means that the initial temperature of the hot liquid has to be greater than would be expected from constant parameters considerations. Also, oxide layer formation, which may account for a decrease in the hot liquid thermal conductivity by at least an order of magnitude, reduces, as a result, the interface temperature. However, as discussed by Corradini et al.,[56] those arguments may account for some experimental results but not for all of them. As a result, it was suggested that a small projection from the molten metal acts as a cooling fin which can be cooled down more rapidly during the dwell time than the bulk liquid. It cools down below the critical point, makes contact, and initiates an interaction.

III. A MODEL FOR LIQUID-LIQUID CONTACT--
SQUEEZING OF VAPOR BETWEEN A DROP AND A SURFACE

Dropping experiments have been conducted by Waldram et al.[59] and Ochiai and Bankoff[38] in which low boiling droplets were dropped onto a hot liquid. They investigated the conditions under which liquid-liquid contact was made as a function of physical properties, temperature difference, drop diameter, and drop release height. Drop diameters and heights were 0.24-0.32 cm and <18 cm, respectively.

Three heat transfer modes were observed:

(1) film boiling (Leidenfrost boiling) - the droplet floats on the surface and evaporates smoothly, which implies that a vapor film separates the two liquids.

(2) wetting - coalescence occurs between the liquids.

(3) spattering - explosive vaporization following coalescence.

A sharp threshold for spattering occurs at the homogeneous temperature of pentane, while for alcohols it occurs at surface temperatures 10-35°C higher. It was s found that the critical height (the maximum height which results in film boiling) and the drop Weber number depend strongly on surface temperature and is smaller for acetone and the lower alcohols than for pentane by a factor of about two, indicating better wetting by the oxygen-containing organic compounds of silicone oil than by hydrocarbons.

In modeling the dropping experiments, the assumption that the intervening film, between the drop and the surface, controls the coalescence-rebound process, can be applied, as is usually done in isothermal liquid-liquid systems.[60] Because the inertia of the drop and

the appreciable evaporation from the approaching drop have to be taken into account, it is reasonable to expect that the film thickness may exhibit a minimum with respect to time. One might hope that this minimum would correspond to some critical thickness for a film instability due to the combined effects of London-Van der Waals forces, inertial and viscous forces[61] or free molecule heat conduction,[62] which might be then related to the existence of a critical release height for coalescence or rebound as a function of the system parameters.

3.1 Model Formulation

A cold drop of a volatile liquid at its saturation temperature falls from initial height h_o under gravity, towards the surface of a pool of a hot nonvolatile liquid. Initially the drop motion is governed entirely by gravity, but as the drop begins to penetrate the pool surface, a thin gas film of thickness h(t) forms, which governs the further approach of the two liquid surfaces. When the film thickness is equal to the thickness of the preexisting thermal boundary layer above the pool surface, evaporation commences. The film is here assumed to be flat, so that the drop takes the shape of a spherical zone (Fig. 3.1). One might expect that the film thickness would be a function of radial position under impact conditions, but to avoid a detailed solution of the flow fields in the three regions, a uniform film thickness is assumed. Evaporation takes uniformly from the flat drop surface into the film with the normal velocity v_e. Mass and heat transfer from the remainder of the drop are considered to be negligible. Using cylindrical coordinates, the equations describing the motion of the film are:

$$\frac{\partial u}{\partial t} + \frac{1}{r}\frac{\partial}{\partial r}(ru^2) + \frac{\partial (uv)}{\partial z} = -\frac{\partial \psi}{\partial r} + \nu \frac{\partial}{\partial z}\left(\frac{\partial u}{\partial z} - \frac{\partial v}{\partial r}\right) \qquad (3.1)$$

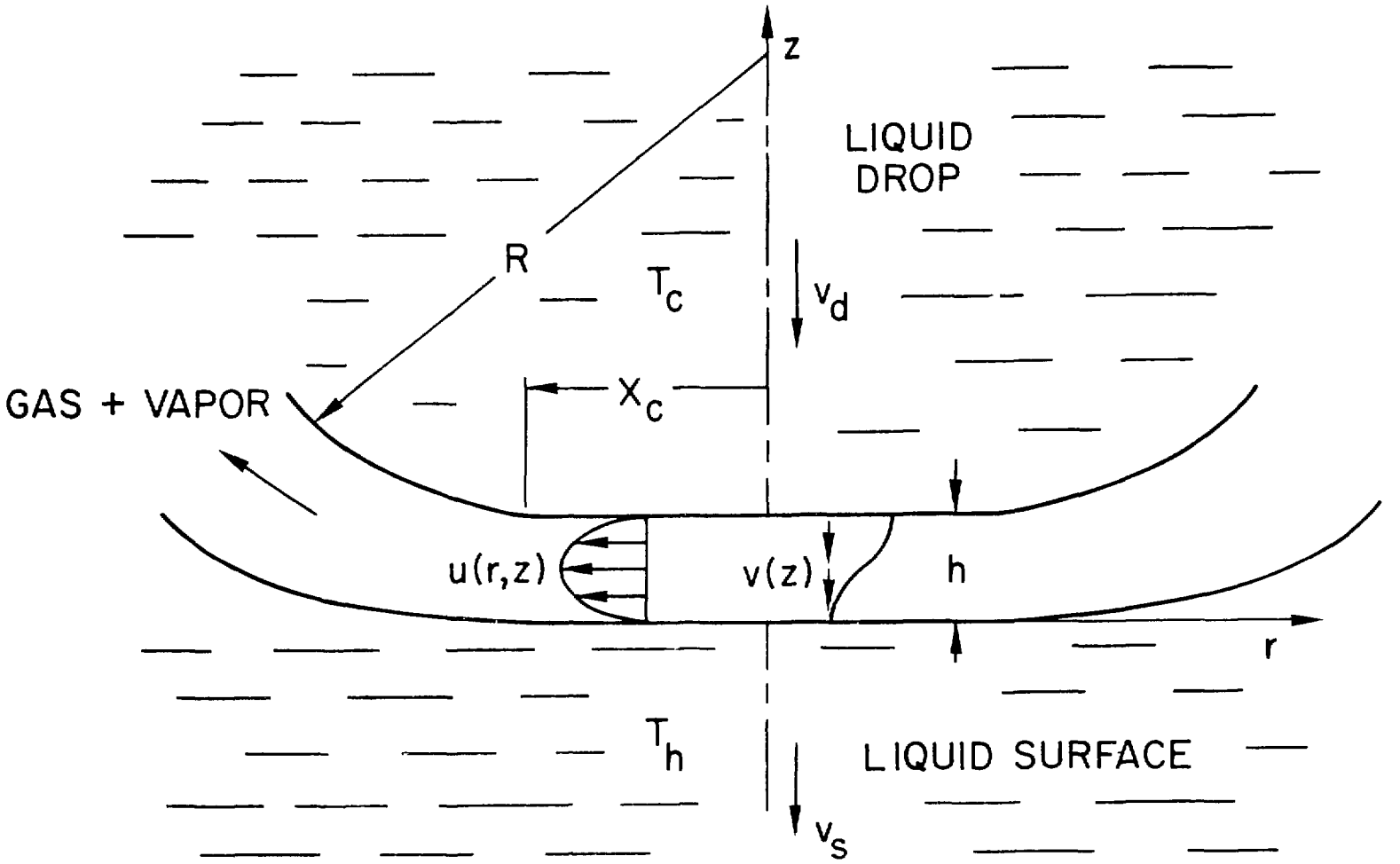

Fig. 3.1 A Model for Squeezing a Vapor Film Between a Falling Drop and a Hot Liquid Surface

$$\frac{\partial v}{\partial t} + \frac{\partial}{\partial r}(ruv) + \frac{\partial v^2}{\partial z} = g - \frac{\partial \psi}{\partial z} - \frac{\nu}{r}\frac{\partial}{\partial r}\left[r\left(\frac{\partial u}{\partial z} - \frac{\partial v}{\partial r}\right)\right] \tag{3.2}$$

$$\frac{1}{r}\frac{\partial (ru)}{\partial r} + \frac{\partial v}{\partial z} = 0 \tag{3.3}$$

where u, v are velocity components in the r, z directions, respectively, and $\psi \equiv \frac{P}{\rho}$ for incompressible flow. We assume that inertial and gravitational forces are small compared to viscous and pressure forces within the gas film, so that:

$$\frac{\partial \psi}{\partial r} = \mu \frac{\partial}{\partial z}\left(\frac{\partial u}{\partial z} - \frac{\partial v}{\partial r}\right) \tag{3.4}$$

$$\frac{\partial \psi}{\partial z} = -\frac{\nu}{r}\frac{\partial}{\partial r}\left[r\left(\frac{\partial u}{\partial z} - \frac{\partial v}{\partial r}\right)\right] \tag{3.5}$$

$$\frac{1}{r}\frac{\partial (ur)}{\partial r} + \frac{\partial v}{\partial z} = 0 \tag{3.6}$$

The boundary conditions are:

$$z = h; \quad u = 0; \quad v = -v_o; \quad T = T_c \tag{3.7}$$

$$z = 0; \quad u = 0; \quad v = -v_s; \quad T = T_h \tag{3.8}$$

where v_o and v_s are the velocities at the film upper and lower surfaces, respectively, and T_c and T_h are temperatures of the cold and hot surfaces, respectively. It is acceptable to assume zero tangential velocity at both edges of the film in view of the low gas velocity and viscosity. We thus look for a solution of the form:

$$v = -f(z), \tag{3.9}$$

upon substituting Eq. 3.9 into Eq. 3.6 and integrating:

$$u = \frac{1}{2} rf'(z) \tag{3.10}$$

After substituting Eq. 3.10 into Eqs. 3.4 and 3.5 we get:

$$\frac{\partial \psi}{\partial r} = \frac{\nu}{2} rf'''(z) \tag{3.11}$$

$$\frac{\partial \psi}{\partial z} = -\nu f''(z) \tag{3.12}$$

Integration of Eq. 3.12 leads to:

$$\psi = -\nu f'(z) + g(r) \tag{3.13}$$

whence:

$$\frac{\partial \psi}{\partial r} = g'(r) \tag{3.14}$$

Comparing Eq. 3.11 to 3.14:

$$\frac{g'(r)}{r} = \frac{\nu}{2} f'''(z) = C_\infty \tag{3.15}$$

where C_∞ is a constant to be determined. Integrating Eq. 3.15 three times leads to:

$$f = \frac{C_o z^3}{6} + C_1 \frac{z^2}{2} + C_2 z + C_3 \tag{3.16}$$

where $C_o = 2C_\infty$. From Eqs. 3.9 and 3.10 it then follows that

$$u = \frac{1}{2} r \left(\frac{1}{2} C_o z^2 + C_1 z + C_2 \right) \tag{3.17}$$

$$v = -\left(\frac{1}{6} C_o z^3 + \frac{1}{2} C_1 z^2 + C_2 z + C_3 \right) \tag{3.18}$$

Introducing the boundary conditions one obtains:

$$u = \frac{3\bar{v}_o rz}{h^2}\left(1 - \frac{z}{h}\right) \tag{3.19}$$

$$v = \frac{\bar{v}_o z^2}{h^2}\left(\frac{2z}{h} - 3\right) \tag{3.20}$$

The velocity $\bar{v}_o$ is equal to:

$$\bar{v}_o = v_d + v_e - v_s \tag{3.21}$$

where v_d is the drop velocity

$$v_d = -\frac{dh}{dt} + v_s \tag{3.22}$$

and v_e is the velocity of the vapor evaporating from the drop:

$$v_e = \frac{-k_v \left.\frac{\partial T}{\partial z}\right|_{z=h}}{\rho_v \lambda} \tag{3.23}$$

Substitution of $f'(z)$ and $g(r)$ (the latter from integration of Eq. 3.15) into Eq. 3.13 results in the pressure in the film;

$$P = P_\infty - \frac{3\bar{v}_o \mu_v}{h^2}\left[2z\left(\frac{z}{h} - 1\right) - \frac{r^2}{h}\right] \tag{3.24}$$

The force due to pressure acting on the drop is;

$$F = 2\pi \int_o^{x_c} (P - P_\infty)\, r\, dr \tag{3.25}$$

where X_c is the flat surface radius given by:

$$X_c = \left[\frac{2}{3}\,\frac{(\rho_d - \rho_v)\cdot g}{\sigma_{eq}}\right]^{1/2} \cdot R^2 \tag{3.26}$$

and σ_{eq} is given by:

$$\sigma_{eq} = \frac{\sigma_d \cdot \sigma_s}{\sigma_d + \sigma_s} \tag{3.27}$$

Integrating Eq. 3.25 one obtains:

$$F = \frac{3}{2} \frac{\pi \bar{v}_o \mu_v X_c^4}{h^3} \tag{3.28}$$

The force balance on the drop takes the form:

$$F - mg + \pi \rho_v v_e^2 X_c^2 = -m \frac{d v_d}{dt} \tag{3.29}$$

where m is the drop mass, and London forces have been neglected.

Upon substituting Eqs. 3.22 and 3.28 into Eq. 3.29, one obtains the nonlinear ordinary differential equation:

$$\frac{d^2h}{dt^2} - \frac{K_2}{h^3}\left(-\frac{dh}{dt} + v_e\right) - K_1 v_e^2 + g - \frac{dv_s}{dt} = 0 \tag{3.30}$$

where

$$K_2 \equiv \frac{9}{8} \frac{\mu_v}{\rho_d} \frac{X_c^4}{R^3} \; ; \quad K_1 \equiv \frac{3\rho_v X_c^2}{4R^3 \rho_d} \tag{3.31}$$

Here ρ_d and R are the drop density and radius, respectively.

We now assume the gas temperature to be a function of axial position only, in view of the requirements that the film thickness be less than the thermal boundary layer thickness and the uniform constant temperatures at both surfaces of the film. With the above assumptions the energy equation becomes:

$$v \frac{dT}{dz} = \alpha \frac{d^2T}{dz^2} \tag{3.32}$$

where v, from Eqs. 3.20-3.23 is given by

$$v = \frac{z^2}{h^2} \left(\frac{2z}{h} - 3 \right) \left(v_d - \frac{k_v}{\rho_v \lambda} \left. \frac{dT}{dz} \right|_{z=h} \right) \tag{3.33}$$

The surface acceleration term in Eq. 3.30 has to be obtained by the use of another differential equation describing the surface motion upon impact. The main problem arising in formulating such an equation is the unknown amount of energy transferred from the drop to the surface and what is the energy distribution to kinetic, potential, and surface energies. For high surface tension materials, such as liquid metals the surface acceleration term can be ignored. Thus, Eq. 3.30 becomes:

$$\frac{d^2h}{dt^2} - \frac{K_2}{h^3} \left(- \frac{dh}{dt} + v_e \right) - K_1 v_e^2 + g = 0 \tag{3.34}$$

Two important special cases can be derived from Eq. 3.34. For isothermal system and negligible drop inertia we get:

$$- \frac{1}{h^3} \frac{dh}{dt} = \frac{g}{K_2} \tag{3.35}$$

which is the known Stefan-Reynolds equation[63] used frequently in lubrication theory, for which an explicit solution can be found.

For a nonisothermal system with negligible drop inertia Eq. 3.34 becomes:

$$\frac{K_2}{h^3} \left(- \frac{dh}{dt} + v_e \right) = g - K_1 v_e^2 \tag{3.36}$$

If it is assumed that $-\left.\frac{dT}{dz}\right|_{z=h} = \frac{T_h - T_c}{h}$ and $g >> K_1 v_e^2$, this becomes:

$$\frac{dh}{dt} = \frac{K_3}{h} - K_4 h^3 \tag{3.37}$$

where:

$$K_3 \equiv \frac{K_v(T_h - T_c)}{\lambda \rho_g} \; ; \quad K_4 \equiv \frac{g}{K_2} \tag{3.38}$$

For large times this gives the result:

$$h \to \left[\frac{9k_v(T_h - T_c)\mu_v X_c^4}{8\rho_v \rho_d \lambda g R^3}\right]^{1/4} = \left(\frac{K_3}{K_4}\right)^{1/4} \tag{3.39}$$

which agrees with the expression derived for stable Leidenfrost boiling,[64] when $X_c = R$

3.2 Results

Equations 3.32 and 3.34 were numerically integrated for the experimental critical release height for droplets to rebound. It can be seen from the form of Eq. 3.34, which corresponds to a strongly nonlinear oscillator, that the film thickness goes through a minimum. There is a relatively slow approach to this minimum thickness, followed by a rapid jump in the film thickness once the critical thickness, δ, has been reached. If this corresponds to the neutral stability thickness for the gas film, this should be nearly independent of the drop diameter. However, the computations indicate that the minimum film thickness for droplets originating at the critical release height is nearly proportional to the diameter. As might be expected, this would indicate that

short-range attractive forces are not sufficiently strong at the calculated minimum thickness ($\sim 10^4$ Å) to result in coalescence in a time scale shorter than that for rebound. A similar dependency was found by Jayaratne and Mason[65] although for entirely different reasons, since their analysis took into account mechanical energy transfer in the rebound phase, which has not been considered here.

A dimensionless correlation for the data was found in the form

$$\zeta \equiv \frac{\delta}{\sqrt{\sigma_{eq}/(\rho_d - \rho_v)g}} = s_b \tag{3.40}$$

where:

$$s_b = \bar{h}_o^{-1.02} \left(\frac{\rho_v}{\rho_d}\right)^{0.472} N_{We}^{0.671} \; N_1^{0.291} \tag{3.41}$$

In this equation the dimensionless critical release height and temperature difference, as well as the droplet Weber number, are given by:

$$\bar{h}_o = h_o/R; \quad N_1 = C_v(T_h - T_c)/\lambda; \quad N_{We} = \rho_d g h_o R/\sigma_d. \tag{3.42}$$

From Fig. 3.2 we see that the experimental results collapse into a straight line, for silicone oil serving as the surface and s_b is given in Eq. 3.41. For the same s_b, the thickness calculated for the glycerol surface data differs from the thickness calculated for the silicone oil data but also collapses into one line (Fig. 3.3). This difference is attributed to the difference in the wetting and thermal properties of the two liquids. If a least-squares procedure is applied to both liquids, s_b is given now as:

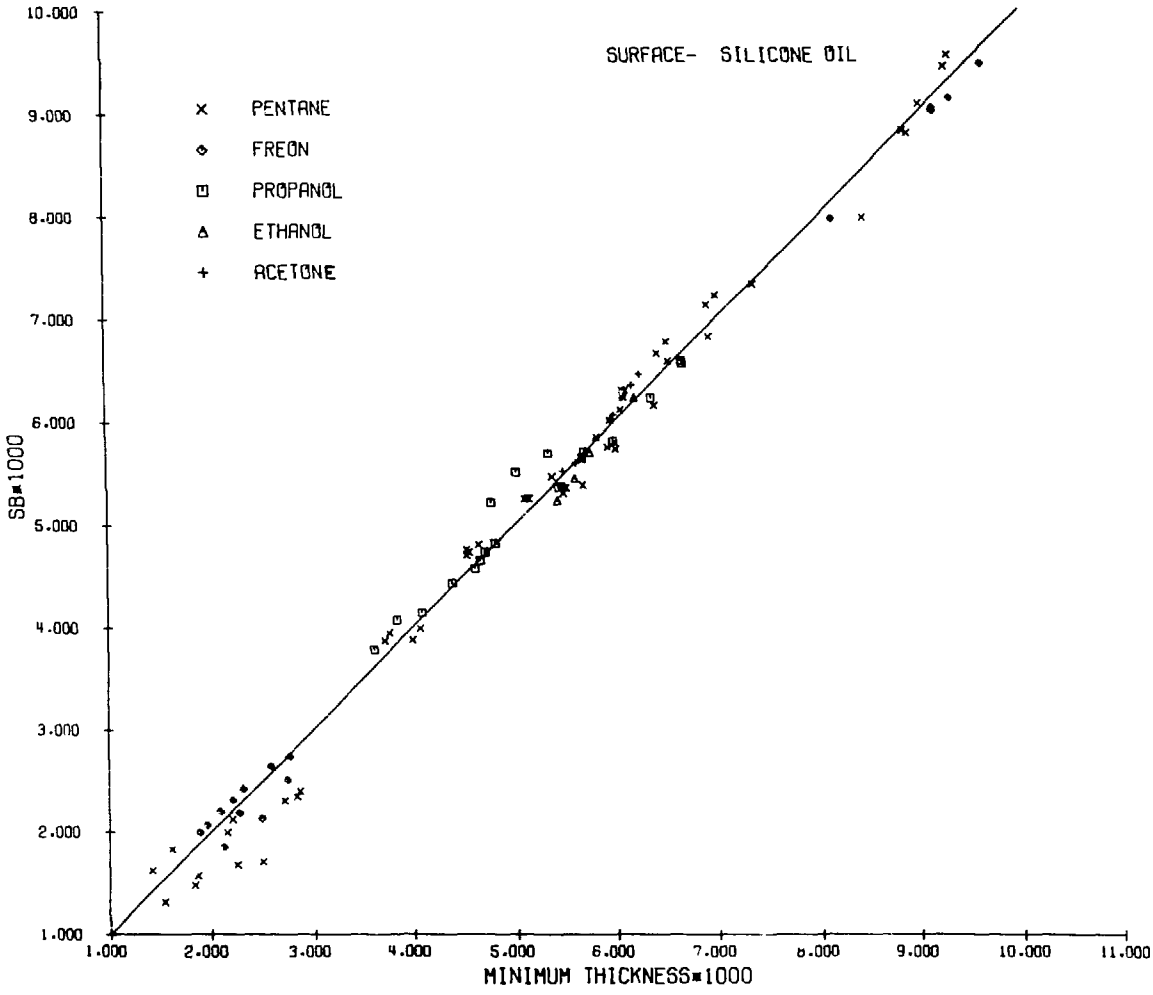

Fig. 3.2 Calculated Minimum Vapor Film Thickness upon Dropping Various Liquids onto Silicone Oil

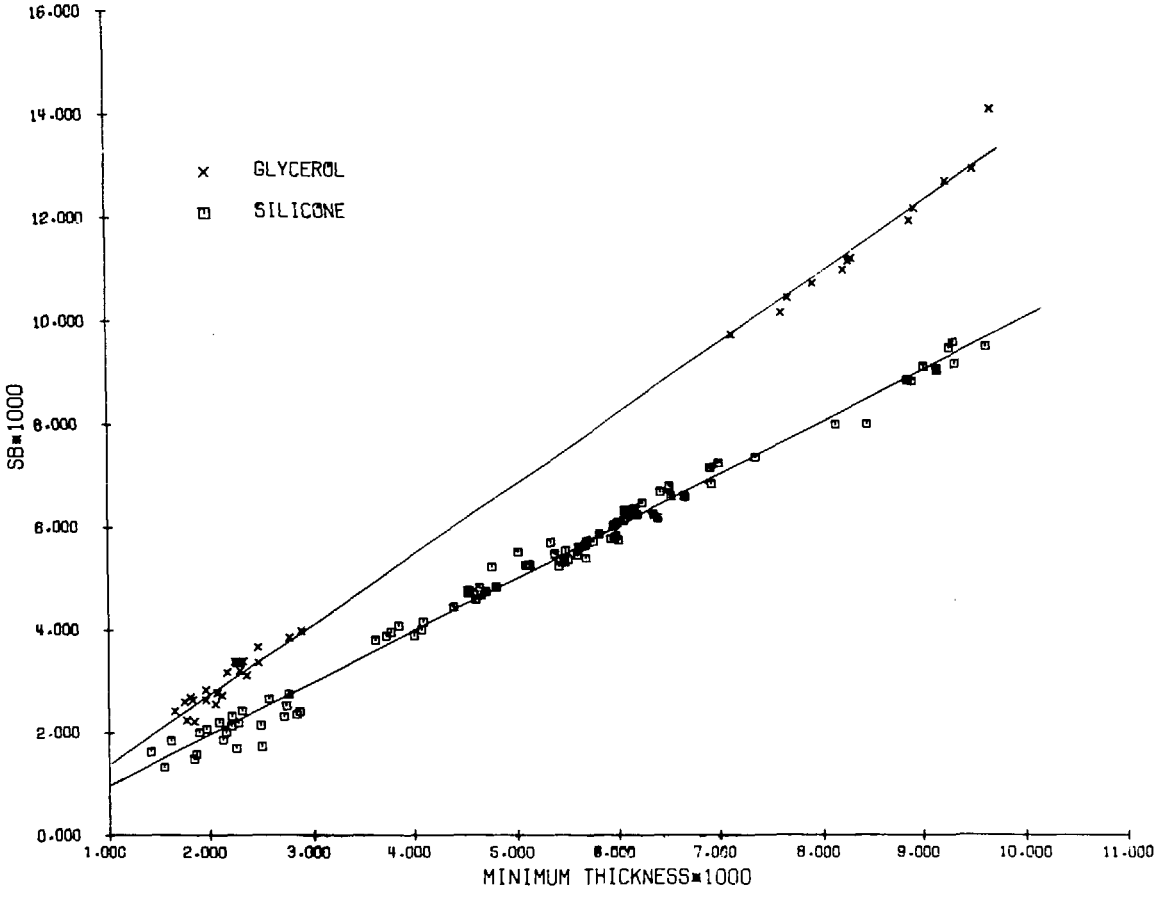

Fig. 3.3 Calculated Minimum Film Thickness for Liquids Dropped onto Silicone or Glycerol

$$s_b = \bar{h}_o^{-0.957} \left(\frac{\rho_v}{\rho_d}\right)^{0.556} N_{We}^{0.721} N_l^{0.258} \qquad (3.43)$$

and the results, shown in Fig. 3.4, yield more scatter of data. However, the differences between the corresponding powers in Eqs. 3.41 and 3.43 are relatively small.

The experimental correlation indicates that the minimum thickness of the film does not acquire a constant value, depending on the system properties, as in free, stationary isothermal thin films. The combined effects of velocity and mass transfer are of considerable importance, and are nonlinear with respect to the calculated minimum thickness. Thus, a coalescence mechanism depending solely on acquiring the neutral thickness of the film is not suitable. Thus, random drop surface motion, high local hydrodynamic acceleration in the liquid surface, drop oscillations inducing disturbances in the film and roughness of surfaces (when applied to solid surfaces), may all be part of the coalescence mechanism resulting in thinner films. In the computation process a thinner film may result if X_c is about 1% of the calculated one. Obviously, in reality X_c changes as a function of time during the film drainage; however, it does not seem likely that the equivalent X_c will be so low.

Even if the experimental correlations do not predict the exact film thickness values, they describe the relative effect of temperature and inertia and may be used in predicting the critical system parameters, such as critical release height, surface temperature or drop diameter. Note that even though the creeping flow assumption is applicable only for a small range of the drop motion, the equations can be applied for larger ranges with a fairly good accuracy because of the very weak dependency on h_o.

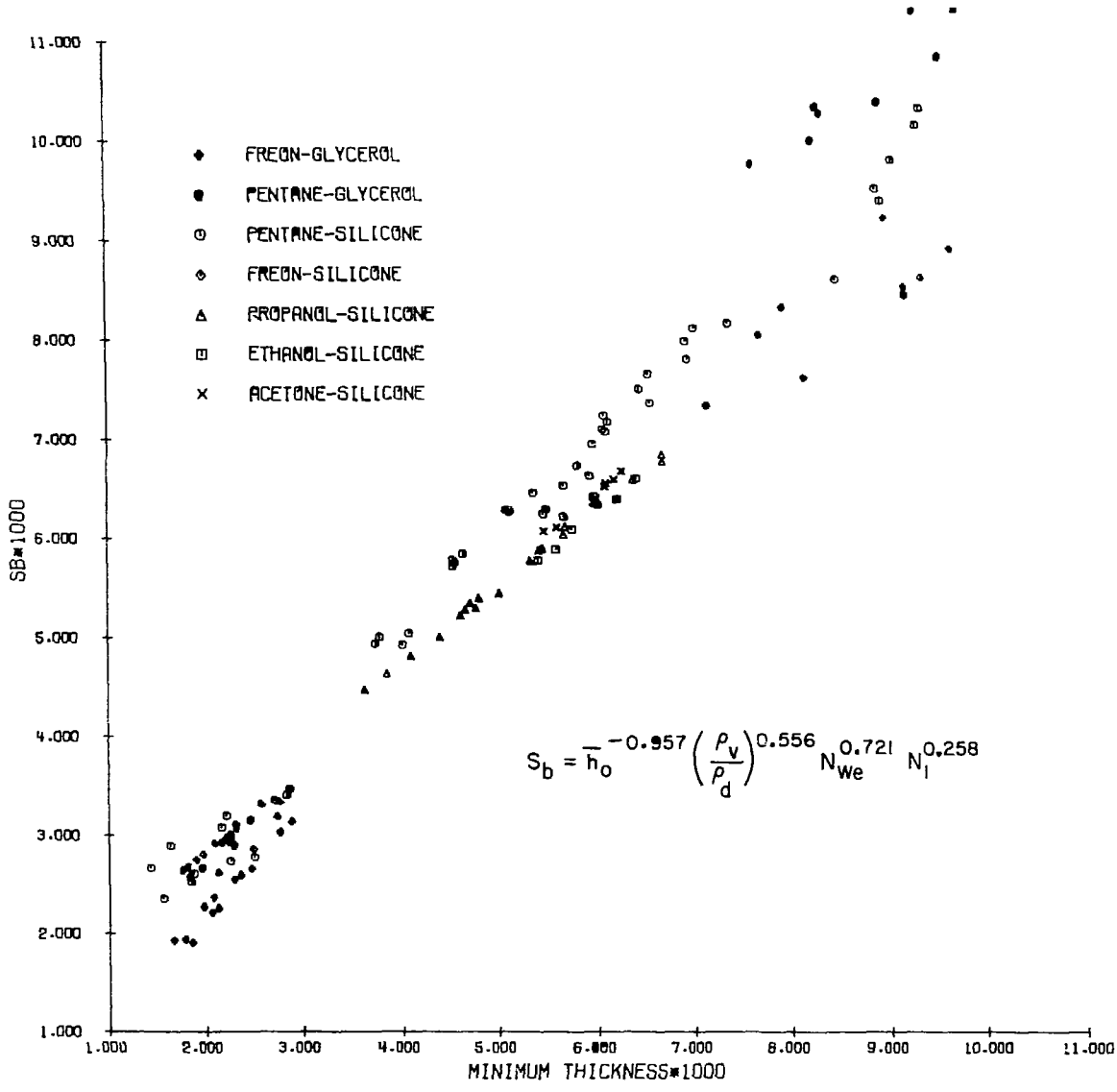

Fig. 3.4 Correlation for the Minimum Vapor Film Thickness

3.3 Discussion

Using experimental data, the minimum thickness of the film at which coalescence occurs was determined by applying the slow viscous flow equations. In the limiting cases, the analysis reduced to those for droplet coalescence in isothermal liquid-liquid systems and stable Leidenfrost boiling of droplets on a hot surface. It has been shown that the critical film thickness increases with temperature, drop diameter, and kinetic energy and it is at least one order of magnitude larger than those required for any conceivable coalescence mechanisms. Since for a specific system no critical film thickness was found, it is suggested that coalescence is a two-stage process. In the first stage, the vapor film is squeezed and the process depends mainly on Weber number. Due to thermal and mechanical instabilities, small tongues of liquid reach the surface. The leading edge radius of these tongues is in order of ~ 10 μ (to permit squeezing of film up to ~ 1000 $\mathring{A}$). The second stage, the controlling one, depends mainly on temperature and surface properties and can be described as the ability of cold liquid to wet a hot surface. So, in modeling the MFB phenomenon one has to find what are the conditions for a small contact to be sustained and spread on the surface.

IV. EXPERIMENTAL INVESTIGATION--LIQUID-LIQUID CONTACT IN SHOCK TUBE CONFIGURATION

As discussed in Section 2.1.2 the impaction of cold liquid onto hot liquid surface in a shock tube configuration has resulted in pressures greater than the cold liquid critical pressure. To date, all shock tube experiments involve hot liquids at temperatures well above the boiling point of the cold liquid. Also, there has not been a systematic work which analyzes the effects of some of the major variables, as the liquid physical and chemical properties, temperatures of liquids, and hydrodynamic effects.

It is the purpose of the present experimental work to contribute to the present knowledge by using different pairs of liquids and to analyze the effects of temperature variations of the hot liquid and the initial system pressure on the thermal and hydrodynamic behavior.

4.1 Description of Experimental Setup

The experimental setup constructed is shown schematically in Fig. 4.1. The apparatus is similar to those described in Chapter II and it consists of three 25.4-mm ID stainless steel tubes (6.35-mm wall thickness) where the middle section (compression chamber), 1406 mm long, holds the cold liquid, and the lower tube (interaction chamber), 117 mm long, contains the hot liquid. The upper tube, 143 mm long, serves as a volume in which gas is introduced to compress the cold liquid column. A diaphragm, which is clamped between two flanges and sealed by an O-ring separates the compression and interaction chambers. The entire assembly is supported below the lower flange by two unistrut beams.

As discussed by Wright et al.[21] a diaphragm rupture by a needle

generally does not produce a good diaphragm opening and this results in many precursor jets which contact the lower surface, which provide vaporization, and cushion the impact. A scoring method (i.e., scoring an x shape in the diaphragm by a die) was used, but with aluminum, copper, stainless steel, and Mylar this technique did not prove satisfactory because the rupture pressure was not reproducible. The simplest, and usually the best, rupture method is to burst the diaphragm by overpressure. This method was used in the present experiments, with a Kapton diaphragm, made from a polyimide film (its operable temperature range is -73 to 260°C and its elongation is 70-100%). The diaphragm ruptured at a specific and repeatable pressure depending on its thickness. The diaphragms used were 0.0127, 0.0254, 0.0508, or 0.0762 mm in thickness (0.0005, 0.001, 0.002 or 0.003 in., respectively) which result in rupture pressures of 0.2, 0.55, 1.1, or 1.7 MPa, respectively. The accuracy in rupture pressure was $\sim\pm$15%. Since most of the runs were performed with the 0.0127 and 0.0254 mm thick diaphragms, we will term them as the "thin" and "thick" diaphragms, respectively, throughout the text. As will be discussed later, the advancing liquid interface following the rupture was not completely flat and usually jets or drops impacted the surface before the main column.

Three piezoelectric pressure transducers (PCB #112A05) with a 2.0 μsec rise time were flush-mounted in the test chambers, two in the cold liquid (PT-2 and PT-3) and one in the hot liquid pool (PT-1). The pertinent dimensions for these transducers are given in Fig. 4.1. For series of tests in which the hot liquid temperature exceeded the 315°C operation limit, the transducer in the hot liquid was removed. The

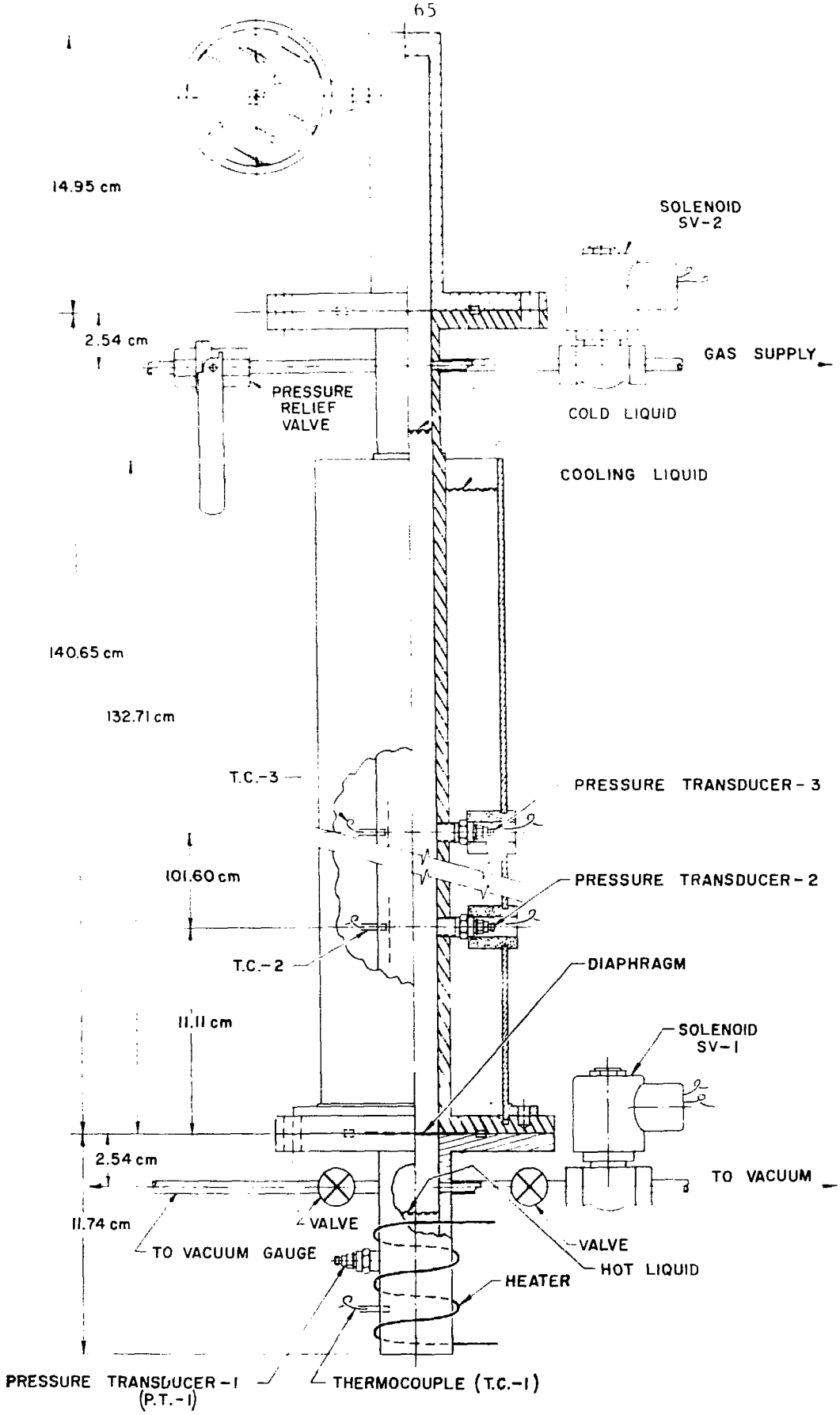

Fig. 4.1 LIQUID-LIQUID SHOCK-TUBE

transducers were calibrated in a separate pressure calibration apparatus where steady pressures (in the range of 0-3.5 MPa) and transient pressures (steps of 0-1.0 MPa in 5 msec rise time) were applied. The transient calibration was performed in a dynamic pressure calibrator, PCB model 903A02. The scales on the charge amplifiers (PCB model 462A) were adjusted so 1 mv output was equivalent to 6.9 KPa (1 psia). The discharge time constant of the charge amplifier, which establish the low frequency response, was set on "long," i.e., at least 500 sec.

Three chromel-alumel thermocouples were used to monitor the system temperatures, two thermocouples are located at different elevations (see Fig. 4.1) in the cold liquid (TC-2 and TC-3), to assure that there is no appreciable stratification throughout the liquid and the third thermocouple was located ~10 mm below the surface of the hot liquid. When it was physically possible, the hot liquid was thoroughly stirred by a magnetic stirrer prior to each run.

A tube surrounding the compression chamber served as a cooling jacket. When below ambient temperatures were desired, a mixture of dry ice and Freon-11 is introduced into the cooling jacket resulting in cold liquid temperature of about -80°C which was maintained reasonably uniform (<5°C difference between TC2 and TC3). Even when no cooling was required, Freon-11 was poured into the cooling jacket to serve as a heat sink, so that the cold liquid remains at room temperature.

4.2 Experimental Procedure

The test procedure was as follows: the lower tube was carefully cleaned and filled with liquid which was then heated after the diaphragm and the compression chamber had been assembled. During the heating

period the cold liquid is poured into the upper tube and is supported by the diaphragm. The volume below the diaphragm is evacuated through a cold trap after sealing the system. When using metal or salt as the hot liquid, it was melted first in the lower tube, after which the apparatus was assembled and sealed and the space above the hot liquid was evacuated. The molten metal or salt was then heated to the desired temperature under vacuum, which also minimized oxidation of the metallic melts. The resulting vacuum is measured by a mercury manometer and a Hastings vacuum gauge (0-133 Pa). If the vapor of the cold liquid was desired in the interaction chamber, it was introduced through a two-way valve which was connected to the vacuum gauge line and a flask containing the cold liquid (in case of Freon-22 it was connected to a Freon-22 cylinder). All lines were evacuated beforehand, so that no noncondensible gases were present. Once the initial conditions are achieved, the valves leading to the vacuum pump and vacuum gauge are turned off, the pressure transducers are set (by ungrounding them) and the test is conducted by opening a valve (SV-2) connected to gas supply (argon). The gas pressurizes the cold liquid and, at a specific pressure depending on the diaphragm thickness, the diaphragm ruptures. No significant differences were observed for rapid or slow pressurization. The pressure history resulting from the impact and the thermal interaction (if any) were recorded on a multichannel FM tape recorder having a frequency response of 20 kHz. These signals were then played back through a visicorder. Since the response time of the thermocouples was too long compared to the interaction time scale, the fast time response of the tape recorder was not required. Hence, the thermocouples output was recorded on a Honeywell strip chart, with paper velocity of 2.5 cm/sec (1 in./sec).

Two hundred thirty-nine runs were performed with the following cold/hot liquid combinations:

1) water-solid surface
2) water-water
3) Freon-22-mineral oil
4) Freon-22-silicone oil
5) Freon-11-silicone oil
6) Freon-22-mercury
7) Freon-11-mercury
8) Freon-22-water
9) water-Wood's metal
10) n-butanol-Wood's metal
11) water-eutectic mixture of LiCl + KCl

For a given system the primary variables investigated were the initial temperature of the hot liquid and the initial driving pressure.

V. EXPERIMENTAL RESULTS

5.1 Hydrodynamic Behavior

A number of runs were conducted to study the hydrodynamic behavior of the cold liquid column upon diaphragm rupture and the consequent impact. Theoretically, following the diaphragm rupture at t = 0 a rarefaction wave from the bottom is transmitted along the liquid column. As the wave travels vertically upward through the liquid, it initiates a downward motion with a velocity u given by (see Fig. 5.1a).

$$u = \frac{\Delta P}{\rho_\ell c} \tag{5.1}$$

When the rarefaction wave reaches the upper liquid/gas interface it is reflected as a compression wave with a pressure essentially equal to the pressure in the gas volume. At the time of this reflection, the pressure along the liquid column is essentially the interaction chamber pressure and all liquid particles are moving at velocity u. When the compression wave moves down through the liquid it increases the liquid velocity by an increment u, i.e., the liquid velocity relative to the tube is 2 u (Fig. 5.1b). When the wave reaches the lower surface of the liquid column, the compression wave is reflected as a rarefaction wave which increases the downward velocity by another interval of u. Therefore, the lower surface of the column moves with $\Delta u = 2u$ velocity increments, each of them lasting a relief time period given by:

$$t_a = \frac{2L}{c} \tag{5.2}$$

The acoustic acceleration of the liquid column is illustrated in Fig. 5.2. The overall behavior can be approximated by an inertial formulation,

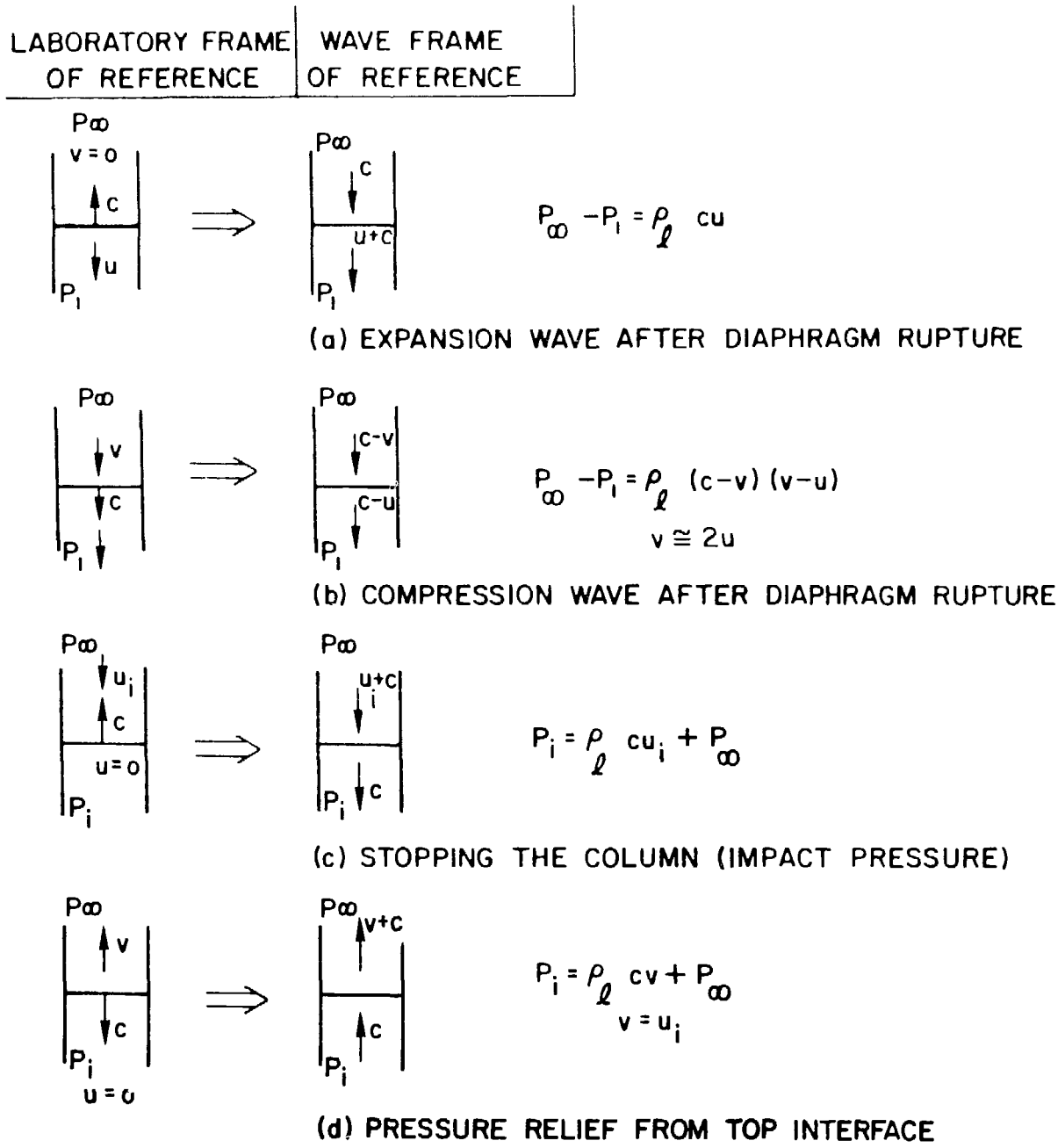

Fig. 5.1 Hydrodynamic Behavior in Shock Tube

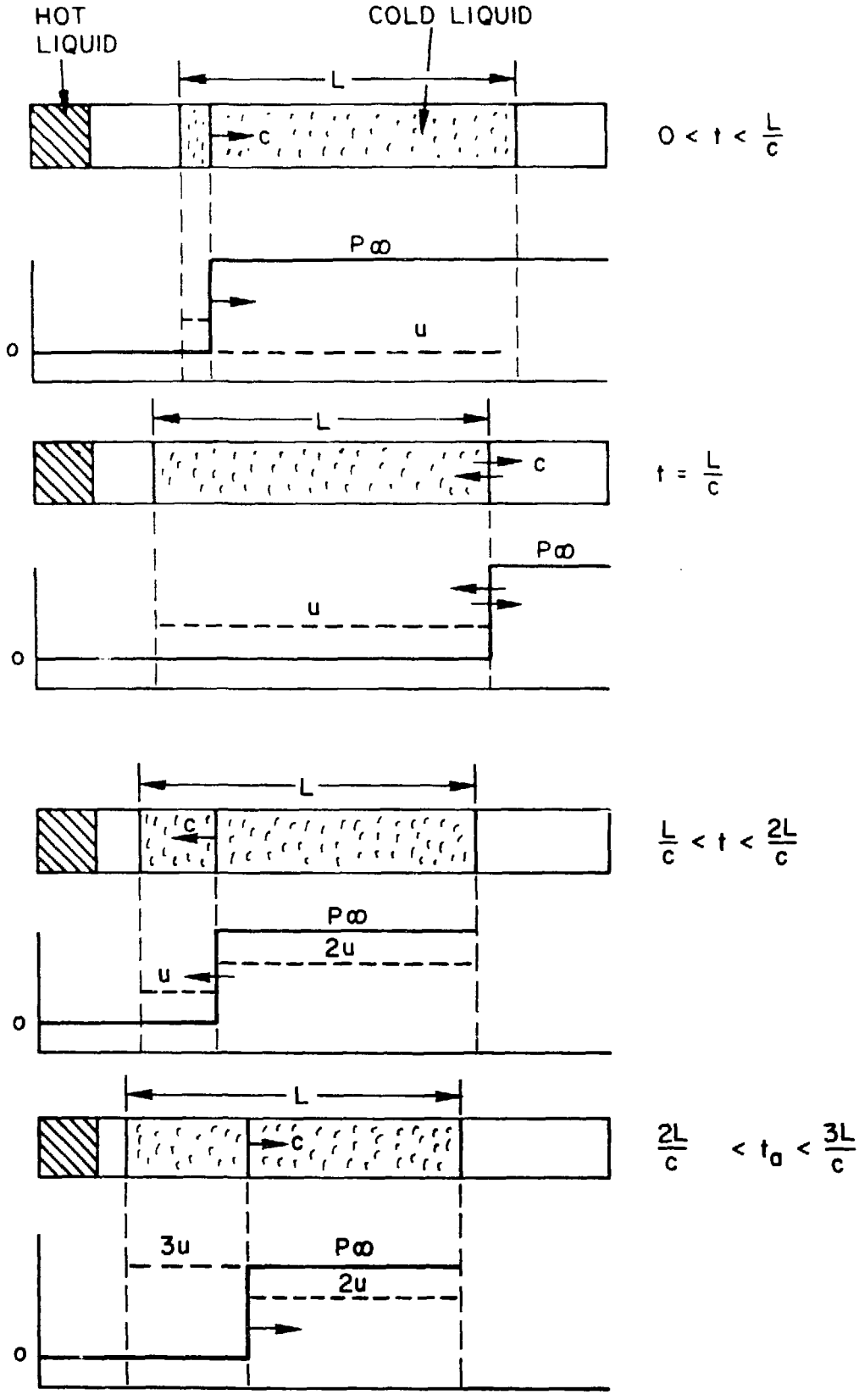

Fig. 5.2 Acoustic Acceleration of Liquid Column

in which the acceleration is assumed to be constant and uniform along the column and is given by:

$$a = \frac{\Delta P}{\rho_\ell L} \tag{5.3}$$

The relationship between the acoustic and inertial accelerations is shown in Fig. 5.3. The inertial form describes the average column behavior and after several reflections, the system velocities predicted by both representations will be in close agreement.

Assuming that there is no compression of gas and/or vapor as the column approaches a rigid boundary, the column will be brought to rest by a compression wave developed at impact. This "water hammer" pressure is given by (Fig. 5.1c)

$$P_i = \rho_\ell \, c \, u_i + P_\infty \tag{5.4}$$

where u_i is the impact velocity and P_∞ is the liquid pressure.

Using the inertial approximation u_i is given by

$$u_i = \frac{\Delta P}{\rho_\ell L} \, t_i \tag{5.5}$$

where t_i is the time from diaphragm rupture to impact. Substituting u_i into Eq. 5.4 the "water hammer" pressure for an ideal instantaneous impact is given by

$$P_i = \frac{c \, \Delta P}{L} \, t_i + P_\infty \tag{5.6}$$

After the column has been stopped, the impact pressure is relieved from the upper interface and the column moves upward at the velocity of u_i (Fig. 5.1d).

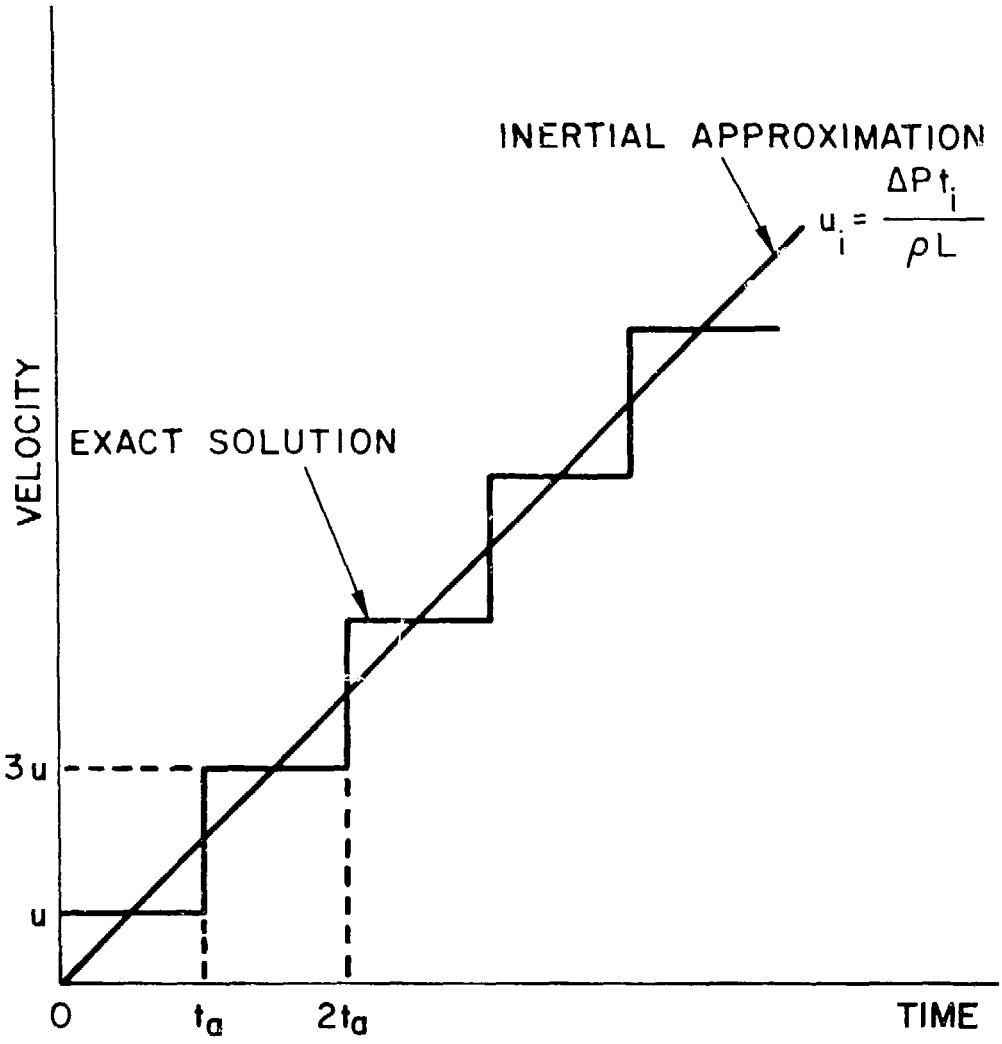

Fig. 5.3 Relationship Between Acoustic and Inertial Accelerations

The experimental impulse per unit area (I_{exp}) measured by a pressure transducer is given by:

$$I_{exp} = \int_{o}^{t_p} P \, dt \tag{5.7}$$

where time t_p is the pulse duration. If that pressure transducer is located at the bottom of the liquid column, t_p is essentially the relief time t_a. Since the process of stopping the column is happening during the time the water hammer pressure travels, i.e., $t_a/2$, the measured impulse per unit area at the bottom is twice the impulse I required to stop the column (Fig. 5.4). Thus, we define I_{th} as

$$I_{th} \equiv 2I \tag{5.8}$$

or

$$I_{th} = 2 \rho_{\ell} L u_i \tag{5.9}$$

Substituting Eq. 5.5 into Eq. 5.9 and replacing t_i by an experimentally measured value, t_{exp}, yields:

$$I_{th} = 2 \Delta P \, t_{exp} \tag{5.10}$$

After the rarefaction wave reaches the lower surface it reflects. If the surface is free from nucleation sites, the liquid behind this reflected wave is at rest and negative pressures are developed.[66] Thus, no bouncing will occur and only oscillations due to liquid compressibility are possible. However, if nucleation sites do exist, the liquid will flash and bouncing of the column occurs. Bouncing also may occur when a significant amount of vapor is initially introduced into

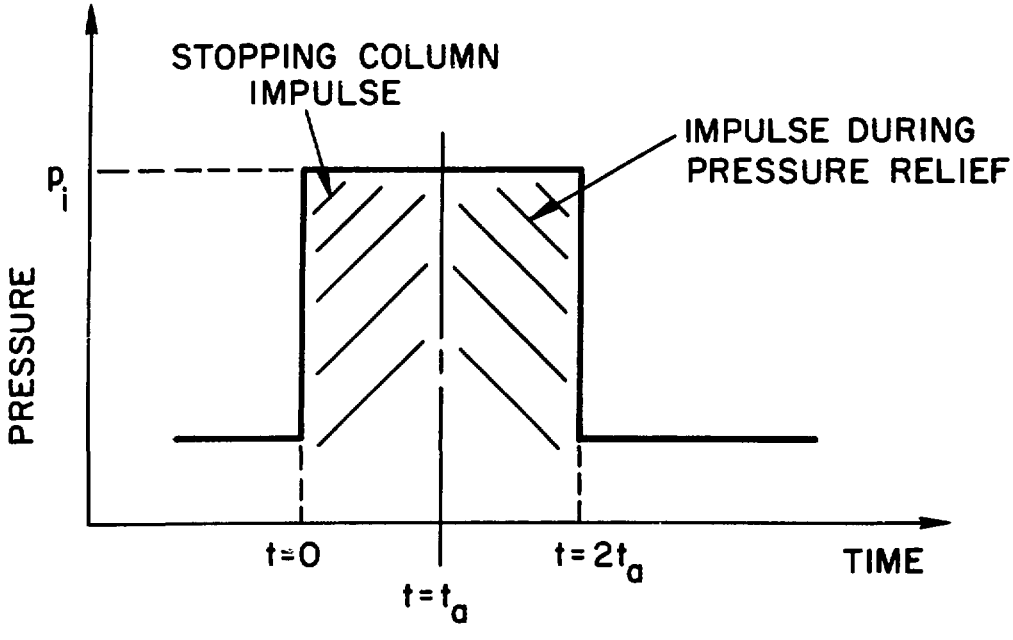

Fig. 5.4 Pressure Pulse Generated upon Instantaneous Stoppage of Column Measured at the Bottom

the interaction chamber since the vapor collapse may not be completed in the time scale we are concerned with.

5.2 Water-Solid Surface Contacts

In runs 71-86 water was impacted on the lower tube surface where both media were at room temperature, and the distance between the diaphragm and the solid surface was 10 cm. Runs 71-74 were performed when the volume below the diaphragm was evacuated to below 66 Pa, and for runs 75-76, 18 mm Hg (2394 Pa) of water vapor was introduced into the lower tube prior to rupturing the diaphragm (18 mm Hg is water vapor pressure at room temperature). This eliminated flashing of the water column following diaphragm rupture. In runs 77-86 controlled amounts of noncondensible gas (air) were introduced in order to study any changes of the pressure pulse shape, magnitude, and frequency. The initial conditions and the results of all those runs, as well as the pressure histories, are given in Appendix C.

Figure 5.5 shows the pressure history of Run 71. In Fig. 5.5a the diaphragm rupture is noticed in P.T.-2 where a sharp dip in pressure occurs. After 26.0 msec from diaphragm rupture the first impact is shown, which is followed by many bounces with progressively lower maximum pressure and longer pulse duration. The details of the first three bounces are shown in Fig. 5.5b. The rise time of the first pulse is very short ($\sim$0.2 msec) and it has a composite shape; after a first plateau the pressure wave travels along the column until it is relieved from the upper water/air interface. This is followed by a rarefaction wave traveling down the column relieving the pressure. A second pulse, larger than the first, is experienced and it exhibits the same compression-

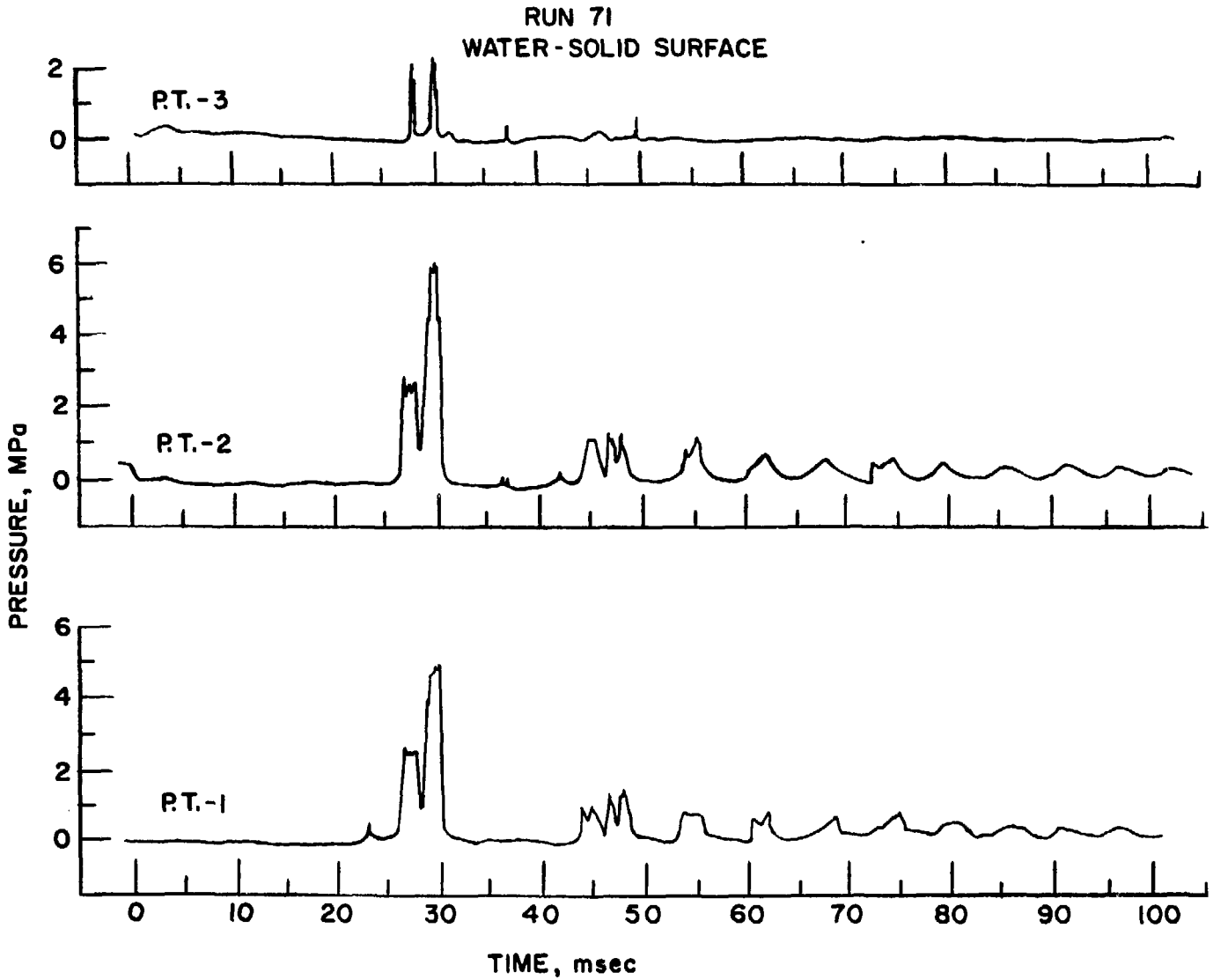

Fig. 5.5a Pressure History of Run 71

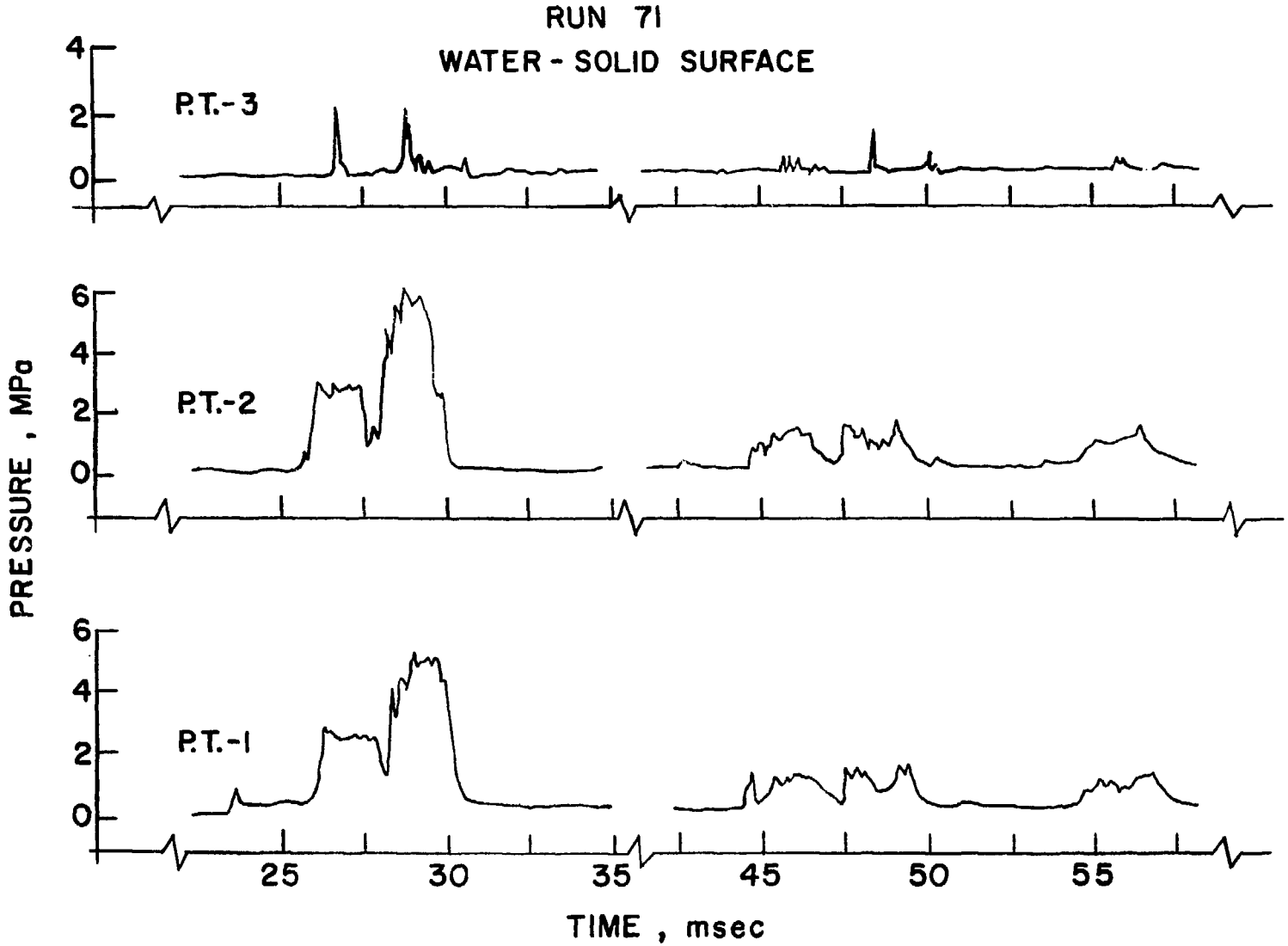

Fig. 5.5b Detail of First Three Pressure Pulses of Run 71

expansion behavior as before. Calculating the sound velocity yields a value of 1450 m/sec which is in good agreement with reported values. The maximum pressure is 46% of the theoretical instantaneous impact value, and the total impulse is 62.5% of the theoretical impulse to stop and rebound the column. The composite shape of the pressure pulse indicates that the impact behavior is complicated and it does not consist of the single pulse which was described theoretically (see discussion in Sect. 6.2). Note that when a small precursor jet impacts on a surface, only a sharp and short pressure pulse would be seen in P.T.-1 since it would be relieved very quickly by the surrounding gas space. A pressure pulse originated by a small jet is seen in P.T.-1 of Fig. 5.5 about 2.5 msec before the main impact.

Introducing vapor pressure below the diaphragm eliminates the pressure relief after the first pulse, as is the case in Run 77 where 33 mm Hg of water vapor was introduced (Fig. 5.6). The general shape and characteristics of this run are similar to those in Run 71.

By introducing noncondensible gases, the relief pressure was also eliminated. See for example run 86 with 270 mm Hg of air (Fig. 5.7). As is shown in the figures in Appendix C and in Table C-1, when more gas is placed below the diaphragm, the duration of the pressure pulses and their rise time are longer, and the frequency of bouncing and the maximum pressure are reduced.

All the impact characteristics discussed are also evident when water impacts water or mercury (Figs. 5.8-5.11).

5.3 Contacts with Freons

A set of experiments was conducted with Freon-11 (23.8°C b.p.) and Freon-22 (-40.75°C b.p.) as cold liquids and oils (mineral oil or

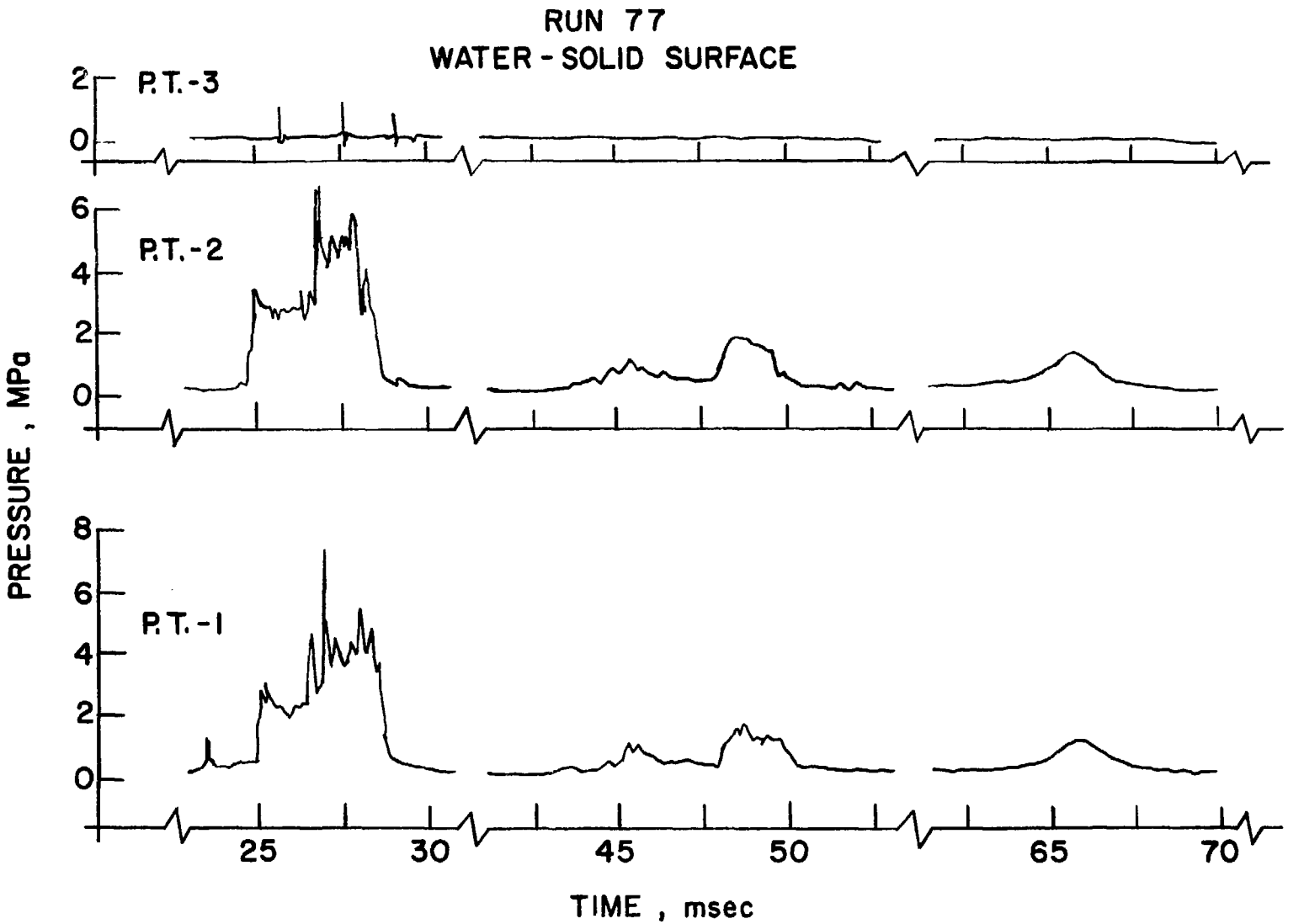

Fig. 5.6 Pressure History of Run 77

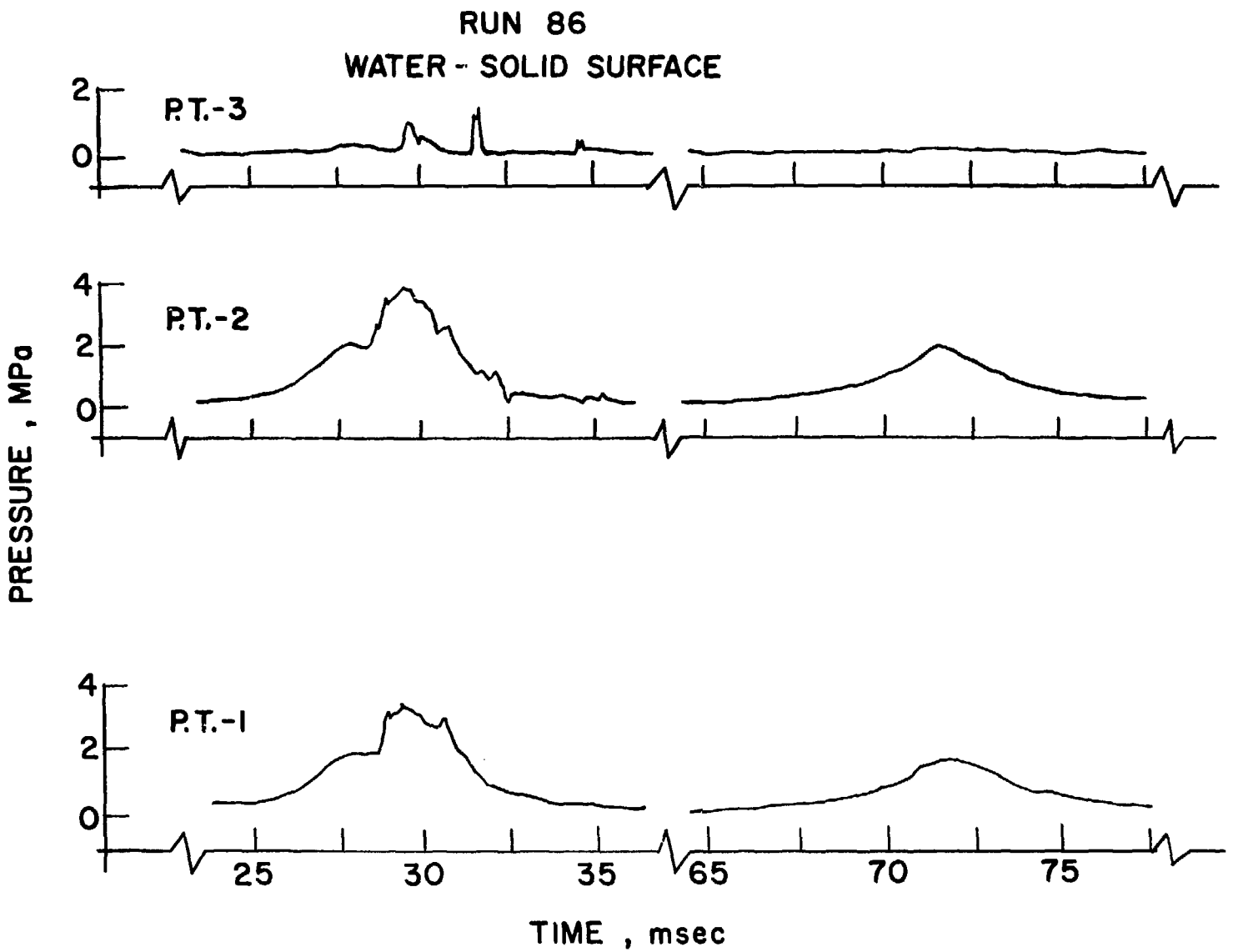

Fig. 5.7 Pressure History of Run 86

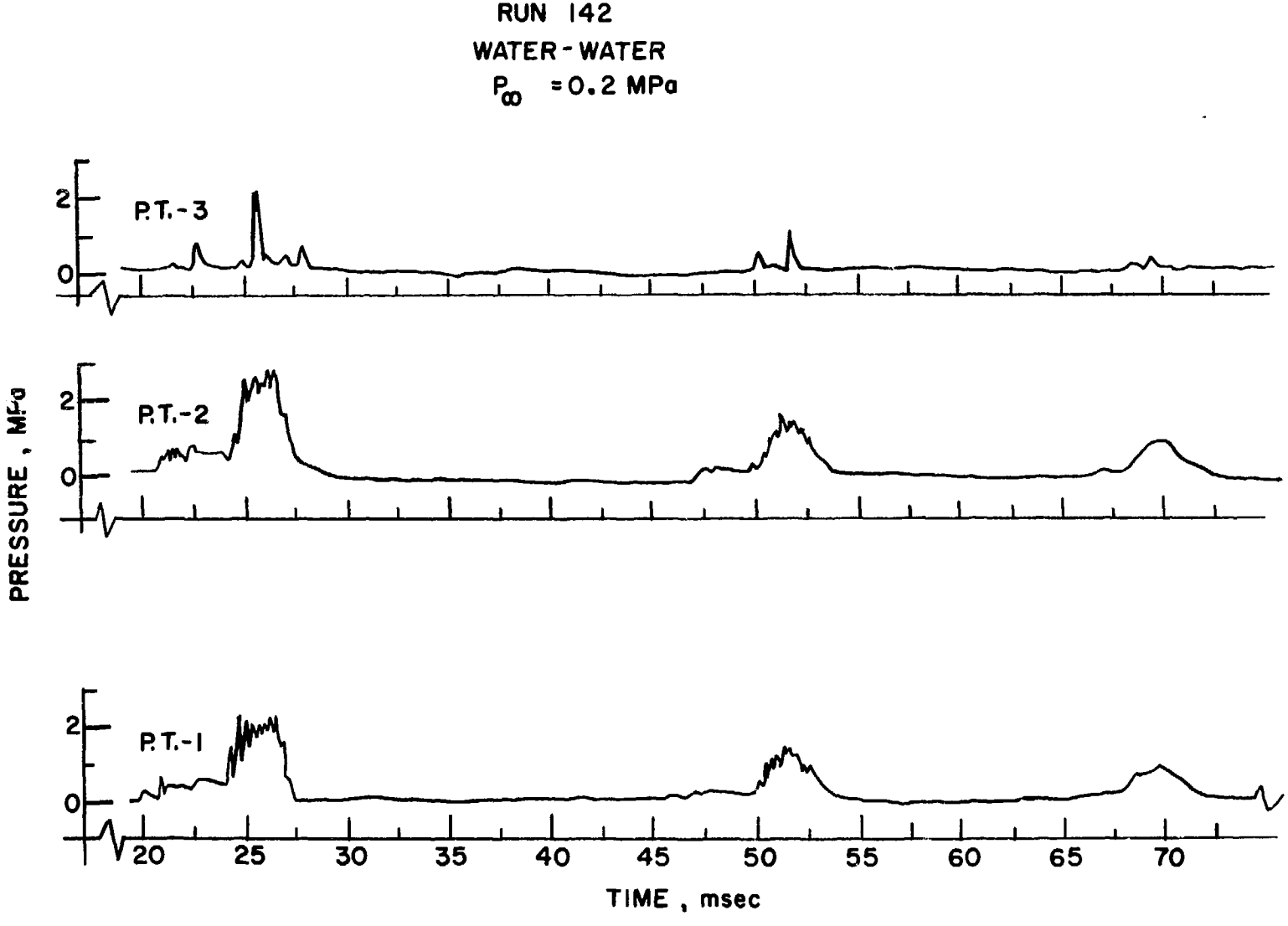

Fig. 5.8 Pressure History of Run 142

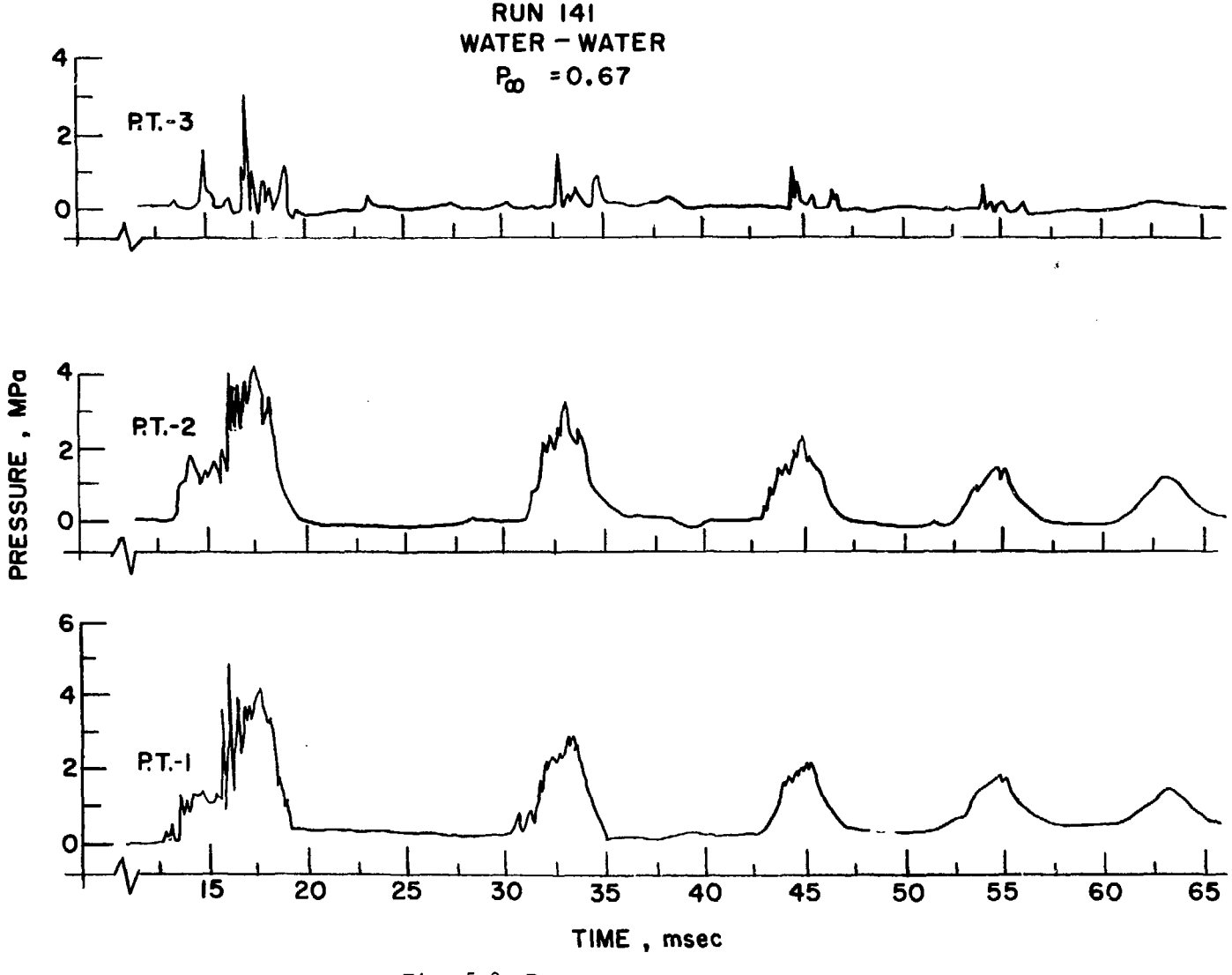

Fig. 5.9 Pressure History of Run 141

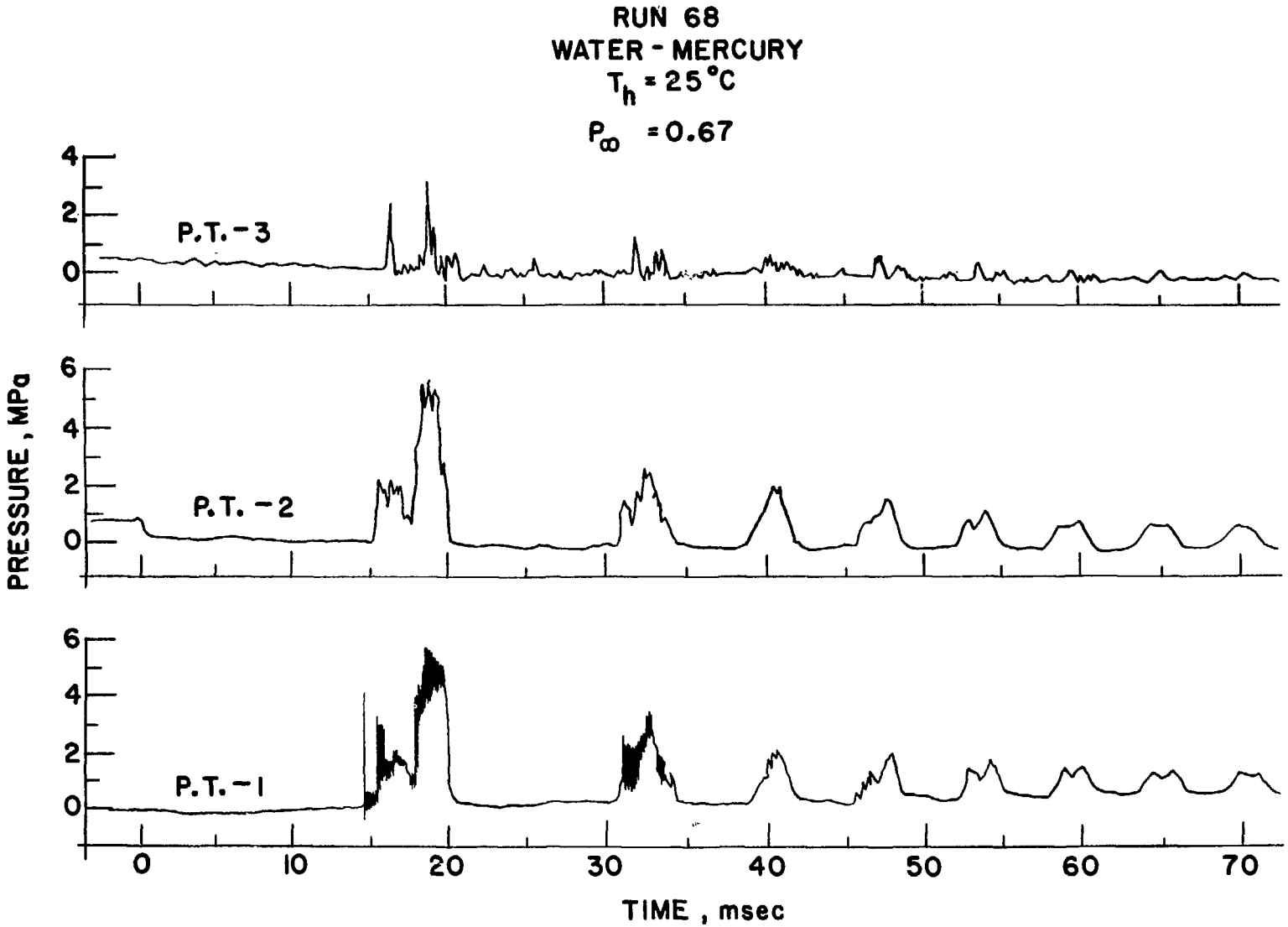

Fig. 5.10 Pressure History of Run 68

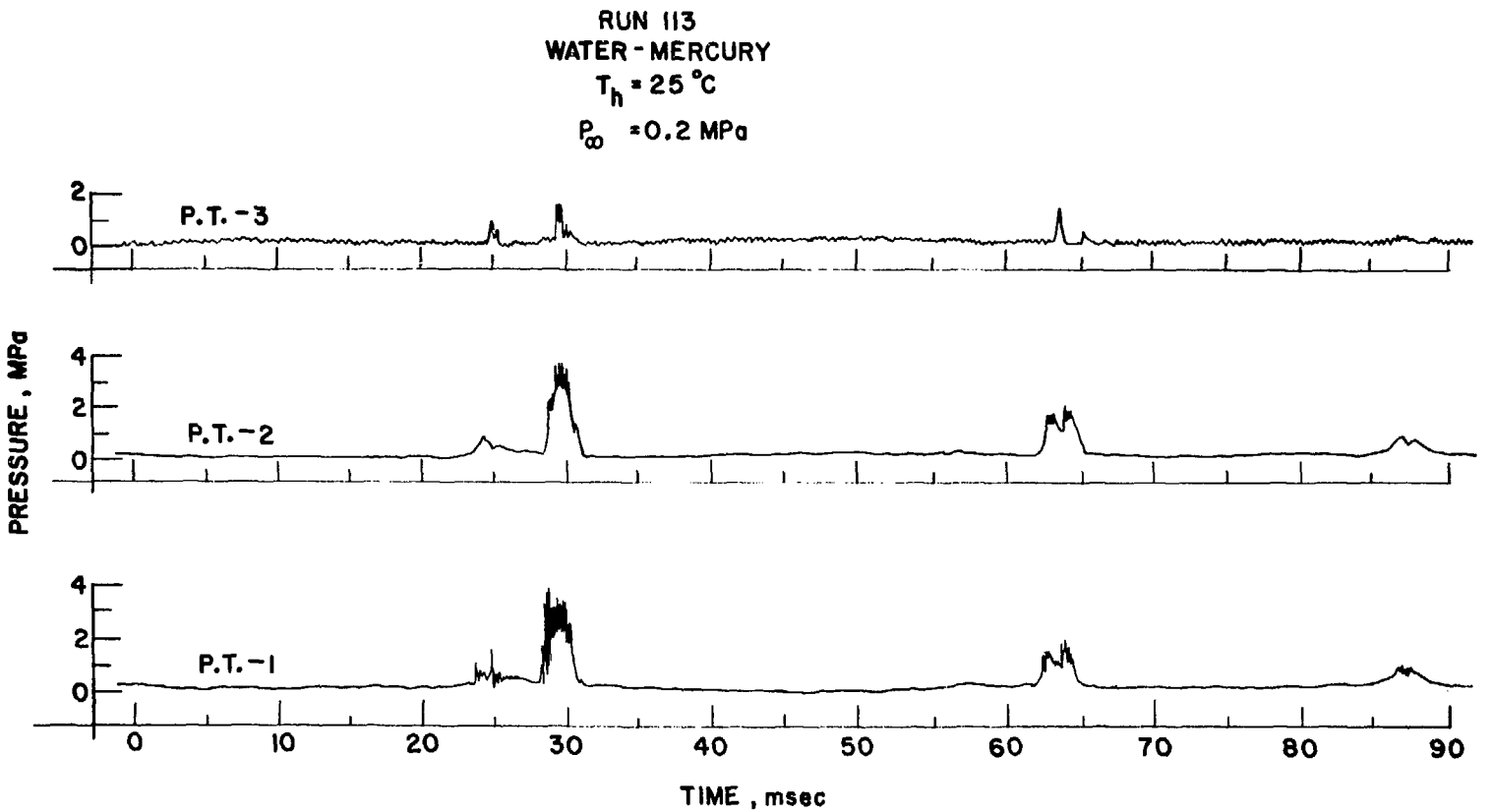

Fig. 5.11 Pressure History of Run 113

silicone oil), water and mercury as the hot liquids. Freon 11-mineral oil, Freon 22-mineral oil, and Freon 22-water are known consistently to produce large-scale vapor explosions in a free mode of contact (i.e., dropping experiments) when the interface temperature is in a specific range.[53],[55] However, it was shown that when the mechanical constraint in the system is increased, e.g., smaller relief ports, the explosive yield decreases,[67] or is zero when the initial pressure in the system is increased from 0.1 MPa to 0.2 MPa (Freon 22-mineral oil).[57] On the other hand, it was reported[49] that explosions can be produced under high impact velocities at temperatures which under gentle mode of contact (dropping) no explosions occur (ethane-water and methane-water). Thus, the objective in performing this set of experiments was to study the possibility of explosions occurring under large mechanical constraint, i.e., a pressurized system, and high driving velocities, when noncondensible gases are not present. The thin (0.0127 mm) and thick (0.0259 mm) diaphragms were used which ruptured at $\sim$0.2 and $\sim$0.6 MPa, respectively. In these experiments a pressure transducer (P.T.-1) was located at the interaction chamber and a magnetic stirrer was used to stir the hot liquid. The distance between the diaphragm and the hot liquid upper interface was $\sim$5.0 cm. In all runs, the Freons were subcooled by a mixture of dry ice and Freon-11 in the cooling jacket. Thus, their initial temperature was maintained at -80°C. The pressure was reduced to <103 Pa before heating the bottom liquid. At high temperatures vapor had to be introduced to minimize evaporation of the hot liquid (since Freon vapor readily dissolved in mineral oil, no vapor was introduced in that system). A tabulated list of experiments performed using Freons as cold liquid is given in Appendix D.

For these systems the thin diaphragm frequently resulted in a premature rupture. Thus, the majority of the runs were performed with the thick diaphragm. In these runs the wave pattern ("ringing") in the cold liquid following diaphragm rupture is usually shown clearly in the pressure history of P.T.-2 and P.T.-3 pressure. As an example, the theoretical and experimental wave behavior is shown in Fig. 5.12. The sound velocity in the Freon-22 was taken as 1100 m/sec and the agreement is excellent. The same wave pattern is also noticed in all the other liquids used, when the driving pressure is sufficiently large (see Sect. 5.7).

Representative results from Freon 22-mineral oil impacts are shown in Figs. 5.13 and 5.14. No sharp impacts are observed, but rather small pressurizations lasting about 20 msec, which indicates a vapor compression by the liquid column. In Fig. 5.13 it is clear that the vapor is compressed by the moving liquid column. The compression is evident from the pressure rise, both in P.T.-1 and P.T.-2, and the "ringing" observed in P.T.-2 and P.T.-3 indicates that the column is still moving down. An even lower pressure is shown in Fig. 5.15 when the thin diaphragm was used and the cold liquid amount was reduced to 100 cm^3 (from the normal amount of $\sim$700 cm^3). It was hypothesized that in addition to vaporization of Freon droplets and precursor jets which may reach the oil before the column, flashing from Freon-22 and the high vapor pressure of oil inhibit the possibility of impact. However, by increasing the impact velocity by using a thick diaphragm and a reduced amount (100 cm^3), an impact was achieved as shown in Fig. 5.16. The boiling behavior is also evident from the temperature history of T.C.-1 (Fig. 5.17). Assuming

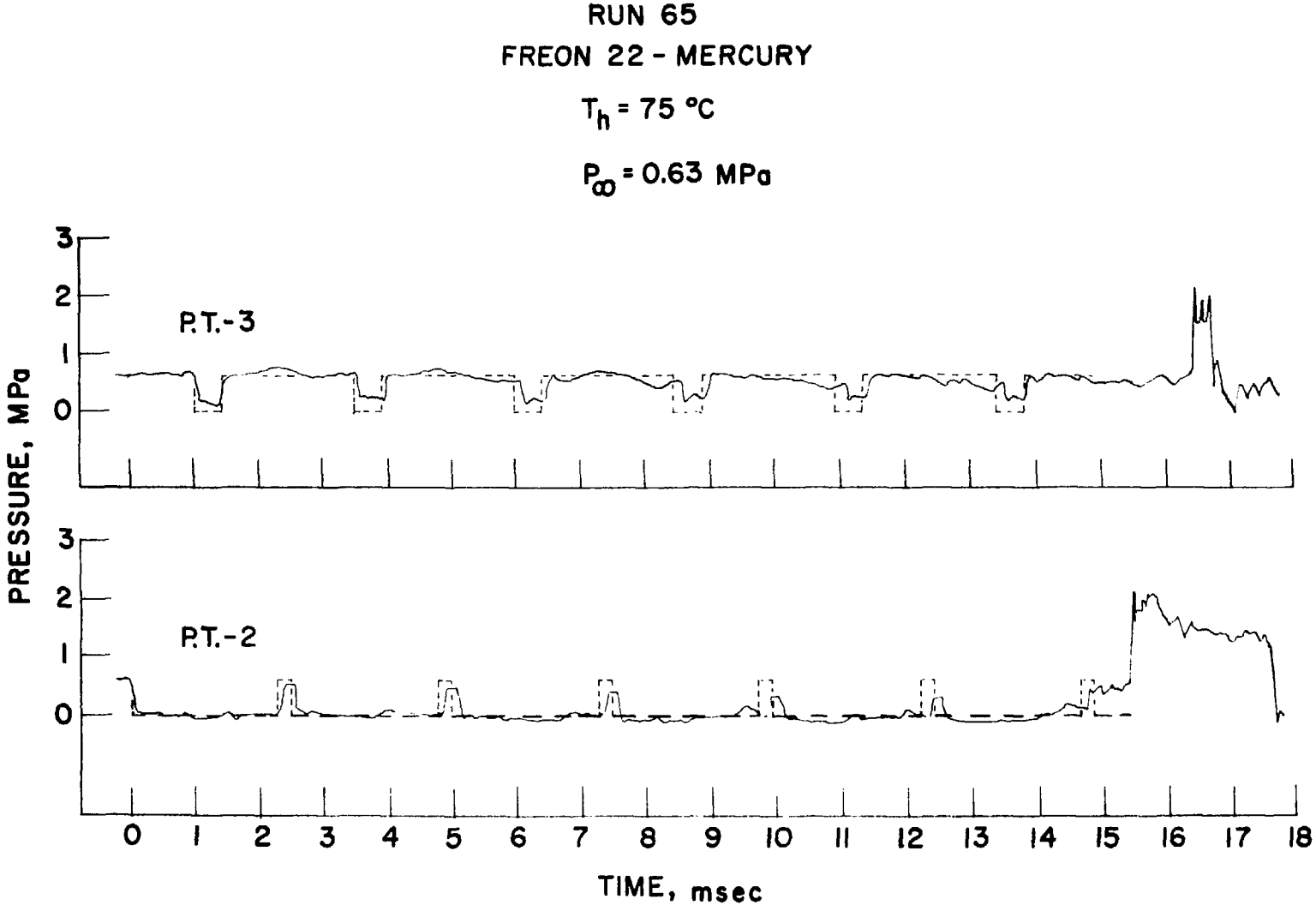

Fig. 5.12 Theoretical and Experimental Wave Behavior ("ringing") during Acceleration Stage

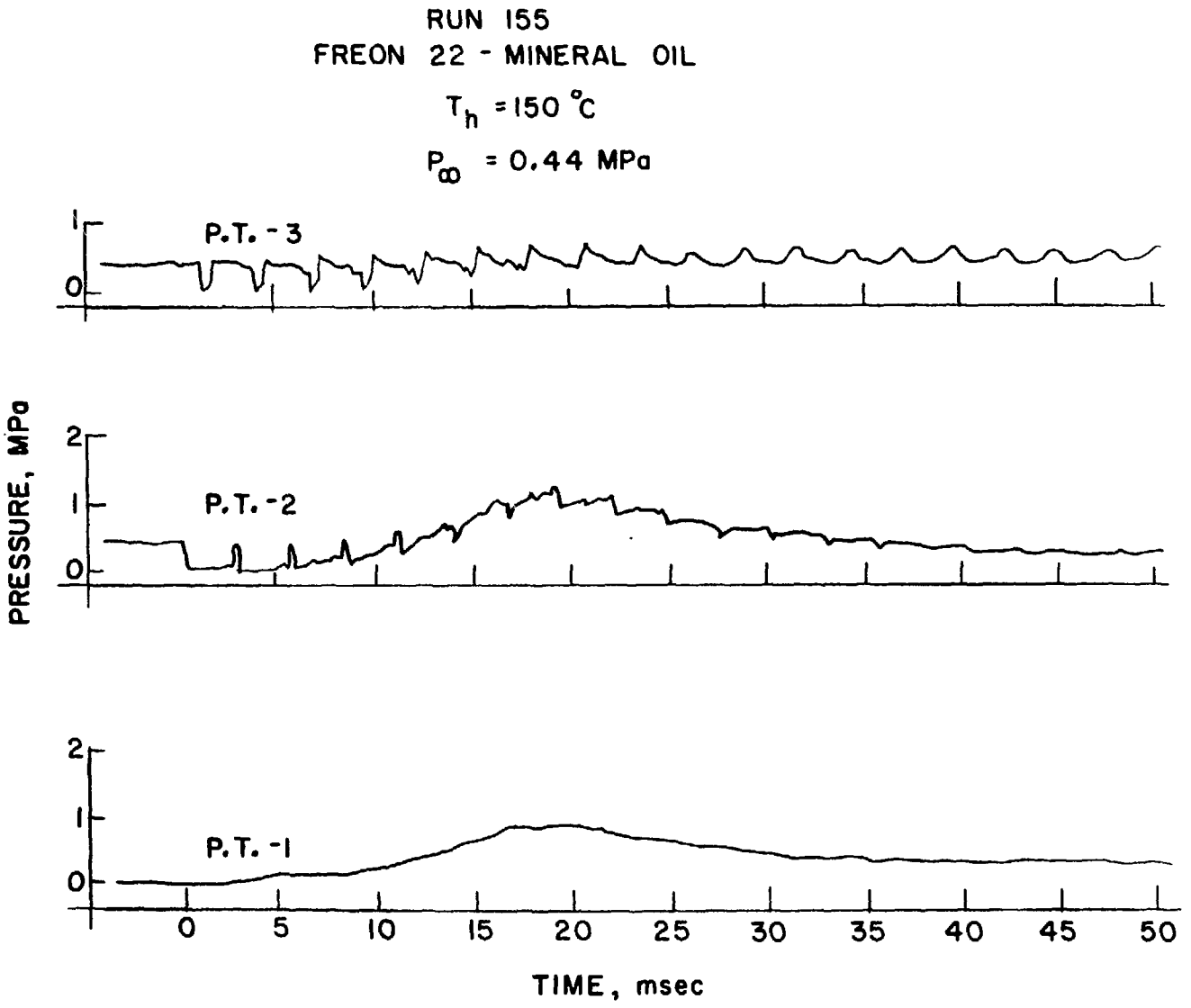

Fig. 5.13 Pressure History of Run 155

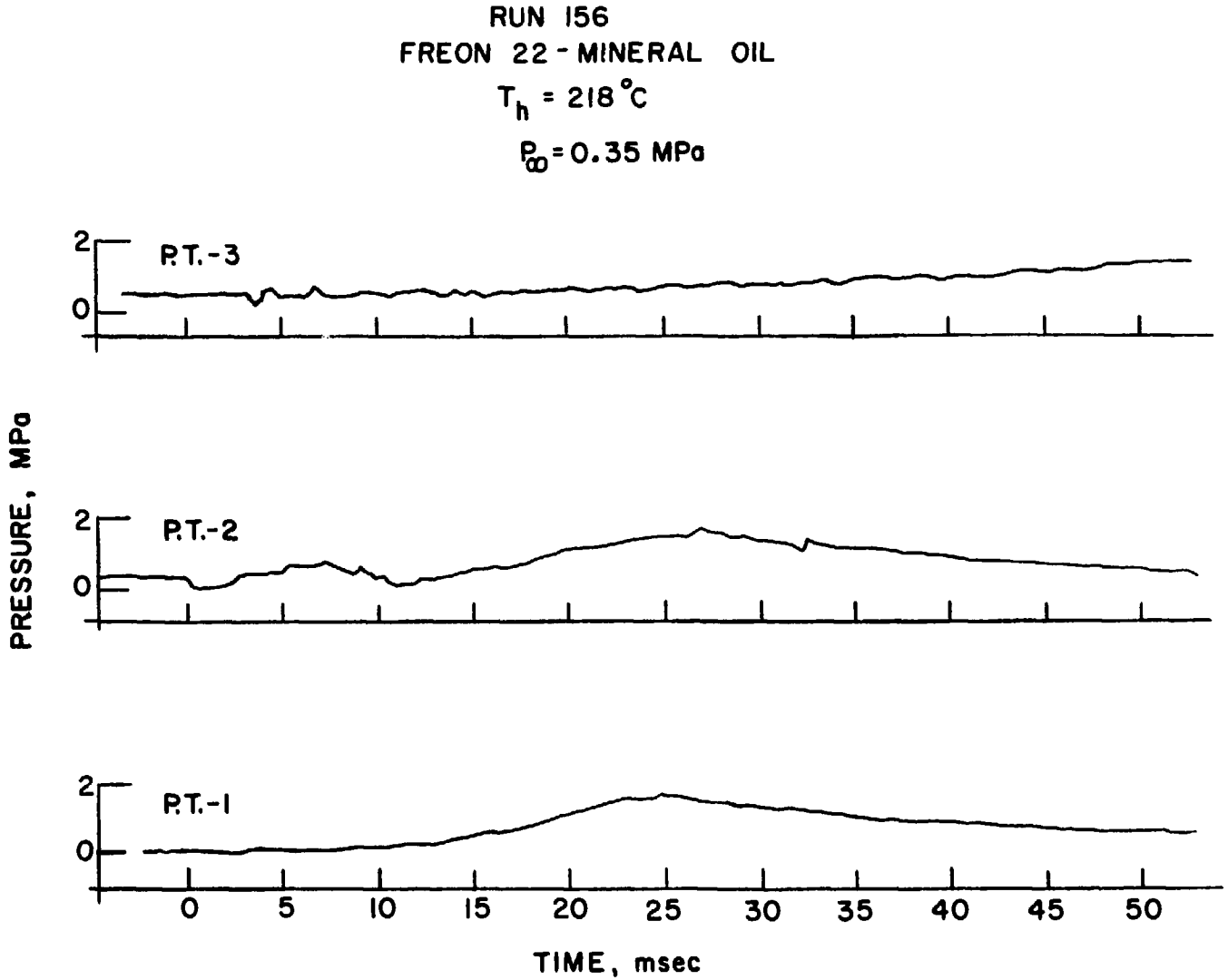

Fig. 5.14 Pressure History of Run 156

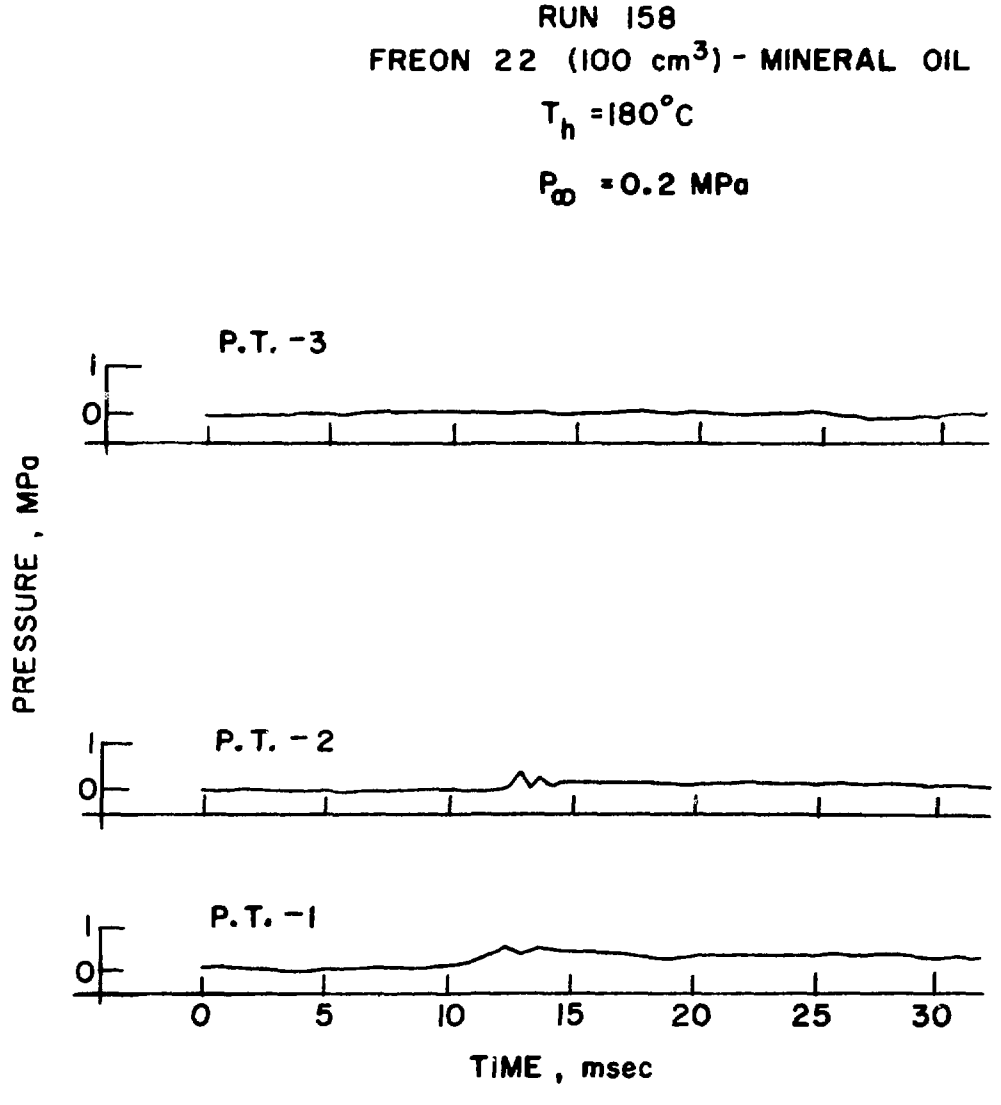

Fig. 5.15 Pressure History of Run 158

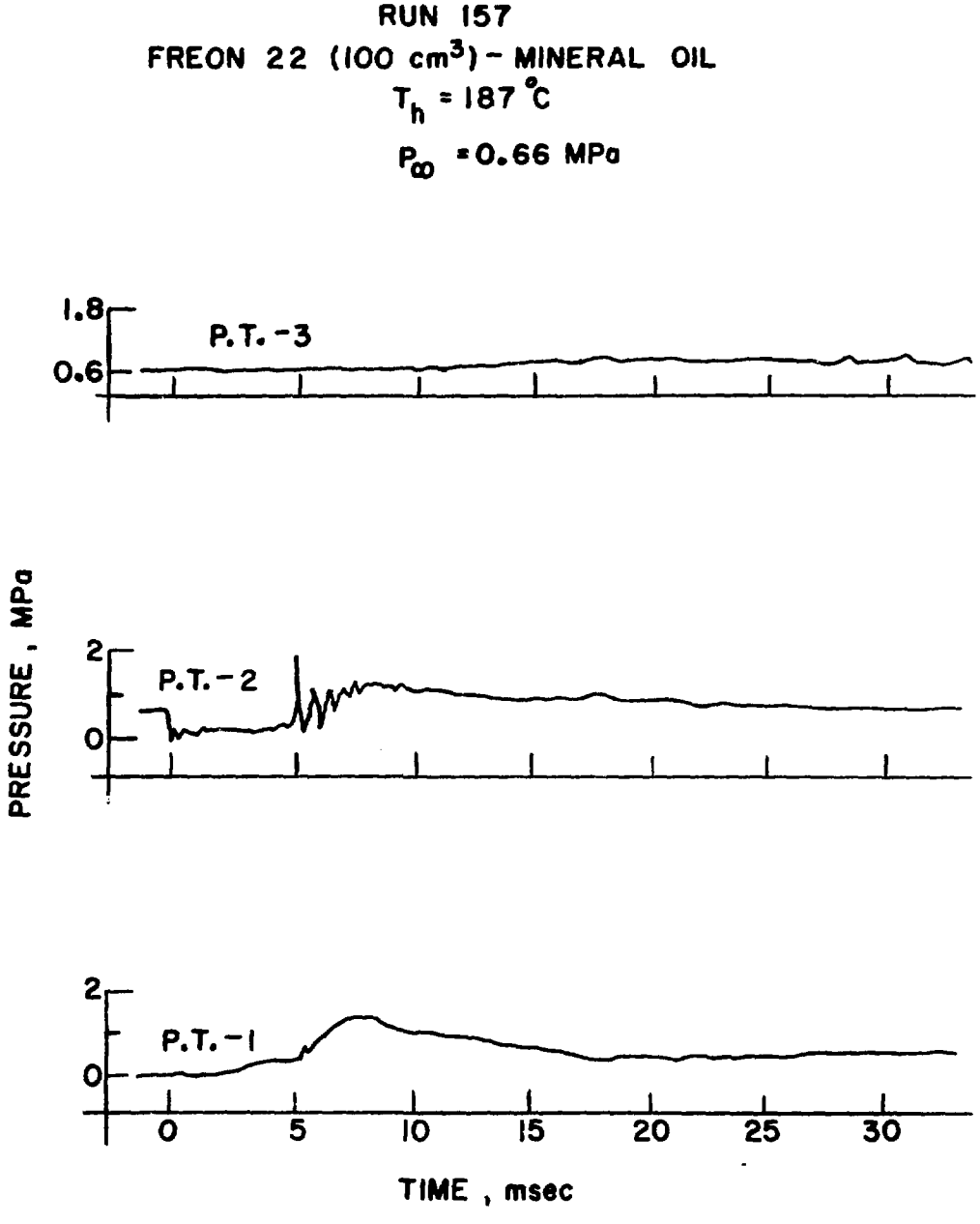

Fig. 5.16 Pressure History of Run 157

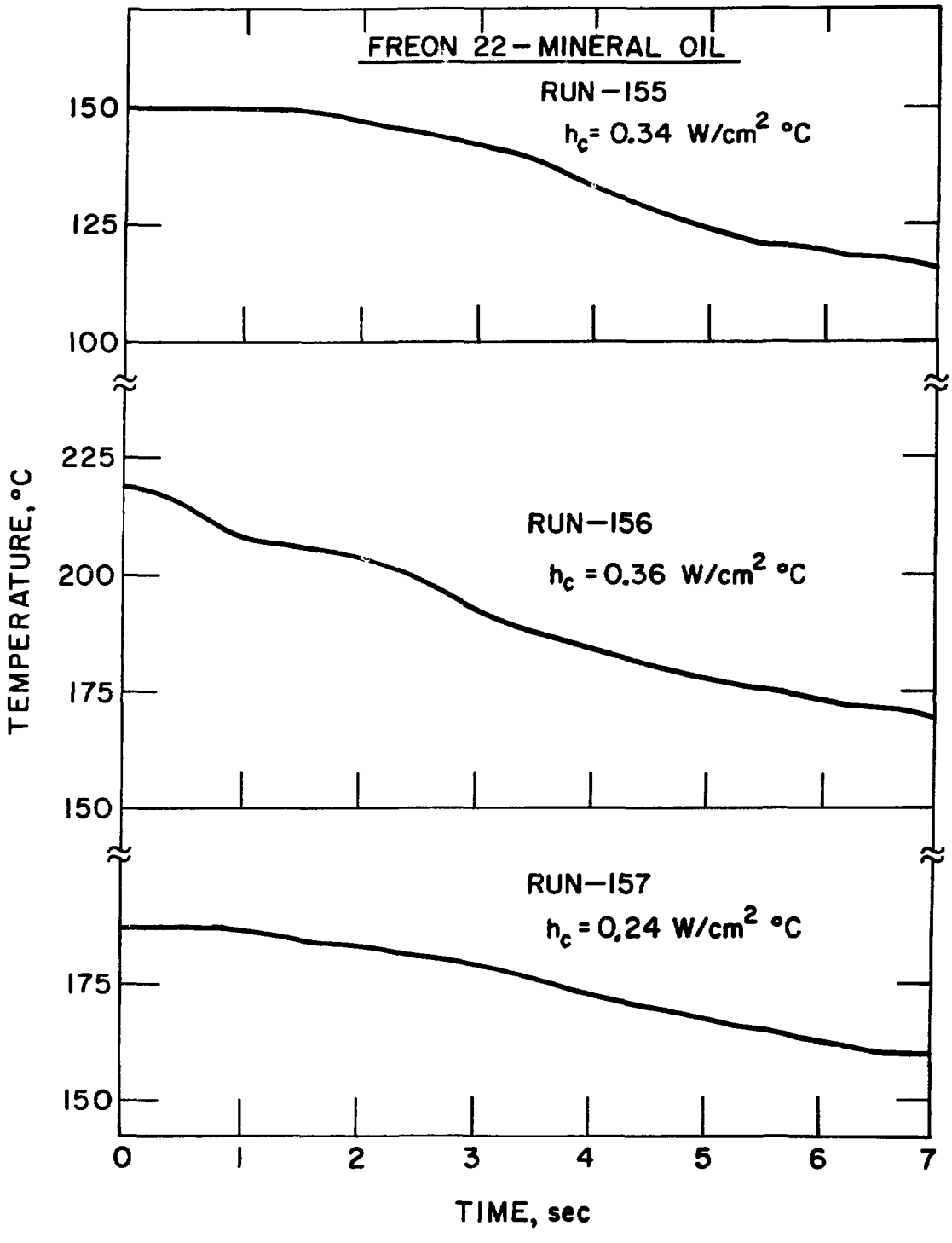

Fig. 5.17 Temperature History of Several Freon-22-Mineral Oil Runs

the oil to be homogeneous and space-wise isothermal the heat transfer coefficient (h_c) was calculated for Freon-22-mineral oil and was found to be in the order of $\sim$0.3 W/cm^2 °C which is well in the film boiling region. Since the resultant impulses were always lower than the theoretical hydrodynamic impulse for instantaneous stoppage of the cold liquid column, one concludes that no significant explosive thermal interaction has occurred and the pressure developed is due to water-hammer pressure (see discussion in Sect. 6.1).

To minimize the effect of the hot liquid vapor pressure silicone oil (Dow Corning 710) was used with Freon-22 and Freon-11. No detectable pressure events were obtained when these fluids were used in a large-scale experiment[68] which may be due to the large amount of dissolved air in the oil. In the present apparatus, the amount of dissolved gases was considerably reduced by evacuating the interaction chamber prior to, and during, the heat-up period. The evacuation procedure was performed initially by using the thin diaphragm which was pressed by hand against the lower flange. The evacuation was continued in that manner until the frothy look of the oil disappeared. After assembling the apparatus, the oil was heated up to $\sim$300°C and the regular evacuation procedure was applied, until the pressure was reduced to <103 Pa. Freon-11 experiments with hot surface temperatures ranging from 30°C to 300°C ($30 \leq T_h \leq 300$°C) and Freon-22 ($25 \leq T_h \leq 272$°C), using the thin and the thick diaphragms produced no explosions. Only the first impact was observed as shown in Fig. 5.18 which represents the data in those systems, using the thick diaphragm. The results are very similar to those obtained from Freon-22-water contacts (Fig. 5.19). When using the thin diaphragm

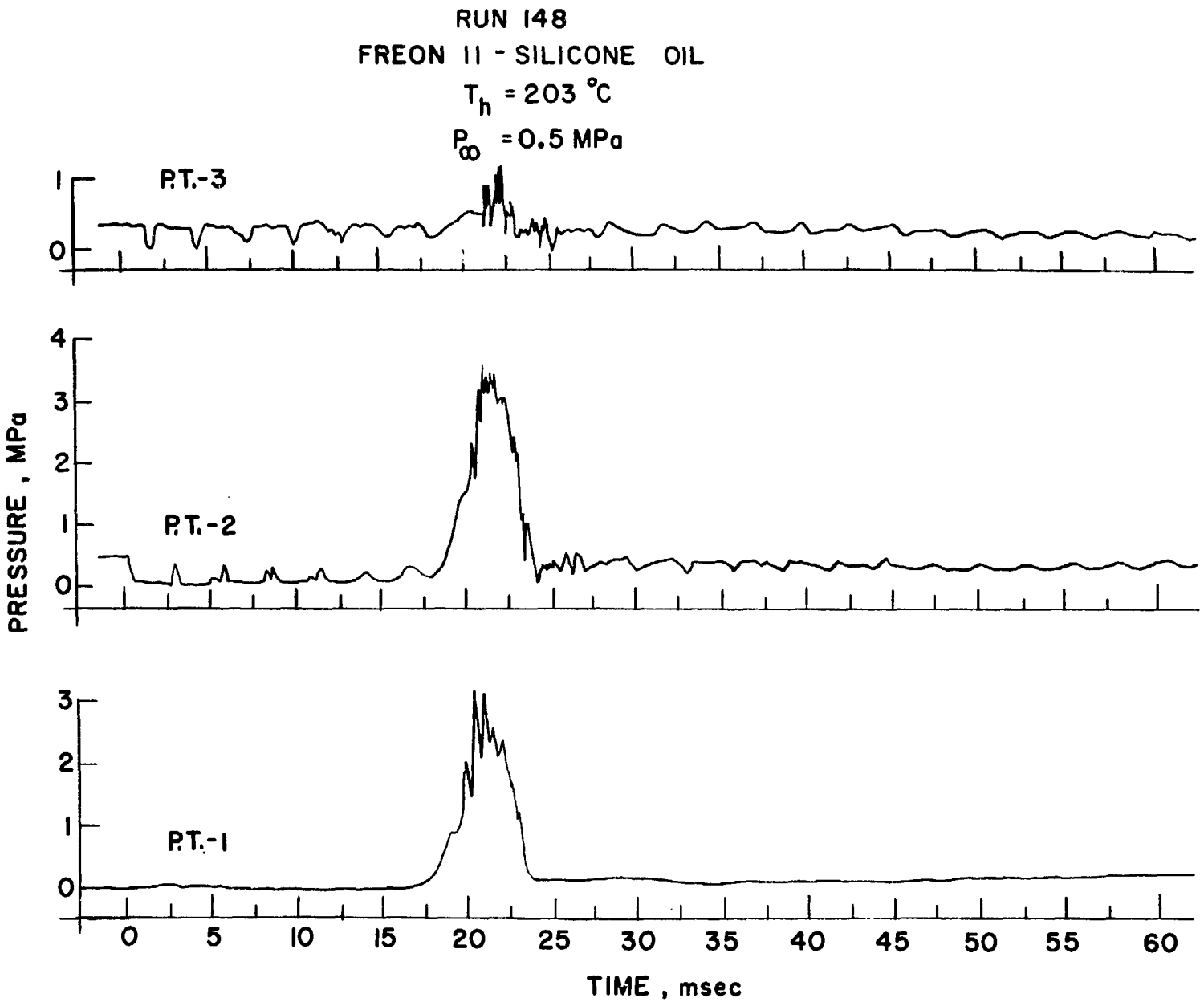

Fig. 5.18 Pressure History of Run 148

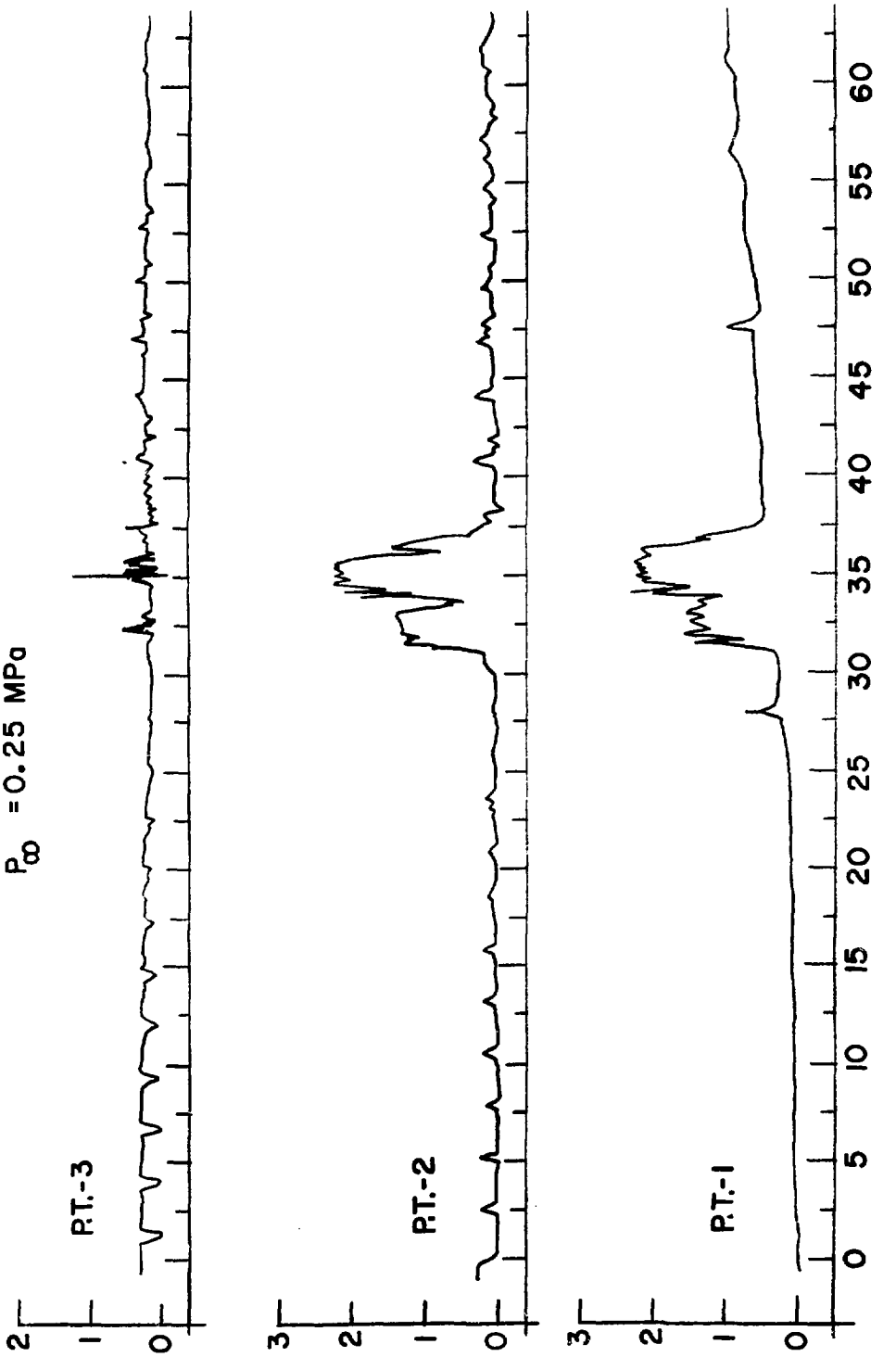

Fig. 5.19 Pressure History of Run 127

with oil or water, the impact was observed at low temperatures but only slow vaporization at higher temperatures (Fig. 5.20).

The first impact and the consecutive bounces were shown very clearly when the Freons were impacted upon mercury ($10 \leq T_h \leq 230$ for Freon-22 and $11 \leq T_h \leq 249$ for Freon-11). Typical pressure measurements are given in Figs. 5.21-5.23.

5.4 Water-Wood's Metal Interactions

Twenty-nine runs were performed with water at room temperature interacting with 250 g of Wood's metal (50% Bi, 25% Pb, 12.5% Cd, and 12.5% Sn) over the temperature range of 90-551°C. Wood's metal melts at 70°C and at higher temperatures (~150°C) it tends to oxidize very quickly, forming a black layer of oxide. At temperatures higher than ~350°C some fine metallic powder was collected in the cold trap after evacuating to about 103 Pa, which indicates a significant vapor pressure. Hence, to reduce the metal vapor pressure above the Wood's metal, water vapor was always introduced when $T_h > 350$°C. This is similar to the procedure employed in previous shock tube experiments (see Sect. 2.1.2).

The majority of the runs were performed with the thin diaphragm which burst at about 0.2 MPa ±15% differential pressure. The theoretical impulse per unit area required to instantaneously stop the water column for this absolute pressure with complete vacuum below the diaphragm is 10.5 KPa.sec and the theoretical water hammer pressure for instantaneous stoppage of the column is 6.20 MPa. The experimental results are tabulated in Appendix E.

In Fig. 5.24 the impulses of all pulses for each run are shown, where in Fig. 5.25 only the maximum impulse is shown. The maximum pressure obtained in each run is shown in Fig. 5.26. In general, when

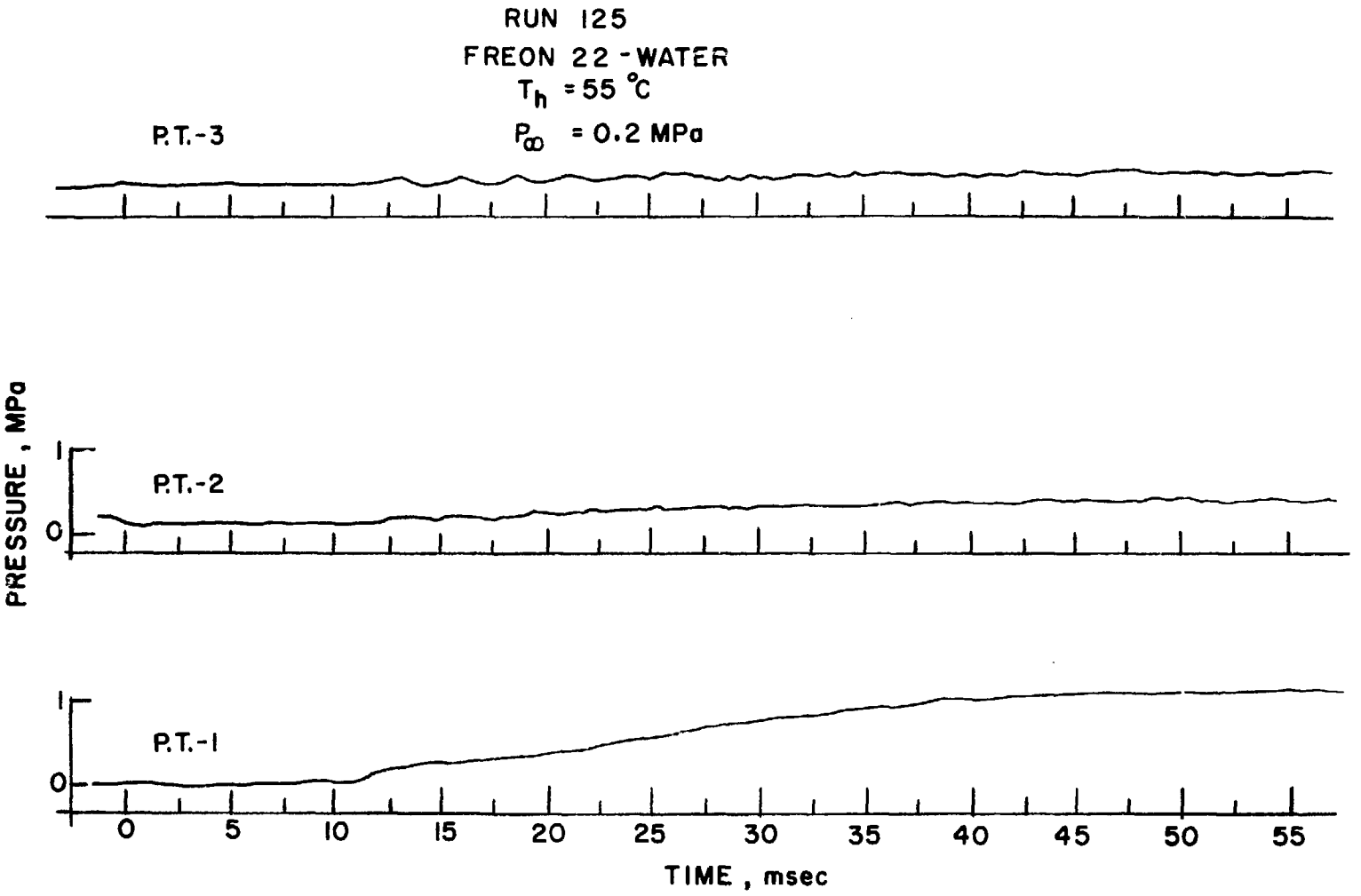

Fig. 5.20 Pressure History of Run 125

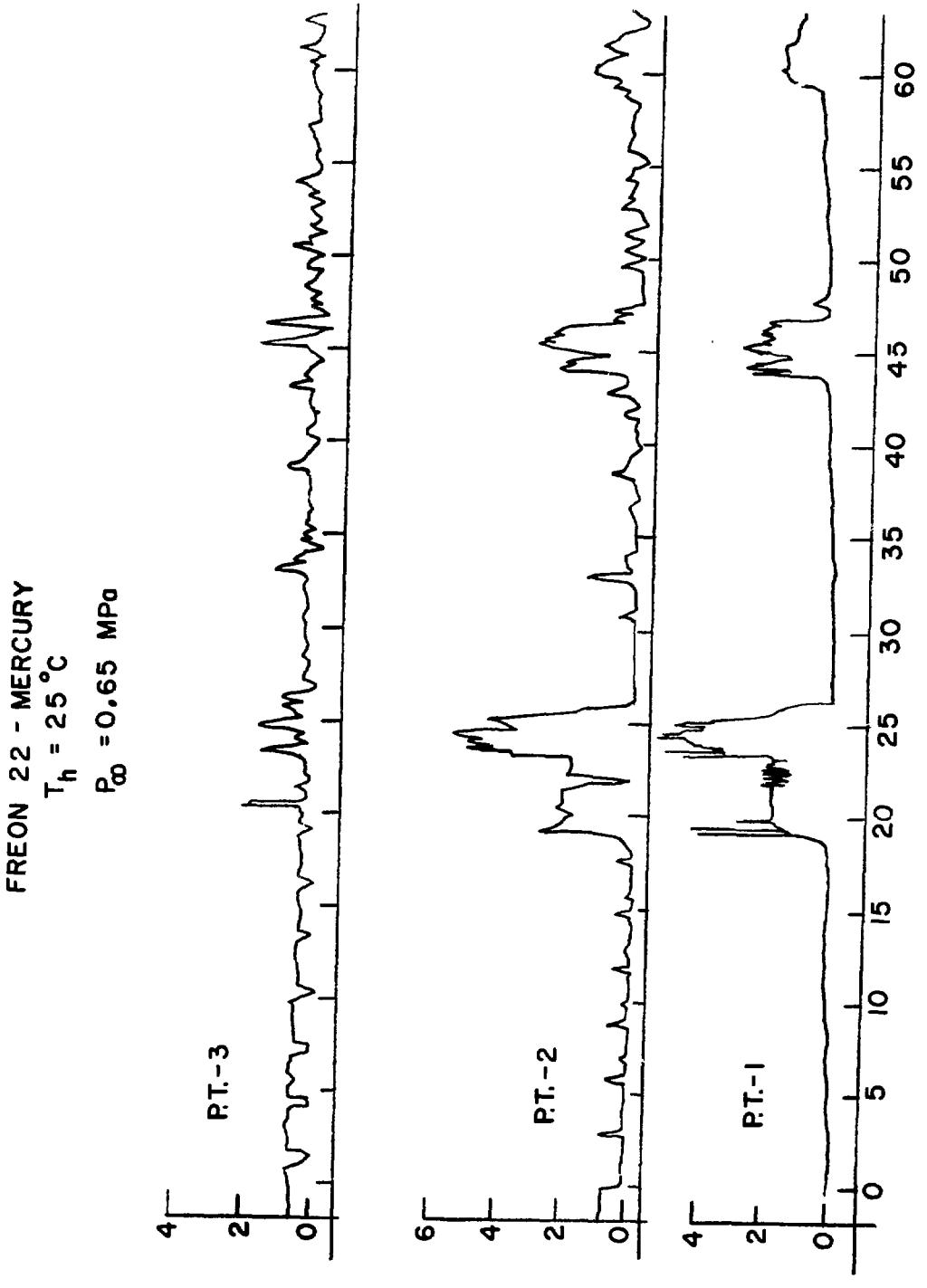

Fig. 5.21 Pressure History of Run 63

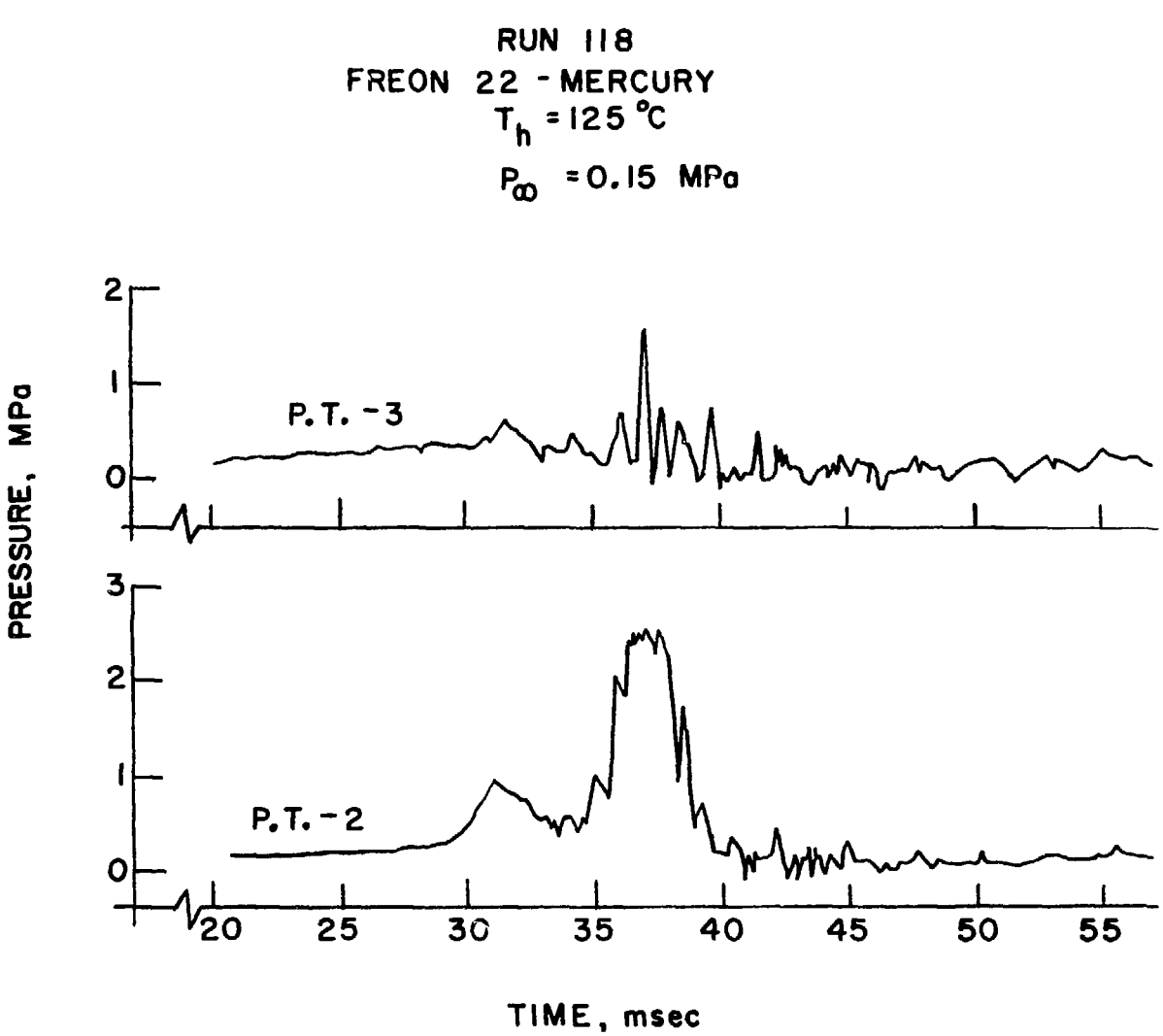

Fig. 5.22 Pressure History of Run 118

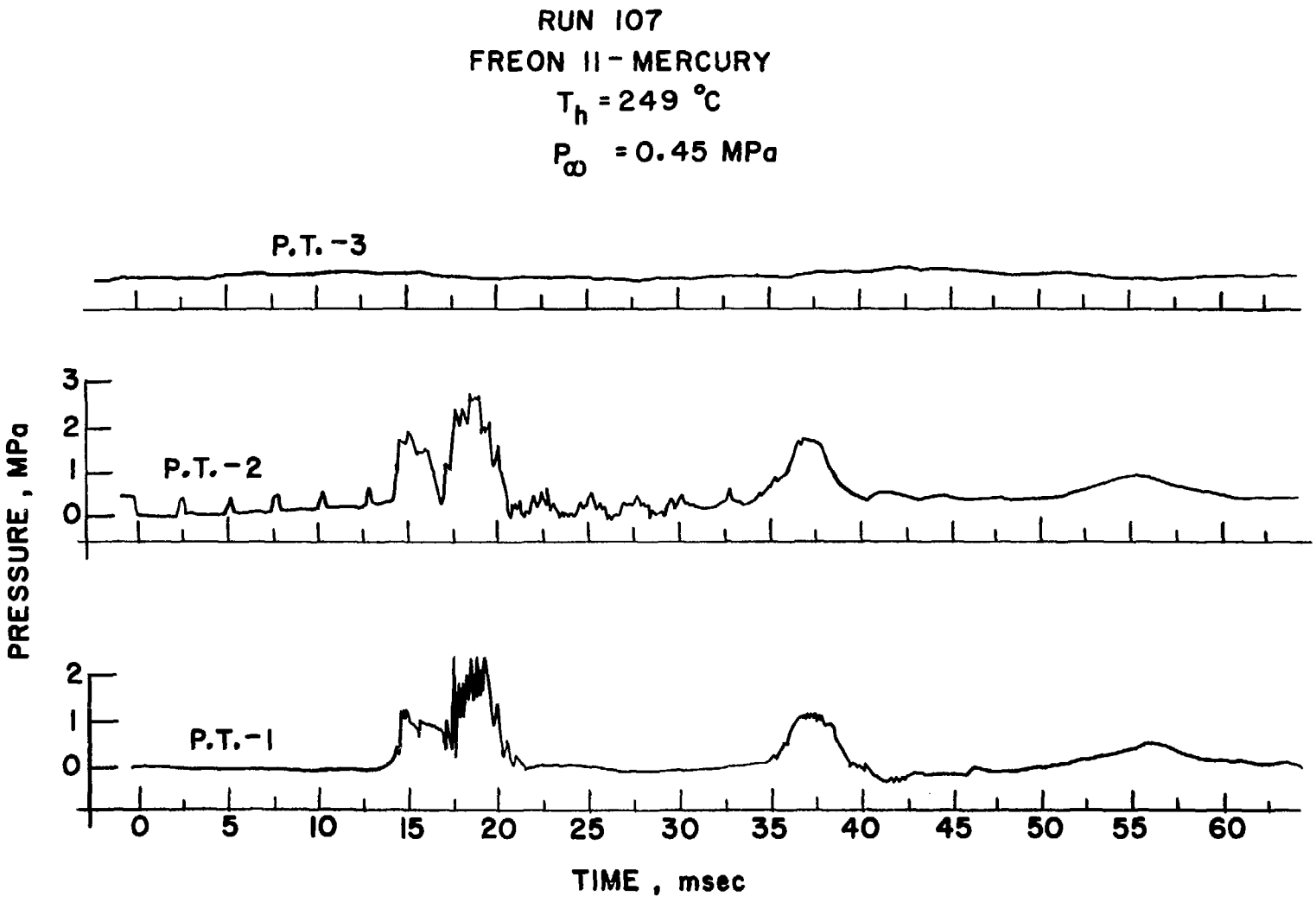

Fig. 5.23 Pressure History of Run 107

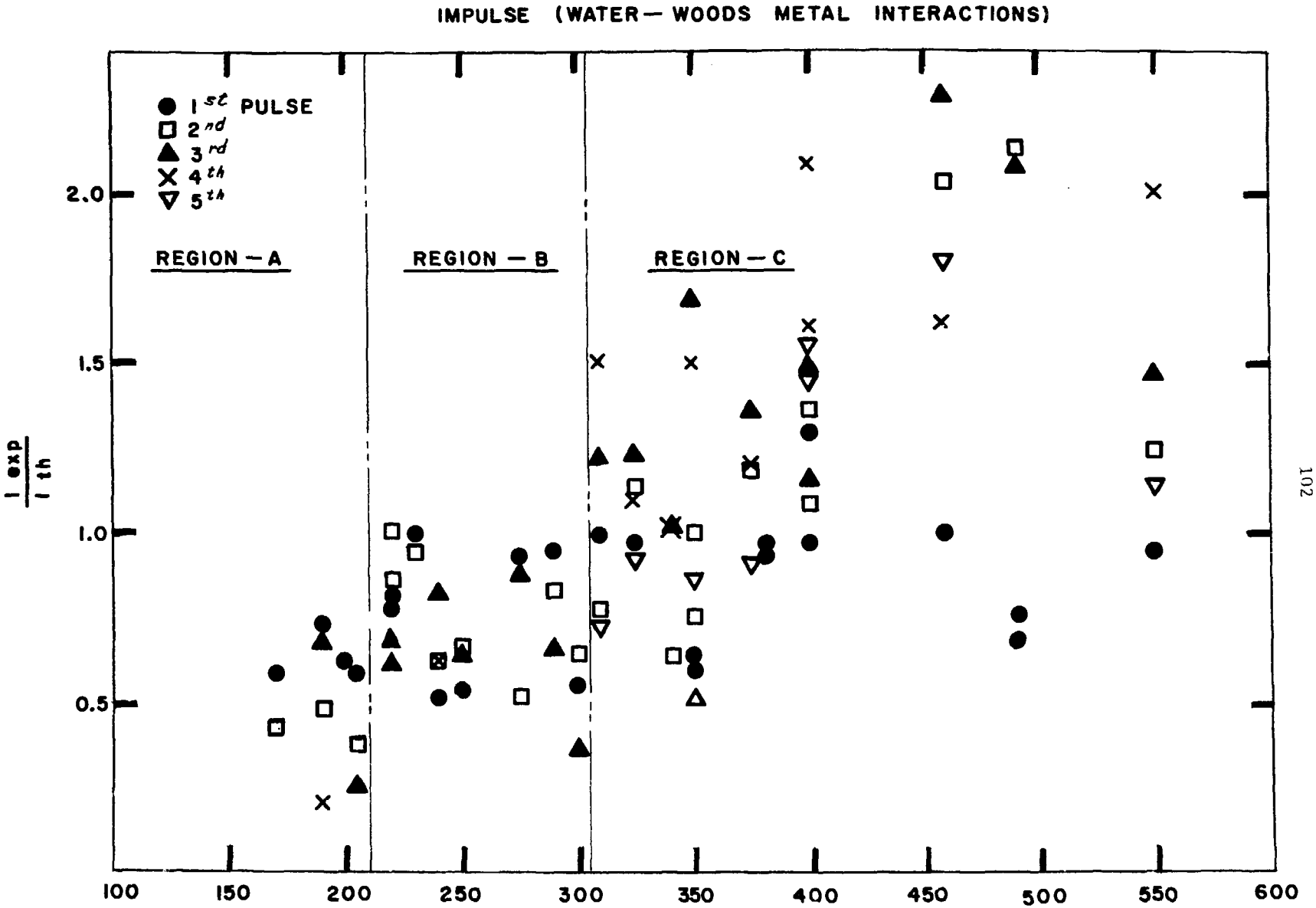

Fig. 5.24 Impulse of Water-Wood's Metal Interactions

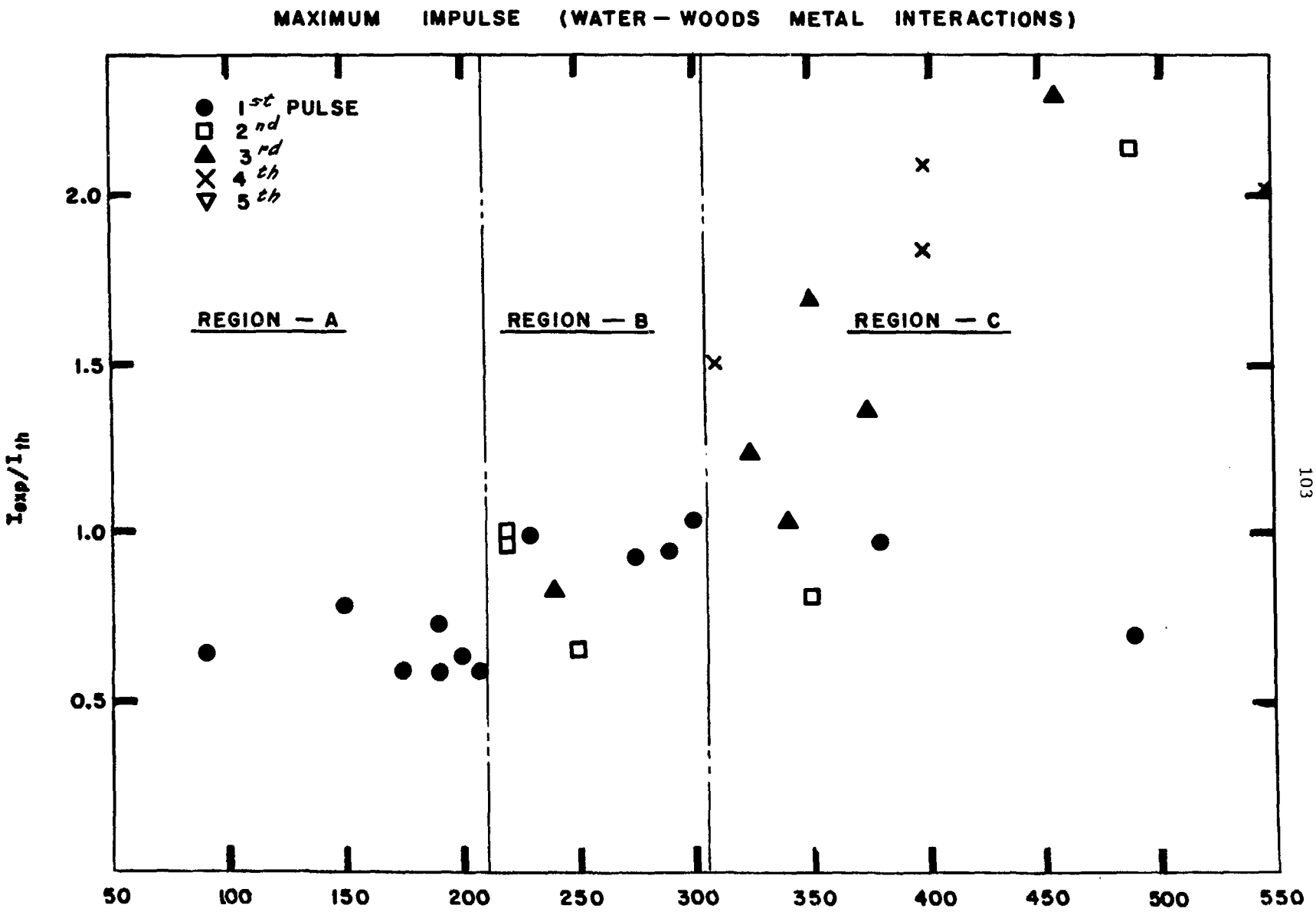
MAXIMUM IMPULSE (WATER — WOODS METAL INTERACTIONS)
1st PULSE
2nd
3rd
4th
5th
REGION — A
REGION — B
REGION — C
I_{exp}/I_{th}
2.0
1.5
1.0
0.5
50
100
150
200
250
300
350
400
450
500
550

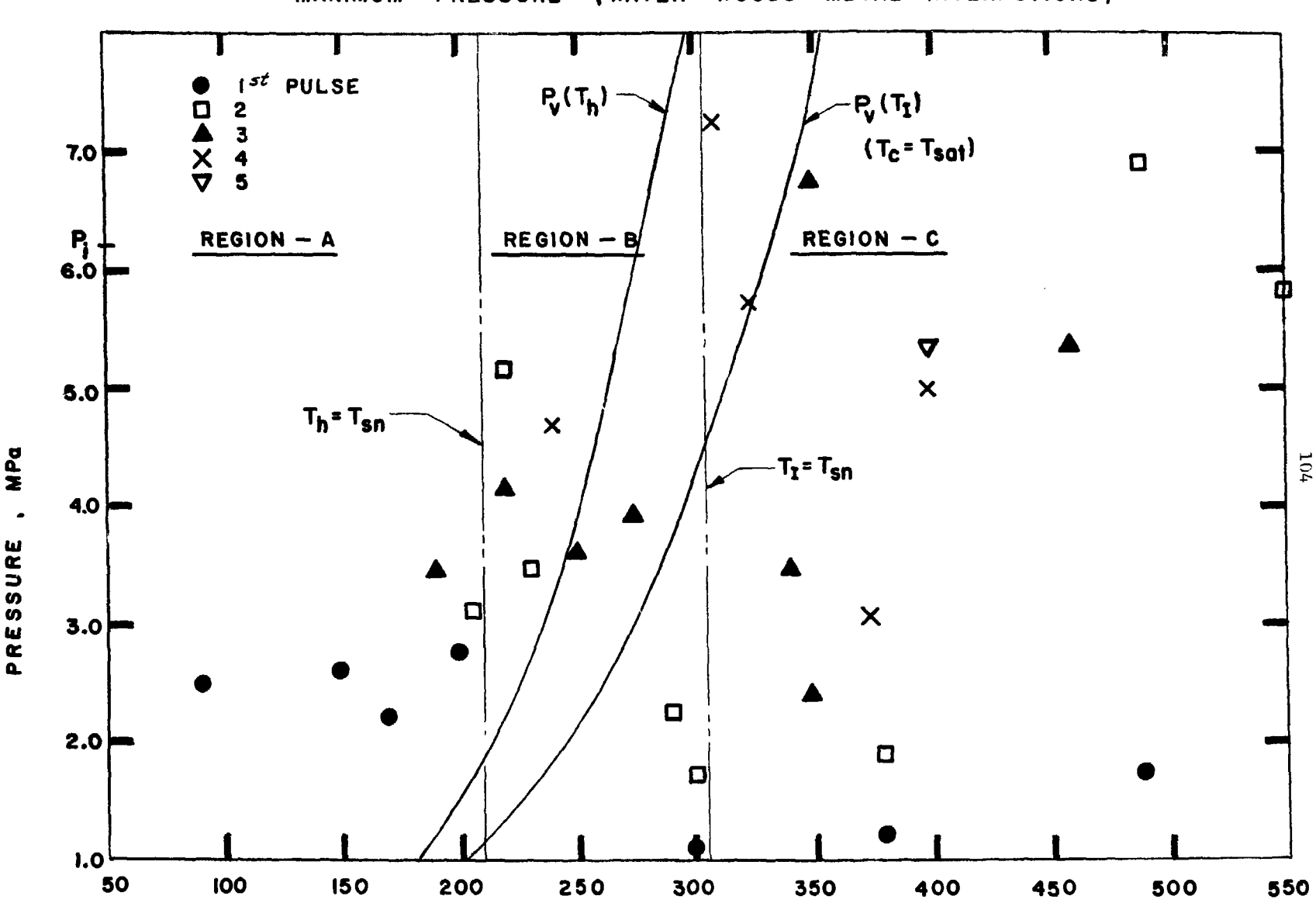

Fig. 5.26 Maximum Pressure of Water-Wood's Metal Interactions

no multiple interaction occurred, only a low level "boom" could be heard which was probably the sound of diaphragm rupture or first impact, the thermocouples (TC-1 and TC-2) did not exhibit rapid changes, the resulting pressures were relatively low and no fragments were found in the pipes and the valves leading to the vacuum pump and vacuum gauge, or on the diaphragm. However, when multiple interactions occurred, definite multiple "booms" were heard which could be correlated with the existence of numerous pressure pulses. The thermocouples indicated a significant energy transfer as shown in Fig. 5.27 for run 216. TC-1 dropped rapidly to about 120°C and after a few seconds increased to a new level, and TC-2 rose sharply to about 80°C, oscillated strongly and maintained a level of about 70°C after a few seconds. The pressures were high with a very short rise time and many fragments were found on the diaphragm and on the flange surface (this surface was below the diaphragm since the diaphragm rested on an O-ring mounted on the flange surface). The valves and pipes to the vacuum pump and gauge were always blocked by frozen fragments.

From the impulse graph (Fig. 5.25), it can be seen that up to 210°C ("region A"), the maximum impulse is less than the theoretical one and it always occurs on the first impact. Any subsequent bounce has an impulse less than the first one. The magnitude of the maximum impulses is similar to the impulse at 90°C and to the isothermal water-solid surface runs, suggesting that no additional energy is transferred. However, the maximum pressure magnitude exhibits a rather unexpected behavior with the addition of water vapor below the diaphragm. One would assume that if no thermal interaction occurred and no thermal

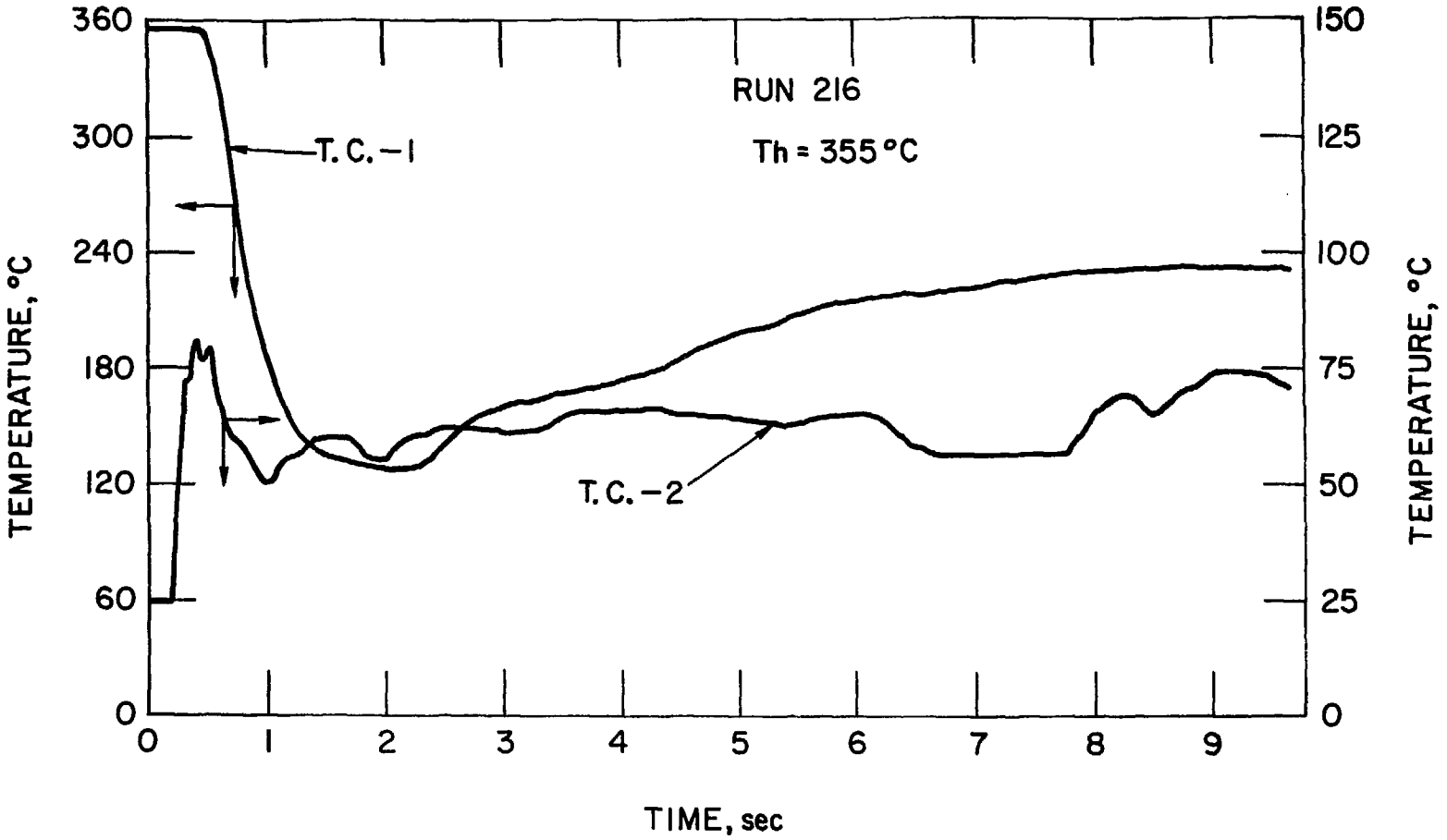

Fig. 5.27 Temperature History of Run 216

energy has been transferred, the water consecutive bounces would be smaller in their impulse and pressure, as was shown in the isothermal water-solid surface experiments. However at temperatures 174°C (Run 192), 188°C (Run 189) (Fig. 5.28), and 207°C (Run 188), where water vapor (∿2.5 cm Hg) had been introduced prior to the interaction, the system exhibited bouncing with large and sharp pressure pulses, contrary to Runs 163 (150°C) and 164 (200°C) (Fig. 5.29) where no water vapor was present and no bouncing was noticed. Also, the impact pressure (the first pulse) in runs with water vapor was considerably less than the impact pressures obtained in those runs without preexisting vapor (see discussion in Sect. 6.2).

In the temperature range from ∿210 to 305°C ("region B") the maximum impulse magnitude is close to the theoretical value based on the initial driving pressure and column displacement. A typical result is shown in Fig. 5.30 for run 187 (220°C). The maximum impulse in some of the runs occurs on the first impact, for other tests it is on the second bounce (e.g., Runs 187 and 202), and for still others on the third bounce (Run 186). The maximum pressures in each run are higher in this temperature range than the lower temperature range (<210°C), except the abnormally low pressures in three runs around 300°C. The maximum pressure of a run never occurred on the first impact but rather on the second, third, or fourth bounce. The maximum pressure magnitude of some of the runs in this temperature range was higher than the cold liquid vapor pressure corresponding to the hot liquid temperature.

The third temperature range which can be observed is temperatures above ∿305°C ("region C"). A typical result is shown in Fig. 5.31 for

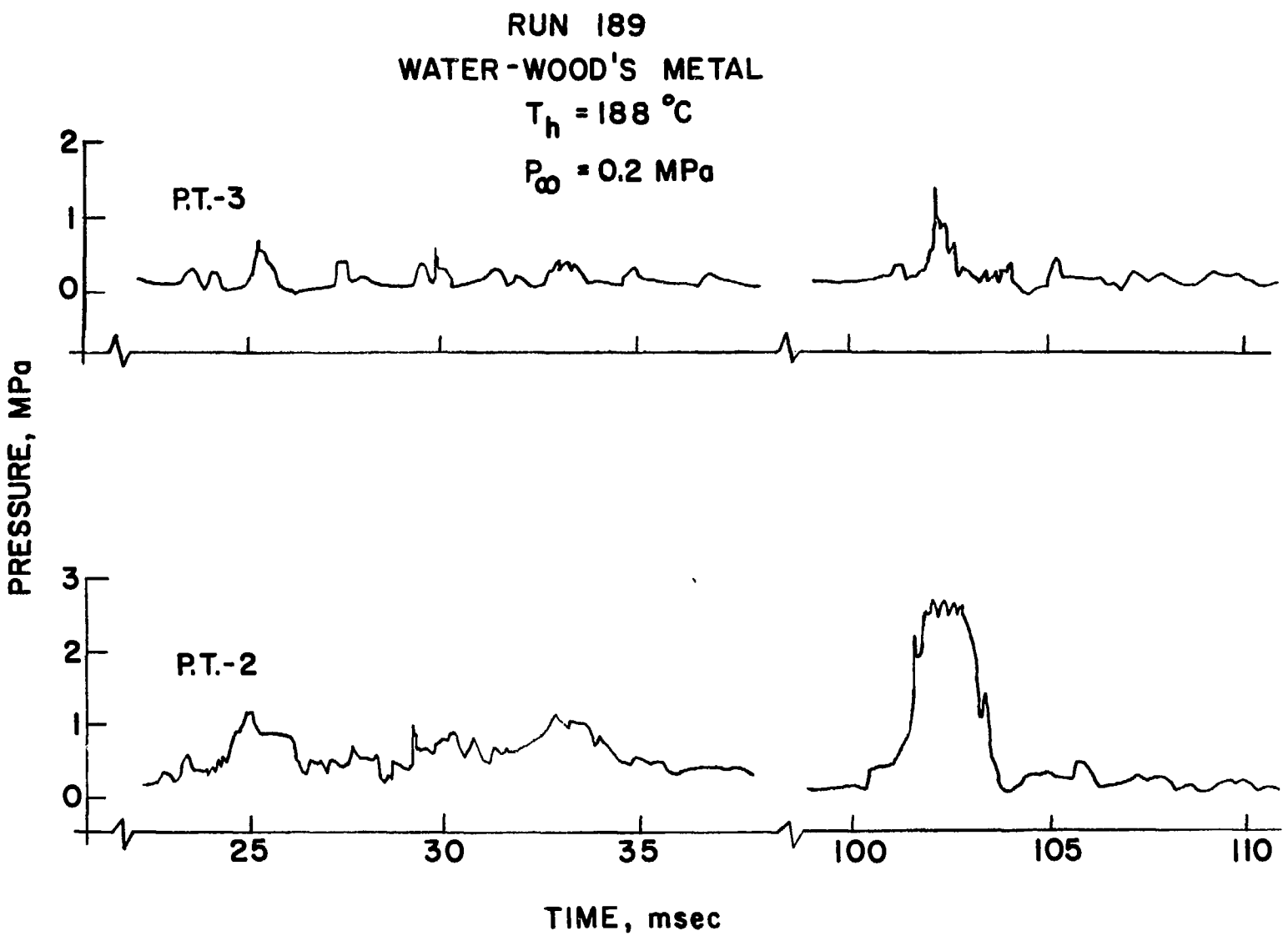

Fig. 5.28 Pressure History of Run 189

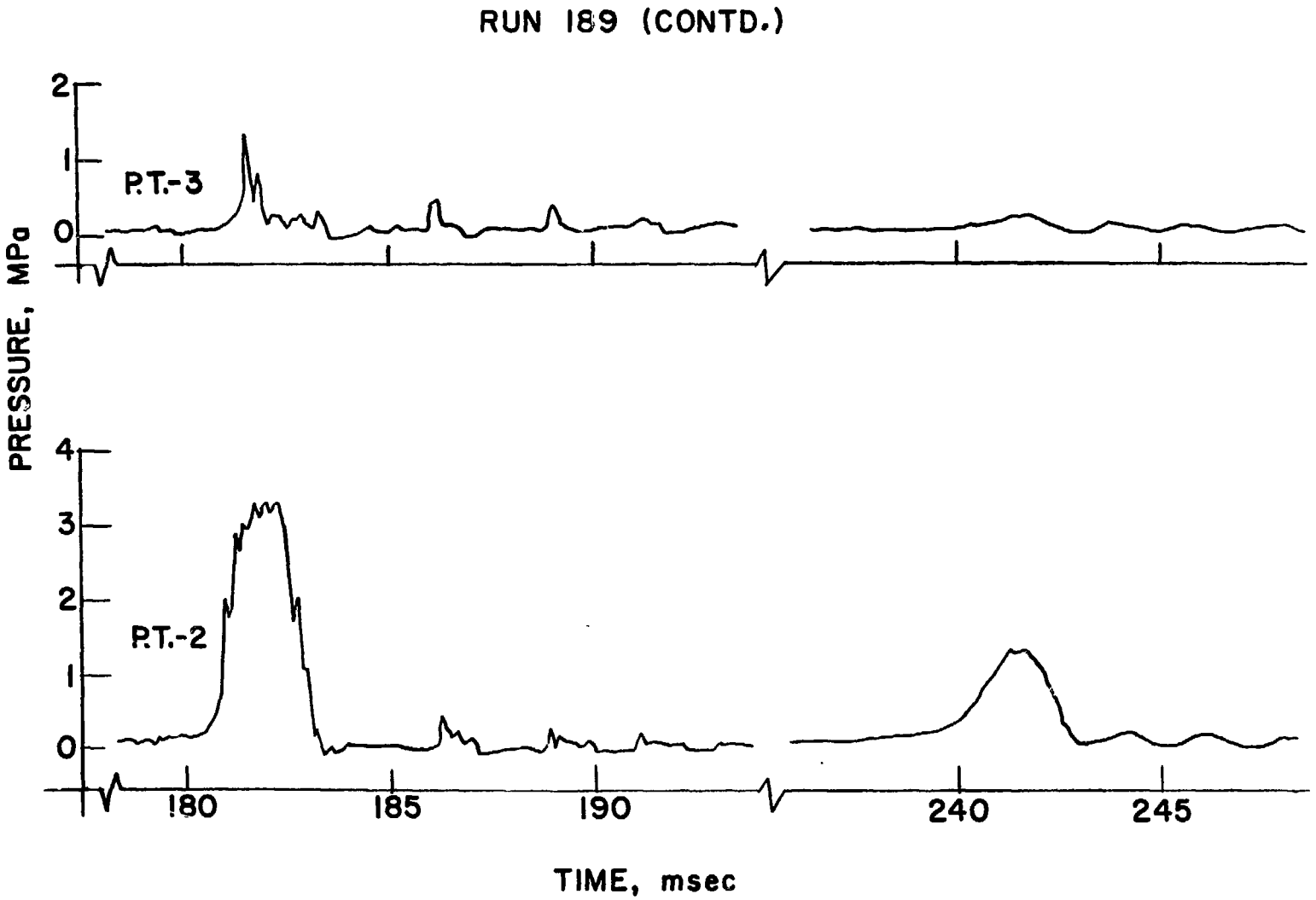

Fig. 5.28 Pressure History of Run 189 (contd.)

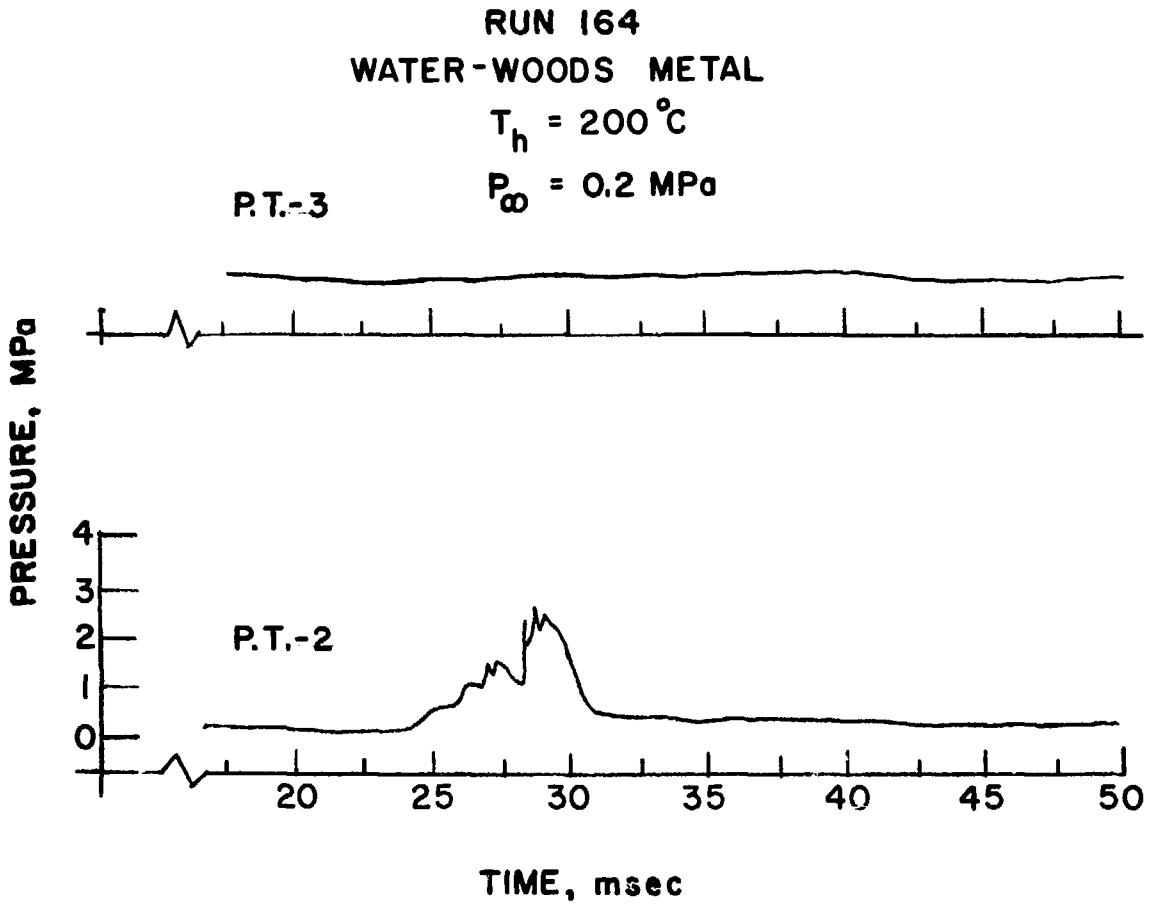

Fig. 5.29 Pressure History of Run 164

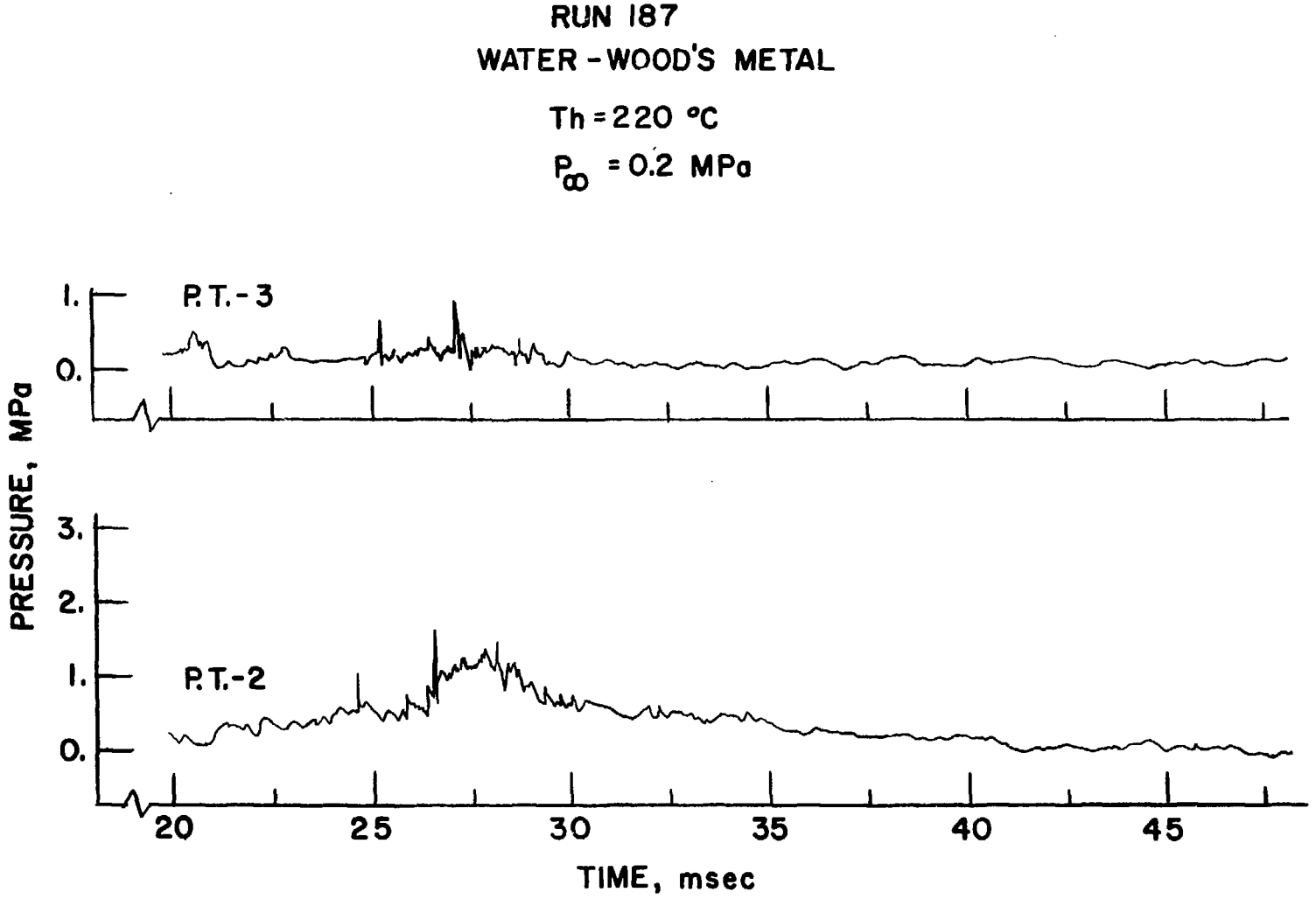

Fig. 5.30 Pressure History of Run 187

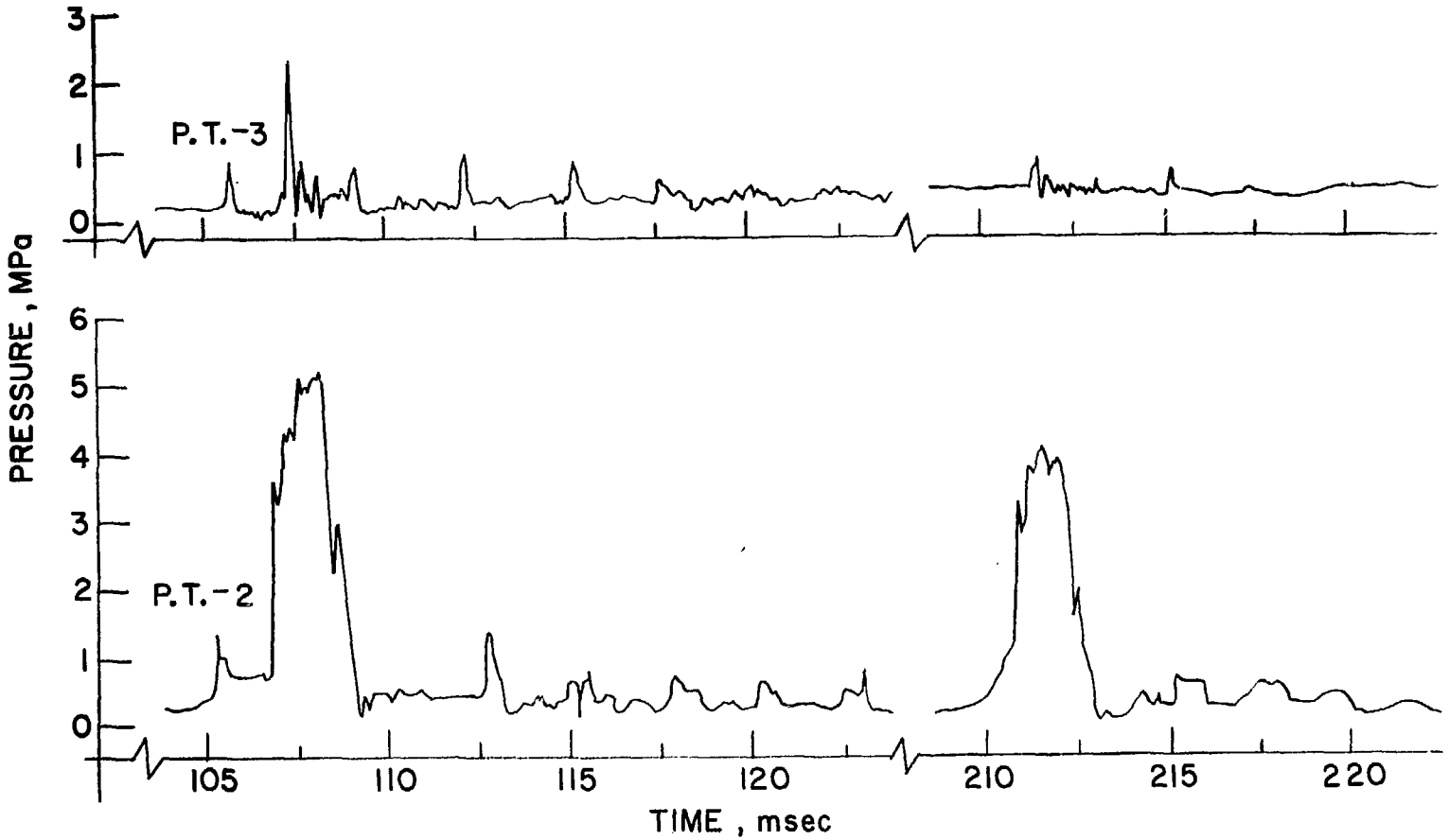

Fig. 5.30 Pressure History of Run 187 (contd.)

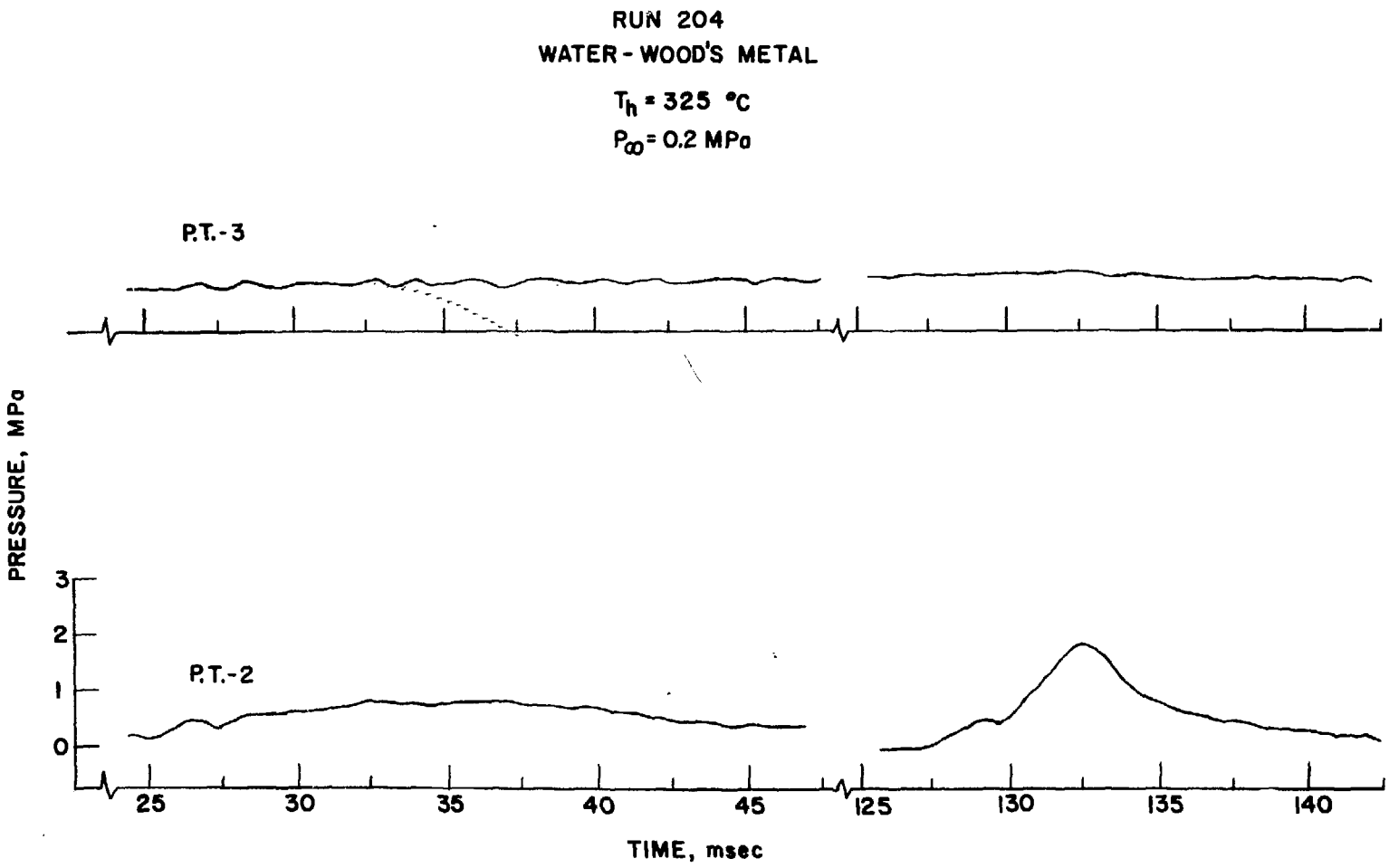

Fig. 5.31 Pressure History of Run 204

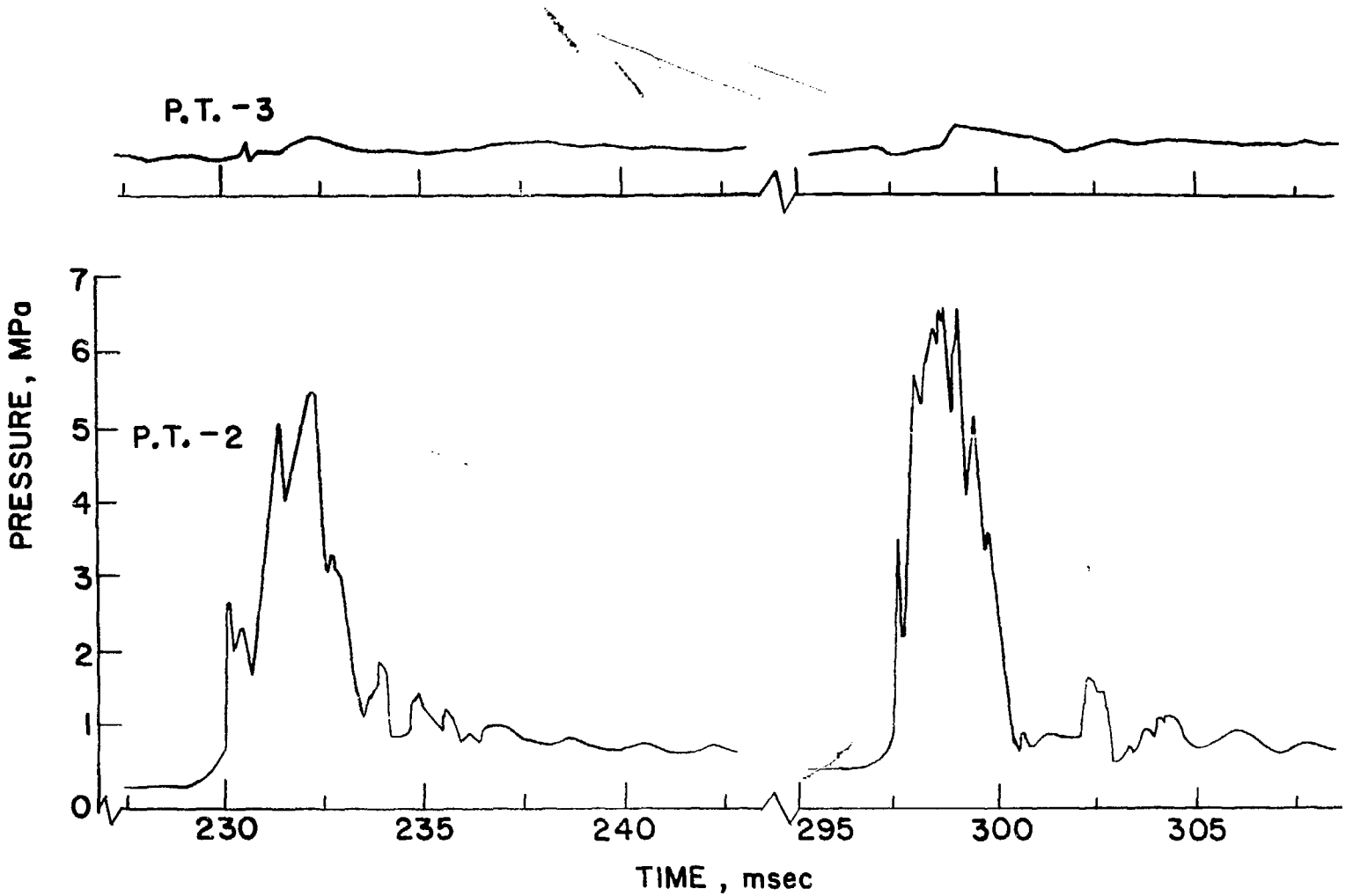

Fig. 5.31 Pressure History of Run 204 (contd.)

RUN 204 (cont.)

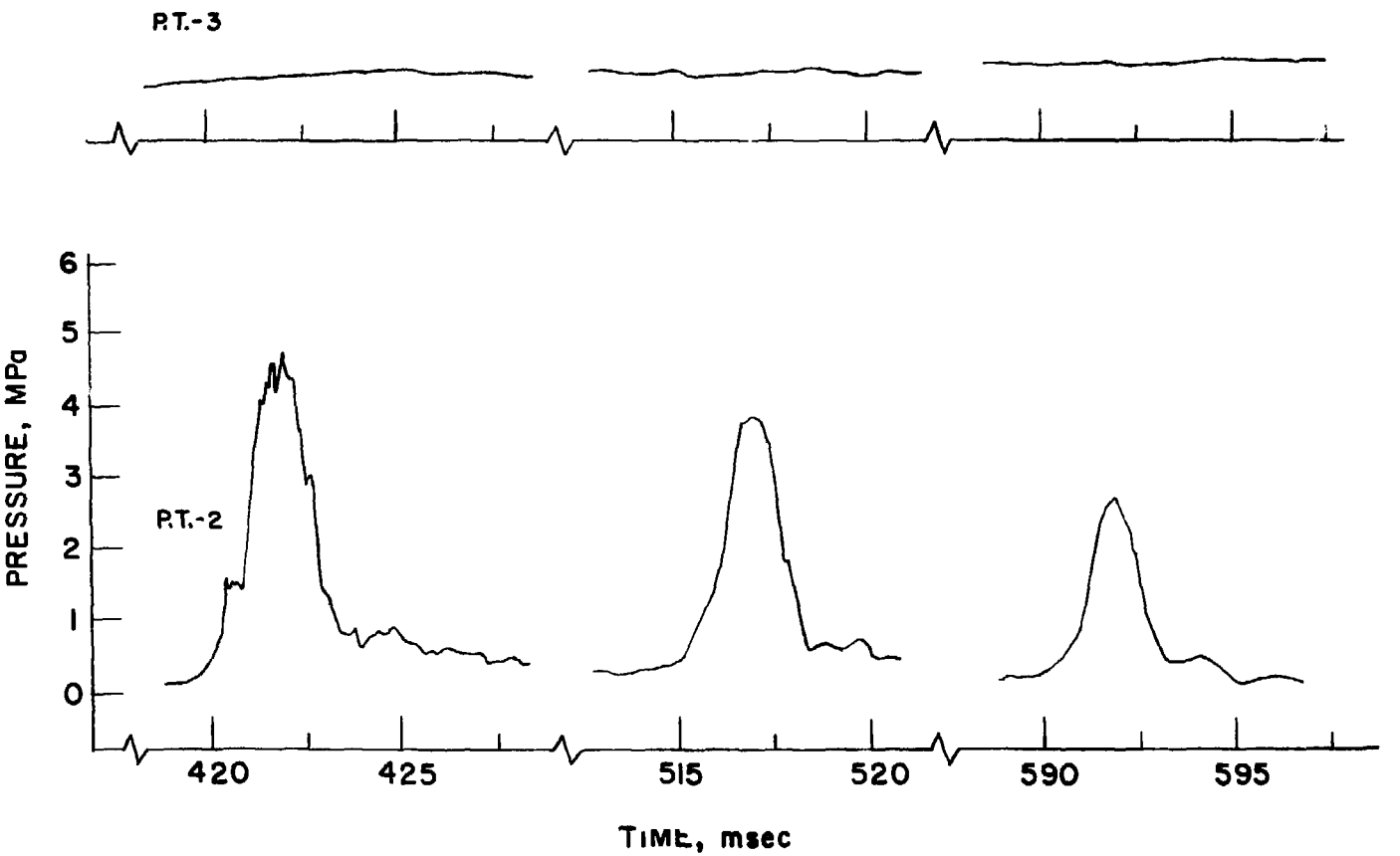

Fig. 5.31 Pressure History of Run 204 (contd.)

run 204 (325°C). In this range the maximum impulse is significantly higher than the theoretical one, and never occurs on the first impact. The same temperature threshold is observed also in the pressure graph. Above 305°C the pressures obtained are high, ~7.0 MPa, through the whole temperature range. At 400°C two runs were performed, Run 169 where no prior vapor pressure was present and Run 198 where vapor pressure was present, and the results of these two runs are very similar in maximum impulse and pressure produced. Thus, it seems that a preexisting oxide layer (which is likely formed on the surface before Run 198) did not change the general system behavior.

5.5 Butanol-Wood's Metal Interactions

Butanol was also used as a cold liquid. The objective in using butanol was to investigate the possibility of interactions with an organic liquid, which has lower oxidation potential than water. The normal boiling point of butanol (117.5°C) and the critical temperature (288°C) are comparable to the respective water temperatures (100°C and 374°C) and it also results in a rather wide temperature range. However, the butanol thermal properties differ from those of water, as is shown in Appendix A.

The experimental procedure for the butanol interactions was the same as for water (butanol vapor was introduced below the diaphragm prior to the runs in which $T_h > 350°C$), and the complete experimental results are tabulated in Appendix E. The Wood's metal temperature range covered is 113-505°C, and the impulses and maximum pressures of each run, as a function of temperature are given in Figs. 5.32 and 5.33, respectively.

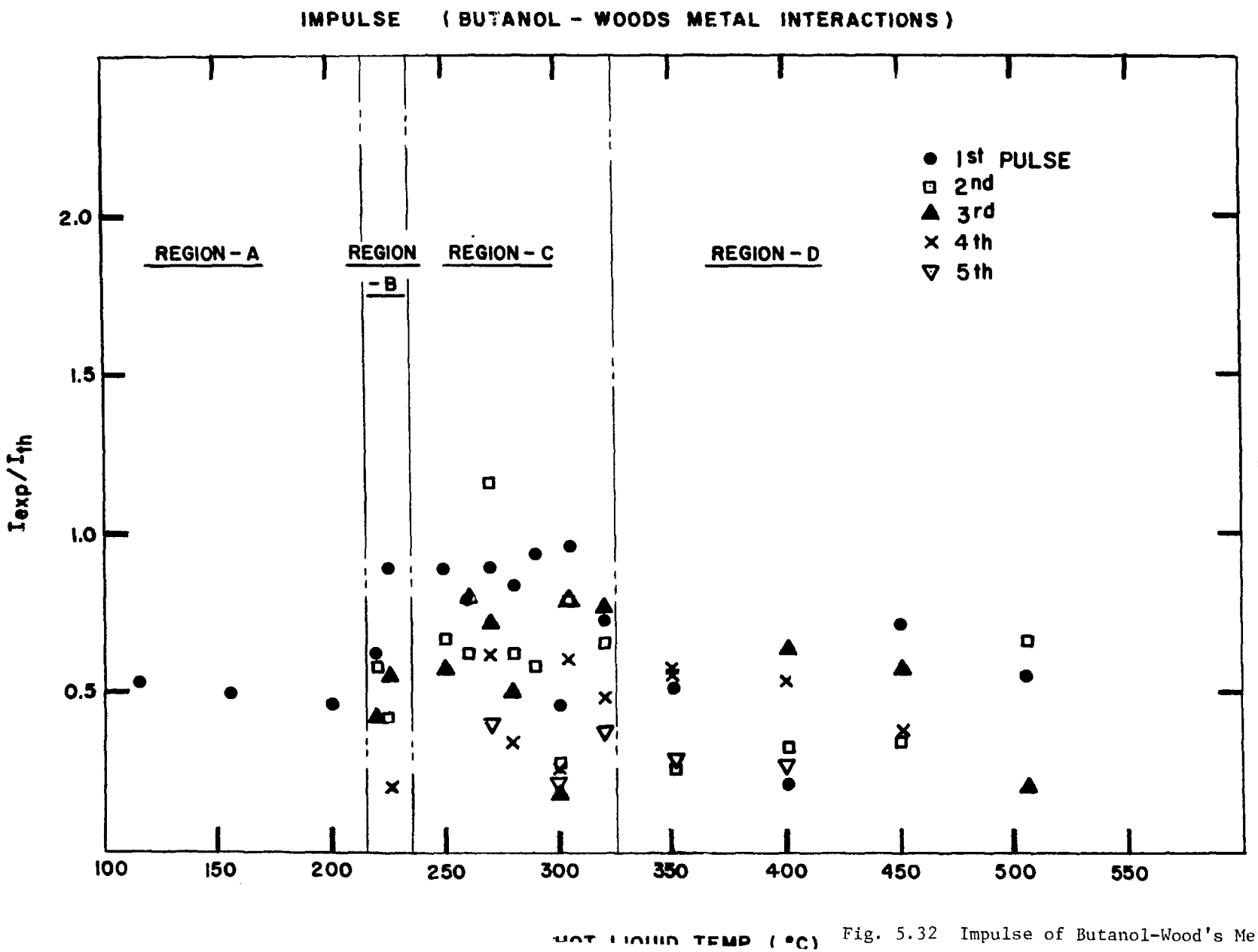

Fig. 5.32 Impulse of Butanol-Wood's Metal

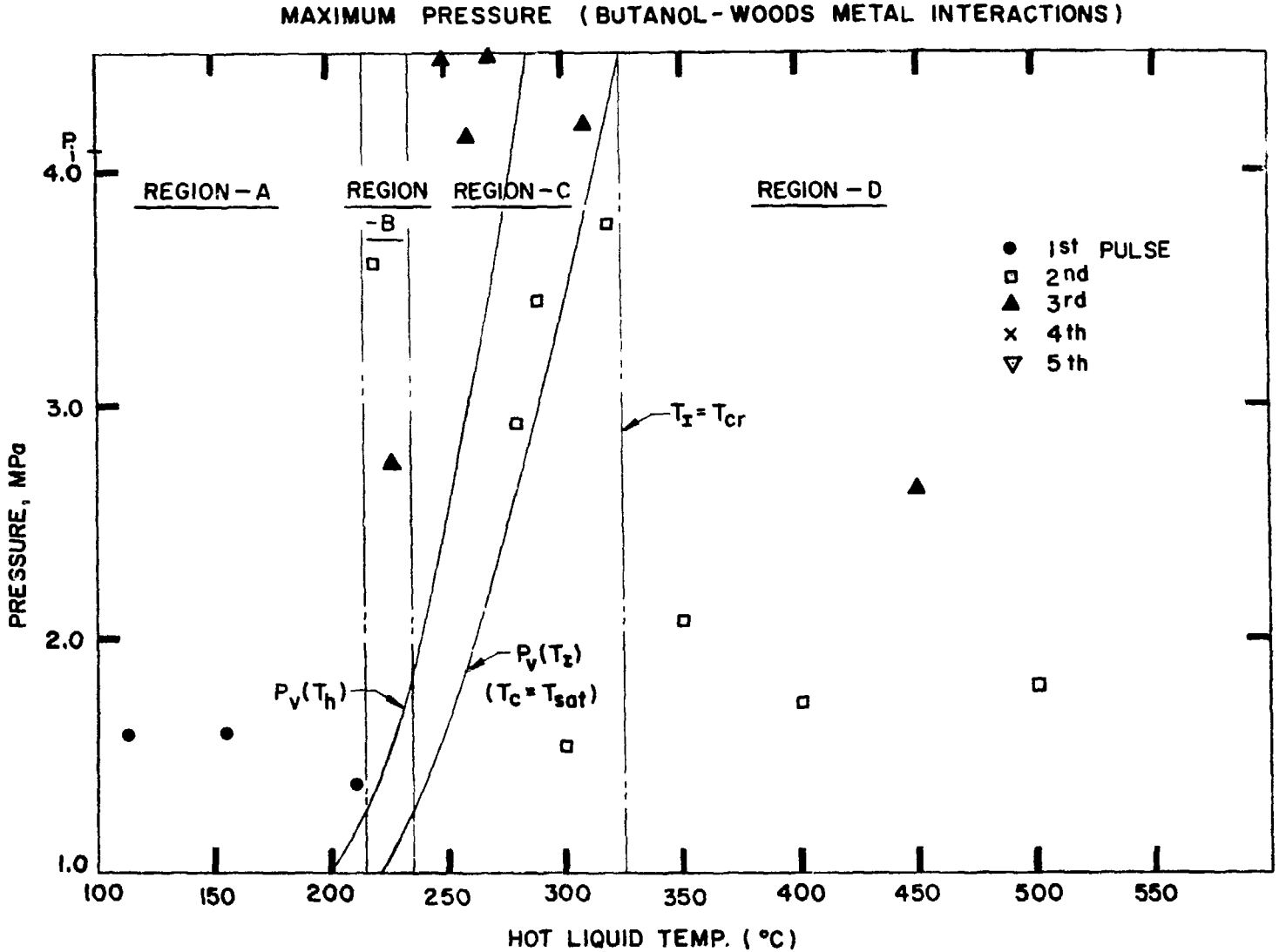

Fig. 5.33 Maximum Pressure of Butanol-Wood's Metal Interactions

Up to ∿215°C, this fluid pair did not exhibit bouncing, and only first impacts were recorded (Region A) which is similar to the behavior exhibited by water, when no vapor was present initially. The impulses and the impact pressures in this region were ∿0.5 and 0.3 of the theoretical respective values for instantaneous stoppage of the column. In the range from ∿215°C to ∿325°C, there is an increase in the impulse magnitude and only one experiment (run 233, Fig. 5.34) produced an impulse greater than the theoretical impact value. There is a definite sharp increase in pressure on the lower boundary of the temperature range, and a sharp decrease on the other end. It is difficult to distinguish between low yield and high yield thermal interaction, which is obvious in the case of water. However, with some uncertainty one can separate the range of 215-235°C ("region B") from "region C" (235-325°C). In region B the pressures are somewhat lower than in region C (the maximum pressure in region B is 3.6 MPa compared to 4.5 MPa in region C) and the impulses of the "bouncing" pulses (not the impact pulse) are lower in region B than the impulses in region C.

Above 325°C another region is observed ("region D") which is not observed in the water interactions. In this region the pressures are much lower than in region C and the impulses are somewhat lower, but the most significant difference between regions C and D is the shape of pulses. When in region C the pressure pulse is sharp with short rise time, the pulses in region D are more gradual in growth and decay as is shown in Run 185 (Fig. 5.35).

5.6 Water-Molten Salt (LiCl/KCl) Interactions

In this set of experiments, 50 g of an eutectic mixture of LiCl and

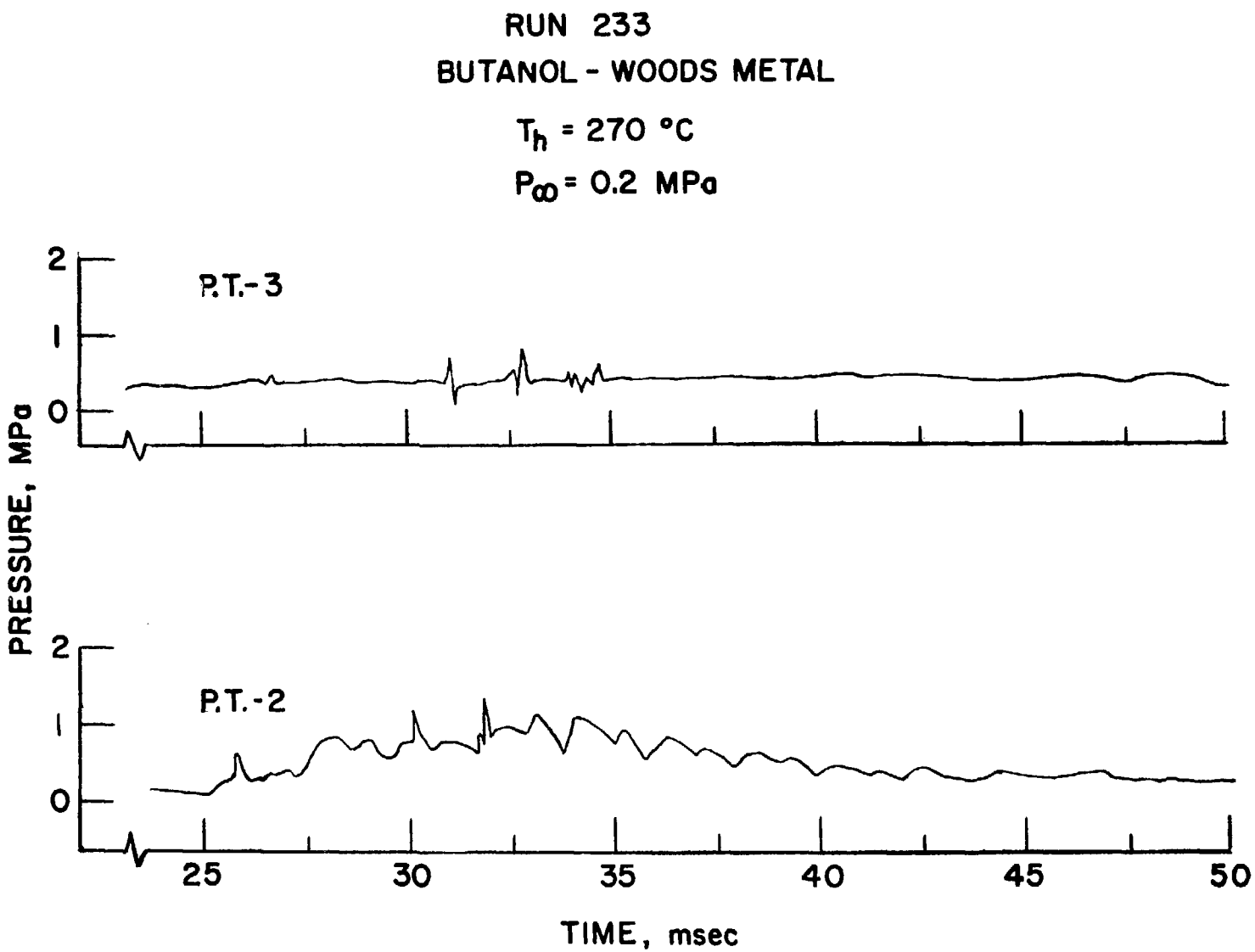

Fig. 5.34 Pressure History of Run 233

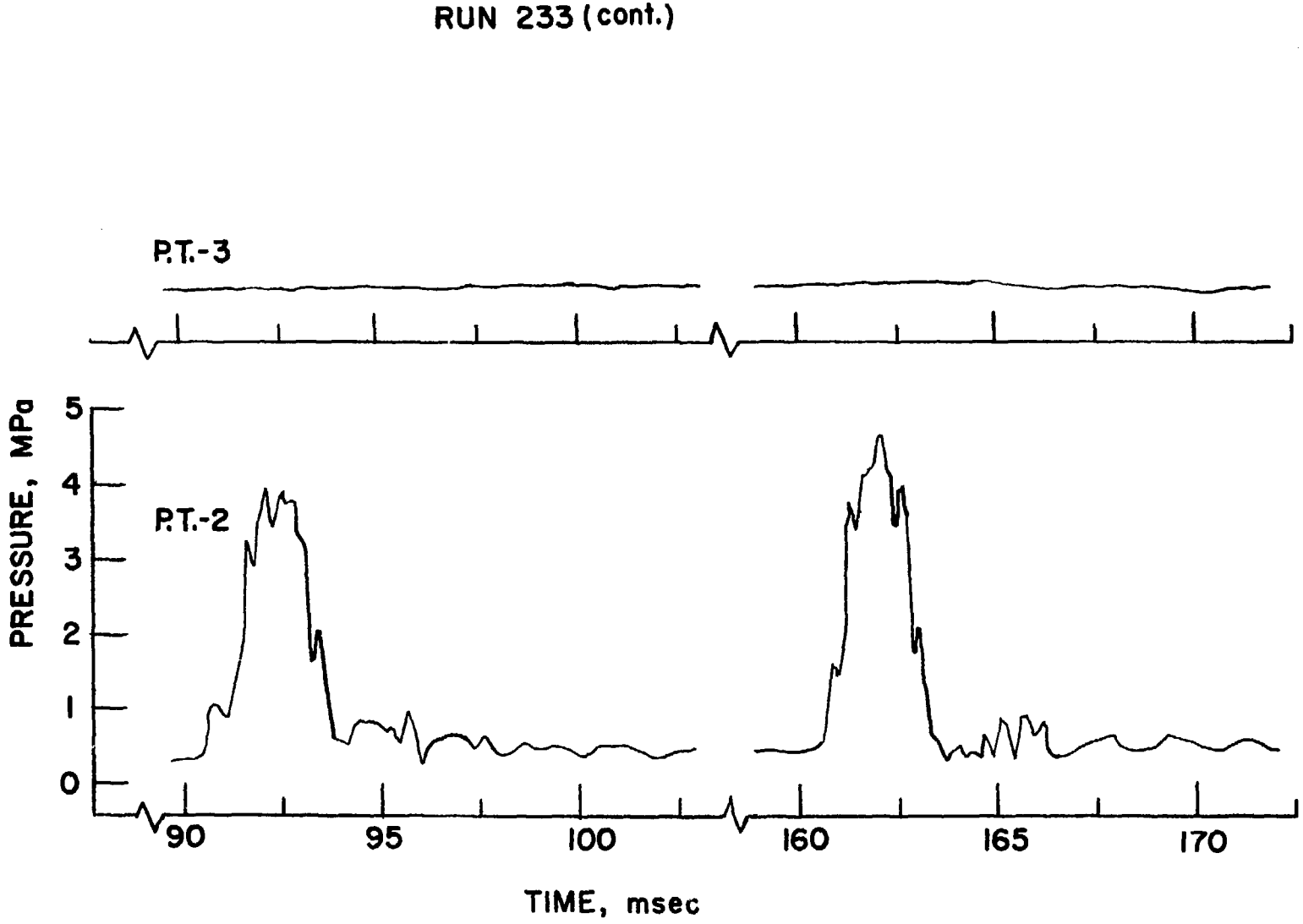

Fig. 5.34 Pressure History of Run 233 (contd.)

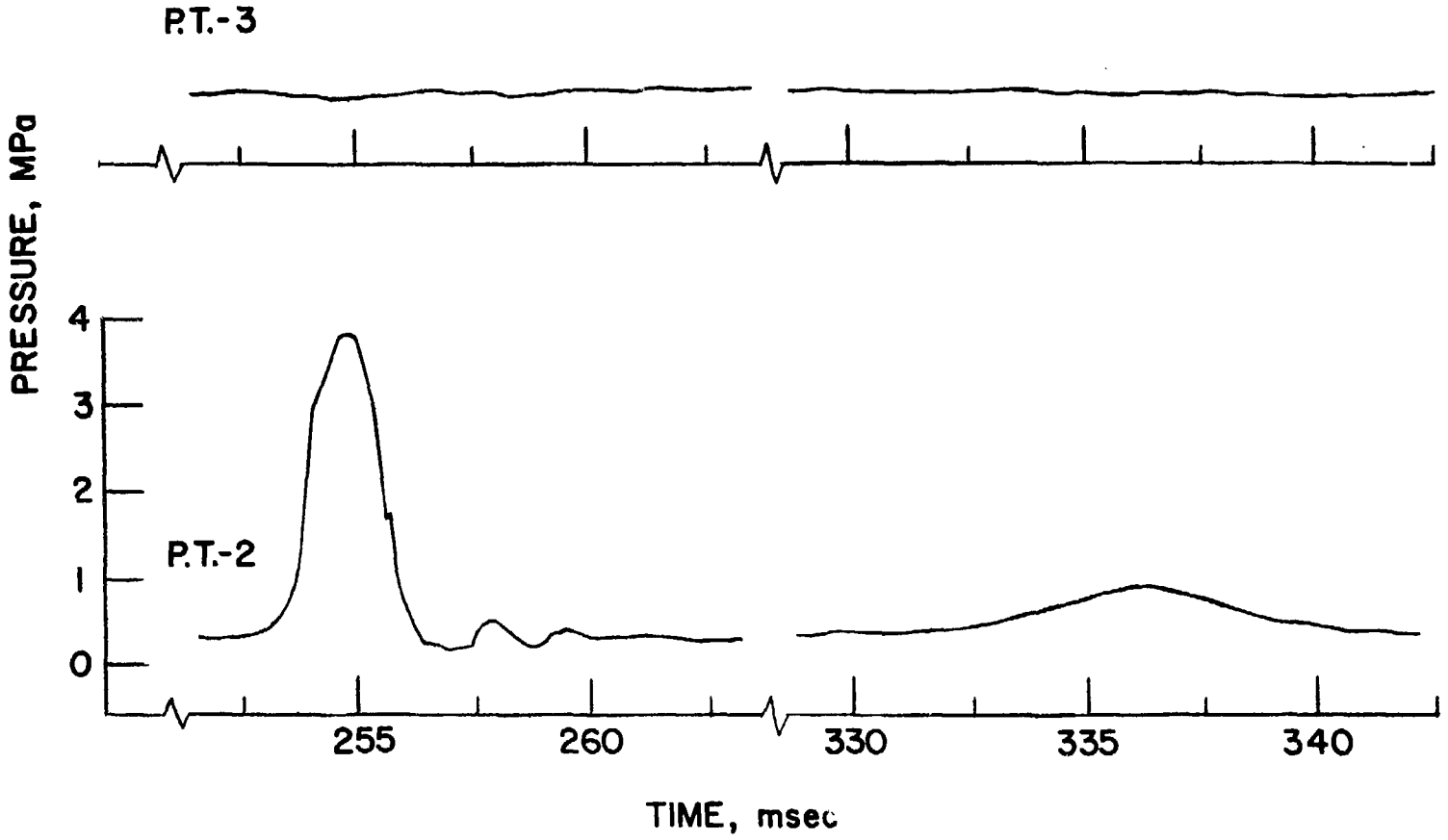

Fig. 5.34 Pressure History of Run 233 (contd.)

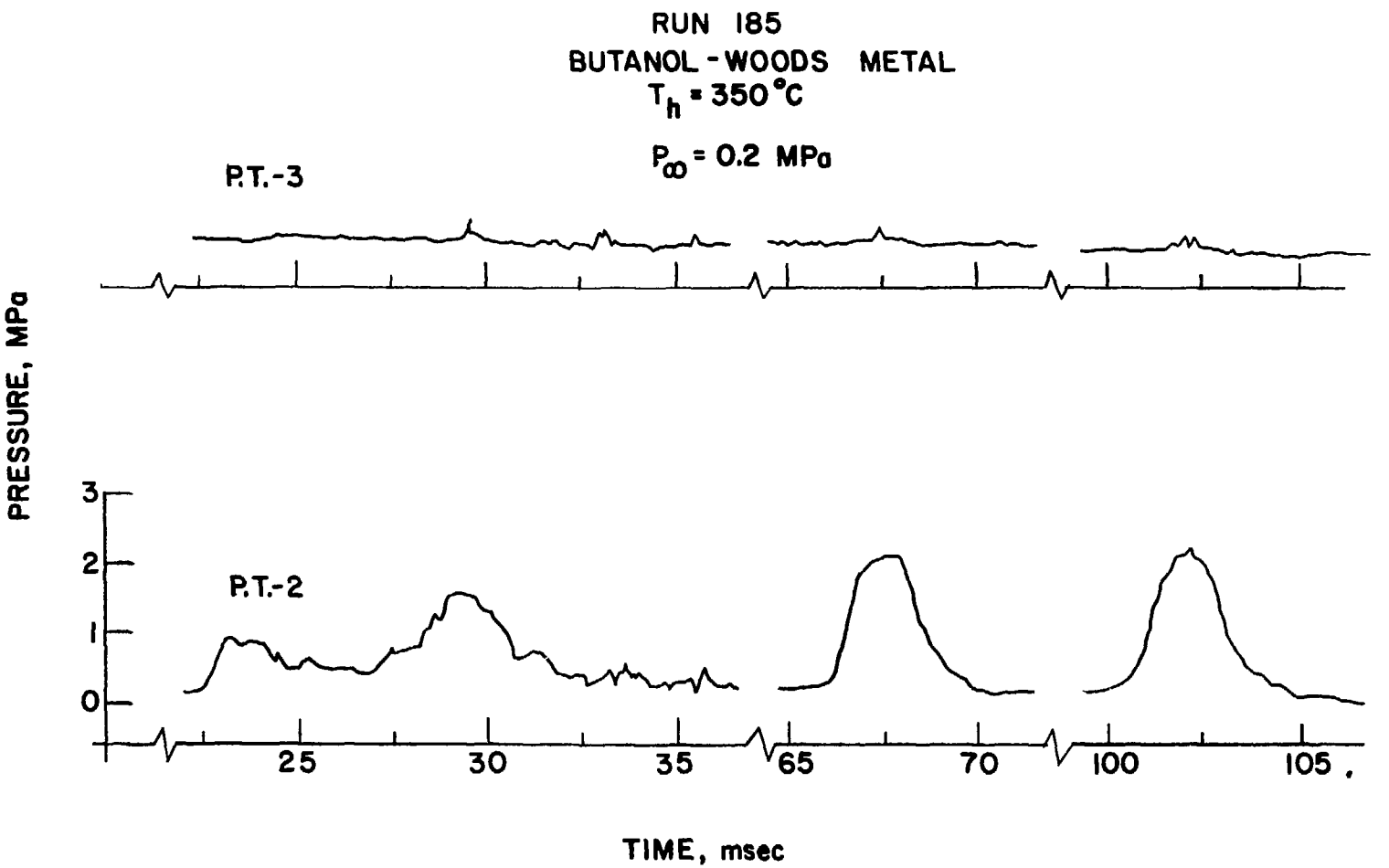

Fig. 5.35 Pressure History of Run 185

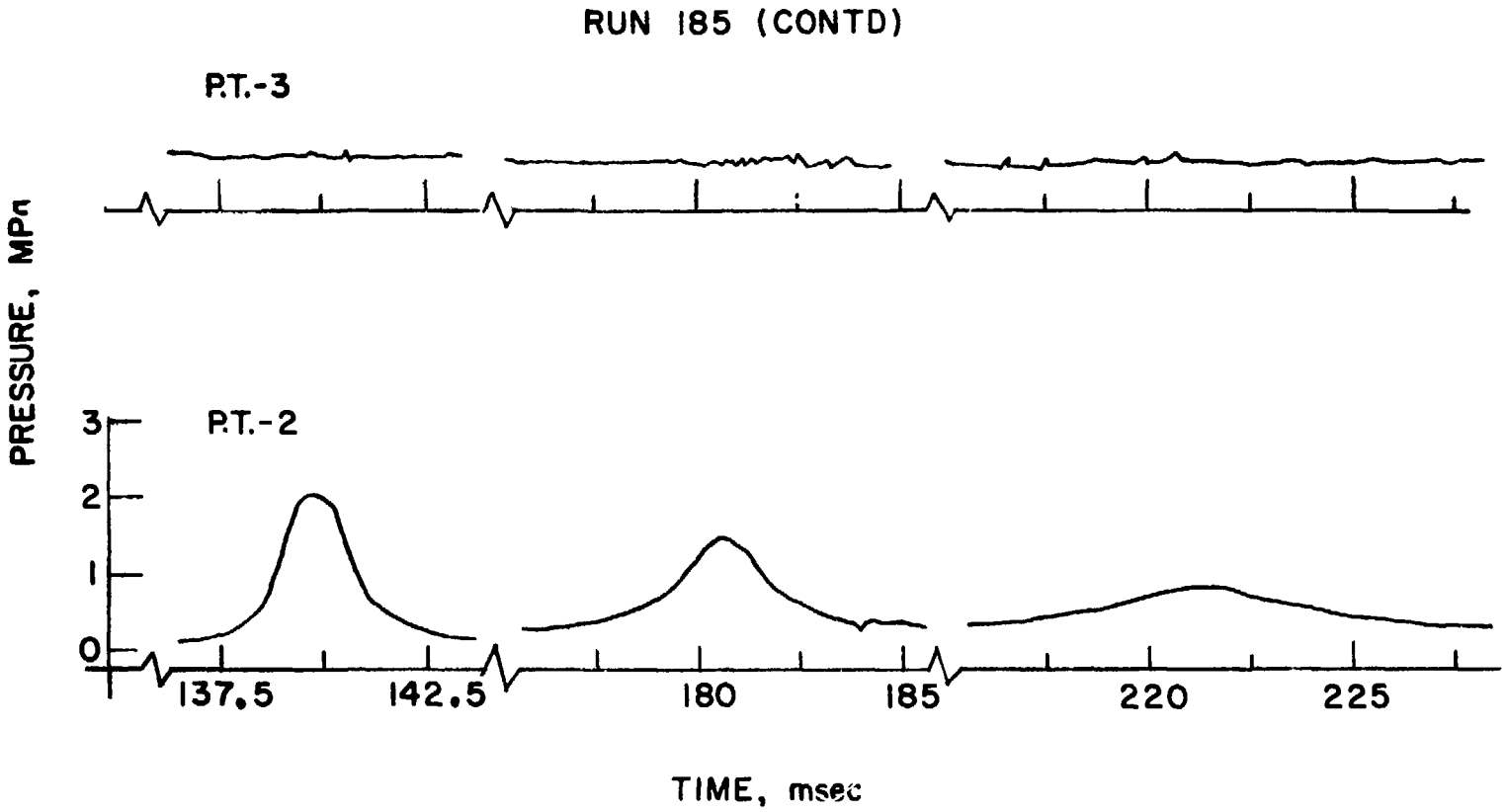

Fig. 5.35 Pressure History of Run 185 (contd

KCl was used as the hot liquid. The eutectic mixture is 44.2 wt % LiCl and 55.8 wt % KCl with a melting point of 352°C and it was kept in a glove box under an argon atmosphere.

The usual procedure of melting, assembling, and heating under vacuum to the desired temperature, resulted in premature rupture of the thin diaphragm. This most likely resulted from corrosion which weakened the diaphragm. To minimize corrosion, the salt was melted in the lower tube and was heated to the desired temperature. Only then the set up was assembled, vacuum was pulled, and the run was conducted.

Since the major interest was not to find the threshold temperatures, but rather the possibility of depressing an interaction under pressure (see Sect. 5.7), only four experiments were conducted with the thin diaphragm. The results of those runs are also tabulated in Appendix E. One run was conducted at a salt temperature of 410°C (run 220) and resulted in low yield thermal interaction. At 600°C, three runs were conducted, which resulted in thermal interaction. The shapes of all those pulses are given in Fig. 5.36. In all the runs the interactions had a considerable delay time after the first impact and produced a sharp pulse with $\sim$0.2 msec rise time and duration of $\sim$0.3 msec which is considerably less than the acoustic relief time of the system. The temperature history of two runs (226 and 228) is shown in Fig. 5.37. In run 224 (T_h = 600°C) the volume below the diaphragm was evacuated only to $\sim$0.5 Bar, which resulted in a very long delay time before interaction was observed (1108.75 msec), but here also the pulse was very sharp and short. The pressures produced by these interactions were relatively very low (0.86-1.93 MPa).

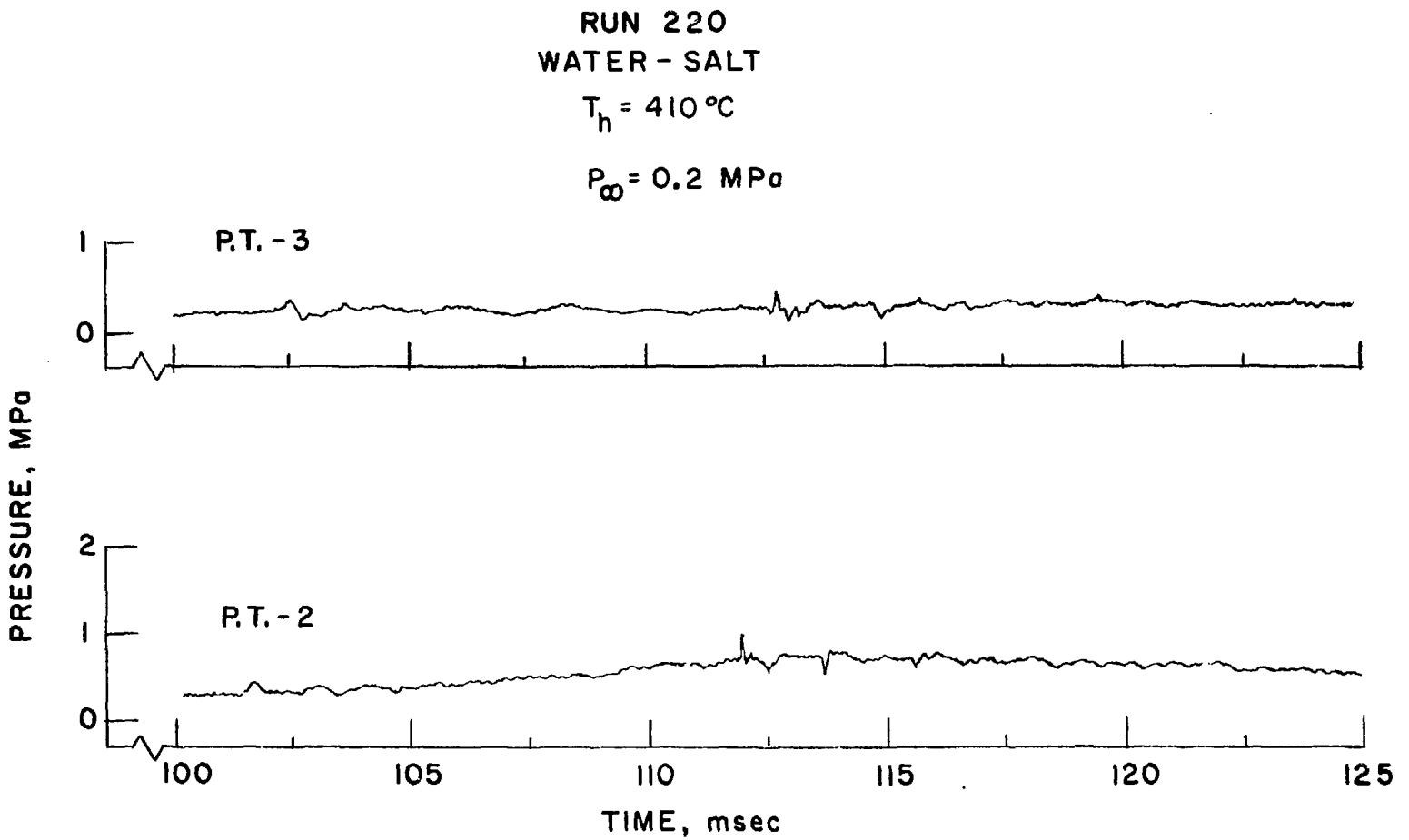

Fig. 5.36a Pressure History of Run 220

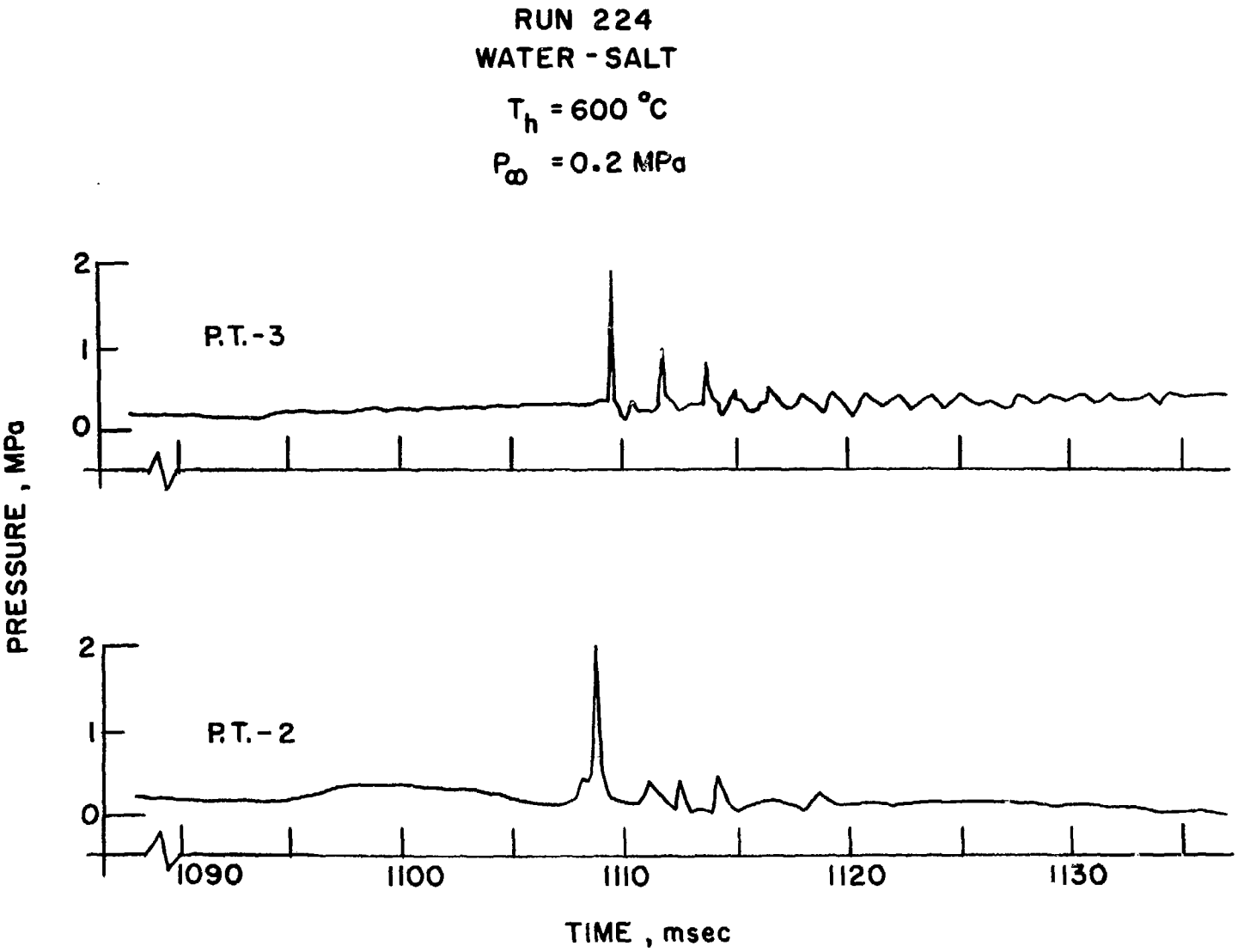

Fig. 5.36b Pressure History of Run 224

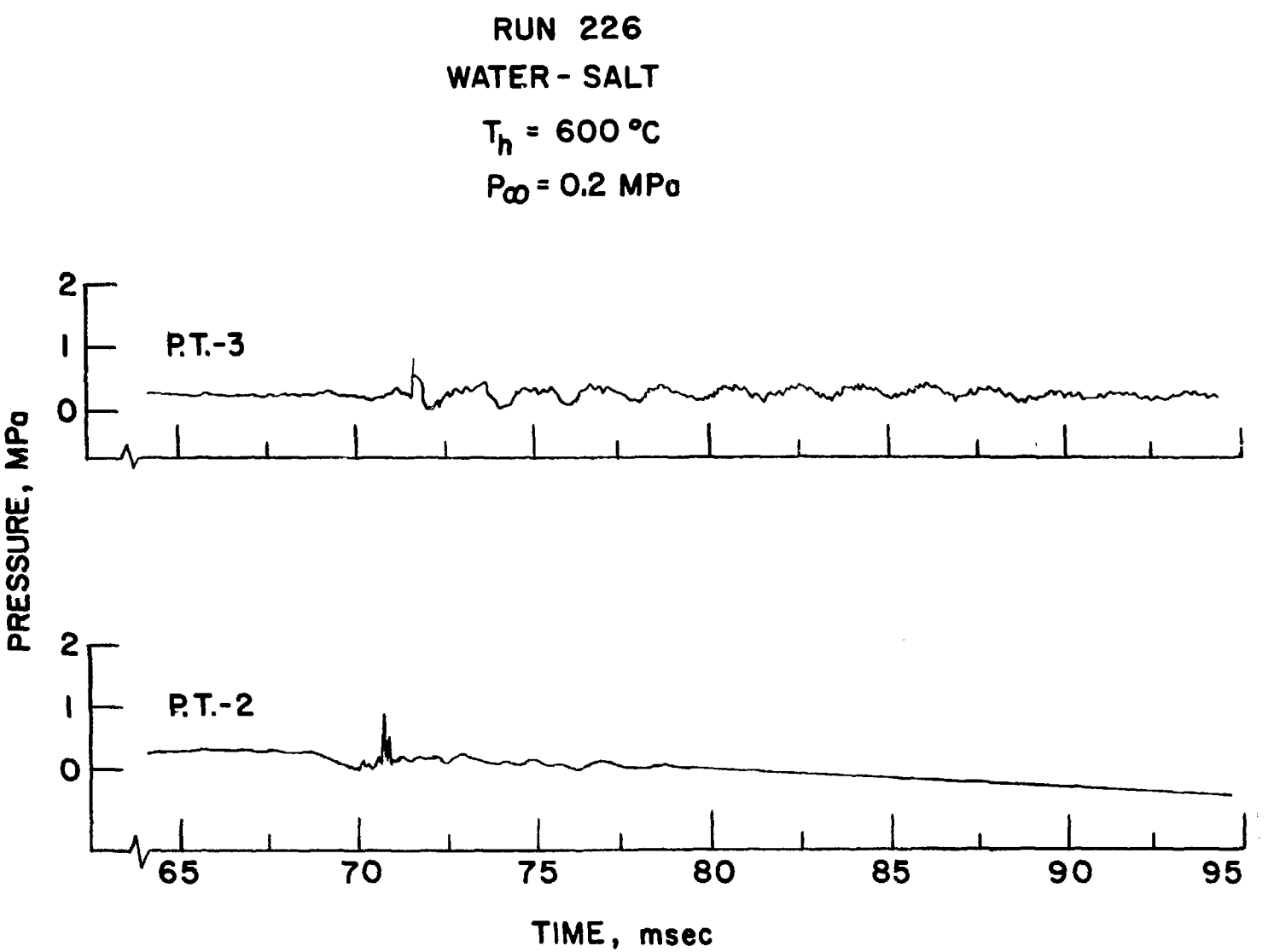

Fig. 5.36c Pressure History of Run 226

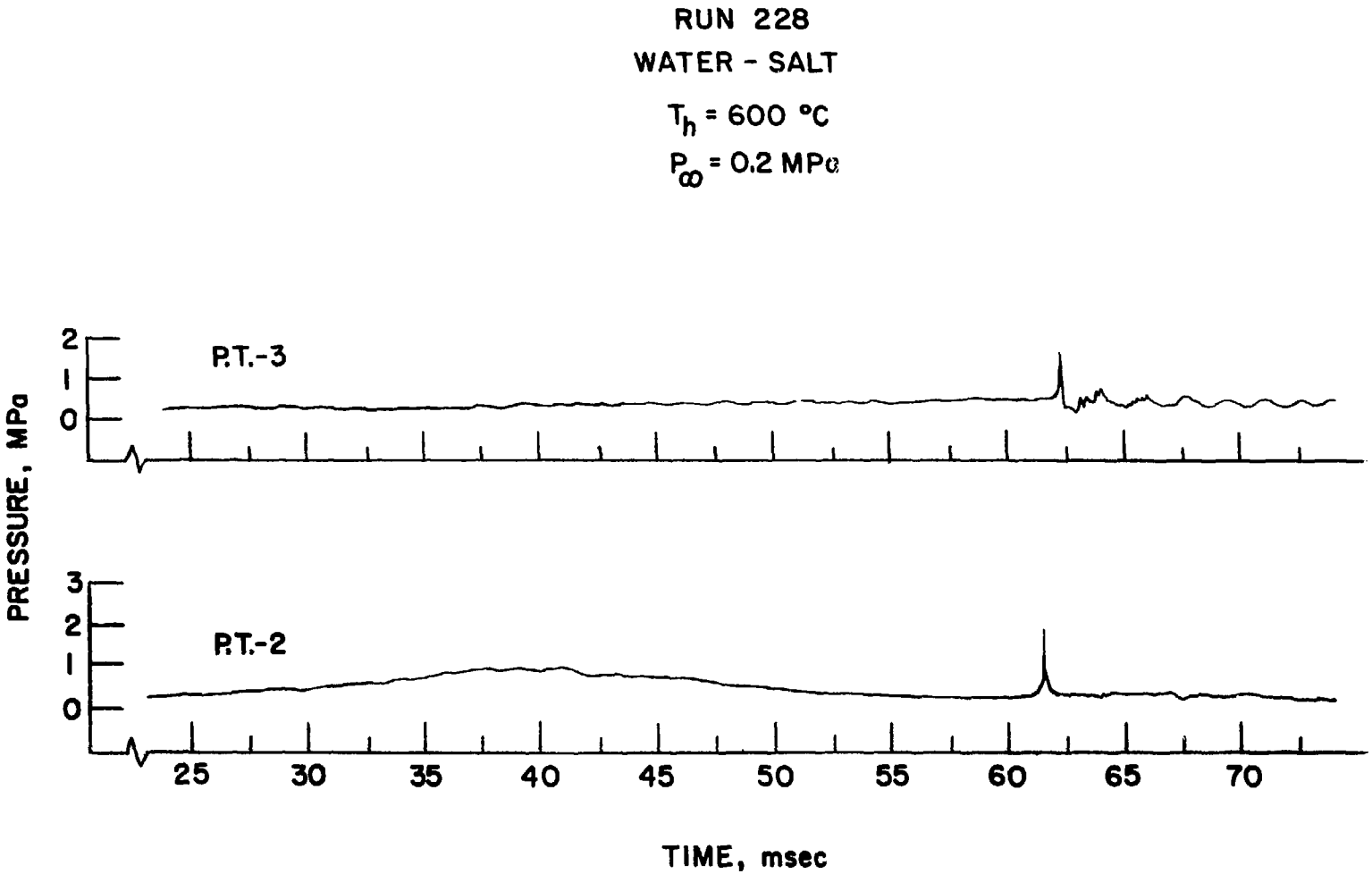

Fig. 5.36d Pressure History of Run 228

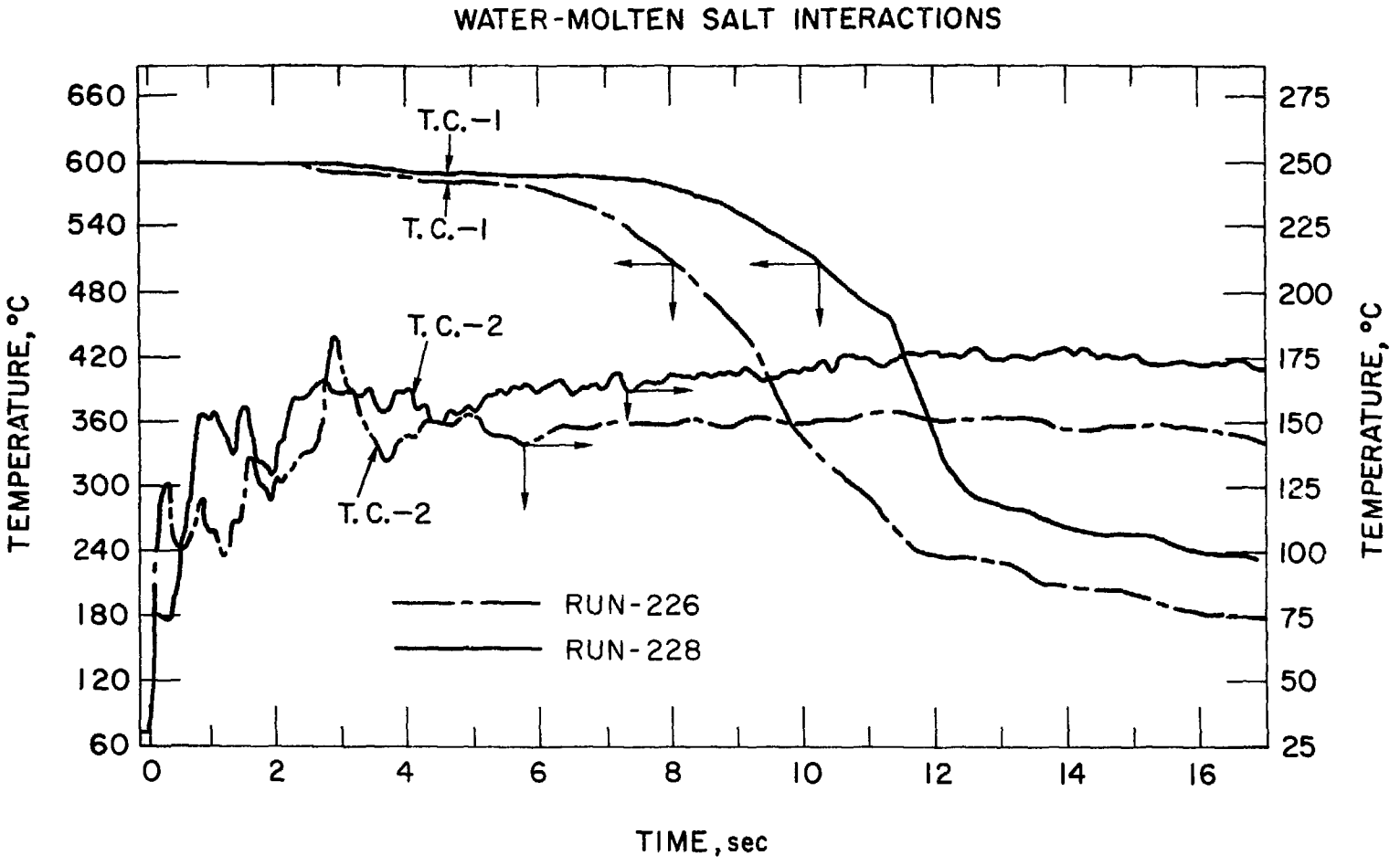

Fig. 5.37 Temperature History of Runs 226 and 228

5.7 Experiments at Elevated Pressures

Experiments were conducted using different diaphragm thicknesses which resulted in various initial pressures in the system (driving pressure). Experiments were conducted with water-Wood's metal, n-butanol-Wood's metal, and water-molten salt (LiCl + KCl) and the results are given in Appendix F.

The water-Wood's metal runs were performed in Region C (T_h > 305°C) where large-scale interactions had occurred for a low system pressure (0.2 MPa). As is clearly evident from Table F.1, the number of bounces is reduced to two or three only, and the pressure pulses corresponding to these bounces have a much longer rise time than was observed in the low pressure data, e.g., Fig. 5.38. Plotting P_{max}/P_i and I_{exp}/I_{th} as a function of bulk temperature for water-Wood's metal (Figs. 5.39-5.40) show that the elevated driving pressure experiments yield lower pressures and impulses than those performed with a 0.2 MPa driving pressure. Experiments at elevated pressures with butanol-Wood's metal resulted in similar features as with water, i.e., the number of bounces was reduced, and the pressure magnitude and pulse duration indicated that no thermal interaction had occurred (Figs. 5.41-5.43). However, when plotting the relative pressures and impulses (Figs. 5.44-5.45) the result is not as clear-cut as for water, which is what was expected recalling the relatively low pressures and impulses obtained for butanol with 0.2 MPa driving pressure. Considering the temperature history of runs 229 and 231 shown in Fig. 5.46 and comparing the pressure shapes to the one obtained at T_h = 110°C (Fig. 5.47) it is highly suggestive that no explosive thermal interactions have occurred with butanol at elevated pressures.

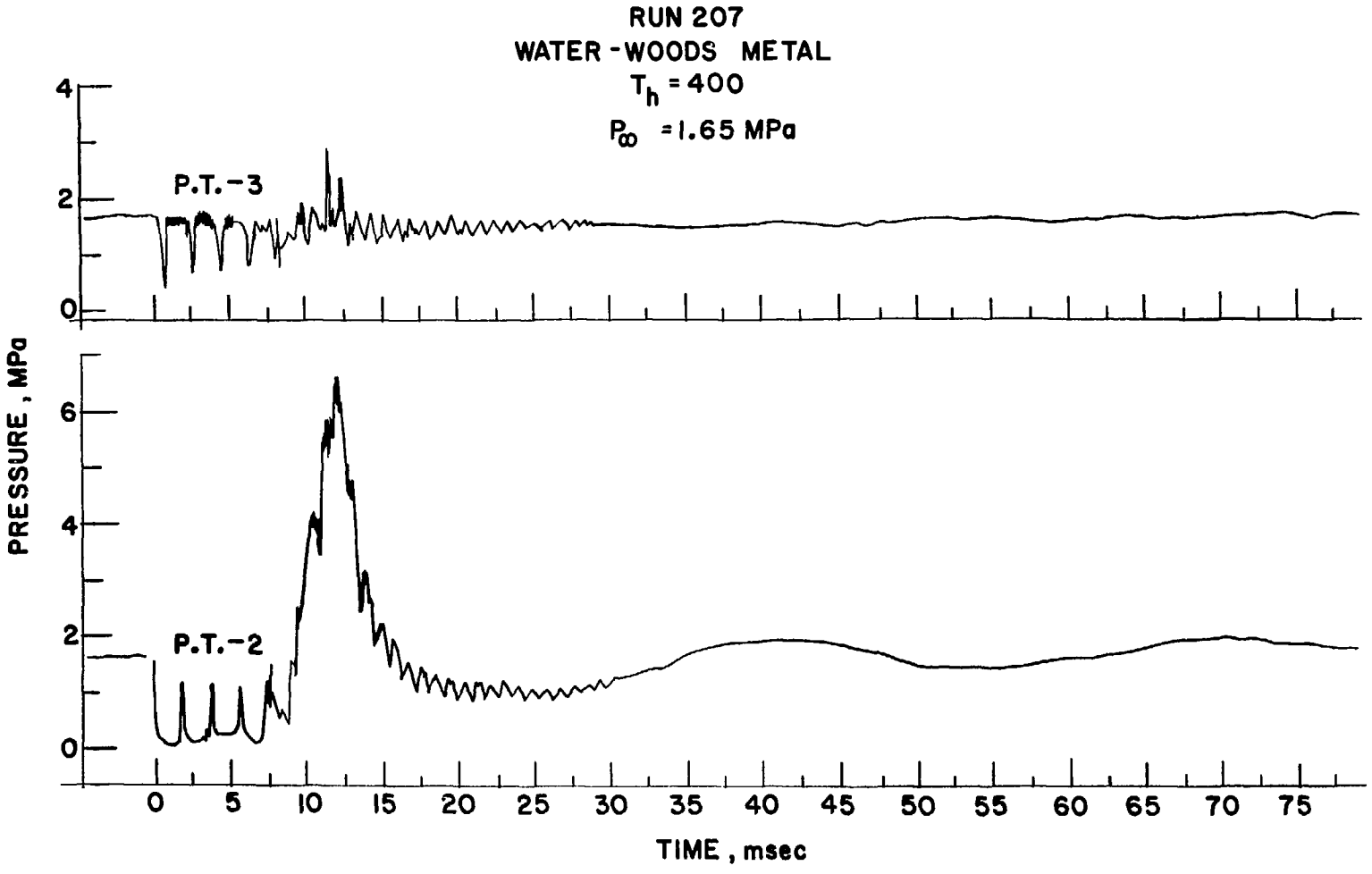

Fig. 5.38 Pressure History of Run 207

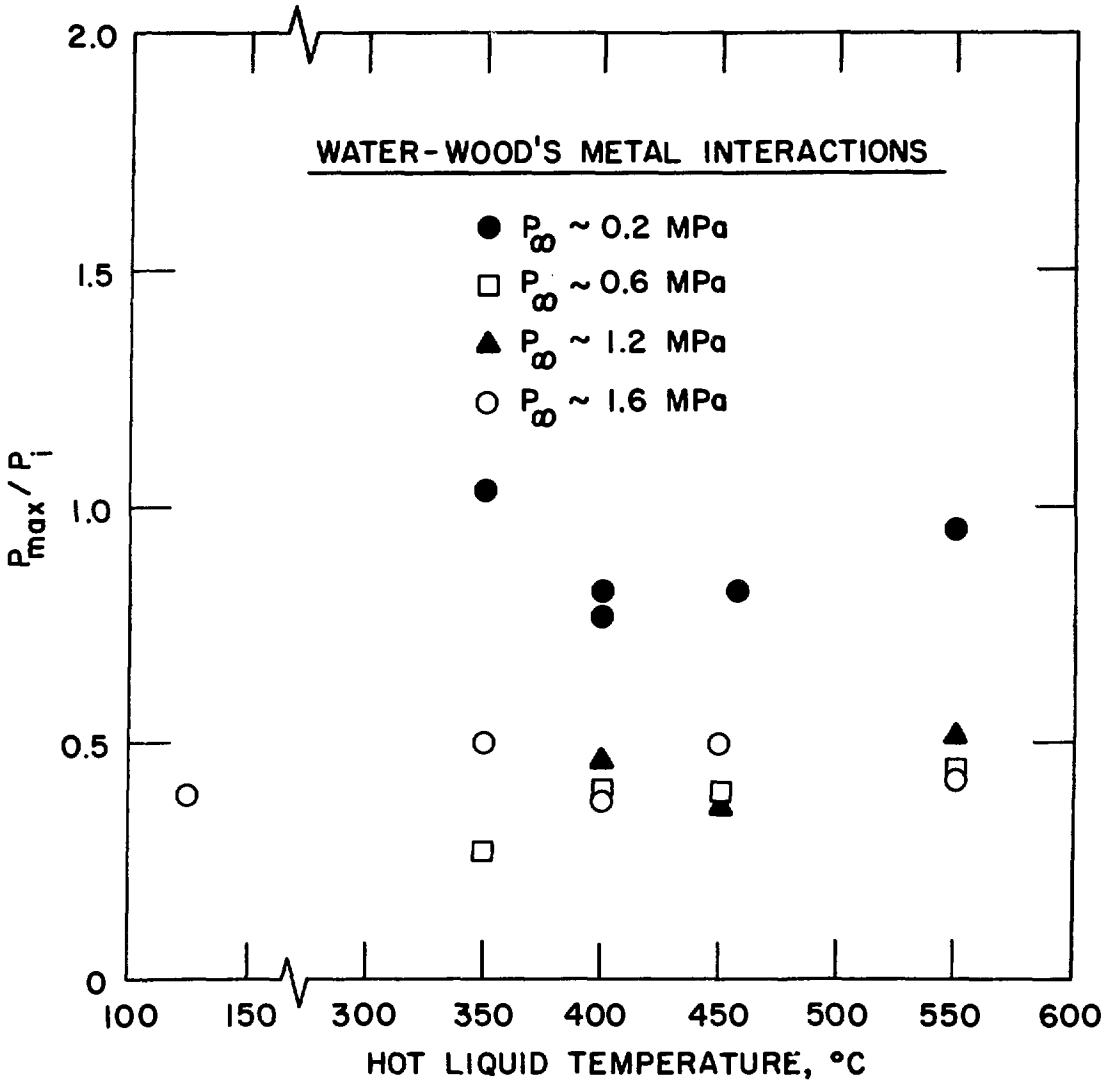

Fig. 5.39 Pressure of Water-Wood's Metal Interactions at Elevated Driving Pressure

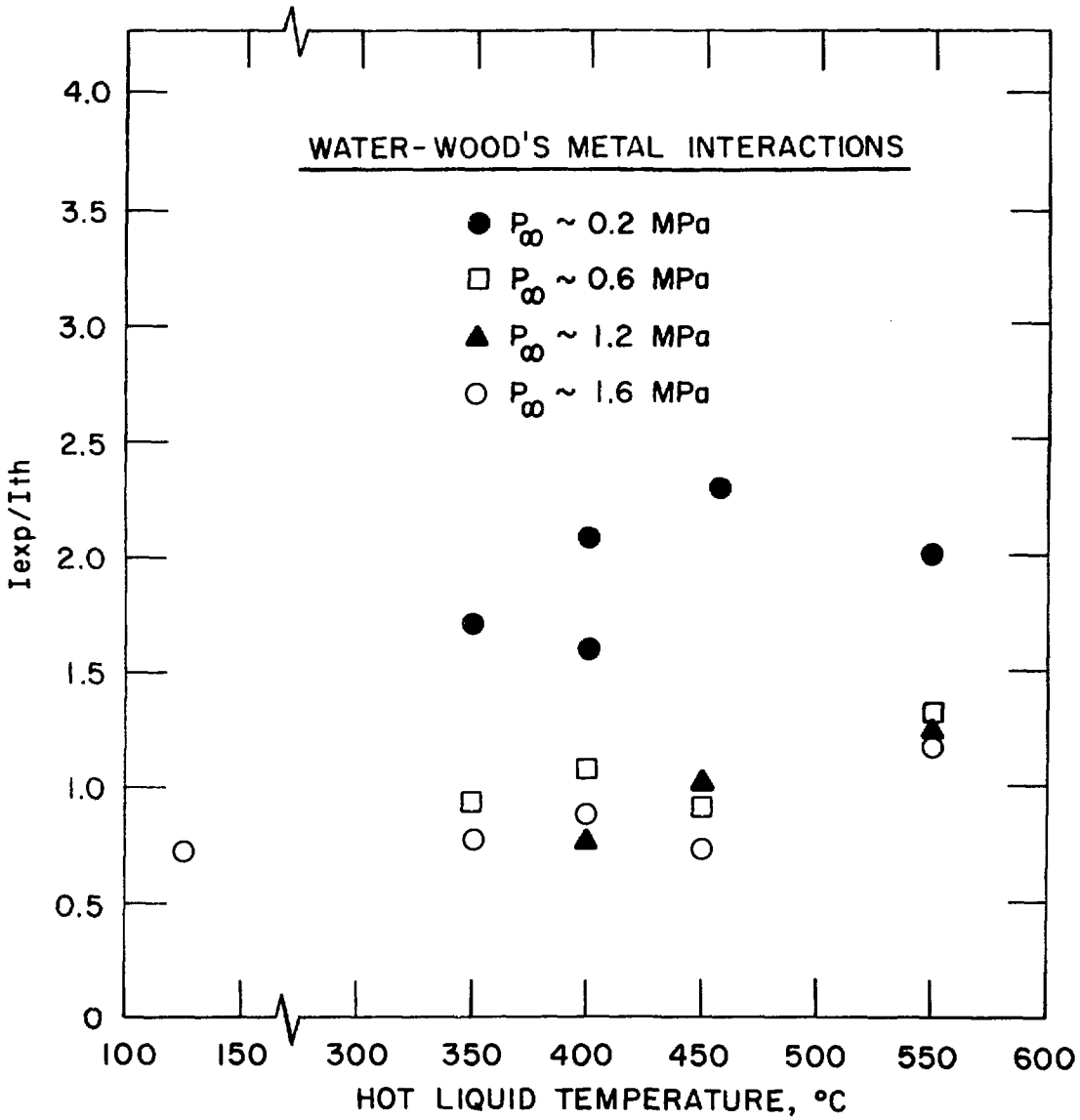

Fig. 5.40 Impulse of Water-Wood's Metal Interactions at Elevated Driving Pressure

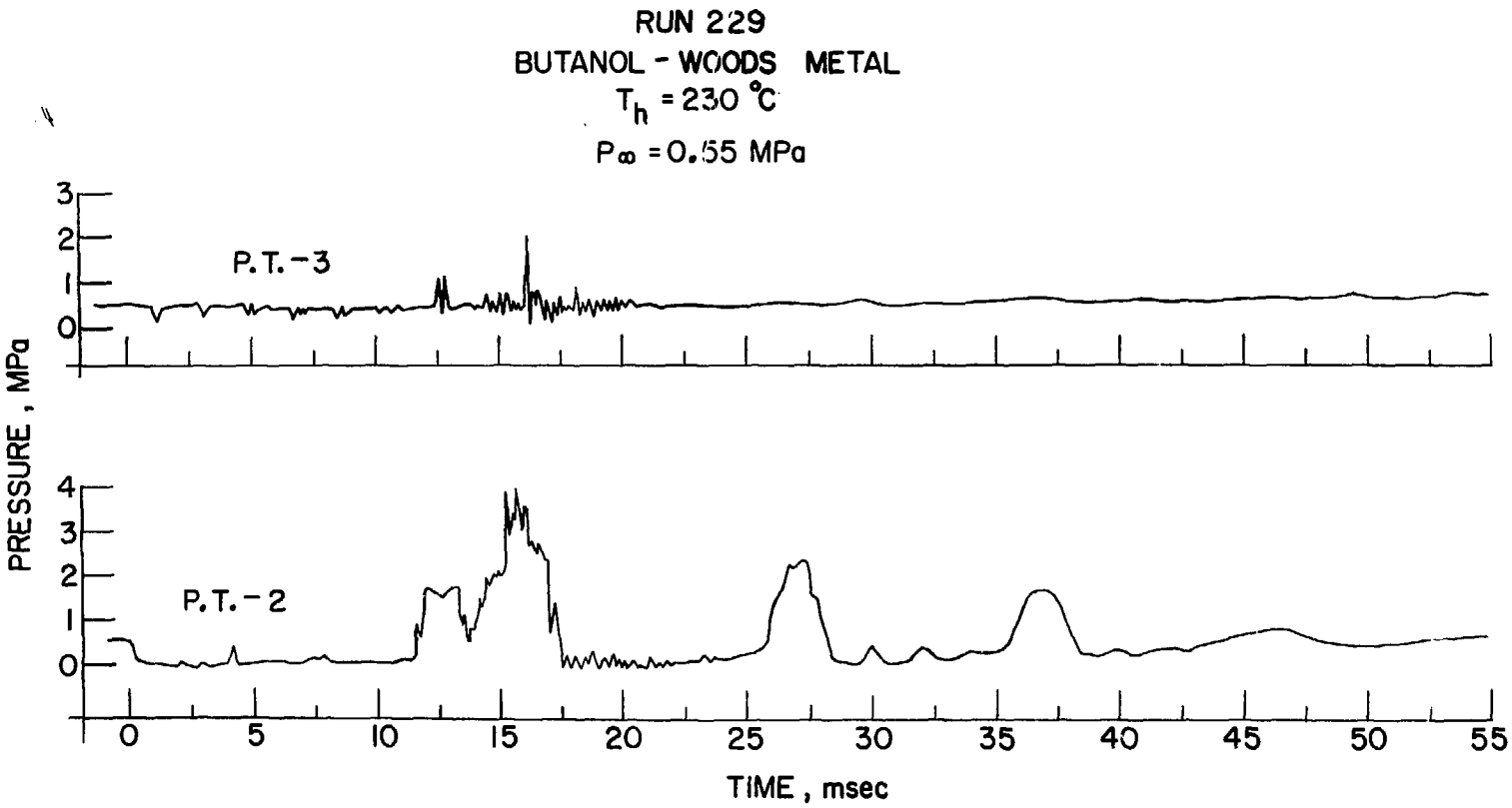

Fig. 5.41 Pressure History of Run 229

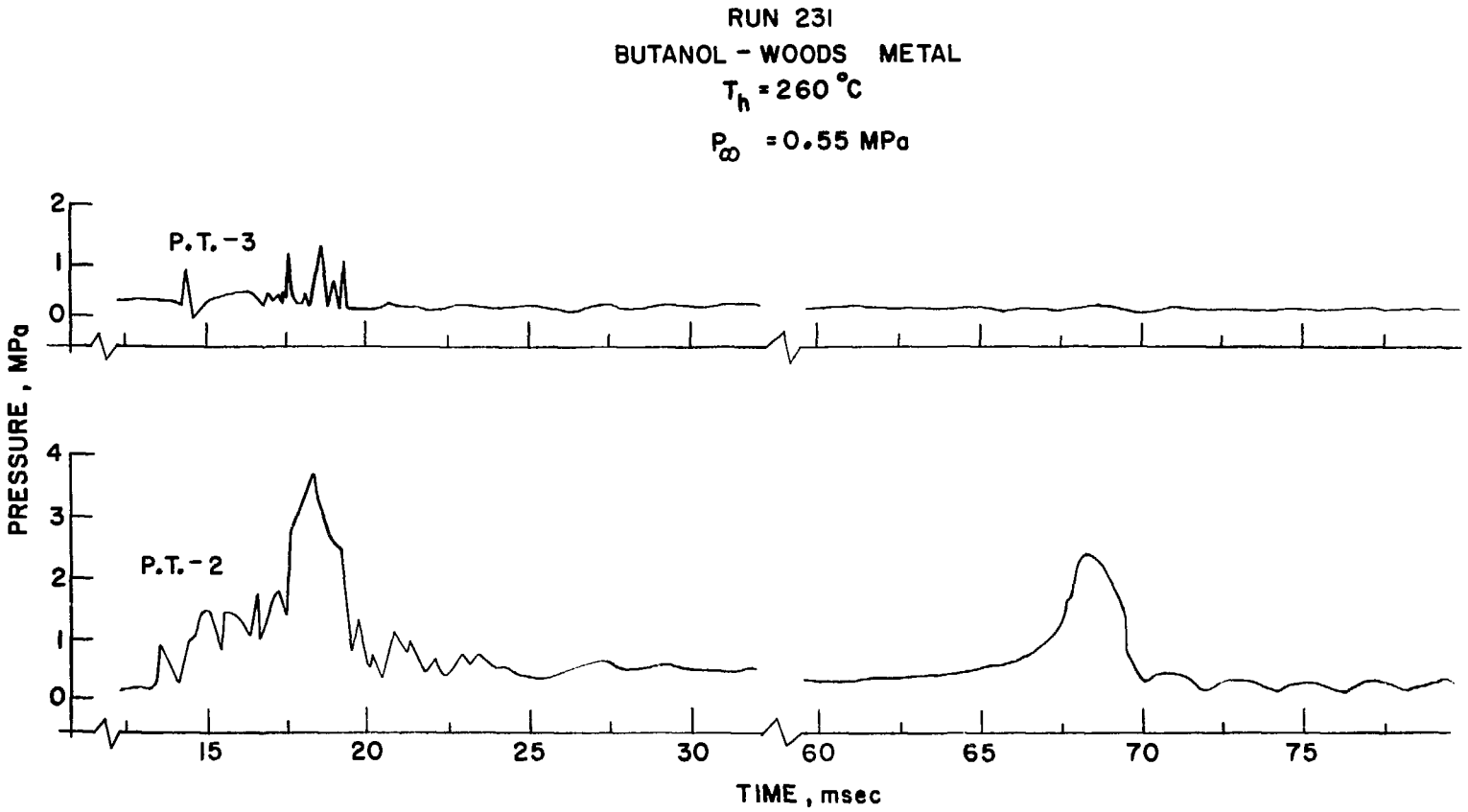

Fig. 5.42 Pressure History of Run 231

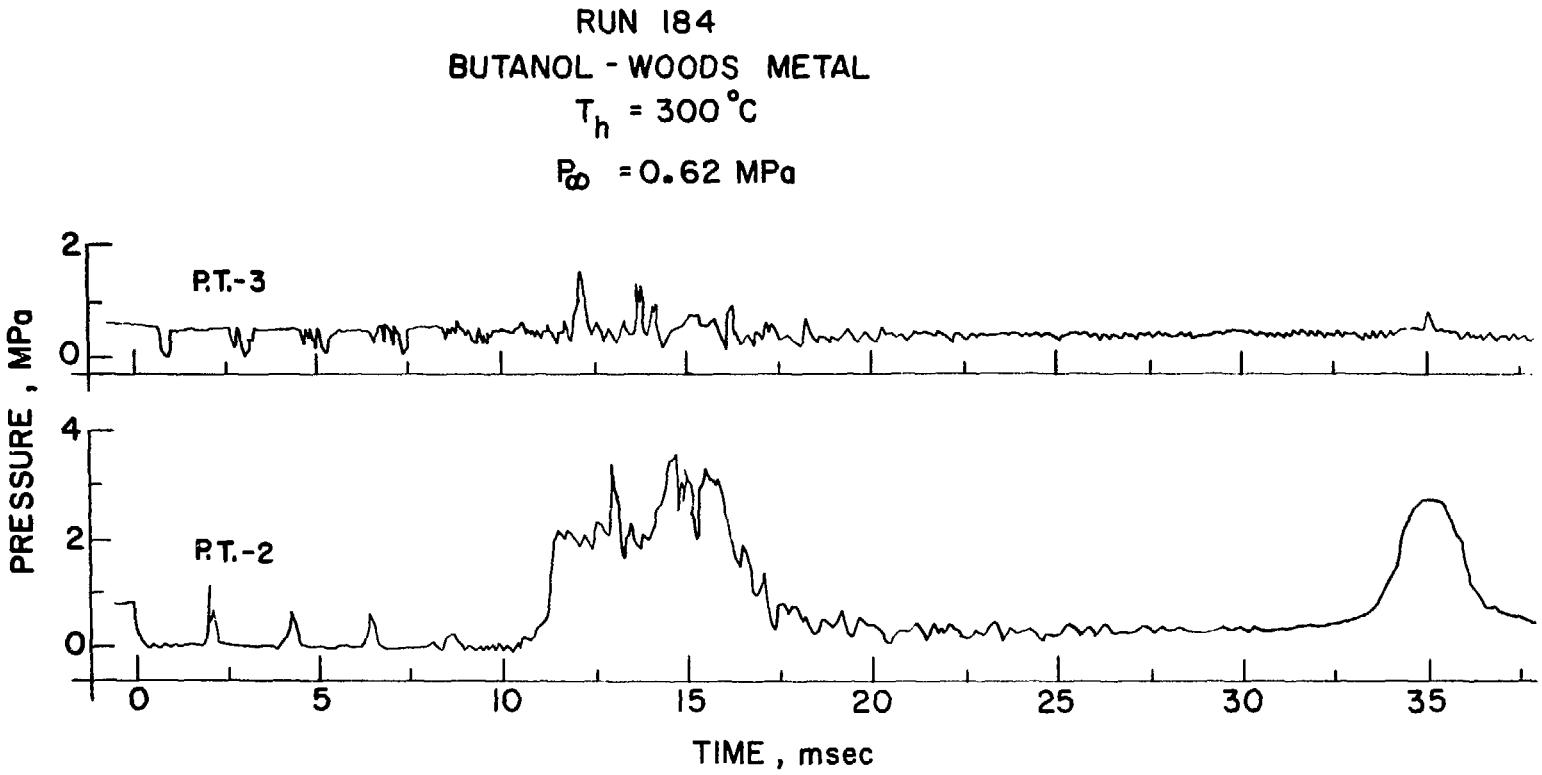

Fig. 5.43 Pressure History of Run 184

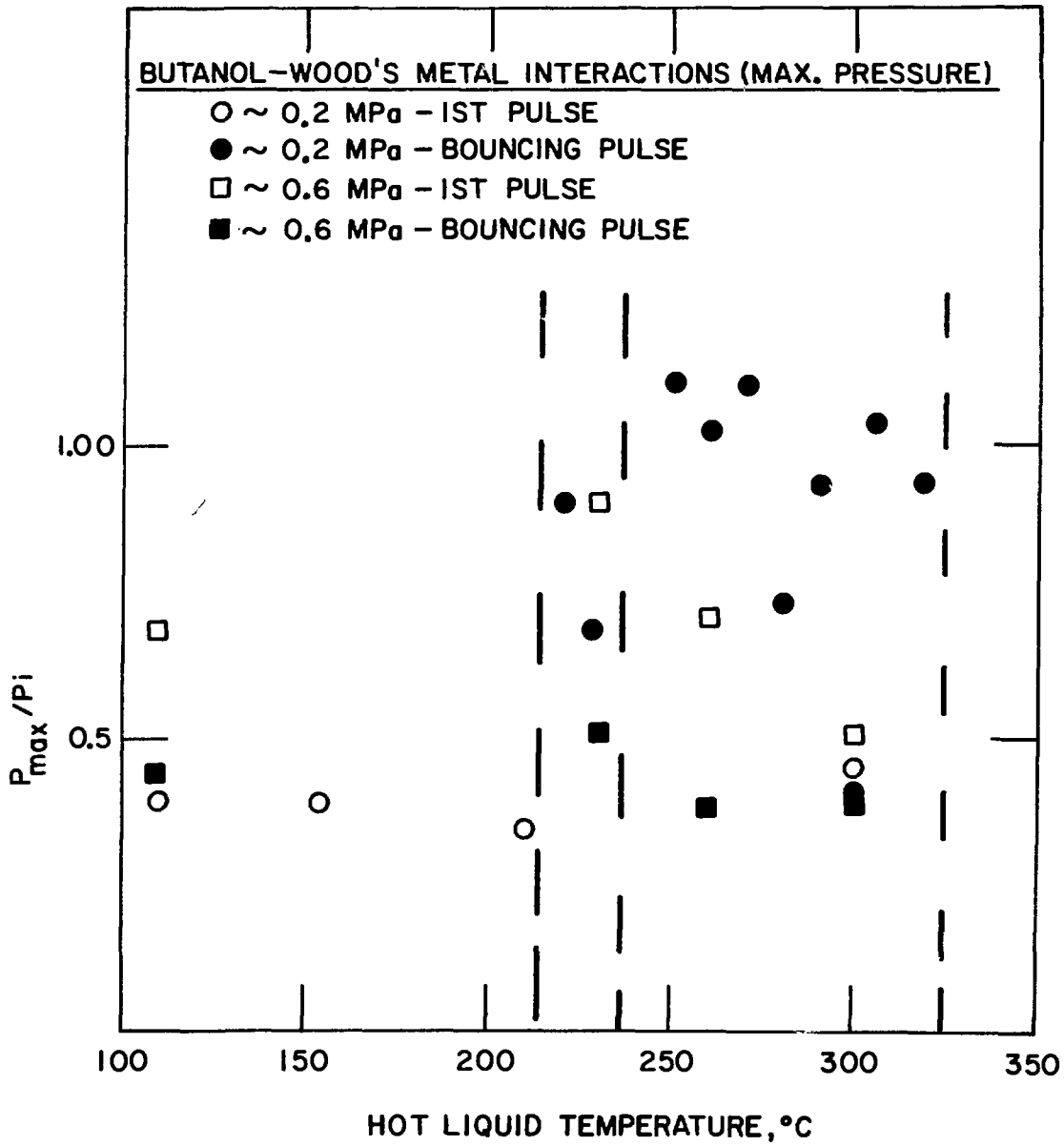

Fig. 5.44 Pressure of Butanol-Wood's Metal Interactions at Elevated Driving Pressure

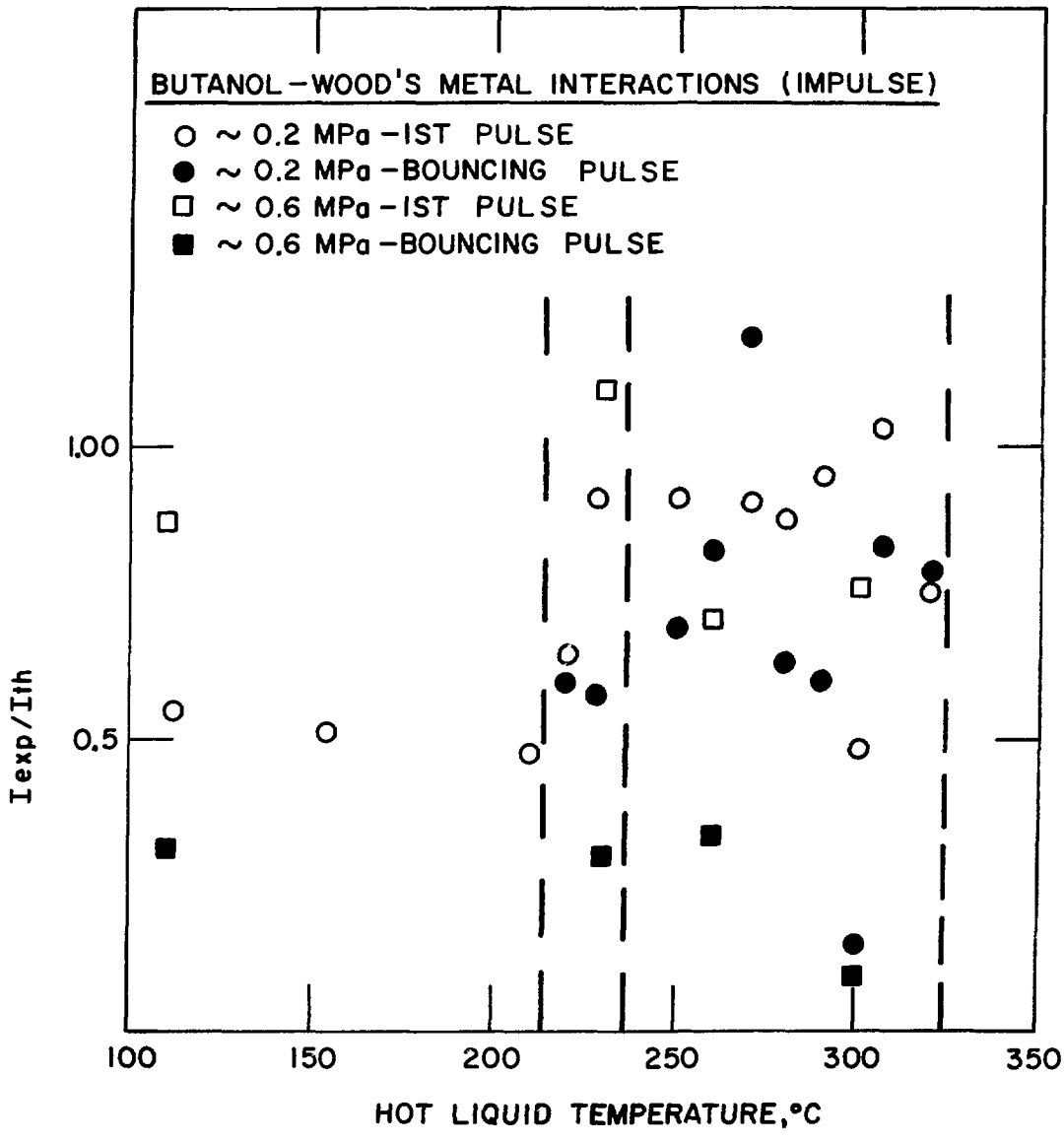

Fig. 5.45 Impulse of Butanol-Wood's Metal Interactions at Elevated Driving Pressure

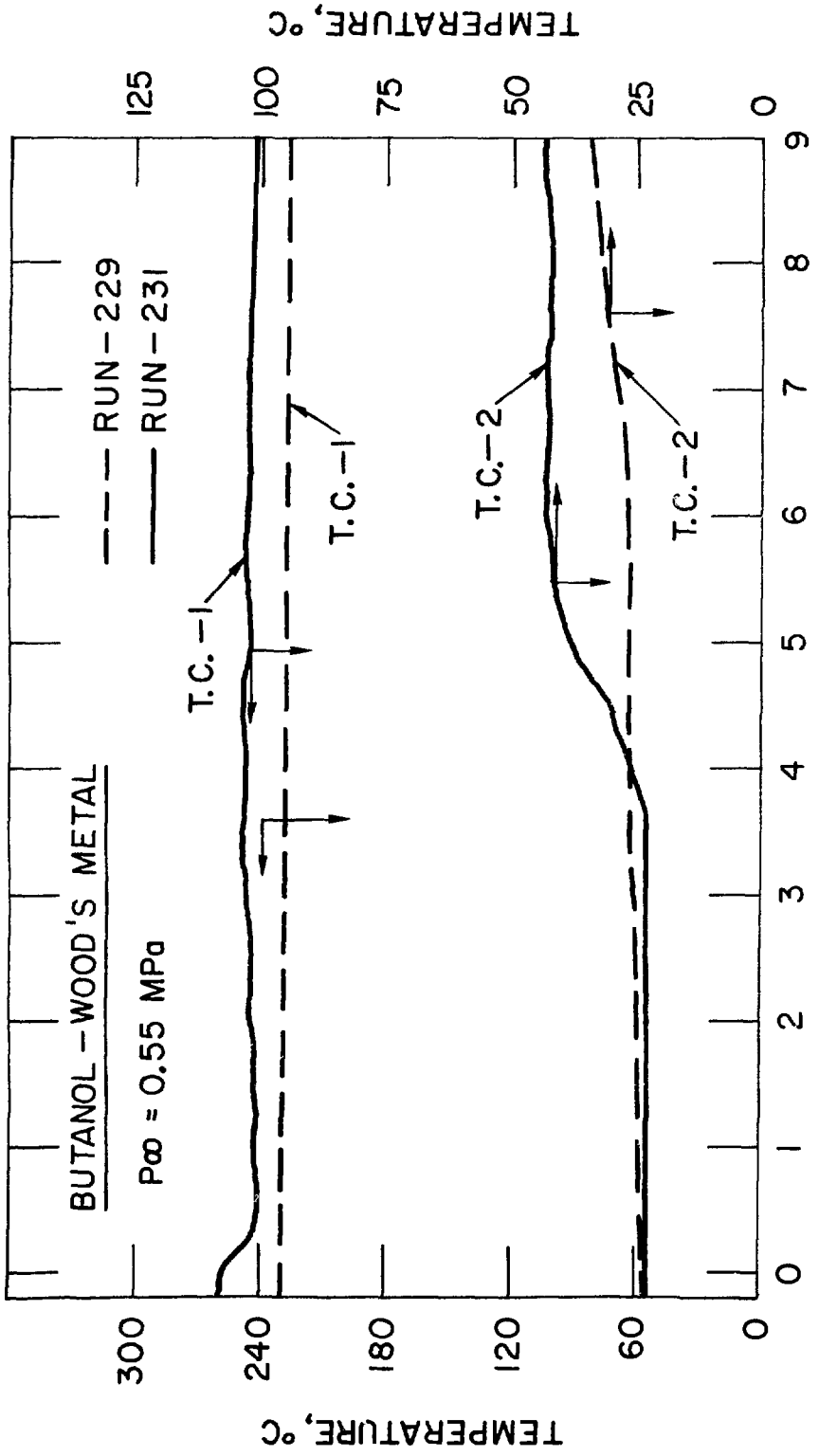

Fig. 5.46 Temperature History of Runs 229 and 231

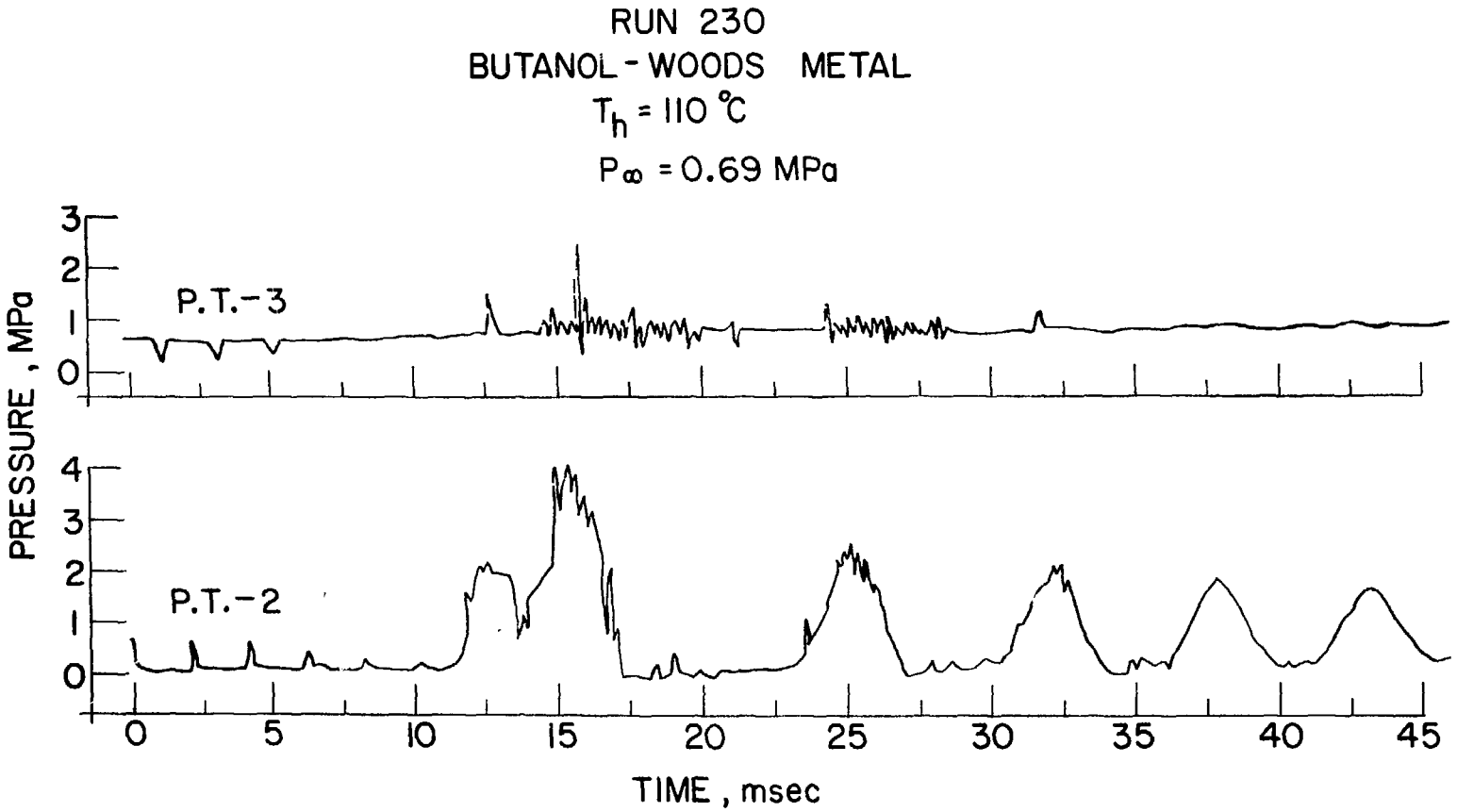

Fig. 5.47 Pressure History of Run 230

With water-molten salt it is clear that no explosive thermal interaction occurred, but rather slow vaporization, as is shown in Figs. 5.48-5.49. The results obtained with this system at elevated pressures (Table F.3 in Appendix F) are a good example of a large impulse production which does not indicate an explosive thermal interaction.

In the elevated pressure experiments we can notice the "ringing" process in the water and butanol. As is shown in Figs. 5.47, 5.49, and 5.50, the pressure magnitude of the expansion waves (shown in P.T.3), which are traveling from the lower column interface, are increasing on each consecutive reflection. The compression waves (shown in P.T.2) which are traveling from the upper column interface, are decreasing on each consecutive reflection. Thus, after few reflections the pressure profile in the column is almost linear, as was assumed by the inertial representation of the column acceleration behavior (Sect. 5.1). The rapid decay of the acoustic waves explains why the "ringing" process was not noticed in experiments with low driving pressures, i.e., P_{∞} = 0.2 MPa. The wave attenuation is probably because of dissipation in bubbles nucleated from previously dissolved air, wall friction and/or interferences by the liquid boundary layer, instrumentation, and vacuum lines. Note that the wave attenuation is not due to pressure changes in the interaction and upper chambers (during most of the liquid motion the pressures remain constant as is evident from the pressure output). However, in the last stage of the liquid motion in some of the runs the pressure in the interaction chamber increases, which is due to existing vapor compression (see discussion in Sect. 6.2).

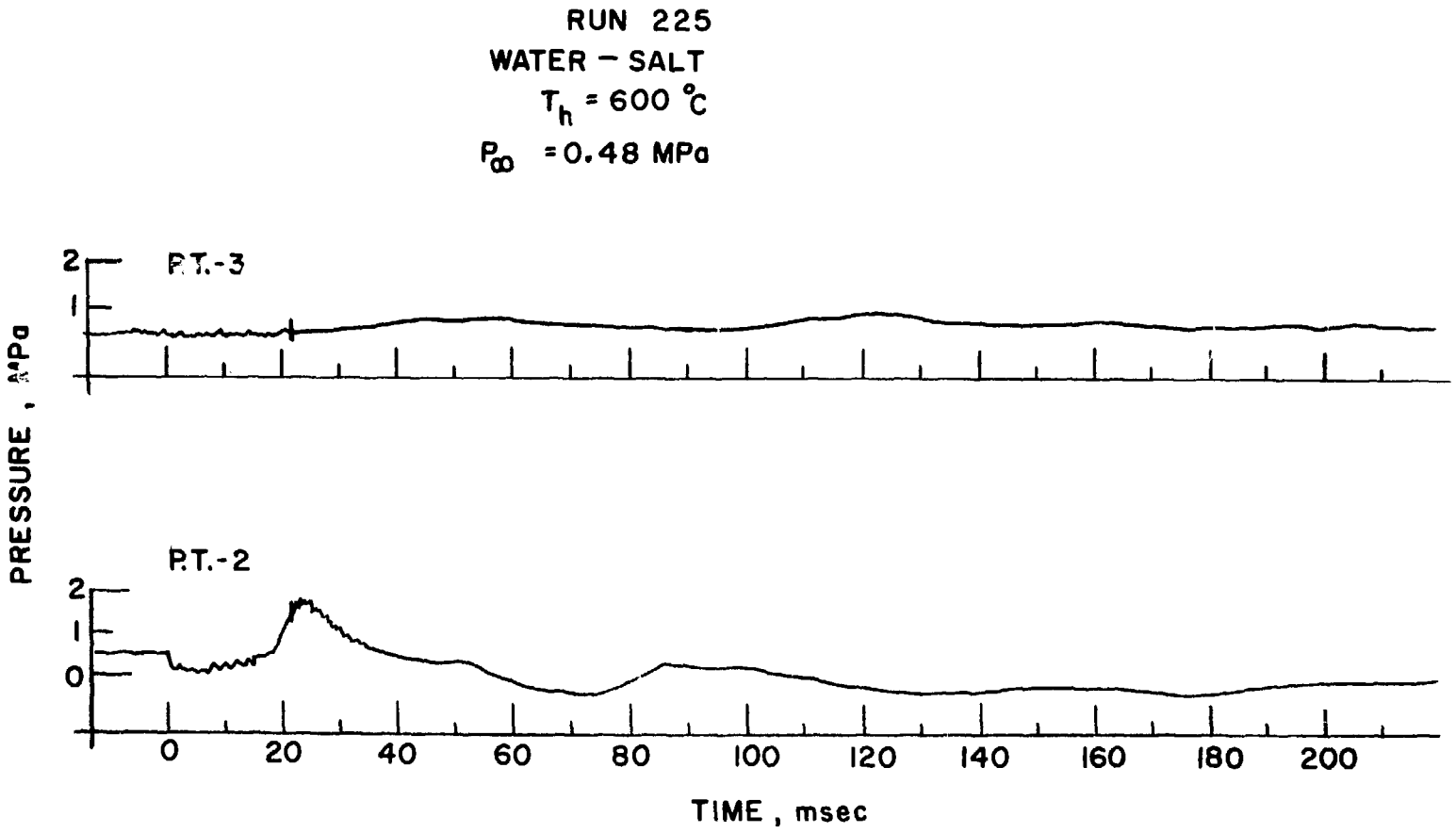

Fig. 5.48 Pressure History of Run 225

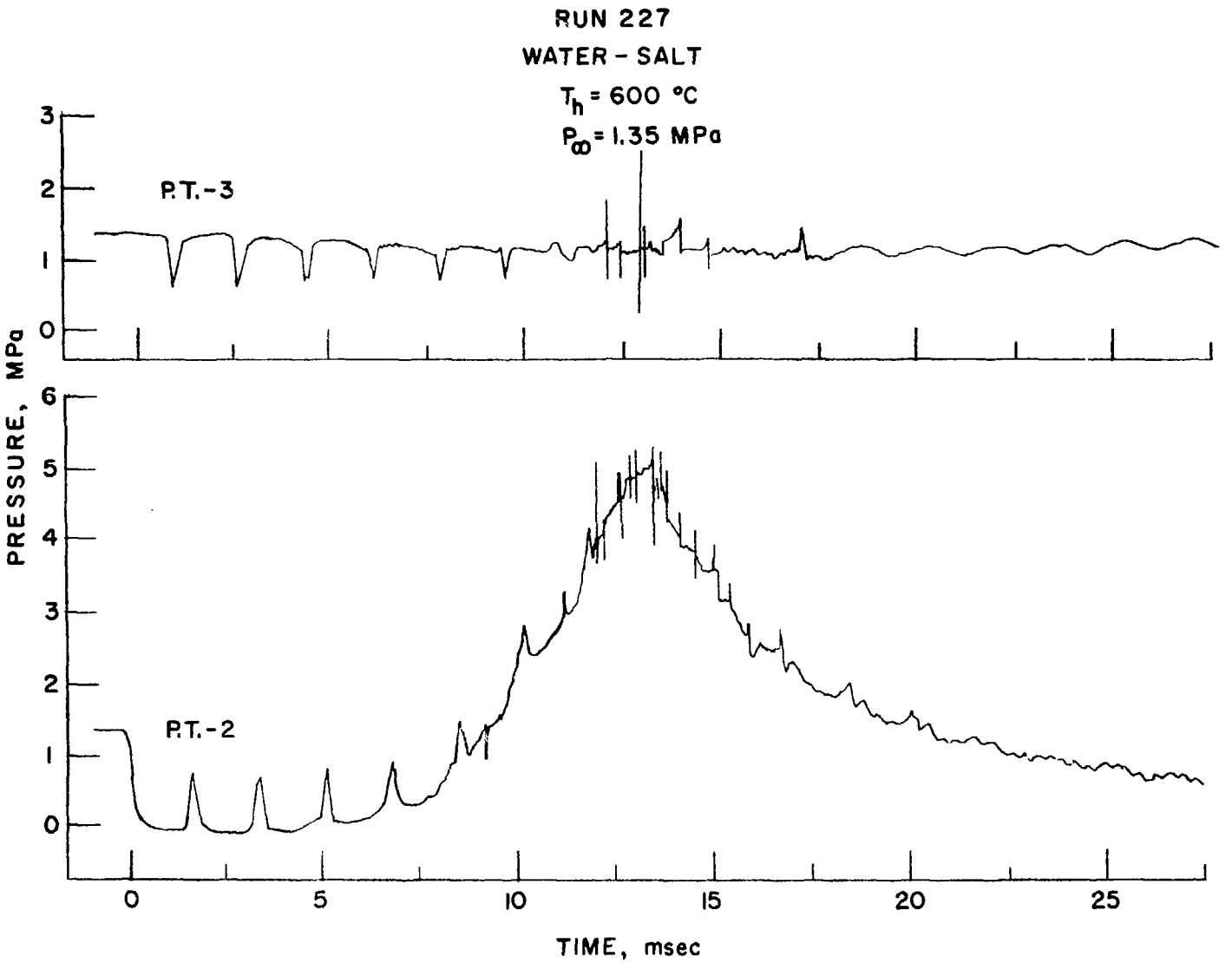

Fig. 5.49 Pressure History of Run 227

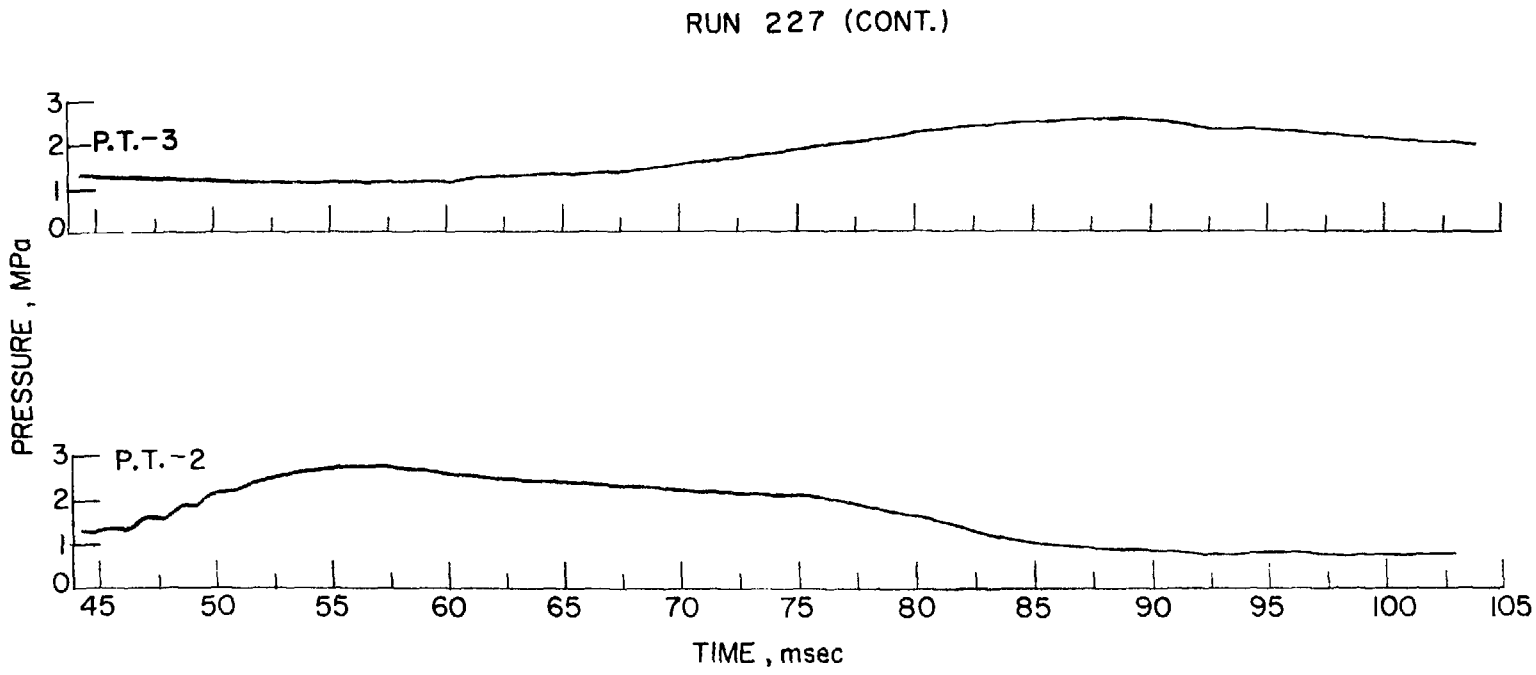

Fig. 5.49 Pressure History of Run 227 (contd.)

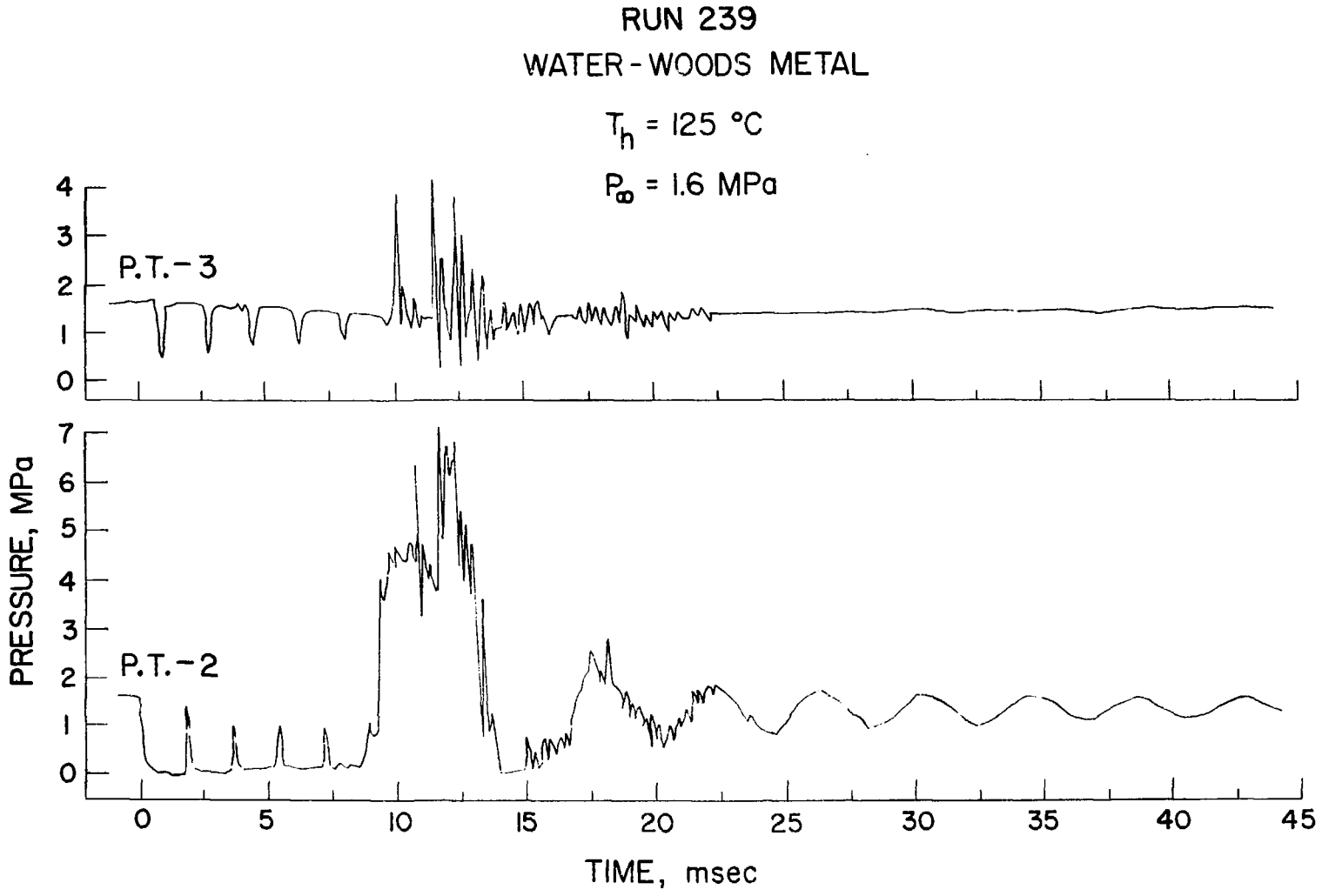

Fig. 5.50 Pressure History of Run 239

VI. DISCUSSION

In this chapter we will discuss the present experimental results in regard to possible mechanisms, temperature thresholds, and system pressure dependency.

6.1 Pressure Magnitude

Consider that a volume of coolant is intermixed with the hot liquid resulting in an equilibrium temperature, T_{eq}, which is given by:

$$T_{eq} = \frac{T_h + \gamma T_c}{1 + \gamma} \tag{6.1}$$

where

$$\gamma \equiv \frac{\rho_c \ell_c C_c}{\rho_h \ell_h C_h} \tag{6.2}$$

where ℓ_c and ℓ_h are the length of the intermixed coolant and hot liquid columns, respectively. Due to the temperature change of the coolant it expands, resulting in compression of the entire coolant column ("single-phase pressurization" or "constant volume heating"). The expansion process is described by:

$$dv = \left(\frac{\partial v}{\partial P}\right)_T dP + \left(\frac{\partial v}{\partial T}\right)_P dT \tag{6.3}$$

or

$$\frac{d\ell_c}{\ell_c} = -\beta_T \, dP + \alpha_P \, dT \tag{6.4}$$

where

$$\beta_T = -\frac{1}{v}\left(\frac{\partial v}{\partial P}\right)_T \tag{6.5}$$

$$\alpha_P = \frac{1}{v}\left(\frac{\partial v}{\partial T}\right)_P \tag{6.6}$$

To evaluate the maximum pressure which can be developed by constant volume heating we assume that the hot liquid contraction is negligible compared to the expansion of the coolant. From Eq. 6.3 the coolant column compression is given by:

$$d(L - \ell_c) = -\beta_T(L - \ell_c)dP \tag{6.7}$$

where L is the initial column length. If the compression is made in constant volume, i.e., dL = 0, the pressure in the liquid can be found from Eqs. 6.4 and 6.7:

$$\Delta P = \frac{\alpha_P \ell_c}{\beta_T L}\ \Delta T \tag{6.8}$$

where $\Delta T = T_{eq} - T_c$.

For water-Wood's metal, T_{eq} is given as:

$$T_{eq} = \frac{1.71\ T_h + \ell_c T_c}{1.71 + \ell_c} \tag{6.9}$$

where ℓ_h is taken as the entire length of the Wood's metal, i.e., $\ell_h = 5.0$ cm. (ℓ_c and temperatures are in centimeters and °C, respectively.) The pressure was thus calculated, assuming $T_c = 20°C$, $\beta_T = 4.8 \cdot 10^{-5}$ 1/bar, and $\alpha_P = \alpha_P(T_{eq})$. The results are shown in Table 6.1 for different values of ℓ_c, at $T_h = 220°C$ and 400°C. It is shown that even assuming all the hot material instantaneously intermixes results in a pressure magnitude at $T_h = 220°C$ that is significantly less than that

TABLE 6.1 Single-Phase Pressurization of Water Contacting Wood's Metal

T_h °C	ℓ_c cm	T_{eq} °C	dp MPa
220	0.25	194	0.93
	1.25	135	2.27
	2.5	101	2.5
	5.0	71	2.45
	10	48	2.1
	20	35	1.72
	50	27	1.38
	75	24	1.29
	100	23.5	1.30
400	0.25	351	6.48
	1.25	240	7.82
	2.5	174	7.44
	5.0	117	6.58
	10	75.5	5.33
	20	50	4.41
	50	32.5	3.22
	75	28.5	2.86
	100	26	4.66

observed experimentally. Consequently the measured pressures in region B are greater than the maximum possible pressure that could be generated by constant volume heating.

In Figs. 5.26 and 5.33 the maximum interaction pressure is shown as a function of the hot liquid temperature for water and butanol. Also shown is the vapor pressure of the cold liquid at the bulk and interface temperatures. In the case of water, the vapor pressure for both temperatures in the lower part of the region B is lower than the interaction pressure. For butanol, almost up to the critical point, the vapor pressure is lower than the interaction pressure. Since the maximum pressure which can be achieved, when vapor is regarded as the pressure source, is the vapor pressure, vaporization cannot be the source for these experimental measurements. So, the large pressures in region B for the water-Wood's metal system cannot be explained by vapor pressure or single-phase pressurization. This suggests that the hydrodynamic component is very important in this region, i.e., the observed pressures are impact pressures due to reentry. This conclusion is similar to the computer model developed by Goldammer and Kottowski[69,70] in which they introduced the hydrodynamic component for describing the interaction pattern, i.e., bouncing behavior, and the pressure magnitude. This model is based on the assumption that the first pulse is a result of constant volume heating and vaporization proceeds when the resulting wave is reflected from the upper interface and reaches the interaction zone. The vapor sets the column into motion, which is controlled by the vapor pressure at the coolant lower interface, which in turn depends on the heat flux from the hot material, vaporization or condensation. When

the column reenters it is stopped by the hot liquid if condensation is complete, or by a vapor layer. So, the pressure developed is a result of water-hammer pressure or vapor pressure whichever is larger. Good agreement between the theory and experimental results was found concerning the interaction pattern, but the calculated pressure was much larger than the experimental pressure.

A simple model was suggested by Board et al.[71] in which the pressure developed is a result of energy transfer to a nonequilibrium two-phase coolant, expanding against the acoustic loading of the coolant column. The pressure is given by:

$$P = \rho_\infty c \frac{S}{S_o} (u_v + u_\ell) + P_\infty \qquad (6.10)$$

where

- S - debris area
- S_o - shock tube area
- u_v - growth rate of vapor
- u_ℓ - expansion rate of heated water

An agreement with Wright's experiment was found, but the pressure calculated is very sensitive to the assumed initial distribution of energy between the vapor and liquid phases. This model and the computer codes which are based on it (e.g., Ref. 72) are concerned only with the energy transfer phase and the consequent pressure developed.

In the present experiments the impulse and pressure graphs for the water-Wood's metal system show that all pulses which produced pressures higher than the vapor pressure have approximately the theoretical hydrodynamic pressure and impulse (region B), based on initial conditions,

which indicate that the hydrodynamic component is the important one in this region. Pulses which produced pressures lower than the vapor pressure acquired larger impulses than theoretically expected from initial hydrodynamic considerations (region C). Those results as well as the composite shape of the pulses in region C suggest that both hydrodynamic and thermal interactions are involved in each pulse at the high temperature runs but it is difficult to differentiate between them. Since the pressures produced are the same order as impact pressures, the only indication for significant thermal interaction is a large increase in the resultant impulse.

For butanol-Wood's metal system the impulses and pressures are close to the theoretical values expected from hydrodynamic considerations which suggest that hydrodynamic effects are significant. However, some of the runs produced pressures which were lower than the vapor pressure corresponding to the hot liquid temperature, and are close to the vapor pressure corresponding to the interface temperature.

From the discussion above, one would expect that the pressure pulses would be amplified since any impact produces more vapor resulting in higher pressures for accelerating the liquid column. This is true so long as the hot liquid surface remains at the same temperature. Actually, the hot liquid temperature decreases during the entire interaction (especially during the multiple mixing stage) so that the pressure amplification is limited and eventually the pressure decreases. Also, especially at high temperatures, the amount of vapor in the system after several bounces becomes so large that condensation cannot be completed and the column is stopped due to vapor compression, a process which is

relatively long (e.g., region D in the butanol-Wood's metal system and the water-salt experiments). Thus, impact is eliminated and the pressure magnitude decreases. The pressure magnitudes of consecutive bounces in a specific run are shown in Fig. 6.1. We can see the pressure magnitude increase in the early bounces, presumably because of larger impact velocities, and afterwards decreases due to the cooling effect or to incomplete condensation.

The present experimental results have shown that by increasing the column velocity impact may be achieved in cases where no impact was observed under low velocities. Those results are consistent with dropping experiments discussed in Chapter III. For example, in the Freon-22-mineral oil system impact was achieved when the driving pressure was P_∞ = 0.66 MPa (Fig. 5.14), whereas in run 158 (Fig. 5.15) where no impact was observed when P_∞ = 0.2 MPa. Large pressure pulses are also generated with water and butanol impacting Wood's metal when $P_\infty \sim 1.65$ MPa (e.g., Run 207 in Fig. 5.38) or $P_\infty \sim 0.62$ (e.g., Run 184 in Fig. 5.43). It indicates that the vapor layer, which is produced initially by precursor jets, small drops or flashing, is broken down, which enables the column to impact the surface. The breakup of the vapor film may be a result of rapid condensation or vapor entrainment through Taylor instability "pockets" existing on the lower liquid column interface. (Taylor instability may exist when the liquid column decelerates, since the acceleration is from the light fluid to the more dense fluid.) When the velocity is relatively low (corresponds to lower driving pressure) and the amount of vapor is relatively large, the vapor layer is stable and cushions the downcoming column, generating long and low pressure pulses as seen in region D of the butanol-Wood's metal system.

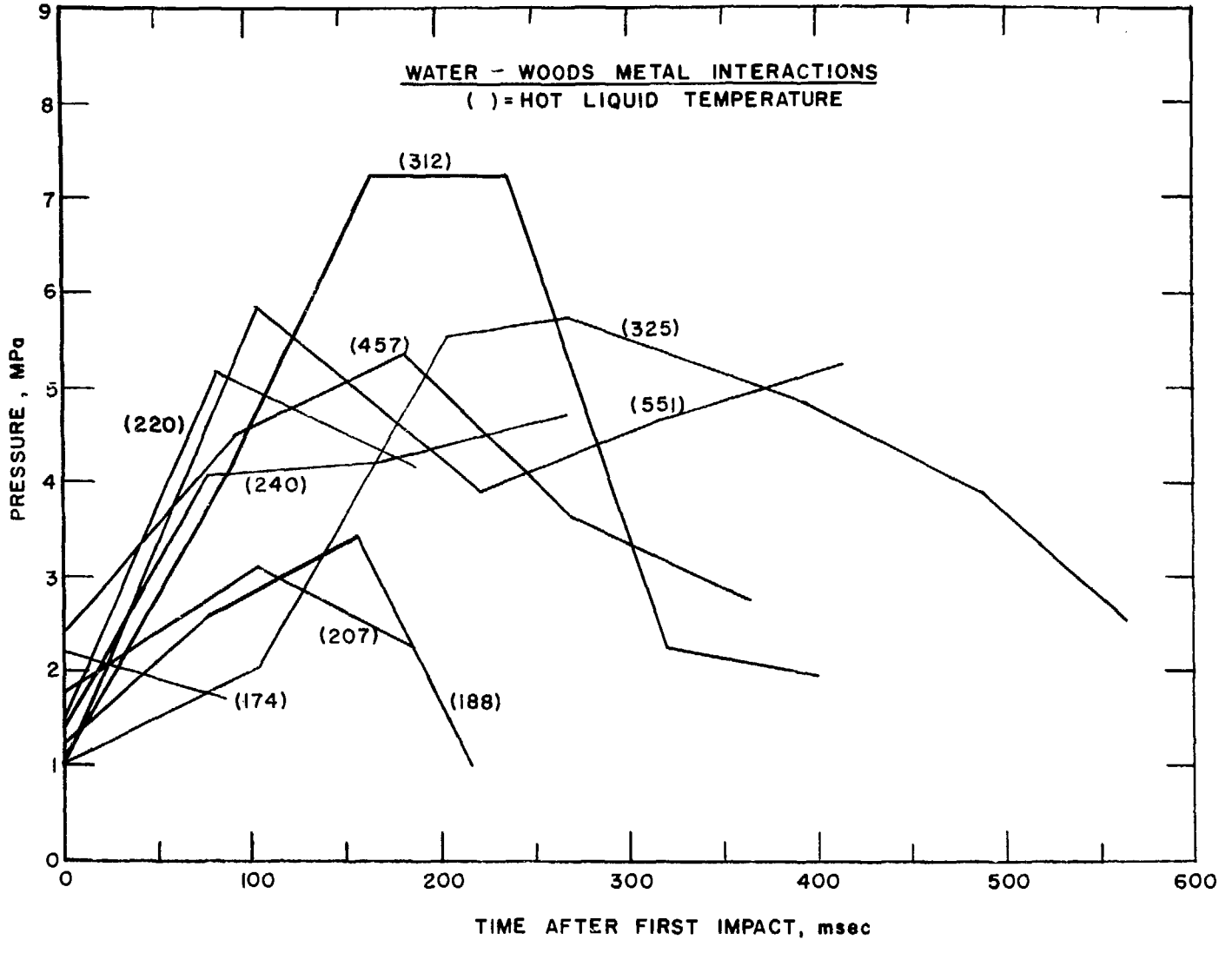

Fig. 6.1 Pressure of Consecutive Bounces As Function of Time

In the nonisothermal experiments, the liquid column approach on the first impact is cushioned by the vapor generated from precursor jets and small drops reaching the surface before the main column. The pressure thus developed is due to vapor compression, and the observed pulse is of a long duration and is considerably less than P_i. When the column accelerates upwards, depressurization and flashing occur, which produces a mixture of vapor and small liquid drops. Also, liquid drops are generated from the Taylor instability of the lower liquid interface. Those drops enhance the rate of condensation as a result of surface area increase when the column reenters and compresses the two-phase mixture. In many cases the condensation is complete as is evident from the sharp impact pressures of the "bouncing pulses," developed from stopping the liquid column. Higher reentry velocities of the column yield larger vapor compression which in turn produce better condensation. Thus, even if the first pulse indicates that no impact had occurred, the vapor generated may cause the column to bounce and reach high velocities, which enables it to condense the film and impact the surface.

6.2 Hydrodynamic Behavior

As was shown in Sect. 5.2, the impact behavior in the isothermal water-solid surface is complicated. It does not consist of a single pressure pulse as would be expected from the simple theory of instantaneous velocity reduction to zero at impact. In the process of developing the model of impact and stopping the column, no vapor was assumed to exist between the liquid and the surface. Taking into consideration the vapor (or air evolved from the coolant) which does exist in reality, because of flashing upon diaphragm rupture or because it was introduced initially, a mechanism for stopping the column may be suggested. As the liquid

column moves down it compresses the vapor, which initially was saturated (in the case of the isothermal water-solid surface experiments the saturation pressure is 2.37 KPa). The shape of the interface may be flat, wavy or any other shape, e.g., parabolic. The small amount of vapor will be pressurized in a very short time when the average vapor film is ∿0.5 mm in thickness resulting in a short rise time pressure pulse which propagates along the column. The pressure developed (P') as well as the rarefaction wave from the upper interface decelerates the downcoming liquid, each by a velocity increment of

$$\Delta u = \frac{P'}{\rho_\ell c} \tag{6.11}$$

(The deceleration by the compression and rarefaction waves is shown in Fig. 6.2.) The liquid column may still move down during the compression stage if condensation takes place on the vapor/liquid interface. This process of condensation ($\dot{m}_c$) and liquid motion (described by the volumetric flow rate $\dot{m}_\ell$) is self limiting. If $\dot{m}_\ell > \dot{m}_c$ the resultant pressure will increase (line "a" in Fig. 6.3) resulting in more condensation. If $\dot{m}_c > \dot{m}_\ell$ the resultant pressure will decrease (line "b" in Fig. 6.3) resulting in less condensation. Thus, the end result of these processes is that the two rates (condensation and volumetric flow) will tend to equalize and the pressure remains approximately constant (line "c" in Fig. 6.3) until all the vapor has been condensed. The process of vapor pressurization and subsequent condensation may explain the pressure pulse developed during the first relief time. An illustration of the proposed mechanism is shown in Fig. 6.4. In step (a) the liquid is coming down and no pressure is observed on the pressure curve.

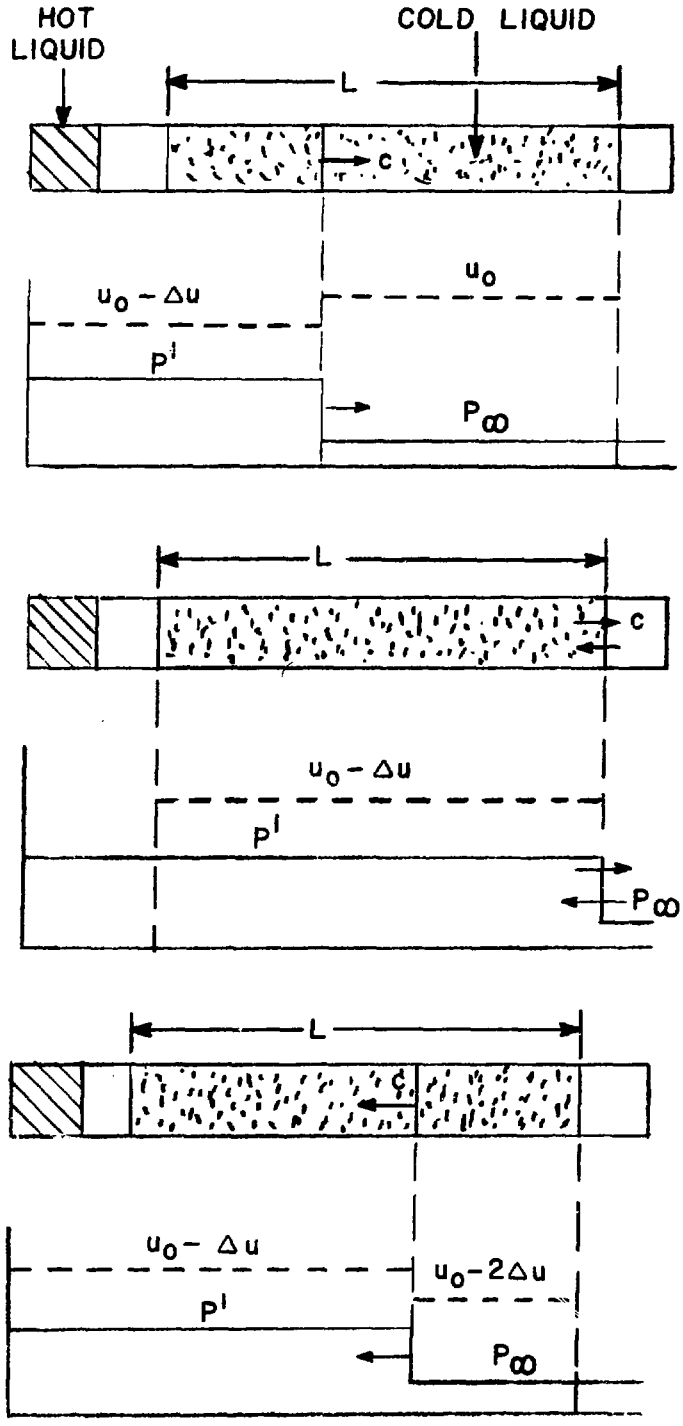

Fig. 6.2 Deceleration of Liquid Column Due to Vapor Compression

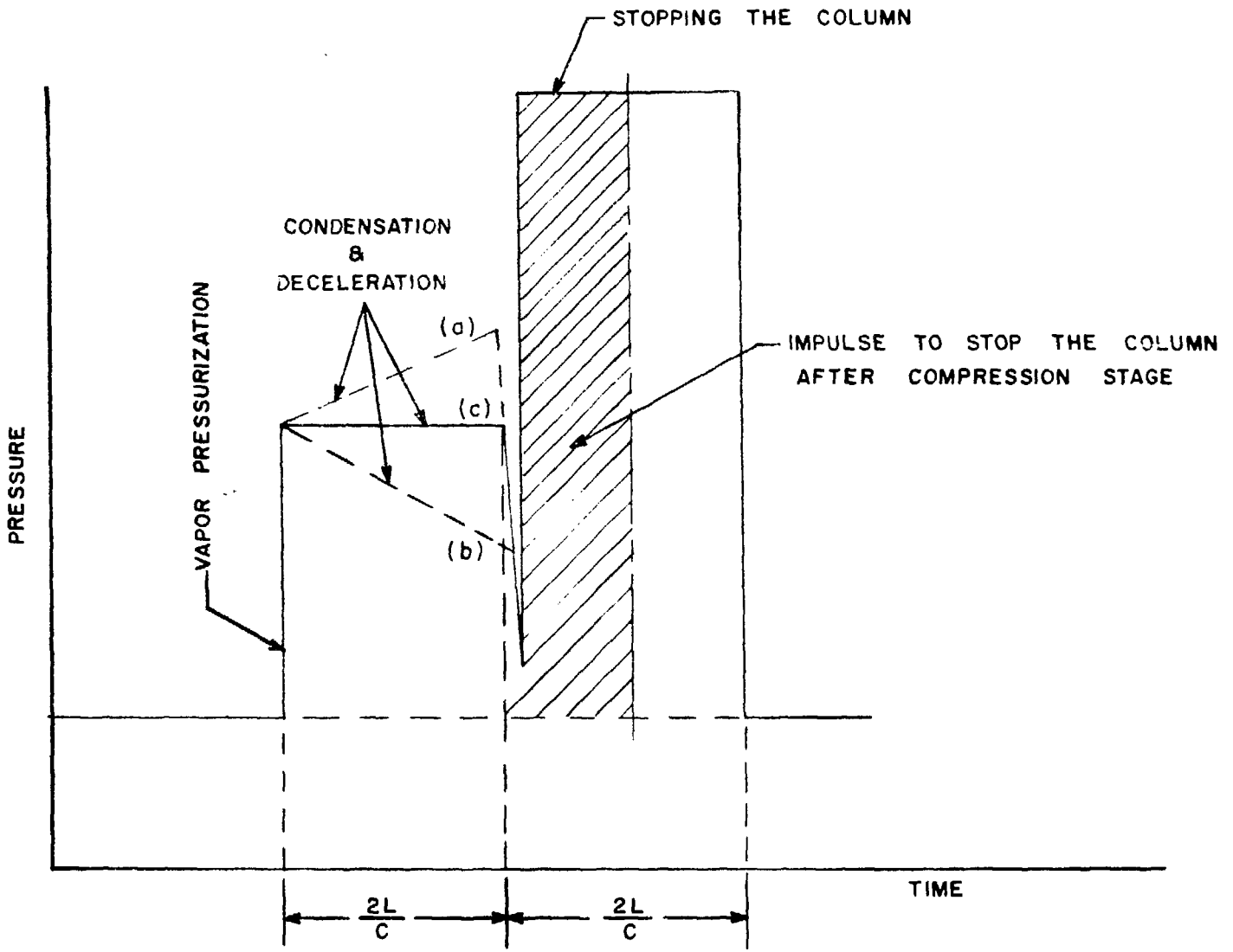

Fig. 6.3 Proposed Mechanism for Stopping a Liquid Column

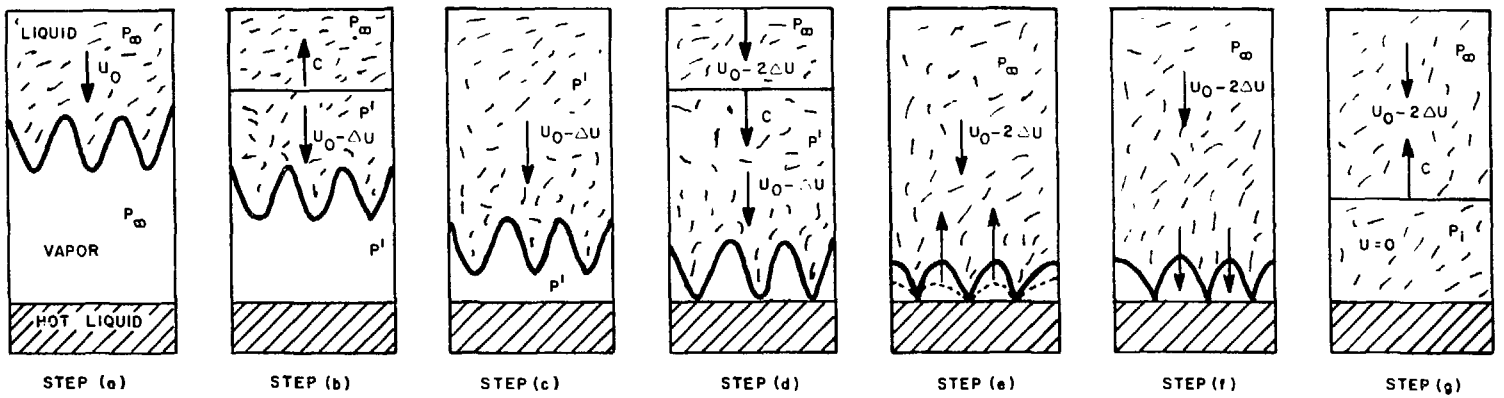

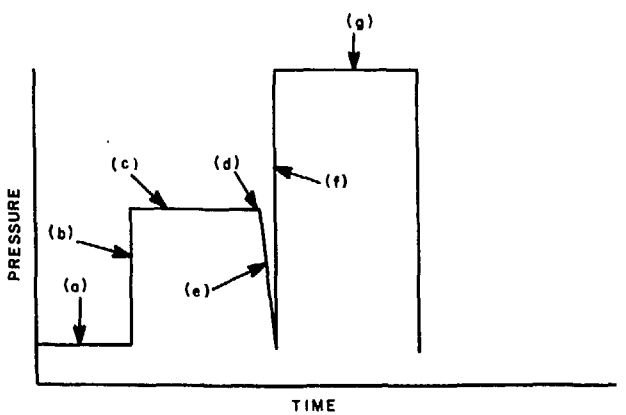

Fig. 6.4 Illustration of Proposed Mechanism for Stopping a Liquid Column

Pressurization commences in step (b) and P' is developed, decelerating the column as does the rarefaction wave in step (d). Steps (e) and (f) illustrate one of the possible mechanisms which results in fast condensation. Due to the arrival of the rarefaction wave to the vapor/liquid interface the pressure in the liquid is the system pressure (P_∞) while the pressure in the vapor is P'. This pressure difference decelerates the liquid (step (e)) and produces Taylor instability (if it did not exist beforehand). The most dangerous wavelength growth rate parameter can be calculated approximately by:

$$b = \left[\frac{4\pi}{3}\left(\frac{\rho_\ell - \rho_v}{\rho_\ell + \rho_v}\right) \cdot \frac{a}{\lambda_{cr}}\right]^{1/2} \tag{6.12}$$

A typical deceleration can be calculated to be 20,000 g's assuming that the pressure difference ($P' - P_\infty$) is ~2.0 MPa and the length of liquid which is subject to this deceleration is about 1.0 cm. Thus, the resultant critical wave length (λ_{cr}) is calculated to be 0.13 mm, the number of bubbles is ($N = S_o/\lambda_{cr}^2$) 30,000, the vapor volume is $3.45.10^{-2}$ cm^3 ($V = N. \frac{4\pi}{3} \frac{\lambda_{cr}}{8}$) and the time for instability growth is 4 μsec. Since the vapor is assumed to be compressed adiabatically, its temperature is high (= 281°C if the compression was from 0.1 MPa to 3.0 MPa). The large increase in surface area due to the instability will increase the condensation rate in a very short time (1/b) resulting in complete condensation by the subcooled liquid (step (f)) followed by water-hammer impact (step (g)). The increase in surface area may also be calculated from Rayleigh's equation (Eq. B.1) assuming bubbles are formed and grow inertially. For example, during a period of 0.1 msec bubbles can grow

to ~3 mm in radius which yield a considerable increase in surface area in view of the initial vapor thickness (~0.5 mm). This kind of process is evident in many experiments, such as the isothermal water-water (Fig. 5.9), water-mercury (Fig. 5.10), and water-solid surface runs (Fig. 5.5) and in the low temperature runs with Wood's metal (e.g., Figs. 5.47 and 5.50), where the pressure P' is sustained during the relief time period.

The vapor may also be condensed if $\dot{m}_\ell$ (and consequently $\dot{m}_c$) is large enough to condense all available vapor before the arrival of the rarefaction wave. In this case the condensation is so rapid that a pressure spike is measured before the main pressure pulse which brings the liquid to rest. Those pressure spikes are evident in many "bouncing pulses" in the nonisothermal runs, since in those experiments large surface area exist as a result of bouncing (see Sect. 6.1) which yields rapid condensation.

After condensing the vapor, the column impacts on the surface with velocity u_i and the column is stopped. The impact velocity can be calculated from the initial velocity u_o, which is reduced by the compression and the rarefaction waves, such as Δu. Thus,

$$u_i = u_o - 2\Delta u \tag{6.13}$$

where u_o is given by

$$u_o = \sqrt{2a\, z_o} \tag{6.14}$$

and the acceleration a is evaluated from Eq. 5.3 (z_o is the initial distance between the surfaces). The calculated values of Δu, u_o, u_i, P_i, and I for three different runs are given in Table 6.2. P_i is calculated by Eq. 5.4 and I is the impulse per unit area calculated by:

TABLE 6.2 Hydrodynamic Impact of Cold Liquid

Run (system)	T_h °C	P' MPa	Δu m/sec	u_o m/sec	u_i m/sec	P_i MPa	I KPa.sec	P_{max}/P_i	I'_{exp}/I
71 (water-solid surface)	20	2.8	1.8	8.8	5.2	7.8	6.76	0.84	0.64
230 (butanol-Wood's metal)	110	2.25	1.5	7.3	4.3	4.73	5.6	0.85	0.85
239 (water-Wood's metal)	125	4.4	2.93	11.5	5.63	8.45	7.32	0.90	0.68

$$I = \rho_{\ell} L u_i \tag{6.15}$$

To compare the theoretical results with the experimental values, P_{max} was taken as the experimental water hammer and I'_{exp} was taken as the impulse per unit area required to stop the column after the compression stage as is shown in Fig. 6.3. Good agreement between the experimental and theoretical values is shown in Table 6.2.

When the driving pressure is relatively low, e.g., P_{∞} = 0.19 MPa in run 78, or when appreciable amount of gas/vapor exist below the liquid column (run 86) the deceleration process resulting from the gas/vapor compression is relatively slow. Thus, the column is stopped in a continuous manner and no "water-hammer" pressure (a result of discontinuity in liquid velocity) is developed.

Note that the discussion above was not limited to two plane surfaces approaching each other or any particular configuration. It can be assumed that the liquid interface is deformed according to Taylor instability in regard to the large deceleration acting on the column by the pressure in the vapor, or the column may come as a liquid bulb. In any case, as long as a compressible volume exists in the system the basic features of the mechanism described are still applicable.

To analyze the hydrodynamic behavior in the nonisothermal runs, let us assume that on the first impact vapor is produced which acts on the coolant column. Assuming negligible effects of friction, the upward movement of the coolant column in the tube is given by:

$$\ddot{z} = \frac{P_v - P_{\infty}}{\rho_{\ell} L} - g \tag{6.16}$$

with the initial conditions:

$$z(0) = 0$$

$$\dot{z}(0) = U_o \tag{6.17}$$

where U_o is the initial velocity of the column due to the momentum transferred to it during the expansion phase (the time in which the rarefaction wave travels along the column and sets it into motion). Thus:

$$U_o = \frac{I'_{exp}}{\rho_\ell L} \tag{6.18}$$

For a rough estimation let us assume that no additional pressure is acting at the bottom (i.e., $P_v = 0$) the column is subjected to gravity and the system pressure. Hence the period between two consecutive bounces is given by:

$$\Delta t = \frac{2U_o}{a} \tag{6.19}$$

or:

$$\Delta t = \frac{2I'_{exp}}{P_\infty + g\rho_\ell L} \tag{6.20}$$

A typical result is (e.g., Run 187 where $I'_{exp} = 3.88$ KPa.sec and $P_\infty =$ 0.2 MPa) $\Delta t = 36$ msec. The measured momentum on the next impact (assuming the column is stopped by one compression wave) is the same as before because of motion symmetry if no energy is transferred or dissipated. Actually, P_v is not equal to zero during the liquid motion up. The pressure in the vapor is shown experimentally as a "tail" following the main impact (e.g., Run 187) of the "bouncing pulses." The pressure of

the tail as a function of time can be approximated by the linear relation:

$$P_v = P_o\left(1 - \frac{t}{t_o}\right) \tag{6.21}$$

where t_o is the "tail" duration and P_o is the initial pressure of the "tail." The equation of motion can be written as:

$$\frac{d^2z}{dt^2} = \frac{P_o - P_\infty}{\rho_\ell L} - \frac{P_o t}{\rho_\ell L\, t_o} \tag{6.22}$$

Introducing new variables given as:

$$\eta \quad \frac{z}{L} \tag{6.23}$$

$$\tau \quad \frac{t}{\sqrt{\rho_\ell L^2/P_\infty}} \tag{6.24}$$

we get:

$$\frac{d^2\eta}{d\tau^2} = P^* - \tau^* t \tag{6.25}$$

where

$$P^* = \frac{P_o}{P_\infty} - 1 \tag{6.26}$$

$$t^* = \frac{P_o}{P_\infty t_o}\sqrt{\frac{\rho_\ell L^2}{P_\infty}} \tag{6.27}$$

The initial conditions are:

$$\eta(0) = 0 \tag{6.28}$$

$$\frac{d\eta}{d\tau}(0) = U^*$$

where

$$U^* = U_o \sqrt{\frac{\rho_2}{P_\infty}} \tag{6.29}$$

The solution obtained is:

$$\eta = \frac{P^*\tau^2}{2} - \frac{t^*\tau^3}{6} + U^*\tau \tag{6.30}$$

The maximum height the column reaches can be obtained from

$$\frac{d\eta}{d\tau} = 0 \tag{6.31}$$

or:

$$t^*\tau^2 - 2P^*\tau - 2U^* = 0 \tag{6.32}$$

For I'_{exp} = 3.88 kPa.sec; P_o = 1.0 MPa; P_∞ = 0.2 MPa and t_o = 10 msec, which are the values of the first impact of Run 187, we get:

$$\tau_{max} = 0.23,$$

or

$$z_{max} = 10 \text{ cm}; \quad t_{max} = 20 \text{ msec}.$$

Assuming the motion down is controlled by the upper plenum pressure and all vapor is condensed ($P_v \tilde{\sim} 0$), then the lower bound for time down is:

$$t_{do} = \sqrt{\frac{2z_{max}}{a}} \tag{6.33}$$

or

$$t_{do} = \sqrt{\frac{2 z_m \rho_\ell L}{P_\infty}} \tag{6.34}$$

The lower bound for the total time is

$\Delta t_{th} = t_{max} + t_{do} = 55$ msec compared to the experimental value of $\Delta t_{exp} = 82.5$ msec. Also, $I_{th} = 14.0$ KPa.sec ($I_{exp} = 10.08$ KPa.sec) and $P_i = 8.25$ MPa ($P_{exp} = 5.17$ MPa).

Plotting the time between bounces for water and Wood's metal as a function of bulk temperature (Fig. 6.5) reveals that $50 \lesssim \Delta t_{exp} \lesssim 100$ msec which is the same order as Δt_{th}.

6.3 Temperature Thresholds of Interactions

In the systems which exhibit an interaction potential (water-Wood's metal and butanol-Wood's metal), different modes of interaction were observed, depending on the hot liquid temperature. (The water-salt system will be discussed later since experiments covered only a small temperature range.)

In the water-Wood's metal system the upper bound of region B is at $T_h = 305°$, which corresponds to an interface temperature of $T_I \sim 210°C$ when $T_c = 20°C$, which agrees with the lower bound of region B ($T_h \sim 210°C$) taking into account the uncertainties in the Wood's metal properties. If one assumes that the spontaneous nucleation temperature of the system is $T_{sn} = 210°C$ then the temperature thresholds for regions B and C are $T_h = T_{sn}$ and $T_I = T_{sn}$, respectively. Those results agree with the spontaneous nucleation model prediction if the low rate of vaporization observed in region B is described as small scale events (in which a thin layer of coolant is heated up to T_{sn} during the intermixing stage which lasts 2L/c sec), and the fast vapor production in region C is described as large scale events in which instantaneous vaporization

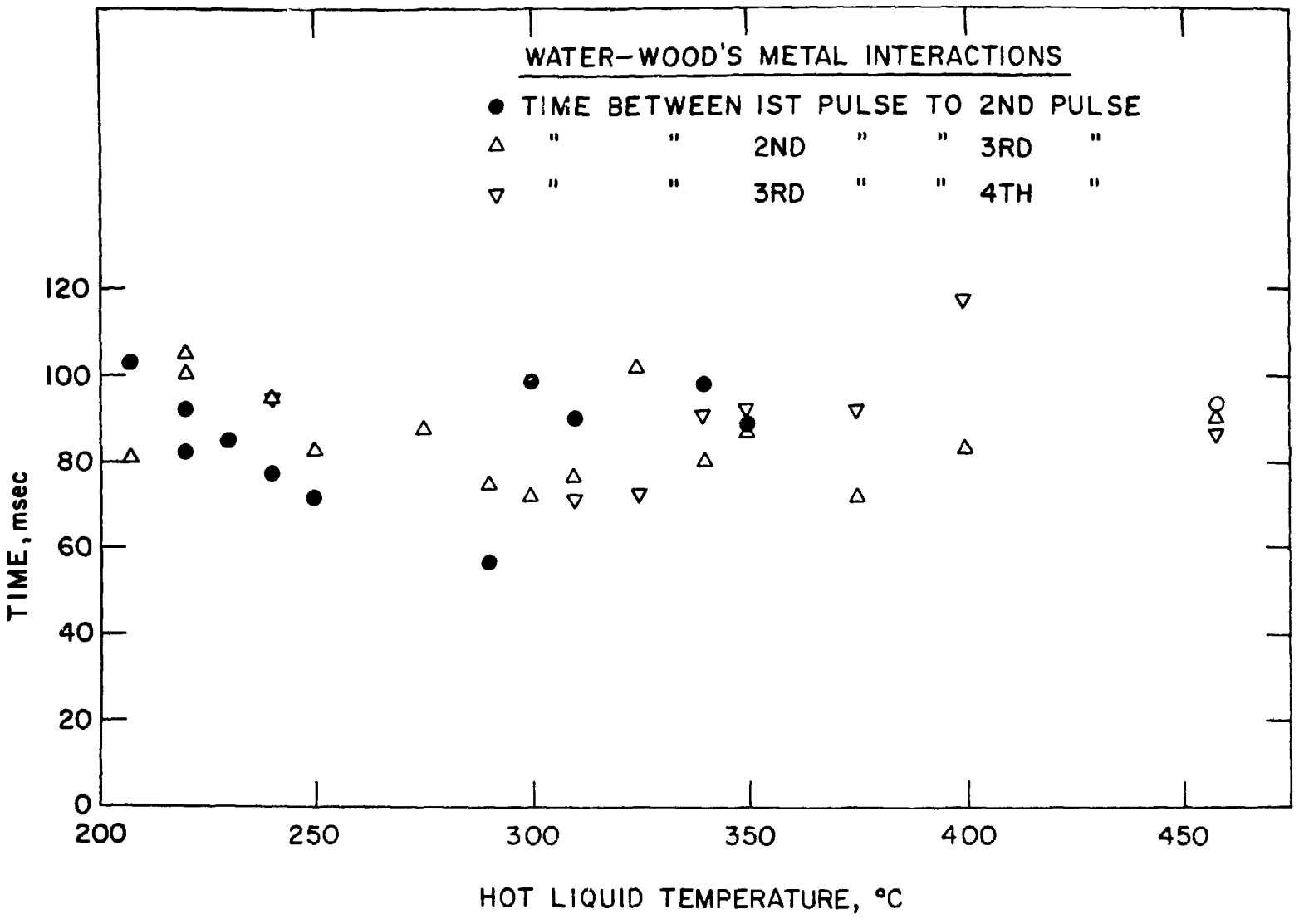

Fig. 6.5 Time Between Bounces As Function of Hot Liquid Temperature

occurs upon contact.

For butanol-Wood's metal system, the homogeneous nucleation temperature is T_{hn} = 240°C. The hot liquid temperature which results in an interface temperature $T_I = T_{hn}$ is T_h = 260°C. Experimentally, the temperature thresholds are 25°C lower than those predicted by the homogeneous nucleation model. It seems likely that this system as with water is also not perfectly wetted but with a smaller wetting angle than the water-Wood's metal system.

In this particular system, region D is observed in which multiple bounces are still obtained but significantly weaker interactions than in region C. The temperature threshold for region D is T_h = 325°C which corresponds to T_I = 290°C. This high temperature cutoff ($T_I \tilde{=} T_{cr}$) is in agreement with the experimental observations for the free contacting mode (Freon-oil system) and the capture theory which predicts that the upper temperature threshold for explosions corresponds to an interface temperature which is approximately the thermodynamic critical point. On the other hand, in water-Wood's metal system, even at interface temperatures above the critical point interactions do occur. The difference between those systems is in the thermal properties (especially the heat of evaporation), the wetting characteristics, and the oxidation potential (which was found to play an important role in determining an explosion occurrence in the dropping experiments).

Calculating the interface temperature for the water-salt (LiCl-KCl) interactions yields $T_I \tilde{=}$ 270°C for T_h = 600°C and $T_I \tilde{=}$ 190°C for T_h = 410°C (see Appendix A for molten salt properties). In view of the large affinity of these liquids to each other, we assume that the wetting in

this system is perfect, so $T_{sn} = T_{hn} \tilde{=} 305°C$. Thus, $T_h > T_{sn}$ but $T_I < T_{sn}$, and the expected result is a small scale event, which was confirmed experimentally (Fig. 5.36).

6.4 System Pressure Dependency

Increasing the initial system pressure, i.e., the driving pressure, resulted in suppression of thermal interaction for water and butanol with Wood's metal as well as for water with molten salt. No thermal interactions were observed when $P_\infty = 0.56$ MPa for all these systems. The same phenomenon was shown to occur with Freon-22 and mineral oil in dropping experiments,[57] when $P_\infty = 0.2$ MPa. The present experiments with Freons, which were performed when $P_\infty = 0.2$ MPa and did not result in any energetic events, are in this category. i.e., explosions were suppressed.

The suppression of Freon-22 interactions was predicted in Ref. 57 by plotting the transition diameter and comparing it to the predicted drop stability line (Appendix B). Even though the capture theory was developed for free contact mode and should be regarded as an order of magnitude estimation, it is interesting to compare the present results to the capture theory prediction. Following the approximate method for predicting the stability line given in Appendix B, for water, assuming $N = 10^9$ sites/cm ($D_B = 3160$ A° and $T^* = 145°C$), we get:

$$t_n = 1.497.10^{-7} \left(\frac{T_I - 100}{T_I - 145} \right)^2 \qquad (6.35)$$

where α_c was taken as $1.67.10^{-7}$ m^2/sec. The stability line as well as the transition diameter for $P_\infty = 0.1$, 0.21, 0.56 and 1.0 MPa is shown in Fig. 6.6. For $P_\infty = 0.1$ and 0.21 MPa, the bubbles in the captured drop are inertially dominated, resulting in explosions. At $P_\infty = 0.56$ and 1.0

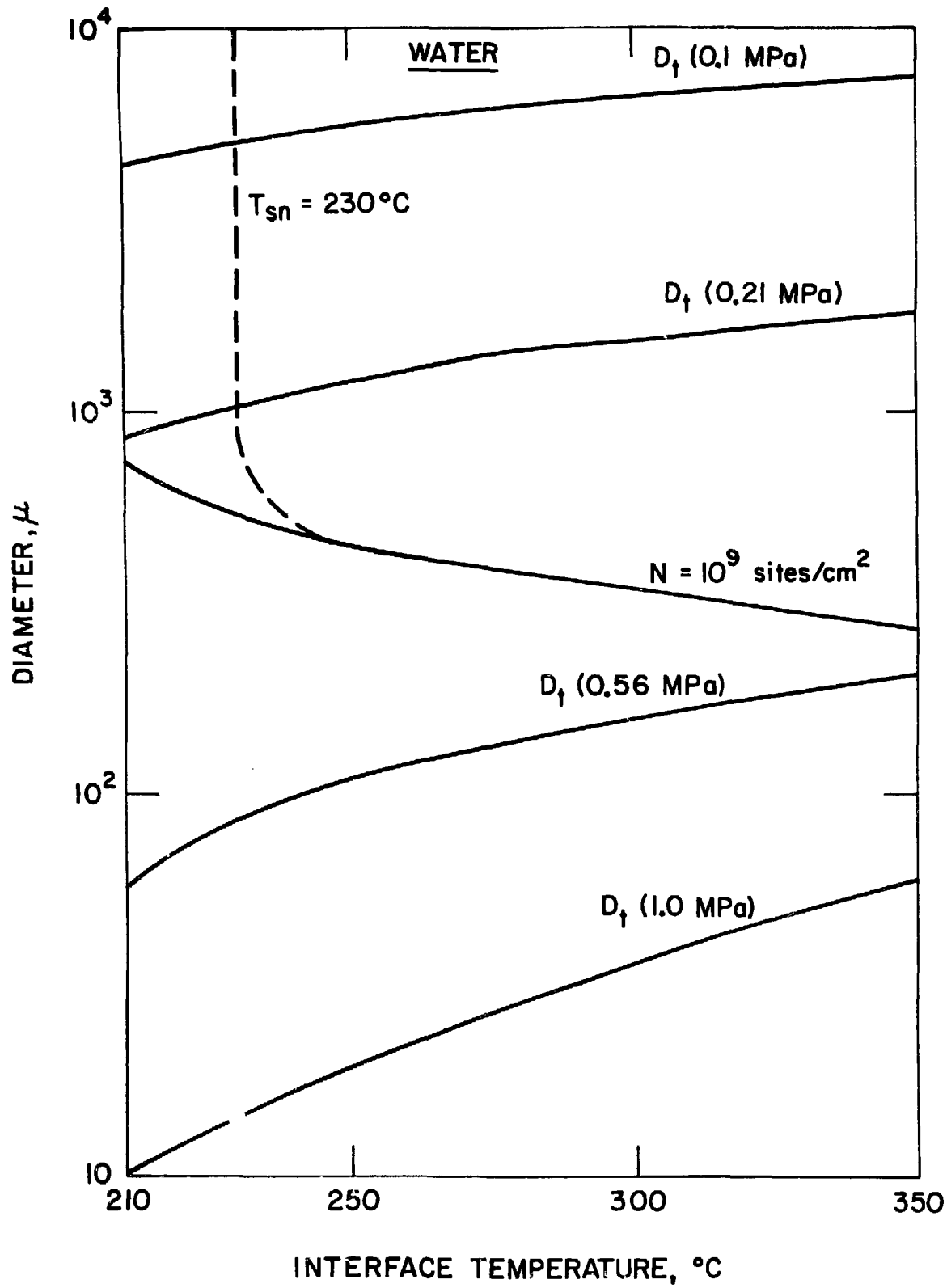

Fig. 6.6 Stability Line and Transition Diameters for Water

MPa, the bubbles are thermally controlled at capture time; thus, no explosion can occur at those or higher pressures without a specific external trigger. There is a good agreement between the theoretical prediction and the experimental results in this case.

For butanol ($\alpha_c = 1.01.10^{-7}$ m^2/sec) assuming N = 10^9 sites/cm^2 (D_B = 3160 A°, T* = 152°C) the stability line is predicted by:

$$t_n = 2.47.10^{-7}\left(\frac{T_I - 117.5}{T_I - 152}\right)^2 \tag{6.36}$$

and for N = 10^{10} sites/cm^2 (D_B = 1000 A°, T* = 174°C),

$$t_n = 2.5.10^{-8}\left(\frac{T_I - 117.5}{T_I - 174}\right)^2 \tag{6.37}$$

The predictions of the stability lines for butanol are given in Fig. 6.7 as well as the transition diameter for P_∞ = 0.1 and 0.2 MPa. For N = 10^9 sites/cm^2 it is predicted that explosions may occur for P_∞ = 0.1 since the transition diameter and the stability line are of the same order of magnitude. For N = 10^{10} sites/cm^2 explosions are possible at P_∞ = 0.2 MPa but are impossible for P_∞ = 0.56 MPa. It should be noted for butanol that its Jakob number, which mainly affects the transition diameter, is similar to that of Freons and all organic liquids. On the other hand, the stability line for N = 10^9 sites/cm^2 depends essentially on the thermal diffusivity which is much larger for butanol than Freons but is similar to water.

The experimental observations of depressing interaction by increasing the pressure is a major argument against the assumed mechanism of single-phase pressurization (constant volume heating). The fact that no explosions were produced with Freons in the present experiments, which

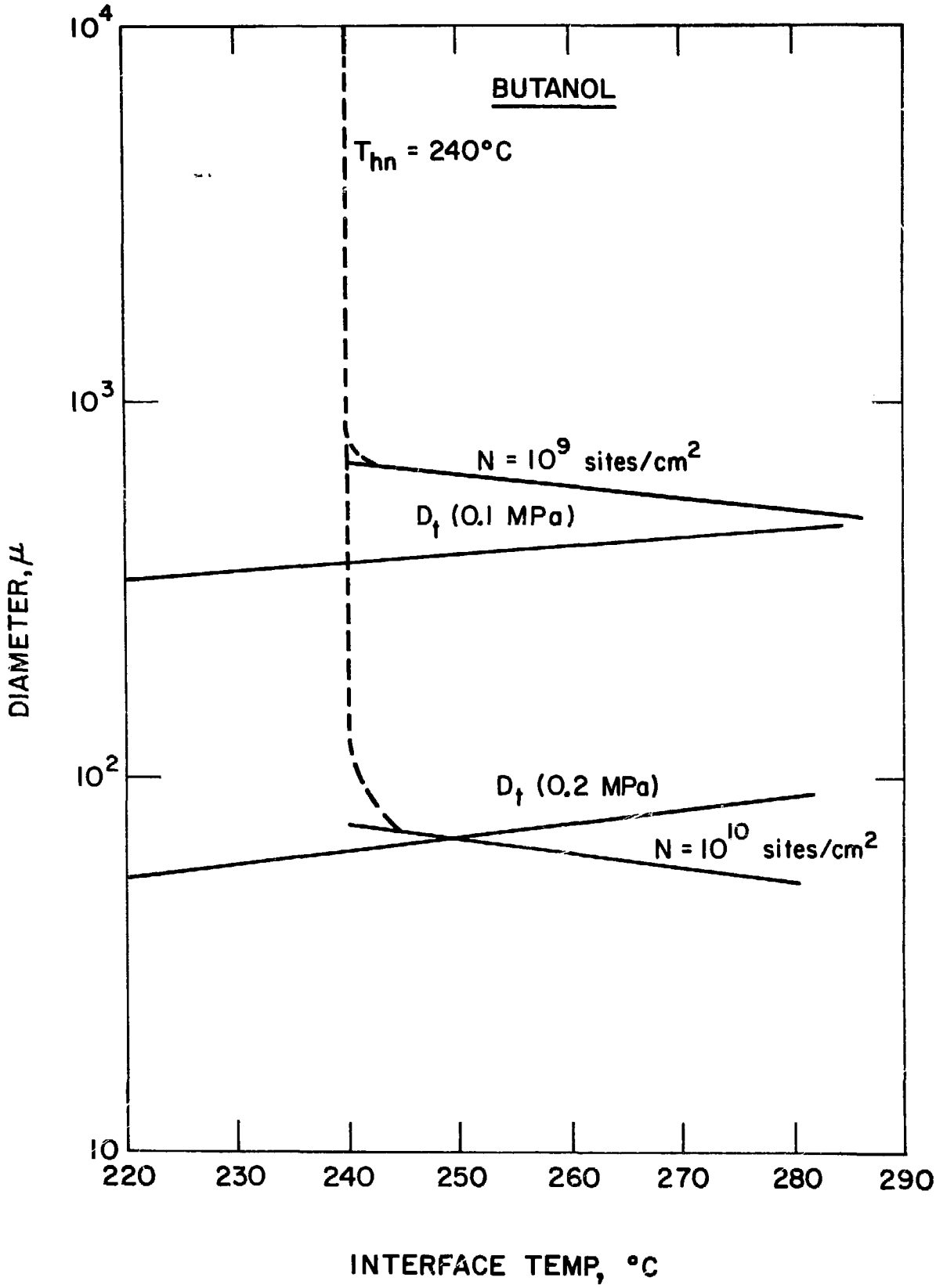

Fig. 6.7 Stability Lines (N = 10^9 and 10^{10} sites/cm^2) and Transition Diameters for Butanol

is similar to the behavior observed in pouring experiments, suggest that the same necessary condition for explosion is missing in both experimental modes.

6.5 Mixing and Heat Transfer Considerations

Contrary to most experimental results of shock tube experiments, reported here and in the literature, the maximum interaction pressures reported by Wright et al.[21] occurred on the first impact. It is most probable that the pressure generated in Wright's experiment was not due to hydrodynamic impact in view of the low driving pressure and impact experiments on solid aluminum. In this section, we will show from mixing and heat transfer considerations, that the energy stored in the aluminum was sufficient to pressurize the whole column via energy transfer to the cold liquid in contact with the hot surface.

Consider a mixing process in which volume V of hot liquid is intermixed with an equal volume of coolant. Assume that all the kinetic energy of the coolant (E_k) is imparted to the hot liquid as mixing energy (E_m). As discussed by Cho et al.,[73] in practical situations the mixing energy is due mainly to the frictional dissipation and other contributions, as surface and kinetic energies, may be ignored. Thus,

$$E_k(\text{coolant}) = E_m \tag{6.38}$$

The mixing is assumed to be a one-step mixing process, thus, E_m is the maximum mixing energy, which yields the largest particle size, and is given by:

$$E_m = N_h C_D \pi R_h^2 (1/2\ \rho_c u_m^2) L_m \tag{6.39}$$

where the mixing zone (L_m) and the number of hot liquid particles (N_h) are:

$$L_m = u_m t_m \tag{6.40}$$

$$N_h = \frac{V}{4/3\ \pi R_h^3} \tag{6.41}$$

Assuming a one-dimensional description (see Fig. 6.8) the volumes of hot liquid and coolant which intermixed are given by:

$$V = L_m\ S_o \tag{6.42}$$

The kinetic energy lost by the coolant at any point in time is;

$$E_k = \frac{1}{2}\ \rho_\ell L' S_o u_i^2 \tag{6.43}$$

where L' is the distance a wave moved through the coolant with sonic velocity (c) during the intermixing period (t_m):

$$L' = ct_m \tag{6.44}$$

Substituting into and rearranging Eq. 6.39 yields

$$R_h = \frac{3}{4}\ C_D\ \frac{u_m^4}{u_i^2 c}\ t_m \tag{6.45}$$

Taking the upper bound for the particle size we assume that $u_m = u_i$ thus

$$R_h = \frac{3}{4}\ C_D\ \frac{u_i^2}{c}\ t_m \tag{6.46}$$

Calculating the particle radius in the present apparatus for water-Wood's metal system ($u_i \overset{\sim}{>} 4$ m/sec) assuming $t_m = 1$ msec and $C_D = 50$, which is a typical value for equal volume systems,

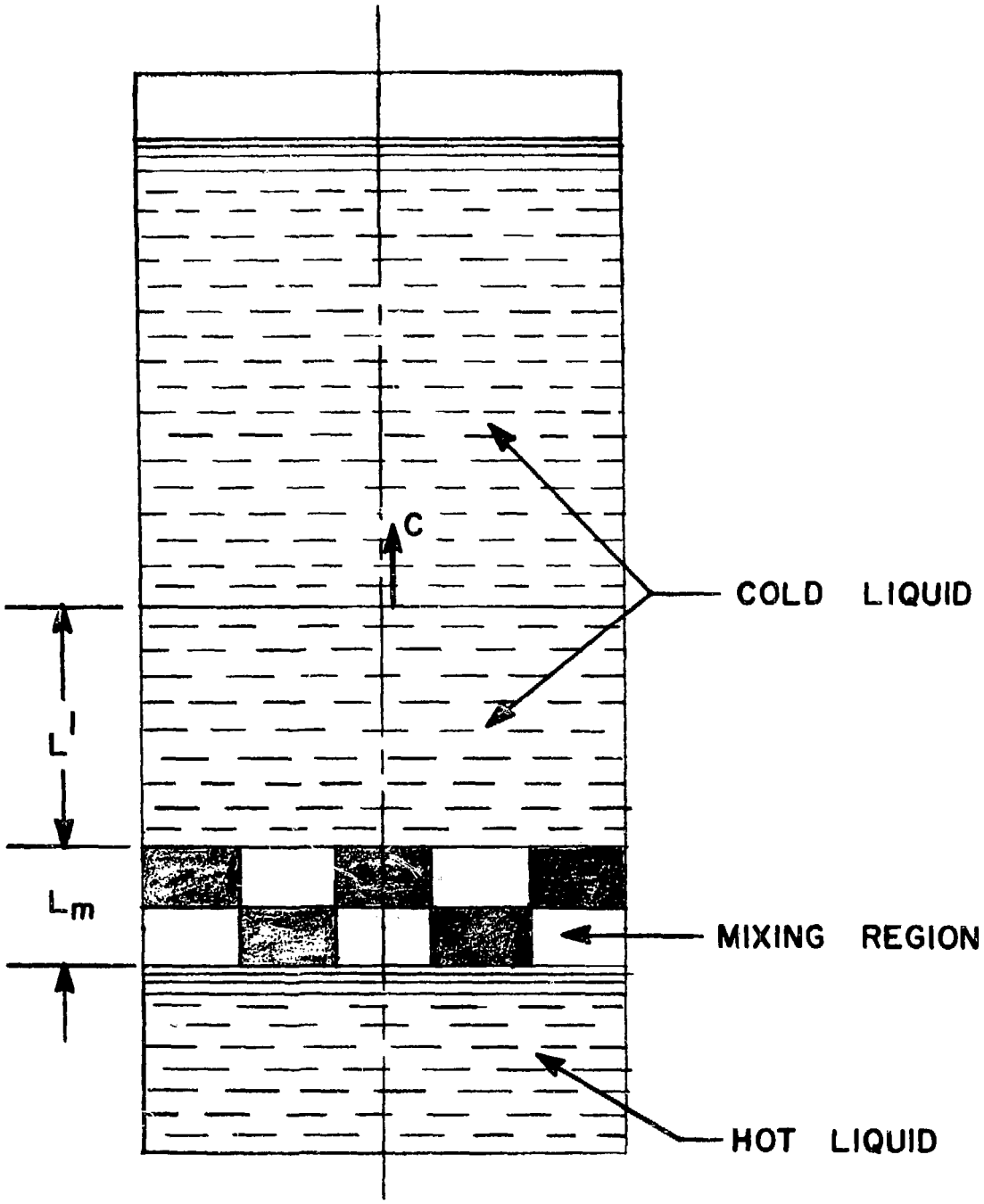

Fig. 6.8 One-Dimensional Description of Mixing Process

$R_h \sim 0.4$ mm

$L_m = 4$ mm

This mixing length is an order of magnitude less than that used in calculating the single-phase pressurization values listed in Table 6.1. Therefore, the pressures listed in that table are approximately an order of magnitude greater than those which could be obtained from mixing considerations.

The new surface area is given by

$$S = \frac{3L_m S_o}{R_h} \tag{6.47}$$

or, the increase in heat transfer area is

$$\frac{S}{S_o} = \frac{3u_i t_m}{R_h} \tag{6.48}$$

In this case, $\frac{S}{S_o} = 30$.

Note that by considering a one-step mixing process and by assuming that $u_m = u_i$, we evaluated the maximum mixing energy. Thus, the increase in area given by Eq. 6.48 is the lower bound, and evaluating the interfacial area from the minimum mixing method of Ref. 73 would increase the heat transfer area.

For Wright's experiments, $t_m = 0.2$ msec (mixing time as observed in Fig. 2.2) and $u_i = 1.36$ m/sec (calculated from the known impact pressure and corresponds closely to free fall behavior) we get:

$R_h \sim 9$ μ

$L_m = 0.27$ mm

and

$$\frac{S}{S_o} \overset{\sim}{=} 90$$

Assuming the liquid is saturated at the maximum pressure shown in Wright's experimental trace (Fig. 2.2) i.e., $T_c \sim 350°C$, the energy stored in the intermixed aluminum

$$Q = \rho_h L_m S_o C_h (T_h - T_c) \tag{6.49}$$

and is evaluated to be 49 cal for an initial temperature of 950°C (ρ_h = 2.3 g/cm^3 and C_h = 0.26 cal/g °C). If vapor is produced in Wright's experiment and it is saturated at 350°C, the displacement required to pressurize the whole column is $d\ell_c$ = 6.76 mm calculated from Eq. 6.7 assuming $\ell_c \ll L$ and $\beta_T = 4.83.10^{-5}$ 1/bar (L is known to be 0.9 m). The heat required to vaporize that amount of vapor is evaluated from

$$Q = \rho_v \, d\ell_c \, S_o \lambda \tag{6.50}$$

and is 78.5 cal, which is the same order as the energy calculated to be stored in the aluminum.

Assuming that the heat for vaporizing the water is transferred from the aluminum to the water during the intermixing stage and is conduction limited in the aluminum, neglecting any contribution from the heat of fusion for aluminum, and chemical reaction or the kinetic energy of the column (∿0.1 cal), the required debris area is;

$$S = \frac{Q}{2k_h \, \Delta T \sqrt{\frac{t_m}{\pi \alpha_h}}} \tag{6.51}$$

and we find that

$$\frac{S}{S_o} = 2.58$$

Solving the same with the assumption that the energy transfer is conduction limited in the water, we find that ($\Delta T = 350 - 20 = 330°C$)

$$\frac{S}{S_o} = 79$$

In both cases the required heat transfer area is of the order or less than the debris area calculated from the intermixing considerations. Thus, a heat transfer mechanism in which intermixing results in a limited amount of hot liquid to transfer its energy to the cold liquid during the intermixing stage, may exist and produce the observed pressurization in the liquid column. Note that we assumed here that the cold liquid is saturated at 350°C and the hot liquid temperature is reduced considerably during the intermixing stage (from 950°C to 350°C), otherwise the heat could not be transferred directly to the cold liquid but rather through a vapor layer. Also, we assumed that the interface temperature is not established according to the classical conduction theory (Eq. A.2) which results in $T_I \sim 850°C$.

6.6 Summary

After the diaphragm bursts, small drops and precursor jets reach the hot surface and produce vapor, the amount of which depends on the hot liquid temperature. The pressure in the vapor volume acts on the coolant and accelerates it upward. During this motion the pressure in the vapor volume decreases and it falls below the system pressure, causing the coolant to decelerate and to reenter. When the column is

stopped pressures generated may be much larger than the first one, since during the ejection stage the liquid column may reach distances larger than the original distance. For example, in the present apparatus, if the column reaches the top of the upper section, the possible impact pressure is about 13.5 MPa when P_∞ = 0.2 MPa. As the impact pressure is relieved, thermal interaction occurs and the process repeats. When the interface temperature is larger than T_{sn} a large amount of vapor is produced which results in large hydrodynamic and thermal effects. When $T_I < T_{sn}$ but $T_h > T_{sn}$ low rate of vaporization occurs which results only in impact pressures without a significant increase in the measured impulses. In order to observe the process of large bouncing, the pressure in the vapor should be larger than the ambient pressure, which means that the vapor produced is a result of bubbles growing inertially, i.e., the pressure is the vapor pressure. So, any mechanism which decreases or eliminates the inertial stage will affect the resultant interaction. This was shown to happen when the pressure system is increased.

In Wright's experiment, the first impact exhibits a very large pressure peak and cannot be considered as hydrodynamic pressure. However, other aluminum experiments exhibit the bouncing behavior. Since the column may be ejected to a large distance along the tube, hydrodynamic impact may be significant. Thus, a careful analysis is necessary in order to evaluate the origin of the high pressures in shock tube experiments.

VII. CONCLUSIONS

1. When any condensible or noncondensible vapor precedes the liquid column, which is always the practical case, the column does not stop instantaneously upon contact.
2. Hydrodynamic and/or thermal interactions, accompanied by bouncing of the liquid column, were observed with water and Wood's metal. The lower temperature threshold for those interactions is $T_h \tilde{=}$ 210°C which may be identified with T_{sn}. When temperatures were in the range of $T_h > T_{sn}$ and $T_I < T_{sn}$ subsequent bounces may produce impact pressures of the order of "water hammer" pressures (induced thermal interactions).
3. Large pressures and impulses are observed when $T_I > T_{sn}$. The mechanism for producing the high pressures is a combination of hydrodynamic impact and thermal interaction.
4. For butanol the measured impulses and pressures are of the same order as the respective theoretical hydrodynamic values. Thus it is highly suggestive that the pressures generated are a result of water hammer action.
5. Impaction of Freons (Freon-11 and Freon-22) on oils (mineral and silicone), water, and mercury have not produced significant thermal interactions which may be due to the high system pressure.
6. The suppression of interactions by large initial system pressures may indicate that bubbles growing inertially are the controlling mechanism for large scale thermal interactions.
7. To analyze shock tube data one should regard carefully the hydrodynamic effects which may be very significant, especially when multiple interactions are observed.

APPENDIX A

Homogeneous Nucleation and Interface Temperature

The range of existence of a liquid extends from the melting point of its solid to its critical temperature, above which point the liquid is indistinguishable from the vapor. Between the boiling and the critical temperatures of the cold liquid lie a number of spontaneous nucleation temperatures due to statistical density fluctuations which depend on the exact nature of the system. The highest spontaneous nucleation temperature will be the homogeneous nucleation temperature, at which point bubbles will be generated with high probability from a metastable superheated state in the absence of heterogeneities and other nucleants.

The spontaneous nucleation rate J (sites/cm^3 sec)can be calculated from[74]

$$J = A(T)\ \exp\left[-\ \frac{16\pi\sigma^3 f(\theta)}{3(P_v - P_\ell)^2 KT}\right] \qquad (A.1)$$

where K is Boltzmann's constant, T is the absolute temperature, σ is liquid surface tension, P_ℓ and P_v are liquid and vapor pressures, respectively, and $f(\theta)$ is a functional relationship involving the contact angle θ ($0 \leq f(\theta) \leq 1$). A(T) describes the exact details of the nucleation process and its value is $\sim 10^{33}$. An error by several orders of magnitude in estimation J/A(T) has little effect on the calculated temperature. Equation A.1 exhibits a very strong temperature threshold as illustrated in Tables A.1 to A.5 for homogeneous nucleation of Freon-22, water, butanol, and sodium ($f(\theta) = 1$). Difficulties arise if one wants to calculate the spontaneous nucleation temperature ($f(\theta) \neq 1$).

In the liquid-solid case, the most severe limitation is inadequate knowledge or means of measuring the liquid-solid and the solid-vapor interfacial tensions. In the liquid-liquid case, extrapolating measurable surface and interfacial tensions into temperature ranges over which the liquid is metastable remains a major constraint on the precision of theoretical predictions. After displacement of the gas layer, equilibration of the characteristic contact angle (or interfacial tension) following direct liquid-liquid contact requires a finite time, i.e., the contact angle θ varies with time. It therefore follows from Eq. A.1 that the spontaneous nucleation temperature for a given liquid-liquid system varies with time. If the interfacial temperature (T_I) at the instant of contact is below the homogeneous nucleation temperature, then the spontaneous nucleation temperature threshold depends upon the heating rate. If the time constant for contact angle equilibration is less than the characteristic heating rate, then the threshold temperature is determined by the characteristic equilibrium contact angle of the system. If this value is near or equal to zero, homogeneous nucleation is possible. On the other hand, if the heating rate exceeds the characteristic time constant for contact-angle equilibration, spontaneous nucleation occurs at the liquid-liquid interface, rather than homogeneous nucleation.

The sudden contact between a hot and cold liquid is an example of rapid heating, where the contact temperature T_I will be established instantaneously according to the classical equation:[75]

$$\frac{T_I - T_c}{T_h - T_I} = \left(\frac{k_h \rho_h C_h}{k_c \rho_c C_c}\right)^{1/2} \qquad (A.2)$$

The basic assumptions for yielding Eq. A.2 are very ideal when applied to liquid-liquid contact. Many uncertainties arise, such as the effects of temperature on thermal parameters, especially near the critical temperature of the cold liquid, and the importance of interfacial structure and of phase changes which could liberate large quantities of heat at the interface.

The thermal properties of some of the liquids used in the present experimental study are given in Table A.5. The molten salt (LiCl-KCl) properties are:

$k = 1.65.10^{-3}$ cal/sec cm °C (Ref. 78)

$\rho = 1.766 - 0.4328.10^{-3}\ T(g/cm^3)$ (Ref. 79)

$C = 1.465 - 3.77.10^{-4}\ T + 1.69.10^{-7}\ T^2$ (J/g °C) (Ref. 80) where T is the temperature in °C.

Table A1. HOMOGENEOUS NUCLEATION FOR FREON-22

P_ℓ = 0.1 MPa

T_ℓ	P_v	σ	R_{cr}	J
°C	MPa	N/m	A°	sites/cm^3 sec
50	1.94	0.0047	49	$3.9 \cdot 10^{-18}$
52	2.03	0.0045	44	2.0×10^{-6}
54	2.12	0.0042	40	2.4×10^{3}
56	2.23	0.0040	36	7.2×10^{10}
58	2.32	0.0037	32	1.6×10^{16}
60	2.43	0.0035	29	3.7×10^{20}

Table A2. HOMOGENEOUS NUCLEATION FOR WATER

P_ℓ = 0.1 MPa

T_ℓ °C	P_v MPa	σ N/M	R_{cr} Å	J sites/cm^3 sec
290	7.44	0.0167	45.6	5.2×10^{-49}
300	8.59	0.0143	33.9	7.8×10^{-6}
310	9.87	0.0121	24.8	1.2×10^{16}
320	11.29	0.0099	17.7	1.1×10^{26}
330	12.86	0.0078	12.2	2.9×10^{30}

Table A3. HOMOGENEOUS NUCLEATION FOR BUTANOL

T_ℓ	P_v	σ	P_ℓ	R_{cr}	J
°C	MPa	N/M	MPa	°A	sites/cm^3 sec
230	1.82	0.0053	0.10	61.6	1.28×10^{-20}
			0.20	65.4	2.26×10^{-27}
235	1.97	0.0048	0.10	51.3	1.14
			0.20	54.2	1.66×10^{-4}
237	2.03	0.0046	0.10	47.7	7.76×10^{5}
			0.20	50.3	6.9×10^{4}
240	2.16	0.0043	0.10	41.7	5.7×10^{13}
			0.20	43.9	5.52×10^{11}
250	2.62	0.0033	0.10	26.2	2.07×10^{27}

Table A4. HOMOGENEOUS NUCLEATION FOR SODIUM

P_ℓ = 0.1 MPa

T_ℓ °C	P_v MPa	σ N/m	R_{cr} Å	J sites/cm^3 sec
1830	11.14	0.0245	42	2.3×10^5
1835	11.30	0.0240	41	6×10^7
1840	11.40	0.0234	40	9×10^9
1860	12.03	0.0213	34	1.5×10^7
1880	12.70	0.0193	30	1.7×10^{22}
1900	13.40	0.0172	25	1×10^{25}
2000	17.12	0.0069	7	5×10^{30}

Table A5. THERMAL PROPERTIES

Liquid	k cal/sec cm °C	ρ g/cm^3	C cal/g °C
Water[76]	0.00139	1.0	1.0
Butanol[76]	0.00037	0.81	0.296
Wood's metal[77]	0.0319	9.70	0.0352

APPENDIX B

Transition Radius of Bubble Growth and Stability Line for "Capture Theory"

For a first order approximation, the bubble growth mechanism can be regarded as consisting of two basic regimes; the inertially dominated growth regime and the thermally dominated regime. In inertially dominated systems, the temperature inside the bubble is essentially equal to the surrounding liquid, and the pressure within the bubble equals the vapor pressure corresponding to the liquid temperature, and is higher than the liquid pressure far removed from the bubble surface. The bubble growth in this regime is calculated from Rayleigh's equation:

$$R - R_{cr} = \sqrt{\frac{2}{3}\,\frac{P_v - P_\ell}{\rho_\ell}}\; t \qquad (B.1)$$

In the thermally dominated regime, the bubble growth is limited by the rate at which thermal energy can be conducted from the liquid to the interface. In this regime the bubble temperature is different than the liquid temperature far removed from the liquid-vapor interface and the bubble pressure essentially equals the liquid pressure. The bubble growth equation in this regime is given by:

$$R = 2Ja\sqrt{\alpha_\ell t} \qquad (B.2)$$

where Ja is Jakob number defined as:

$$Ja = \frac{\left(T_h - T_{sat}\right)\rho_\ell C_\ell}{\rho_v \lambda} \qquad (B.3)$$

The inertial and thermal dominated bubble growth behavior is shown in Fig. B.1. The actual growth is always limited by the slowest growth rate between the two mechanisms and for some conditions it is limited by both thermal and inertial considerations. These two growth behaviors can be viewed as asymptotic limits, i.e., the growth is inertially dominated early in time and thermally dominated late in the growth. By equating Eqs. B.1 and B.2 one can find the approximate transition radius where the growth behavior changes from inertial to thermal domination. This transition radius is given by:

$$R_t = \frac{4Ja^2\alpha_\ell}{\frac{2}{3}\left(\frac{P_v - P_\ell}{\rho_\ell}\right)^{1/2}} \qquad (B.4)$$

Equation B.4 is a reasonable approximation, following the criteria given in Ref. 81 which indicate that R_t given in Eq. B.4 is in the center of the intermediate regime.

As discussed in Sect. 2.2.2 the capture theory[37] predicts the sizes of drops which would remain in contact with a hot surface, as a function of the interface temperature. A computer code has been developed for the purpose of predicting a stability line for a given cold liquid. The main features of the code are:

1) uses tabulated values for P_v, σ, and ρ_ℓ.
2) calculates the intersection between the bubble mechanical stability line and the thermal boundary layer after waiting time consisting of: single phase relief time and waiting time for the first nuclei and acoustic relief time for bubble.
3) the thermal boundary layer is calculated by the standard error function solution.

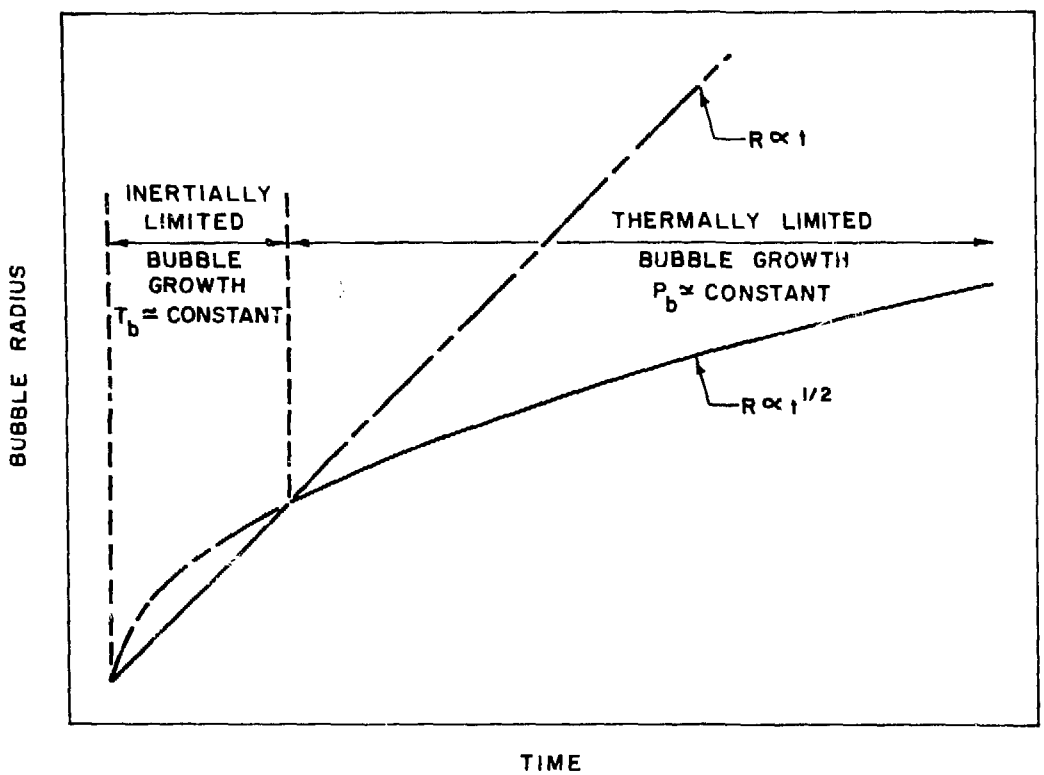

Fig. B.1 Inertial and Thermal Dominated Bubble Growth Behaviors (after Henry and McUmber[57])

4) it is easy to recalculate if a change in parameters is desired e.g., N.

A prediction of the stability line for Freon-22 is given in Fig. B.2. It is shown that for N = 10^9 sites/cm^2 the predicted drop diameters here differ by a factor of ∿4 from those given in Ref. 37 (Fig. B.3). Also, the vertical portion of the line is shifted from ∿58°C in Ref. 37 to 60°C, which may be a result of a more refined calculation, i.e., using the error function instead of the approximate form of it. Another interesting point is the sensitivity of the predicted diameter to the assumed maximum N. However, the vertical portion of the line is the same for N = 10^8, 10^9, and 10^{10} sites/cm^2, which indicate that above 60°C capture essentially is limited by maximum number of sites assumed. Below 60°C, J at point A is reduced considerably and consequently, N. Thus, bubble growth time for mutual pressurization is rather long, which results in capture. Hence, an approximate method can be derived for predicting the stability line.

Approximating the thermal boundary layer equation yields:

$$\frac{T_I - T}{T_I - T_c} = \frac{x}{2\sqrt{\alpha_c \, t_n}} \tag{B.5}$$

where $t_n = t_{sf} + t_a + t_w$ (B.6)

$$t_{s_f} = \begin{cases} 10^{-7} \text{ sec} & t_a > 10^{-7} \text{ sec} \\ t_a & t_a < 10^{-7} \text{ sec} \end{cases} \tag{B.7}$$

$$t_a = \frac{2\ell}{c} \tag{B.8}$$

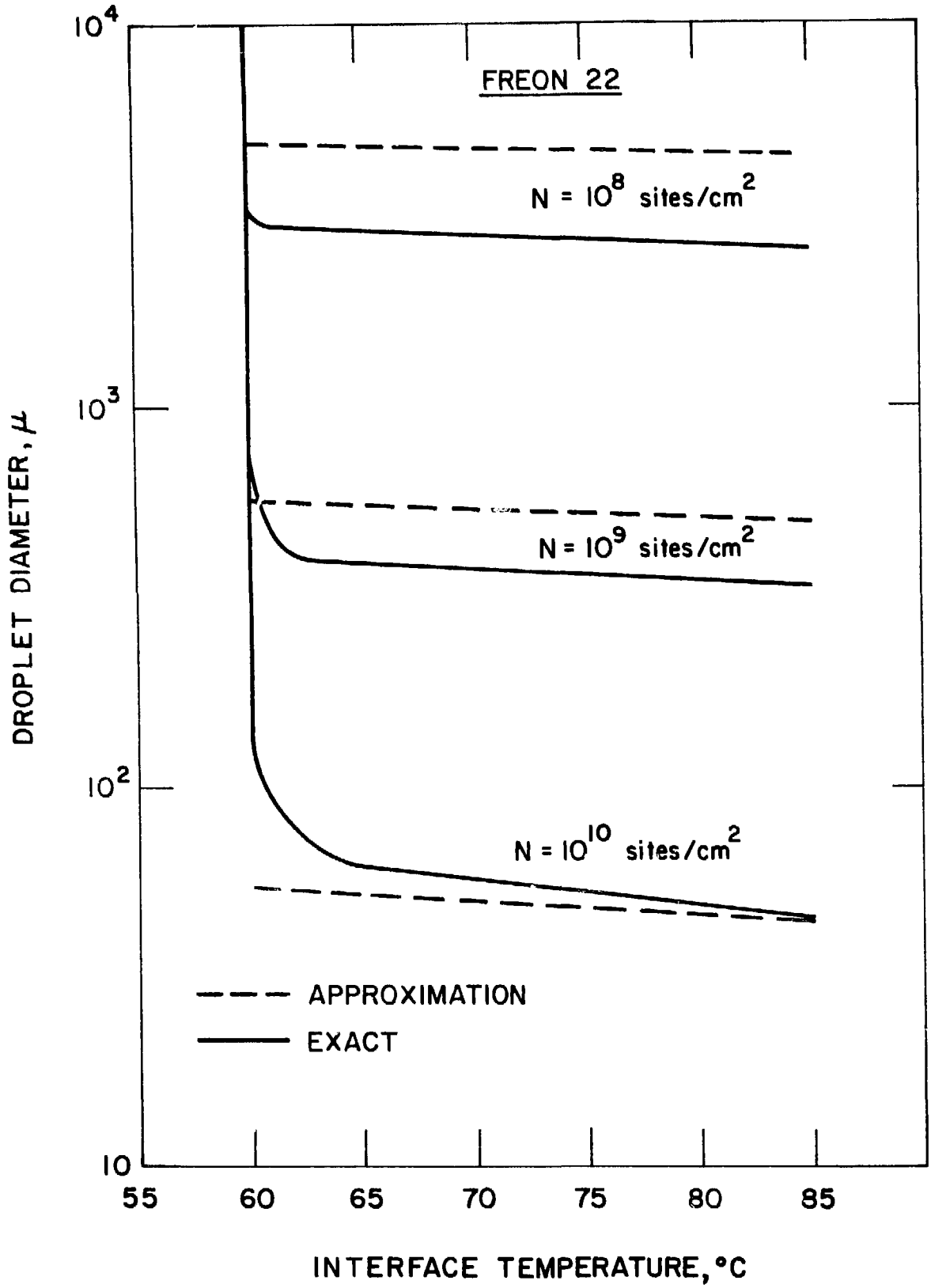

Fig. B.2 Stability Line of Freon-22 at a Pressure of 0.1 MPa

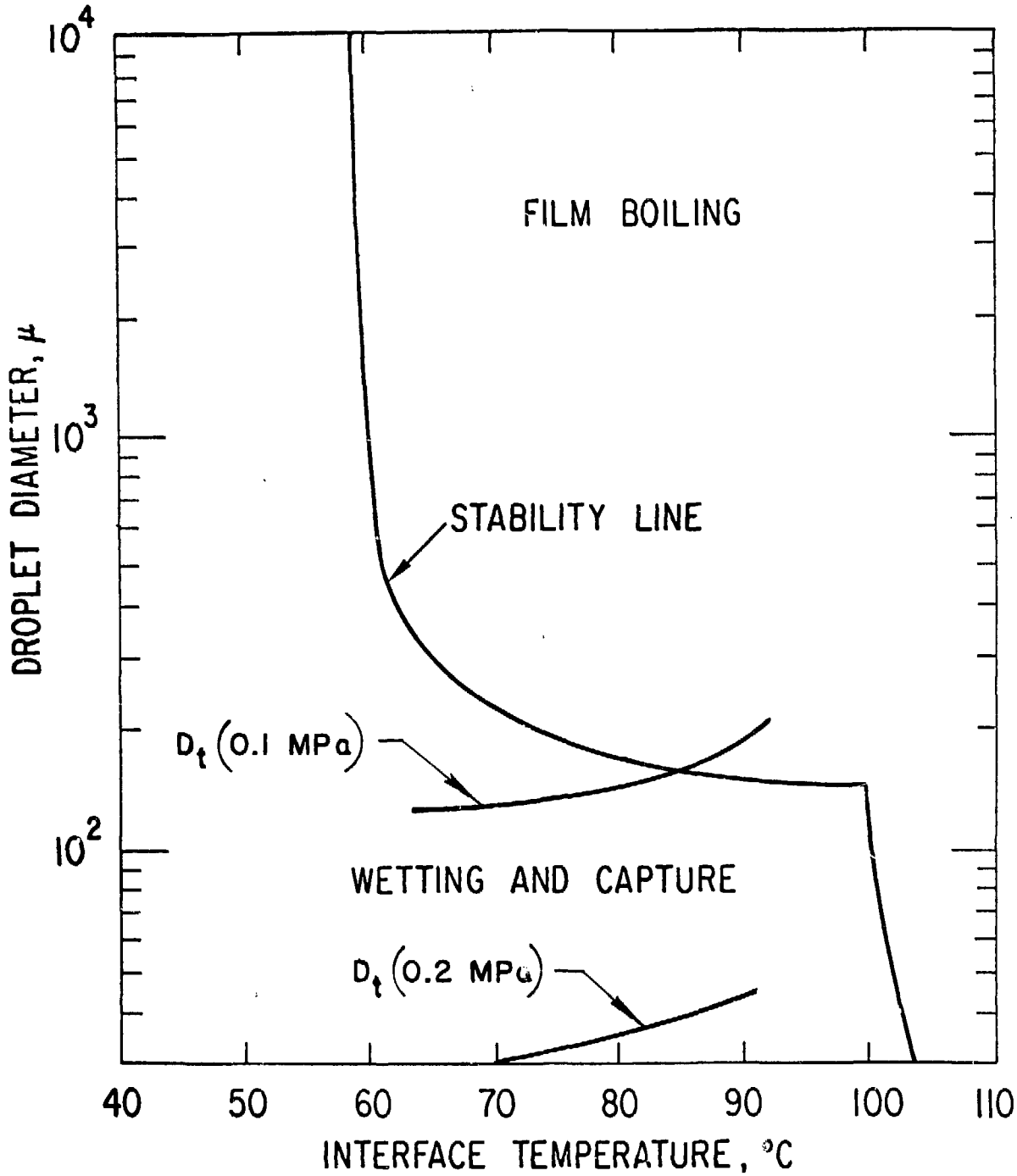

Fig. B.3 Freon-22 Capture Diameters Versus Interface Temperature at a Pressure of 0.1 MPa (after Henry and McUmber[57])

$$t_w = 1/(JV) \tag{B.9}$$

The crucial point for determining capture/film boiling is the intersection at point B, where $x = D_B$ and $T = T^*$. Hence, Eq. B.5 has the form:

$$\frac{T_I - T^*}{T_I - T_{sat}} = \frac{D_B}{2\sqrt{\alpha_c t_n}} \tag{B.10}$$

D_B can be calculated by:

$$D_B = \frac{1}{\sqrt{N}} \tag{B.11}$$

and T^* can be found from the explicit relation:

$$D_B = \frac{4\sigma(T^*)}{P_v(T^*) - P_\ell} \tag{B.12}$$

When calculating for temperature well above the spontaneous nucleation, $t_w << t_a$, or,

$$t_n = t_{sf} + t_a \tag{B.13}$$

Hence,

$$t_n = \begin{cases} \frac{4\ell}{c} & t_a < 10^{-7} \text{ sec} \\ 10^{-7} + \frac{2\ell}{c} & t_a > 10^{-7} \text{ sec} \end{cases} \tag{B.14}$$

and an implicit relation between ℓ and T_I can be derived (here we assume $i = D/3$).

For Freon-22, assuming $N = 10^9$ sites/cm^2 yields $D_B = 3160$ Å which corresponds to $T^* = -16.4°C$. Taking $\alpha_c = 6.7.10^{-8}$ m^2/sec and

rearranging e.g., (B.10) we get:

$$t_n = 3.726.10^{-7} \left(\frac{T_I + 40.75}{T_I + 16.4} \right)^2 \text{ sec} \qquad \text{(B.15)}$$

The predicted stability lines for different assumed values of N are also shown in Fig. B.2. The results compare quite well with those predicted using a computer code, when interface temperature is higher than T_{sn}. From Eqs. B.10 and B.11 one can notice that the captured drop diameter depends on 1/N, as shown in Fig. B.2.

APPENDIX C

Water-Solid Surface Contacts

Pressure histories of water impacting on solid surface are given in this appendix, as well as data on the first three pulses (Table C1). The symbols used in the table are:

P_∞ the pressure in the upper tube before diaphragm rupture.

t_{exp} time from diaphragm rupture to first impact, measured from pressure graph

Δt time from beginning of first impact to the beginning of i^{th} pulse.

P_{max} maximum measured pressure of i^{th} pulse

t_p pulse duration

I_{exp} measured impulse by P.T.-1 of i^{th} pulse

P_i, I_{th} theoretical pressure and impulse to stop instantaneously the liquid column, based on initial conditions.

TABLE C1. Isothermal Impacts of Water on Solid Surface

Run	Vacuum (mm Hg)	ΔP_∞ (MPa)	t_{exp} (msec)	Δt (msec)	P_{max} (MPa)	t_p (msec)	P_{max}/P_i	I_{exp} KPa.sec	I_{exp}/I_{th}
71	0.15	0.41	26.0	0	6.00	4.4	0.46	13.5	0.62
				18.5	1.72	5.0	0.12	5.2	0.24
				28.5	1.45	3.75	0.10	3.6	0.17
72	0.5	0.55	20.75	0	10.3	4.0	0.68	17.5	0.76
				16.5	2.21	4.0	0.14	5.5	0.24
				25.0	1.65	3.0	0.11	2.5	0.11
73	0.5	0.55	22.5	0	5.86	4.25	0.35	16.4	0.66
				14.25	1.72	4.25	0.10	3.7	0.15
				21.25	0.69	3.0	0.04	1.0	0.04
74	0.5	0.45	27.5	0	5.52	4.5	0.33	11.7	0.47
				20.25	3.45	3.0	0.21	5.2	0.21
				32.5	2.45	3.0	0.15	3.7	0.15
75	18	0.62	25.25	0	4.83	5.0	0.23	14.5	0.46
				17.75	3.79	2.75	0.18	5.2	0.17
				30.0	2.76	3.50	0.13	4.8	0.15
76	18	0.50	25.5	0	6.34	4.5	0.37	11.2	0.44
				15.75	1.38	5.5	0.08	3.8	0.15
				25.5	0.55	2.5	0.03	0.7	0.03
77	33	0.52	25.0	0	7.45	4.12	0.39	11.9	0.46
				18.75	1.65	6.50	0.09	4.3	0.16
				38.0	1.03	5.62	0.06	1.5	0.06
78	64	0.19	42.5	0	3.45	7.5	0.31	8.0	0.49
				50.0	1.52	9.0	0.14	2.4	0.14
				92.5	0.83	15.0	0.07	2.1	0.13

TABLE C1. Isothermal Impacts of Water on Solid Surface (cont'd.)

Run	Vacuum (mm Hg)	ΔP_∞ (MPa)	t_{exp} (msec)	Δt (msec)	P_{max} (MPa)	t_p (msec)	P_{max}/P_i	I_{exp} KPa.sec	I_{exp}/I_{th}
79	43	0.48	25.25	0	7.65	4.4	0.47	11.3	0.46
				20.0	2.76	6.25	0.17	3.5	0.14
				36.25	2.21	5.0	0.13	2.8	0.11
80	35	0.52	25.0	0	6.90	5.0	0.40	11.9	0.46
				21.25	2.41	4.37	0.14	5.2	0.20
				37.5	1.38	5.62	0.08	3.9	0.15
81	80	0.34	26.25	0	5.52	7.5	0.46	10.4	0.57
				27.5	2.76	5.0	0.23	5.2	0.28
				52.5	1.72	7.5	0.14	3.8	0.21
82	110	0.62	21.25	0	6.20	8.12	6.35	13.2	0.50
				27.5	2.45	9.37	0.14	5.4	0.21
				50.0	1.52	10.0	0.09	3.8	0.14
83	140	0.48	22.5	0	6.69	7.5	0.46	12.1	0.55
				30.0	2.76	7.5	0.19	6.9	0.32
				55.0	1.38	7.5	0.09	5.2	0.24
84	170	0.41	22.5	0	5.65	7.5	0.45	13.5	0.72
				35.0	2.41	8.75	0.19	6.0	0.32
				62.5	1.24	10.0	0.10	4.6	0.25
85	220	0.48	25.0	0	3.86	7.5	0.24	14.5	0.6
				32.5	1.72	12.5	0.11	10.7	0.44
				60.0	0.83	15.0	0.05	6.2	0.26
86	270	0.41	25.0	0	3.79	8.12	0.27	10.4	0.50
				40.0	1.72	12.5	0.12	6.5	0.31
				100.0	0.83	15.0	0.06	4.1	0.2

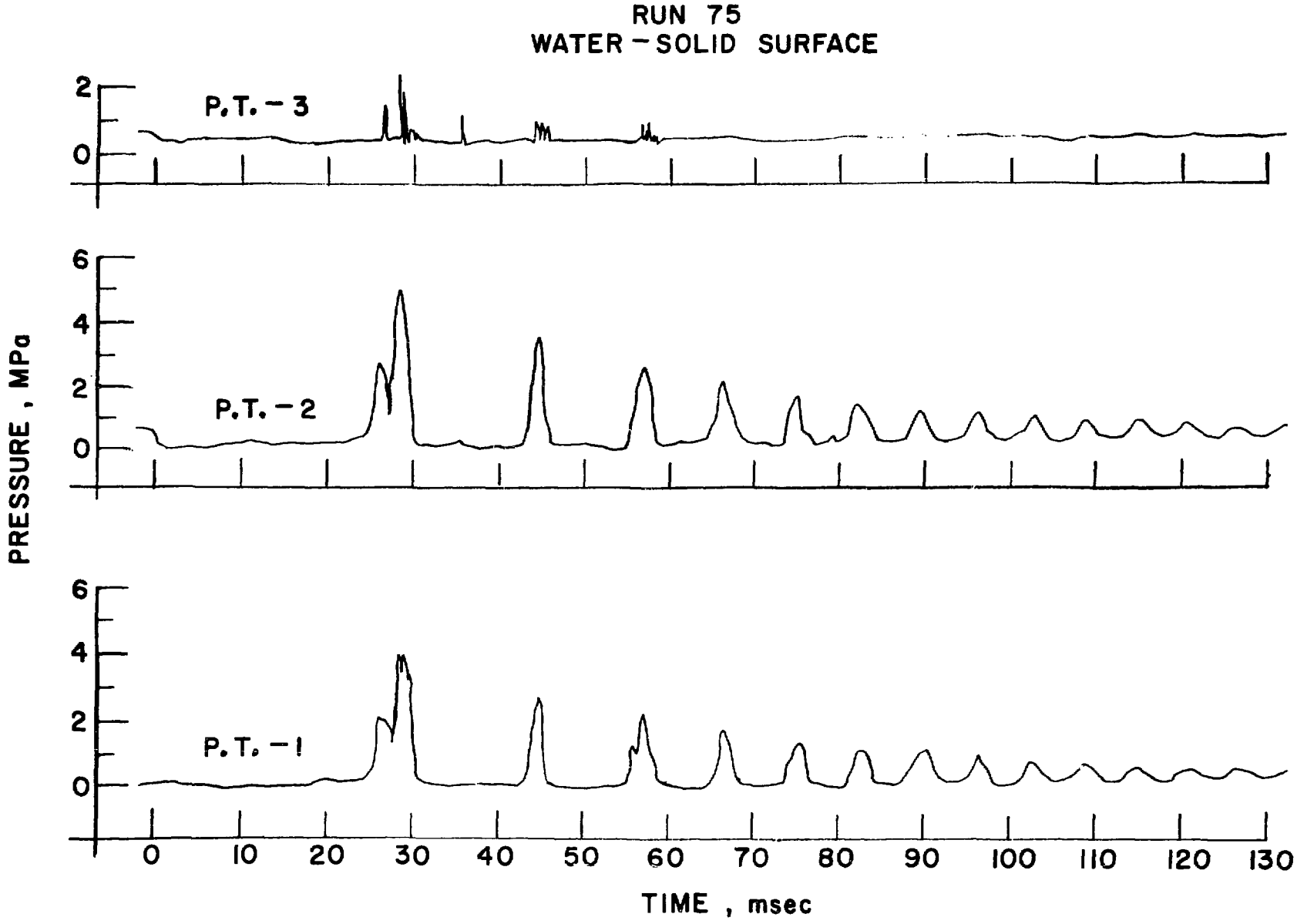

Fig. C.1 Pressure History of Run 75

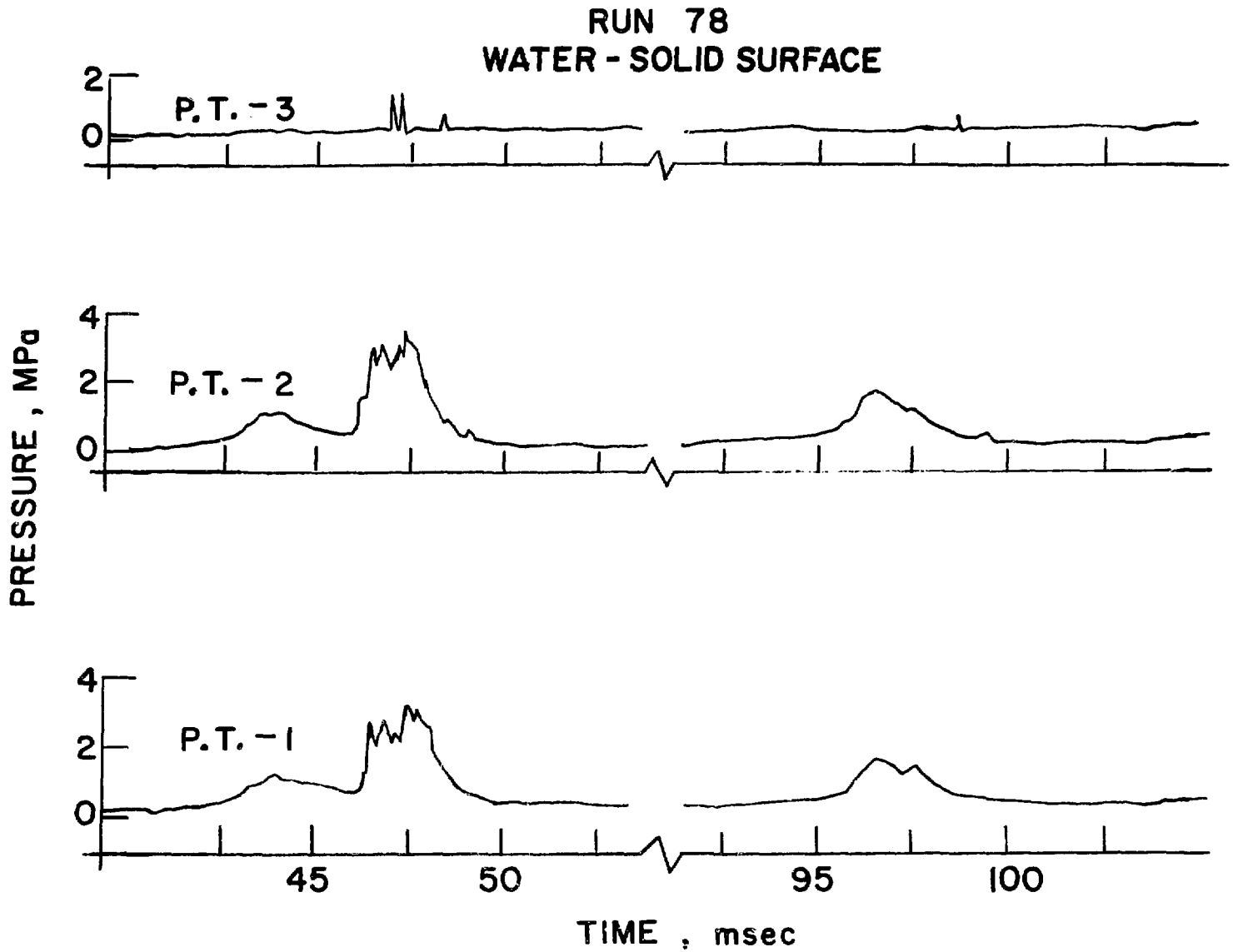

Fig. C.2 Pressure History of Run 78

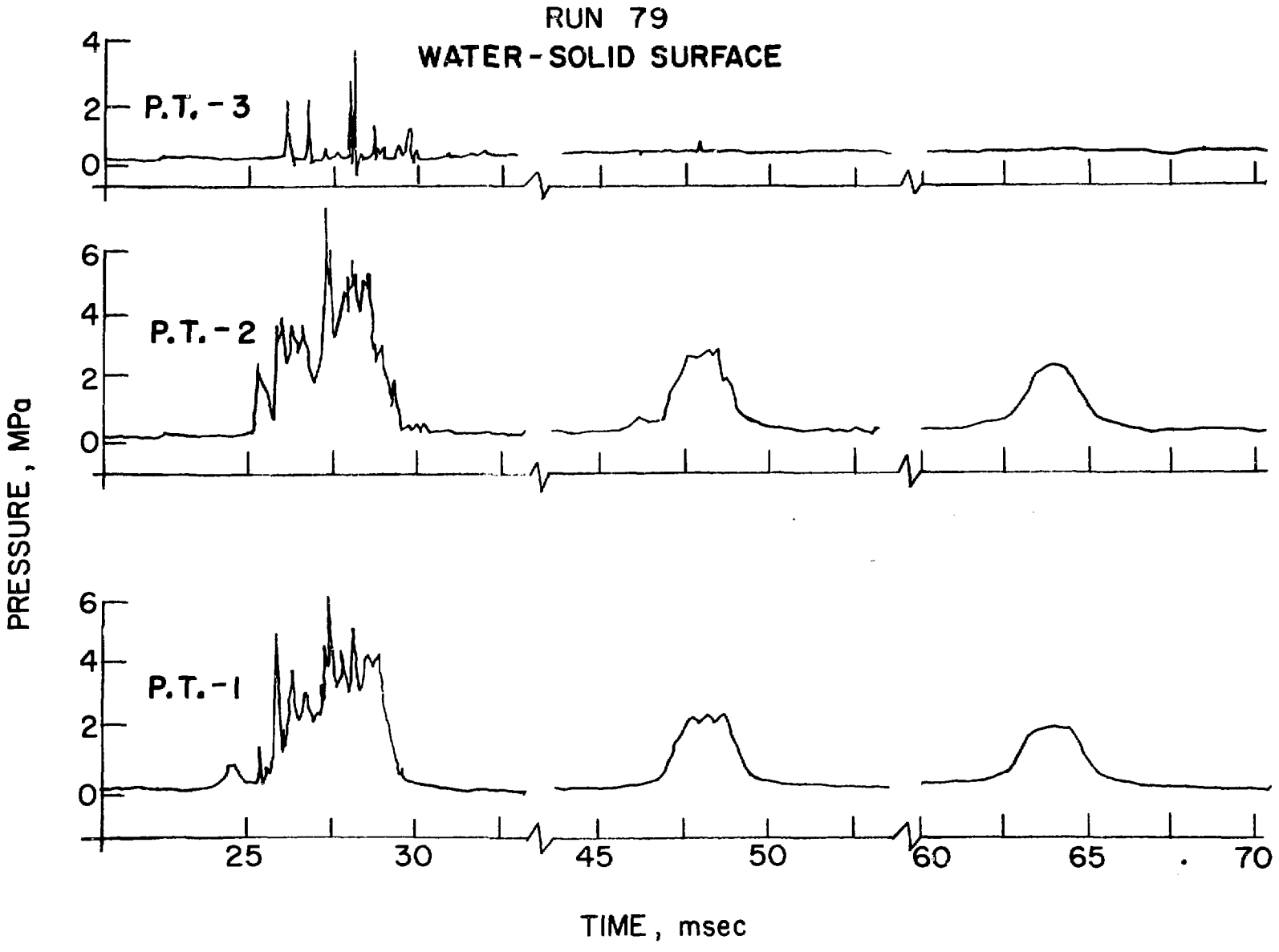

Fig. C.3 Pressure History of Run 79

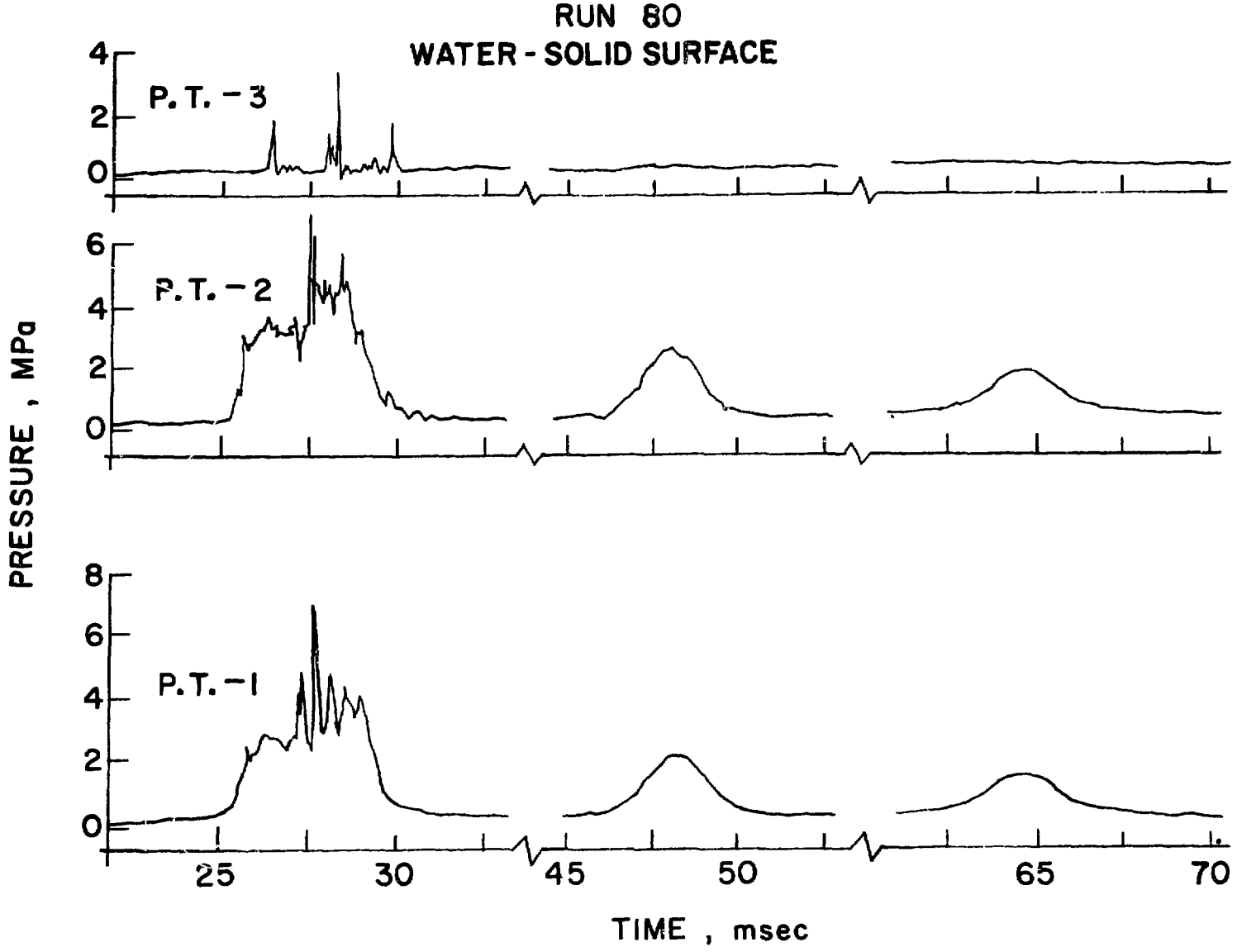

Fig. C.4 Pressure History of Run 80

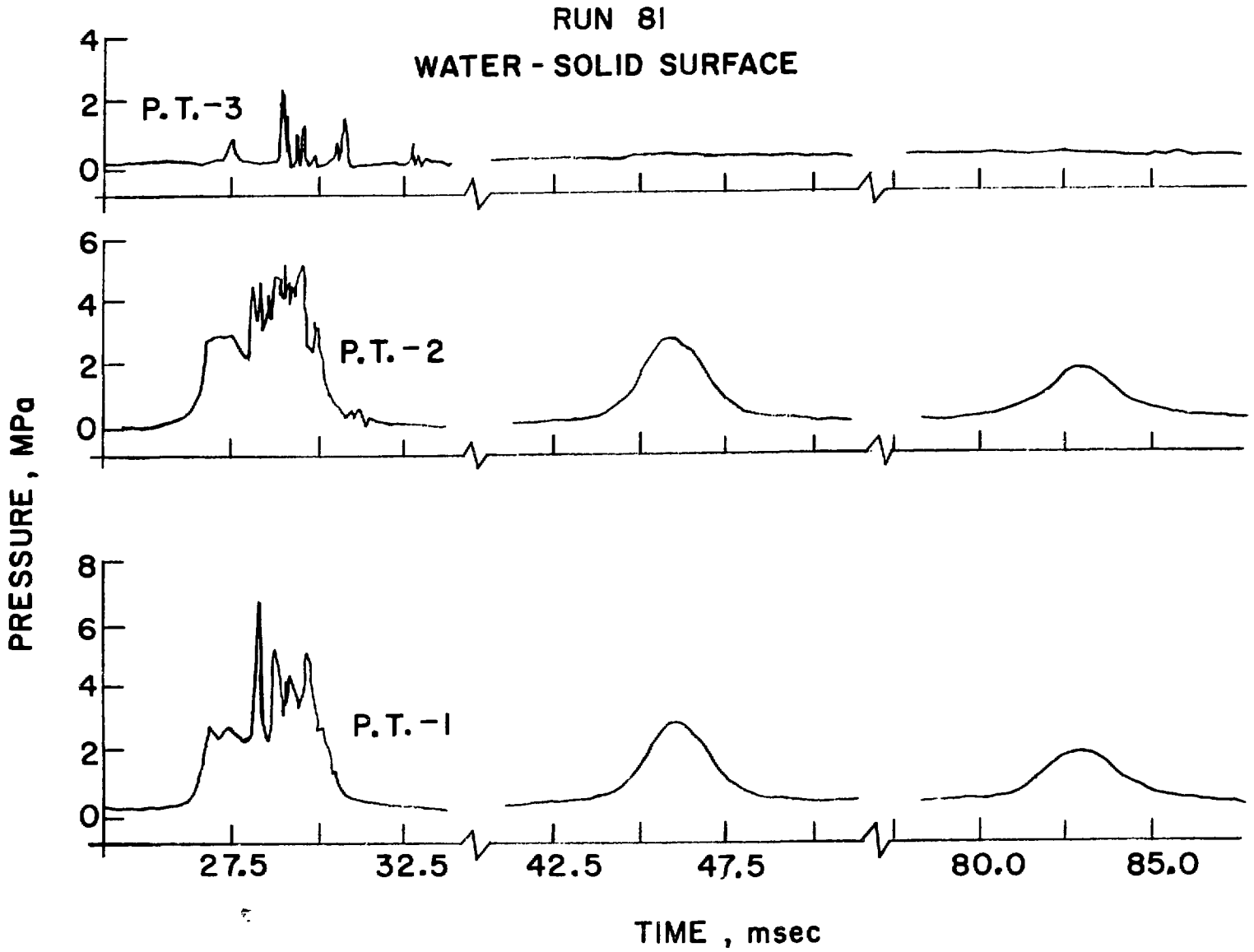

Fig. C.5 Pressure History of Run 81

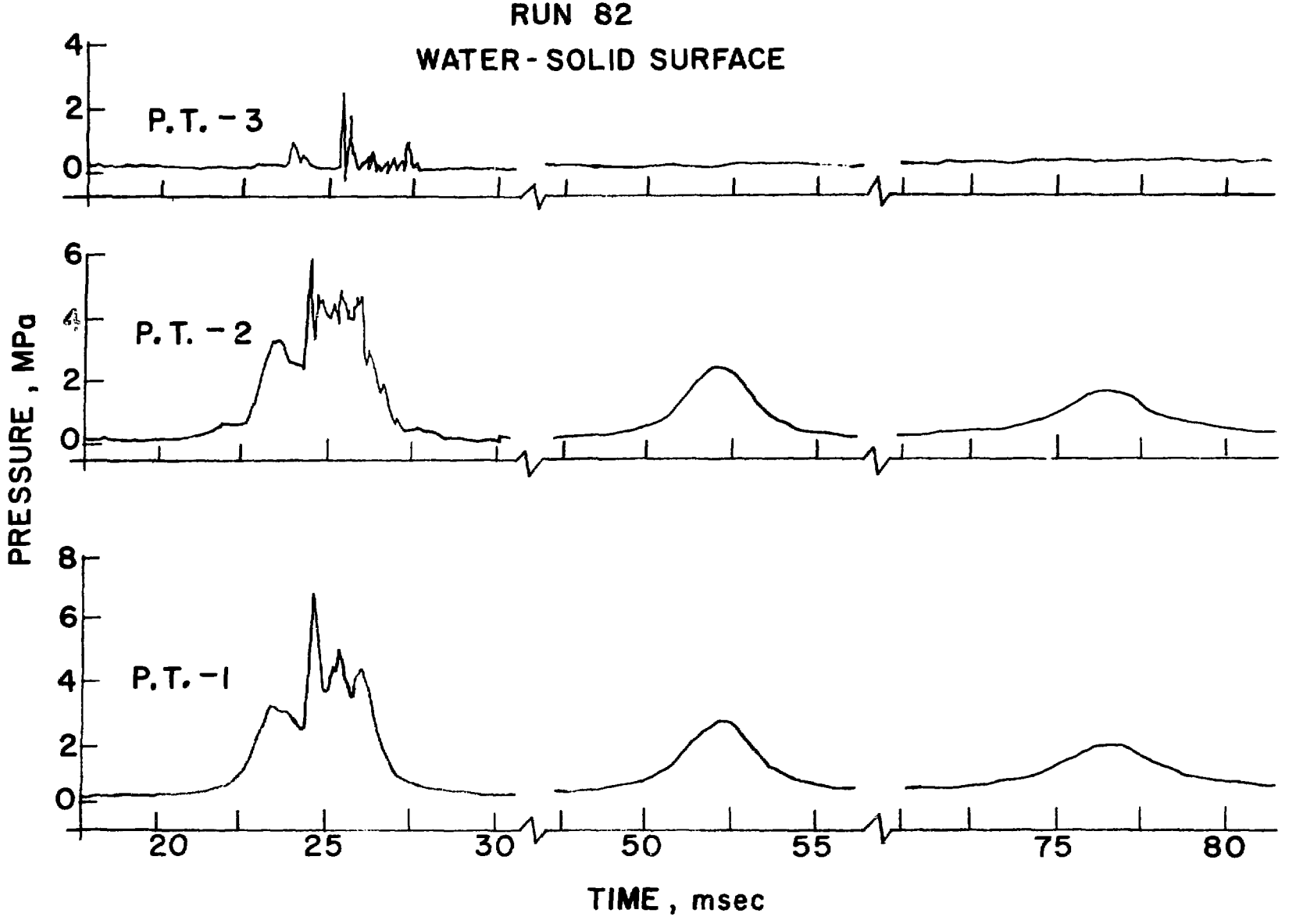

Fig. C.6 Pressure History of Run 82

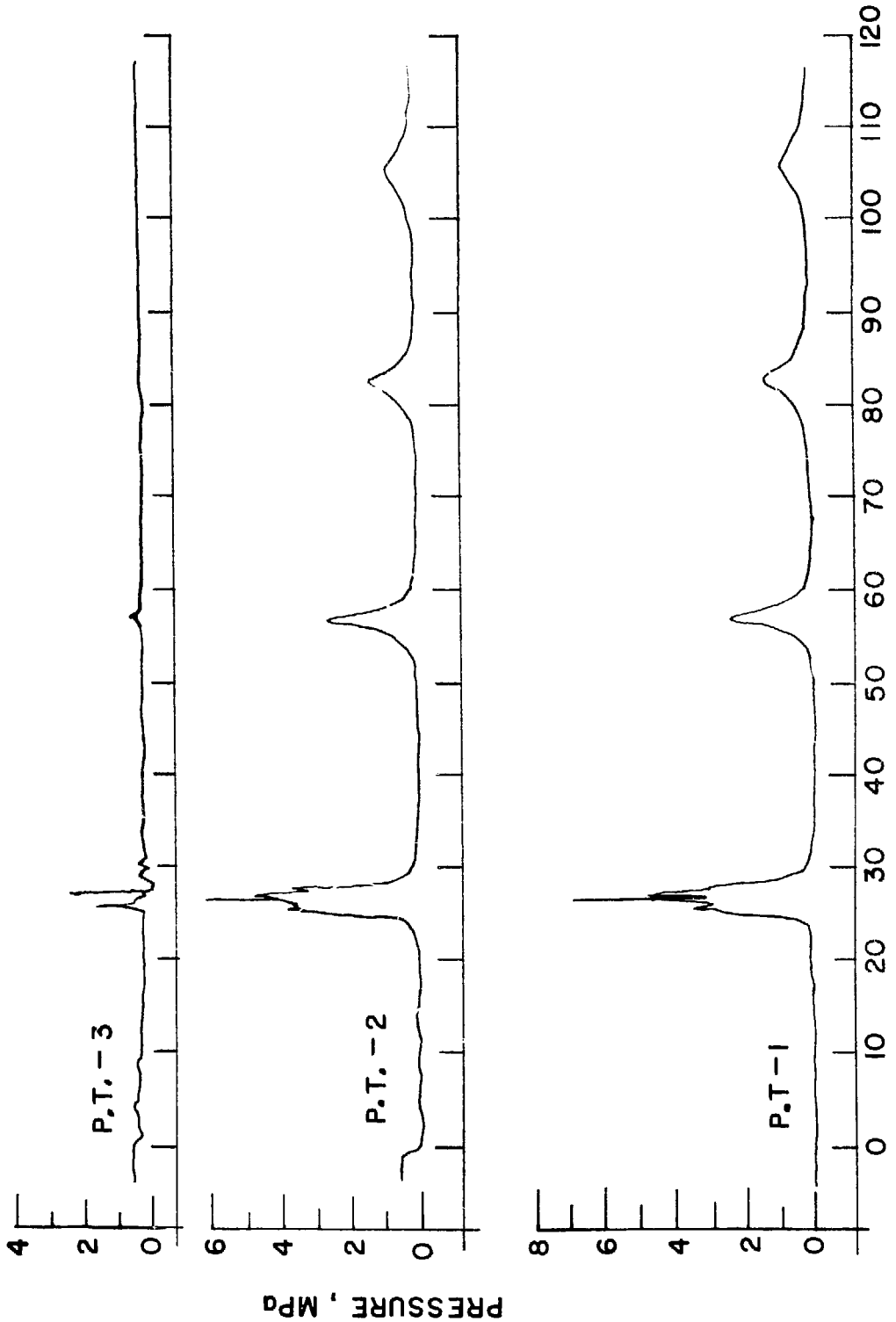

Fig. C.7 Pressure History of Run 83

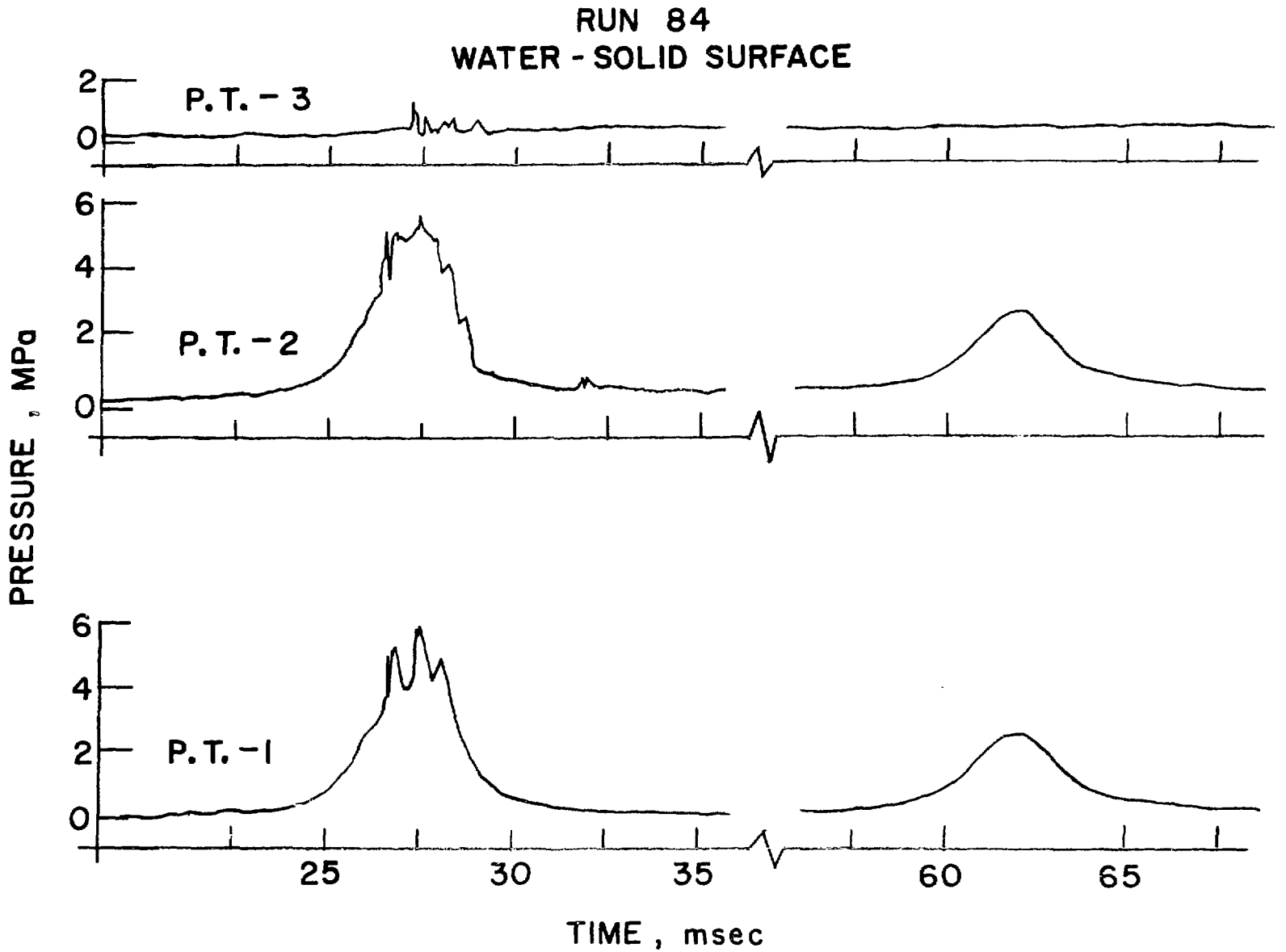

Fig. C.8 Pressure History of Run 84

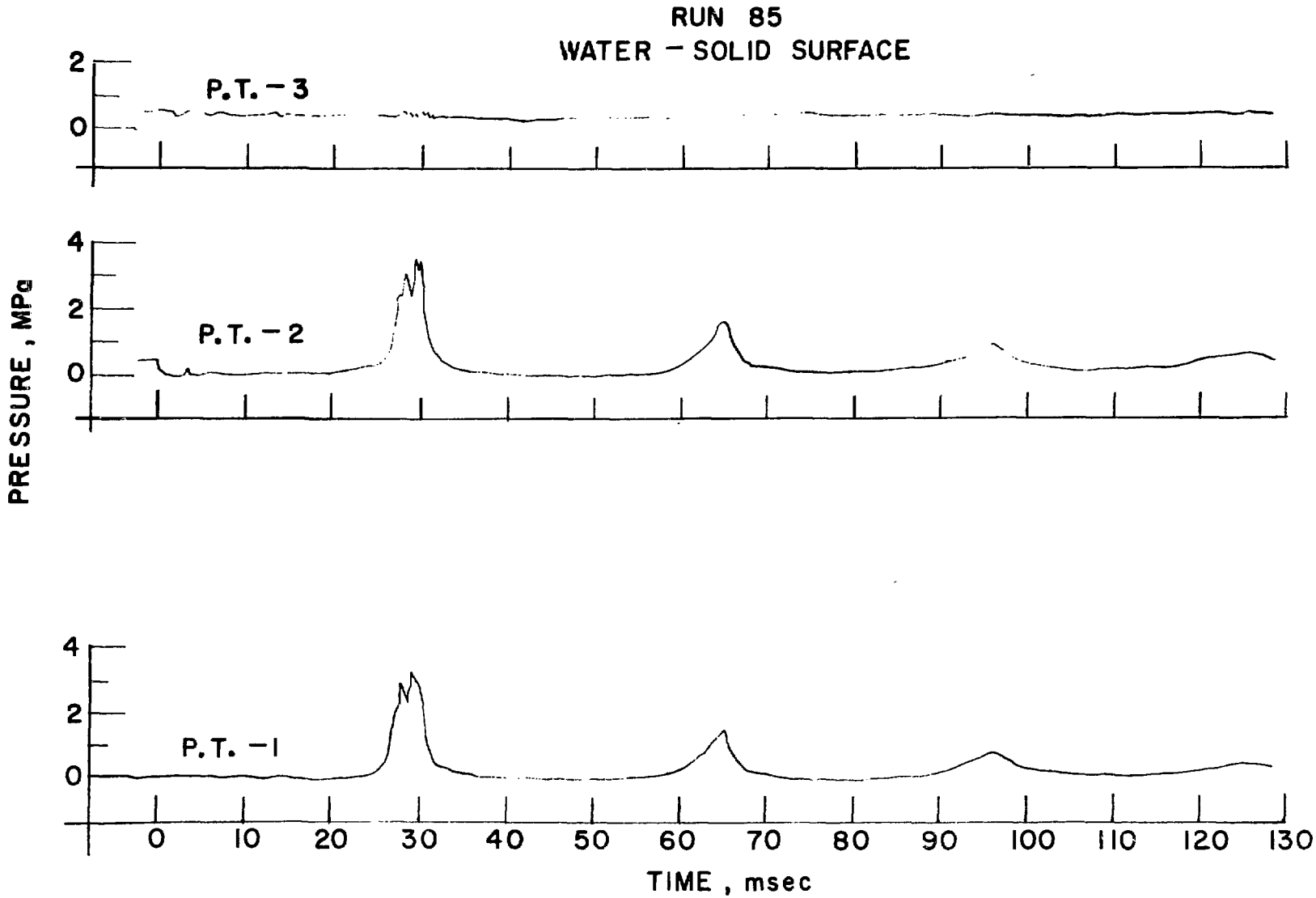

Fig. C.9 Pressure History of Run 85

APPENDIX D

Contacts of Freons

Experiments conducted with Freon-22 and Freon-11 are listed in Table D1. The hot liquids used are: silicone oil, mineral oil, water, and mercury.

TABLE D1. Contacts of Freons

System	Diaphragm	Hot Liquid Temperature °C	Run Number	Remarks
Freon-11-	thin	40	131	
Silicone oil		150	134	
		152	132	
		250	140	100 CC
		250	133	
		250	135	
		250	137	
		250	139	40 CC
		300	138	
	thick	30	144	
		100	143	
		152	145	
		203	148	
		215	151	
		222	152	
		225	153	
		230	149	
		260	146	
		300	147	
Freon-22-	thin	36	130	
silicone oil	thick	25	47	
		45	53	
		108	42	
		110	43	
		110	48	
		115	37	
		120	38	
		122	44	
		138	46	
		160	49	
		161	58	
		170	54	
		170	55	
		178	45	
		178	57	
		185	50	
		186	59	
		200	51	
		217	56	
		220	52	
		232	60	
		239	62	
		243	61	
		249	39	
		252	41	
		272	40	

TABLE D1. Contacts of Freons (contd.)

System	Diaphragm	Hot Liquid Temperature °C	Run Number	Remarks
Freon-22-mineral oil	thin	180	158	100 CC
	thick	0	32	
		100	33	
		100	34	
		150	155	
		187	157	100 CC
		218	156	
Freon-22-solid surface	thick	21	35	
		100	36	
Freon-11-solid surface		200	150	
		320	154	40 CC
Freon-22-water	thin	50	125	
		50	129	
		84	121	
	thick	26	126	
		43	161	
		50	127	
		59	122	
		60	160	
		80	128	
		80	159	
Freon-22-mercury	thin	10	116	
		18	119	
		125	118	
		128	117	
	thick	12	87-89	different vapor pressure
		25	63	
		27	108	
		35	91	
		41	92	
		51	64	
		68	93	
		70	90	
		75	65	
		82	95	
		83	96	
		94	97	
		96	98	
		100	66	
		118	94	
		156	99	
		163	100	
		173	101	

TABLE D1. Contacts of Freons (contd.)

System	Diaphragm	Hot Liquid Temperature °C	Run Number	Remarks
		197	102	
		210	103	
		230	109	
Freon-11-mercury	thin	25	114	
		165	120	
		232	115	
	thick	11	67	
		172	106	
		207	104	
		222	105	
		249	107	

APPENDIX E

Experimental Results of Water-Wood's Metal, Butanol-Wood's Metal, and Water-Molten Salt Interactions

TABLE E1. Water-Wood's Metal Interactions

Run	Hot Liquid Temperature (°C) T_h	Time from First Impact (msec) Δt	Pressure MPa P_{max}	Pulse Duration (msec) t_p	Impulse KPa/sec I_{exp}
162	90	0	2.48	8.0	6.46
163	150	0	2.58	7.5	7.85
192	174	0	2.20	10.0	5.86
		87.5	1.72	5.25	4.31
189	188	0	1.24	13.25	7.31
		77.5	2.59	3.75	4.82
		157.5	3.45	2.75	6.90
		216.25	1.03	3.75	1.94
164	200	0	2.76	6.75	6.29
188	207	0	1.72	15.0	5.86
		103.0	3.10	2.5	3.79
		184.0	2.27	2.75	2.59
187	220	0	1.55	20.0	7.76
		82.5	5.17	4.125	10.08
		187.5	4.14	3.125	6.21
202	220	0	1.90	12.5	9.48
		92.5	3.45	2.875	4.97
		192.5	4.14	3.125	6.72
201	230	0	2.24	9.5	9.93
		85.0	3.45	4.5	9.48
186	240	0	1.38	7.5	5.17
		77.5	4.07	2.5	6.21
		172.5	4.21	3.0	8.28
		267.5	4.69	2.75	6.21
165	250	0	2.07	6.75	5.41
		72.5	2.41	7.50	6.55
		155.0	3.89	3.00	6.07
203	275	0	1.31	25.0	9.31
		87.5	3.79	2.75	5.21
		175.0	3.97	8.75	9.03
218	290	0	1.38	27.5	9.48
		57.5	2.24	17.5	8.40
		132.5	0.86	15.5	6.55
167	300	0	0.52	16.25	5.60
		97.5	1.72	10.0	6.46
		180.0	1.21	17.5	3.62
166	300	0	1.03	37.5	10.34
217	312	0	1.03	19.25	9.93
		90.0	4.14	11.25	7.76
		166.25	7.24	6.87	12.21
		237.5	7.24	6.62	15.08
		320.0	2.24	10.6	7.28
		400.0	1.93	10.12	3.62
204	325	0	1.03	22.9	9.72
		102.5	2.07	13.12	11.42

TABLE E1. Water-Wood's Metal Interactions (contd.)

Run	Hot Liquid Temperature (°C) T_h	Time from First Impact (msec) Δt	Pressure MPa P_{max}	Pulse Duration (msec) t_p	Impulse KPa/sec I_{exp}
		205.0	5.52	15.0	12.38
		272.5	5.72	5.62	11.10
		395.?	4.83	10.0	9.05
		490.0	3.86	5.0	7.24
		565.0	2.55	5.0	3.51
205	340	0	1.03	24.5	9.66
		97.5	3.10	10.25	6.40
		177.5	3.45	12.75	10.38
		267.5	2.48	11.25	10.34
168	350	0	0.69	17.5	6.03
		75.0	1.72	17.25	8.10
		165.0	2.41	12.5	5.17
216	355	0	0.69	17.5	6.46
		87.5	1.79	11.87	10.08
		173.25	6.76	10.62	17.01
		247.5	6.90	4.125	15.03
		332.5	1.72	10.0	8.62
219	375	0	1.03	15.25	8.62
		72.5	2.76	11.25	11.86
219	375	147.5	2.07	17.5	13.59
		240.0	3.03	20.0	10.43
		325.0	0.69	16.25	5.60
		435.0	1.86	15.0	4.65
200	380	0	1.21	24.0	9.72
193	381	0	0.69	27.5	9.48
169	400	0	1.55	13.25	9.59
		84.0	2.41	9.18	10.94
		168.25	3.28	12.75	11.59
		285.75	5.00	10.75	20.86
		347.5	2.93	26.25	15.59
198	400	0	1.03	35.0	12.07
		95.0	2.93	12.37	13.62
		187.5	4.31	14.12	16.07
		285.0	4.83	12.5	18.34
		392.5	5.34	24.0	15.10
		500.0	3.45	17.5	11.90
		630.0	0.69	7.5	2.59
		782.5	1.72	10.0	8.62
		900.0	1.38	12.5	5.17
		1022.5	0.69	12.5	4.31
190	457	0	2.41	12.5	10.0
		93.0	4.48	13.75	20.27
		182.5	5.34	12.5	22.30

TABLE E1. Water-Wood's Metal Interactions (contd.)

Run	Hot Liquid Temperature (°C) T_h	Time from First Impact (msec) Δt	Pressure MPa P_{max}	Pulse Duration (msec) t_p	Impulse KPa/sec I_{exp}
		268.5	3.62	16.25	16.28
		365.5	2.76	22.5	17.93
170	490	0	1.72	12.5	6.90
171	490	0	2.24	15.65	7.54
		85.0	6.90	13.75	21.45
		165.0	1.38	37.5	21.03
191	551	0	1.03	30.0	9.48
		104.0	5.86	13.75	12.48
191	551	222.0	3.90	10.875	14.70
		317.5	4.65	20.0	20.08
		415.0	5.24	19.375	11.38

TABLE E2. Butanol-Wood's Metal Interactions

Run	Hot Liquid Temperature, °C T_h	Time from First Impact (msec) Δt	Maximum Pressure (MPa) P_{max}	Pulse Duration (msec) t_p	Impulse KPa.sec I_{exp}
174	113	0	1.59	8.5	5.17
175	154	0	1.59	8.75	4.82
183	210	0	1.38	7.5	4.48
234	220	0	1.93	8.375	6.05
		87.5	3.62	3.125	5.65
		162.5	2.62	3.75	4.14
176	227	0	1.24	12.5	8.62
		30.0	2.41	3.375	4.07
		122.5	2.76	3.875	5.39
		195.0	1.21	7.5	1.96
232	250	0	1.59	18.1	8.62
		74.75	3.45	3.75	6.50
		164.0	4.48	2.5	5.59
178	260	0	1.03	17.5	7.76
		57.5	3.10	3.625	6.03
		127.5	4.14	3.25	7.79
233	270	0	1.34	26.25	8.62
		65.5	4.00	5.625	11.24
		134.75	4.48	2.75	6.96
		226.5	3.79	3.125	5.93
196	280	0	1.21	19.25	8.23
		70.75	2.93	8.75	6.00
		150.0	2.76	5.625	4.82
		253.75	2.07	5.0	3.36
235	290	0	2.93	10.25	9.14
		57.87	3.45	2.75	5.69
182	300	0	1.90	5.875	4.50
		60.0	1.55	5.0	2.52
		107.5	1.03	5.0	1.81
		152.5	0.86	6.62	2.41
		192.5	0.86	8.125	2.32
236	306	0	1.24	16.25	9.65
		64.25	3.52	4.375	7.72
		129.0	4.21	3.75	7.86
		213.5	2.41	4.625	5.82
237	318	0	1.45	15.25	7.07
		57.5	3.79	3.375	6.46
		102.5	3.72	3.75	7.45
		142.5	2.76	5.0	4.66
		180.0	1.34	7.5	3.70
185	350	0	1.55	9.0	4.96
		43.75	2.07	2.5	2.59
		77.5	2.07	5.0	5.17
		115.0	2.21	5.0	5.52
		153.75	1.38	7.5	2.76
		193.75	0.69	10.0	1.55

TABLE E2. Butanol-Wood's Metal Interactions (contd.)

Run	Hot Liquid Temperature, °C T_h	Time from First Impact (msec) Δt	Maximum Pressure (MPa) P_{max}	Pulse Duration (msec) t_p	Impulse KPa.sec I_{exp}
179	400	0	1.03	12.5	3.27
		70.0	1.72	5.62	3.23
		115.0	1.24	5.0	6.21
		157.5	1.03	7.5	5.17
		197.5	0.69	7.5	2.59
180	450	0	1.24	12.5	6.90
		40.0	1.72	5.0	3.45
		77.5	2.76	7.5	5.52
		115.0	2.07	3.5	3.62
		150.0	1.72	4.4	3.45
		182.5	1.72	7.5	2.07
		215.0	0.86	7.5	0.41
194	505	0	1.24	20.0	5.10
		65.0	1.72	7.5	6.45
		110.0	0.62	10.0	3.10

TABLE E3. Water-LiCl+ KCl Interactions

Run	Hot Liquid Temperature, °C T_h	Time from First Impact (msec) Δt	Maximum Pressure (MPa) P_{max}	Pulse Duration (msec) t_p	Impulse KPa.sec I_{exp}
220	410	0	0.76	27.5	11.48
		112.0	1.00	0.125	0.06
224	600	0	0.48	62.5	10.76
		12.5	1.52	87.5	66.38
		1108.75	1.93	0.5	0.48
226	600	0	0.34	45.5	12.31
		50.0	0.86	0.25	0.11
228	600	0	0.83	37.5	15.52
		40.0	1.72	0.375	0.32

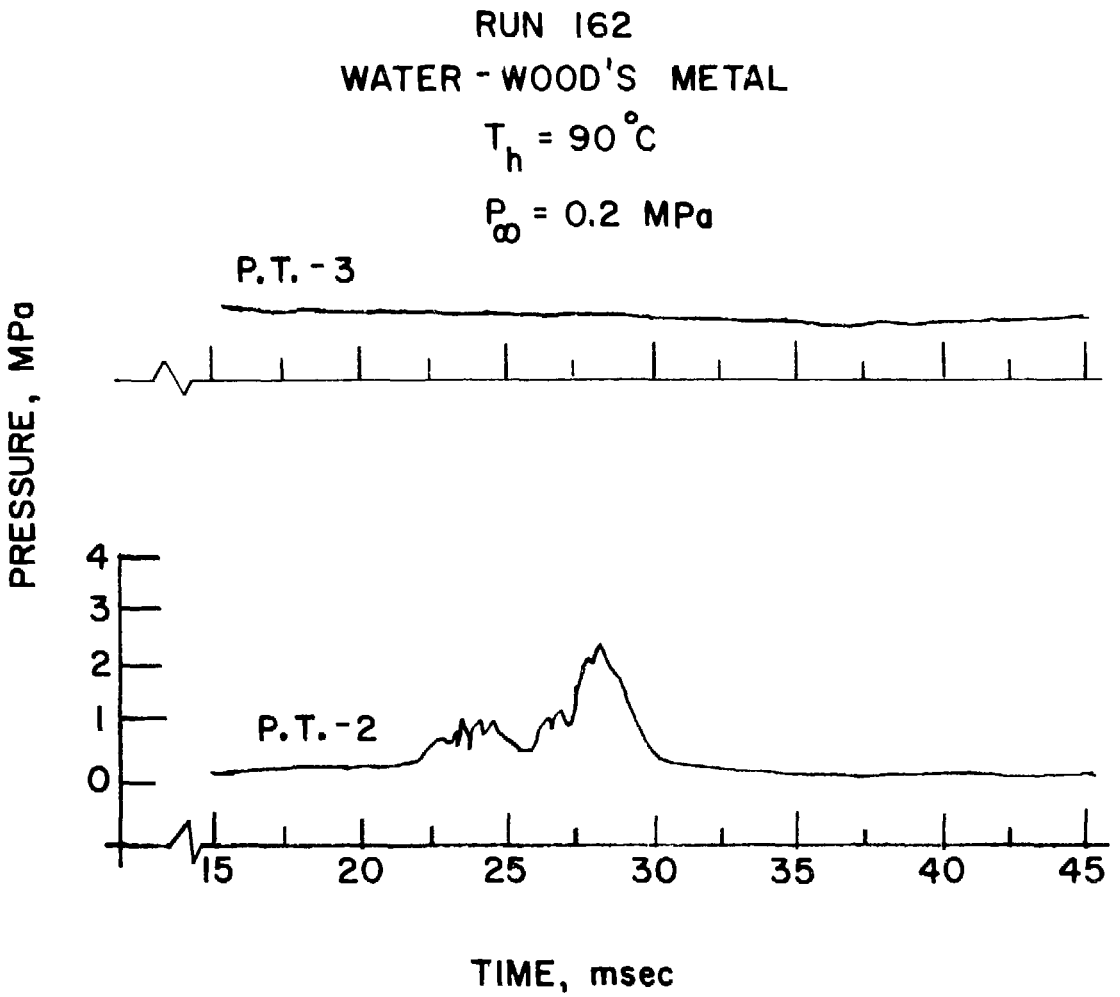

Fig. E.1 Pressure History of Run 162

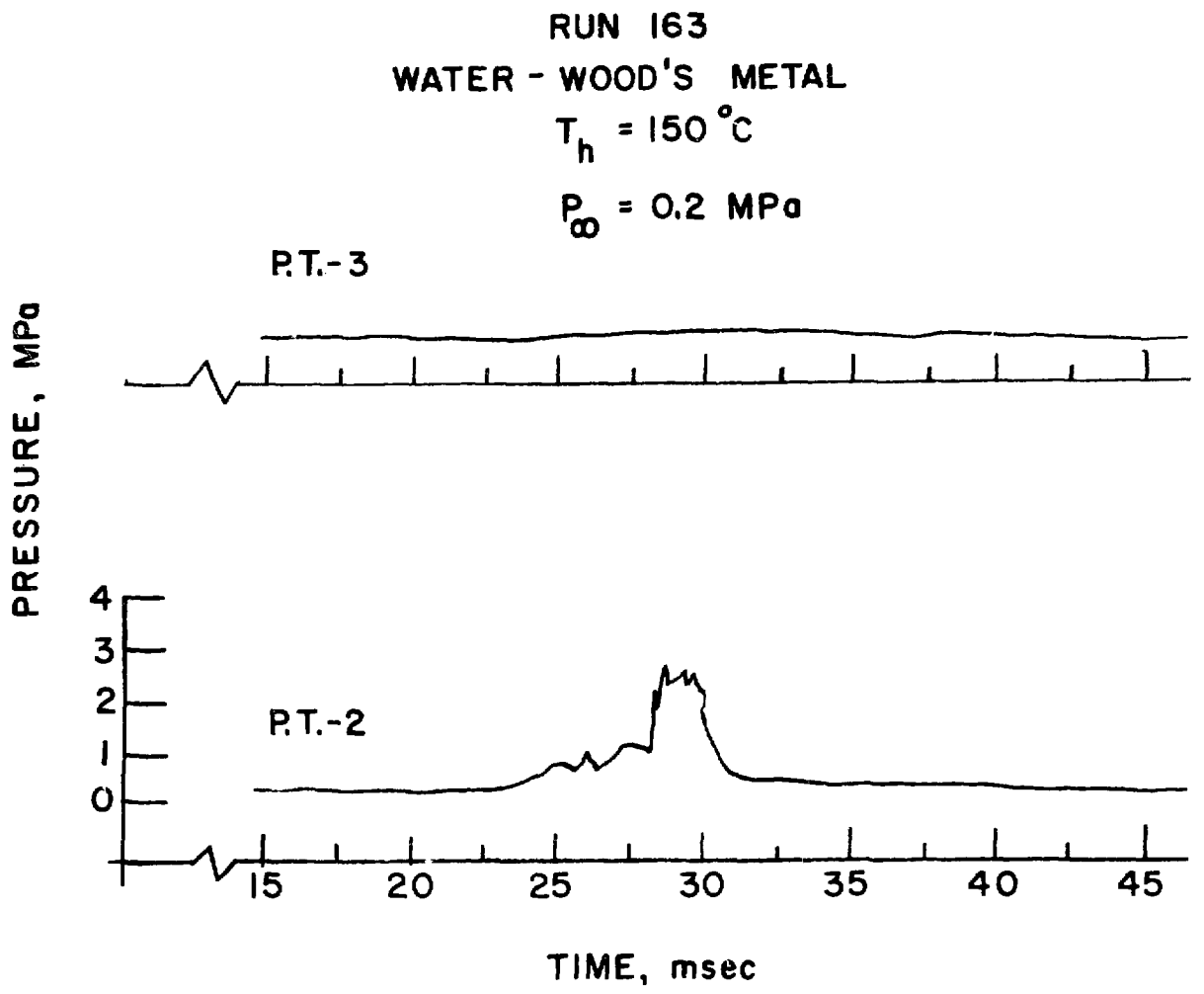

Fig. E.2 Pressure History of Run 163

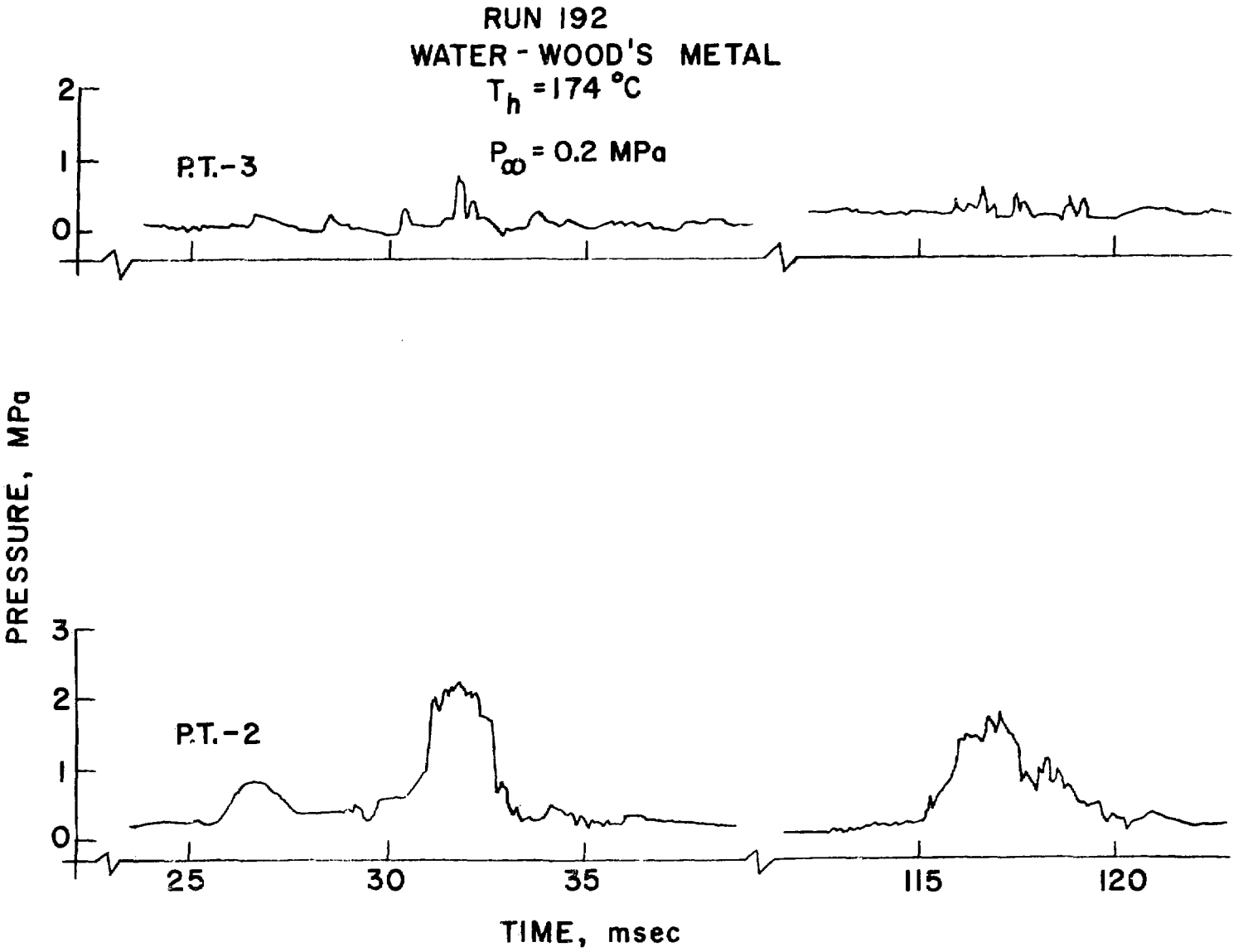

Fig. E.3 Pressure History of Run 192

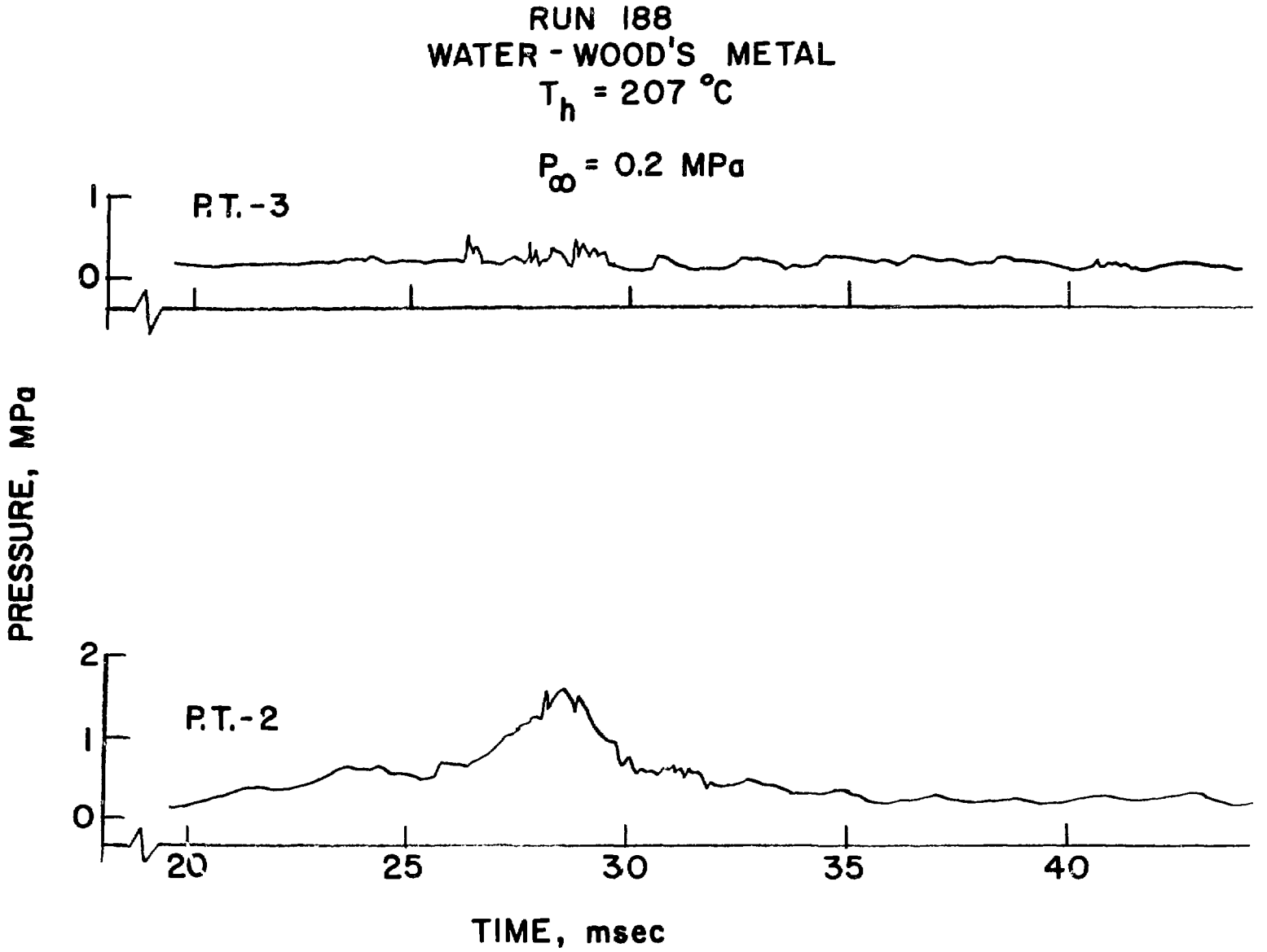

Fig. E.4 Pressure History of Run 188

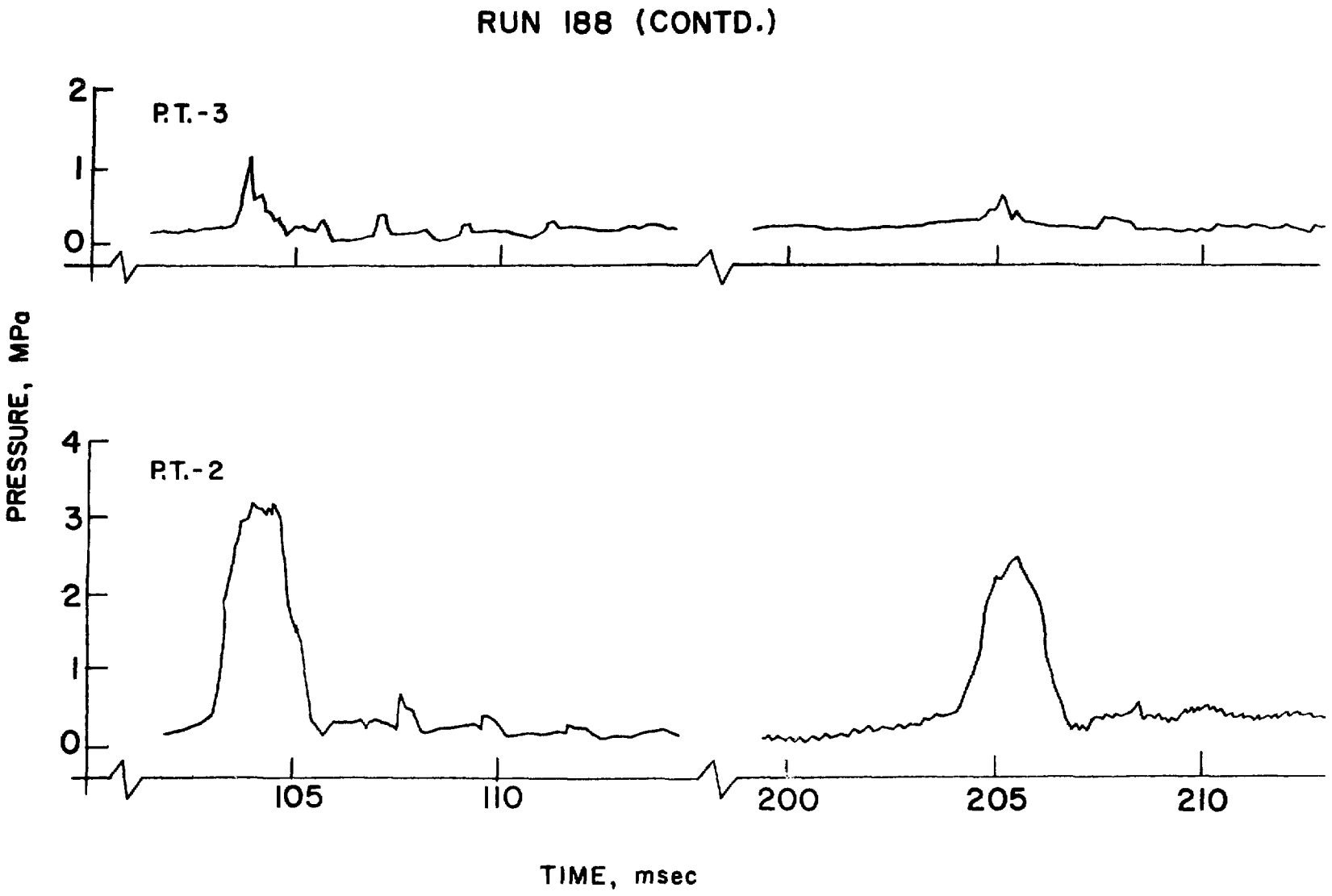

Fig. E.4 Pressure History of Run 188 (contd.)

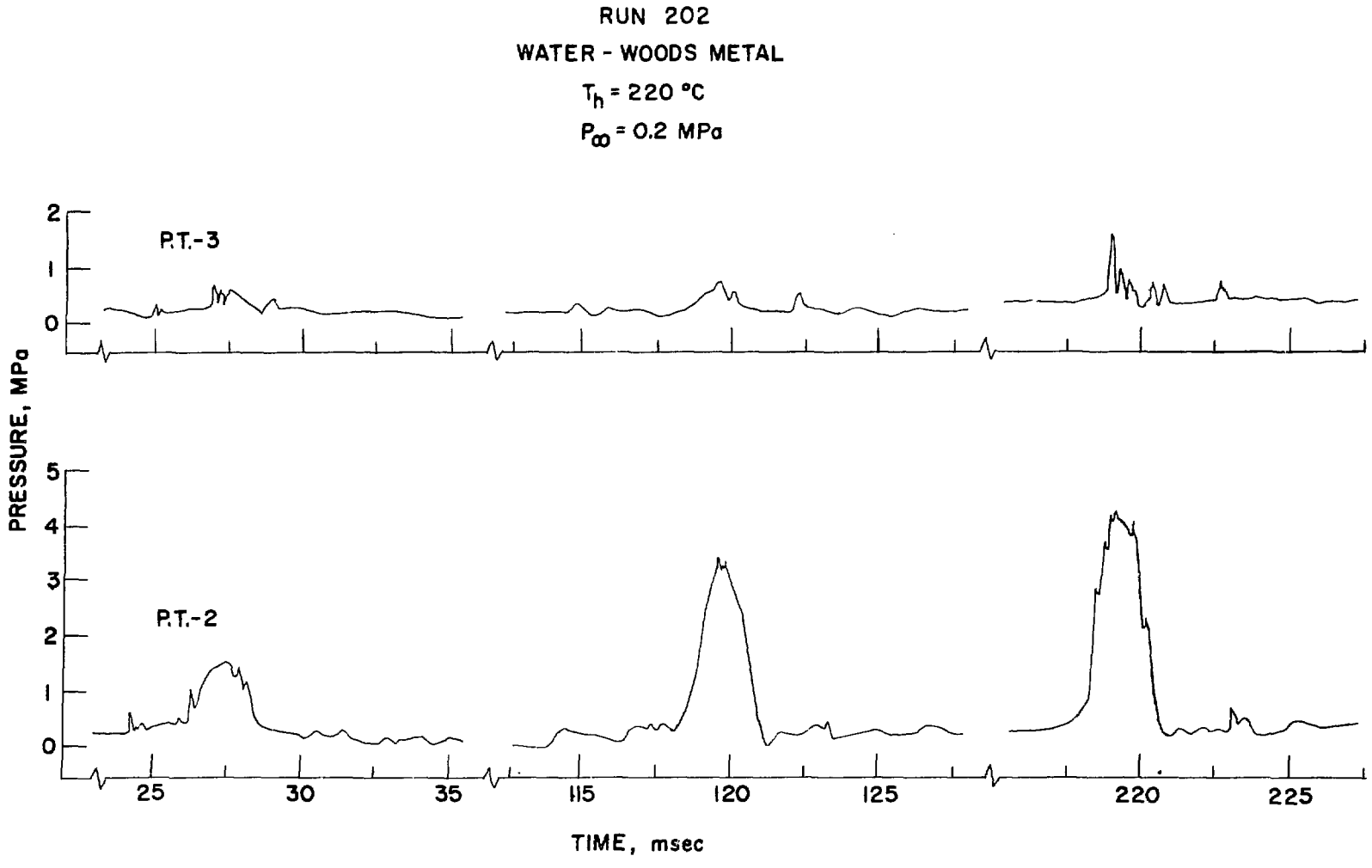

Fig. E.5 Pressure History of Run 202

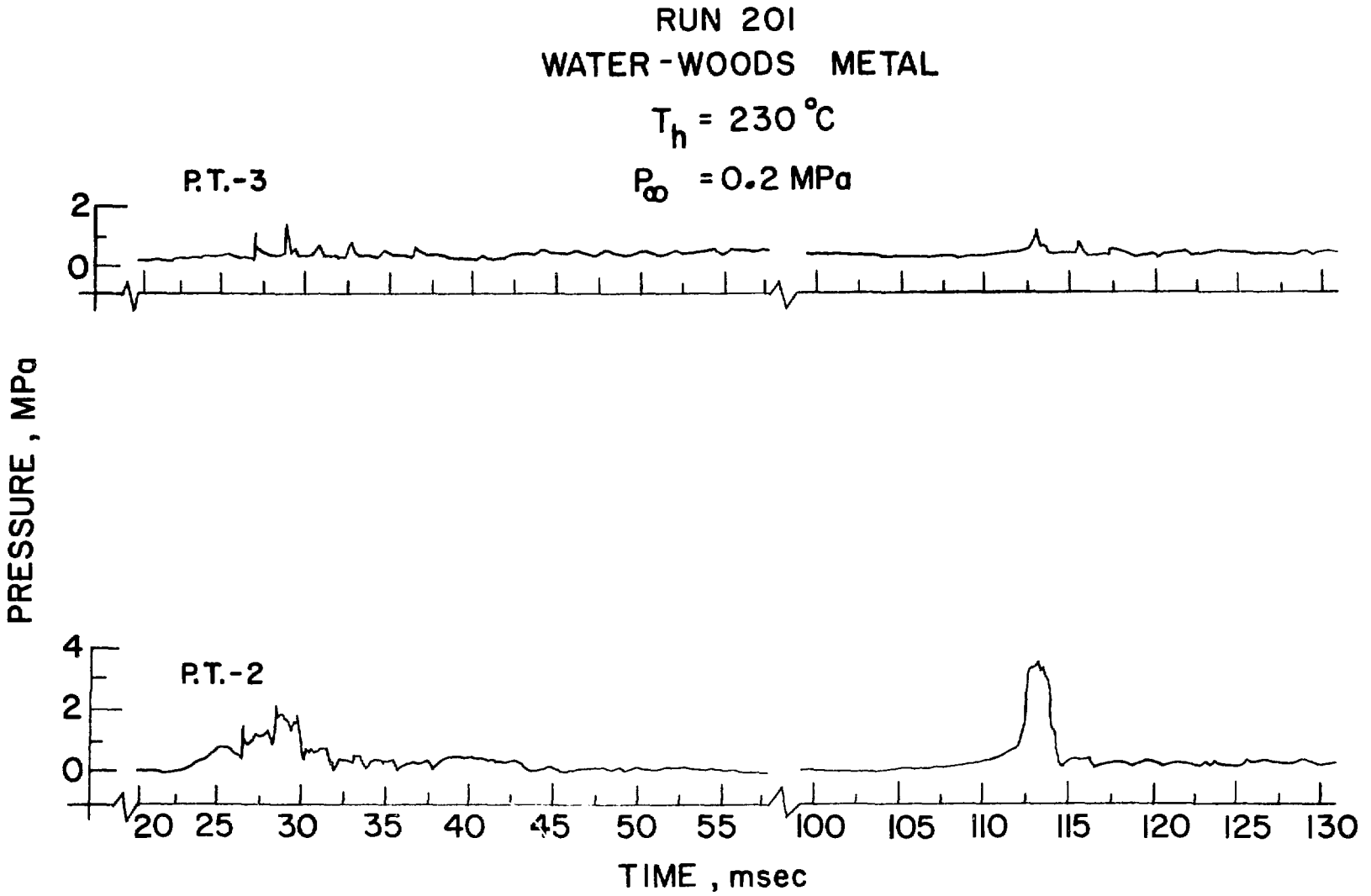

Fig. E.6 Pressure History of Run 201

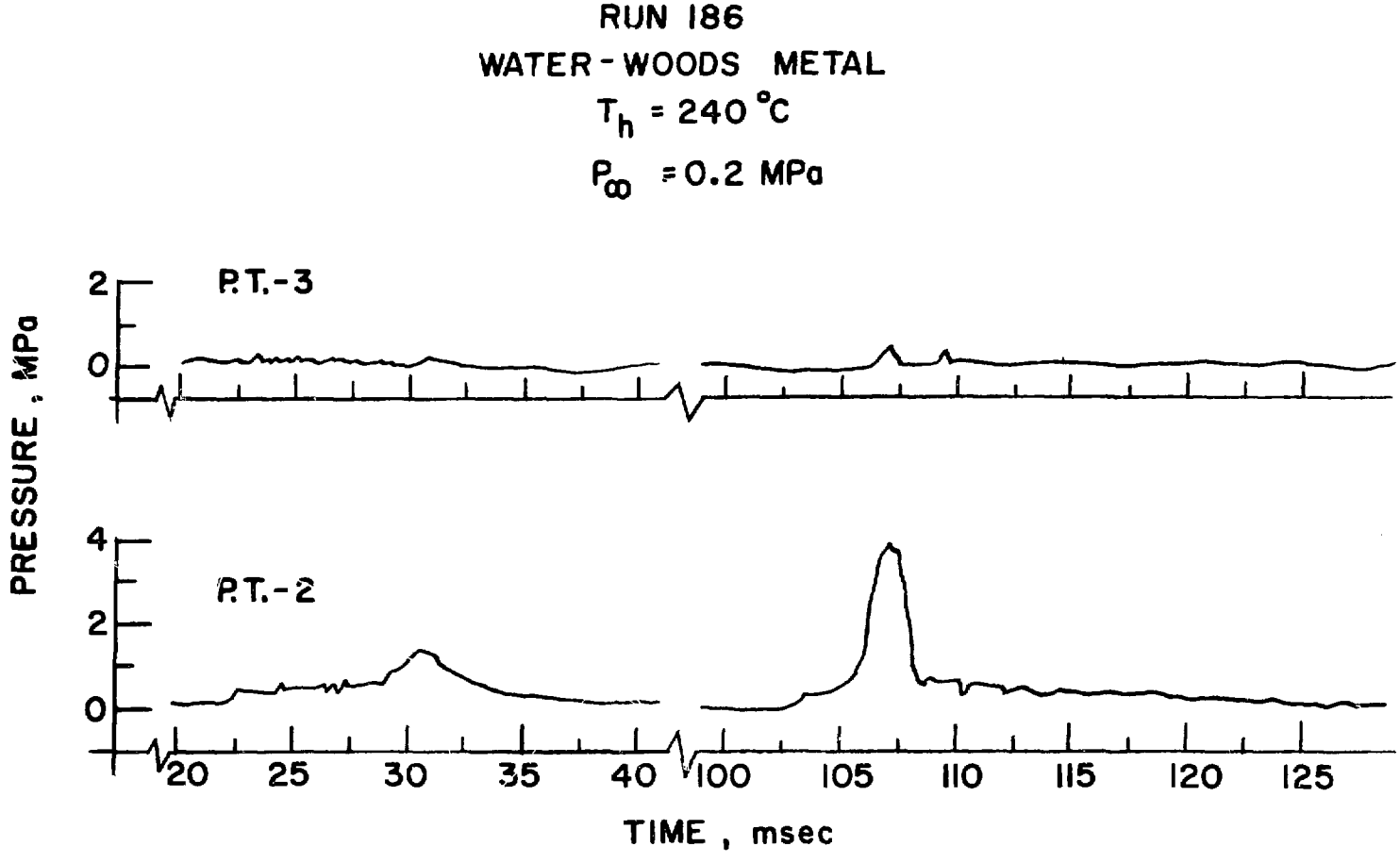

Fig. E.7 Pressure History of Run 186

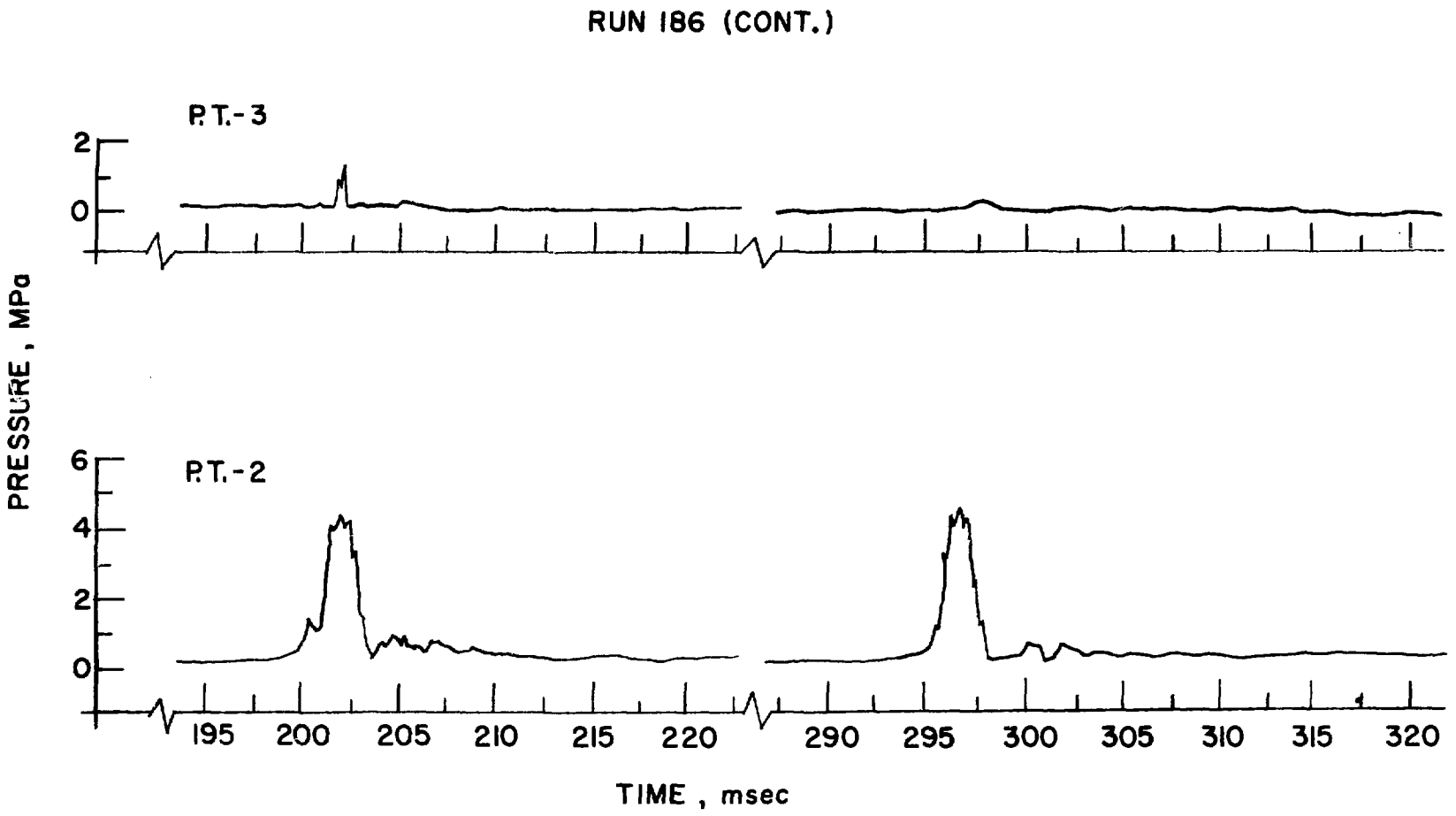

Fig. E.7 Pressure History of Run 186 (contd.)

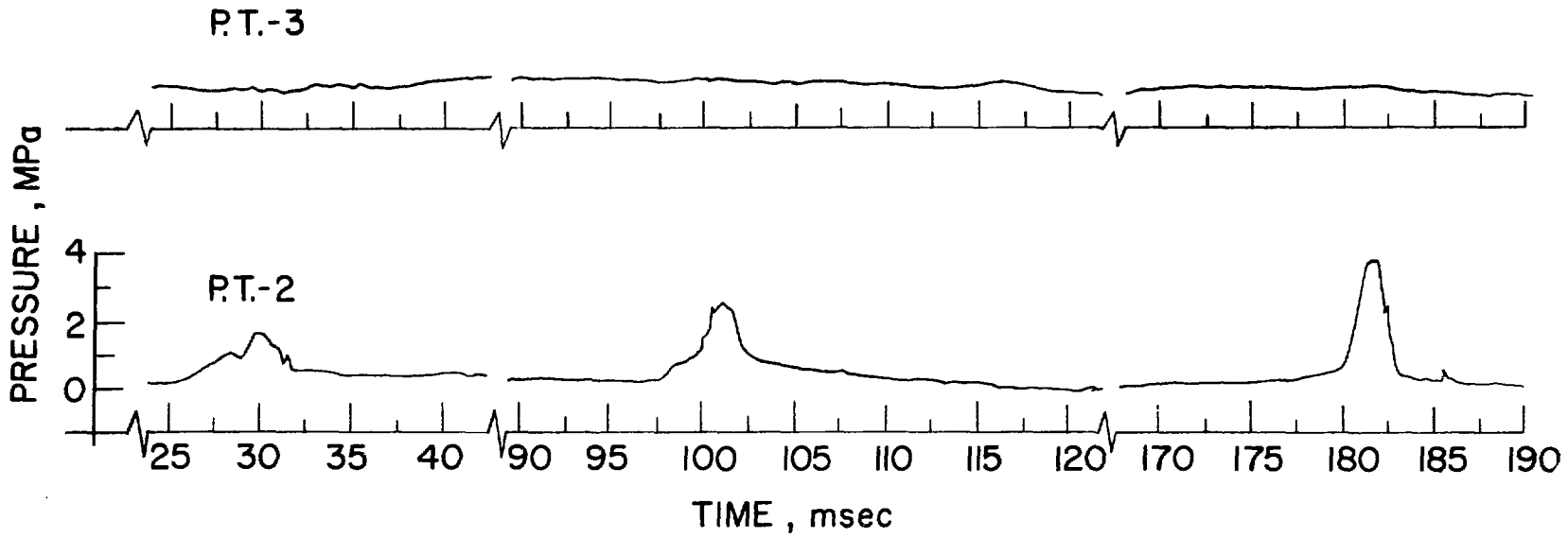

Fig. E.8 Pressure History of Run 165

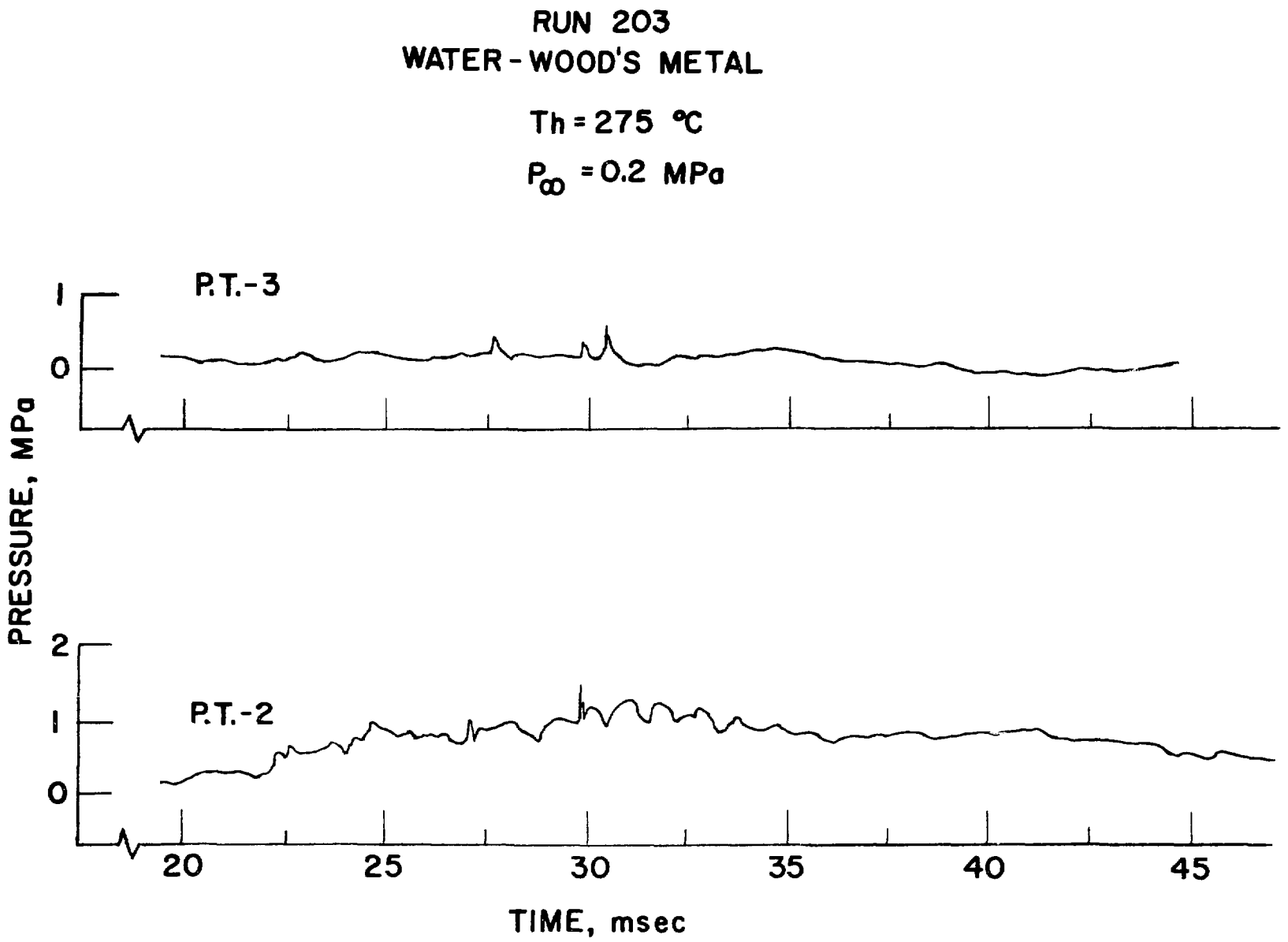

Fig. E.9 Pressure History of Run 203

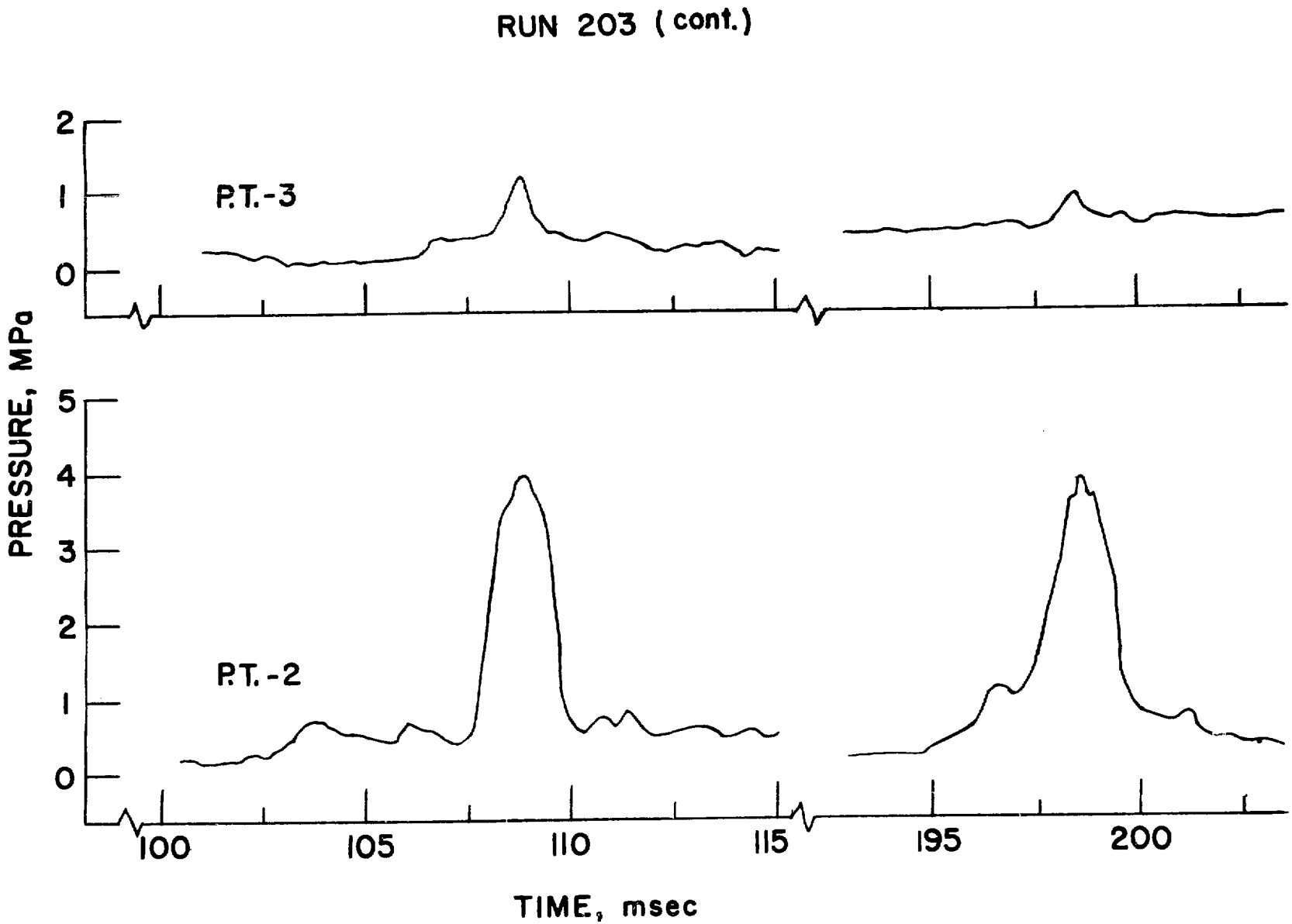

Fig. E.9 Pressure History of Run 203 (contd.)

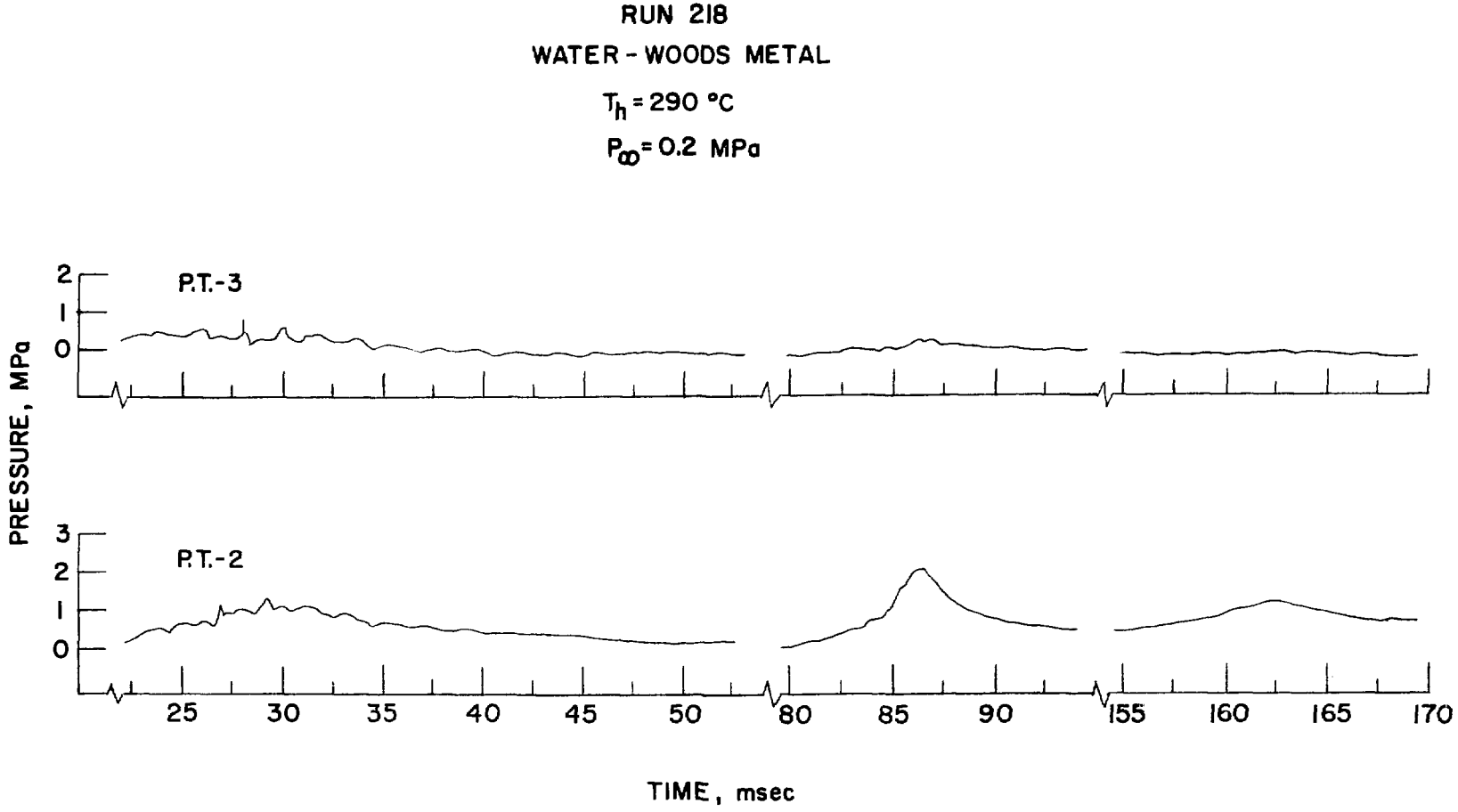

Fig. E.10 Pressure History of Run 218

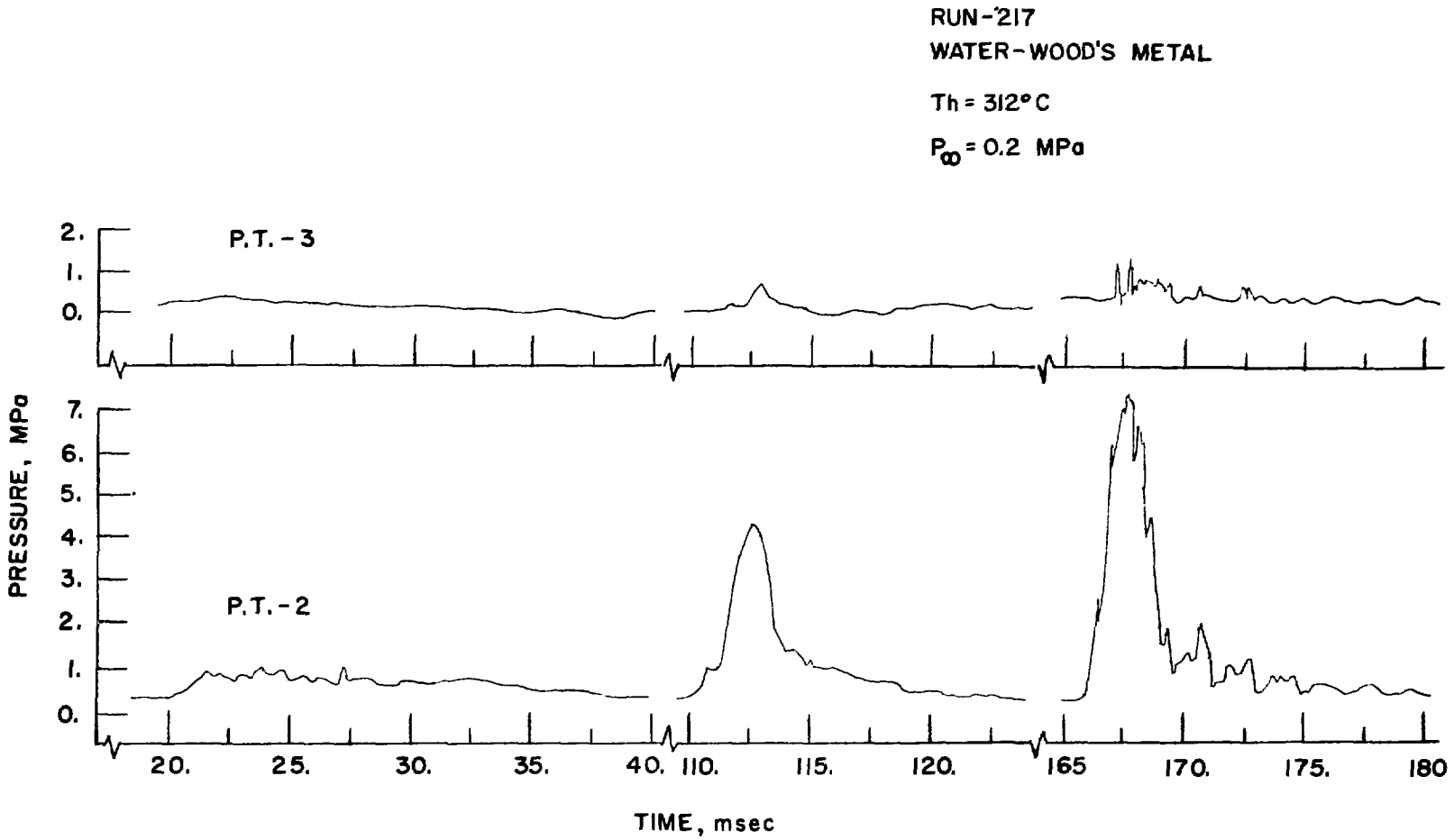

Fig. E.11 Pressure History of Run 217

RUN 217 (cont.)

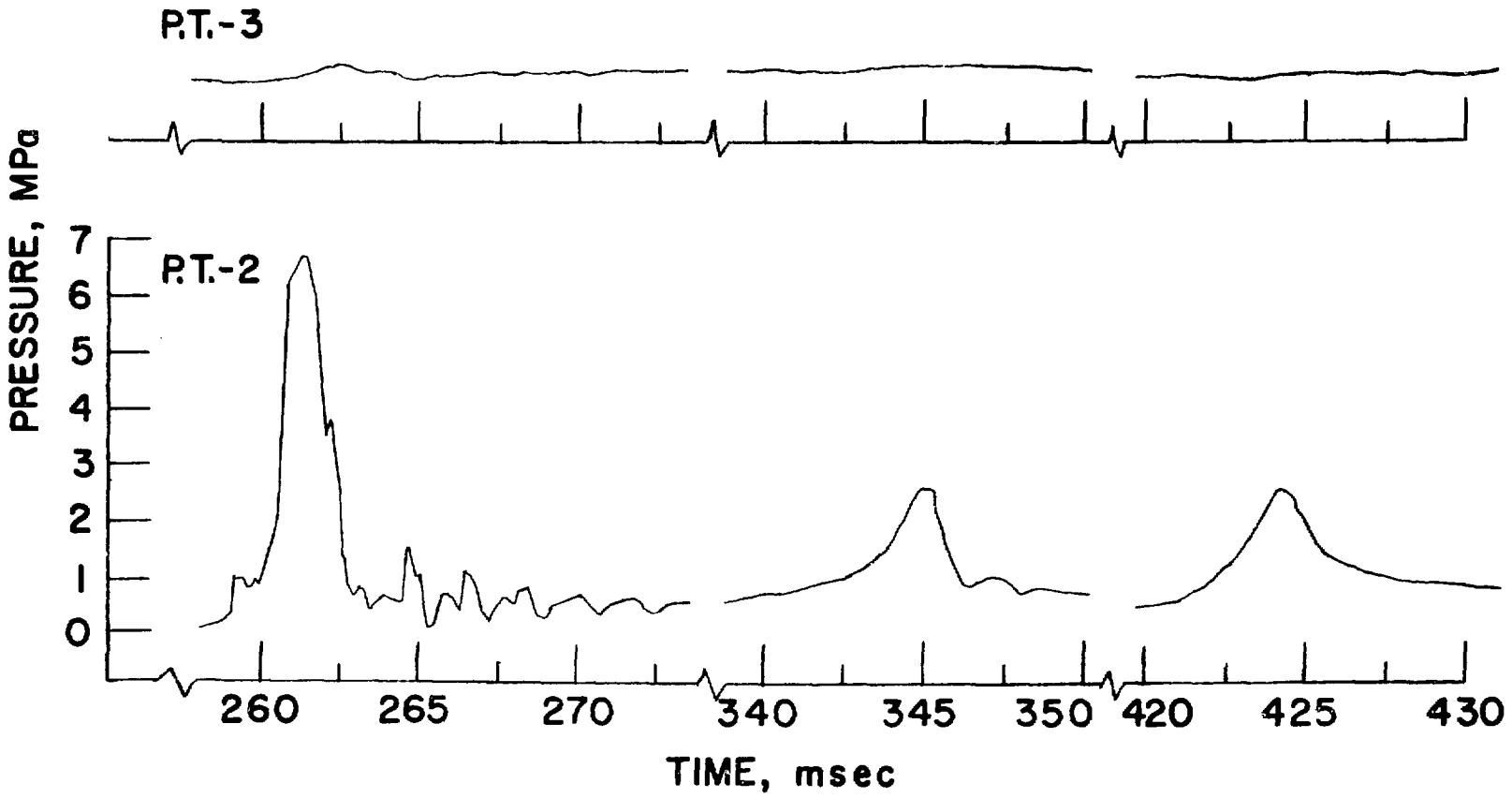

Fig. E.11 Pressure History of Run 217 (contd.)

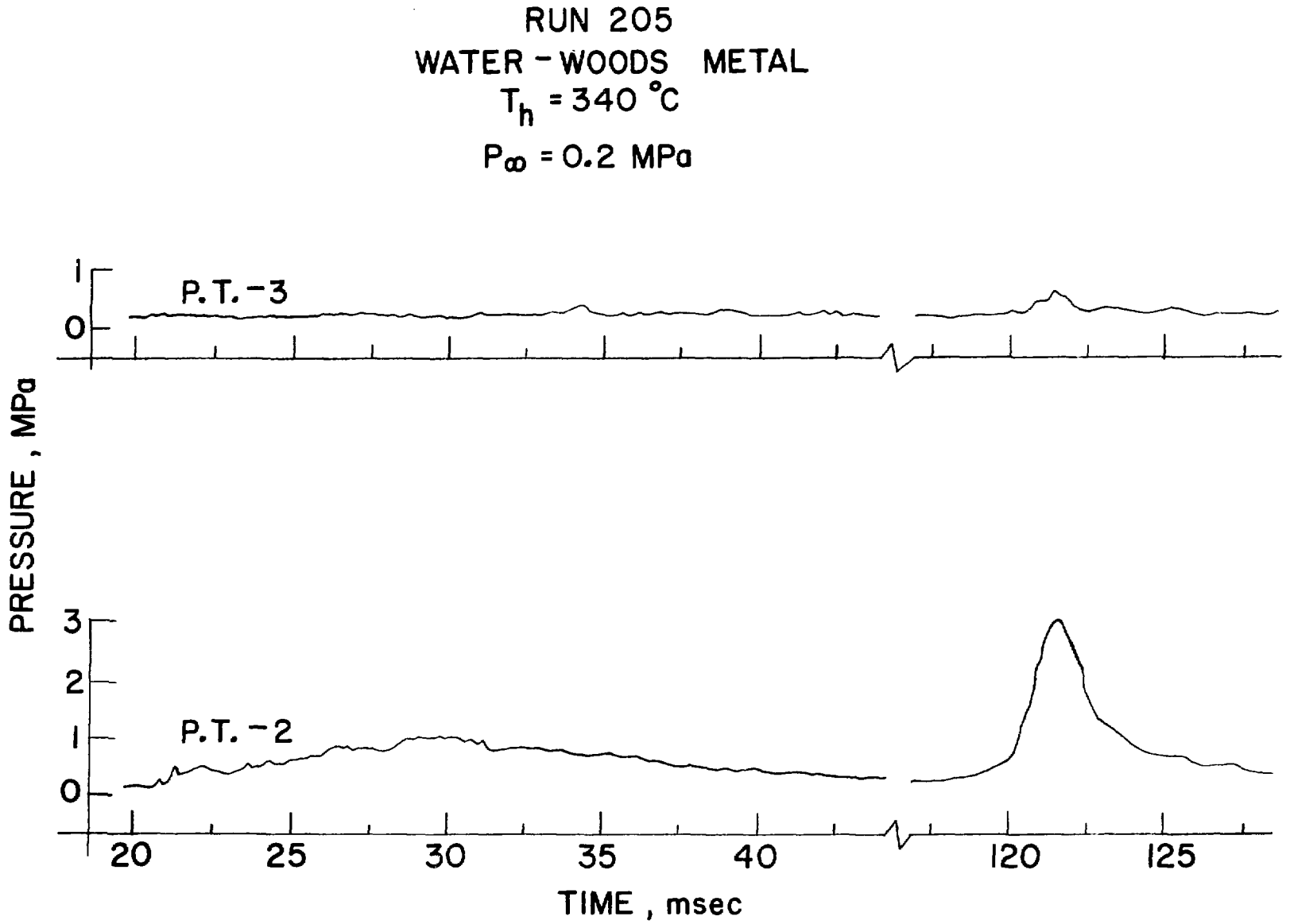

Fig. E.12 Pressure History of Run 205

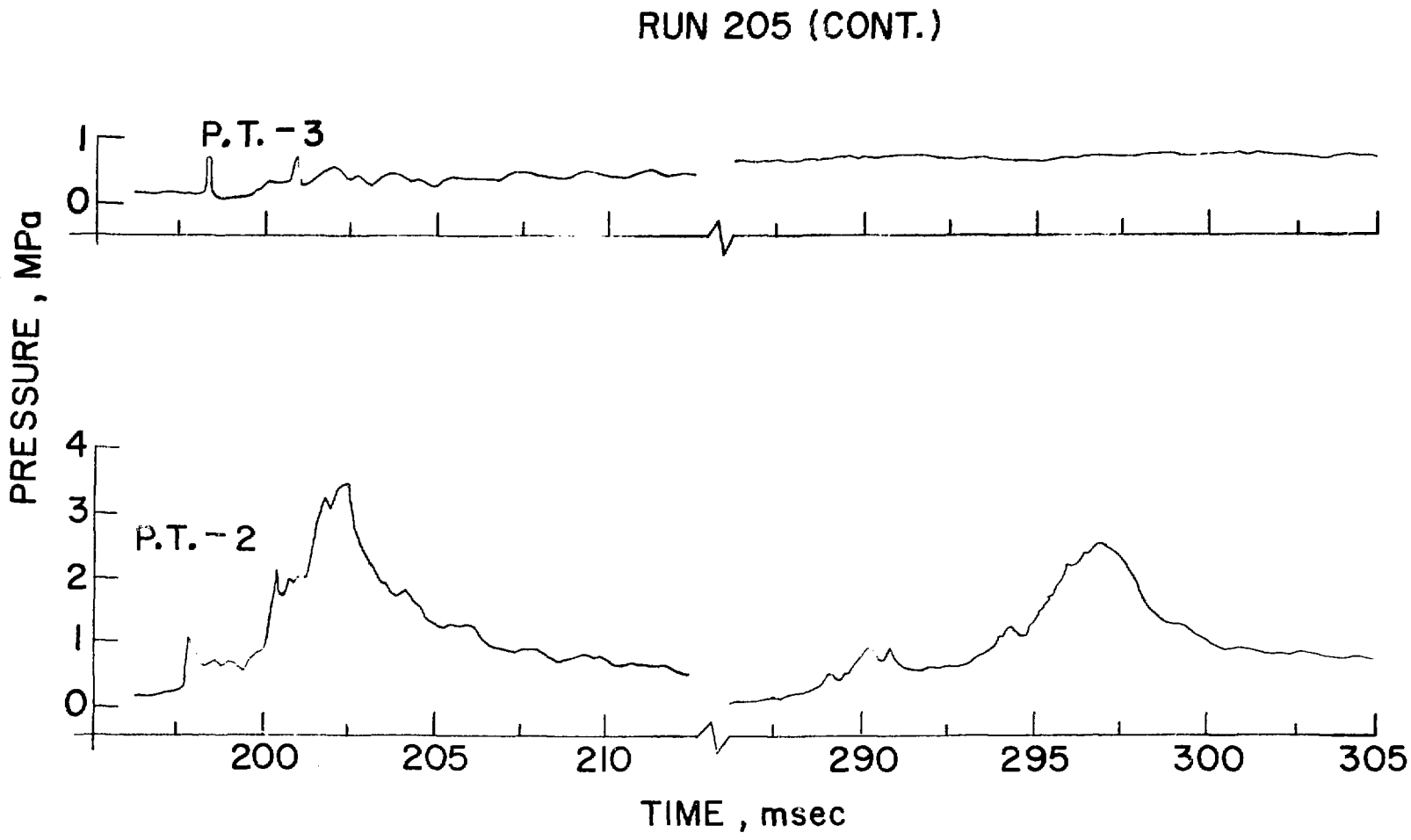

Fig. E.12 Pressure History of Run 205 (contd.)

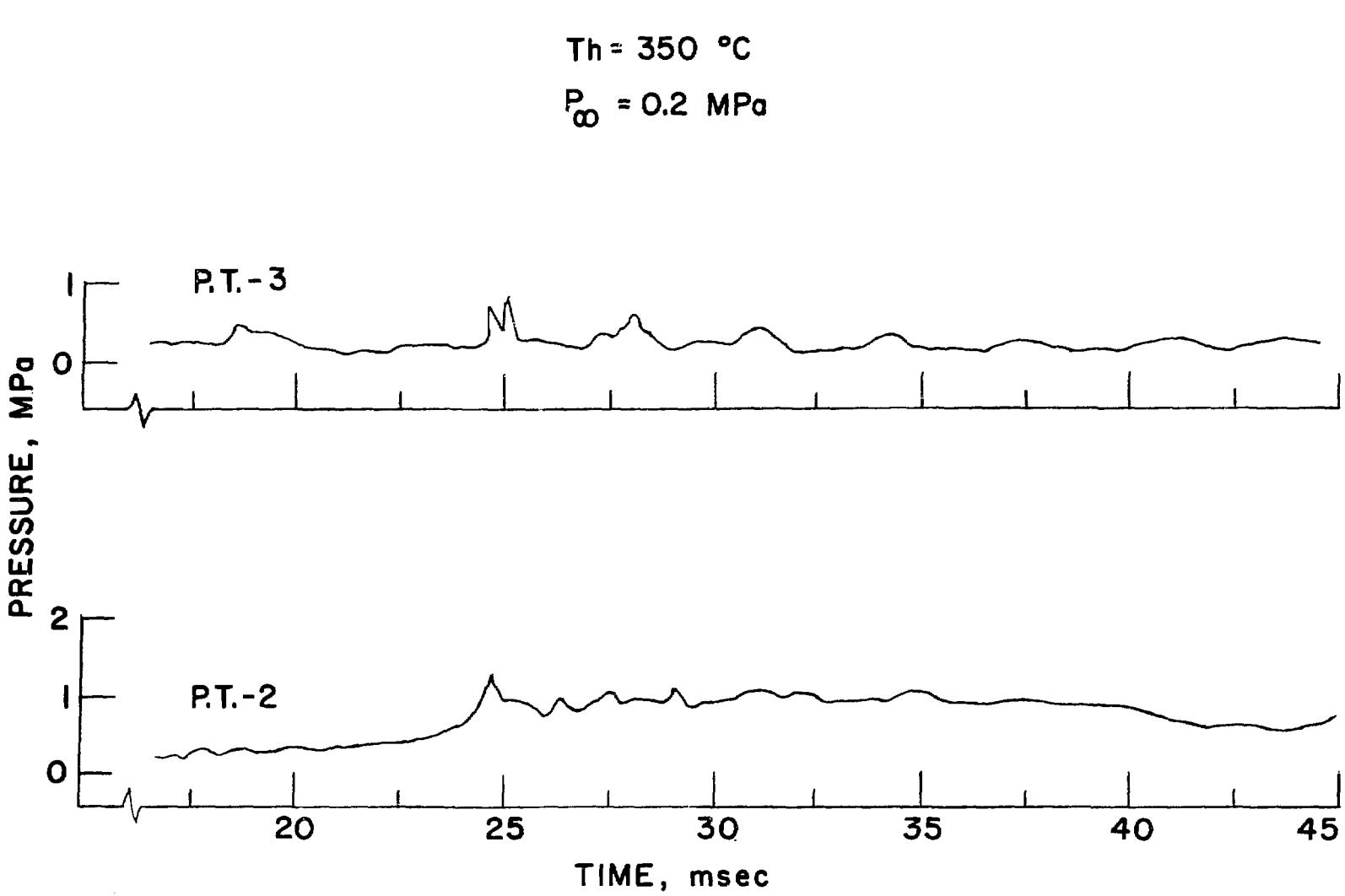

Fig. E.13 Pressure History of Run 168

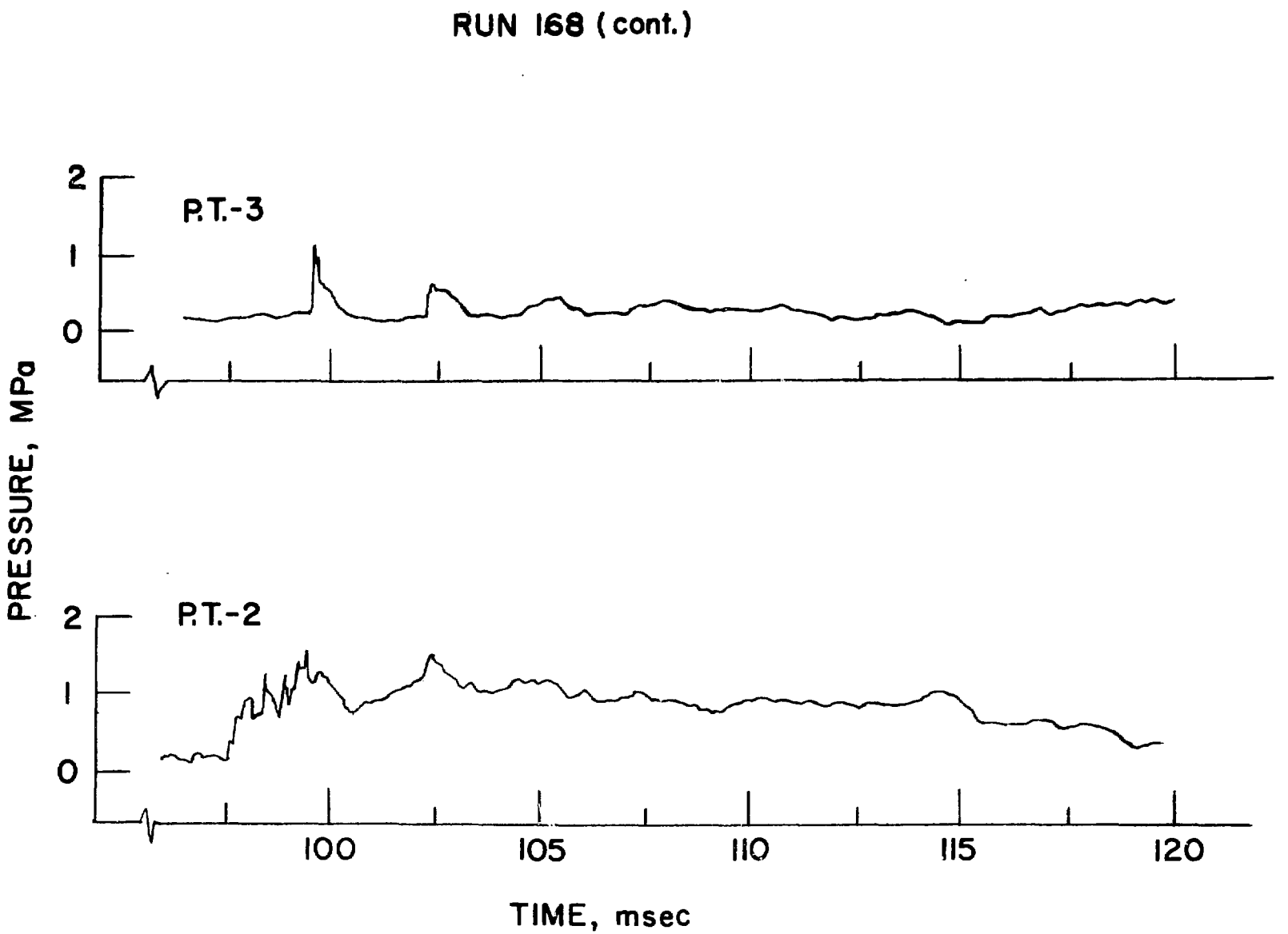

Fig. E.13 Pressure History of Run 168 (contd.)

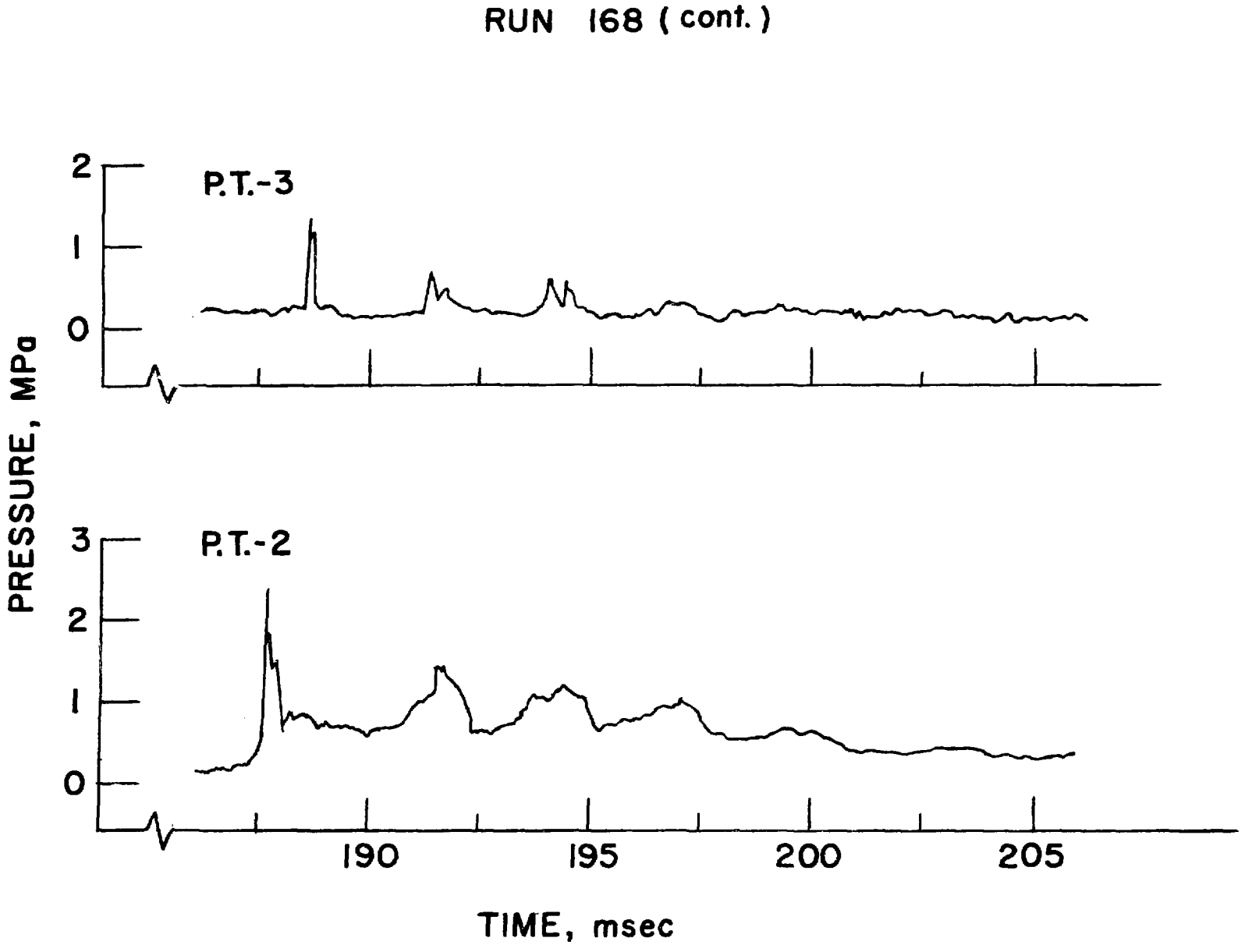

Fig. E.13 Pressure History of Run 168 (contd.)

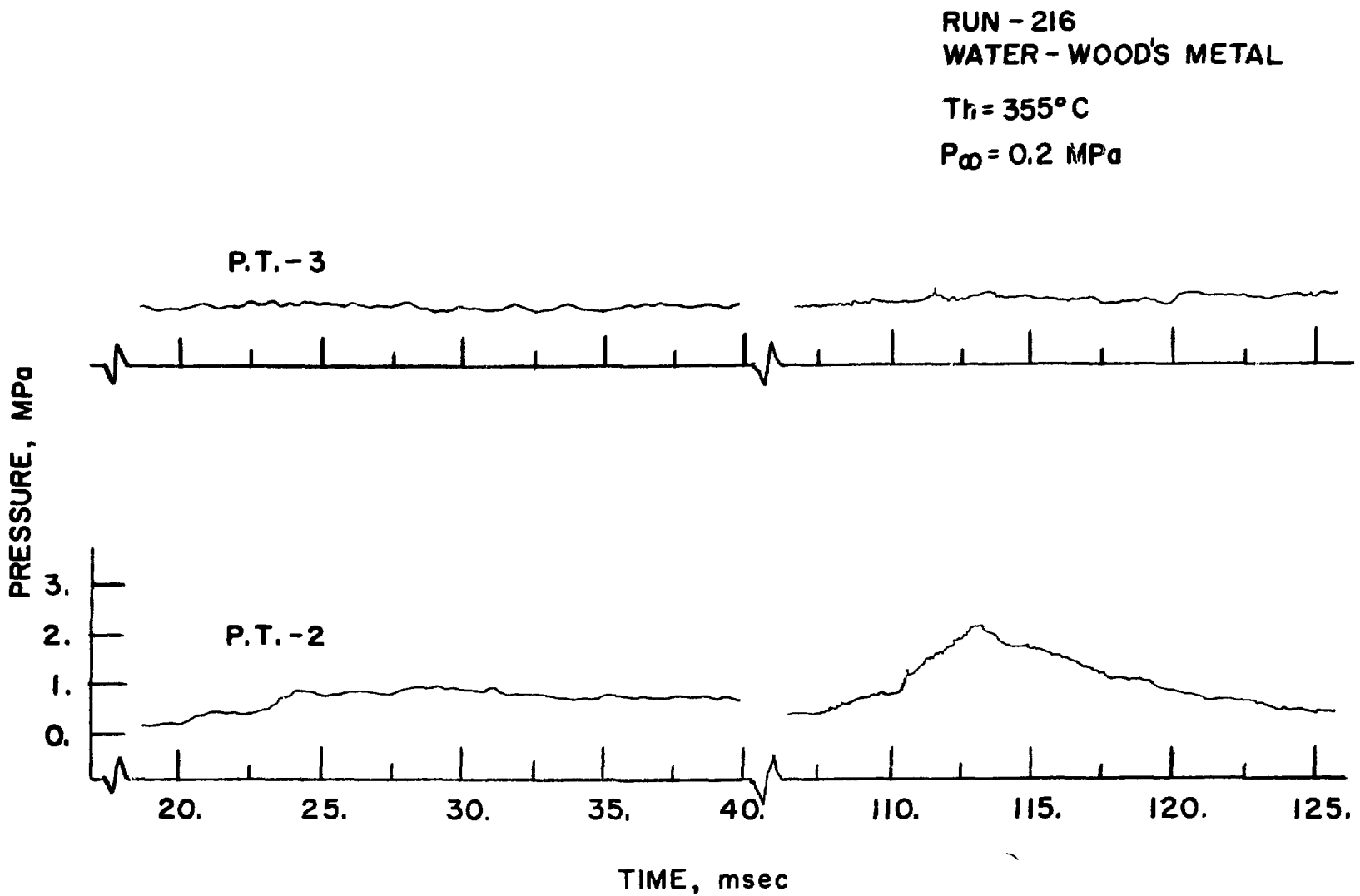

Fig. E.14 Pressure History of Run 216

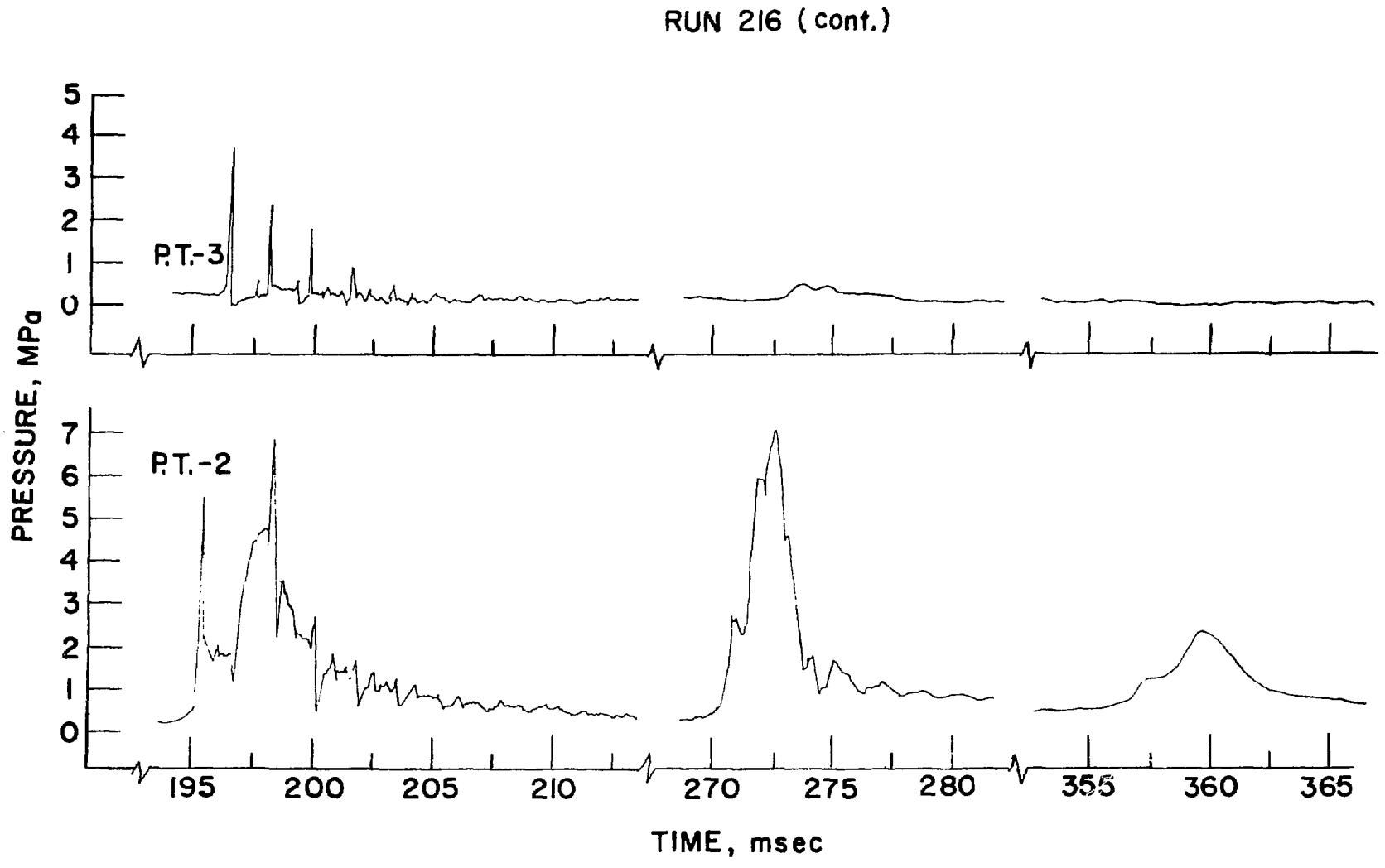

Fig. E.14 Pressure History of Run 216 (contd.)

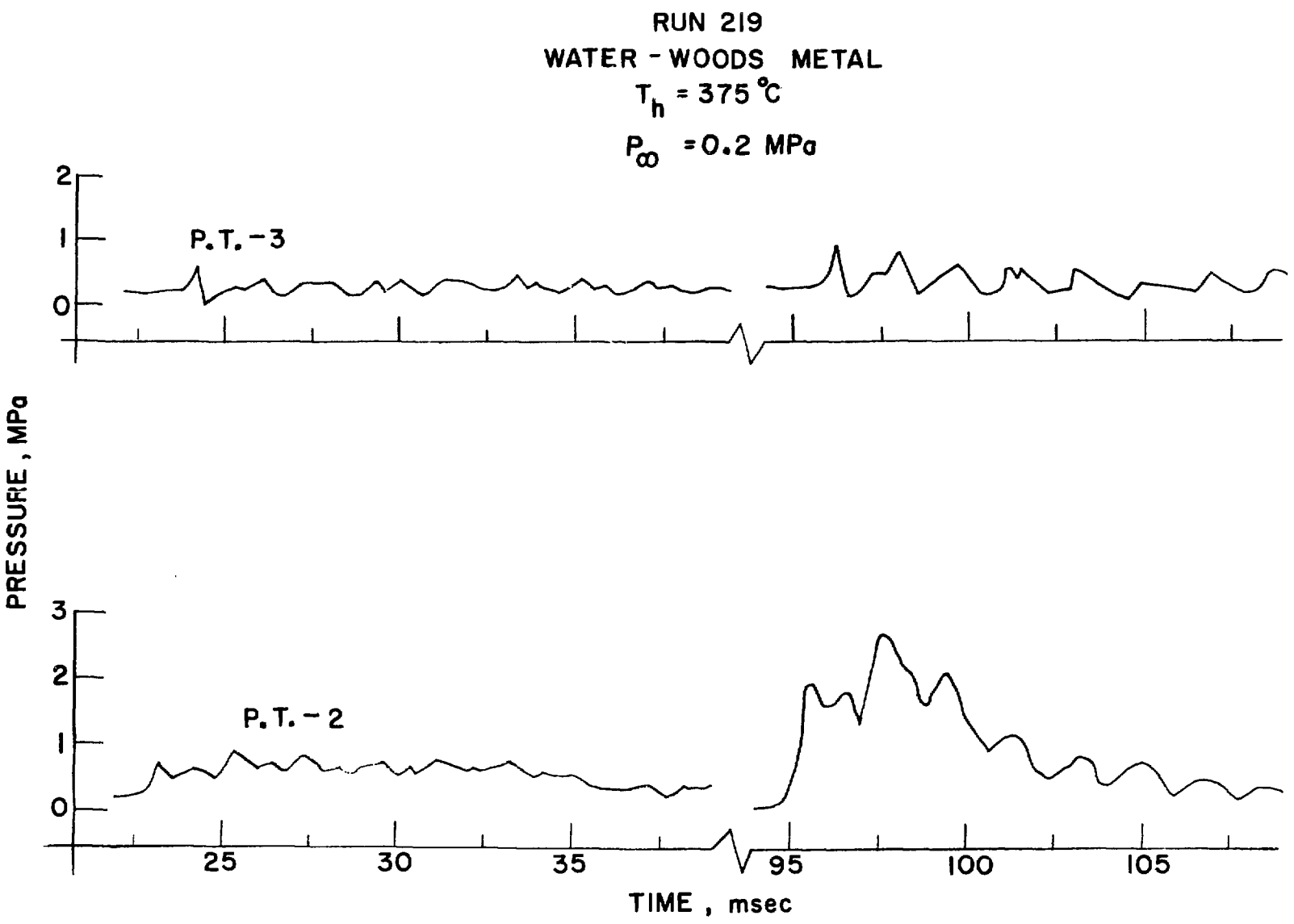

Fig. E.15 Pressure History of Run 219

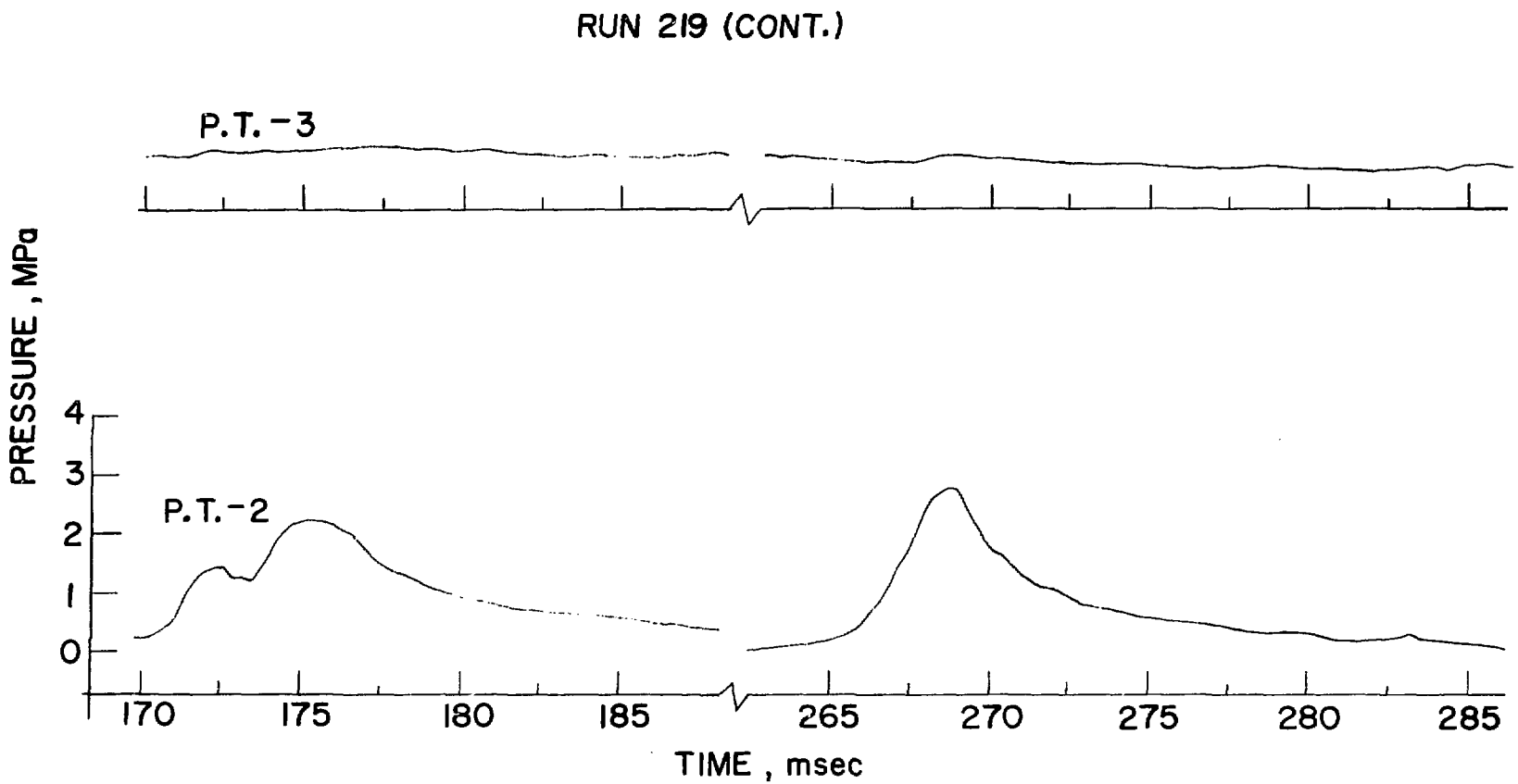

Fig. E.15 Pressure History of Run 219 (contd.)

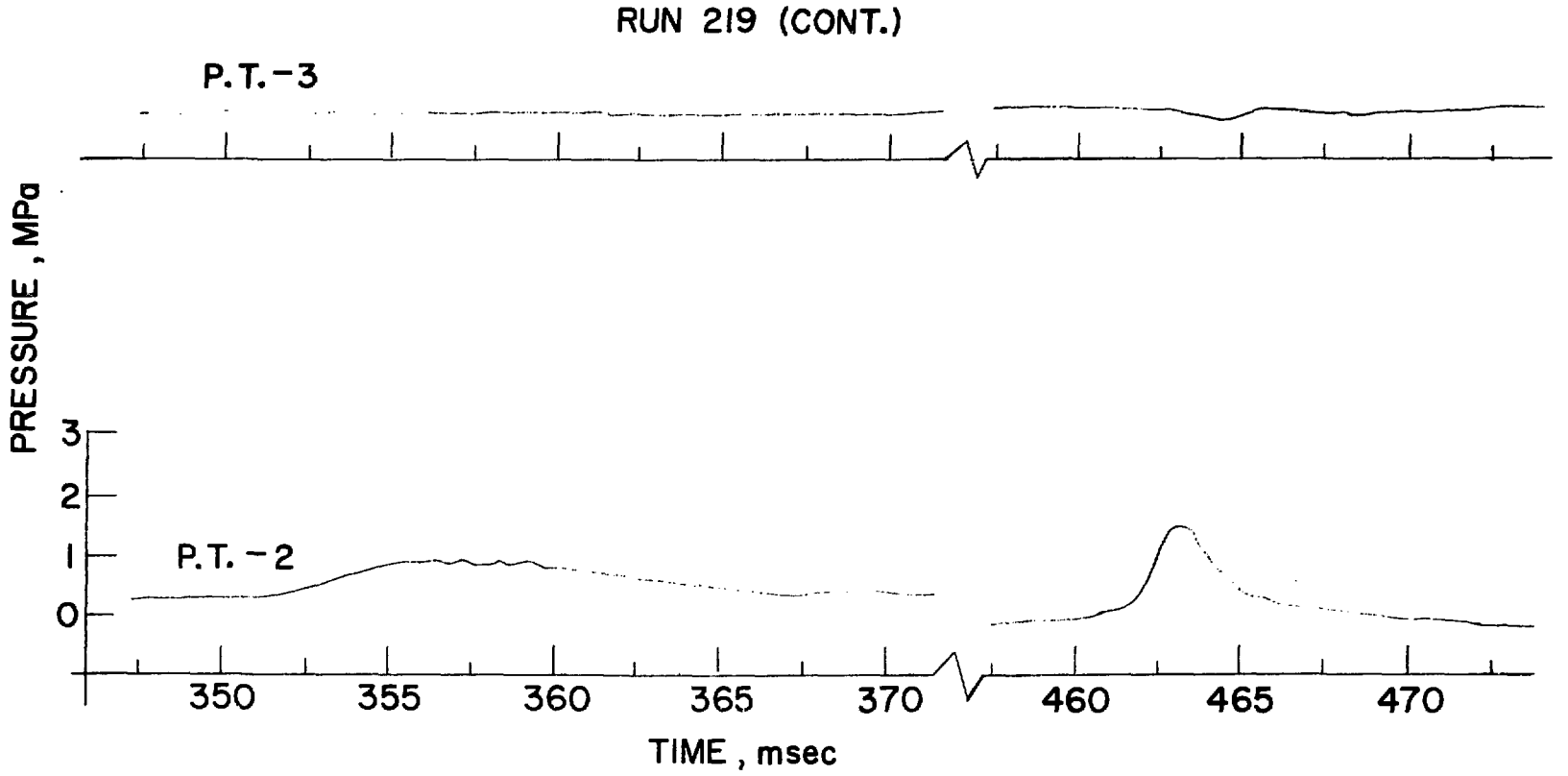

Fig. E.15 Pressure History of Run 219 (contd.)

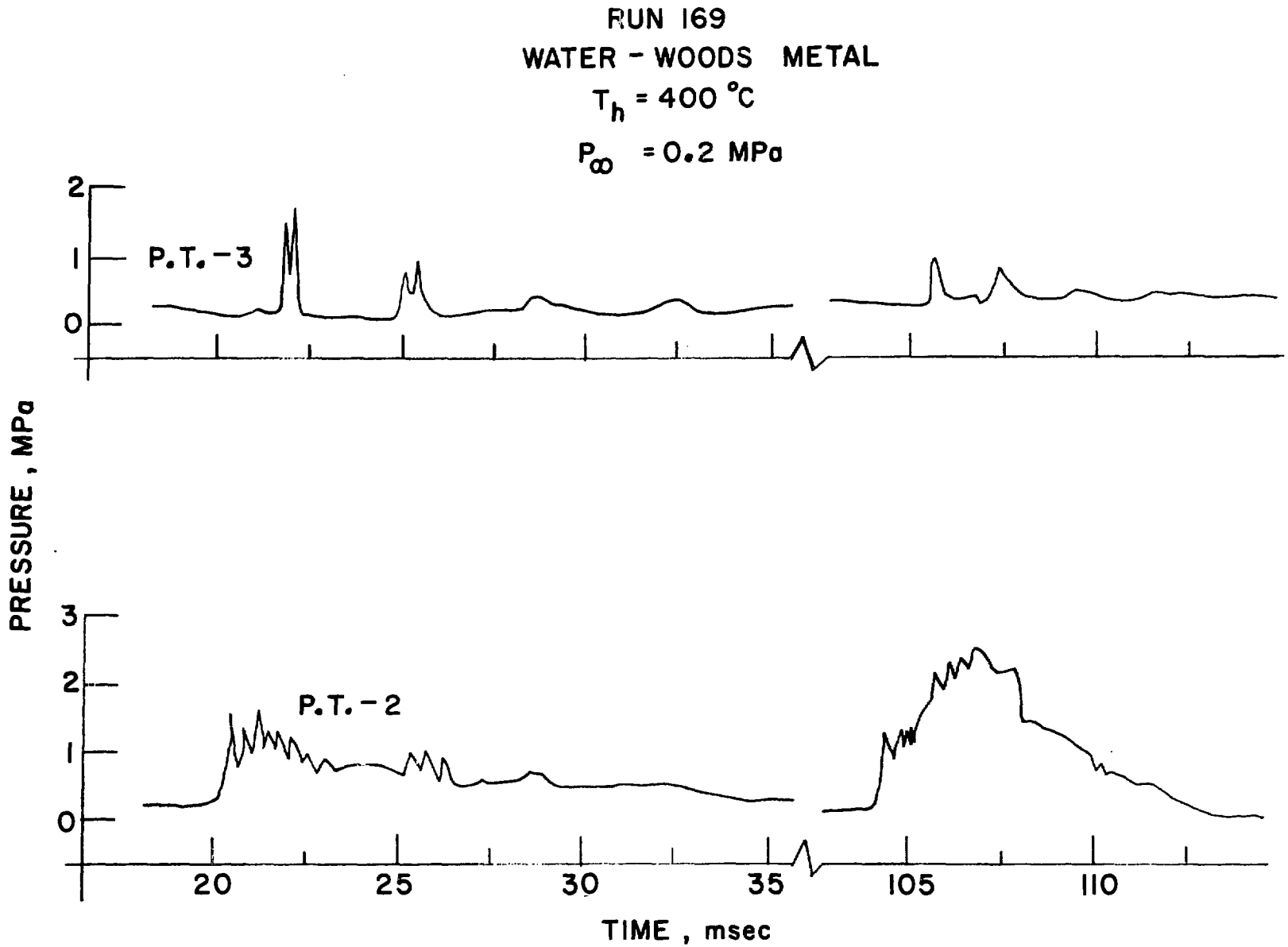

Fig. E.16 Pressure History of Run 169

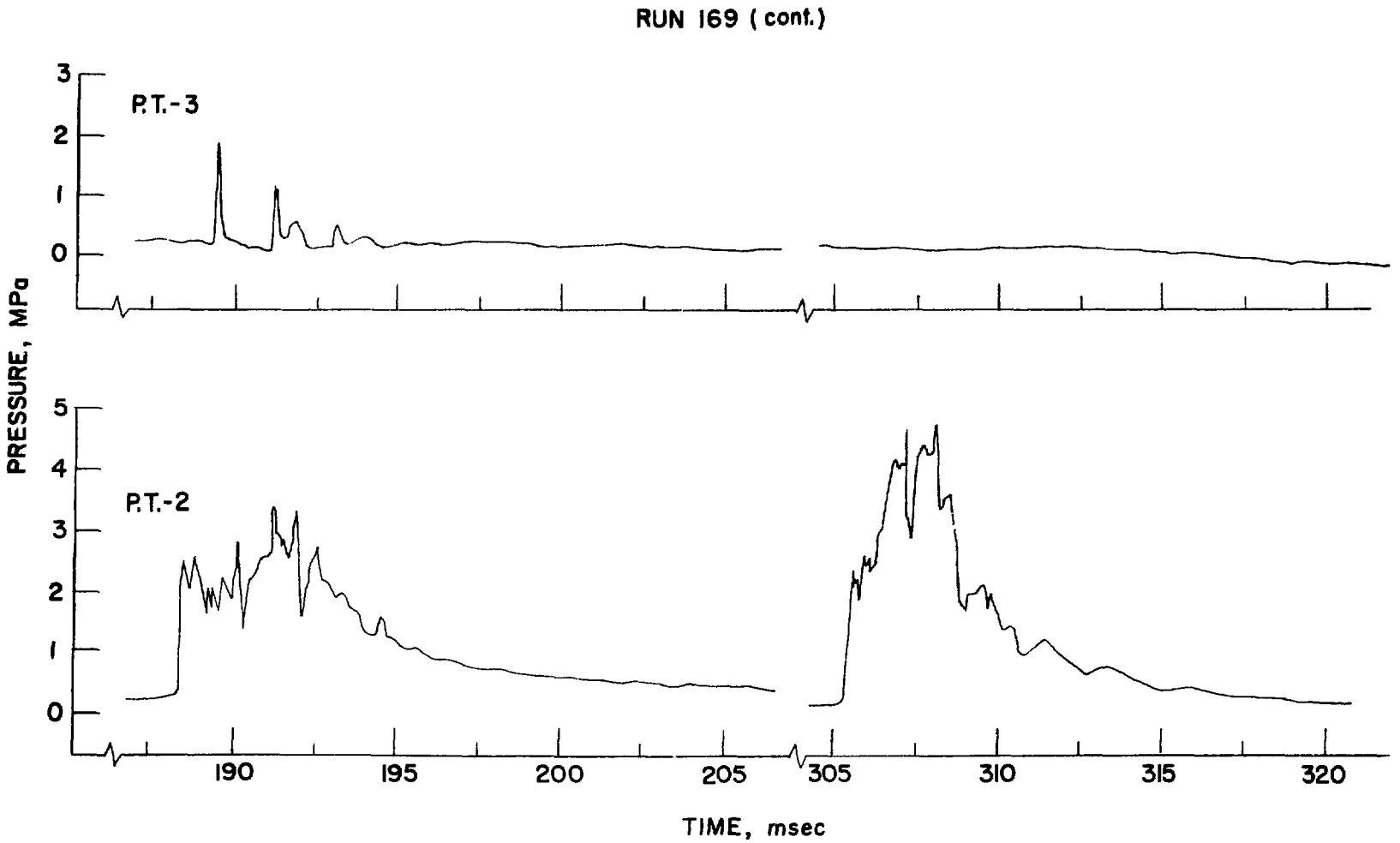

Fig. E.16 Pressure History of Run 169 (contd.)

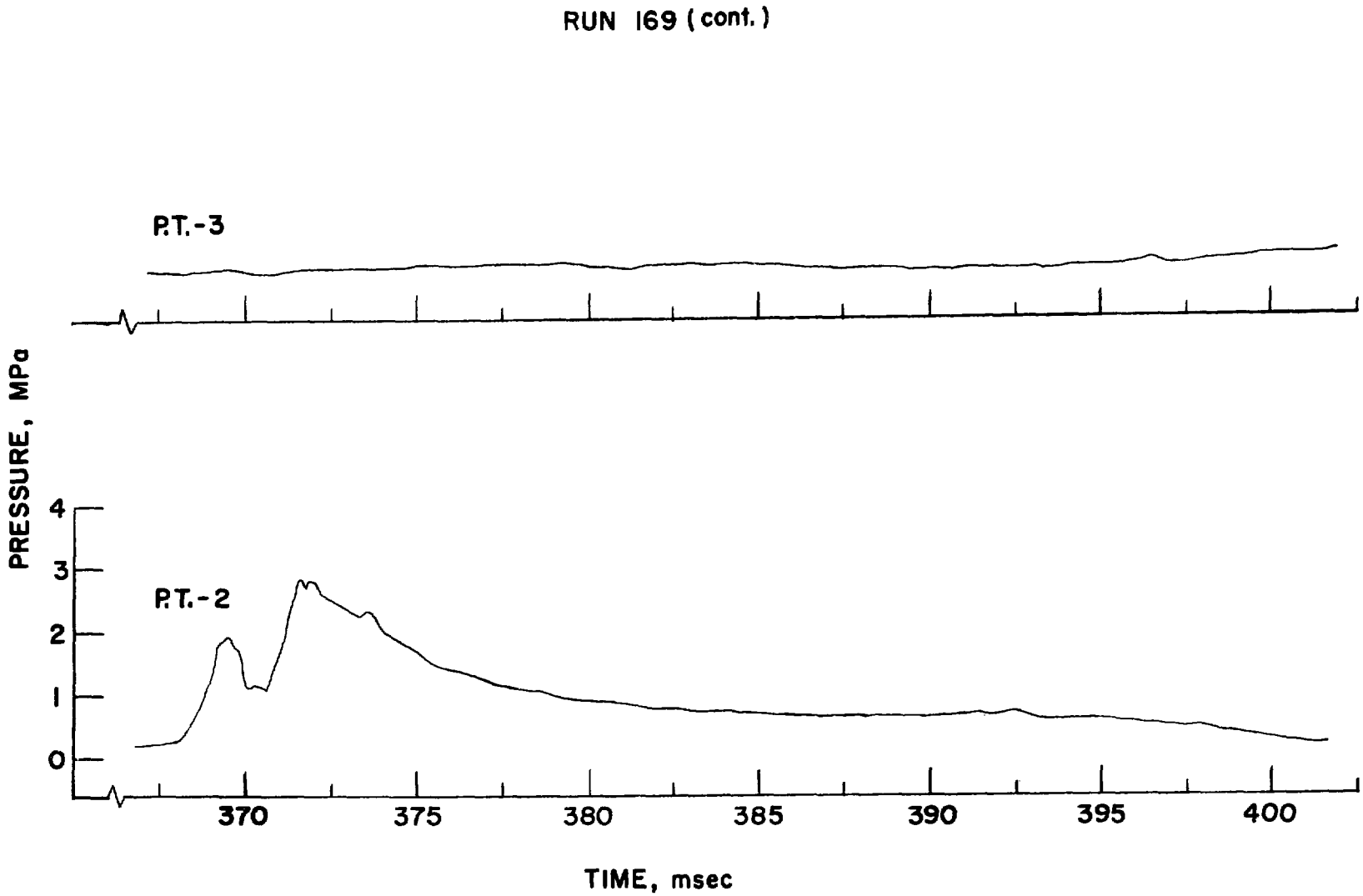

Fig. E.16 Pressure History of Run 169 (contd.)

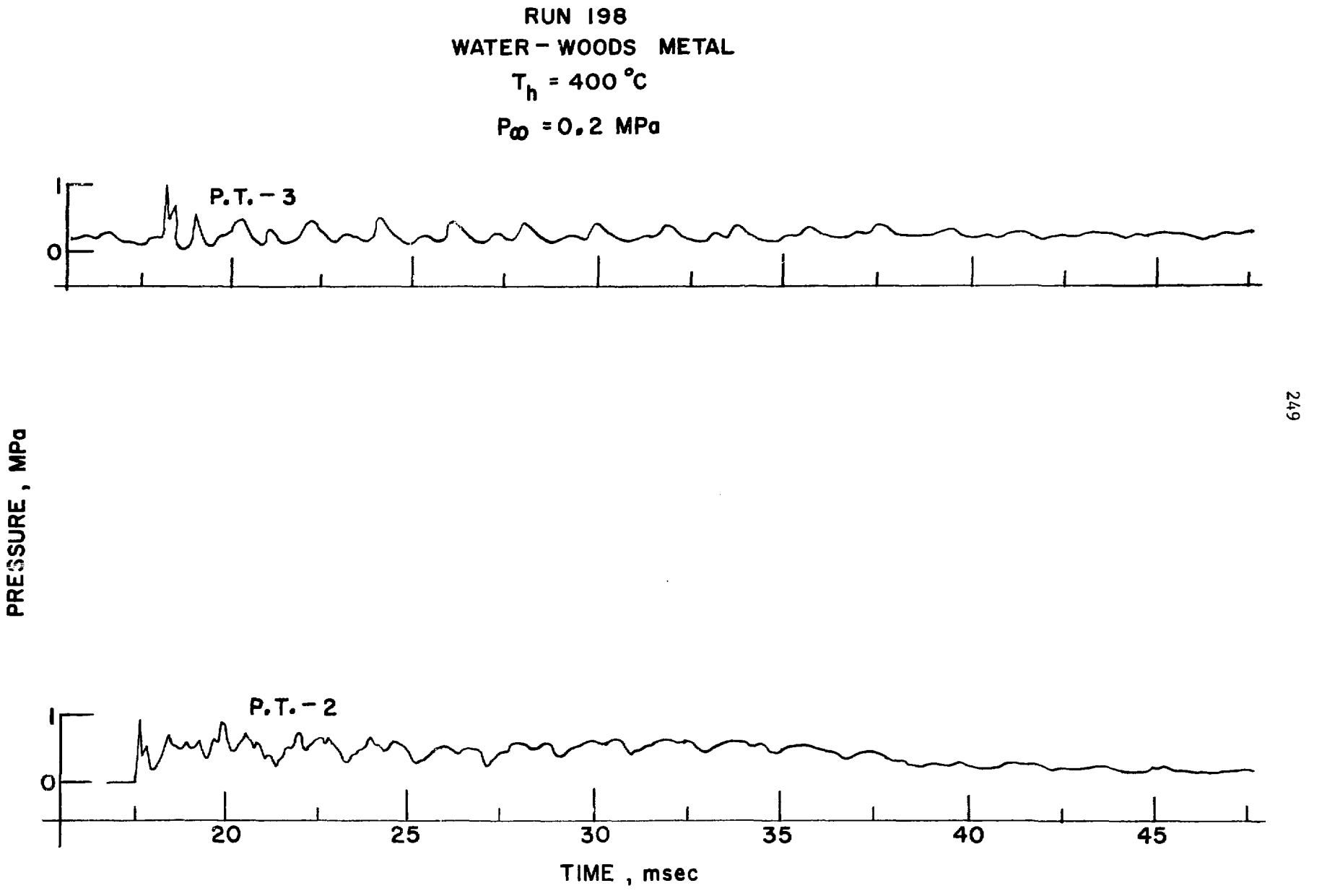

Fig. E.17 Pressure History of Run 198

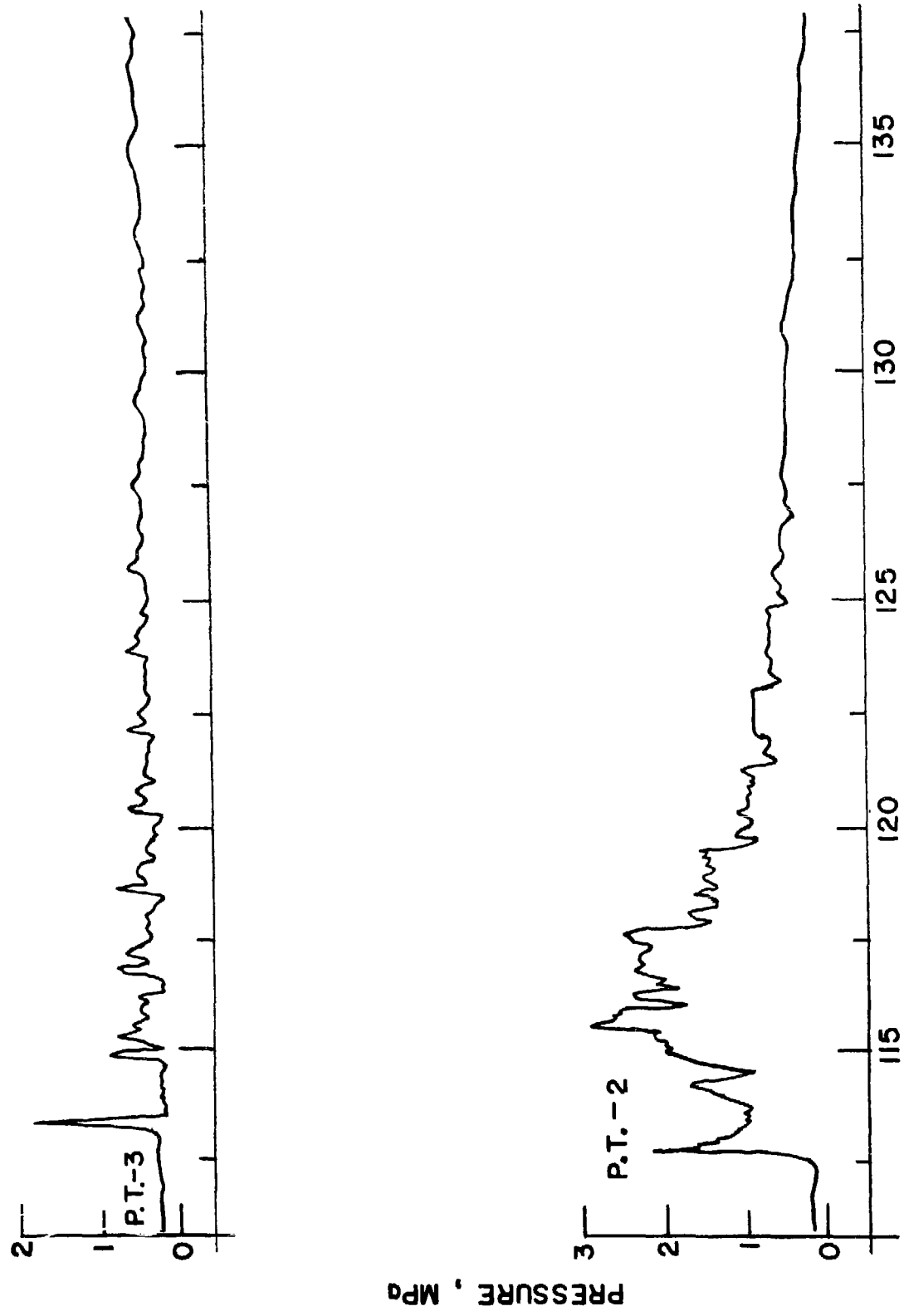

Fig. E.17 Pressure History of Run 198 (contd.)

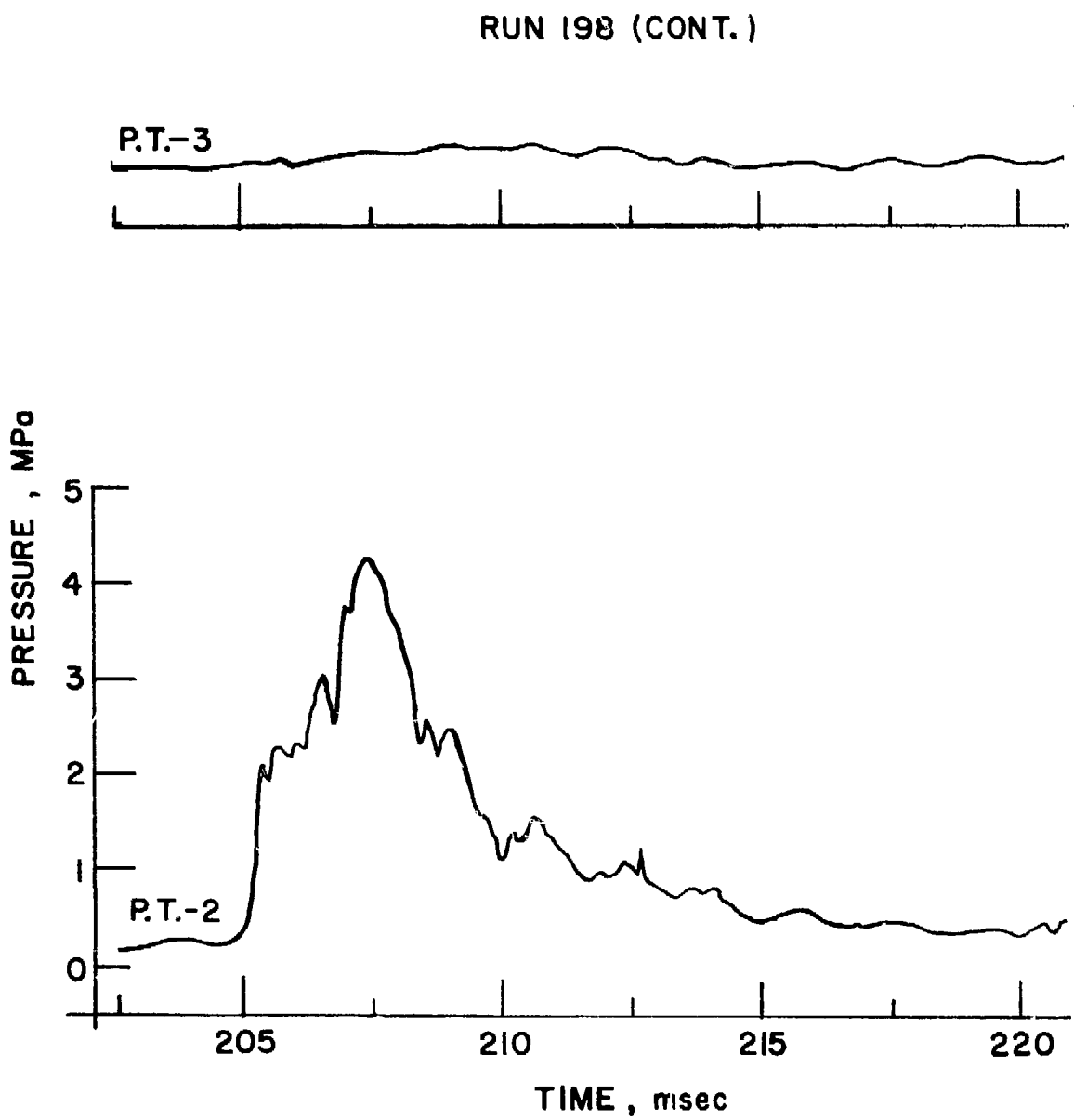

Fig. E.17 Pressure History of Run 198 (contd.)

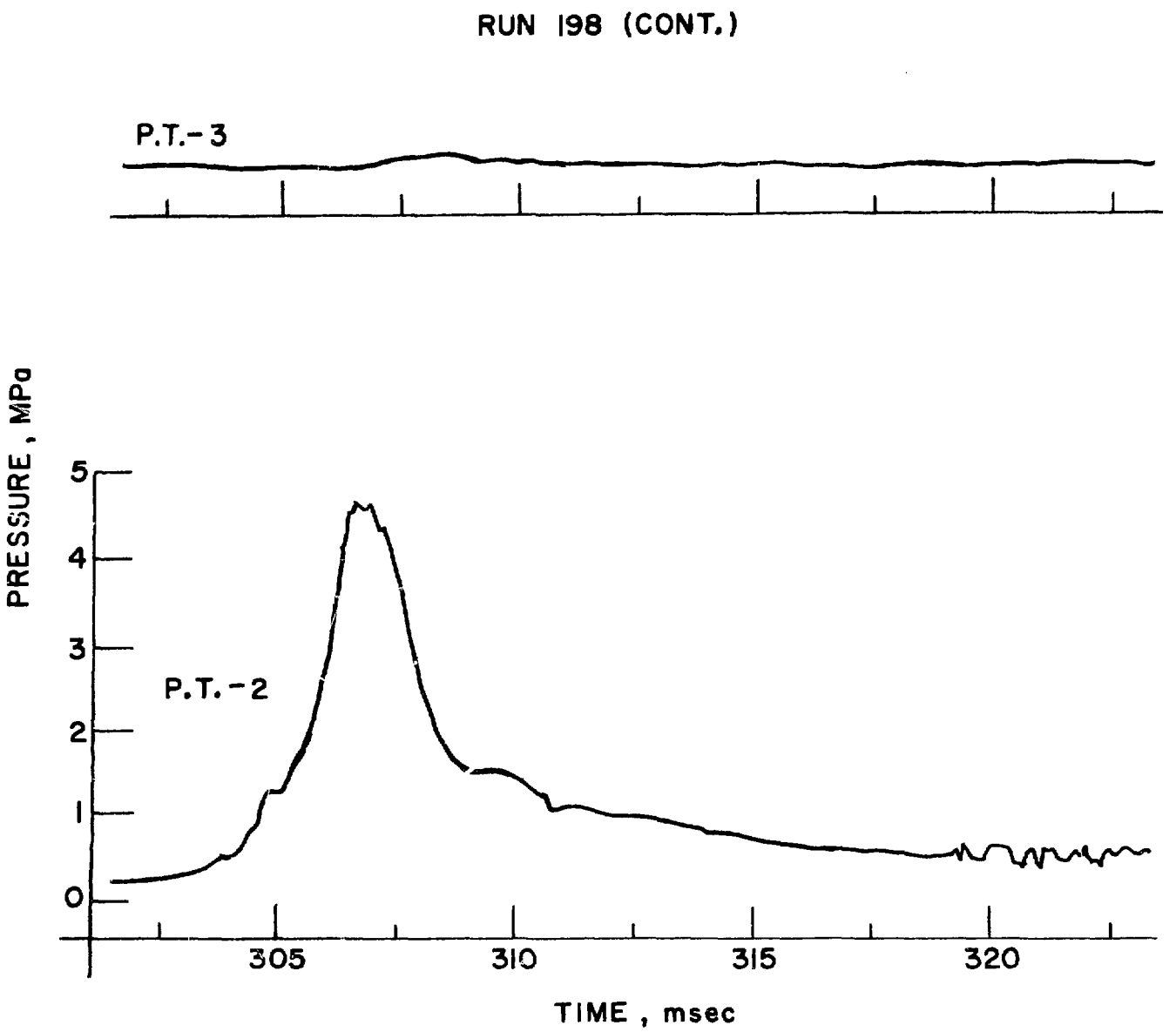

Fig. E.17 Pressure History of Run 198 (contd.)

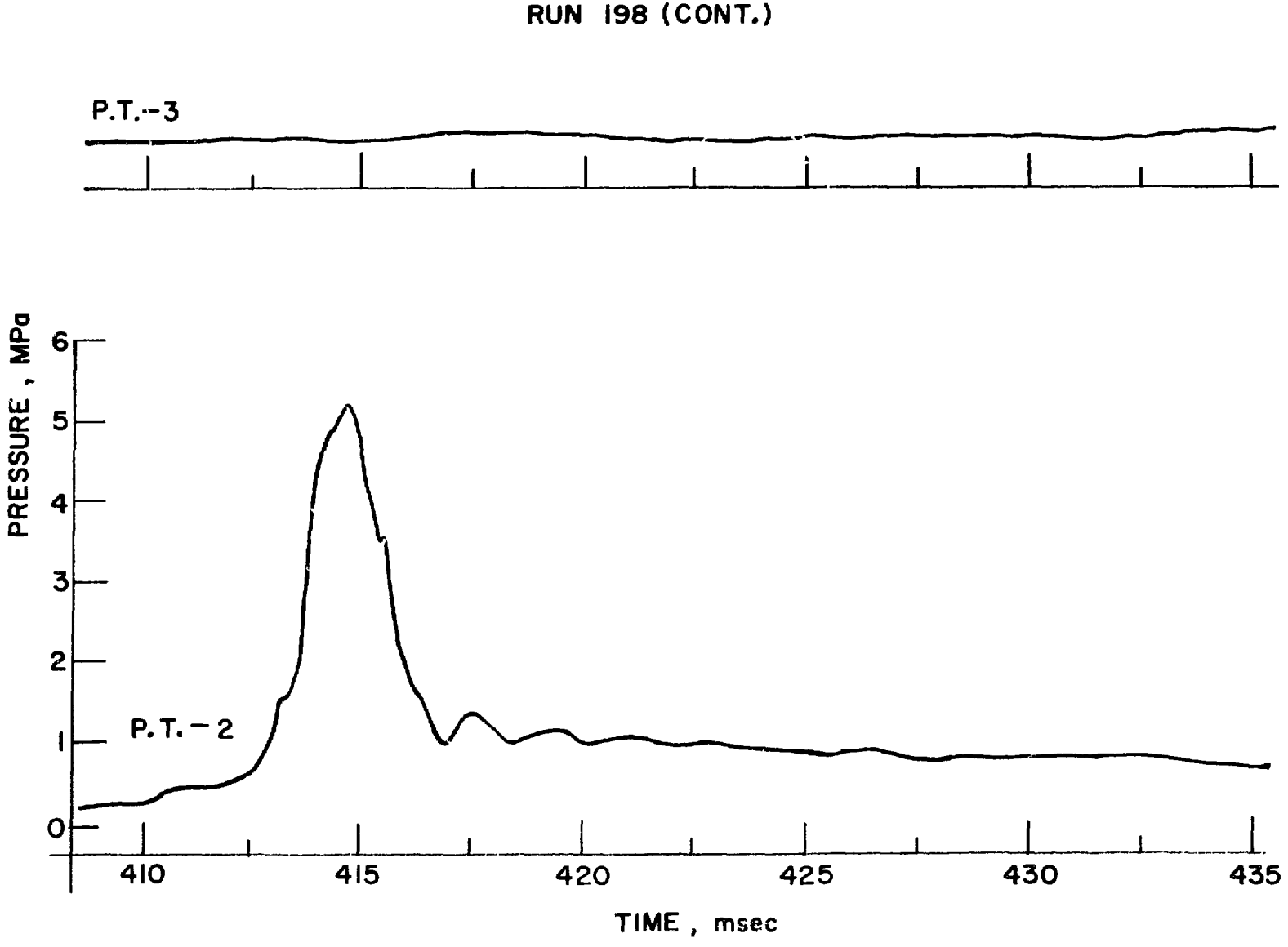

Fig. E.17 Pressure History of Run 198 (contd.)

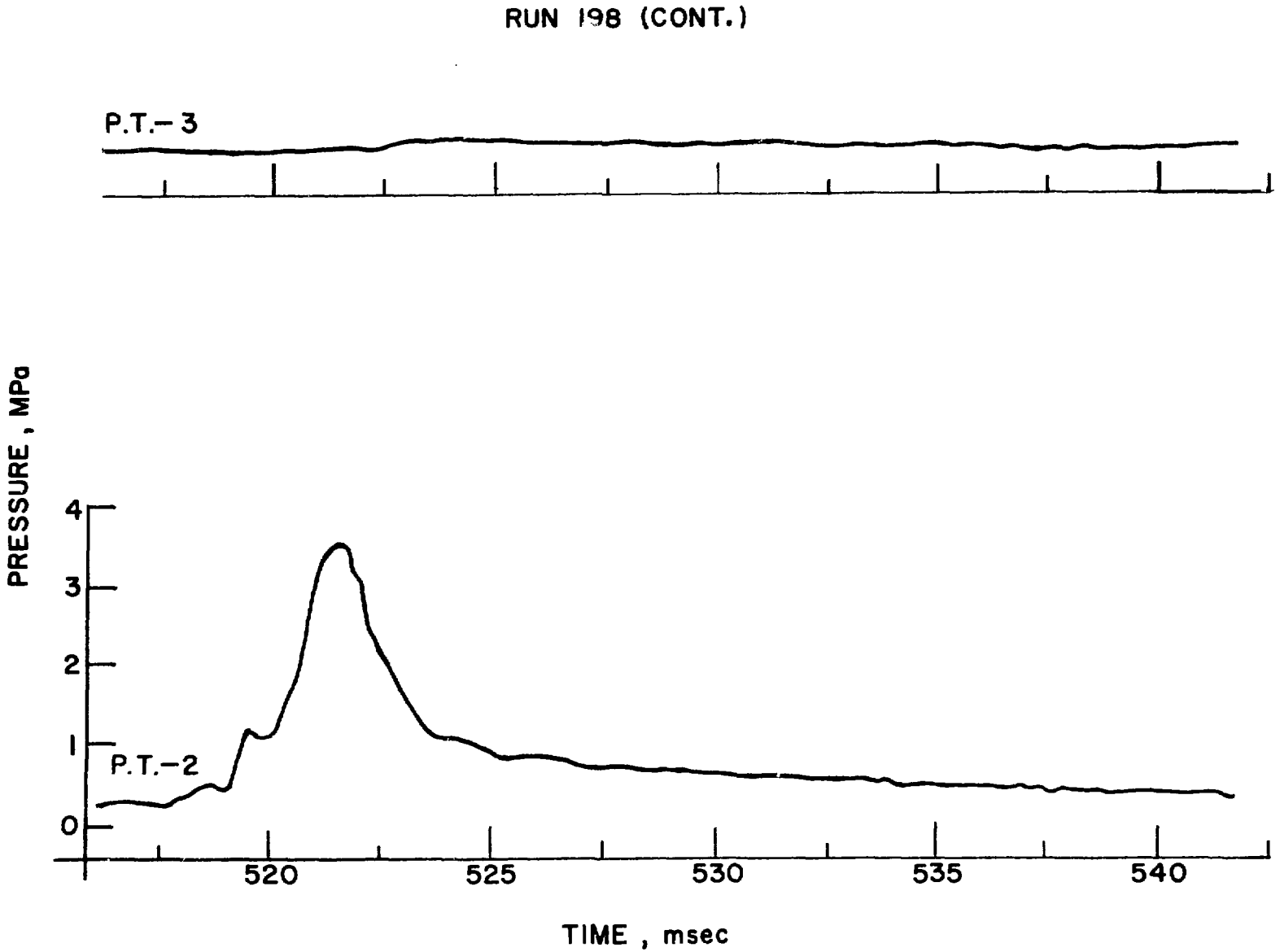

Fig. E.17 Pressure History of Run 198 (contd.)

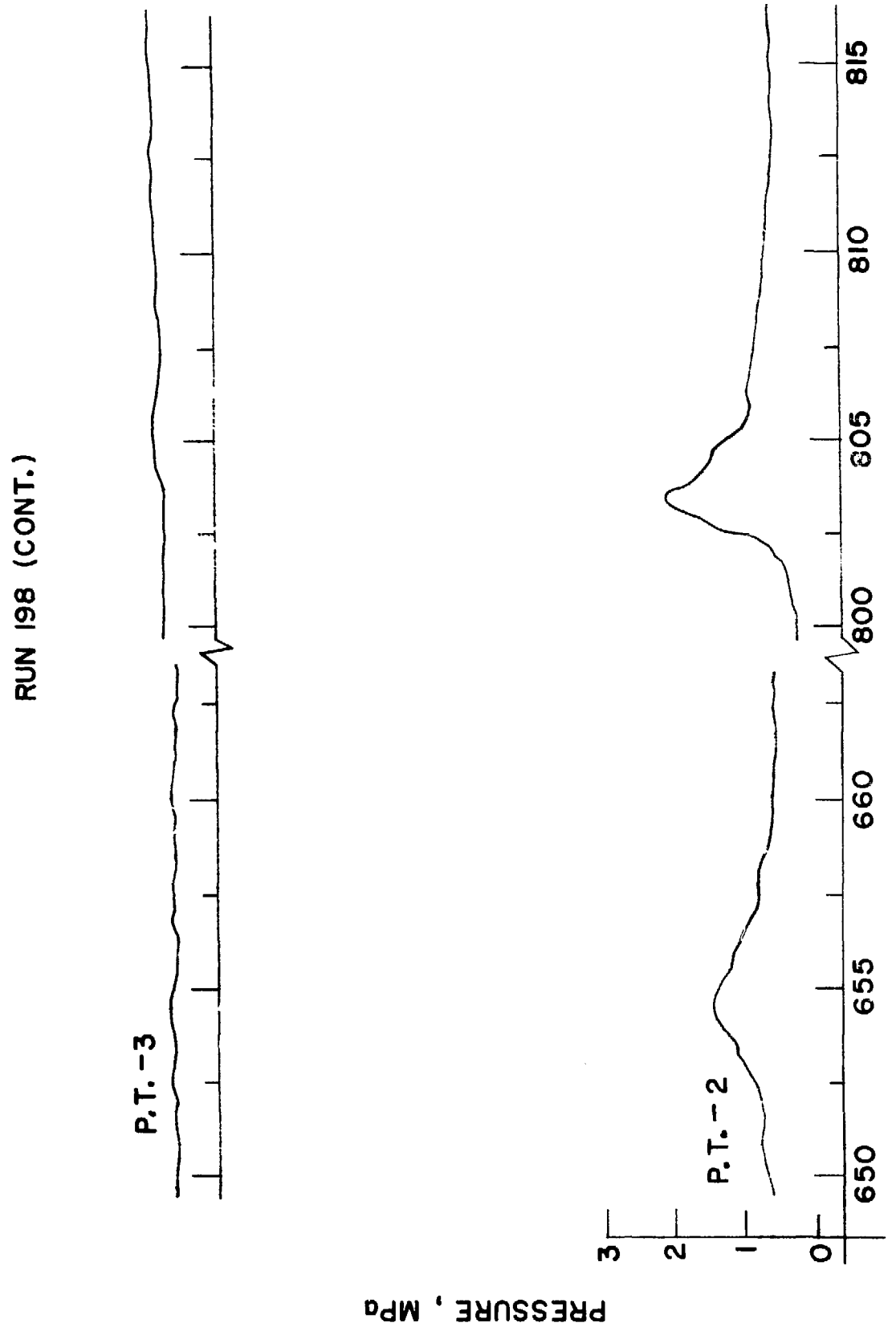

Fig. E.17 Pressure History of Run 198 (contd.)

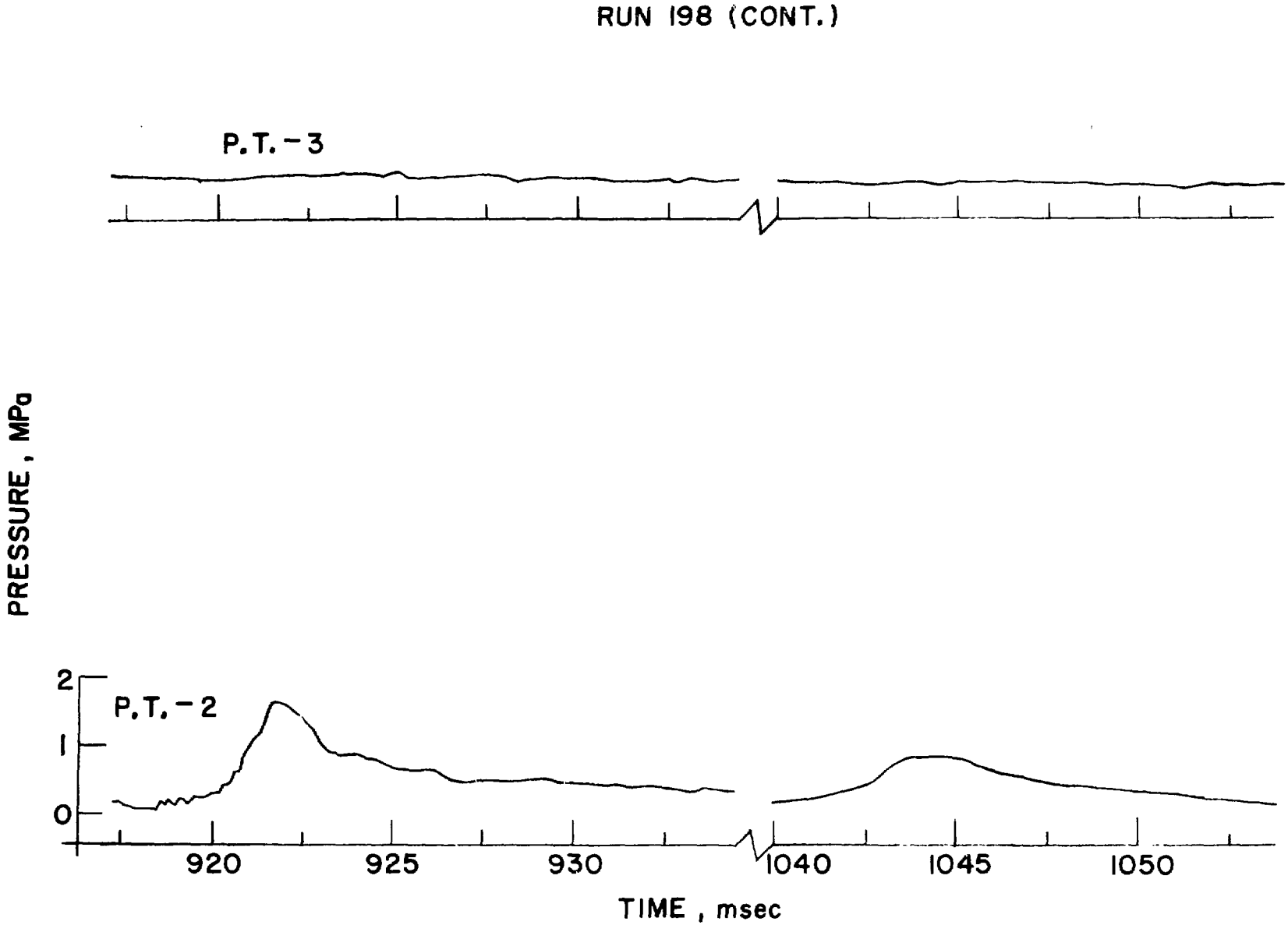

Fig. E.17 Pressure History of Run 198 (contd.)

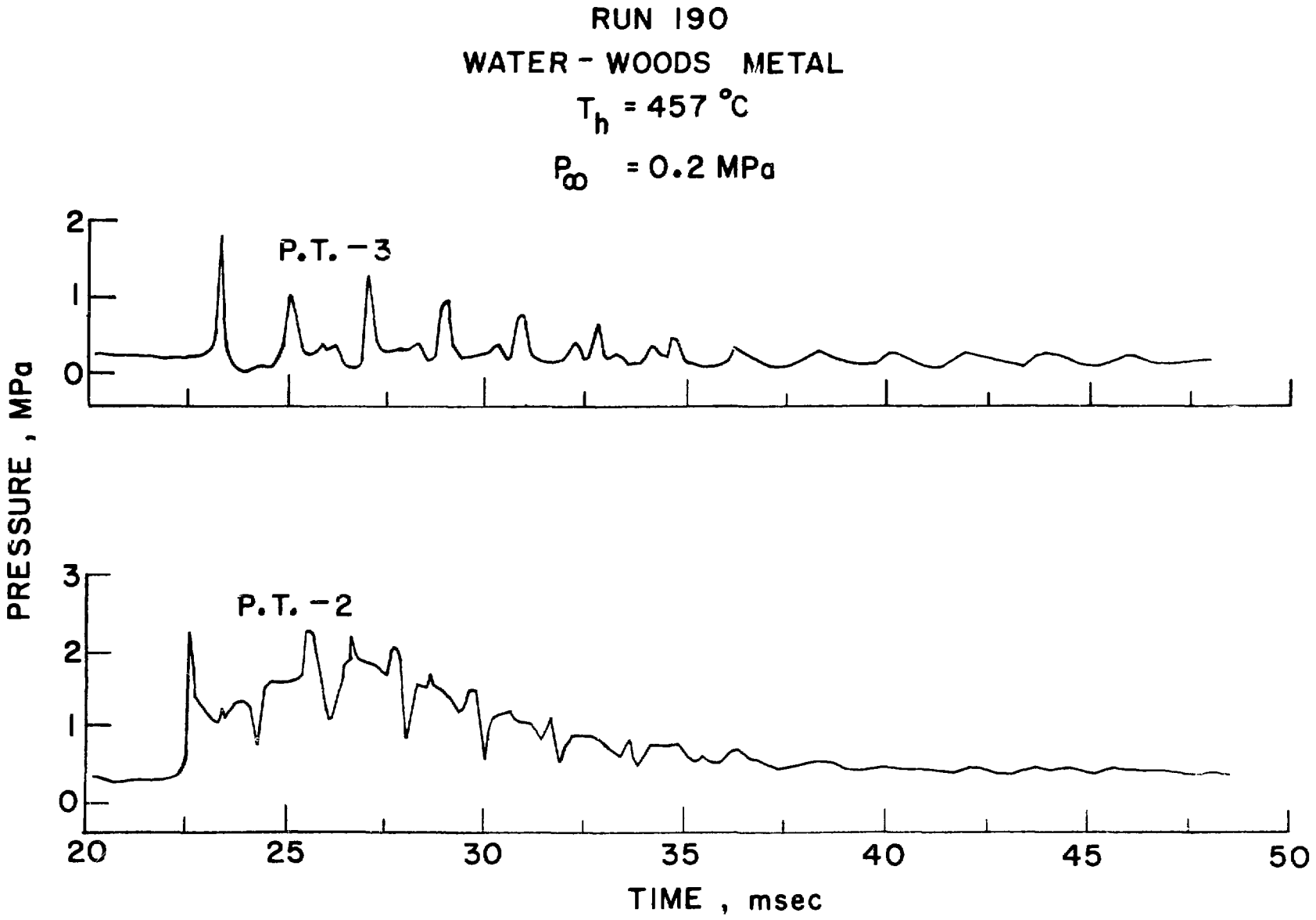

Fig. E.18 Pressure History of Run 190

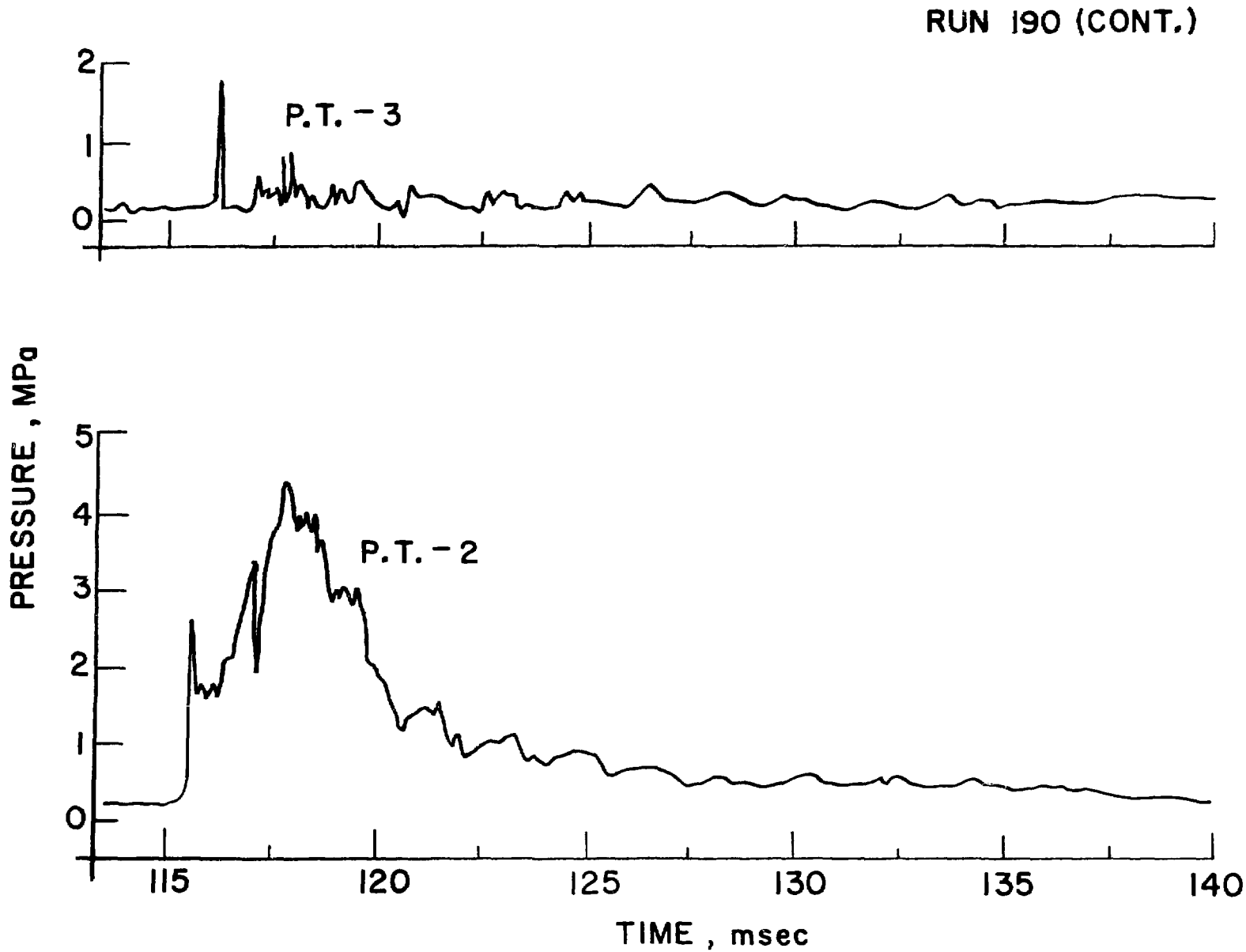

Fig. E.18 Pressure History of Run 190 (contd.)

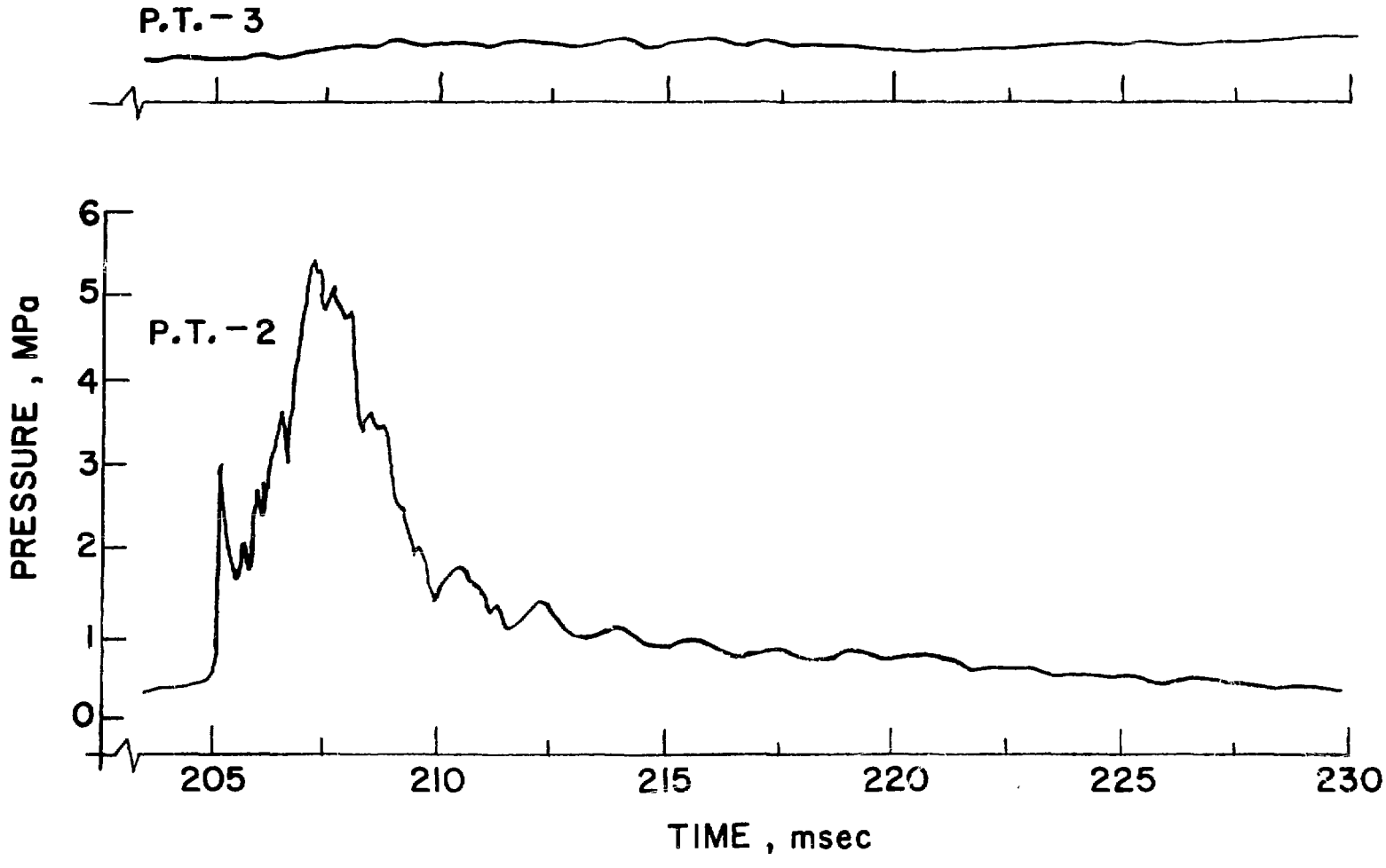

Fig. E.18. Pressure History of Run 190 (contd.)

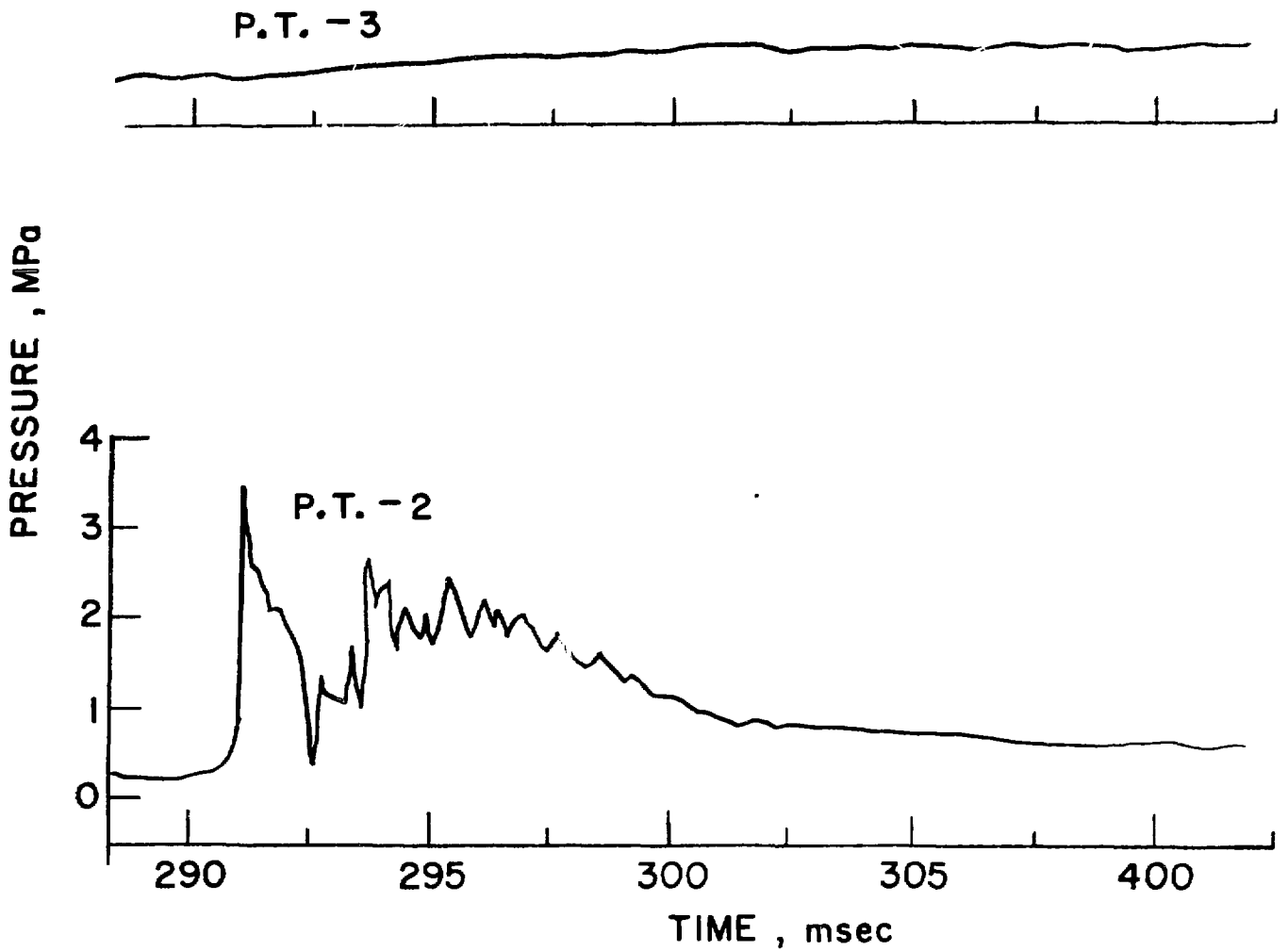

Fig. E.18. Pressure History of Run 190 (contd.

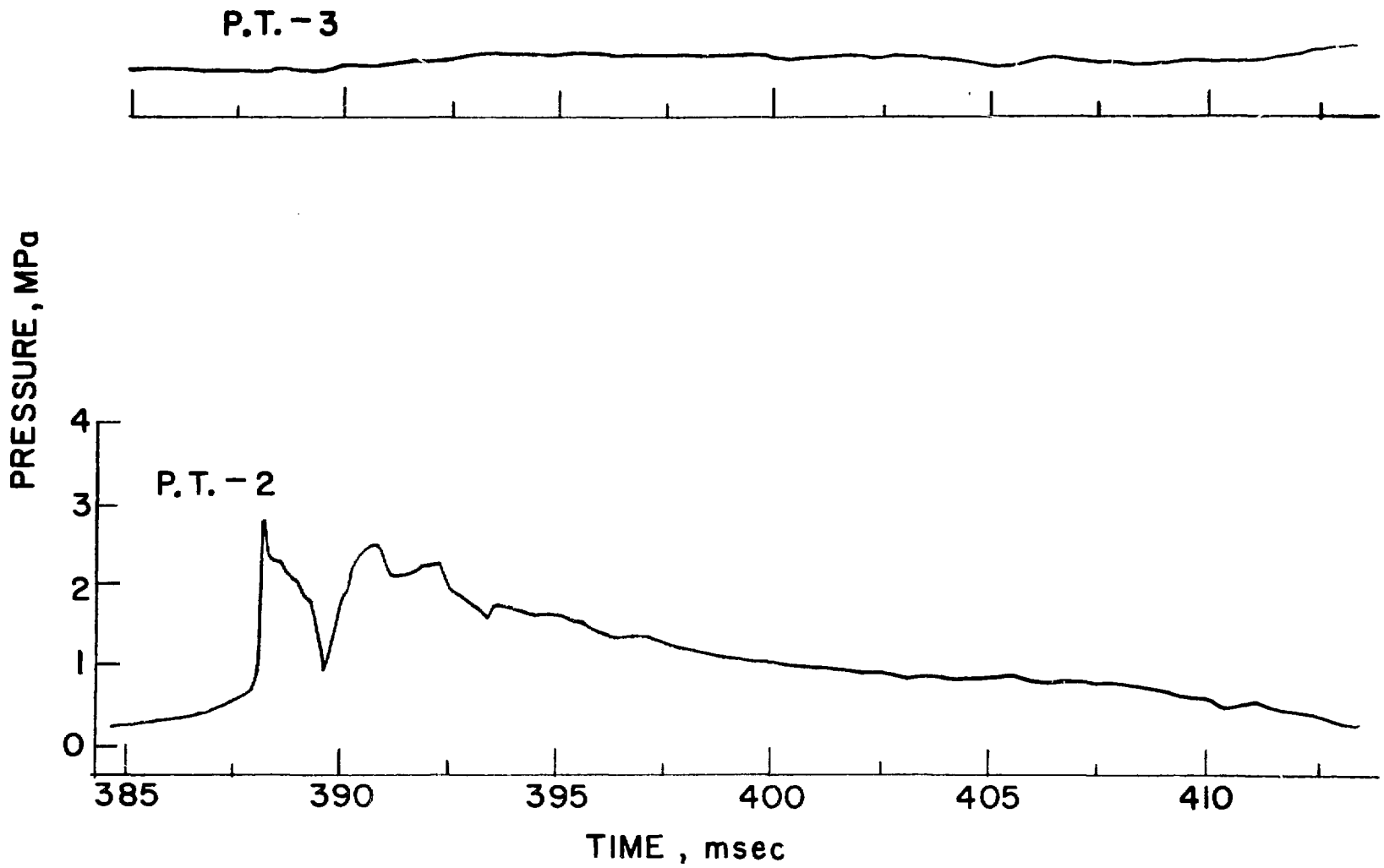

Fig. E.18. Pressure History of Run 190(contd.)

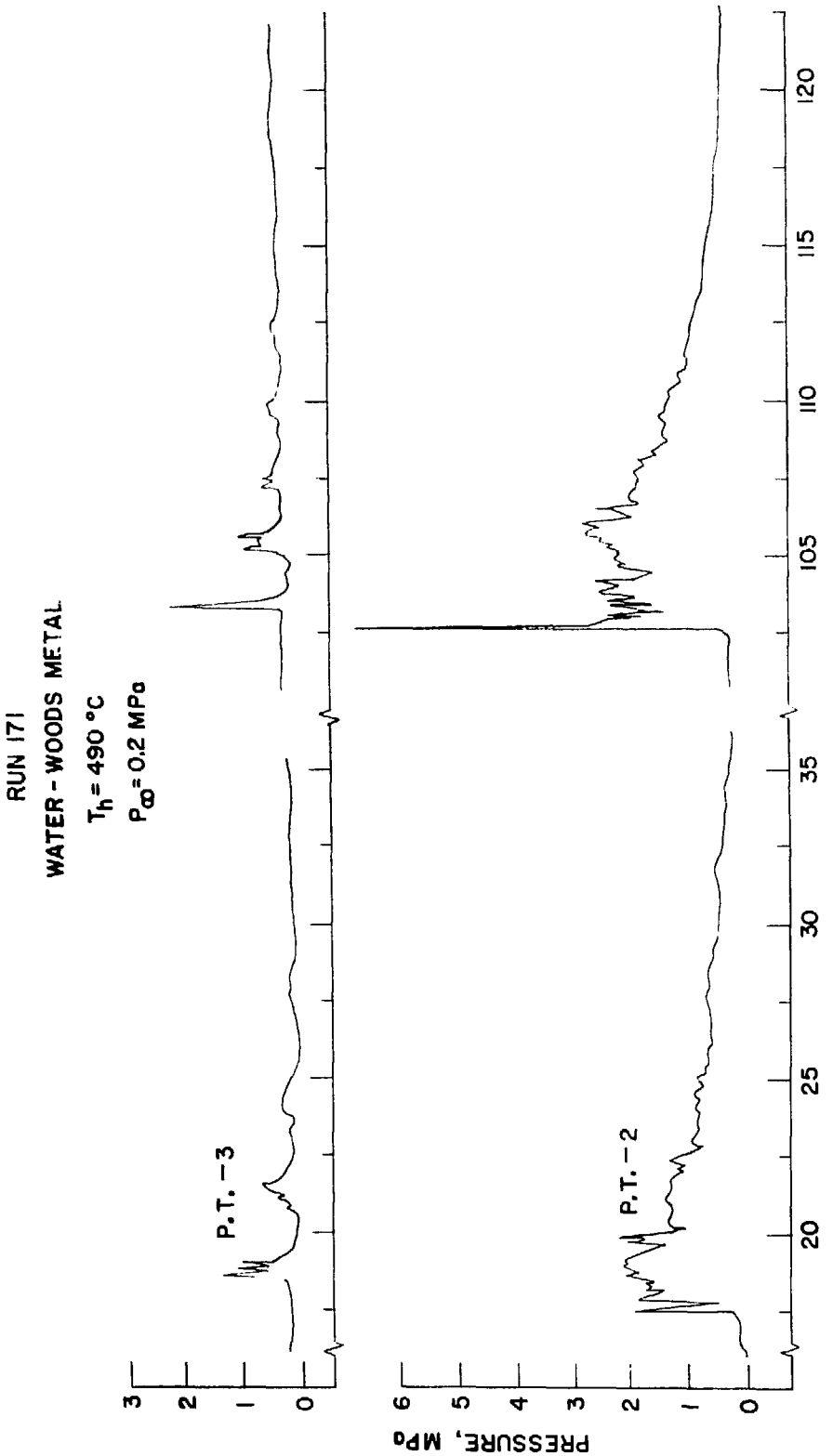

Fig. E.19. Pressure History of Run 171

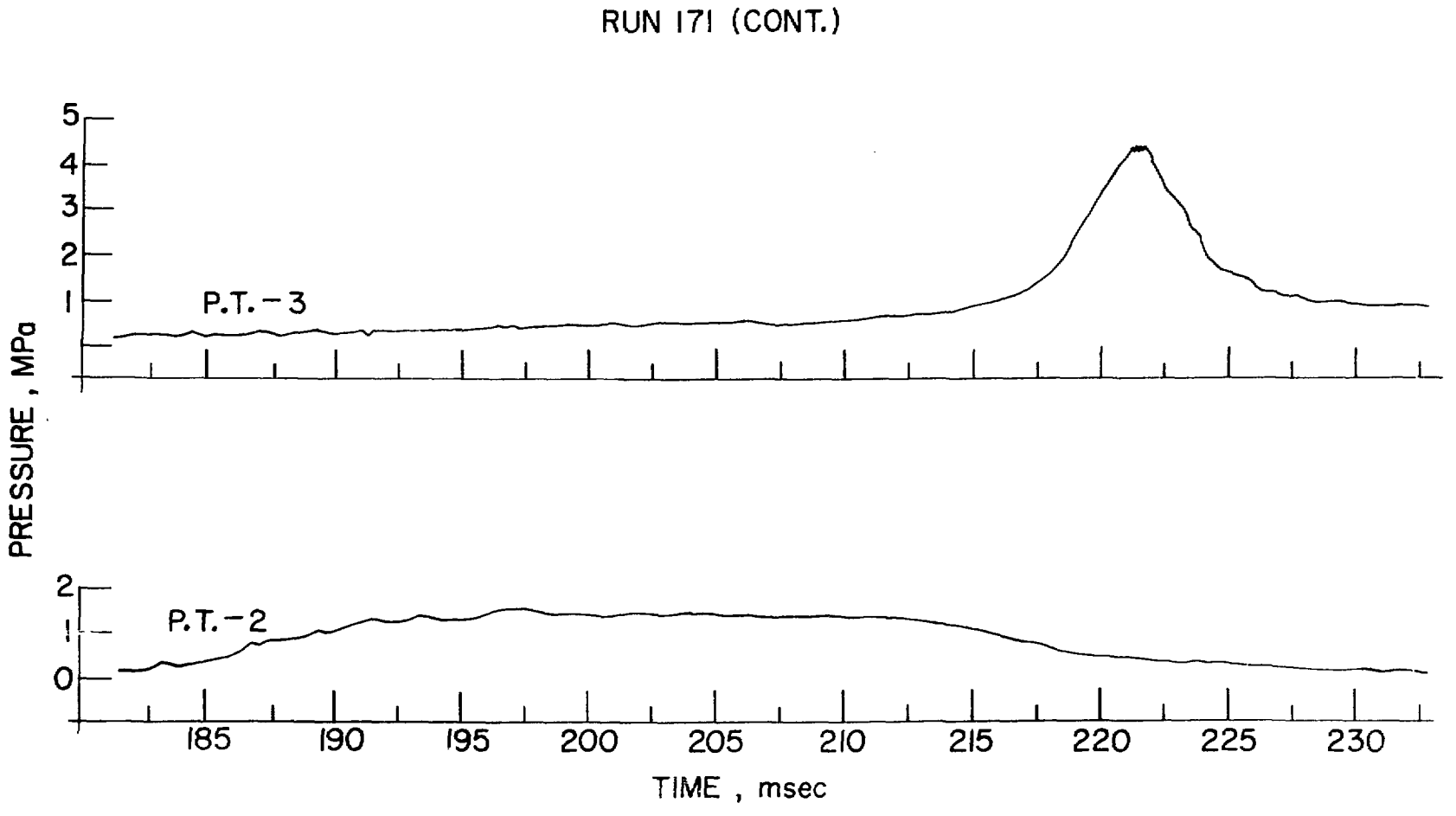

Fig. E.19. Pressure History of Run 171(contd.)

RUN 191
WATER – WOODS METAL
T_h = 551 °C
P_∞ = 0.2 MPa

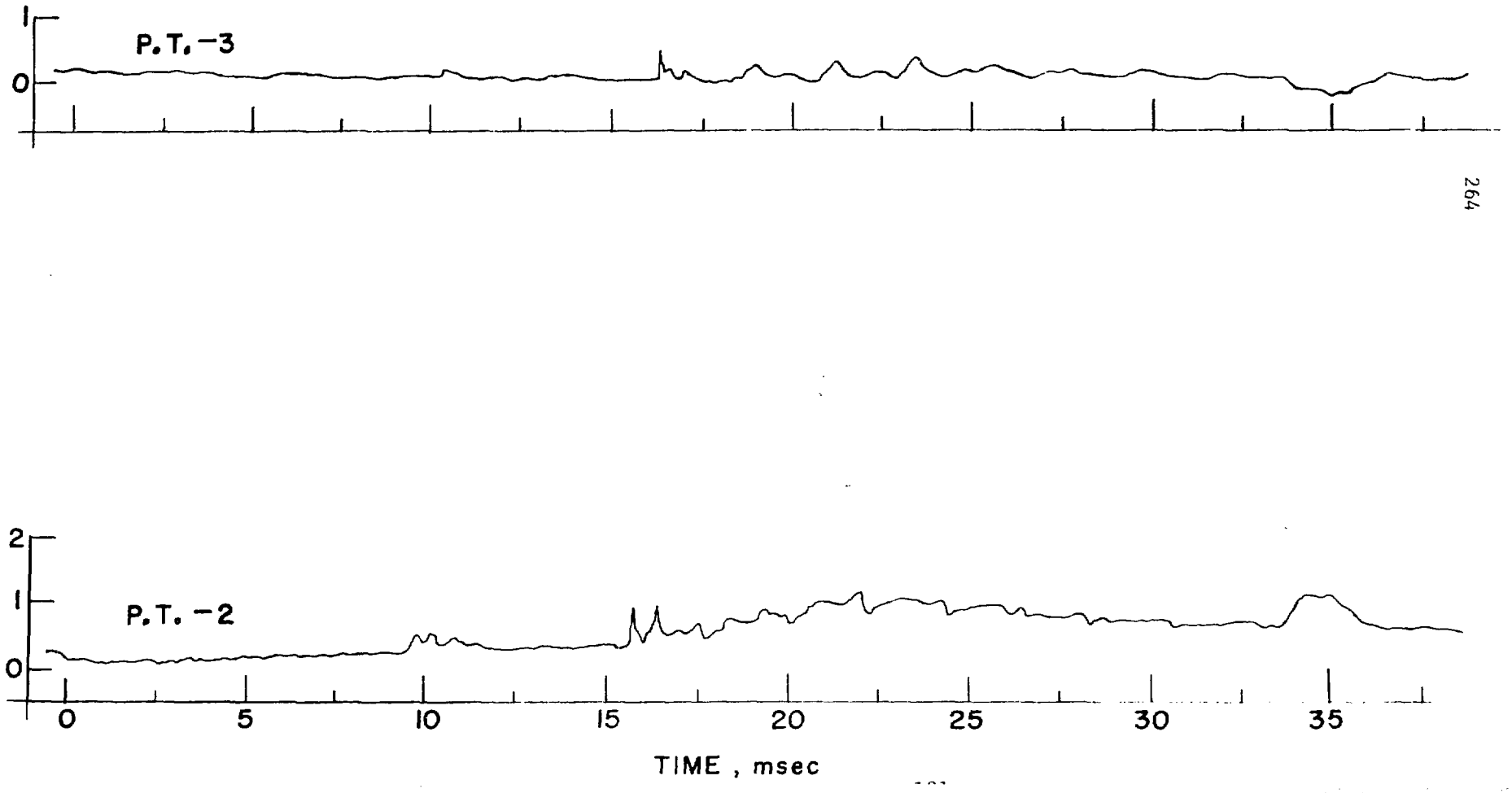

264

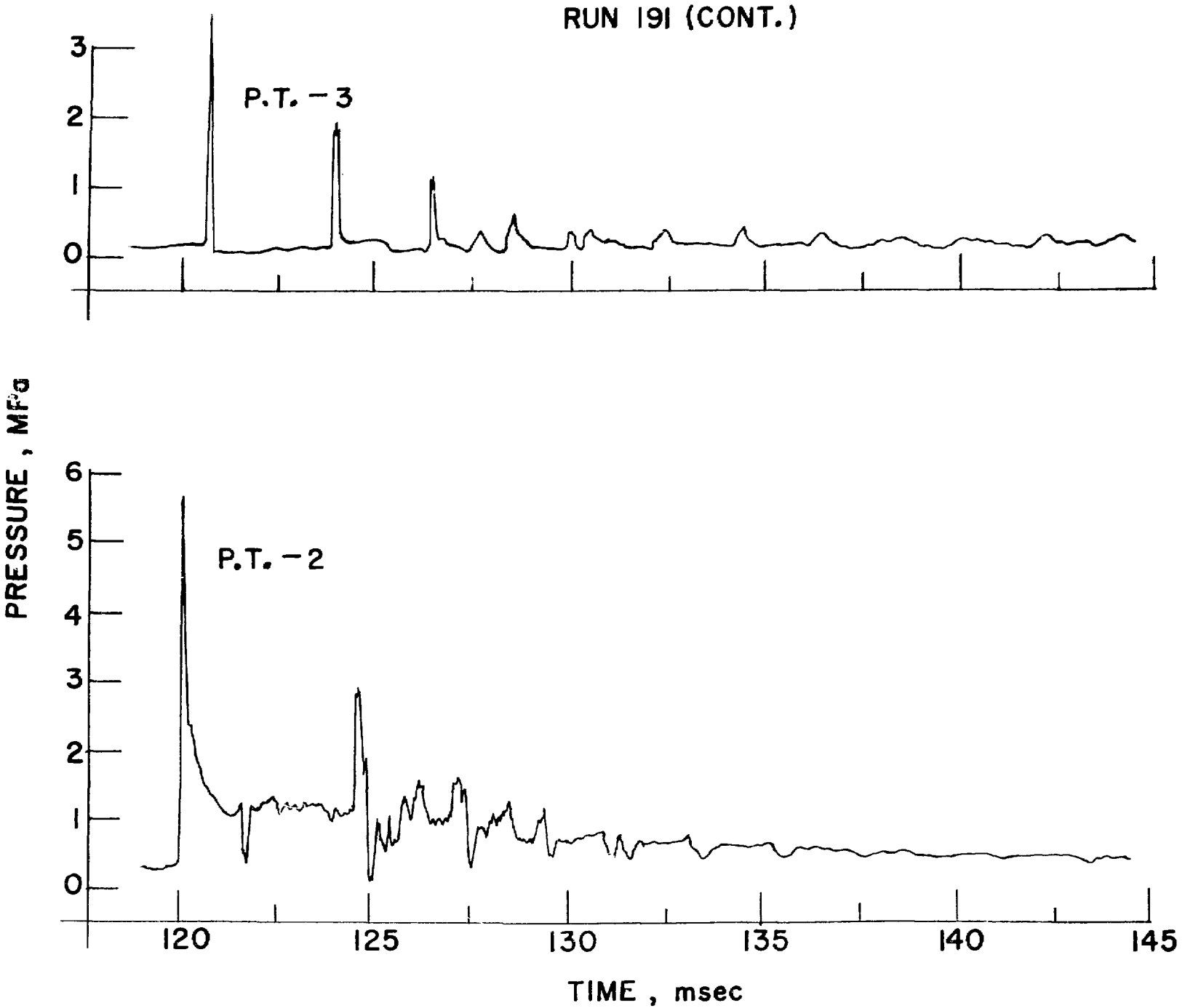

Fig. E.20 Pressure History of Run 191(contd.)

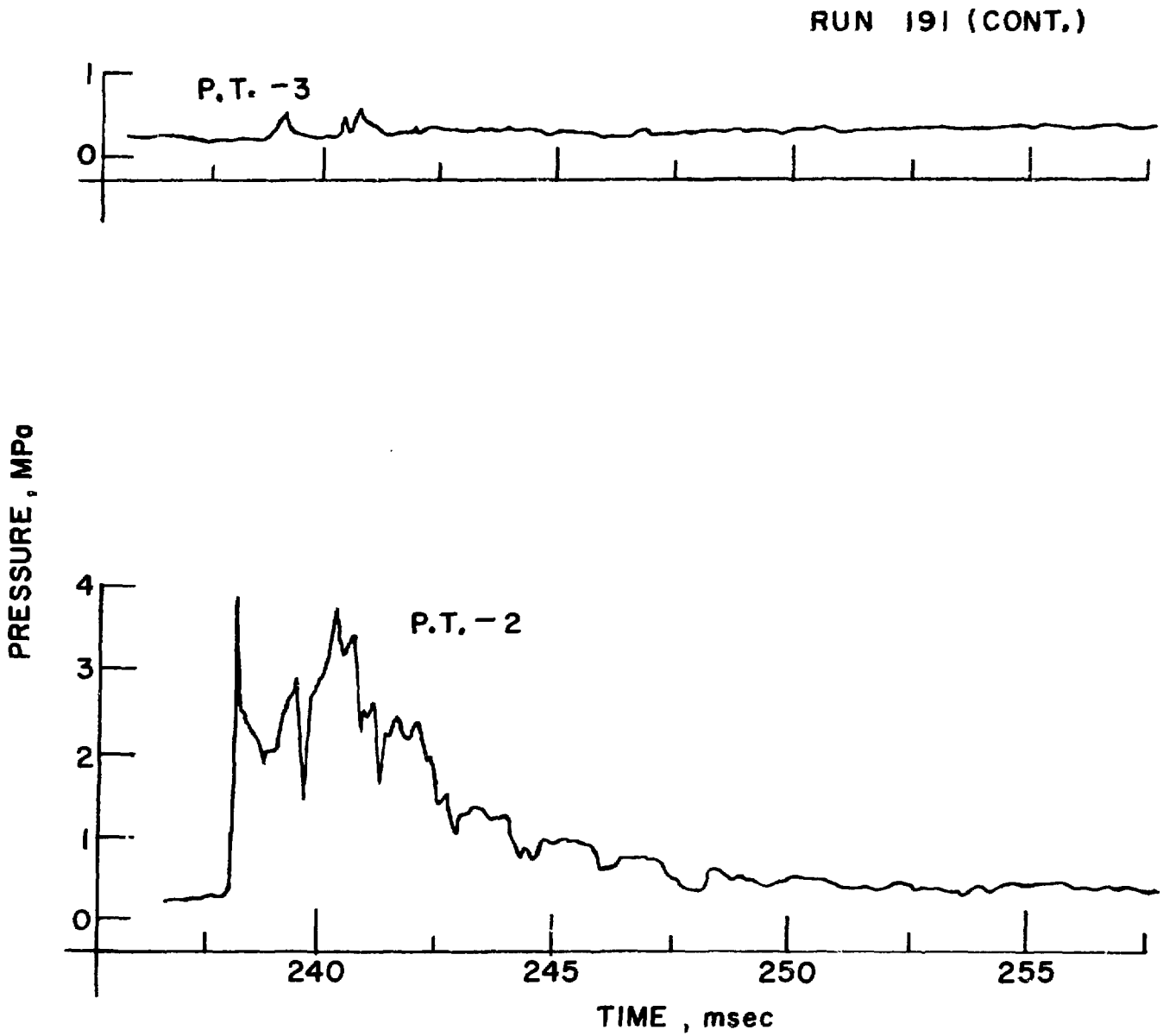

Fig. E.20 Pressure History of Run 191(contd.)

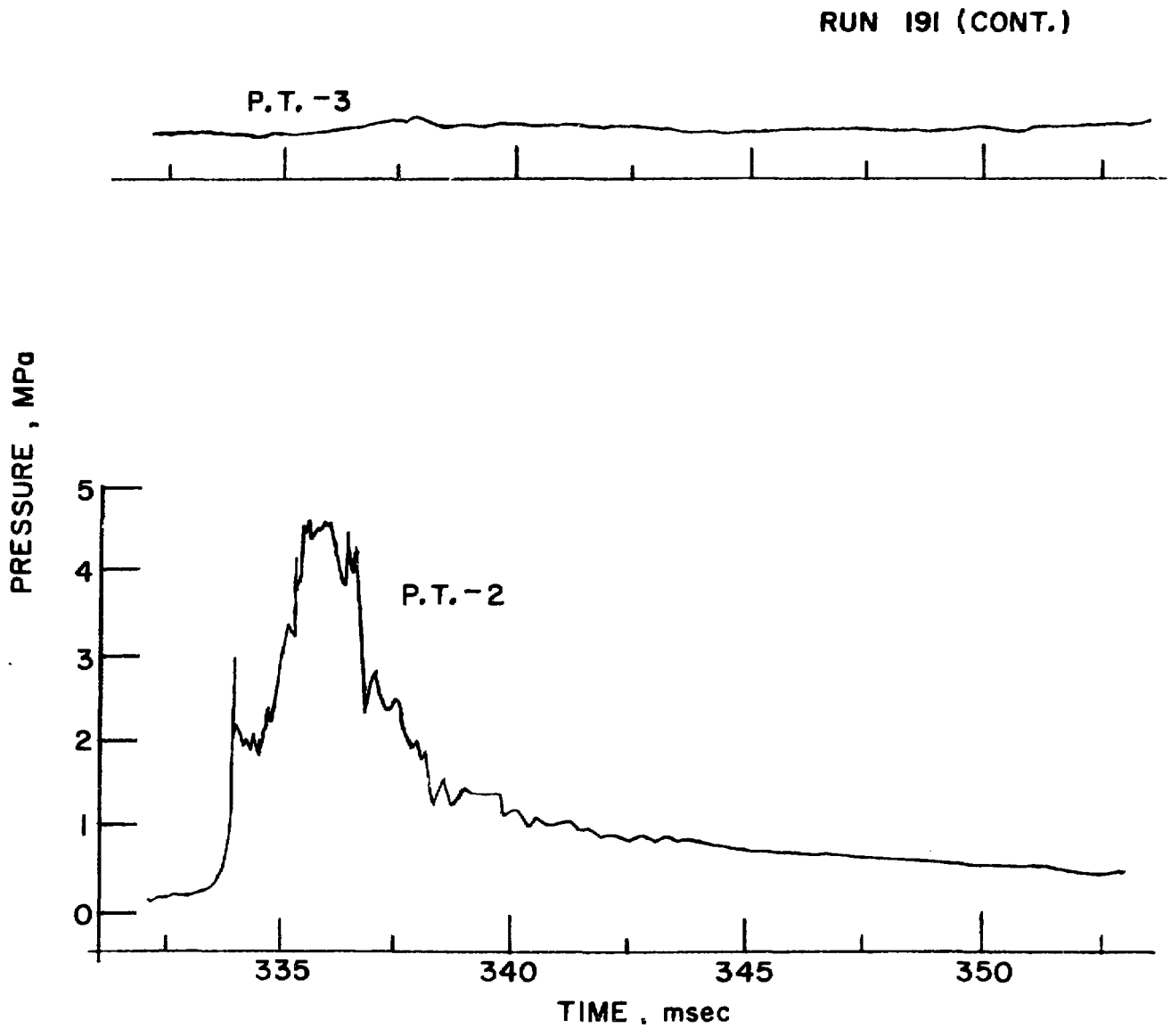

Fig. E.20 Pressure History of Run 191(contd.)

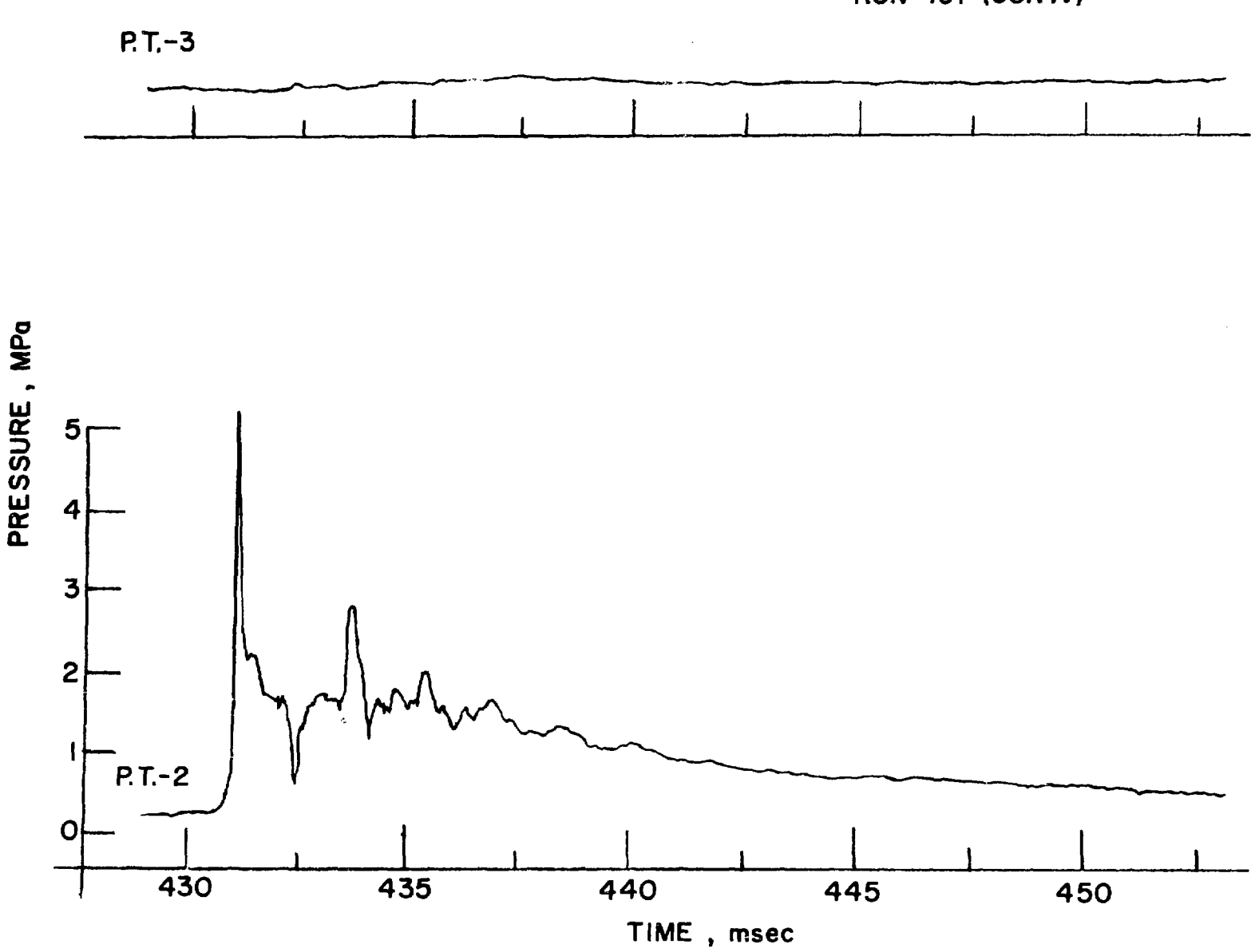

Fig. E.20 Pressure History of Run 191(contd.)

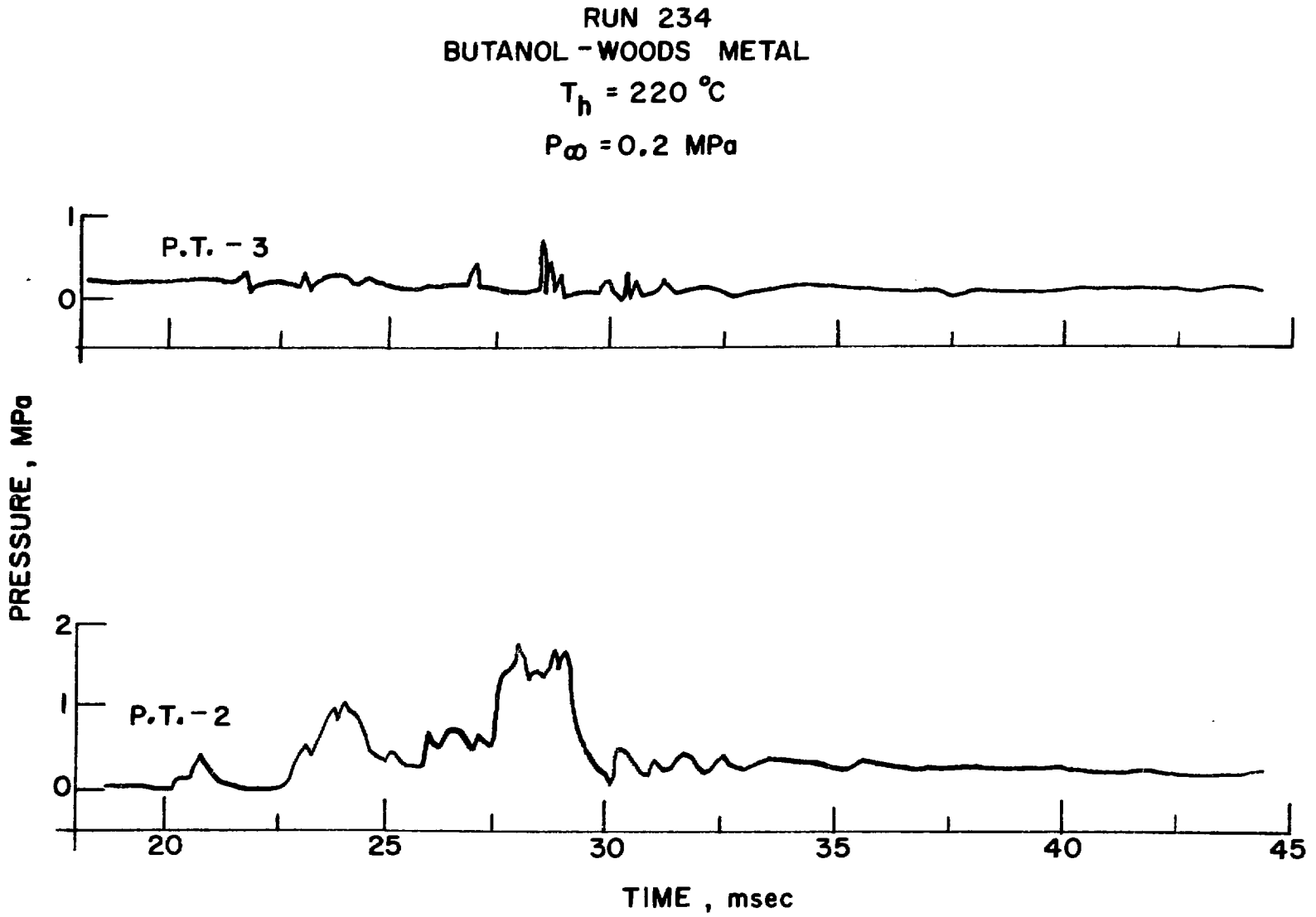

E.21. Pressure History of Run 234

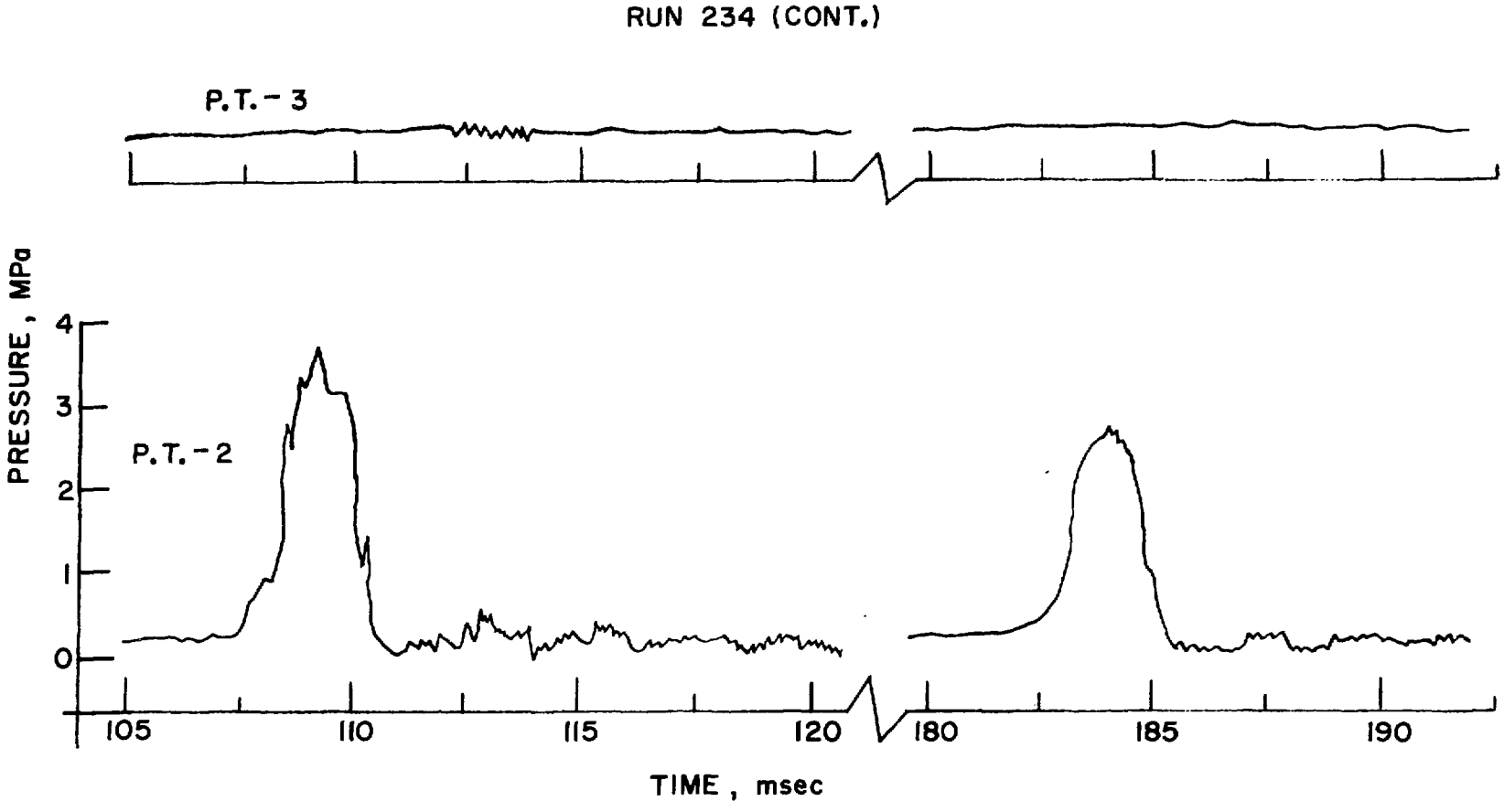

Fig. E.21 Pressure History of Run 234(contd.)

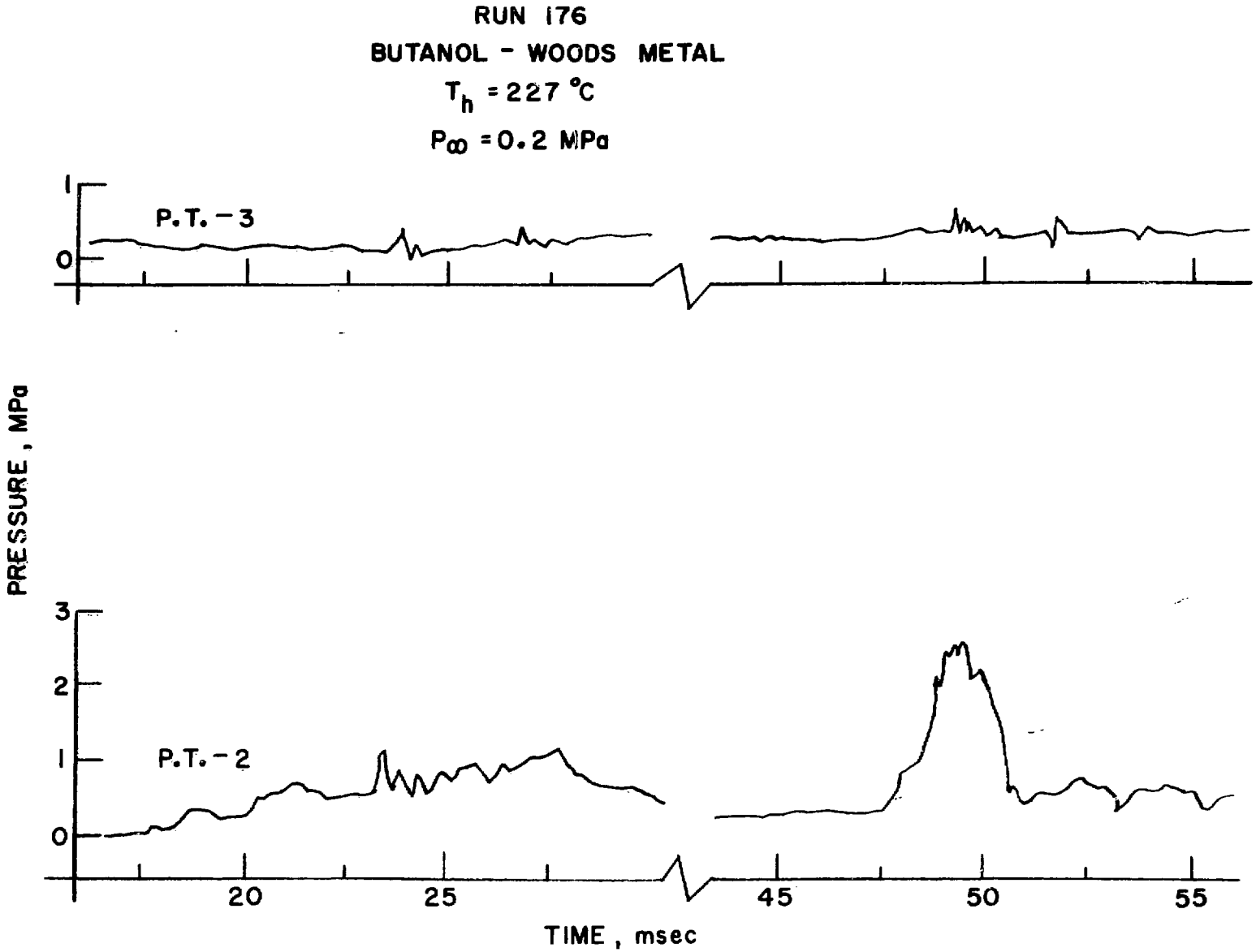

Fig. E.22. Pressure History of Run 176

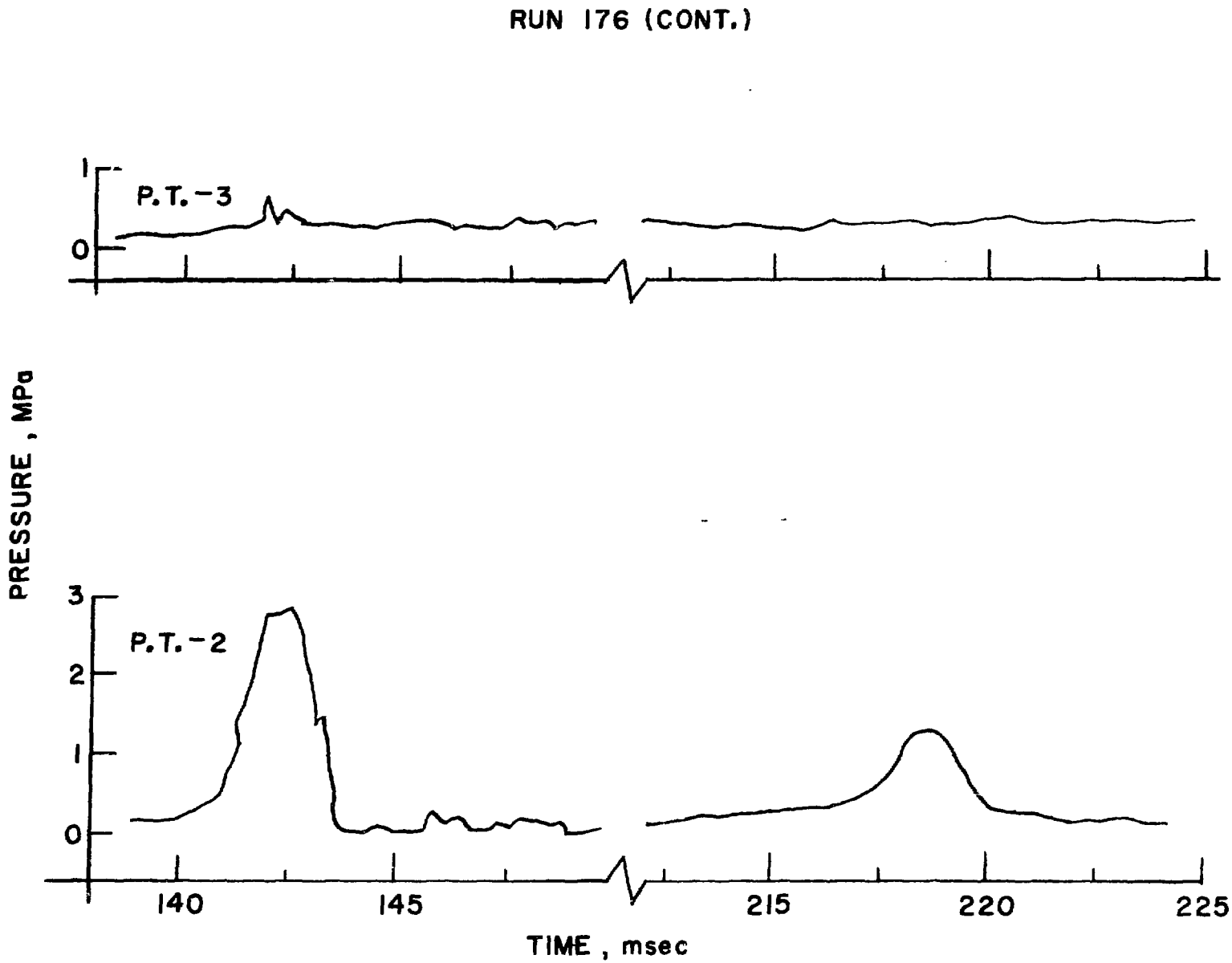

Fig. E.22. Pressure History of Run 176(contd.)

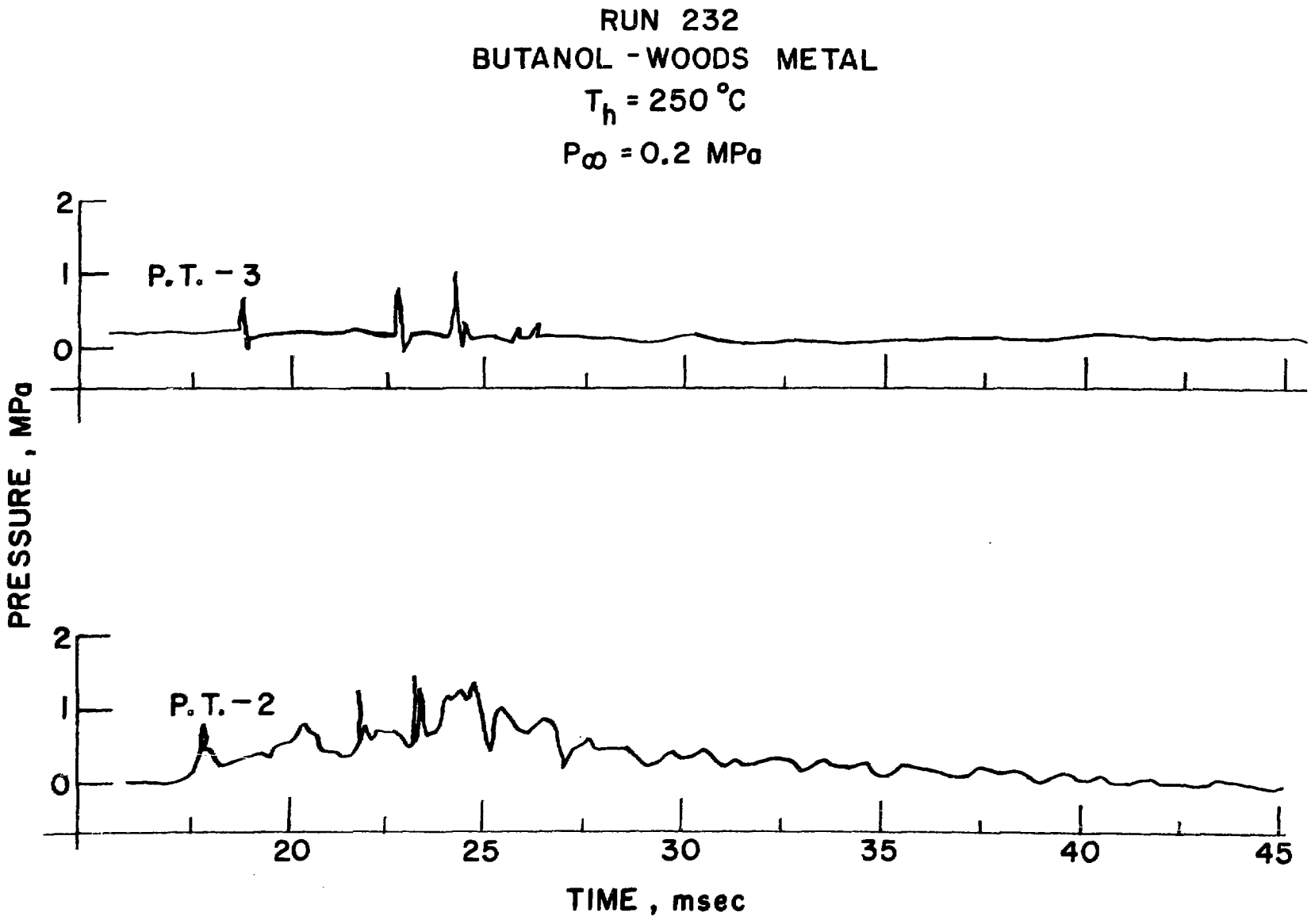

Fig. E.23. Pressure History of Run 232

RUN 232 (cont.)

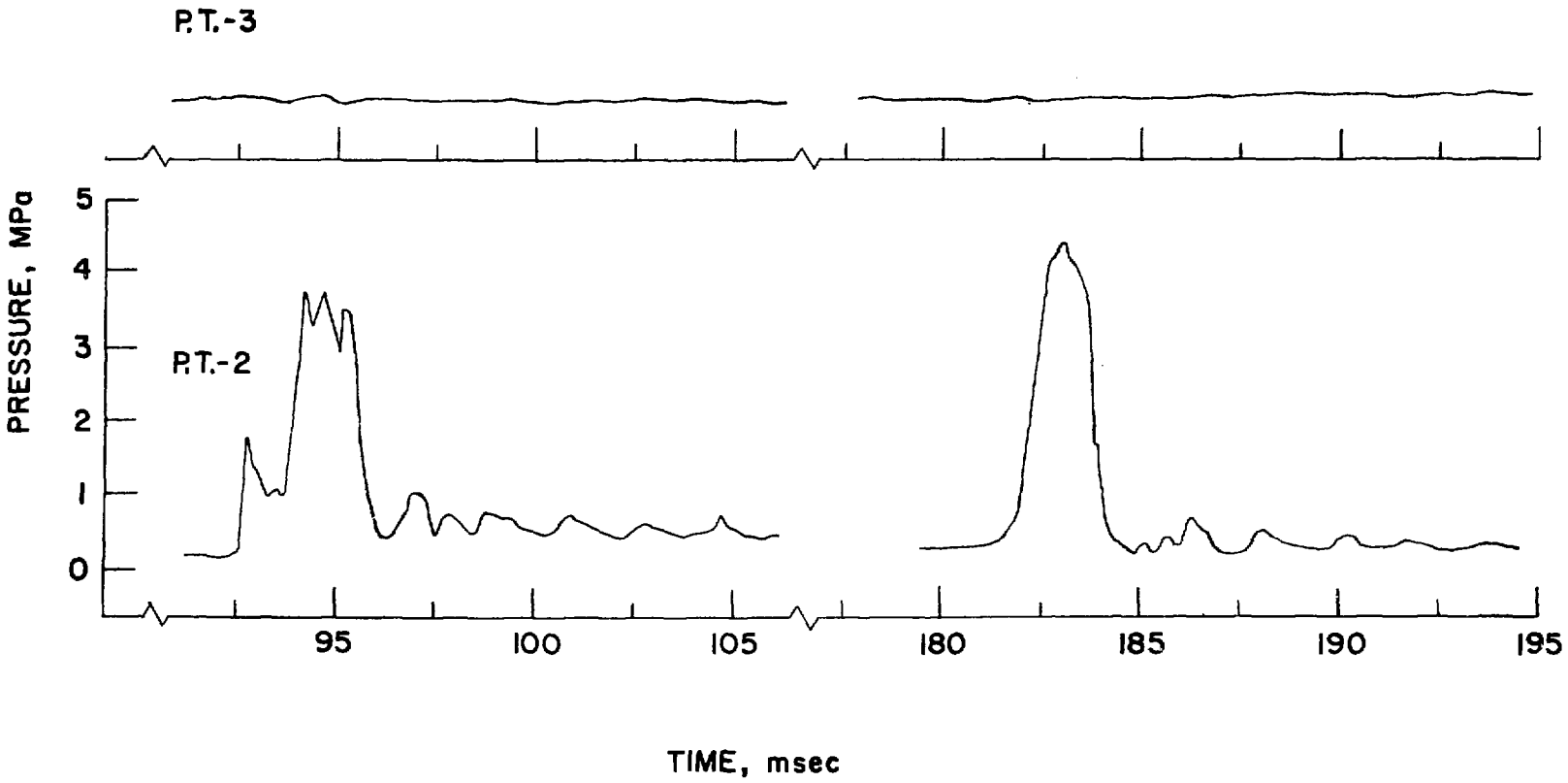

Fig. E.23. Pressure History of Run 232(contd.)

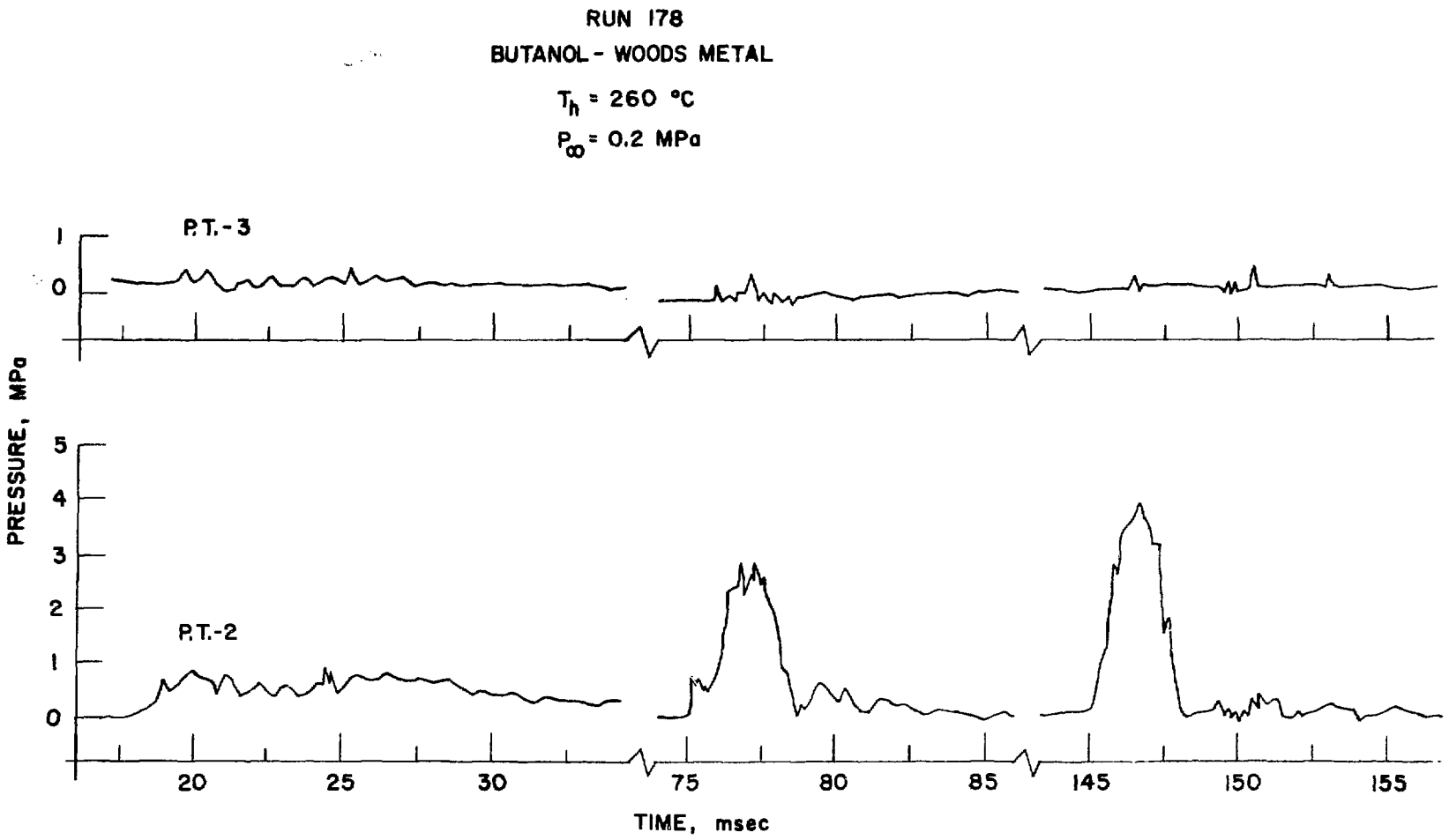

Fig. E.24. Pressure History of Run 178

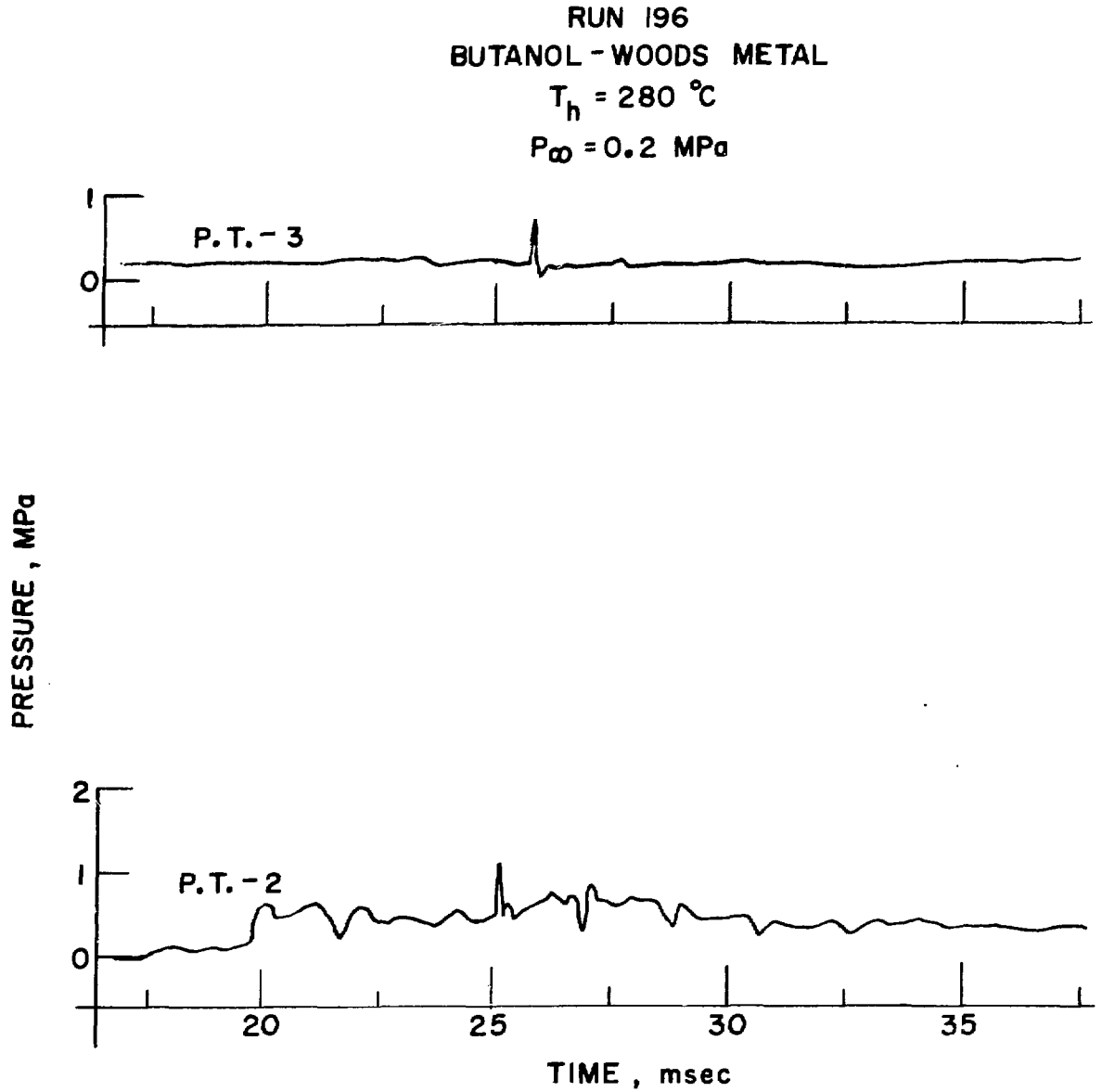

Fig. E.25. Pressure History of Run 196

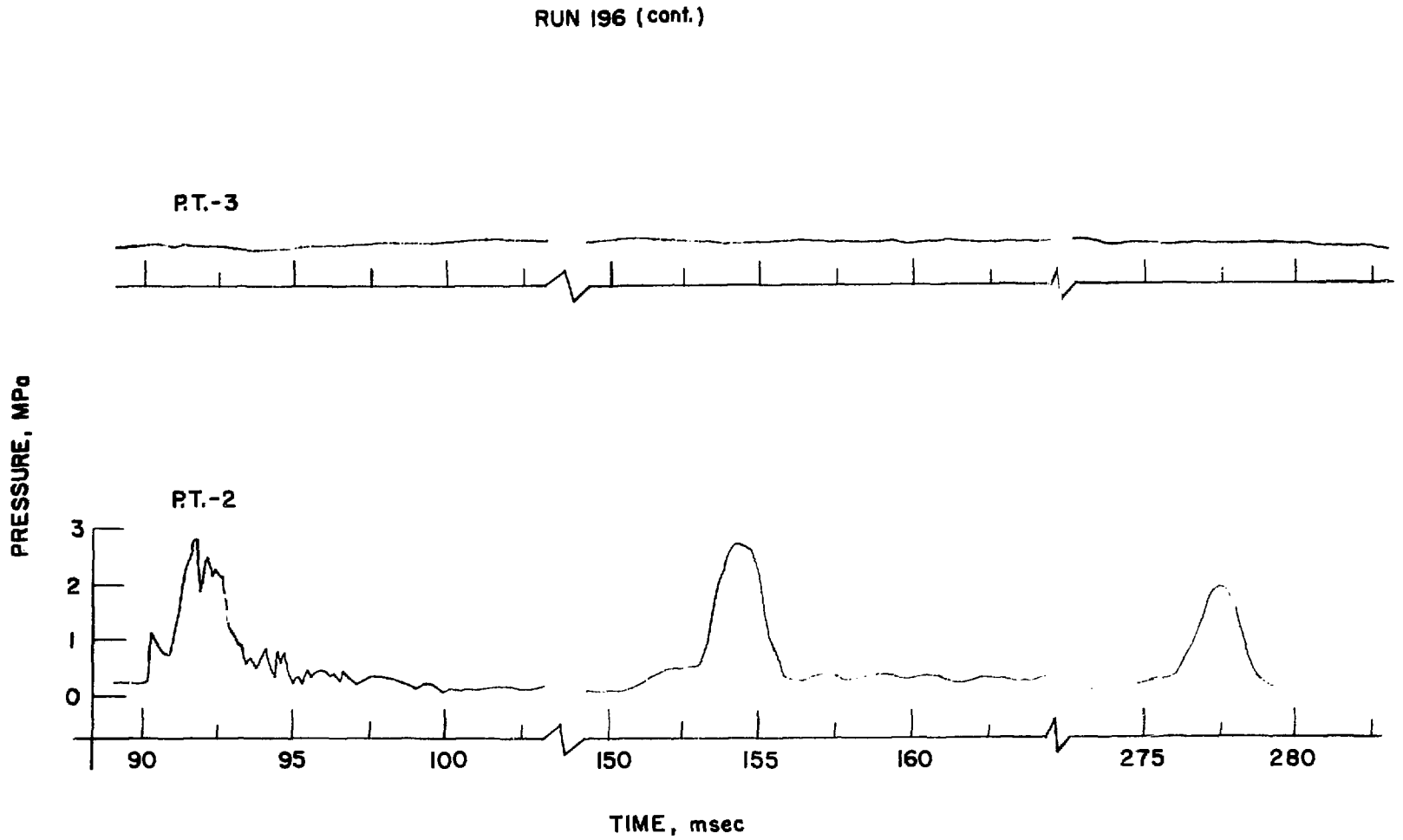

Fig. E.25. Pressure History of Run 196(contd.)

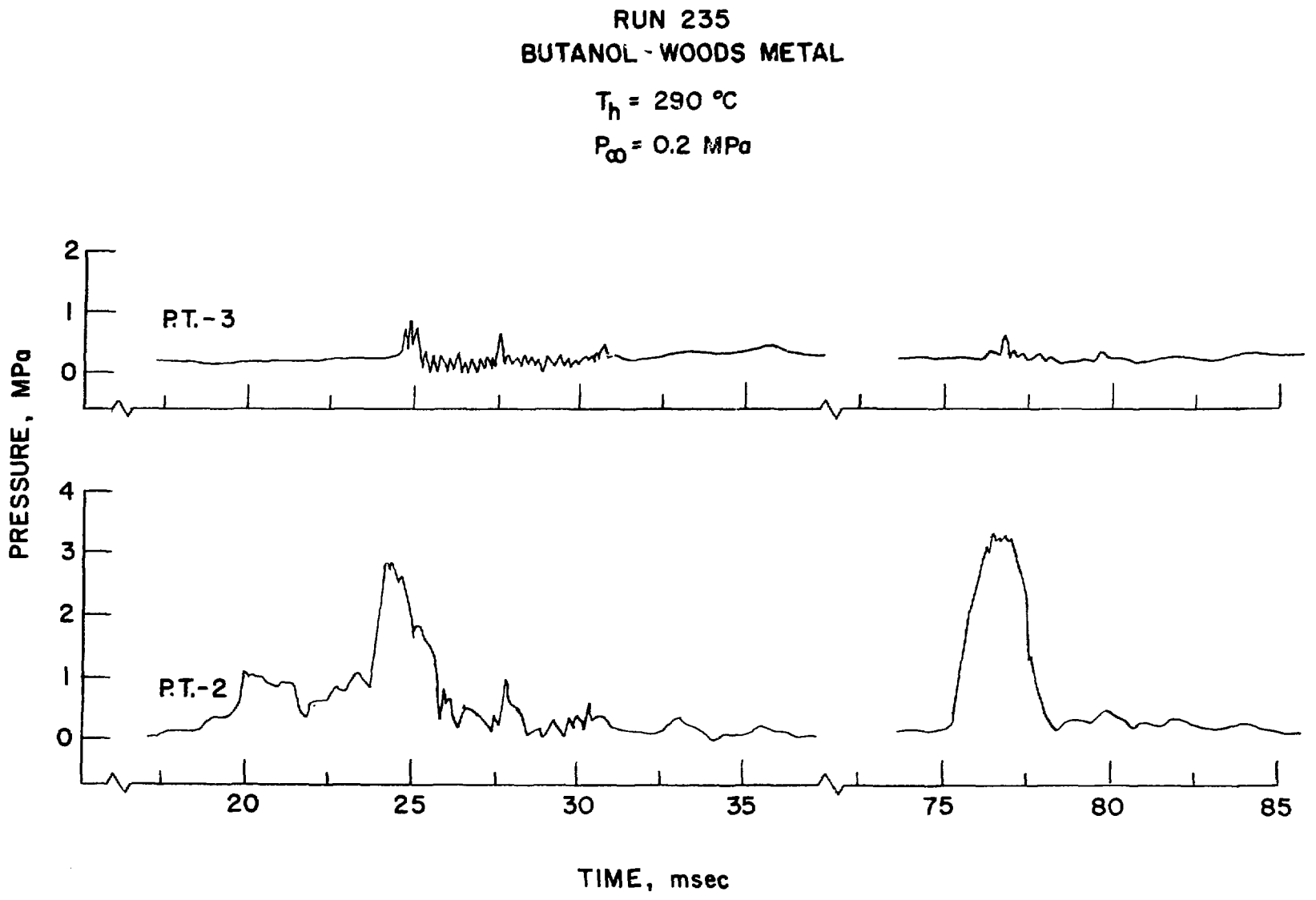

Fig. E.26. Pressure History of Run 235

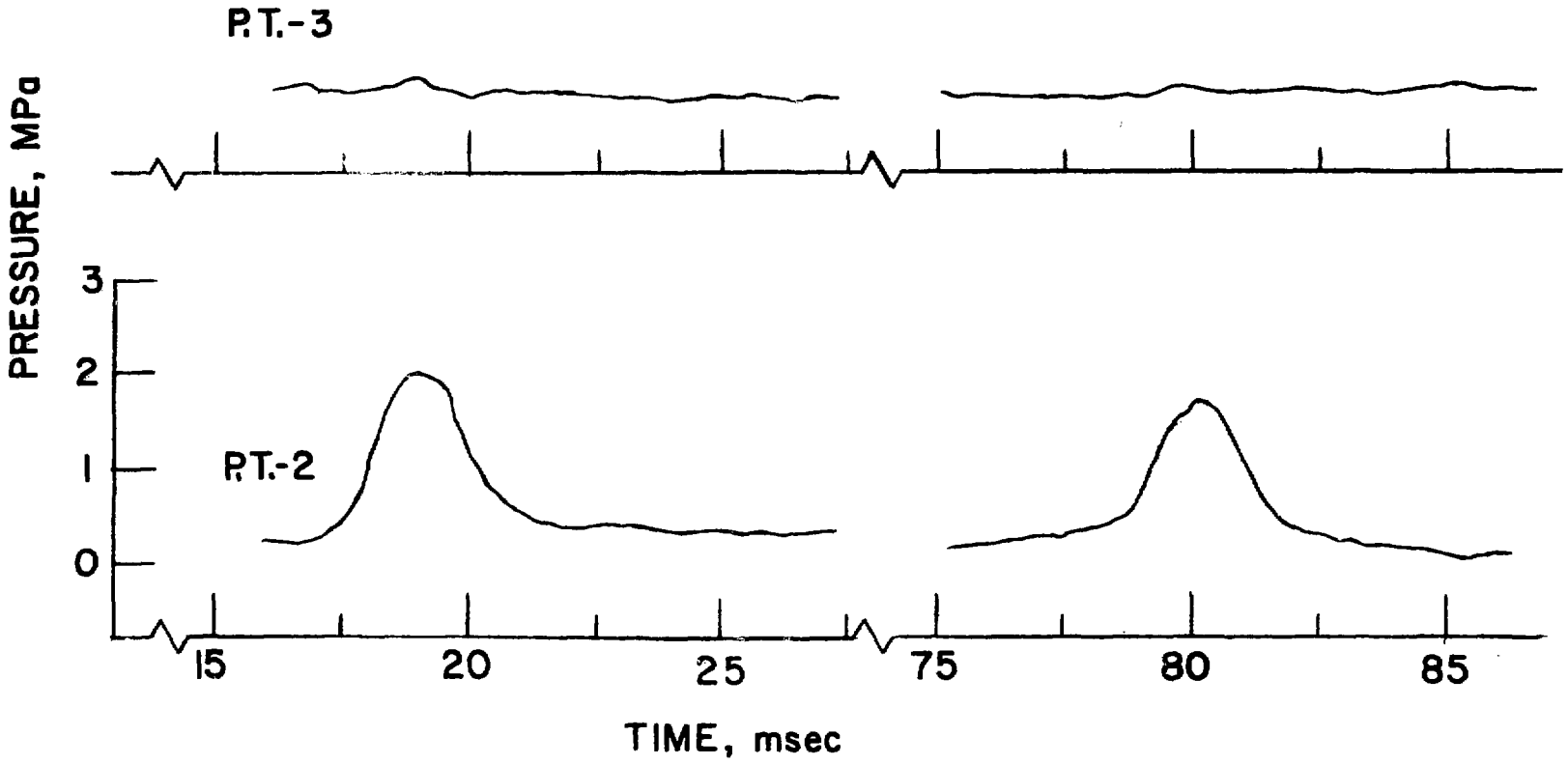

Fig. E.27. Pressure History of Run 182

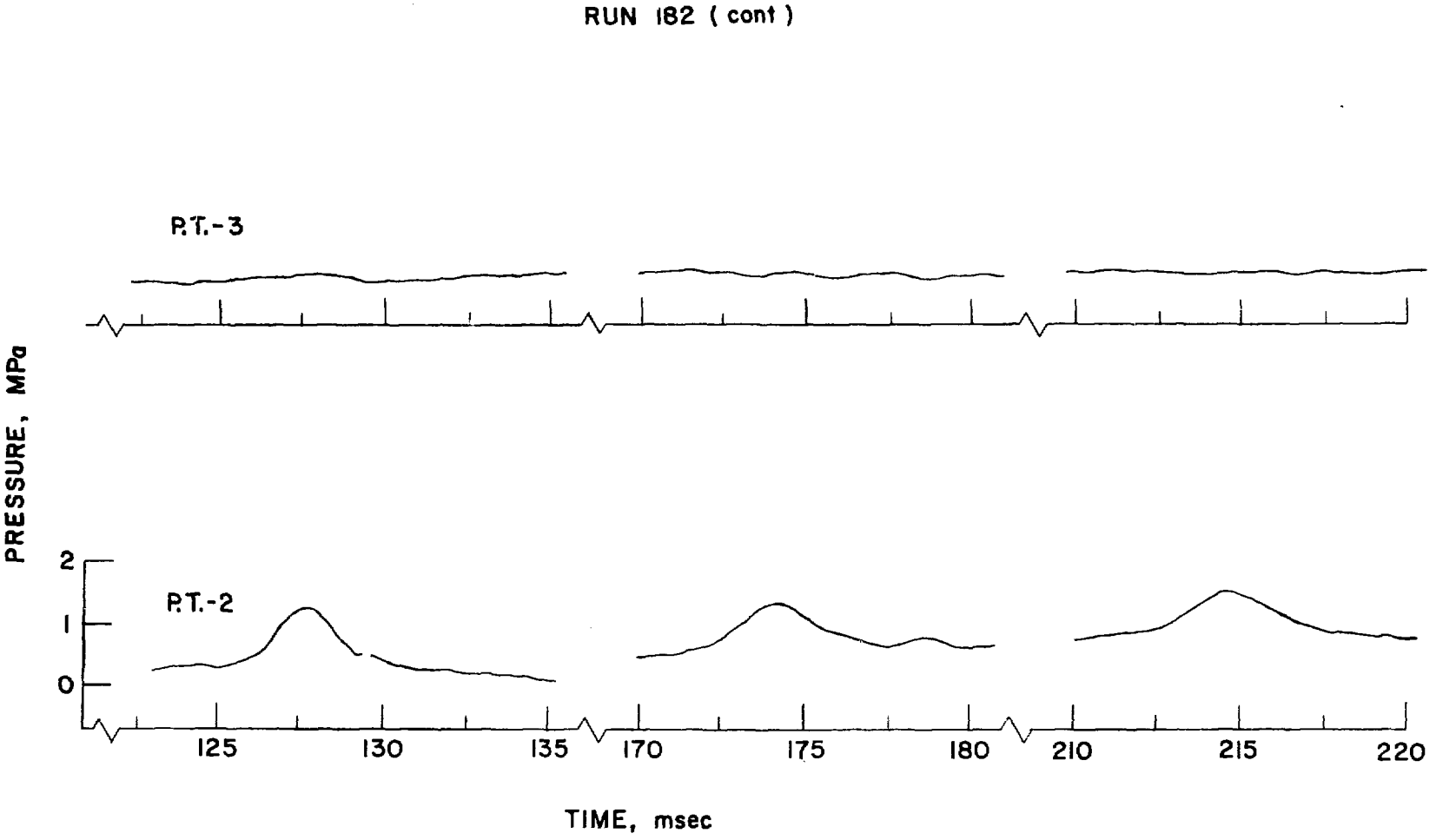

Fig. E.27. Pressure History of Run 182(contd.)

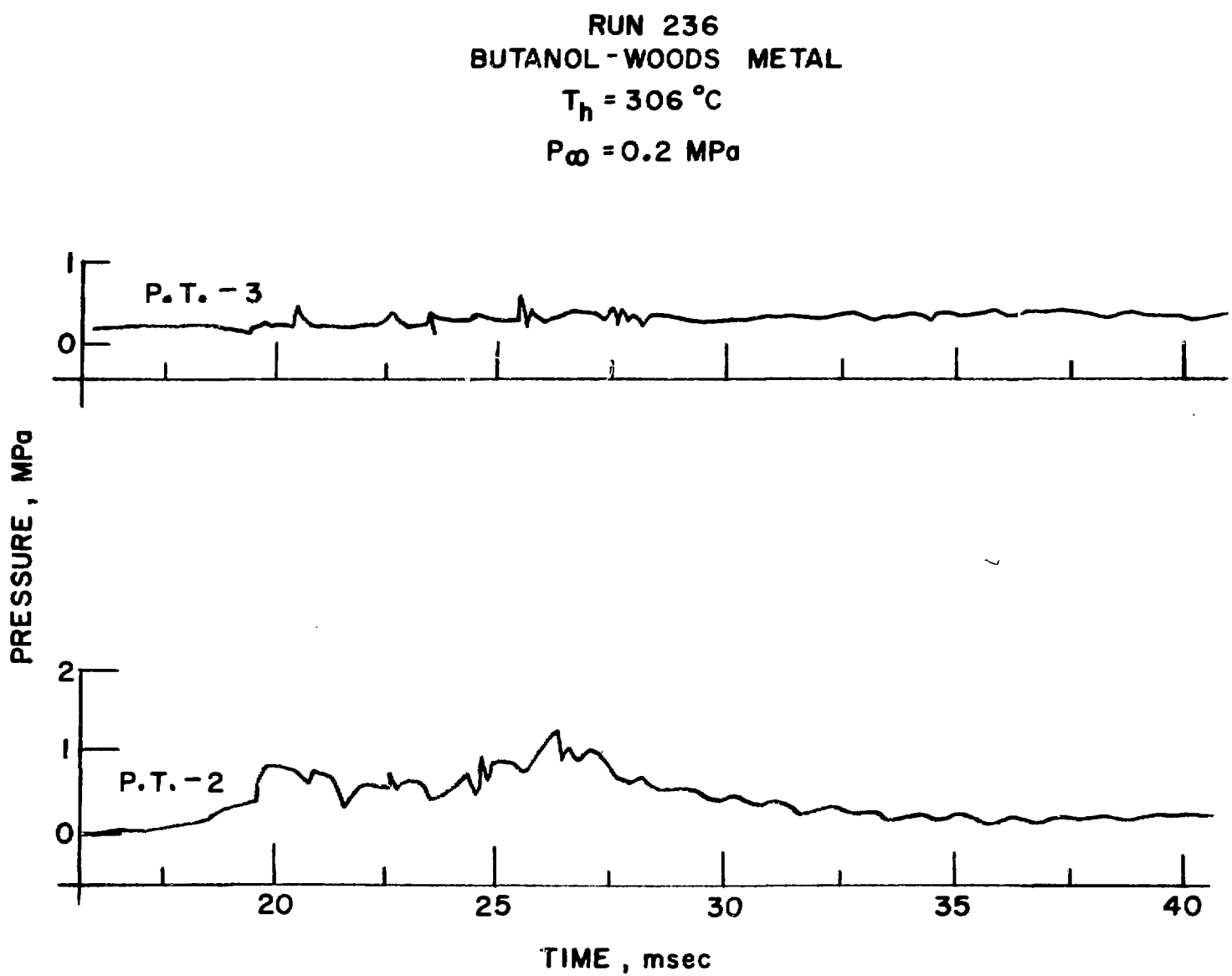

Fig. E.28. Pressure History of Run 236

RUN 236 (CONT.)

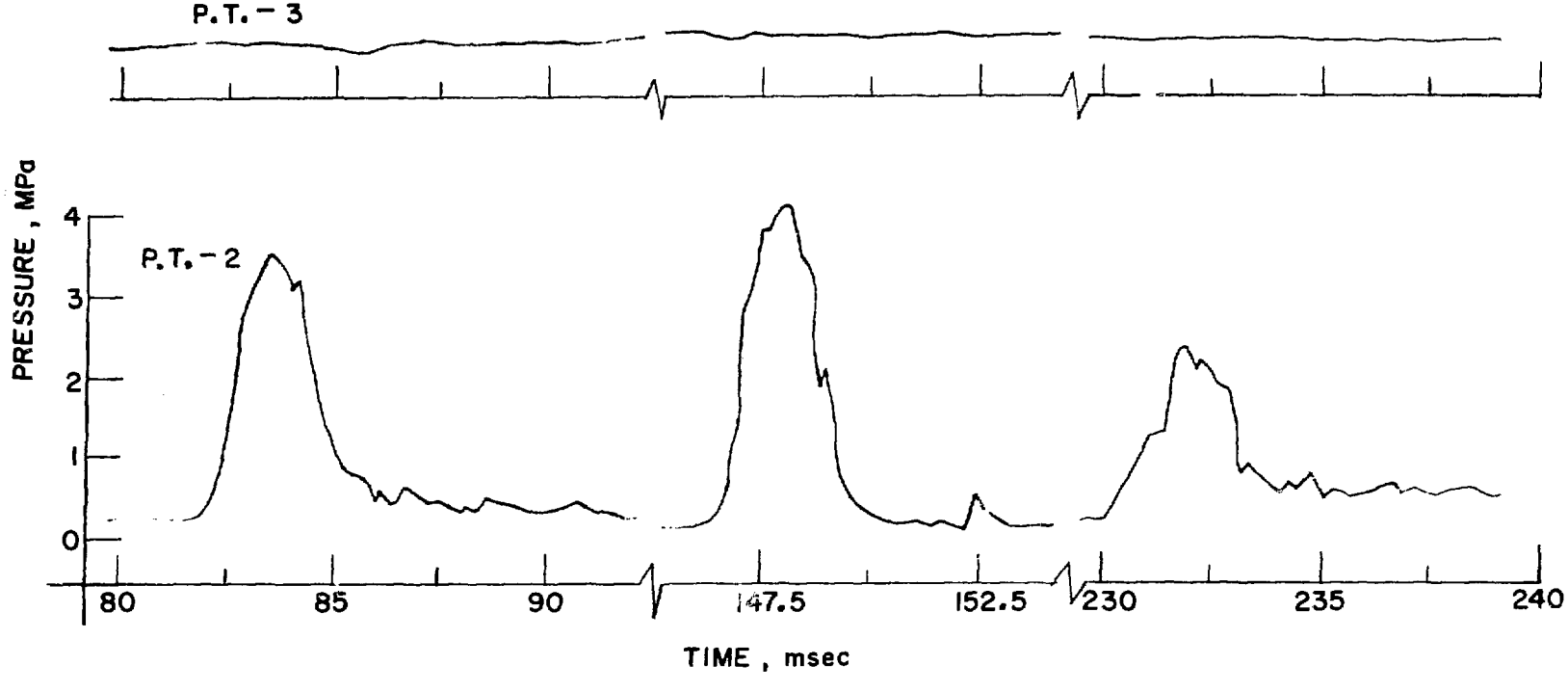

Fig. E.28. Pressure History of Run 236(contd.)

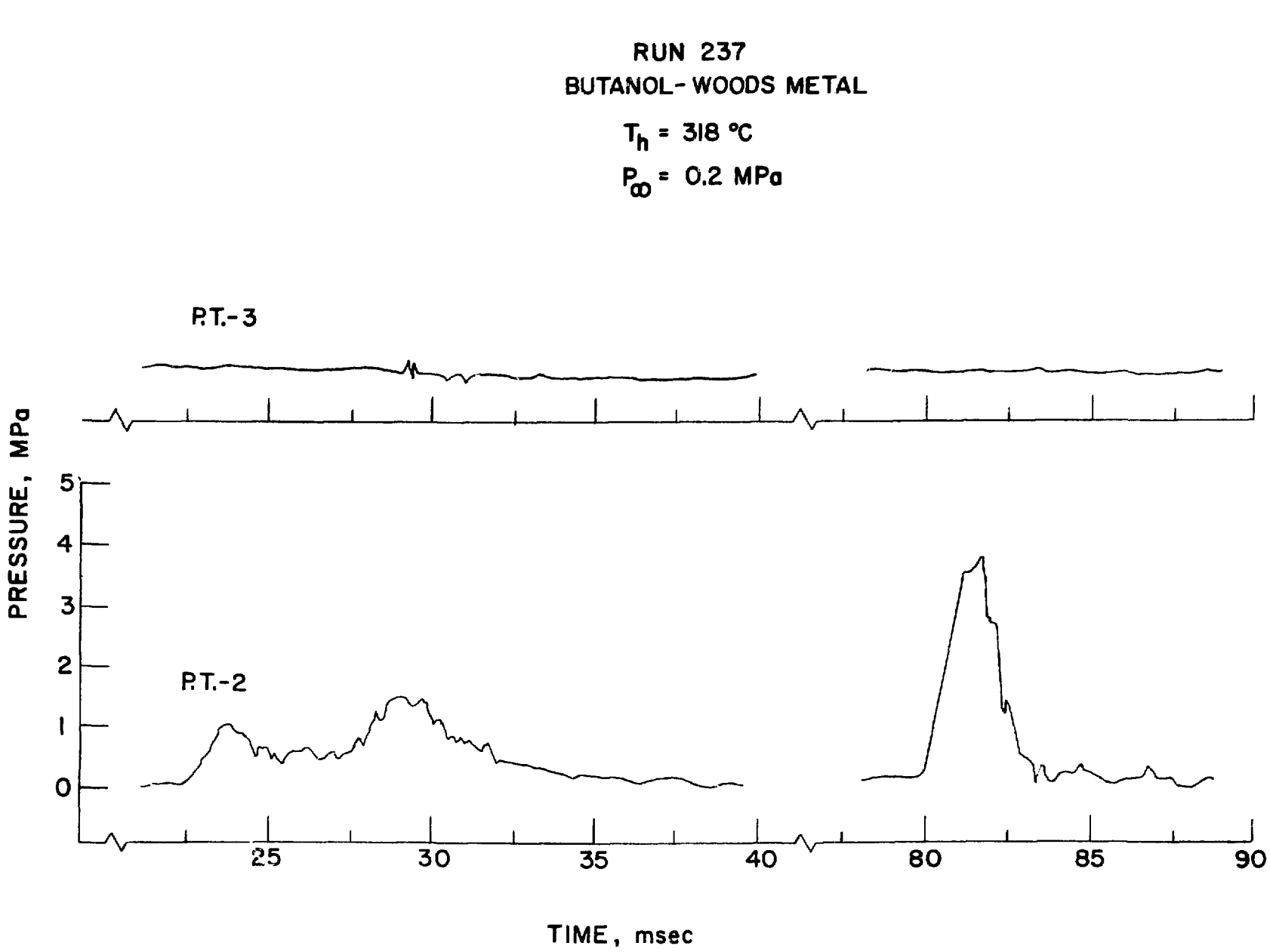

Fig. E.29. Pressure History of Run 237

RUN 237 (cont.)

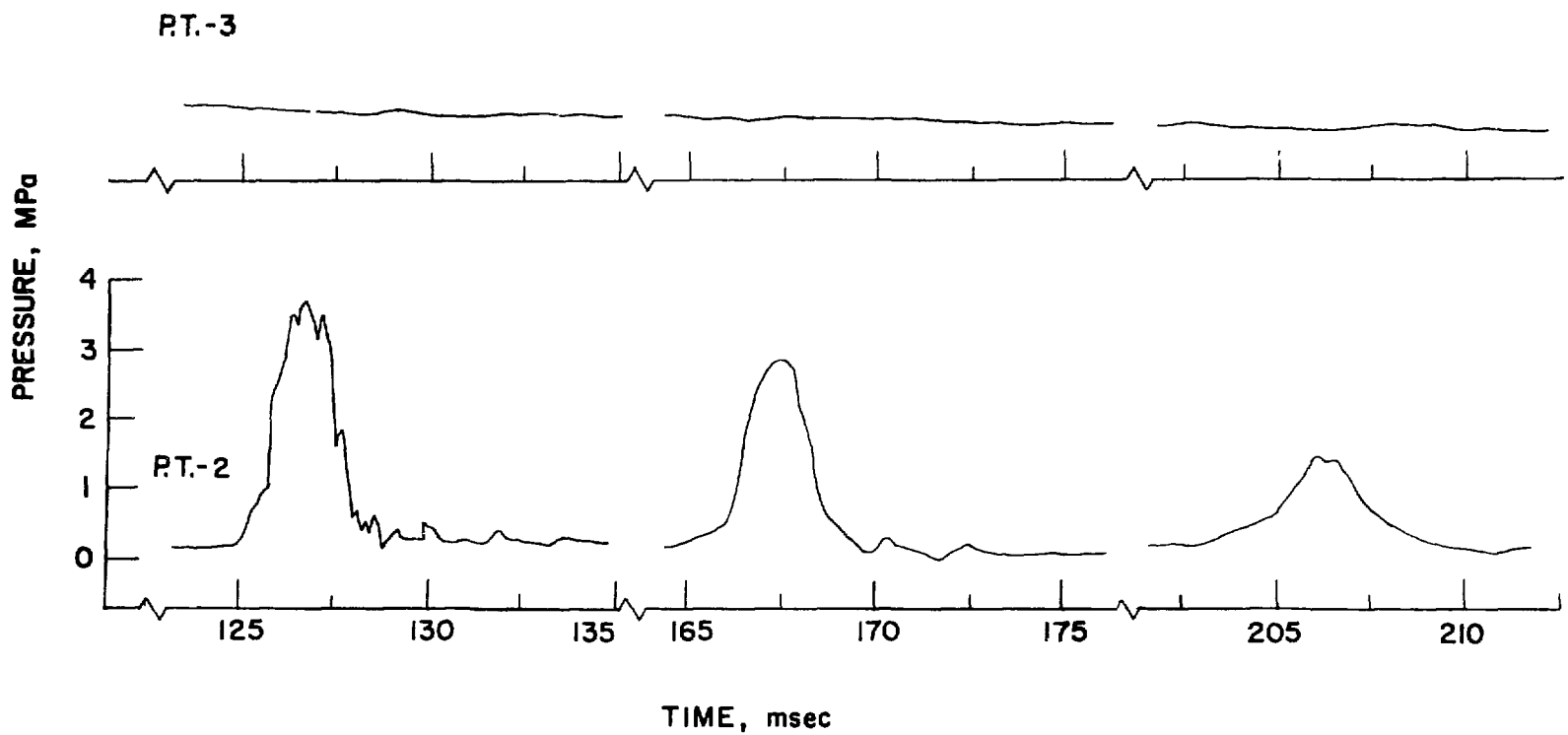

Fig. E.29. Pressure History of Run 237(contd.)

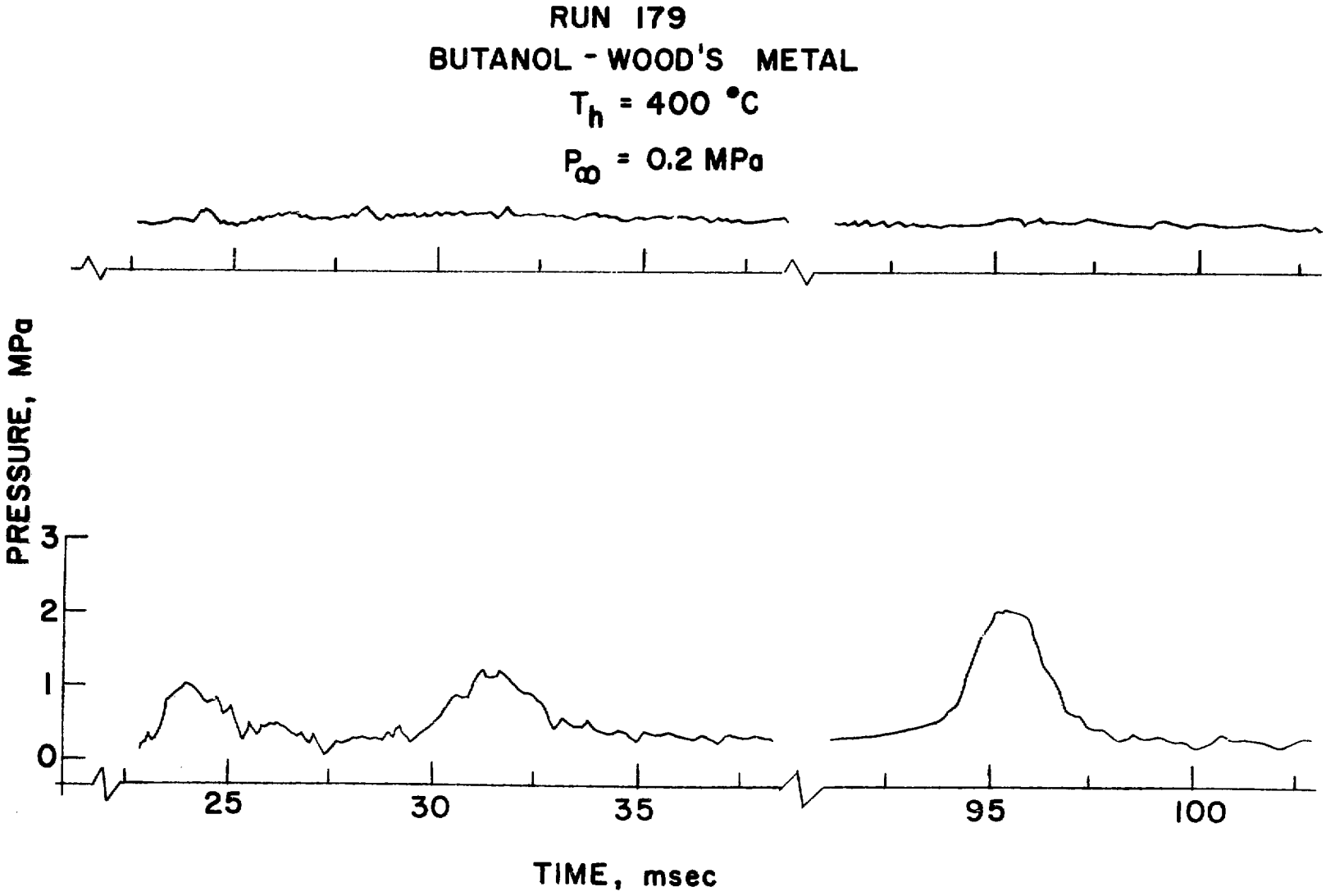

Fig. E.30. Pressure History of Run 179

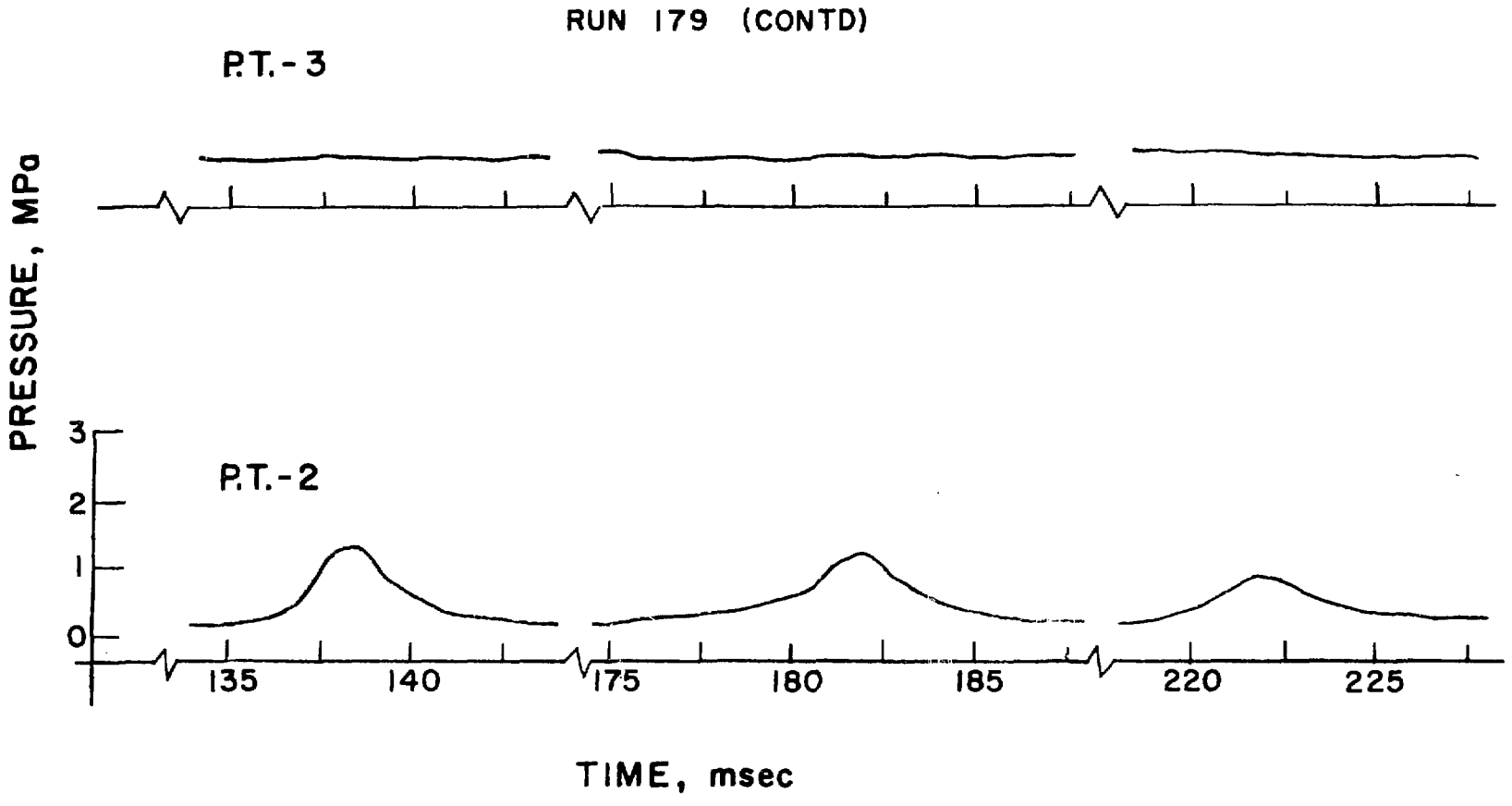

Fig. E.30. Pressure History of Run 179(contd.)

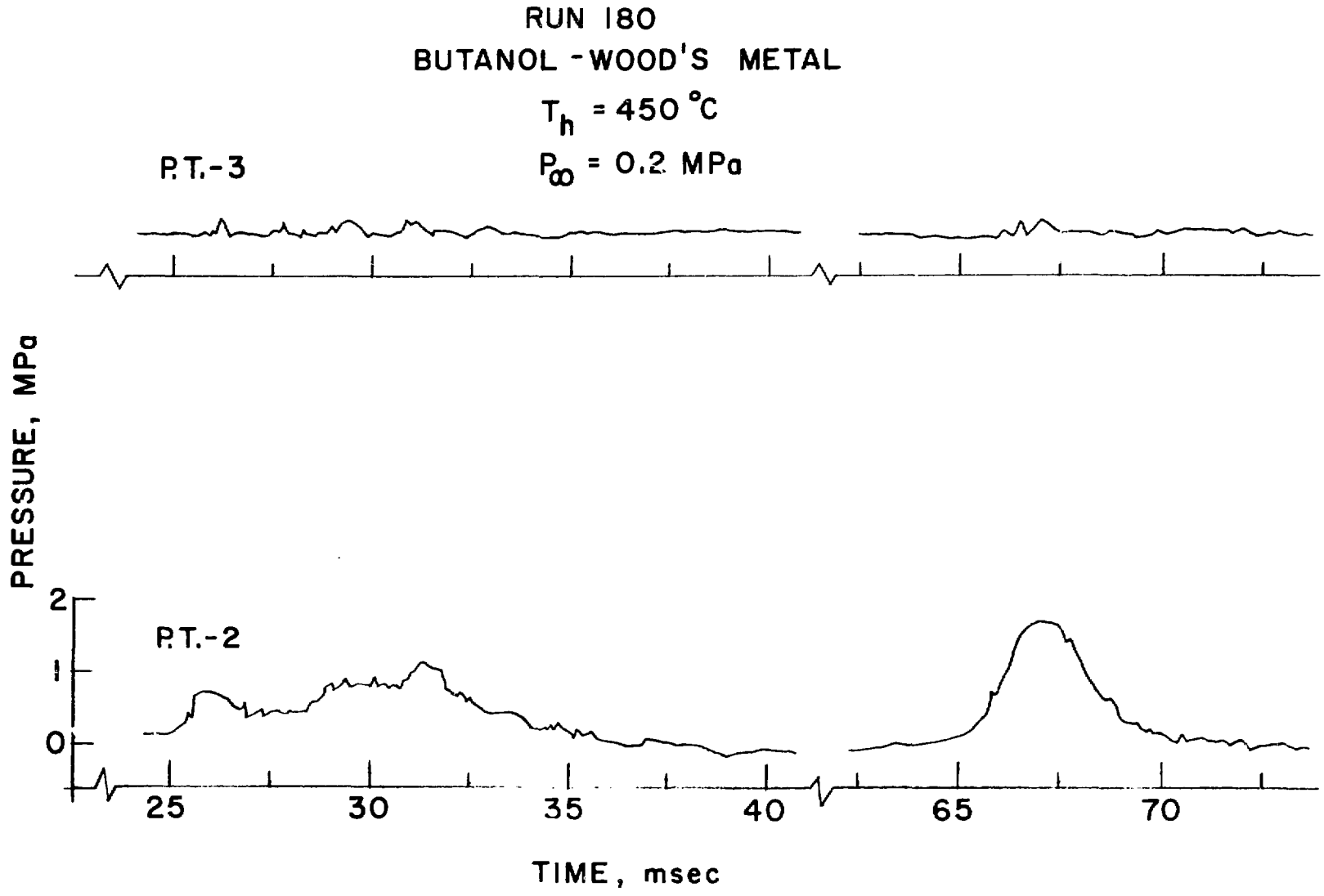

Fig. E.31. Pressure History of Run 180

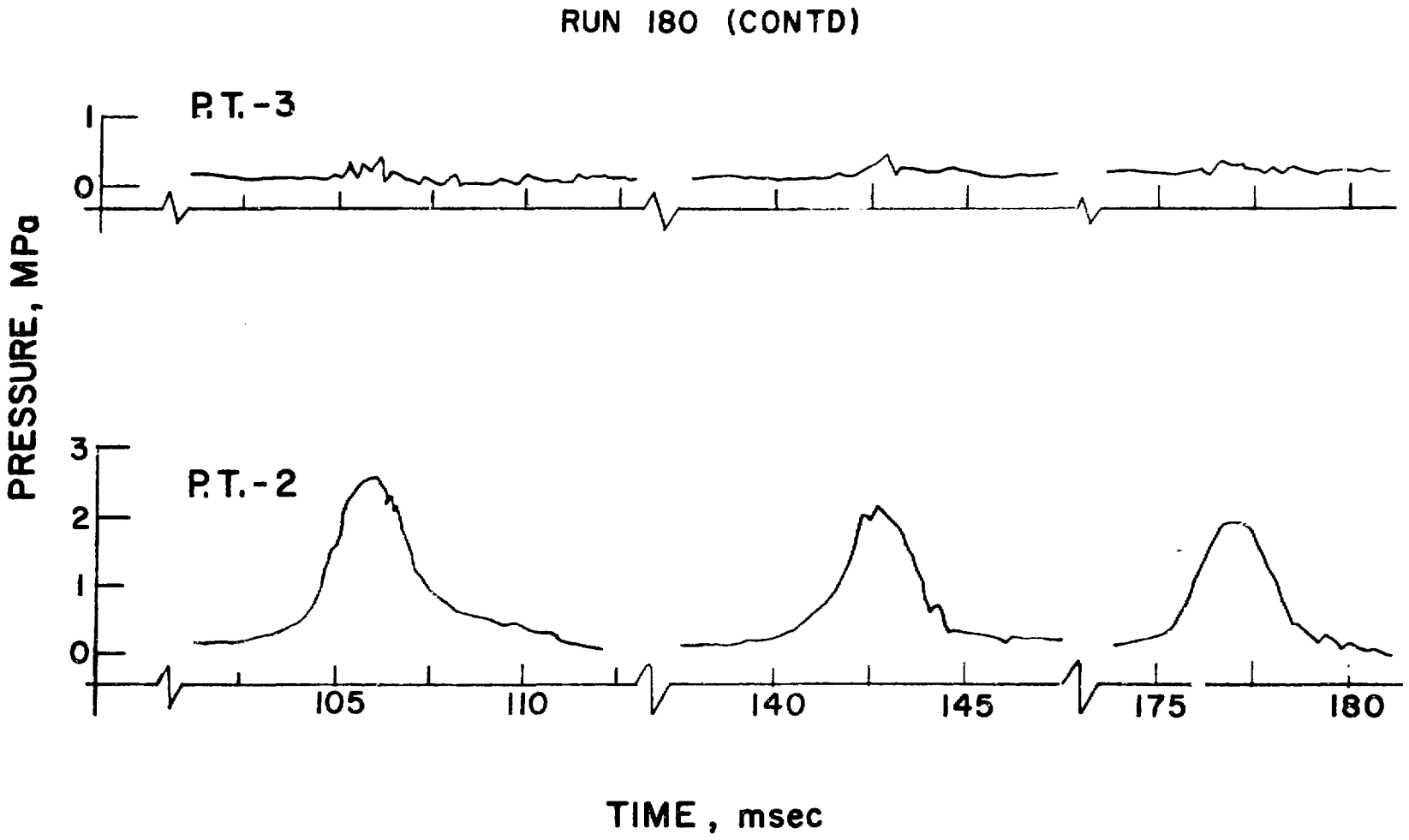

Fig. E.31. Pressure History of Run 180(contd.)

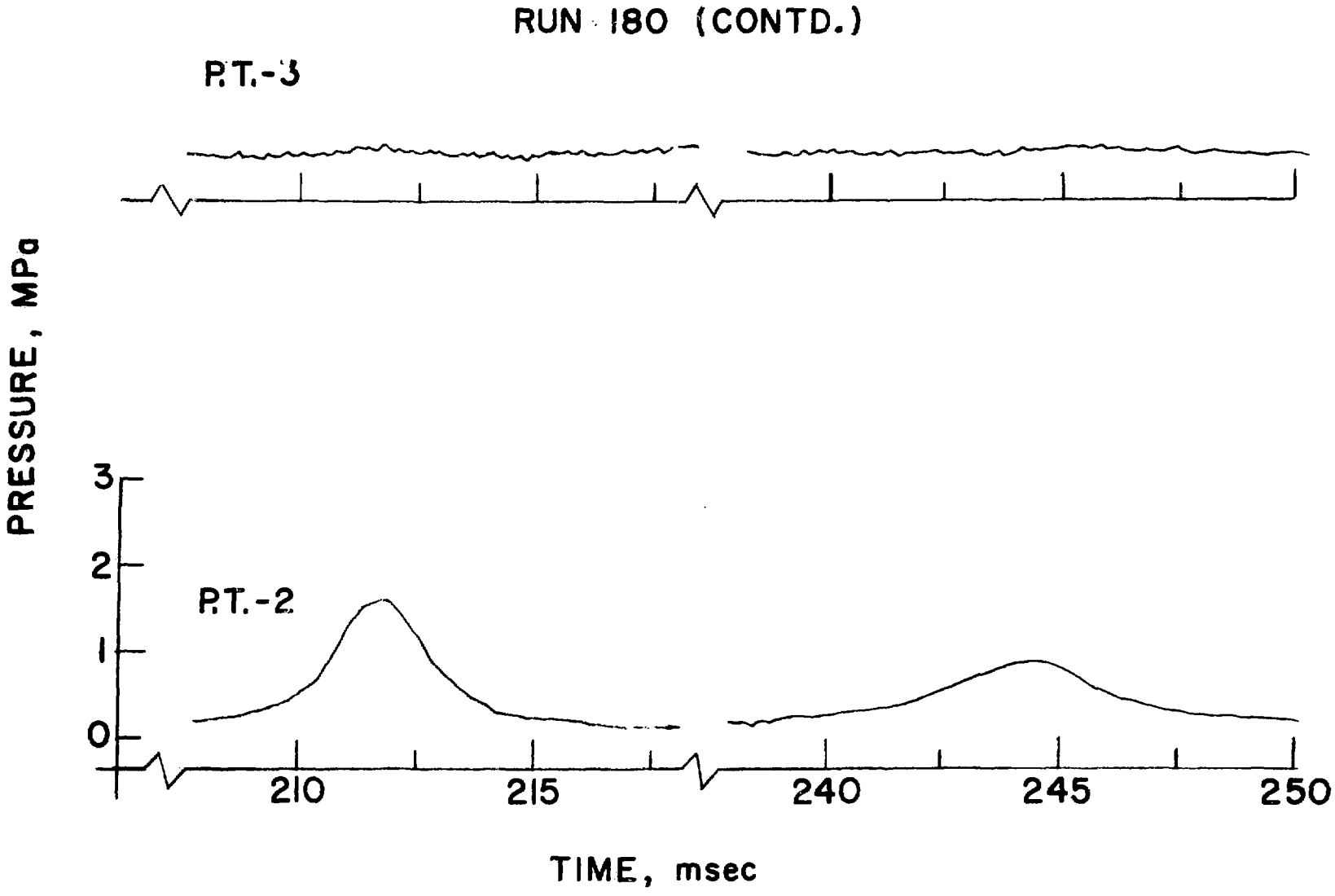

Fig. E.31. Pressure History of Run 180(contd.)

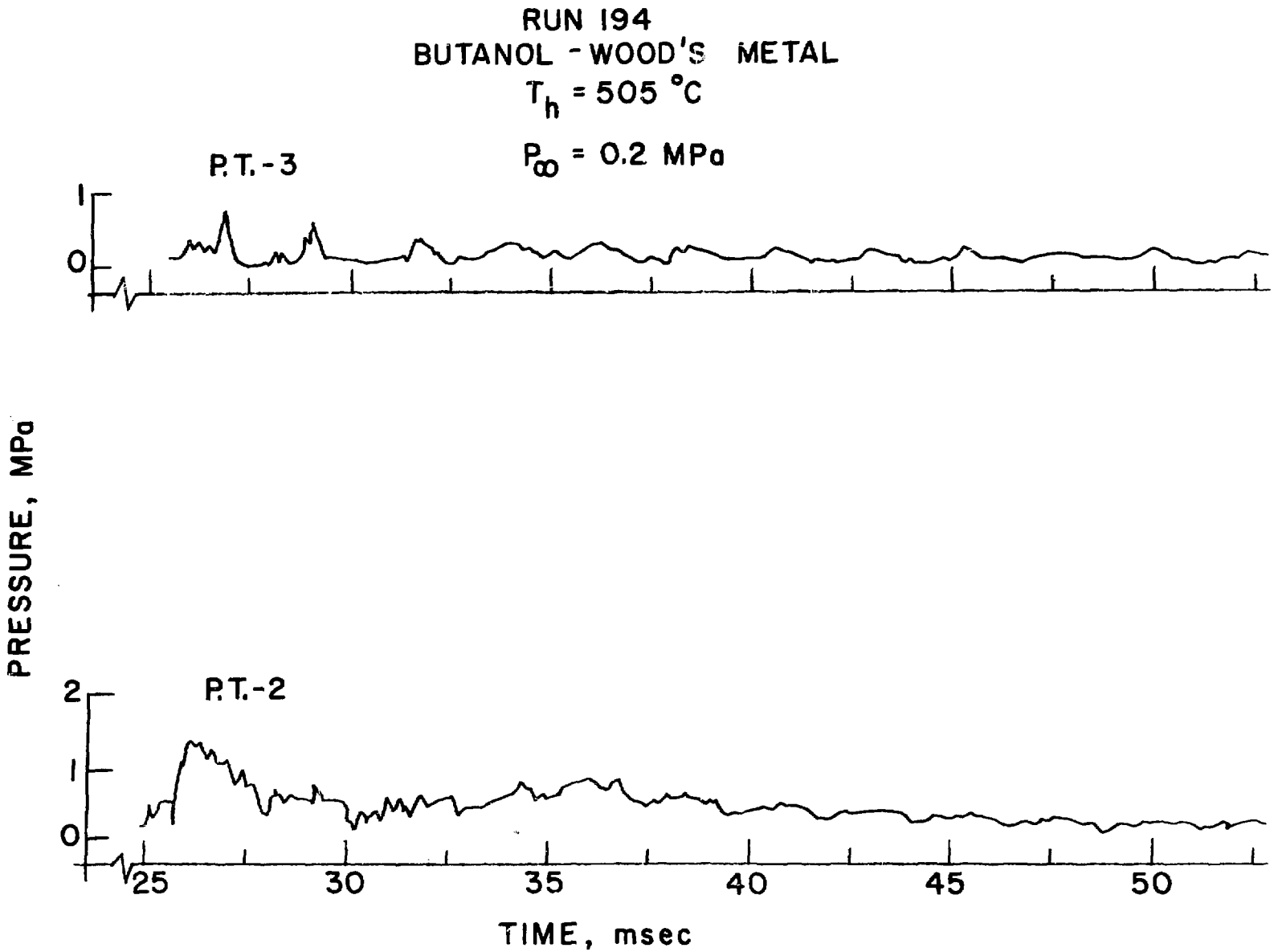

Fig. E.32. Pressure History of Run 194

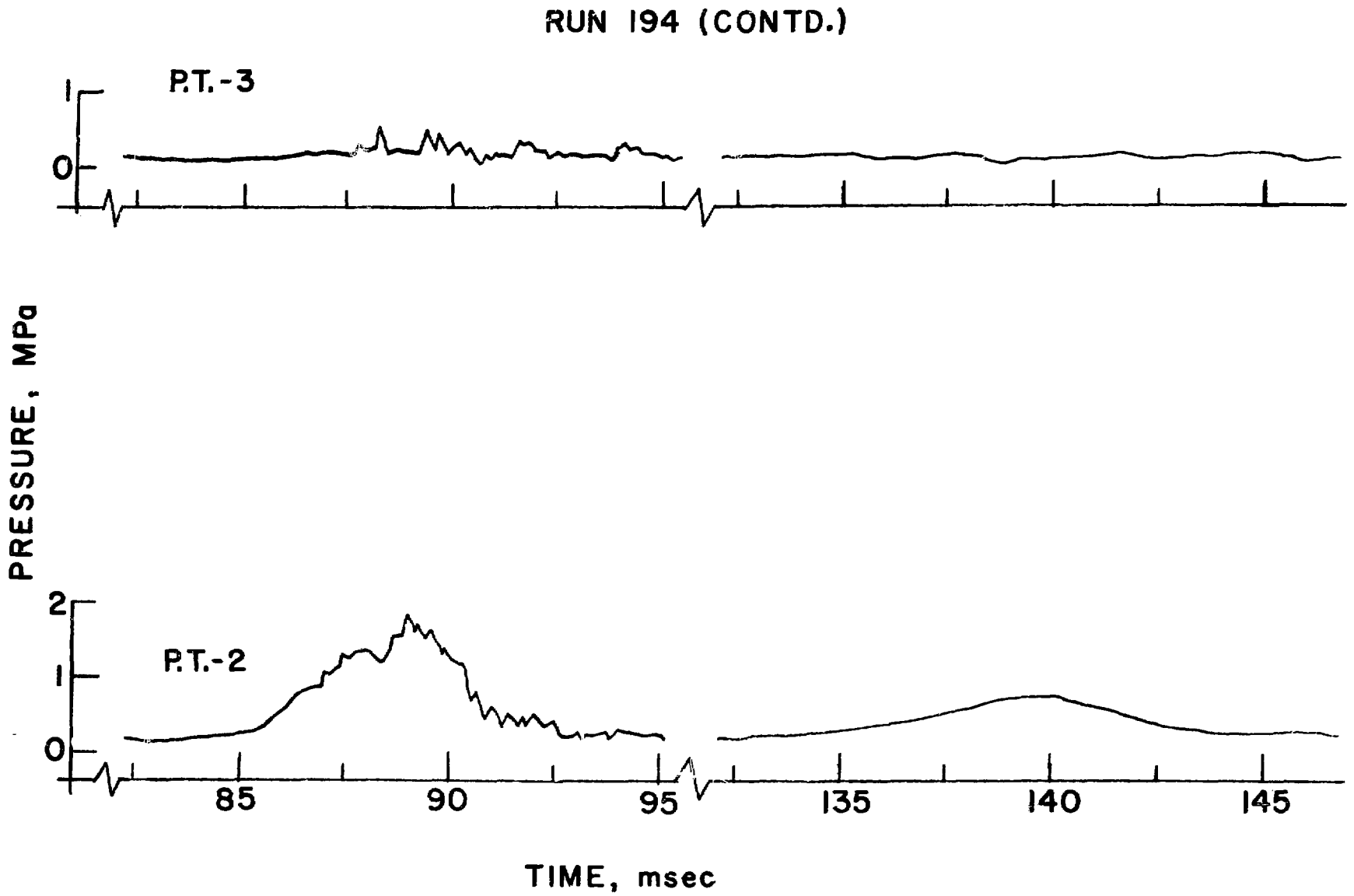

Fig. E.32. Pressure History of Run 194(contd.)

APPENDIX I

Experimental Results of Interactions at Elevated Pressures

Table F.1. Water-Wood's Metal Interactions at Elevated Pressures

Run	Hot Liquid Temperature T_h (°C)	ΔP MPa	t_{exp} msec	Time From First Impact Δt (msec)	Pulse Duration t_p (msec)	Maximum Pressure P_{max} (MPa)	$\frac{P_{max}}{P_i}$	Impulse I_{exp} KPa.sec	$\frac{I_{exp}}{I_{th}}$
239	125	1.60	9.37	0	4.50	7.59	0.39	23.52	0.73
				7.5	3.125	2.97	0.15	4.62	0.143
214	350	0.57	15.62	0	12.5	2.62	0.25	16.38	0.95
				72.5	10.0	2.93	0.28	10.97	0.64
215	350	1.67	8.75	0	6.25	6.76	0.35	21.10	0.673
				32.5	3.75	9.31	0.49	17.45	0.556
199	400	0.55	14.25	0	20.0	2.34	0.24	15.10	0.96
				71.25	15.0	2.69	0.28	12.07	0.767
				97.5	19.25	3.79	0.40	16.97	1.08
206	400	1.10	10.75	0	7.5	6.55	0.45	18.10	0.76
				35.0	9.37	3.97	0.27	9.91	0.42
207	400	1.50	9.0	0	11.25	6.97	0.38	26.55	0.89
208	450	0.55	13.0	0	20.87	2.24	0.26	11.63	0.811
				62.5	10.62	3.28	0.38	13.17	0.92
209	450	1.23	9.37	0	10.0	5.79	0.38	25.86	1.02
				27.5	15.0	3.45	0.22	10.67	0.42
210	450	1.73	8.75	0	7.12	9.17	0.48	23.10	0.74
211	550	0.65	13.75	0	20.75	3.79	0.41	18.21	1.2
				61.25	25.0	3.96	0.43	20.14	1.32
213	550	0.62	9.0	0	8.12	2.76	0.41	12.61	1.13
				35.0	10.0	3.45	0.51	13.79	1.23
				65.0	12.5	2.93	0.43	9.17	0.82
212	550	1.79	8.75	0	16.25	7.17	0.38	33.93	1.08
				33.12	11.25	8.00	0.42	32.3	0.74

TABLE F2. Butanol-Wood's Metal Interactions at Elevated Pressures

Run	Hot Liquid Temperature T_h (°C)	ΔP MPa	t_{exp} msec	Time From First Impact Δt (msec)	Pulse Duration t_p (msec)	Maximum Pressure P_{max} (MPa)	$\frac{P_{max}}{P_i}$	Impulse I_{exp} KPa.sec	$\frac{I_{exp}}{I_{th}}$
230	110	0.69	11.87	0	5.62	4.31	0.69	13.38	0.82
				12.25	3.75	2.76	0.44	5.17	0.32
				19.87	3.12	2.24	0.36	3.52	0.21
				25.5	3.75	1.93	0.31	3.62	0.22
				30.6	4.12	1.72	0.27	3.56	0.22
229	230	0.55	11.62	0	6.00	4.41	0.90	14.07	1.10
				14.37	2.50	2.48	0.51	3.79	0.30
				24.37	3.50	1.79	0.36	3.17	0.25
				32.5	7.50	1.03	0.21	3.86	0.30
231	260	0.55	13.25	0	6.87	3.96	0.71	10.34	0.71
				48.5	8.50	2.14	0.38	4.83	0.33
184	300	0.62	11.25	0	6.25	3.76	0.52	10.76	0.77
				22.5	2.50	3.07	0.39	2.59	0.19

TABLE F3. Water-Molten Salt Interactions at Elevated Pressures

Run	Hot Liquid Temperature T_h (°C)	ΔP MPa	t_{exp} msec	Time From First Impact Δt (msec)	Pulse Duration t_p (msec)	Maximum Pressure P_{max} (MPa)	$\frac{P_{max}}{P_i}$	Impulse I_{exp} KPa.sec	$\frac{I_{exp}}{I_{th}}$
221	460	0.67	18.5	0	25.0	3.45	0.27	20.83	0.91
				38.75	57.5	2.07	0.16	59.48	2.59
223	500	0.57	20.0	0	16.5	2.76	0.26	22.76	1.22
				57.5	42.5	1.72	0.16	36.62	1.96
222	536	0.60	12.5	0	26.87	1.41	0.21	14.65	1.21
				57.5	52.5	0.83	0.12	12.90	1.07
225	600	0.48	17.5	0	22.5	1.93	0.21	21.72	1.29
227	600	1.35	10.0	0	12.5	5.35	0.33	34.48	1.14
				34.5	37.5	3.10	0.18	58.19	1.92

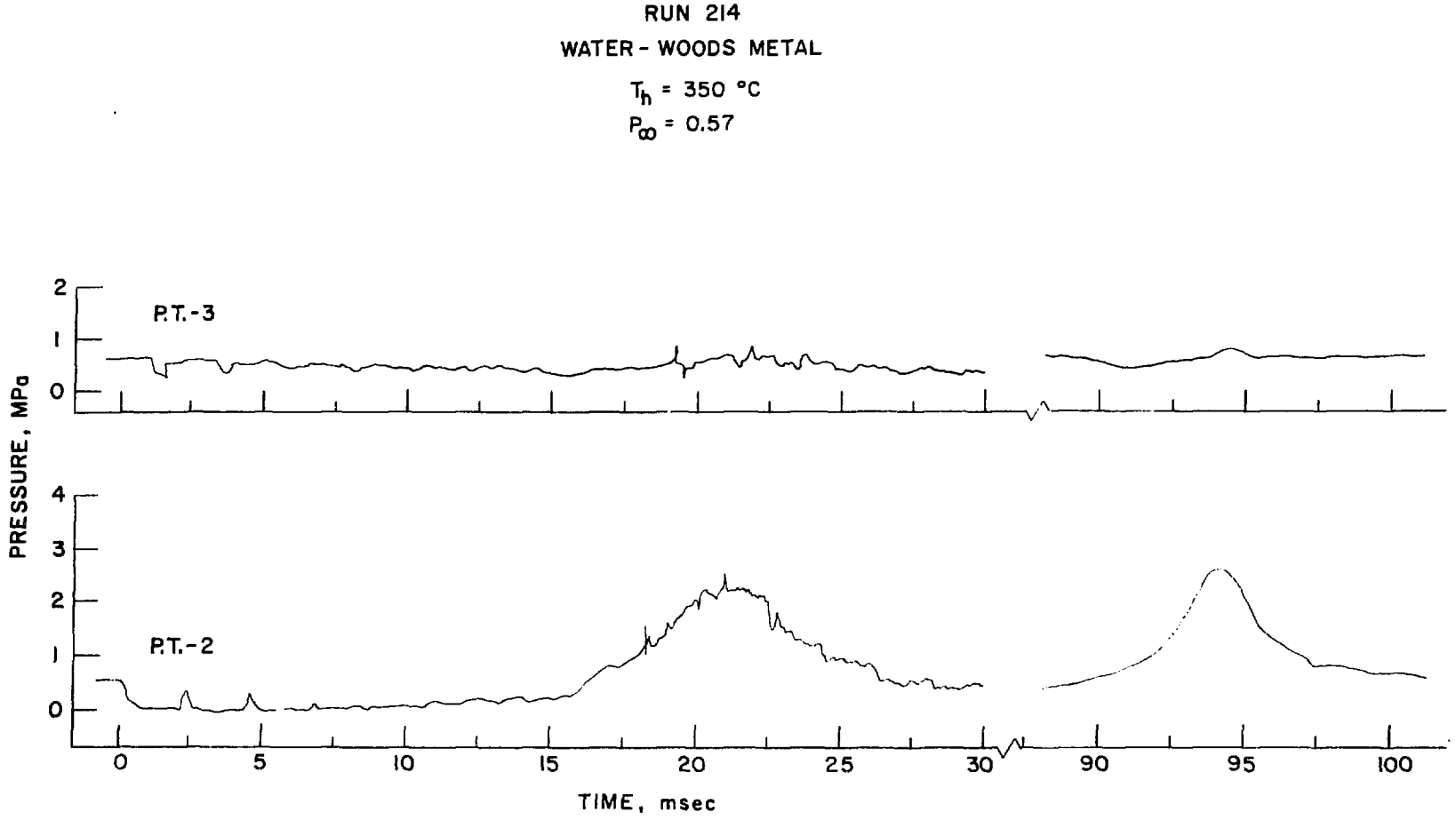

Fig. F.1. Pressure History of Run 214

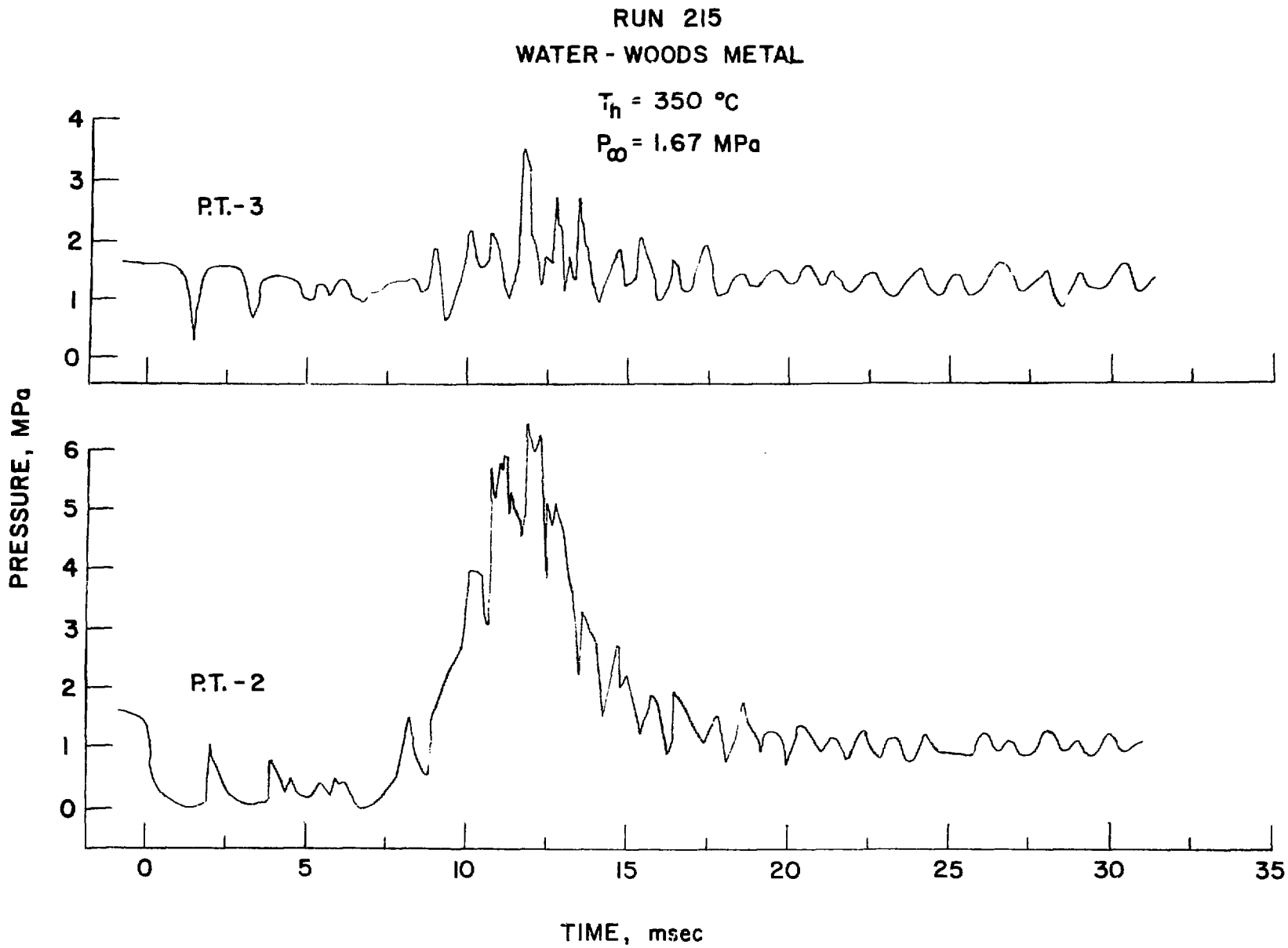

Fig. F.2. Pressure History of Run 215

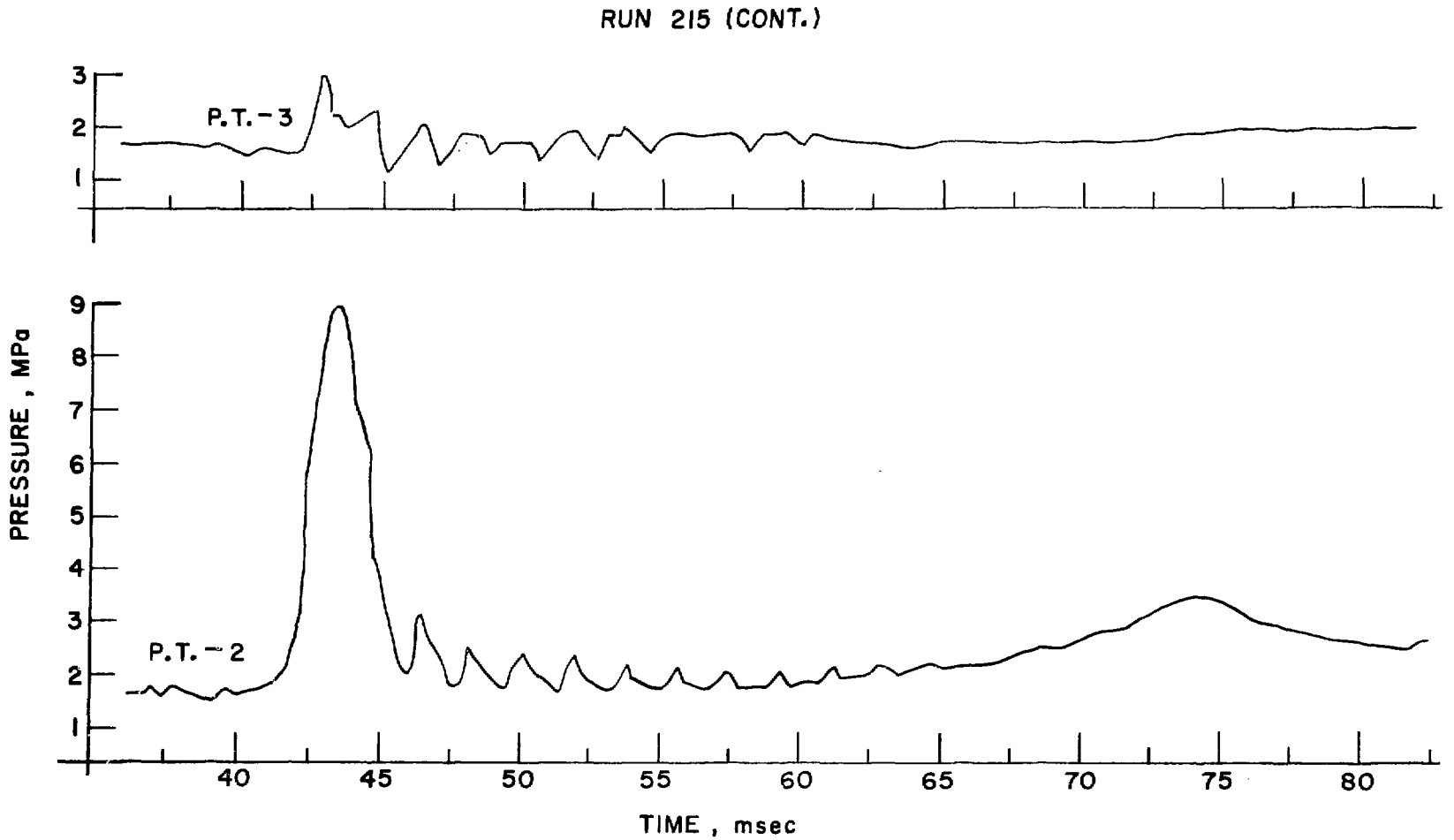

Fig. F.2. Pressure History of Run 215(contd.)

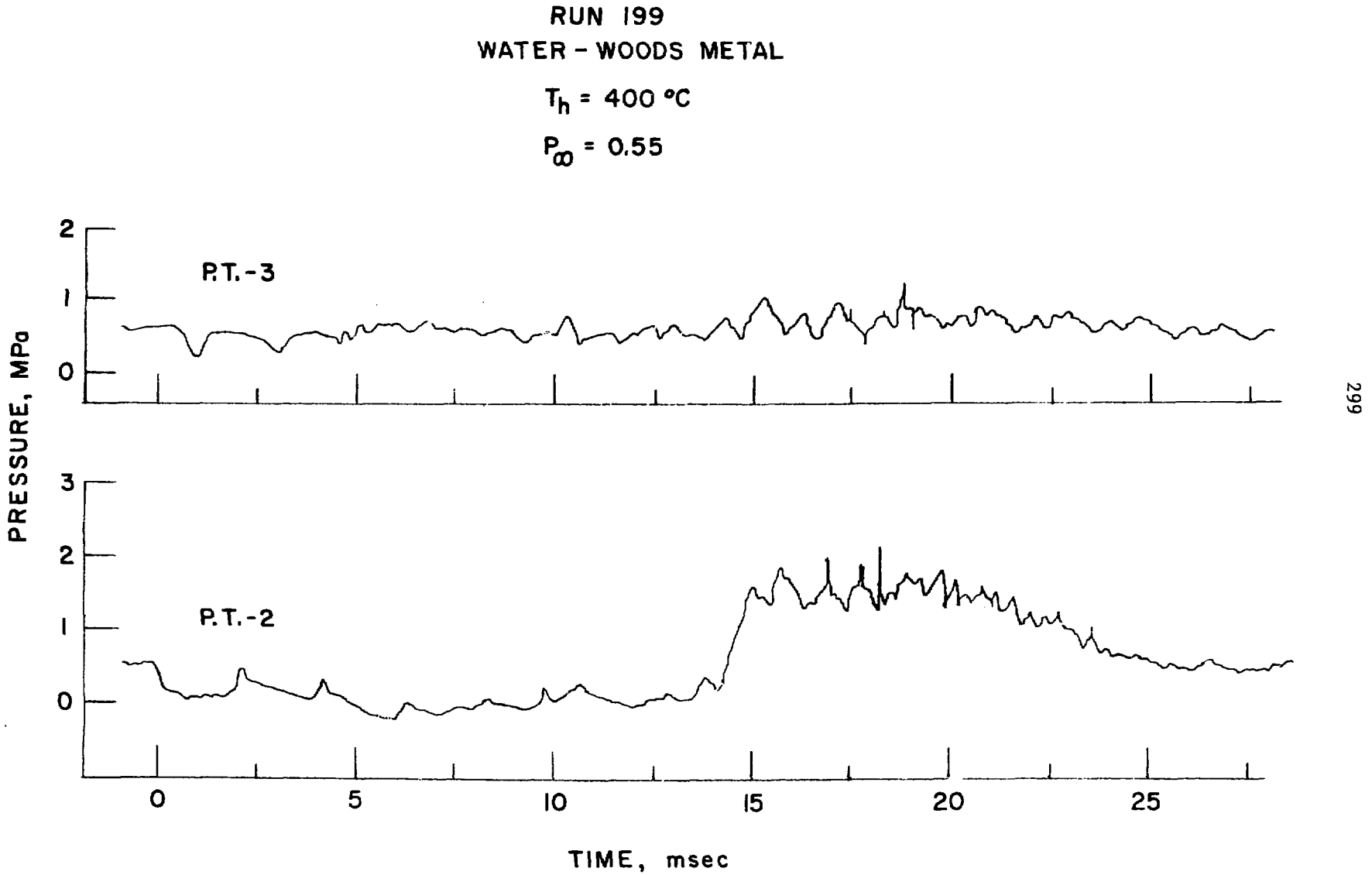

Fig. F.3. Pressure History of Run 199

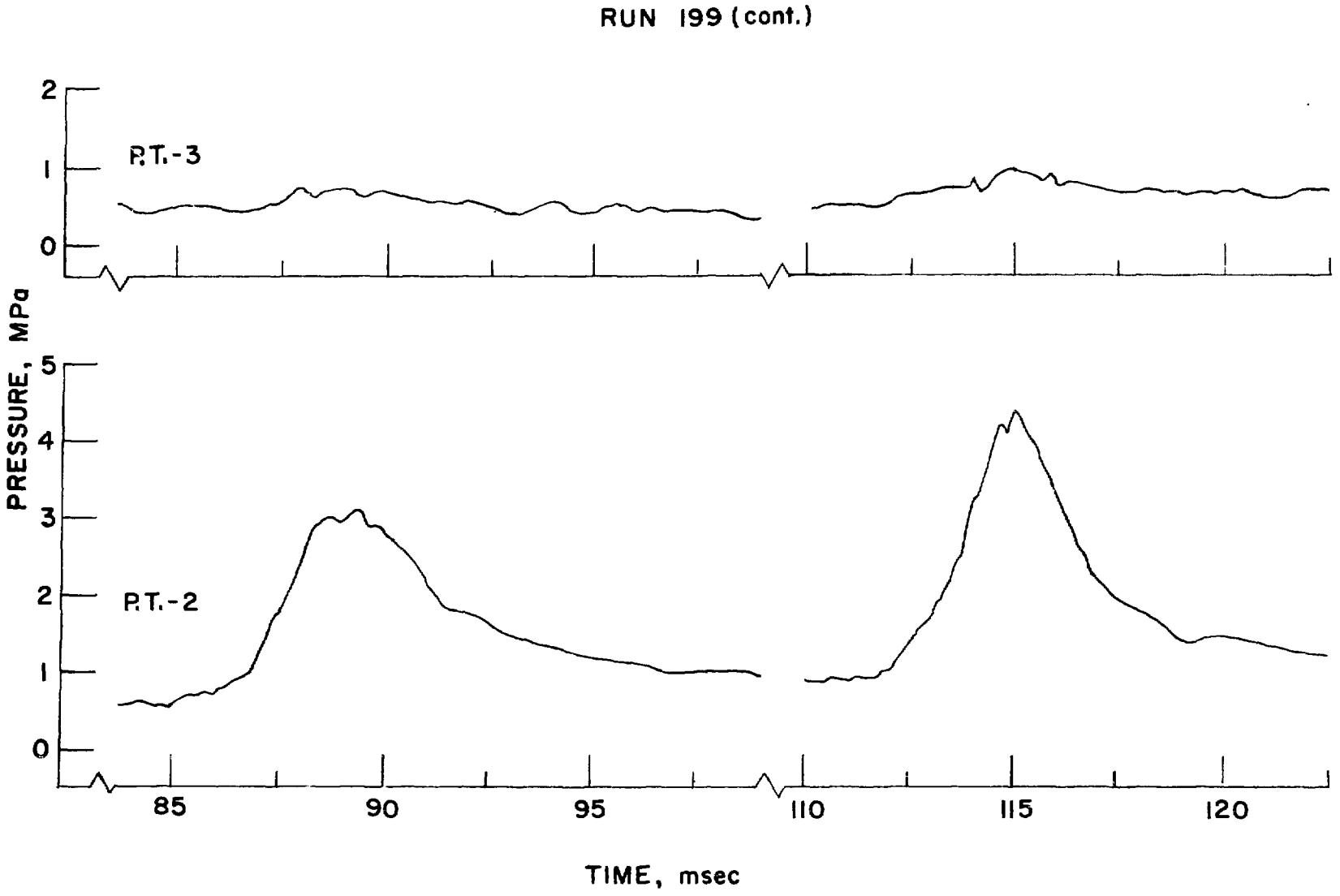

Fig. F.3. Pressure History of Run 199(contd.)

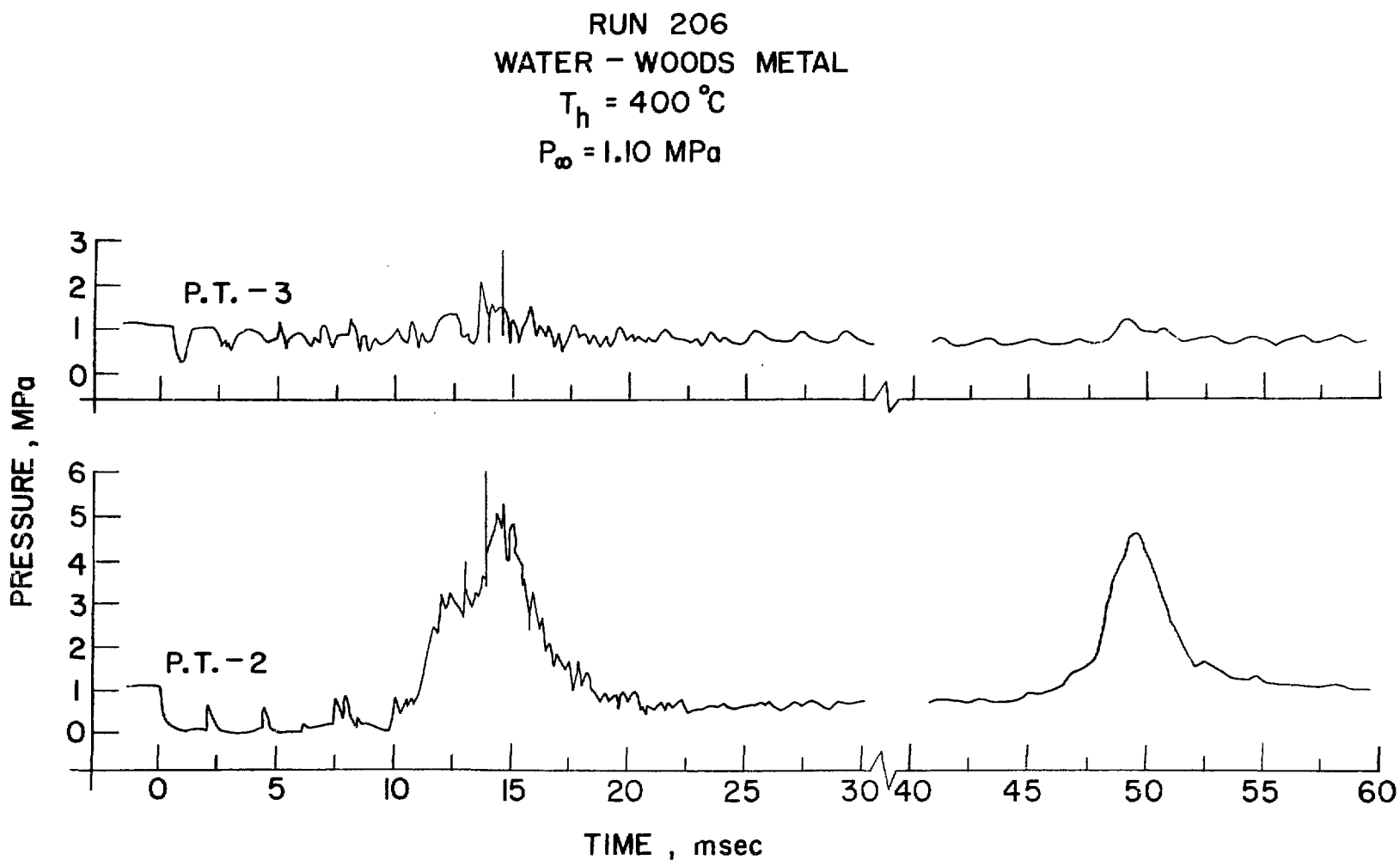

Fig. F.4. Pressure History of Run 206

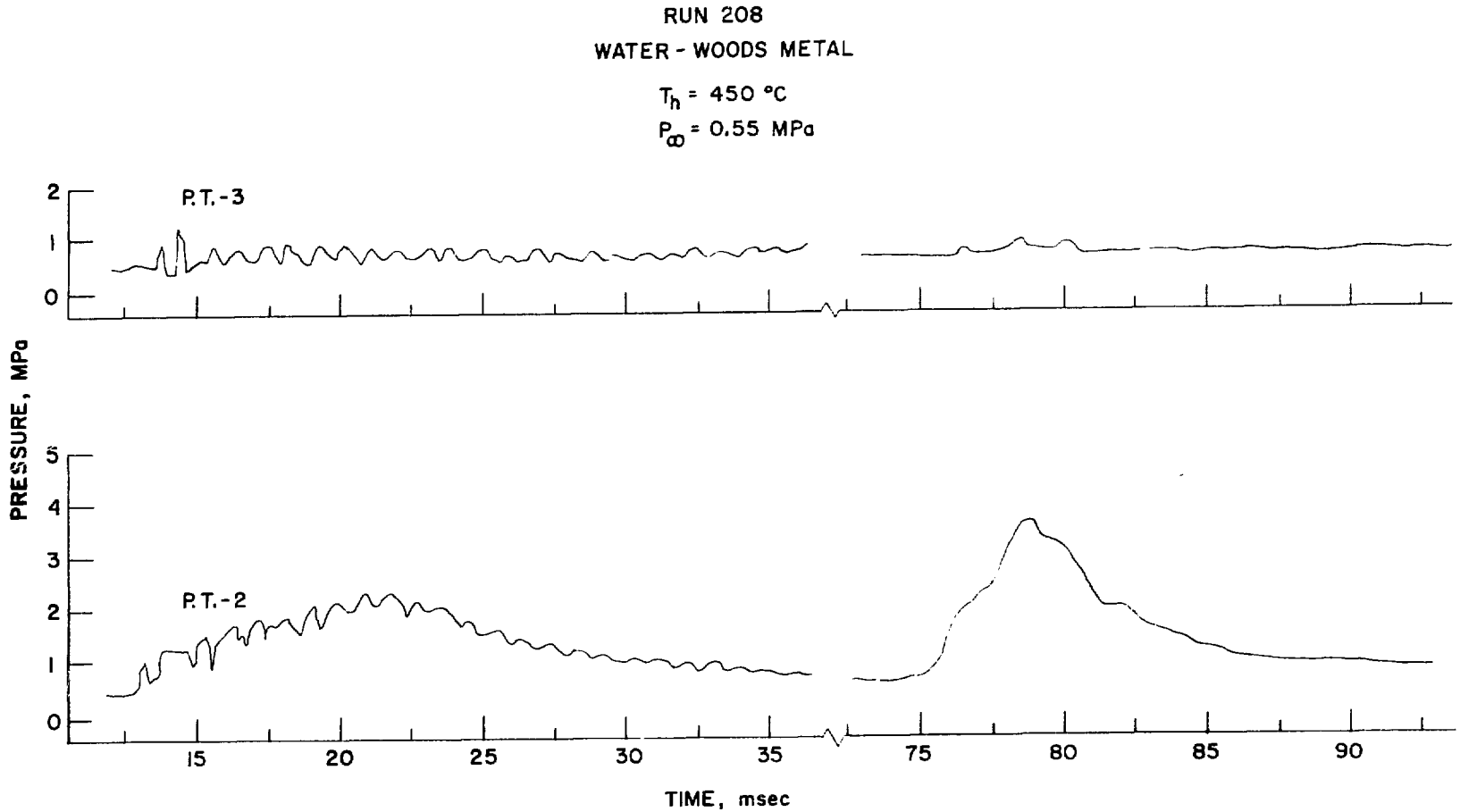

Fig. F.5. Pressure History of Run 208

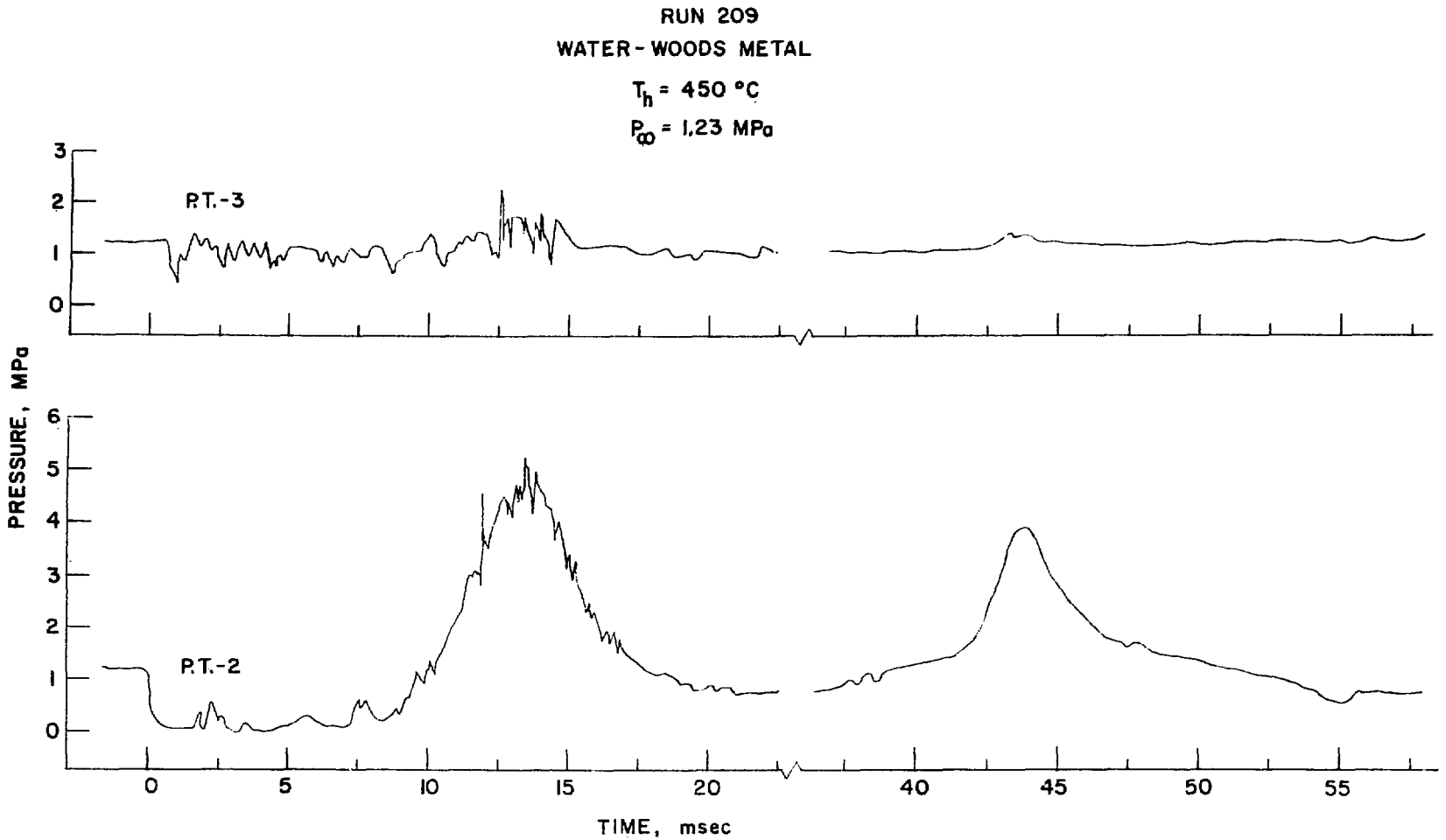

Fig. F.6. Pressure History of Run 209

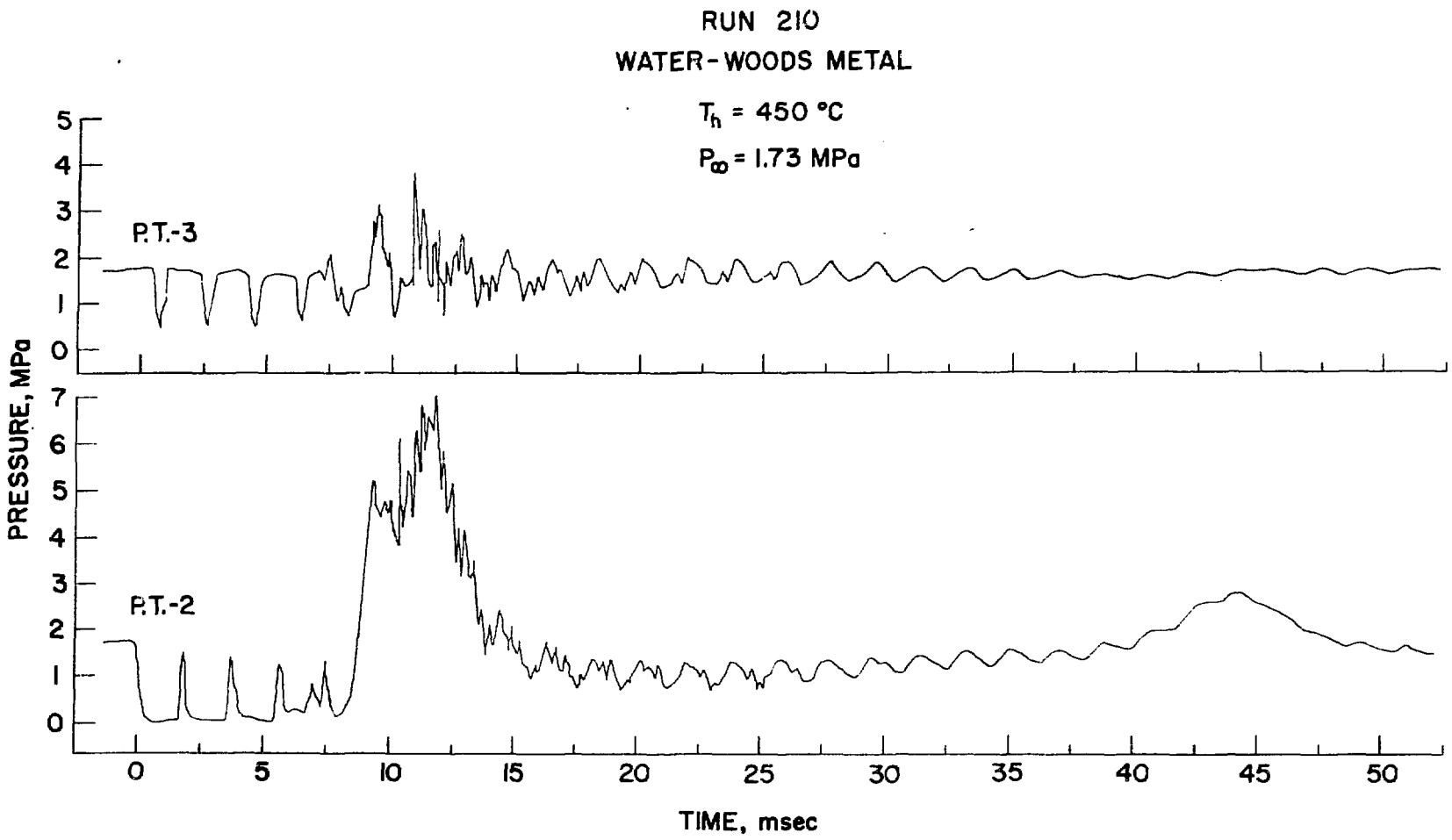

Fig. F.7. Pressure History of Run 210

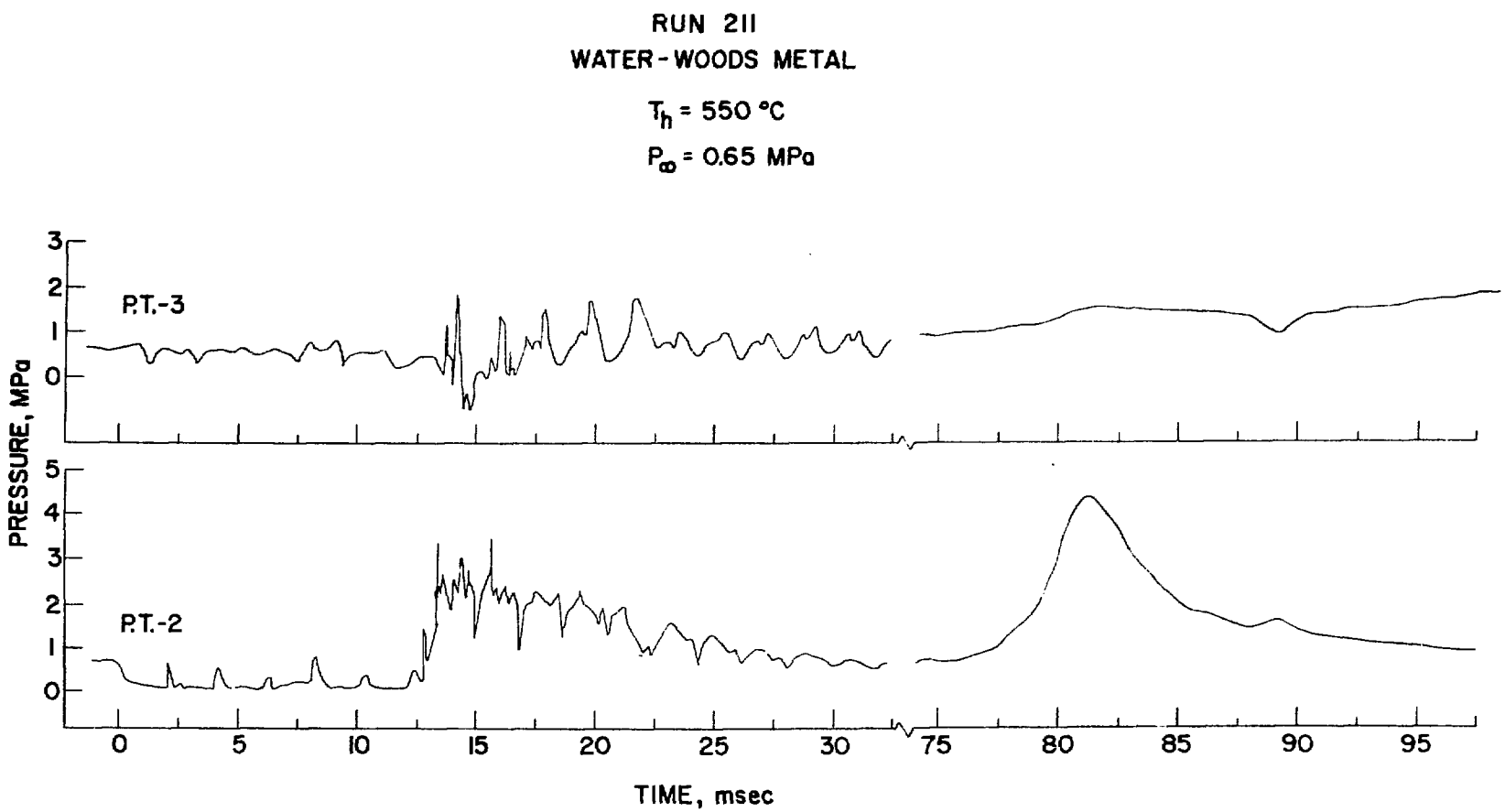

Fig. F.8. Pressure History of Run 211

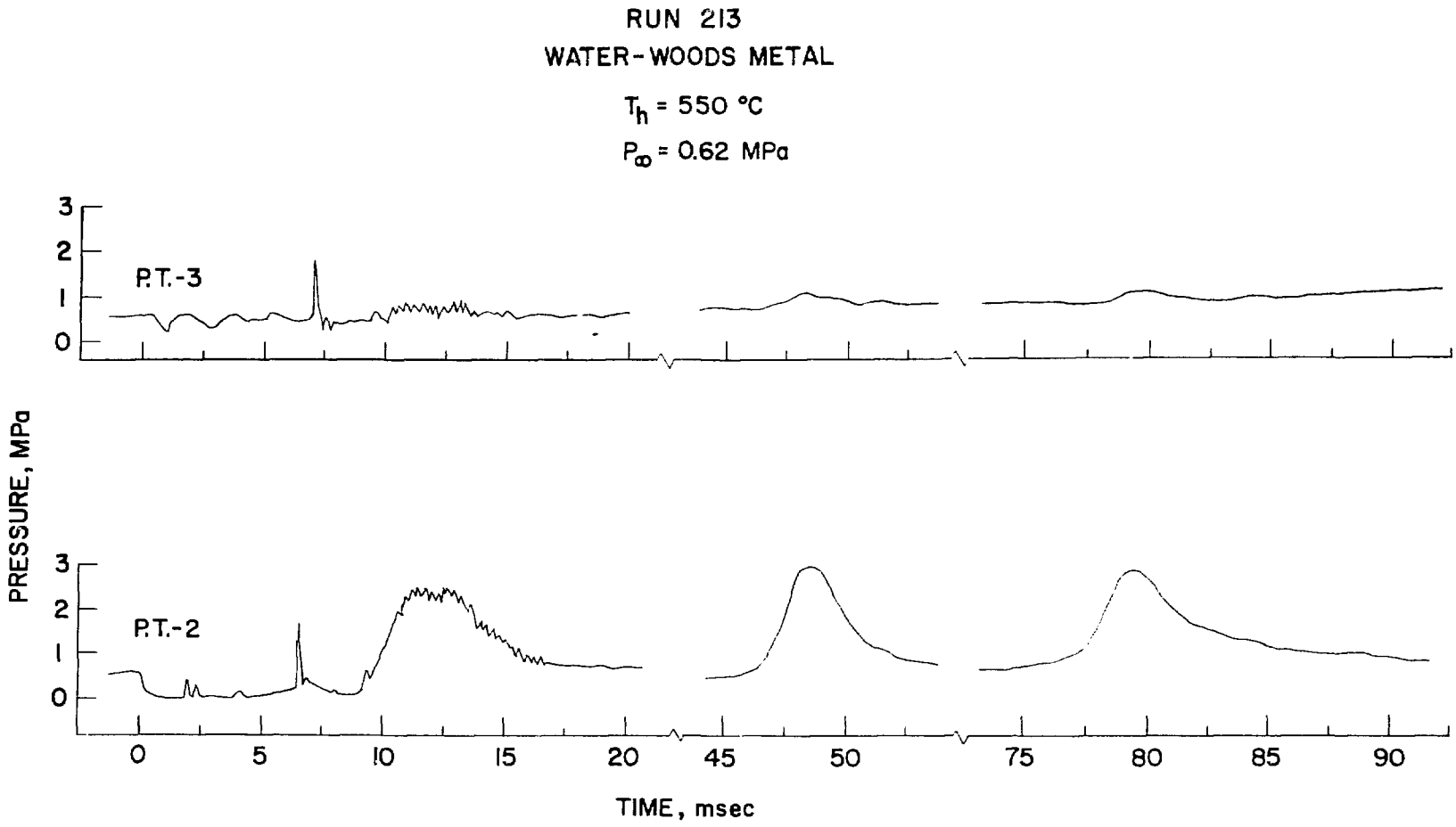

Fig. F.9. Pressure History of Run 213

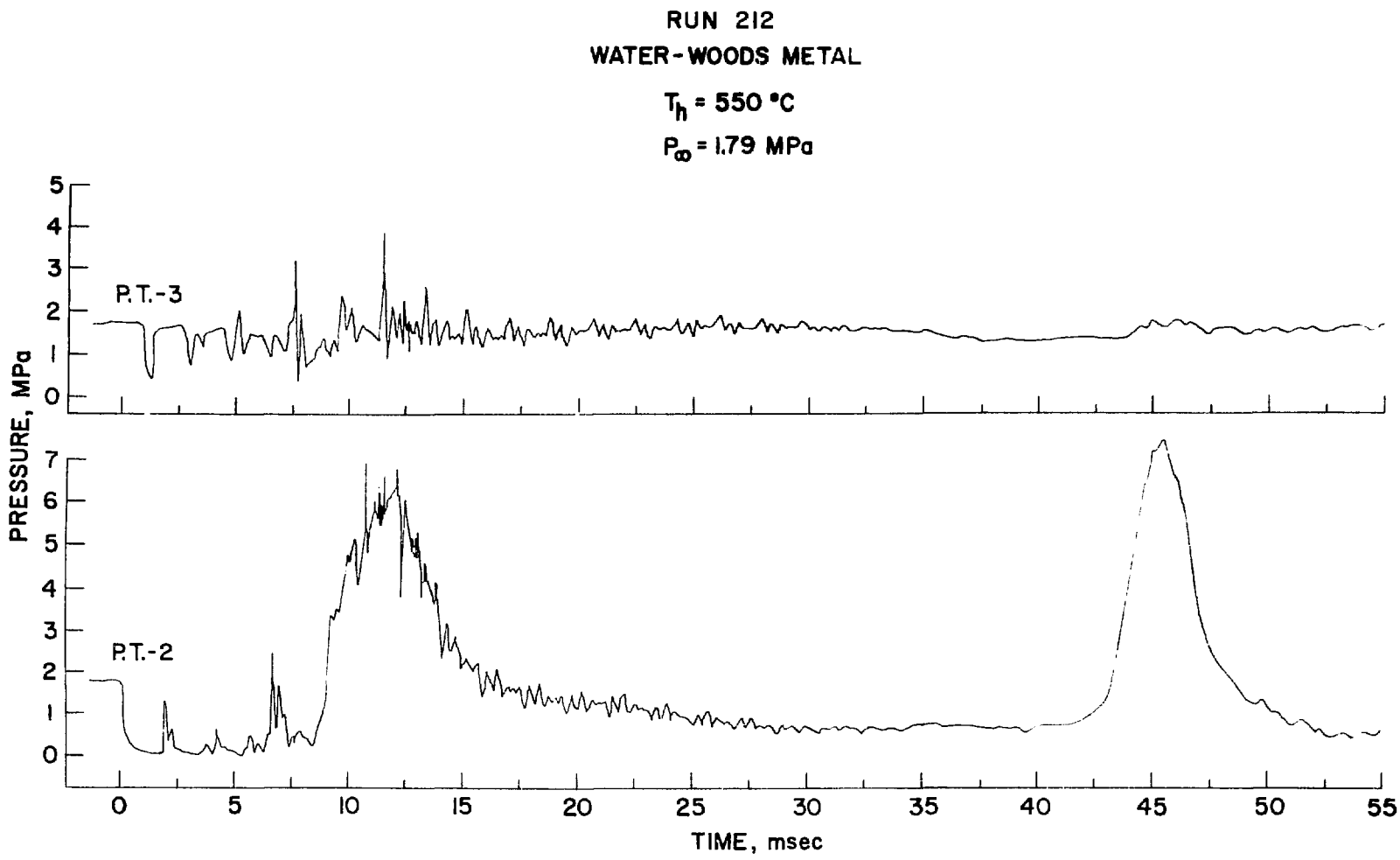

Fig. F.10. Pressure History of Run 212

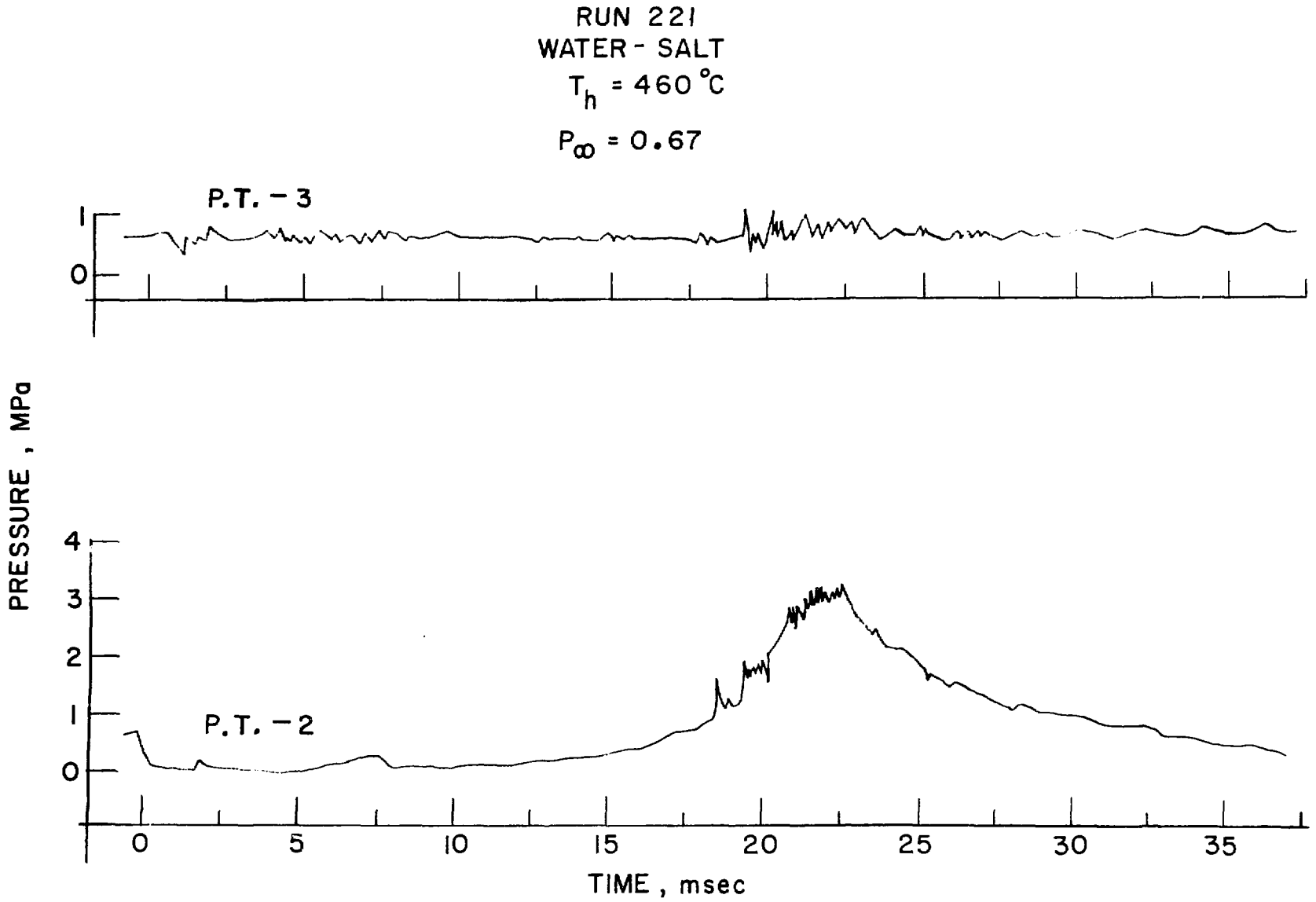

Fig. F.11. Pressure History of Run 221

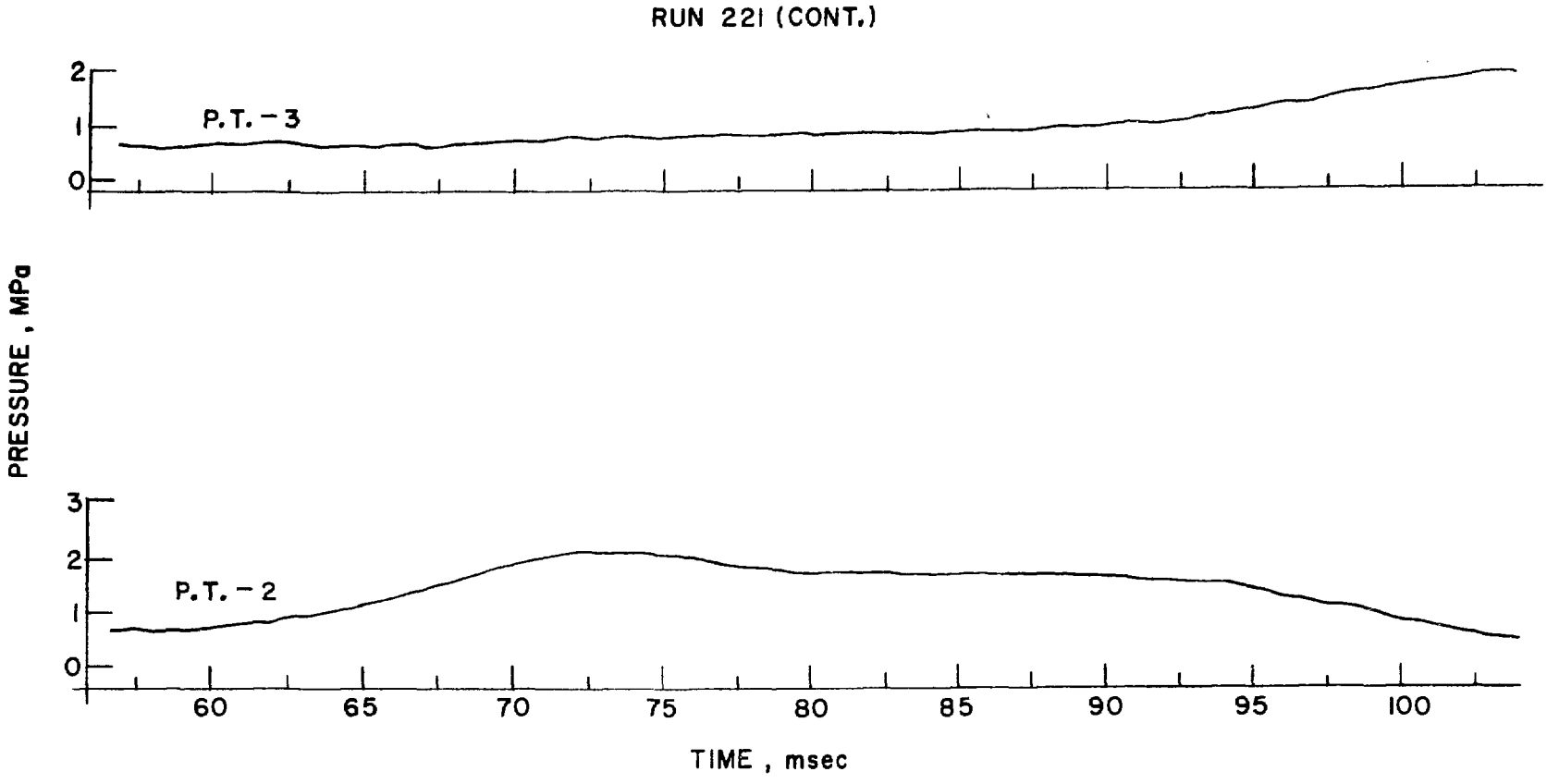

Fig. F.11. Pressure History of Run 221(contd.)

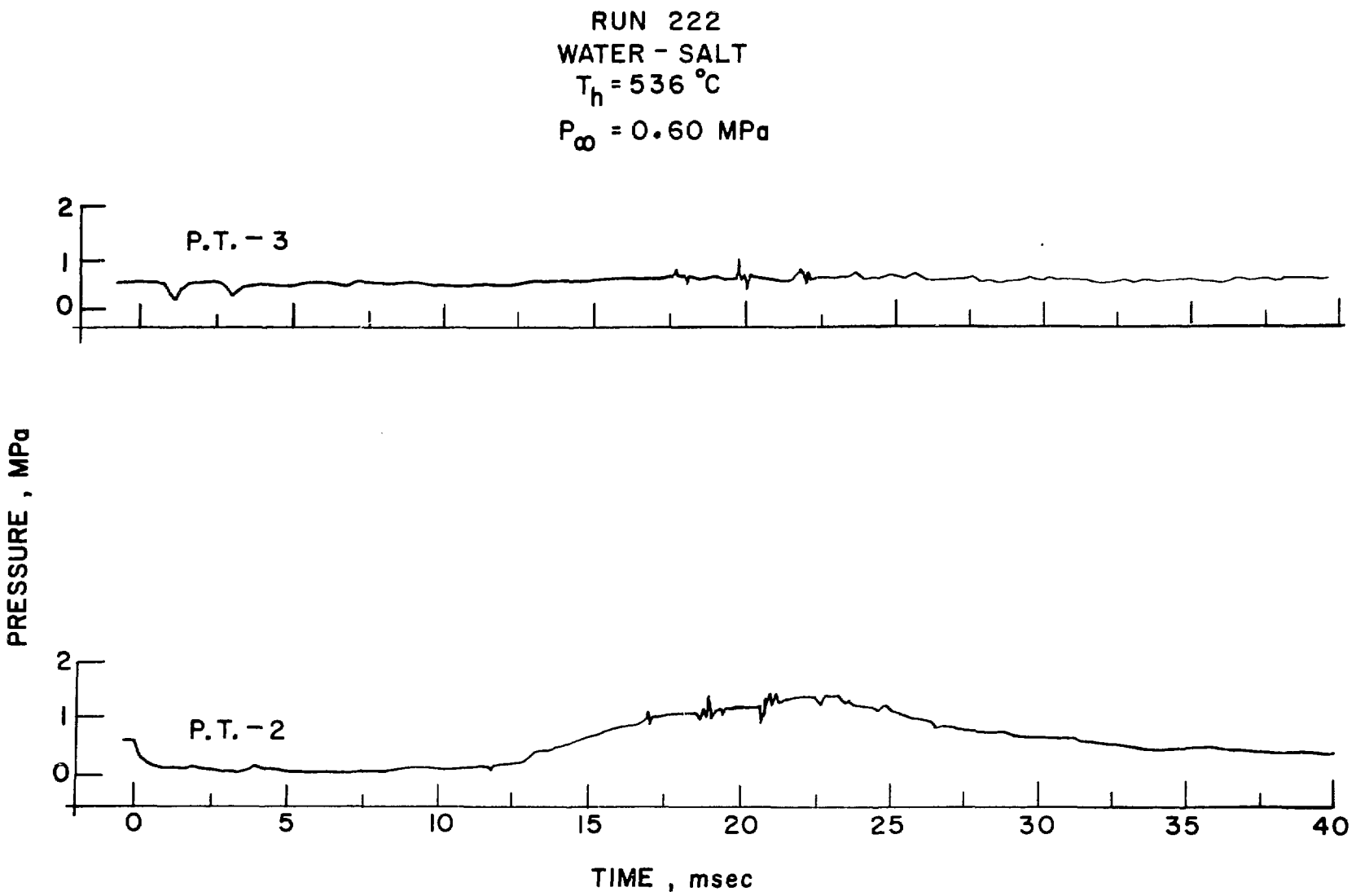

Fig. F.12. Pressure History of Run 222

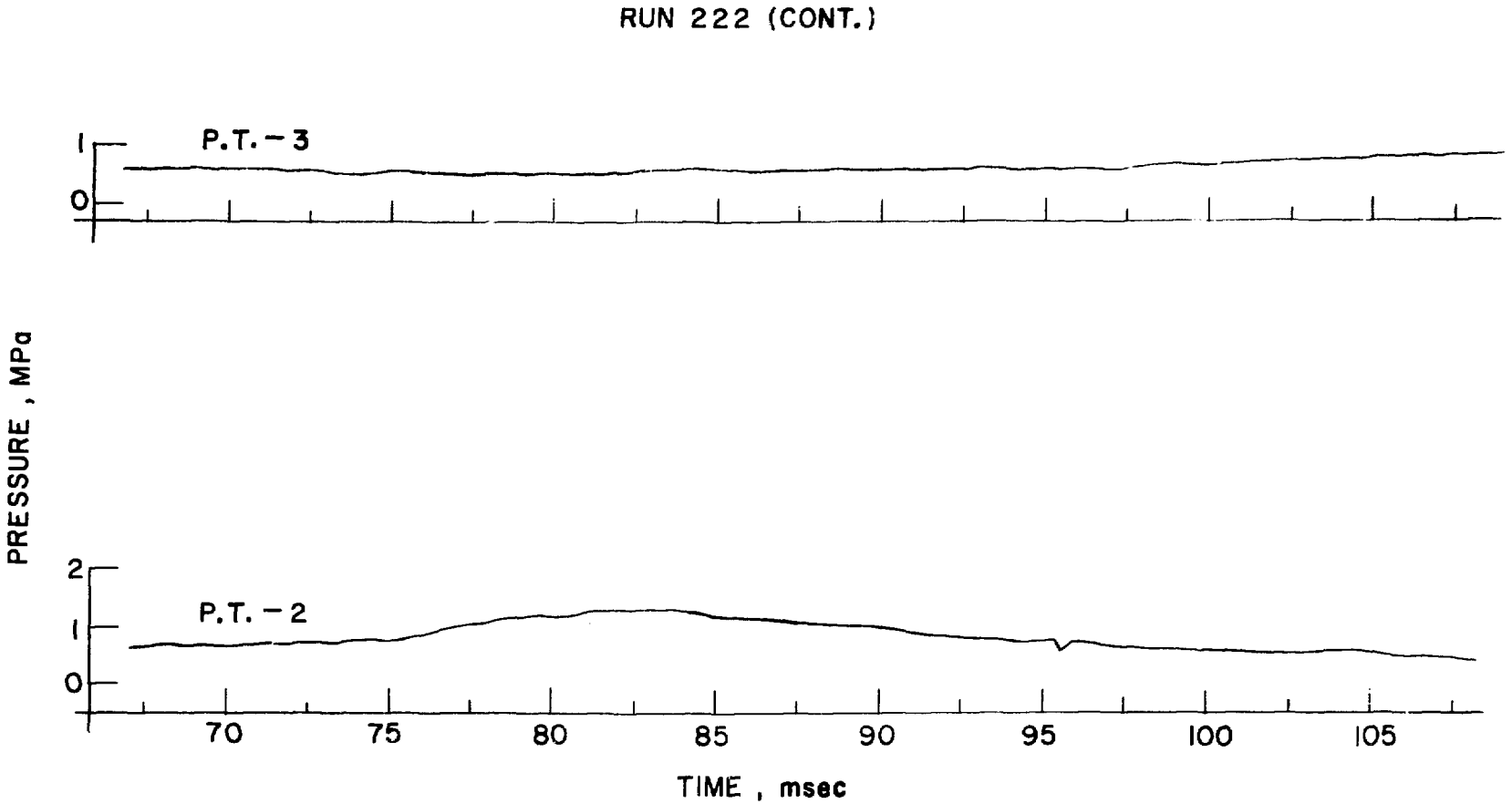

Fig. F.12. Pressure History of Run 222(contd.)

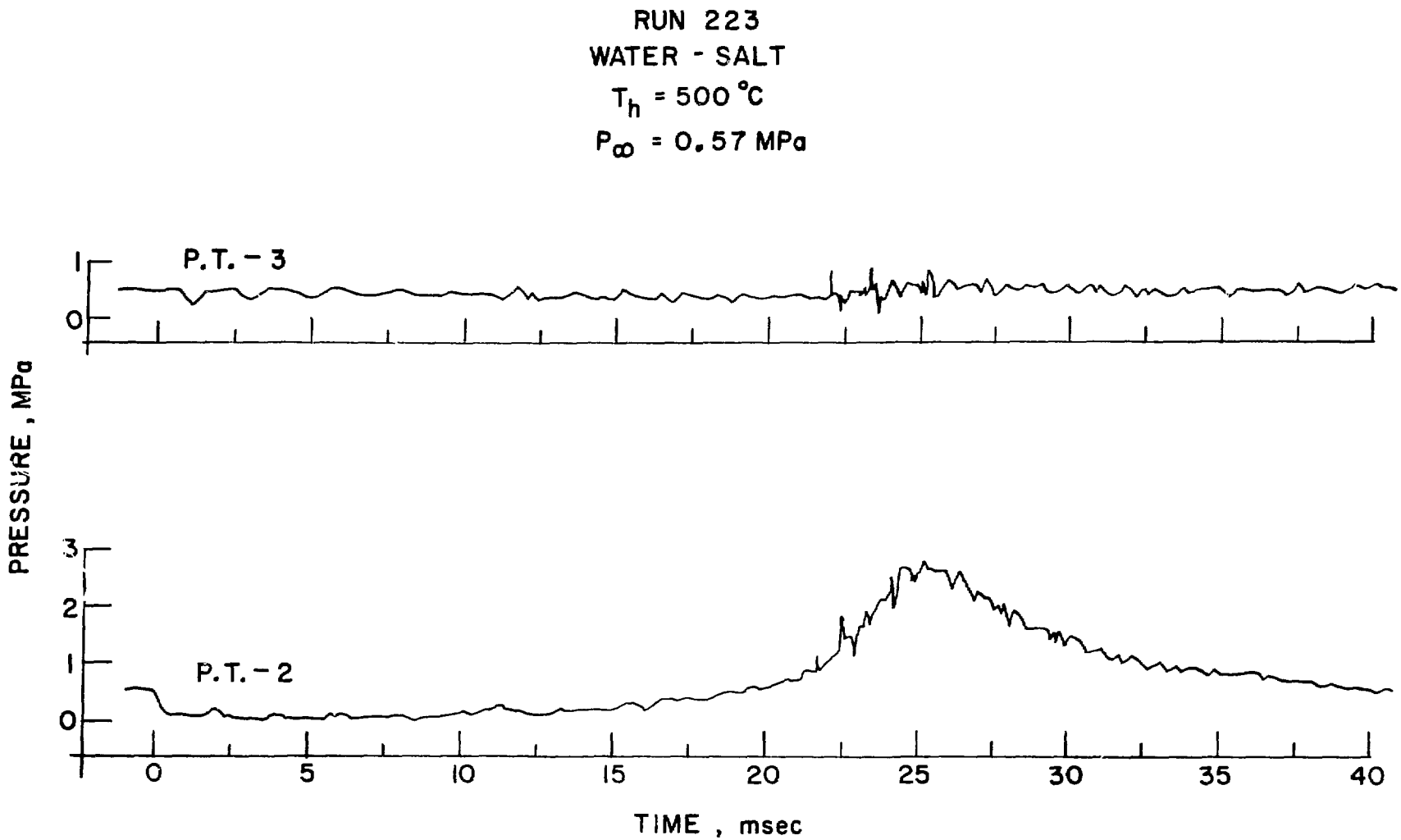

Fig. F.13. Pressure History of Run 223

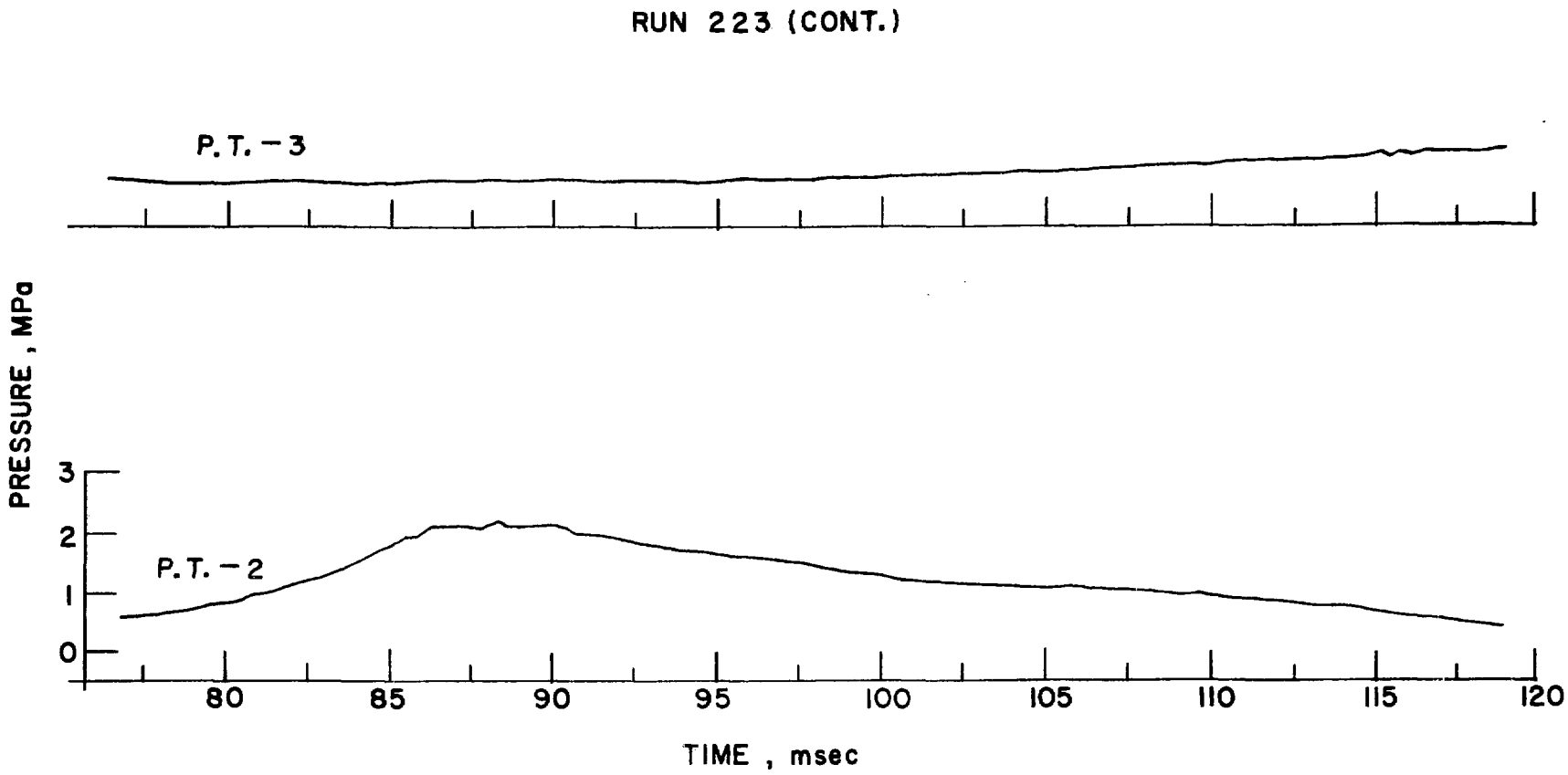

Fig. F.13. Pressure History of Run 223(contd.)

ACKNOWLEDGMENTS

I would like to express my gratitude to my coadvisors, Professor S. G. Bankoff for his helpful discussions and suggestions as a teacher and as a personal friend during my graduate study, and Dr. R. E. Henry for his assistance in time and knowledge and his valuable constructive criticism during the experimental investigation.

My appreciation is extended to Mr. D. J. Quinn and Mr. E. A. Spleha for their all-around assistance and technical advise, to Gregory Zahradnik for his helpful assistance in carrying out this experimental investigation, and to Mrs. Loretta Pavlik for her careful and efficient typing of the manuscript.

Many thanks are extended to the Experimental Modeling Section of the Reactor Analysis and Safety Division of Argonne National Laboratory for supporting the experimental investigation.

Finally, I want to express my deepest gratitude to my wife, Batya, and my sons, Dorry and Gilly, whose love and encouragement supported me during my years of study.

REFERENCES

1. Percy, J., Metallurgy, p. 625, J. Murray, London, 1864.

2. Lipsett, S.G., "Explosions from Molten Materials and Water," Fire Technology, p. 118 (1966).

3. Epstein, L.F., "Metal-Water Reactions: VII. Reactor Safety Aspects of Metal-Water Reactions,"USAEC Report No. GEAP-3335 (Jan 1960).

4. Witte, L.C., Cox, J.E., and Bourvier, J.E., "The Vapor Explosion," J. Metals, 22, p. 39 (1970).

5. Proctor, J.F., "Adequacy of Explosion-Response Data in Estimating Reactor-Vessel Damage," Nuclear Safety, 8, (6), p. 565 (1967).

6. Buxton, L.D., and Nelson, L.S., "Steam Explosions," Ch. 6, Report No. SAND 74-0382 (1975).

7. Anderson, R.P., and Armstrong, D.R., "Comparison Between Vapor Explosion Models and Recent Experimental Results," 14th Natl. Heat Transfer Conf., AIChE-ASME, Atlanta, GA (1973).

8. Cronenberg, A.W., and Grolmes, M.A., "A Review of Fragmentation Models Relative of Molten UO_2 Breakup When Quenched in Sodium Coolant," ASME Winter Annual Mtg., New York, NY (1974).

9. Long, G., "Explosions of Molten Aluminum in Water-Cause and Prevention," Metal Progress, 71, p. 107 (1957).

10. Cho, D.H., Gunther, W.H., and Armstrong, D.R., "Fragmentation of Molten Materials Dropped into Water," ANL-8155 (1974).

11. Cho, D.H., Gunther, W.H., and Armstrong, D.R., "Fragmentation of Molten Materials Dropped into Water," ANL-8155 (1974).

12. McCracken, G.M., "Investigation of Explosions Produced by Dropping Liquid Metals into Aqueous Solutions," Safety Research Bulletin of the Safety and Reliability Directorate, Issue No. 1, p. 20, UKAEA (1973).

13. Reynolds, J.A., Dullforce, T.A., Peckover, R.S., and Vaughan, G.J., "Fuel-Coolant Interactions-Some Basic Studies at the UKAEA Culham Laboratory," Proc. Third Specialist Mtg on SFI in Fast Reactors, PNC N251 76-12, 1, p. 97, Tokyo (1976).

14. Mizuta, H., "Fragmentation of Uranium Dioxide After Molten Uranium Dioxide-Sodium Interaction," J. Nucl. Sci. and Tech., 11, p. 480 (1974).

15. Armstrong, D.R., Testa, F.J., and Raridon, D., Jr., "Interaction of Sodium with Molten UO_2 and Stainless Steel Using a Dropping Mode of Contact," ANL-7890 (1971).

16. Bradley, R. H., and Witte, L. C., "Explosive Interaction of Molten Metals Injected Into Water," Nucl. Sci. Eng., 48, p. 387 (1972).

17. Anderson, R.P., and Bova, L., "Final Report on the Small Scale Vapor-Explosion Experiments Using a Molten NaCl-H_2O System," ANL-76-57 (1976).

18. Armstrong, D.R., Goldfuss, G.T., and Gebner, R.H., "Explosive Interaction of Molten UO_2 and Liquid Sodium," ANL-76-24 (1976).

19. Asher, R.C., Bradshaw, L., Collett, R., and Davies, D., "Experimental Work at Harwell on the Injection of Sodium into Liquid Steel," Proc. Third Specialist Mtg. on SFI in Fast Reactors, Tokyo PNC N251 76-12, 1, p. 341 (1976).

20. Abbey, M.J., Asher, R.C., Bradshaw, L., Davies, D., and Sangwinw, S.J., "The Injection of Sodium into Liquid Stainless Steel: A Report of the Second Experimental Na-SS/1," ibid, p. 363.

21. Wright, R.W., Firstenberg, A.F., and Humberstong, G.H., Neal, L.G., Wentz, L.B., and Zivi, S.M., "Kinetic Studies of Heterogeneous Water Reactors-Annual Summary Report-1966," USAEC Report No. STL-372-50 (1966).

22. Darby, K., Pottinger, R.C., Rees, N.J.M., and Turner, R.G., "The Thermal Interaction Between Water and Molten Aluminum Under Impact Conditions in a Strong Tube," Proc. of the Intl. Conf. on Eng. of Fast Reactors for Safe and Reliable Operation, Oct. 9-13, 1972, Karlsruhe, p. 898.

23. Hillary, J.J., Curry, P., and Taylor, L.R., "Preliminary Experimental Studies of the Interaction of Water and Molten Lead and Molten Salt Mixtures," ibid, p. 852.

24. Hinze, J.O., "Critical Speeds and Sizes of Liquid Globules," App. Sci. Res., A1, p. 273 (1948).

25. Hinze, J.O., "Forced Deformations of Viscous Liquid Globules," Appl. Sci. Res., A1, p. 263 (1948).

26. Board, S.J., and Hall, R.W., "Propagation of Thermal Explosions 1-Tin/Water Experiments," Central Elect. Generation Board Report No. RD/B/N2850 (1974).

27. Zyszkowski, W., "Experimental-Theoretical Investigation of the Thermal Explosions," Second Specialist Mtg. of SFI, Ispra, Italy (1973).

28. Bjornard, T.A., Rohsenow, W.M., and Todreas, N.E., "The Pressure Behavior Accompanying the Fragmentation of Tin in Water," Trans. Am. Nucl. Soc., 19, p. 247 (1974).

29. Bradfield, W.S., "Liquid-Solid Contact in Stable Film Boiling," I & EC Fundamentals, 5, No. 2, p. 200 (1966).

30. Watchters, L.H.J., Bonne, H., and Nouhmis, van, H.J., "The Heat Transfer from a Hot Horizontal Plate to Sessile Water Drops in the Spherodial State," Chem. Eng. Sci., 21, p. 923 (1966).

31. Berenson, P.J., "Film Boiling from a Horizontal Surface," Trans. ASME J. of Heat Transfer, 83, p. 351 (1961).

32. Spiegler, P., Hopenfeld, J., Silberberg, M., Bumpus, C.F., Jr., and Norman, A., "Onset of Stable Film Boiling and the Foam Limit," Intl. J. Heat and Mass Transfer, 6, p. 987 (1963).

33. Henry, R.E., "A Correlation for the Minimum Film Boiling Temperatures," 14th Natl. Heat Transfer Conf., Atlanta, GA (1973).

34. Baumeister, K.J., and Simon, F.F., "Leidenfrost Temperature-Its Correlation for Liquid Metals, Cryogens, Hydrocarbons and Water," Trans. ASME J. Heat Transfer, 95, p. 166 (1973).

35. Gordon, K.F., Singh, T., and Weissman, E.Y., "Boiling Heat Transfer Between Immiscible Liquids," Intl. J. Heat Mass Transfer, 3, p. 90 (1961).

36. Henry, R.E., Quinn, D.J., and Spleha, E.A., "An Experimental Study of the Minimum Film Boiling Point for Liquid-Liquid Systems," Fifth Intl. Heat Transfer Conf., Tokyo (1974).

37. Henry, R.E., and Fauske, H.K., "Energetics of Vapor Explosions," AIChE-ASME Natl. Heat Transfer Conf., San Francisco, CA (1975).

38. Ochiai, M., and Bankoff, S.G., "A Local Propagation Theory for Vapor Explosion," Proc. Third Specialist Mtg. on SFI in Fast Reactors, Tokyo, PNC 76-12, 1, p. 129 (1976).

39. Swift, D.L., and Baker, L., Jr., "Experimental Studies of the High-Temperature Interaction of Fuel and Cladding Materials with Liquid Sodium," Proc. of Conf. on Safety, Fuels, and Core Design in Large Fast Power Reactors, p. 839 (1965) Argonne National Laboratory, ANL-7120.

40. Brauer, F.E., Green, N.W., and Mesler, R.B., "Metal/Water Explosions," Nucl. Sci. Eng., 31, p. 551 (1968).

41. Cronenberg, A.W., Chawla, T.C., and Fauske, H.K., "Thermal Stress Mechanism for the Fragmentation of Molten UO_2 Upon Contact with Sodium Coolant," Nucl. Engr. and Design, 30, p. 434 (1974).

42. Caldarola, L., and Kastenberg, W.E., "On the Mechanism of Fragmentation During Molten Fuel/Coolant Thermal Interactions," Proc. Fast Reactor Safety Mtg., Beverly Hills, CA., p. 937 (1974).

43. Epstein, M., "Thermal Fragmentation--A Gas Release Phenomenon," Nucl. Sci. Eng., 55, p. 462 (1974).

44. Board, S.J., Hall, R.W., and Hall, R.S., "Detonation of Fuel Coolant Explosions," Nature, 254, p. 319 (1975).

45. Hicks, E.P., and Menzies, D.C., "Theoretical Studies on the Fast Reactor Maximum Accident," ANL-7120, p. 654 (1965).

46. Bankoff, S.G., Jo, J.H., ad Gauguli, A., "Mechanisms of Vapor Explosions," Int. Conf. on Fast Reactor Safety, Chicago, IL (1976).

47. Enger, T., and Hartman, D., "Rapid Phase Transformation During LNG Spillage on Water," Proc. Third Intl. Conf. on LNG, Washington, DC (1972).

48. Nakanishi, E., and Reid, R.C., "Liquid Natural Gas-Water Reactions," Chem. Eng. Progress, 67, (12), p. 36 (1971).

49. Porteous, W.M., and Reid, R.C., "Light Hydrocarbon Vapor Explosions," Chem. Eng. Prog., 72(5), p. 83 (1976).

50. Fauske, H.K., "Some Aspects of Liquid-Liquid Heat Transfer and Explosive Boiling," Proc. of Fast Reactor Safety Mtg., Beverly Hills, CA, p. 992 (1974).

51. Wakeshima, H., and Takota, K., "On the Limit of Superheat," J. of Physical Society of Japan, 13, p. 1398 (1958).

52. Henry, R.E., and Cho, D.H., "An Evaluation of the Potential for Energetic Fuel-Coolant Interactions in Hypothetical LMFBR Accidents," ASME Winter Annual Mtg., Atlanta, GA (1977).

53. Henry, R.E., et al., "Large-Scale Vapor Explosions," Proc. Fast Reactor Safety Mtg., Beverly Hills, CA, p. 922 (1974).

54. Board, S.J., Hall, R.W., and Brown, G.E., "The Role of Spontaneous Nucleation in Thermal Explosions: Freon/Water Experiments," ibid, p. 935.

55. Henry, R.E., Fauske, H.K., and McUmber, L.M., "Vapor Explosions in Subcooled Freon," Proc. Third Specialist Mtg. on SFI in Fast Reactors, Tokyo, PNC N251 76-12, 1, p. 231 (1976).

56. Corradini, M., Rohsenhow, W.M., and Todreas, N.E., "Application of Spontaneous Nucleation Theory to Tin-H_2O Interactions," MIT, Dept. Nucl. Eng. Report #COO-2781-11TR (1977).

57. Henry, R.E., and McUmber, L.M., "Vapor Explosion Potentials Under LWR Hypothetical Accident Conditions," ANS Topical Mtg. Thermal Reactor July 31-Aug 4, 1977, Sun Valley, ID.

58. Fauske, H.K., "On the Mechanism of Uranium Dioxide-Sodium Explosive Interactions," Nucl. Sci. Eng., 51, p. 95 (1973).

59. Waldram, K.L., Fauske, H.K., and Bankoff, S.G., "Impaction of Volatile Liquid Droplets onto a Hot Liquid Surface," AIChE-ASME Natl. Heat Transfer Conf., San Francisco, CA (1975).

60. Charles, G.E., and Mason, S.G., "The Coalescence of Liquid Drops with Flat Liquid/Liquid Interfaces," J. Colloid Sci., 15, p. 236 (1960).

61. Vrij, A., "Possible Mechanism for the Spontaneous Rupture of Thin, Free Liquid Films," Disc. Faraday Soc., 42, p. 23 (1966).

62. Marx, J.W., and Davies, B.I., "Film Boiling Mechanism," J. Appl. Phys., 23, (12), p. 1354 (1952).

63. Cameron, A., Basic Lubrication Theory, 2nd Edition, J. Wiley and Sons, Inc., New York (1976).

64. Baumeister, K.J., and Hamill, T.D. "Creeping Flow Solution to the Leidenfrost Phenomenon," NASA TN D-3133 (1965).

65. Jayaratne, O. W., and Mason, B. J., "The Coalescence and Bouncing of Water Drops at an Air/Water Interface," Proc. Roy. Soc., A280, p. 545, (1964).

66. Briggs, L.J., "Maximum Superheating of Water as a Measure of Negative Pressure," J. Appl. Phys., 26, p. 1001 (1955).

67. Henry, R.E., Fauske, H.K., and McUmber, L.M., "Vapor Explosion Experiments with Simulant Fluids," Int. Conf. on Fast Reactor Safety, Chicago, IL (1976).

68. Henry, R.E., private communication.

69. Goldammer, H., and Kottowski, H.M., "Physical Model and Calculation Code for Fuel Coolant Interactions," Proc. Third Specialist Mtg. on SFI in Fast Reactors, Tokyo, PNC N251 76-12, 2, p. 839 (1976).

70. Goldammer, H., and Kottowski, H.M., "Theoretical and Experimental Investigation of Fuel-Coolant Interactions in a Shock Tube Configuration," Int. Conf. on Fast Reactor Safety, Chicago, IL (1976).

71. Board, S.J., Duffey, R.B., Farmer, C.L., and Poole, D.H., "The Analysis of Metal-Water Explosions," Nucl. Sci. and Eng., 52, p. 433 (1973).

72. Hoskin, N. E., and Morgan, K., "Studies of Pressure Generation by Water Impact upon Molten Alunimum with Reference to Fast Reactor Subassembly Accidents," Proc. of Intl. Conf. on Eng. of Fast Reactors for Safe and Reliable Operation, Karlsruhe, Oct. 9-13, 1972, p. 870.

73. Cho, D.H., Fauske, H.K., and Grolmes, M.A., "Mixing Considerations for Large-Mass, Energetic Fuel-Coolant Interactions," Int. Conf. on Fast Reactor Safety, Chicago, IL (1976).

74. Skripov, V.P., Metastable Liquids, J. Wiley and Sons, Inc., New York (1974).

75. Carslaw, H.S., and Jeager, J.C., Conduction of Heat and Solids, 2nd Edition, Clarendon Press, Oxford (1959).

76. Vargaftik, N.B., Tables on the Thermophysical Properties of Liquids and Gases, 2nd Edition, J. Wiley & Sons, Inc. (1974).

77. International Critical Tables, McGraw-Hill (1927).

78. Turnbull, A.G., "The Thermal Conductivity of Molten Salts," Aust. J. Appl. Sci., 12(1), p. 30 (1961).

79. Van Artsdalen, E.R., and Yaffe, I.S., "Electrical Conductance and Density of Molten Salt System: KCl-LiCl, KCl-NaCl, and KCl-KI," J. Phys. Chem., 59, p. 118 (1955).

80. BNL Rep. #249 (1953).

81. Florschuetz, L.W., and Al-Jubouri, A.S., "Generalized Quantitative Criteria for Predicting the Rate-Controlling Mechanism for Vapor Bubble Growth in Superheated Liquids," Int. J. Heat Mass Transfer, 14, p. 587 (1971).

VITA

Name: Aryeh Segev

Place of Birth: France

[redacted]

EDUCATION: Earned B.Sc (August 1972) and M.Sc. (October 1974) in Mechanical Engineering from the Technion, Israel Institute of Technology. Enrolled in the Chemical Engineering Department of Northwestern in January 1975 for graduate work towards the Ph.D. Thesis. Joined the Reactor Analysis and Safety Division of Argonne National Laboratory in June 1976 to conduct the experimental part of this thesis.